Ecologie des foraminifères benthiques, interactions biologiques et géochimiques : approche pluridisciplinaire à différentes échelles

Constance Choquel

▶ **To cite this version:**

Constance Choquel. Ecologie des foraminifères benthiques, interactions biologiques et géochimiques : approche pluridisciplinaire à différentes échelles. Earth Sciences. Université d'Angers, 2021. English. NNT : 2021ANGE0011 . tel-03413987

HAL Id: tel-03413987
https://theses.hal.science/tel-03413987

Submitted on 4 Nov 2021

HAL is a multi-disciplinary open access archive for the deposit and dissemination of scientific research documents, whether they are published or not. The documents may come from teaching and research institutions in France or abroad, or from public or private research centers.

L'archive ouverte pluridisciplinaire **HAL**, est destinée au dépôt et à la diffusion de documents scientifiques de niveau recherche, publiés ou non, émanant des établissements d'enseignement et de recherche français ou étrangers, des laboratoires publics ou privés.

DOCTORAT SCIENCES BRETAGNE DE LA MER LOIRE ET DU LITTORAL

université angers

THESE DE DOCTORAT DE

L'UNIVERSITE D'ANGERS

ECOLE DOCTORALE N° 598
Sciences de la Mer et du Littoral
Spécialité : Ecologie marine

Par

Constance CHOQUEL

Ecologie des foraminifères benthiques, interactions biologiques et géochimiques ; approche pluridisciplinaire à différentes échelles

Thèse présentée et soutenue à Angers, le 9 juillet 2021

Unité de recherche : UMR CNRS 6112 LPG-BIAF : Bioindicateurs Actuels et Fossiles

Rapporteurs avant soutenance :

Petra HEINZ	Professeure Université de Vienne
Lionel DENIS	Professeur Université de Lille

Composition du Jury :

Vincent BOUCHET	Maître de conférences Université de Lille
Vona MELEDER	Maître de conférences Université de Nantes
Pierre ANSCHUTZ	Professeur Université de Bordeaux
Directrice de thèse : Emmanuelle GESLIN	Professeure Université d'Angers
Co-encadrants de thèse : Aurelia MOURET	Maître de conférences Université d'Angers
Bruno JESUS	Maître de conférences Université de Nantes

DOCTORAT SCIENCES BRETAGNE DE LA MER LOIRE ET DU LITTORAL

université angers

THESE DE DOCTORAT DE

L'UNIVERSITE D'ANGERS

ECOLE DOCTORALE N° 598
Sciences de la Mer et du Littoral
Spécialité : Ecologie marine

Par

Constance CHOQUEL

Ecologie des foraminifères benthiques, interactions biologiques et géochimiques ; approche pluridisciplinaire à différentes échelles

Thèse présentée et soutenue à Angers, le 9 juillet 2021

Unité de recherche : UMR CNRS 6112 LPG-BIAF : Bioindicateurs Actuels et Fossiles

Rapporteurs avant soutenance :

Petra HEINZ	Professeure Université de Vienne
Lionel DENIS	Professeur Université de Lille

Composition du Jury :

Vincent BOUCHET	Maître de conférences Université de Lille
Vona MELEDER	Maître de conférences Université de Nantes
Pierre ANSCHUTZ	Professeur Université de Bordeaux
Directrice de thèse : Emmanuelle GESLIN	Professeure Université d'Angers
Co-encadrants de thèse : Aurelia MOURET	Maître de conférences Université d'Angers
Bruno JESUS	Maître de conférences Université de Nantes

REMERCIEMENTS

Merci à mes encadrants de thèse Emmanuelle Geslin, Aurélia Mouret et Bruno Jesus de m'avoir permis de vivre cette aventure de thèse. Merci de m'avoir fait confiance, de m'avoir fait voyager, de m'avoir appris tant de choses. J'ai vécu cette thèse comme un challenge personnel, un dépassement de soi motivé par la prise conscience de faire partie d'un projet scientifique bien plus grand. Merci à tous les co-auteurs de cette thèse pour vos expertises et votre bienveillance, en particulier : Edouard Metzger, Helena Filipsson, Nils Risgaard-Petersen, Patrick Launeau, Liliane Jean-Soro, Aubin Thibault de Chanvalon, Thierry Jauffrais, Emilie Houliez. Merci aux membres de mon jury d'avoir accepté de juger ce travail ainsi qu'aux membres de mon CSI Christine Dupuy et Bruno Deflandre, pour votre soutien et vos conseils.

Famille BIAF, 4 ans et demi se sont écoulés depuis que j'ai débarqué chez vous. Merci à Christine Barras et Briz Parent avec qui l'aventure Foraminifère a commencé pendant mon stage de Master 2. A l'époque j'étais tellement intimidée devant tant de personnes charismatiques au tempérament bien trempé. Vous n'imaginez pas à quel point j'ai dû travailler sur mon for intérieur ! Le chocolat a dû aider un peu aussi… chocolat « géochimiste » (au lait fruits secs) ou chocolat « foraminifériste » (noir aux noisettes) entre les deux mon cœur balance, mais pourquoi choisir ? ☺ Merci à tous les maîtres de conférence/ ingénieurs : Christine, Pia, Meryem, Franz, Hélène, Grégoire, Fabrice, Magali, pour tous ces moments forts de discussions scientifiques et de convivialité. Merci particulièrement à Hélène de m'avoir fait découvrir les coulisses de l'école doctorale. Merci à l'équipe technique Eric, Sophie Q., Sophie S. Merci également à Luzia et Sophie V. pour toute l'aide administrative. Merci aux thésards devenus docteurs avec qui j'ai partagé ma vie de thèse : Matthieu, Briz, Jean-Baptiste, Julien, Sitraka, Louise, j'arrive ! Aux jeunes docteurs lâchés dans le grand bain de la recherche : Charlotte, Laurie, Sandrine, Inge, Christiane, Aurélie, Vivien, Julia et David, merci pour votre soutien et tous vos conseils (l'après-thèse semble être aussi un challenge !). Bon courage aux docteurs en devenir : Marie, Eleonora, Pauline, Corentin, Hélène, je suis de tout cœur avec vous !

Merci également à mes amies de longue date (Léa, Manon, Anne-Hélène, Célia…) pour votre soutien et les appels visio, maudit covid ! De si longues semaines de convalescence n'ont pas facilitée la fin de ma thèse... Merci à mes parents pour leur soutien indéfectible. Merci de m'avoir toujours encouragée et suivie dans le dédale des études universitaires aussi bien moralement et financièrement, je ne serais jamais arrivée aussi loin sans vous <3.

« Je pars pour une aventure » - Bilbon Saquet - *Le Hobbit, un voyage inattendu* [J.R.R Tolkien].

FOREWORD

This thesis work was mainly carried out in the LPG-BIAF laboratory (UMR CNRS 6112) at the University of Angers. This thesis project has received multiple fundings: the FRESCO project (Region Pays de la Loire and University of Angers), the MANGA 2D project (CNRS-INSU), the MUDSURV project (OSUNA and the LPG –BIAF laboratory). Field campaigns in Bourgneuf bay and data analyses were conducted jointly with the MMS laboratory (Nantes), IFSTTAR (Nantes) and the LPG-BIAF laboratory (Nantes and Angers). Field campaigns in the Gullmar fjord and the data analyses (for two months plus one week) were carried out jointly with Pr. Helena L. Filipsson who acknowledges funding from the Swedish Research Council VR. Foraminiferal denitrification analyses (duration of one week) were performed at Aarhus University (Denmark) with Dr. Nils Risgaard-Petersen and were funded by the FRESCO and MANGA 2D projects. Two international congresses (Forams 2018, Edinburgh, Scotland and Goldschmidt 2019, Barcelona, Spain) and one national congress (RST 2019 micropaleontology session, Lille, France) were funded by the LPG-BIAF laboratory, the FRESCO and MANGA-2D projects.

CONTENTS

INTRODUCTION

Introduction

1. State of the art

1.1 Challenges of coastal areas

The ocean provides essential resources such as food and energy and plays a key role in human well-being (Fleming et al., 2019). Our economy and the rapid demographic growth of the world's population are placing increasing pressures on the marine environments (e.g., overfishing, eutrophication, increasing greenhouse gas emissions, warming, ocean acidification, and under-oxygenation of the oceans) (Breitburg et al., 2018; Visbeck, 2018; Jouffray et al., 2020) (Fig. 1).

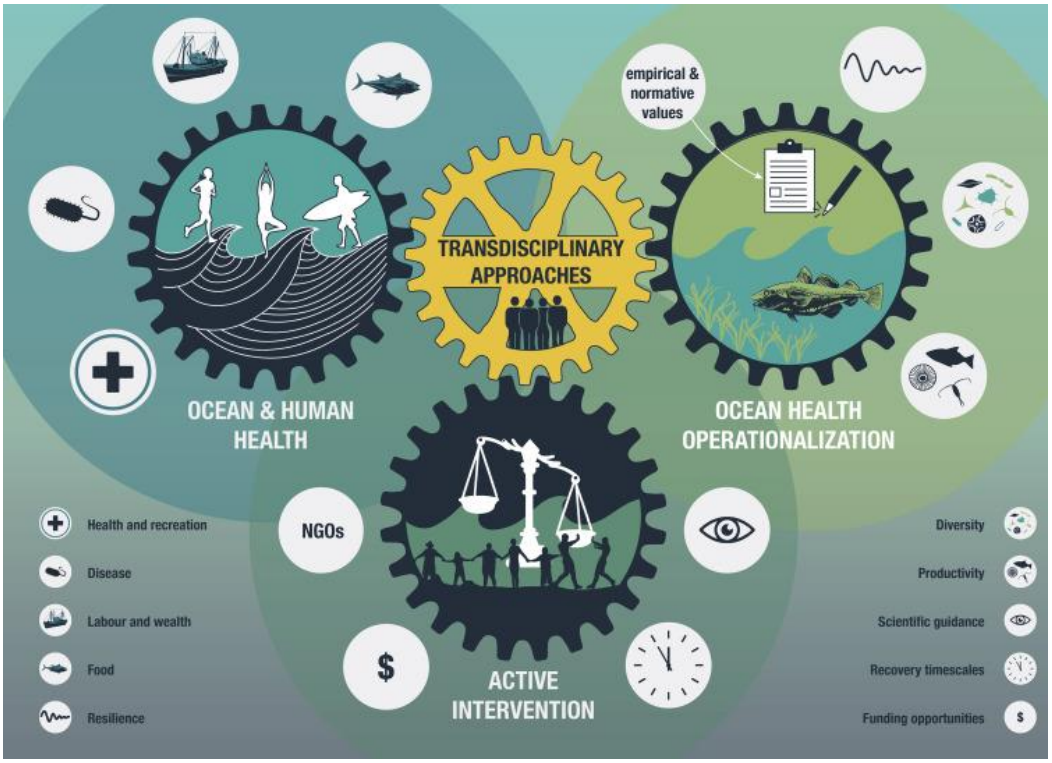

Figure 1: A Transdisciplinary Framework Integrating Ocean and Human Health and Ocean-Health and Recovery Research. From Franke et al., (2020).

In coastal areas, in particular, urban and tourism pressures are increasing, making these areas the most threatened by natural and human-induced climate change. More than 20 % of the world's population currently lives within 30 km of the coast. This represents 3.8 billion people living within 150 km of the shoreline according to the IUCN (International Union for Conservation of Nature). Population projections predict that more than 75% of the world's population will live there by 2035 (Haslett, 2016). One of the last reports of IPCC (Intergovernmental Panel on Climate Change) (Wong et al., 2014) on coastal systems indicates that this high attraction of coastal areas by human populations, generates tensions for the

humans living there (e.g. settlements, infrastructure, food production, tourism and health) and for the coastline which is degraded (e.g. excess of nutrients via the land-sea continuum) (Fig.2).

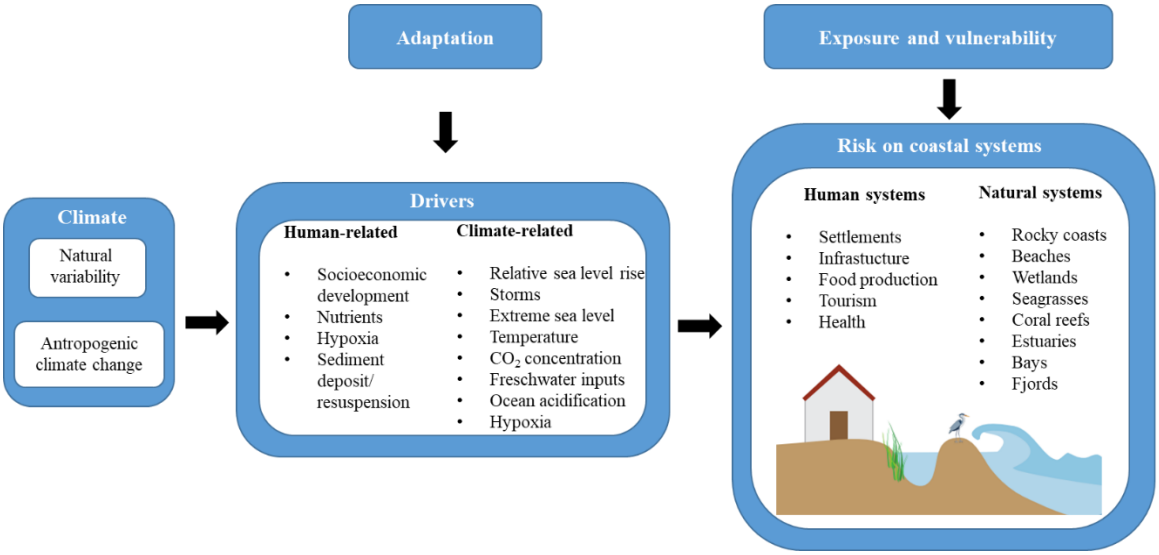

Figure 2: IPCC report on Coastal systems and low-lying areas. Modified from Wong et al., 2014.

One of the main threat for coastal ecosystems is natural/ human-induced hypoxia with a threshold of $[O_2] < 63$ µmol L^{-1} equivalent to 30 % oxygen saturation (Diaz and Rosenberg, 2008; Rabalais et al., 2010; Breitburg et al., 2018). Hypoxia affects both aerobic organisms (Diaz et al., 2013; Riedel et al., 2016) and coastal ecosystems occurring at different spatial (from < 1 km^2 to > 100 000 km^2) and temporal (from hours to decades) scales. The effects of hypoxia also depend on size, geomorphology, freshwater influence and anthropogenic impact on the ecosystem (Fig. 3). Several authors also highlight that hypoxia in coastal waters are increasing in extent, frequency and duration (Diaz and Rosenberg, 1995, 2008; Rabalais et al., 2010; Schmidtko et al., 2017; Richirt, 2020).

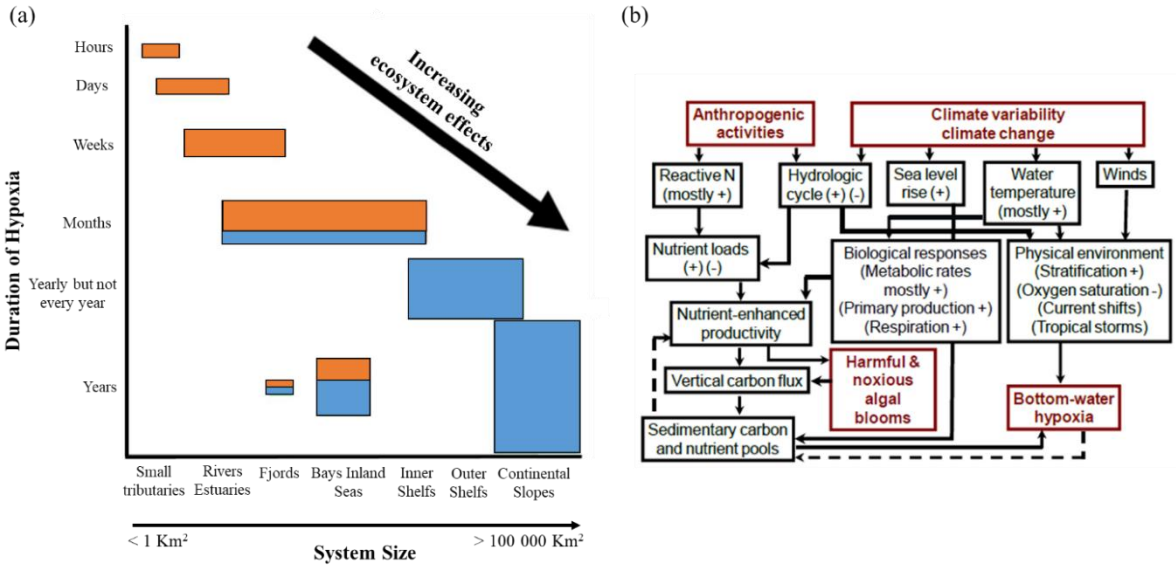

Figure 3: (a) Synthetic scheme of the temporal and spatial variability of hypoxia in different environments. Orange and blue colours correspond respectively to human and natural causes. From Rabalais et al., (2010). (b) Potential physical and hydrological changes resulting from climate change and their interaction with current and future human activities. The dashed lines represent negative feedbacks to the system (from Rabalais et al., 2009).

Coastal zones act as buffer zones between land and ocean (Costanza et al., 1997). The benthic realm is expected to be the most impacted by natural and human-induced stresses, occurring either in the water column and affecting the bottom (e.g., fjord) or directly in bare sediments (e.g., mudflat). Coastal ecosystems strongly influence benthic biological and geochemical processes modulating biogeochemical cycles. Biogeochemical cycles are essential to living organisms, as they transform energy and matter into forms that can be used to support ecosystem functioning (Brusseau, 2019). The main biogeochemical cycles addressed in coastal ecosystems are carbon cycle, nutrient cycles (nitrogen, phosphorus) and metal cycles (iron, manganese). The understanding of the biogeochemical processes operating in marine sediments required a complementarity approach to link the benthic faunal and geochemical compartments. Taking into account the spatial and temporal variabilities of biological and geochemical compartments has become a major challenge to improve our understanding of biogeochemical cycles (impact of benthic fauna on cycles and *vice-versa*). Indeed, the benthic flora/fauna (e.g. microphytobenthos, macrofauna and meiofauna such as foraminifera) is not very mobile and show a panel of more or less tolerant species to changes in environmental conditions (e.g. hypoxia, storms, flood event, tides) (Murray, 2006; Gilbert et al., 2007; Middelburg and Levin, 2009; Serôdio et al., 2020). Therefore, it is possible to detect environmental changes through variations in the specific richness, density, longitudinal (along a gradient) or vertical (in the sediment) distribution and the composition of species assemblages. Several ocean health

assessment tools (Borja et al., 2016; Halpern, 2020) and Framework directives (Water Framework Directive (2000/60/EC) and the Marine Strategy Framework Directive (MSFD, 2008)), were developed to measure resilience, productivity and species diversity. Multidisciplinary approaches involving scientific disciplines, civil society and non-governmental organization are required. The measurements can be either direct (e.g. physico-chemical measurements) or through bioindicators (e.g. benthic macrofauna, benthic meiofauna) (Labrune et al., 2007; Prazeres et al., 2020; Bouchet et al., 2021). To obtain quantitative and qualitative information on the status of marine and especially coastal ecosystems, long-term data sets are essential (temperature, oxygen concentration, nutrients (nitrate, ammonium, phosphate), pH, species composition, density and diversity). These tools for monitoring and assessing coastal ecosystems, allow the identification of changes due to natural and human-induced environmental variabilities. One of the challenges of our time is to acquire a multidisciplinary approach linking diverse knowledge from complementary disciplines (e.g. biology, ecology, geochemistry) to find solutions.

1.2 Geochemistry of coastal areas

1.2.1 Physical properties and transport processes of marine sediments

The space between particles in water saturated sediments is called pore or interstitial water (Meade, 1966). The porosity is defined as the ratio of the volume of water-filled void spaces in a sediment to the total volume of sediment. The porosity is controlled by grain size and mineralogy (Fig. 4 a) (Friedman and Sanders 1978; Berner, 1980). Sediment compaction due to the increase of sedimentary column weight as the particles are buried, generates a decrease of porosity until the better geometrical arrangement is attained. As muddy and sandy particles are not related to the same mineralogical shape, a decrease of porosity can also be interpreted as an increase of sand content in a sedimentary series (Fig. 4 a). Permeability is also related to grain size variations. Permeability is defined as the capacity of a porous medium to transmit fluid in response to a pressure gradient (Lerman, 1979). Pressure-driven flow is governed by Darcy's Law, may be generated by wave action or interactions between bottom currents and surface sediment structures (e.g. macrofaunal burrows) (Fig. 4 b). Thus, in sandy sediments permeability is high and lead to the occurrence of significant pore-water advection (i.e., flux of water through the interstices of the sediment in response to pressure gradients) (Huettel and Webster, 2000). Conversely, muddy sediments indicate much lower permeability, thus diffusion (i.e., response to concentration gradients) or bioturbation (i.e., macrofaunal and meiofaunal activities, (Aller, 1980)) dominate pore-water transport processes. The changes in

porosity (and permeability) profile of muddy sediment are the consequences of major impacts on the sediment diagenesis due to flood deposit/resuspension, tidal cycles, waves, currents and macrofaunal bioturbation.

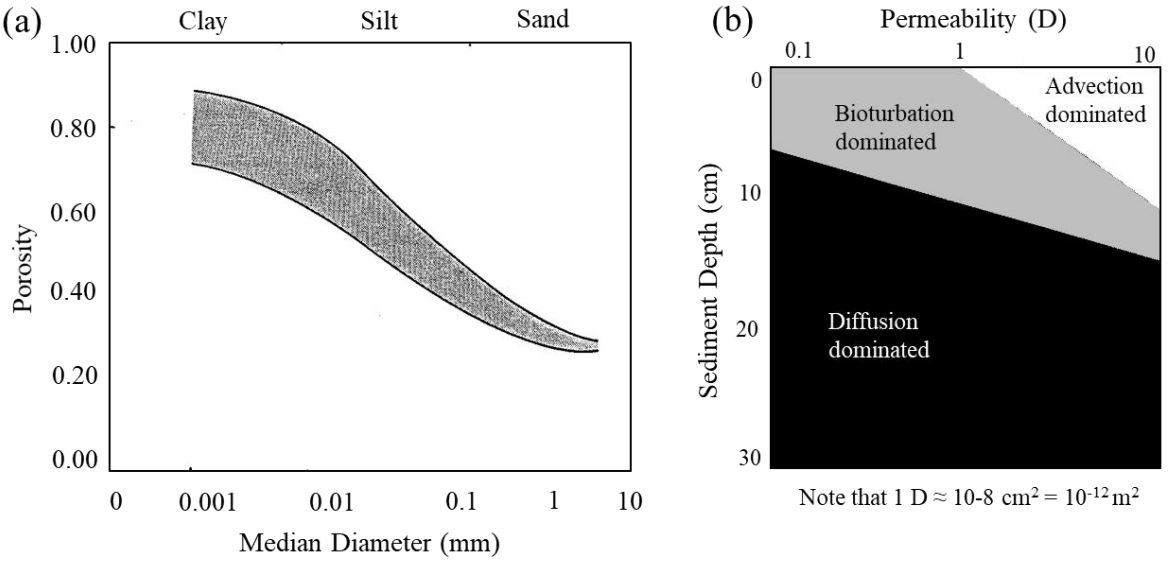

Figure 4: (a) Porosity as a function of medium grain size for surficial marine sediments (from Burdige, 2006 and Berner, 1980). (b) Schematic representation of the possible depth dependence of various pore water transport processes (diffusion, bioturbation and physical advection) as the function of sediment permeability (from Burdige, 2006 and references within).

1.2.2 Early diagenesis at steady-state

Coastal sediments are not only the bottom of the ocean/sea, they can be represented as a succession of layers that can be accumulated or eroded (Sundby, 2006). The sedimentary transformations occurring during the first stages of organic matter (OM) burial correspond to early diagenesis (Froelich et al., 1979; Berner, 1980). Early diagenesis combines chemical reactions (e.g. redox, complexation, adsorption, precipitation), physical processes (e.g. diffusion, advection, mixing) and biological processes (e.g. microbial mineralization, respiration of meiofauna and benthic macrofauna, microphytobenthos photosynthetic activity). Changes in the composition of pore-water create concentration gradients, which result in fluxes of soluble chemical elements across the sediment-water interface (SWI). These changes also impact the composition and properties of the solid phase, thereby altering the information about the state of the ocean contained in the particulate matter that is deposited on the seafloor (Sundby et al., 2006).

In coastal sediments, organic matter (OM) and nutrients (i.e. nitrate (NO_3^-); ammonium (NH_4^+); dissolved reactive phosphorus (DRP)) from the continent and primary production encounter biogeochemical transformations driven by physical (sediment deposit/ resuspension

by tidal cycles, river flood, currents or storms) and biological (activity of benthic meiofauna, macrofauna and microphytobenthos) factors. The study of early diagenesis aims to target the study of recent sediments. The assumption of a steady state must be established to quantify the intensity of the processes. In other words, the steady state assumes that a particulate and dissolved flux between the water column and the sediment column is constant over time. This paradox must be based on an accurate spatio-temporal definition of the observed sedimentary ecosystem.

Primary diagenetic reactions correspond to OM remineralization through aerobic or anaerobic respiration (Table 1). These reactions result in the bacterial OM degradation using the various oxidants contained in the sediment or in pore-waters. Organic matter is the electron donor (reducer) and a series of chemical elements can be used as electron acceptors (oxidants) (Fig. 5). In marine oxygenated environments, oxygen is the first electron acceptor respired by aerobic bacteria in the water column until its complete depletion (Aller, 2004). Oxygen diffusive exchanges occur between the water column and the sediment interface, inducing a stationary state (i.e. equilibrium between SWI diffusive exchanges and aerobic mineralization). Thus, the O_2 concentration decreases linearly in the water column near the sediment interface (diffusion layer ~ 1 mm; (Santschi et al., 1991)), followed by a sharp decrease below the interface, until its disappearance in the uppermost sediment. Once the O_2 is exhausted, other available oxidants degrade OM using firstly the most efficient in terms of energy yield before changing to the next oxidant. The successive oxidants during primary reactions are: O_2 > NO_3^- > Mn oxy-hydroxides (mainly MnO_2), iron oxy-hydroxide (mainly $Fe(OH)_3$), SO_4^{2-} (Froelich et al., 1979; Canfield et al., 1993; Burdige, 1993) (Fig. 5, Fig. 6).

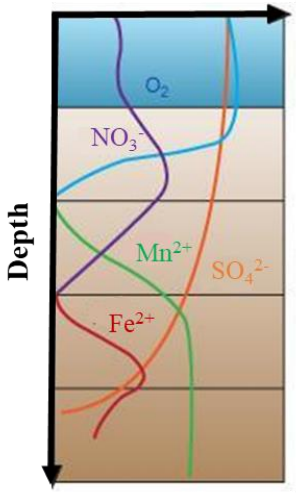

Processes	Electron acceptors	Primary reactions
Aerobic respiration	O_2	(1)
Denitrification	NO_3^-	(2)
Manganese reduction	Mn^{4+} (e.g. MnO_2)	(3)
Iron reduction	Fe^{3+} (e.g. $Fe(OH)_3$)	(4)
Sulfate reduction	SO_4^{2+}	(5)

Figure 5: Pore-water profiles predicted by the successive utilization of inorganic terminal electron acceptors during the remineralization of organic matter in marine sediments. The primary reactions indicated by a number are detailed in Table 1. Modified from Froelich et al., (1979) and Burdige, (1993).

The presence or absence of dissolved oxygen and sulfides in the sediments establishes three vertically organized zones (or redox layers) in the sediments (Fig. 6): 1) a superficial oxic zone where dissolved oxygen is present, 2) a suboxic zone below, where oxygen and sulfides are not detectable (this zone can also be called hypoxic zone by some authors (Middelburg and Levin, 2009)), 3) an anoxic zone located further down where sulfides are present. The subsequent reactions of chemical species produced by the primary redox reactions are referred to secondary redox reactions. The dissolved compounds formed during primary reactions can diffuse through the redox layers and can react with each other, with the sedimentary matrix or with dissolved compounds of the layers they cross. Some secondary redox reactions are detailed in Table 1.

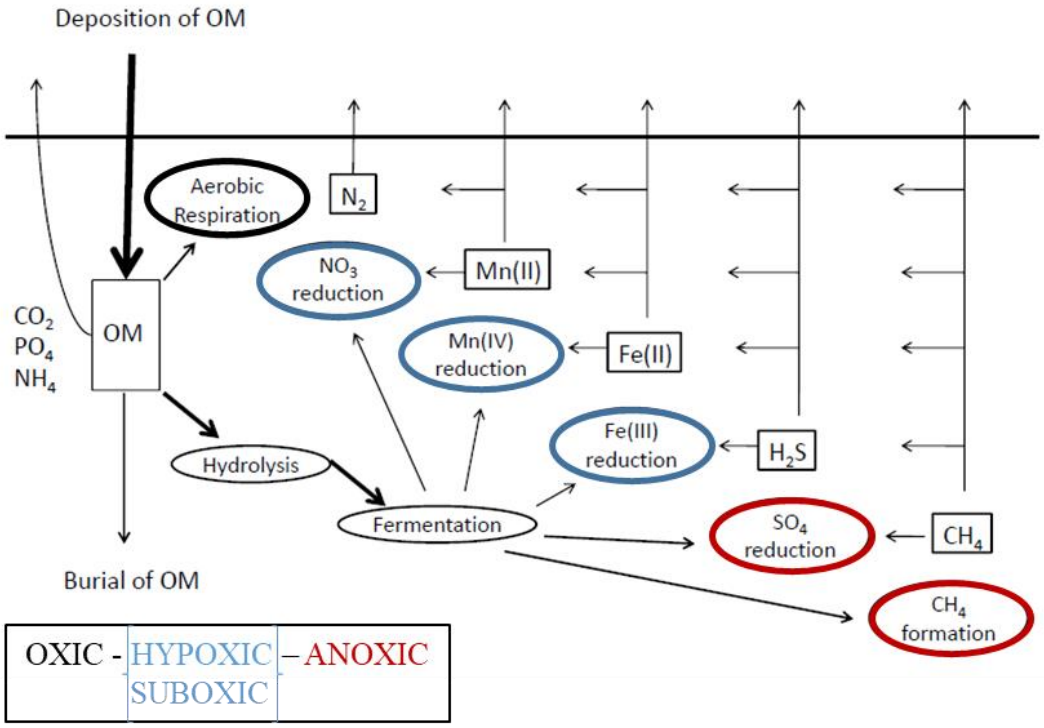

Figure 6: Conceptual model of organic matter (OM) degradation pathways and re-oxidation pathways in oxic, hypoxic and anoxic marine sediments. OM degradation involves hydrolysis of macromolecular OM and fermentation to smaller compounds. These fermentation products are used by respiring micro-organisms and methanogens. Oxidants are utilized sequentially, first oxygen, then nitrate, metal oxides and sulphate. Dissolved reduced products (methane, sulphide, manganese (II) and iron (II)) diffuse upwards and are then oxidized. Sediments underlying oxic bottom waters support aerobic respiration and re-oxidation of Mn (II), Fe (II), H_2S and CH_4 by oxygen; these processes do not occur in hypoxic and anoxic sediments. In sediments underlying permanently anoxic bottom waters reactive manganese and iron oxides stocks have been exhausted and OM degradation occurs by sulphate reduction and methane formation. Modified from Middleburg and Levin, (2009).

Primary or secondary oxidation-reduction reactions promote the precipitation of carbonated (e.g. $CaCO_3$, $MnCO_3$) or sulphated (e.g. HCO_3^-, Fe^{2+}, H_2S) chemical species. These reactions lead to the accumulation of these mineral species in the solid phase and the consumption of dissolved species (Ca^{2+}, Mn^{2+}, Fe^{2+}, or H_2S) in the pore water.

Actually, at steady-state, the surface sediment is constituted of a layer enriched in solid-phases oxidized: Mn and iron Fe (Canfield et al., 1993; Burdige, 1993). Deeper in suboxic sediments, Mn and Fe oxides are reduced to dissolved phases Mn_d and Fe_d, respectively (Burdige, 1993). Due to the concentration gradients, a part of these benthic fluxes of dissolved elements can escape from the suboxic sediment and can be reoxidized at the sediment surface. The presence of a superficial oxide layer can create a cap preventing dissolved elements to escape from sediment (Canfield et al., 1993). However, exchanges exist across the sediment

oxic-anoxic boundary and across the SWI by diffusion from the sediment to the bottom waters and its precipitation in solid phases (Sundby and Silverberg, 1985; Anschutz et al., 2005).

Adsorption / desorption reactions also occur in the sediments. The adsorbed forms are ions, single molecules or crystals retained on the surface or inside crystalline matrices by low intensity forces (physical or chemical bonds). Especially, orthophosphates are adsorbed onto iron oxides at the sub-surface and are released in dissolved reactive phosphorus during the reduction of iron oxides deeper in the anoxic sediment (Krom and Berner, 1980; Sundby et al., 1992; Anschutz et al., 1998, 2007; Thibault de Chanvalon et al., 2016). Understanding these adsorption/desorption mechanisms are crucial because these mechanisms modulate nutrients availability which often controls the intensity of primary production at the sediment surface and in the water column.

The vertical succession of the early diagenesis processes is a paradigm which can be modulated by several physicochemical and biological factors occurring at different spatial and temporal scales. These factors lead to transient states (Sundby, 2006). These transient states may be related to random, short-lived, small-scale disturbances such as benthic faunal bioturbation. Larger scale periodic disturbances also occur, such as those generated in estuarine sediments or intertidal bays by tidal cycles. Large scale random events can occur such as deposition or resuspension of sediments by wind-storms or flood events. These transient states can also be seasonal, linked to variations in temperature, oxygen concentration in the bottom water or the quantity of organic matter. Then, the turnover of oxygen-poor bottom waters by oxygen-rich bottom waters in fjords can disrupt bottom sediment diagenesis on seasonal to decadal time scales.

Table 1: Depth sequence of bacterially-mediated oxidation of organic matter (O.M.=$C_{106}H_{263}O_{110}N_{16}P$, (Redfield, 1963)) in marine sediments (Froelich et al., 1979). Then the secondary reactions produced during the OM burial (Wang and Van Cappellen, 1996; Hyacinthe et al., 2001).

PRIMARY REACTIONS

Oxygen consumption by oxic respiration and nitrate production

$138O_2 + O.M. + 18HCO_3^- \rightarrow 124CO_2 + 16NO_3^- + HPO_4^{2-} + 140H_2O$

Nitrate consumption by denitrification

$94.4NO_3^- + O.M. \rightarrow 13.6CO_2 + 92.4HCO_3^- + 55.2N_2 + 8\ 4.8H_2O + HPO_4^{2-}$

Reduction of Mn-oxides by anaerobic respiration

$236MnO_2 + O.M. + 364CO_2 + 104H_2O \rightarrow 470HCO_3^- + 8N_2 + 236Mn^{2+} + HPO_4^{2-}$

Reduction of Fe-oxides and production of ammonia

$424Fe(OH)_3 + O.M. + 740CO_2 \rightarrow 846HCO_3^- + 424Fe^{2+} + 16NH_3 + 320H_2O + HPO_4^{2-}$

Production of sulfide and ammonia by sulfato reduction

$53SO_4^{2-} + O.M. \rightarrow 39CO_2 + 67HCO_3^- + 16NH_4^+ + 53HS^- + 39H_2O + HPO_4^{2-}$

SOME SECONDARY REACTIONS

Production of nitrate by nitrification

$NH_4^+ + 2O_2 \rightarrow NO_3^- + 2H^+ + H_2O$

Oxidation of Mn^{2+}

$2Mn^{2+} + O_2 + 2H_2O \rightarrow 2MnO_2 + 4H^+$

$4Mn^{2+} + O_2 + 6H_2O \rightarrow 4MnOOH + 8H^+$

$5Mn^{2+} + 2NO_3^- + 4H_2O \rightarrow 5MnO_2 + N_2 + 8H^+$

$10Mn^{2+} + 2NO_3^- + 14H_2O \rightarrow 10MnOOH + N_2 + 18H^+$

Oxidation of Fe^{2+}

$O_2 + 4Fe^{2+} + 10H_2O \rightarrow 8H^+ + 4Fe(OH)_3$

$5Fe^{2+} + NO_3^- + 12H_2O \rightarrow 5Fe(OH)_3 + 1/2N_2 + 9H^+$

Oxidation of Fe^{2+} with Mn-oxides

$Fe^{2+} + MnOOH + H_2O \rightarrow Fe(OH)_3 + Mn^{2+}$

$2Fe^{2+} + MnO_2 + 4H_2O \rightarrow 2Fe(OH)_3 + Mn^{2+} + 2H^+$

Reduction of Mn-oxide with ammonia to give dinitrogen

$3/2MnO_2 + NH_4^+ + 2H^+ \rightarrow 3/2Mn^{2+} + 1/2N_2 + 3H_2O$

$3MnOOH + NH_4^+ + 5H^+ \rightarrow 3Mn^{2+} + 1/2N_2 + 6H_2O$

Reduction of Mn-oxide with ammonia, production of nitrate

$8MnOOH + NH_4^+ + 14H^+ \rightarrow 8Mn^{2+} + NO_3^- + 13H_2O$

$4MnO_2 + NH_4^+ + 6H^+ \rightarrow 4Mn^{2+} + NO_3^- + 5H_2O$

Oxidation of sulphide

$H_2S + 2O_2 + 2HCO_3^- \rightarrow SO_4^{3-} + 2CO_2 + 2H_2O$

$H_2S + 4CO_2 + 2Fe(OH)_3 \rightarrow Fe^{2+} + S + 4HCO_3^- + 2H_2O$

$H_2S + 2CO_2 + MnO_2 \rightarrow Mn^{2+} + S + 2HCO_3^-$

Fe2+ and sulphide precipitation

$Fe^{2+} + H_2S \rightarrow FeS + 2H^+$

$Fe^{2+} + 2H_2S \rightarrow FeS_2 + 2H+$

+ adsorption / desorption, dissolution / precipitation process ($CaCO_3$, $MnCO_3$, FeS)

1.2.3 Water column seasonal hypoxia and impacts on diagenesis

The occurrence of coastal hypoxia (i.e. $[O_2] < 63$ µmol L^{-1} (Diaz and Rosenberg, 2008; Breitburg et al., 2018)) can be natural, human influenced, or result from the interactions of the two processes (Middelburg and Levin, 2009). Natural hypoxia is present in a variety of coastal environments. Thus, in fjords the circulation of deep basin bottom waters may be seasonally restricted (water stratification). In coastal bays close to estuaries, the autotrophic state is maintained by inputs of terrestrial and riverine OM and *in situ* primary production (intense remineralization of OM). Hypoxia induces a transient state of redox boundaries and impacts the early diagenetic pathways (more anaerobic pathways at the expense of aerobic ones). In hypoxic environments, aerobic respiration and aerobic re-oxidation processes are limited. On the other hand, anaerobic re-oxidation processes still occurred. These processes are based on the influx of nitrates (denitrification), sedimentary Mn and Fe oxides stocks (reduction of Mn and Fe oxides), and sulfate (sulfato-reduction). In permanent anoxic environments, sulfato-reduction and methanogenesis dominate mineralization because the stocks of particulate oxidants have been depleted.

The effects of seasonal decreasing dissolved oxygen availability in the bottom water impact redox species and nutrients biogeochemical cycles as; nitrogen cycle (Childs et al., 2002; Kemp et al., 2005; Conley et al., 2007; Diaz and Rosenberg, 2008; Neubacher et al., 2013; Breitburg et al., 2018) and manganese cycle (Burdige, 1993; Aller, 1994; Anschutz et al., 2000; Kristensen et al., 2003; Sundby, 2006).

The nitrogen cycle in marine sediments is a perpetual balance between nitrogen inputs (e.g., terrestrial runoff, atmospheric precipitations) and outputs (e.g., denitrification from sediment and water column) (Galloway et al., 2004; Sigman et al., 2009). At oxic bottom water conditions, nitrification is an aerobic process that converts NH_4^+ to NO_3^- in the oxic sediment and in the oxic water column (Fig. 7) (Rysgaard et al., 1994; Thamdrup and Dalsgaard, 2008). Denitrification and anammox are anaerobic processes, converting NO_2^- or NO_3^- to (nitrogen) N_2 gas (Herbert, 1999; Brandes et al., 2007; Thamdrup and Dalsgaard, 2008). Denitrification depends on NO_3^- transported from the water column and/or sedimentary nitrification zones at the sediment surface. Nitrification and denitrification are thus strongly coupled (Kemp et al., 1990; Cornwell et al., 1999). This dependence on nitrification may imply a reduction in denitrification rates when the bottom waters become hypoxic. Anoxic nitrification is also possible through secondary reactions with the oxidation of NH_4^+ by Mn and Fe oxides (Luther et al., 1997; Cornwell et al., 1999; Mortimer et al., 2004). In reduced sediments, dissimilatory

reduction of nitrate to ammonium (DNRA) can also contribute to NO_3^- depletion, leading to the conversion of NO_3^- to NH_4^+ instead of N_2 (Christensen et al., 2000).

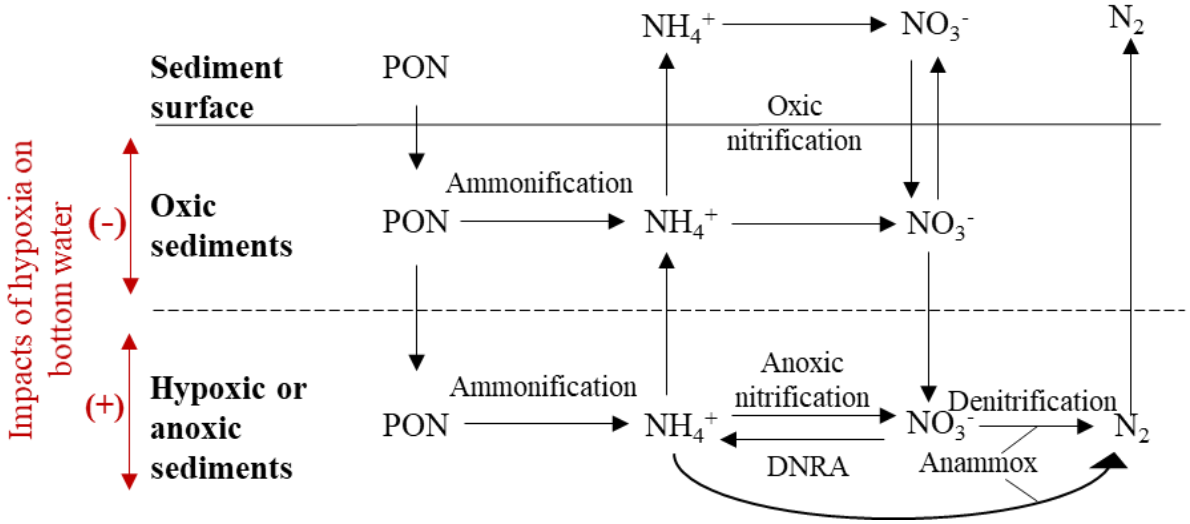

Figure 7: Conceptual model illustrating the processes associated with nitrogen cycling in marine sediments. When the bottom waters become hypoxic the oxic sediment layer reduces (-) and the hypoxic/ anoxic deep layers increase (+). Therefore, the processes occurring in the oxic layer are limited in favour of the processes occurring in the hypoxic/ anoxic layers. (PON = particulate organic nitrogen). Modified from (Burdige, 2006).

Hypoxia leads to a transient state of redox boundaries impacting Mn biogeochemical cycle (Fig. 8) (Burdige, 1993; Aller, 1994; Anschutz et al., 2000; Kristensen et al., 2003; Sundby, 2006). A decrease in the O_2 bottom water concentration decreases the re-oxidation efficiency of the dissolved manganese (Mn_d) which, in well oxygenated bottom water conditions, builds the enrichment in Mn oxides in the oxic sediment layer. The fluxes of reduced compounds as Mn_d from the anoxic sediment to the water column increase (Aller, 1994; Kristiansen et al., 2002; Katsev et al., 2007). The increase of the Mn_d fluxes coincides with the decrease of the oxic sediment layer. Indeed, the impermeability of the oxic layer containing the major part of Mn oxides is exhausted by O_2 depletion and the Mn_d can more easily cross the SWI (Thamdrup et al., 1994). The Mn_d flux released to the water column varies in intensity during hypoxia (Sundby et al., 1986; Thamdrup et al., 1994; Kristiansen et al., 2002; Katsev et al., 2007). At the beginning of a hypoxia event, the Mn_d flux increases rapidly until a maximal Mn_d concentration reached in anoxia. Then, the Mn_d flux decreases progressively corresponding to the depletion of the reservoir (or stock) of Mn_d combined with the low reoxidation of Mn oxides (Sundby et al., 1986).

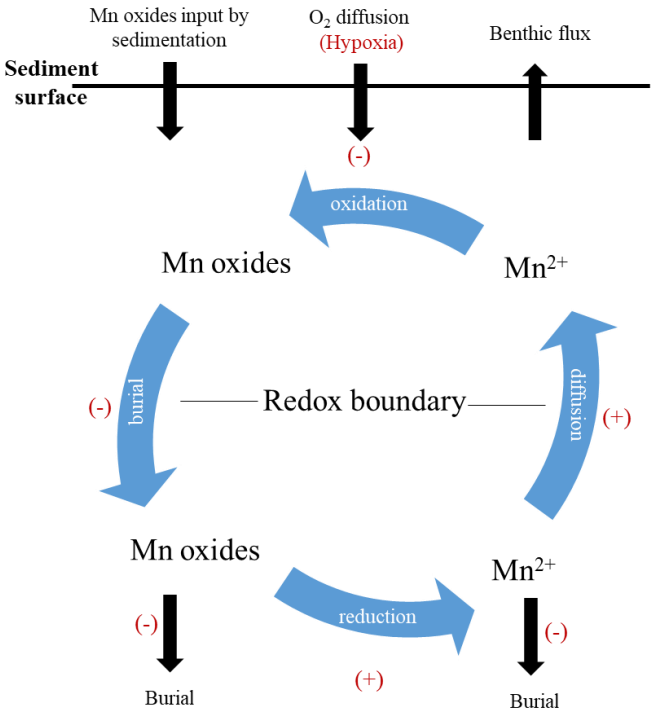

Figure 8: Simplified Mn redox cycle in marine sediments. In the absence of oxygen (i.e., below the redox boundary), Mn oxides are reduced to Mn^{2+}, which then diffuse upward as a result of a Mn^{2+} concentration gradient. When this Mn^{2+} reaches oxygen-containing sediments, it is then oxidized back to particulate Mn oxides. Under steady-state conditions, this cycle results in the concentration in particular, oxidized Mn in the sediments just above the sediment redox boundary. This Mn cycling can be much complicated when hypoxia reaches bottom waters (indicate in red: (+) favored processes, (-) disadvantage processes. Modified from Burdige, (2006).

1.2.4 Impacts of macrofaunal bioturbation on biogeochemical cycles

The OM remineralization intensity depends on: the amount and the quality of OM in the sediments, the oxygenation of the bottom water and the bioturbation induced by the activity of the benthic fauna (Thamdrup, 2000; Burdige, 2006). Faunal bioturbation defined by Kristensen et al., (2012) is: "all transport processes carried out by animals that directly or indirectly affect sediment matrices". The bioturbation involving particles movement is named *biomixing* (or *particle reworking*). The transport process is the burrowing and the transport type of soluble elements is the diffusion in muddy and sandy sediments. The bioturbation involving water mass movement is called *bioirrigation* (or *ventilation*). The pore-water solute transport in sediment surrounding burrows can occur as radial molecular diffusion or pressure-induced advective pore-water flow depending on the sediment type and its permeability (Kristensen et al., 2012).

Specifically, bioturbation can be induced in the sediment by infaunal organisms as; biodiffusors (e.g. bivalve, echinoderma) which randomly rearrange sediment particles and gallery-diffusors (e.g. polychaeta) which dig galleries, tubes and burrows (Austen and Wibdom, 1991; Gerino et al., 2003; Gilbert et al., 2007). The bioturbation creates a three-dimensional mosaic of sediment oxic-anoxic boundaries (Bouchet et al., 2009; Middelburg and Levin, 2009). Bioturbation contributes to disturb the vertical distribution of redox species, inducing a transient state (Aller, 1982; Berner, 1980; Anschutz et al., 2000). This transient state can affect especially the nitrogen cycle (Fig. 9 a) (Aller, 1988; Gilbert et al., 2003) and the Mn cycle (Fig.

9 b) (Aller, 1990). Indeed, benthic infaunal activity impacts solute transport through the passive or active flushing of burrow, generating a network between SWI and deeper sediment, namely bioirrigation (Meile et al., 2001). Bioirrigation may increase dissolved redox elements fluxes across the SWI to the point that the measured benthic fluxes may be mainly due to bioirrigation rather than diffusion (Sundby and Silverberg, 1985; Burdige, 2006; Thibault de Chanvalon et al., 2017). Bioturbation impact strongly redox chemical elements cycles; metal oxides are conveyed downwards in reduced zones and reduced forms are mixed upwards to reoxidation zones (Canfield et al., 1993; Aller, 1994; Thamdrup, 2000; Burdige, 2006).

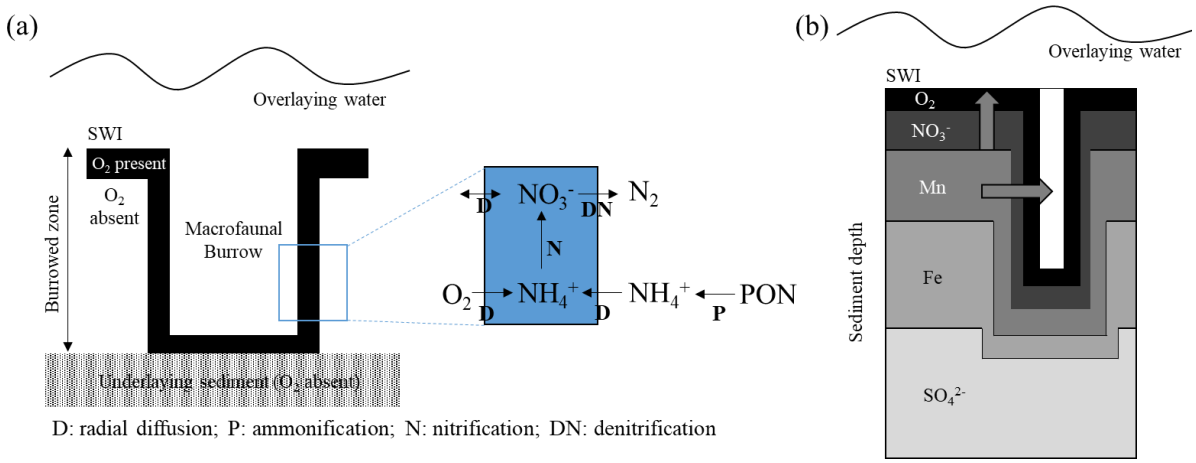

Figure 9: (a) Conceptual model illustrating the processes affecting nitrogen cycling in a bioirrigated sediment. Modified from Aller, (1988); Gilbert et al., (2003); Burdige, (2006). (b) Idealized diagenetic processes affecting the manganese composition of the particles in case of biodiffusion. Modified from Aller, 1982; Thibault de Chanvalon, (2016).

Hypoxia affects the behaviour, physiology, and ecology of the benthic macrofauna (species richness, density, biomass). However, some groups of macrofaunal and meiofaunal species are more or less tolerant to oxygen depletion (Rosenberg et al., 1991; Diaz and Rosenberg, 1995; Jorissen et al., 1995). Particle mixing and bioirrigation are limited to the uppermost layers of the sediment (~ > 10 cm depth). Often hypoxia leads to a reduction in bioirrigation and bioturbation as well as a loss of spatial heterogeneity at the sediment surface (Levin et al., 2003; Duport et al., 2007). A decrease of bioirrigation activity can alter benthic fluxes of nutrients and redox species in both directions (Sundby and Silverberg, 1985; Aller, 2001; Point et al., 2007). Thus, these interactions between hypoxia, benthic fauna, and biogeochemistry remain complex because they are often nonlinear (Aller, 2001).

1.2.5 Impacts of high hydrodynamism and tidal cycles on intertidal sediments

Intertidal mudflats are areas of intense mineralization of particulate OM from terrestrial, riverine and marine origin. The tidal pump indicates hydrostatic pressure gradients at low tide inducing a seeping (negative fluxes) of anoxic pore waters and advection of pore waters through macrofaunal burrows and permeable sediments. This process is a major contributor of solute export from the sediment to the tidal channels (Billerbeck et al., 2006; Taillefert et al., 2007; Deborde et al., 2008; Abril et al., 2010; Delgard et al., 2012; Anschutz et al., 2019). The contrasted hydrological context can fuel the dynamics in oscillatory redox elements generated by tidal pump. The tidal cycles induce a periodic oxic/suboxic oscillation of the redox boundaries due to repetitive cycles of deposit and resuspension of the sediment surface (Froelich et al., 1979; McKee et al., 2004; Aller, 2004; Sundby, 2006). When deposits are constituted of fine particles combined with lower hydrodynamics for bays or other protected coastlines, the particles settle and form transient benthic turbid structures called "fluid mud". (Abril et al., 2010). The height of sediment resuspended and redeposited during the tidal cycle can be estimated between 1 and 5 mm. Seasonal or random disturbances as wind-storms and high rainfall can affect strongly the topography of the sediment surface (Aller et al., 1998; Abril et al., 1999, 2000; Aller, 2004; Goubert et al., 2010; Redzuan and Underwood, 2021). A river flood event can induce a higher quantity (or height) of the deposited sediment (Aller, 2004; McKee et al., 2004; Sundby, 2006; Roy et al., 2013; Thibault de Chanvalon et al., 2016). The intensity of deposition and resuspension of sediment particles modulate different redox stages over several months (Thibault de Chanvalon et al., 2016). Indeed, each oxidant is consumed on different time scales, one of the complexities of river-dominated oceanic margins (RiOMar, Aller, 2004; McKee et al., 2004; Roy et al., 2013) environments is to capture transient states of diagenesis with a time series at the appropriate frequency (Thibault de Chanvalon et al., 2016). Previous studies report time scales of hours for O_2, days to weeks for nutrients and months to years for Mn and Fe oxides consumption (Abril et al., 1999, 2000; Aller, 2004; Thibault de Chanvalon et al., 2016 and reference within). The Loire river estuary indicates periodic winter flood event (GIP, Loire Estuaire). Thibault de Chanvalon et al., (2016) described three redox stages of transient diagenesis in the “Les Brillantes” mudflat after a Loire river flood event. Briefly, during the winter flood period, no manganese (Mn), iron (Fe) and phosphorus (P) are released into pore-waters within the flood-deposited layer. In post-flooding period (~ 1 month later), high Mn-Fe-P oxidized phases are consumed while the dissolved phases increase. Simultaneously, phosphorus is released into pore-water. Finally, in summer conditions (~ 6 months later) redox dissolved phases dominate. Thus according to the intensity of

hydrodynamic conditions, the sediment can be a source or a sink of nutrients (NO_3^-, NH_4^+ and DRP). Phosphates are intimately bound to iron oxides, and are therefore also sensitive to environmental oxygenation. Sedimentary phosphorus cycling involves attention to the anaerobic remineralization of organic phosphorus and the interaction of phosphate with sedimentary iron oxides (Sundby et al., 1992; Slomp et al., 1997; Anschutz et al., 1998). Phosphate can therefore be released to the water column during the reduction of iron oxides or be adsorbed by iron oxides during deposition/re-suspension events. In summer conditions, when the oxides are strongly dissolved, the increase of NH_4^+ can be favoured by the higher anaerobic OM remineralization (higher alkalinity, sulfato-reduction process). In intertidal mudflats, the denitrification is very high and NO_3^- rapidly consumes by microphytobenthos (MPB) and bacteria (Dalsgaard and Thamdrup, 2002; Risgaard-Petersen et al., 2003). The understanding between the combined hydrodynamism/meteorological conditions and transient diagenesis is essential because they modulate the availability of oxygen and nutrients for the benthic fauna (Sundbäck and Granéli, 1988; Seuront and Spilmont, 2002; Méléder et al., 2007; Deborde et al., 2008; Oakes et al., 2020).

1.2.6 Challenges of high resolution technics

The challenge in recent years is to develop high spatial resolution geochemical methods to target the sedimentary microenvironments in order to better understand the impact of benthic fauna on diagenetic processes at the spatial and temporal scales of faunal activities (i.e., millimeter to decimeter and seconds to hours).

Since the pioneering work of Revsbech et al., (1980), the oxygen microprofile technique is widely used with the development of microelectrode microprofilers (Reimers, 1987). This allowed to study oxygen concentration variations at the sediment surface *in situ* (Fig. 10 a) and on sediment cores in the laboratory (Fig. 10 b). These techniques are used to monitor the evolution of oxygen concentrations in pore-waters at a submillimeter scale, such as to understand the behavior of microphytobenthos and quantify its rate of photosynthesis (Glud et al., 1992; Serôdio et al., 2007; Denis and Desreumaux, 2009; Delgard et al., 2012). The use of oxygen (i.e. aerobic respiration) and nitrous oxide (N_2O) (i.e. denitrification) microprofiles was

also adapted to study the respiration of meiofauna such as benthic foraminifera (Fig. 10 c) (Risgaard-Petersen et al., 2006; Geslin et al., 2011).

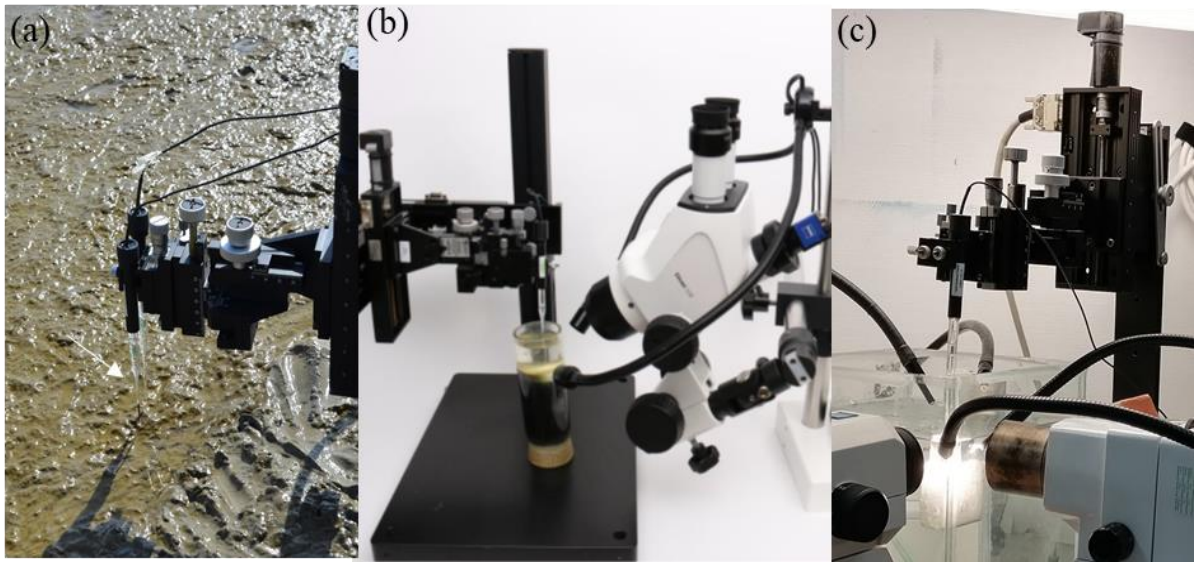

Figure 10: (a) Oxygen microprofiling deployed in situ in the Bourgneuf bay mudflat, (b) oxygen microprofiling in a sediment core performed in laboratory (from Tage Dalsgaard, Unisense), (c) oxygen respiration rate measurement of foraminifera in a microtube.

The 1D (one-dimensional) chemical elements concentration profiles are quickly limited by the spatial variability of the pore-water sediment allowing to study only a fixed point (Schulz, 2006). Thus, 1D profiles require to multiply vertical profiles to apprehend the lateral variability of the sediment pore water. The 1D DET (diffusional equilibrium in thin-film) were first developed by Davison et al., 1991 to measure dissolved iron. This technique was adapted later to dissolved manganese (Davison et al., 1994), nitrate, sulfate (Krom et al., 1994) and other chemical species. The two-dimensional approach developed from DGT (diffusional gradients in thin-film) was then adapted for 2D DET (Shuttleworth et al., 1999). At microenvironment scale, the complex interactions between geochemical and biological compartments can be difficult to observe with conventional technics (Stockdale et al., 2009). More recently, the 2D DET have been coupled with colorimetric methods, the aim being to transpose the colorimetric technique from the spectrophotometric cell to the 2D DET gel for: dissolved iron (Jézéquel et al., 2007), phosphates (Robertson et al., 2008; Pagès et al., 2011) and alkalinity (Bennett et al., 2015). This low-cost approach provides a high-resolution, 2D image of the vertical and lateral distribution of chemical species. Developments of 2D DET gels coupled with colorimetric methods, allow a high resolution at mm and sub-millimeter scales of many dissolved elements as; Fe/ DRP (Cesbron et al., 2014), NO_2^-/ NO_3^- (Metzger et

al., 2016), NH_4^+ (Metzger et al., 2019), Mn (Mouret et al., *in preparation*). Gels equilibrated with reagents can be photographed with a simple scanner. Some chemistries can be performed on the same probe gel with reactive gels targeting two chemical elements (e.g. Fe_d/ DRP). In order to dissociate the concentrations of these two chemicals, the use of the hyperspectral camera was required (Fig. 11, Cesbron et al., 2014). The main advantage of 2D DET gels is to provide information in both horizontal and vertical dimensions simultaneously about biogeochemical processes (e.g. diffusive fluxes, production/ consumptions zones) allowing characterization of microenvironments (Jézéquel et al., 2007; Santner et al., 2015; Thibault de Chanvalon et al., 2017; Moncelon et al., 2021). To characterize the different microenvironments two main analytical approaches have been adapted/developed. For microenvironments with strong vertical gradients and lateral homogeneity, the modeling of production/consumption zones and diffusive fluxes at the SWI can be performed with the PROFILE software (Berg et al., 1998). Some environments show high lateral pore-water heterogeneity generated by the bioturbation activity of macrofauna (Thibault de Chanvalon et al., 2015). To target production/consumption zones around burrows and to differentiate diffusive from bioirrigational fluxes, Thibault de Chanvalon PhD thesis (Thibault de Chanvalon, 2016) developed/adapted the Savitsky-Golay Filter method to pore-water modeling from the 2D DET gels (Thibault de Chanvalon et al., 2017). More recently, 2D-DET gels used to obtain the 2D distribution of Mn_d in pore-waters (Mouret et al., *in preparation*) were combined with a sediment slice, facing the gel probe (Thibault de Chanvalon et al., 2015), and was embedded (Jauffrais et al., *in preparation*) and analyzed for two main objectives: sediment structures in 2D/ 3D as macrofaunal burrows and 2D Mn micro-distribution by µXRF. The methodological and analytical 2D development give the opportunity to apply these high-resolution methods to the understanding of benthic faunal microenvironments.

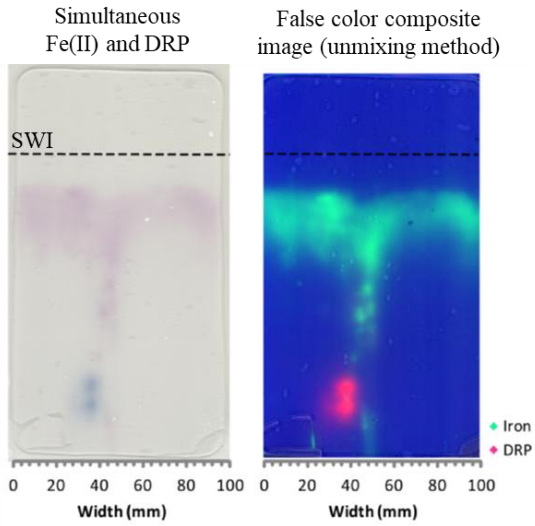

Figure 11: 2D DET gels coupled with colorimetric methods for Fe(II) and DRP and unmixing method used with hyperspectral camera to dissociate the signal of the two chemical elements. Modified from Cesbron et al., (2014)

1.3 Benthic foraminifera and their role in biogeochemical cycles

1.3.1. Biology of benthic foraminifera and their applications

Foraminifera have been observed since antiquity but were accurately described centuries later. Interest in these microorganisms was developed over the 18th and 19th centuries, especially by the naturalist Alcide d' Orbigny who classified Foraminifera within the Cephalopoda (as *Nautilus*) (D'Orbigny, 1826). Shortly afterwards, foraminifera were definitively described as unicellular organisms (Dujardin, 1835). Nowadays, foraminifera are defined as eukaryotic unicellular microorganisms (protists) belonging to the Rhizaria group and one of the most widespread groups of organisms (Adl et al., 2012). Foraminifera live both in the sediment (benthic) and in the water column (planktonic). The size of these organisms varies according to the species and their environments, thus in temperate and sub-polar environments they can range from few micrometers (propagules) to about 1 mm diameter (adults). Foraminifera are characterized by their cell surrounded by a shell, called a test. This test can be subdivided into one or more interconnected compartments or chambers which contain the same single cell. This test can be: organic (also called "naked"), agglutinated (formed of grains selected in the sediment), or carbonated (formed from calcite). In addition, foraminifera are characterized by the possibility of forming reticulated and granular extensions called pseudopodia. These pseudopods can extend up to 1 cm in length through the opening or test openings (Murray et al., 2002) allowing them to move, feed, protect, respire and reproduce (Goldstein, 1999). Figure 12 illustrates different photographs of the widespread intertidal foraminifer *Ammonia tepida* (*Ammonia* sp. T6; (Hayward et al., 2004; Richirt et al., 2019)).

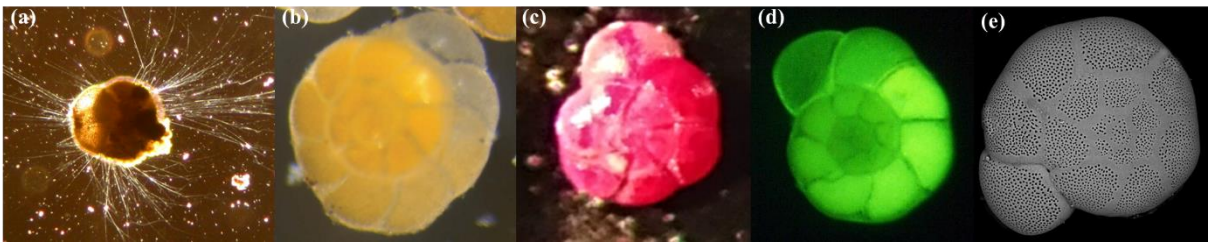

Figure 12: Photographs of Ammonia tepida: (a) light photograph of live Ammonia tepida with pseudopods, (b) light photograph of live Ammonia sp. T6 (natural color)(LeKieffre et al., 2018), (c) light photograph of Ammonia sp. T6 Rose Bengal staining, (d) Ammonia sp. T6 epifluorescence photograph CellTracker Green-labeled, (e) test photograph of Ammonia sp. T6 Scanning Electron Microscope image. (b-e) Ammonia sp. T6 from the Bourgneuf Bay mudflat (West Atlantic coast of France). Individuals of 300 µm wide.

Benthic foraminifera are used in different study contexts. Most foraminifera with a test can be used as fossil record. They are intensively used as biostatigraphic tools and for the

reconstruction of paleoenvironments (Rabalais et al., 2007; Pawlowski et al., 2003; Murray, 2006; Filipsson, 2008). Indeed, benthic foraminifera allow a better understanding of the evolution of climate change (e.g. ocean oxygenation conditions) through the study of the elemental composition of their shells (tests) (i.e. paleoceanographic proxies) (Katz et al., 2010; Petersen et al., 2018; Dijk et al., 2019). Benthic foraminifera are ubiquitous and found in all marine environments, showing high species diversity (Debenay et al., 2000; Murray, 2006) and high abundances, especially in the top first centimeter of coastal sediments (Alve and Murray, 2001; Schönfeld et al., 2012). Thanks to their species-specific tolerance or sensitivity to events (natural or anthropic) affecting the ecosystem they inhabit, foraminifera are good bioindicators of environmental modifications and stresses (e.g. eutrophication, heavy metals, hydrodynamism, oxygen availability, food source, salinity, land-sea continuum) (Debenay and Guillou, 2002; Murray, 2006; Jorissen et al., 2018; Parent et al., 2021; Bouchet et al., 2021).

Foraminiferal reproduction can be alternatively sexual and asexual (Murray, 2006). There is a lack of study showing clearly the different ontogenetic stages of a foraminiferal species. However, knowing the development speed of the specimens allows to better understand the response time between the moment of reproduction (proloculus or propagule stage < 32 µm (Alve and Goldstein, 2010)) and the adult specimens visible in the 150 µm fraction. The PhD thesis of Stouff (1998) give some indications on the "normal" ontogenetic growth of *Ammonia tepida* (Fig. 13) in controlled conditions. Briefly, the proloculus stage (1 chamber) visible with the 32 µm fraction to the numerous juvenile stages of 50 to 110 µm reached according to (Stouff, 1998) after 15 days after the appearance of proloculus. There is no further indication on the following stages until the adult stage (14-20 chambers) reached 3 months after the appearance of the proloculus. However, given the ontogenic speed of the early stages, it can be suggested that the specimens may reach a size of 150 µm after one month. This 150 µm fraction is used to study the population dynamics of adult foraminifera (Schönfeld et al., 2012). The response time lag is complex to estimate, being modulated by the environmental conditions which can be favorable or unfavorable to reproduction event and/or to the development of propagules (Heinz et al., 2002; Ernst et al., 2006; Debenay et al., 2006; Alve and Goldstein, 2003, 2010).

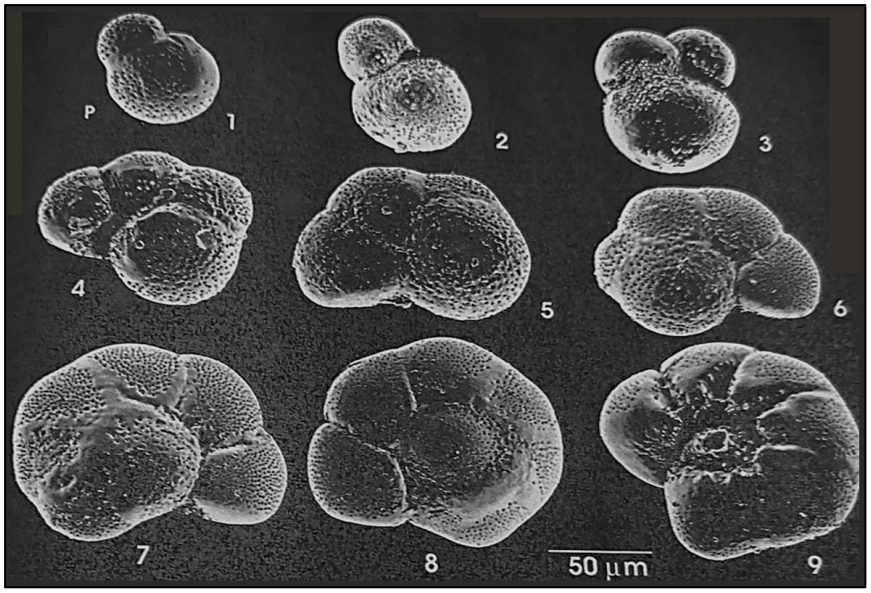

Figure 13: Some stages of ontogenic development of Ammonia tepida. (1-2) Proloculus + 1 loge, (3) 3 loges (24 h later), (4-5) 4 loges, (6) 5 loges, (7) 6 loges (1 week later), (8-9) 8 loges (2 weeks later) the test size reaches 110 µm. From Stouff, (1998).

Foraminifera have multiple adaptations and mechanisms (e.g. store intracellular nitrate to denitrify, symbiosis with chloroplasts (kleptoplasty), dormancy, feeding strategies, move towards a favorable microhabitat) to cope with various environmental conditions, giving them the ability to live in most marine sedimentary environments, from intertidal bays to deep-sea basins. Therefore, study their role and contribution to biogeochemical cycles especially carbon and nitrogen cycles are increasing in the various environments where their abundance is high.

1.3.2. Role and contribution of benthic foraminifera to biogeochemical cycles especially nitrogen cycle

Benthic foraminifera colonize a wide variety of sediments and may play a relevant role in the carbon cycle in sediments from brackish environments (Thibault de Chanvalon et al., 2015). The foraminiferal contribution to aerobic remineralization of OM is relatively low compared to aerobic bacteria (Geslin et al., 2011) and may account up to 7% in mudflat (Cesbron et al., 2016). The diverse feeding strategies of foraminifera (e.g. phytodetritus, bacteria, algae, phyto- and zooplankton, and nematodes) are also involved in the carbon assimilation and its transfer within the trophic web (Moodley et al., 2000; Koho et al., 2008; Nomaki et al., 2008; Chronopoulou et al., 2019; Jauffrais et al., 2016, 2019a; Wukovits et al., 2017; LeKieffre et al., 2018; Lintner et al., 2019, 2021).

High abundance of denitrifying (respiring nitrate) foraminifera in hypoxic and oxygenated marine environments suggest that these species play an important role in the

nitrogen cycle (Risgaard-Petersen et al., 2006; Pina-Ochoa et al., 2010; Bernhard et al., 2012b; Glock et al., 2013; Xu et al., 2017). Estimations of foraminiferal contributions to the denitrification in sediments range from 1 % to 90 % (Høgslund et al., 2008; Pina-Ochoa et al., 2010; Kamp et al., 2015; Dale et al., 2016; Xu et al., 2017) (Table 2).

Table 2: Estimations of foraminiferal contribution to sediment denitrification published in the literature modified from Xu et al., (2017).

References	Location	Foraminiferal denitrification rate (µmol N m^{-2} d^{-1})	Total sediment denitrification rate (µmol N m^{-2} d^{-1})	Foraminiferal contribution to sediment denitrification (%)
(Pina-Ochoa et al., 2010)	Skagerrak	720	1030	70
(Pina-Ochoa et al., 2010)	Bay of Biscay	64	76	84
(Pina-Ochoa et al., 2010)	OMZ Chile	173	250	70
(Pina-Ochoa et al., 2010)	Arabian Sea OMZ	78	510-840	9-15
(Pina-Ochoa et al., 2010)	Tagus Prodelta	72-240	480-960	8-50
(Glud et al., 2009)	Sagami Bay	50	1250	4
(Bernhard et al., 2012b)	Santa Barbara Basin, USA	3000	4500	67
(Glock et al., 2013)	Peruvian OMZ	420-1310 10-90	10-1300	29-50 (OMZ) 2-6 (below OMZ)
(Dale et al., 2016)		1400-1500	1510-2380	62-90 (lower OMZ)
(Larsen et al., 2013)	Jones bank, Celtic Sea	1-13	120	1-11
(Xu et al., 2017)	East China Sea Yellow Sea	64-69 16-88	264 45-144	24-26 36-61

Dissimilatory nitrate reduction (DNR) pathways such as denitrification are well studied in denitrifying bacteria (Knowles, 1982). And some eukaryotes are known to use incomplete denitrification pathways (e.g. freshwater ciliates, *Loxodes* sp.) (Finlay et al., 1983). For example, incomplete denitrification to nitrous oxide was shown to be present in the fungus *Fusarium oxysporum* (Shoun and Tanimoto, 1991; Takaya et al., 1999). Some diatoms are also able to use dissimilatory nitrate reduction to ammonium (DNRA) (e.g. *Amphora coffeaeformis* and *Thalassiosira weissflogii* (Kamp et al., 2011, 2013). However, the nitrate reduction pathway remains unknown for most of the denitrifying eukaryotes such as the Gromiids, Chlorophytes, Haptophytes and Dinoflagellates (Kamp et al., 2015). Benthic foraminifera were the first discovered marine eukaryotes able to perform denitrification (Risgaard-Petersen et al., 2006), but not all foraminifera are able to denitrify (Pina-Ochoa et al., 2010). Denitrifying species of foraminifera are defined as species able to perform a complete denitrification proved by denitrification rates measurements. Risgaard-Petersen et al. (2006) were the first to measure denitrifying rates of two benthic foraminifera species: *Nonionella* cf. *stella* (OMZ, Peru) and

Globobulimina turgida (Gullmar Fjord). Since that, nineteen species have been shown to be denitrifiers (Risgaard-Petersen et al., 2006; Høgslund et al., 2008; Pina-Ochoa et al., 2010; Bernhard et al., 2012b; Woehle et al., 2018; for details see Glock et al., 2019). The nitrate reduction pathway seems to differ from one species to another: some species seem to possess their own cytoplasmic pathway, while others have acquired their denitrifying capacity through symbiosis. For example, *Globobulimina turgida* and *Globobulimina auriculata* have their own eukaryotic denitrification pathways encoded in their genome (Woehle et al., 2018; Stein, 2018). While denitrification in certain species (e.g. allogromiids in Santa Barbara Basin) is carried out by bacterial endobionts and not by the foraminifer itself (Bernhard et al., 2012a; Nomaki et al., 2014). Until 2019, it was accepted that denitrifying species were facultative anaerobes. However, Glock et al. (2019) showed that nitrate was the preferred electron acceptor over oxygen in foraminifera from the Peruvian OMZ.

Foraminifera denitrification rates show wide variability, with the highest rate (2241 ± 1825 pmol N indiv.$^{-1}$ d^{-1}) measured for *Valvulineria inflata* (OMZ, Peru, Glock et al., 2019) and the lowest denitrification rate (7 ± 1 pmol N indiv.$^{-1}$ d^{-1}) measured on *Nonionella auris* (OMZ, Peru, Glock et al., 2019). These two denitrifying species are found mainly in oxygenated depleted environments such as oxygen minimum zones (OMZ) of Peru (Glock et al., 2013) and Chile (Risgaard-Petersen et al., 2006; Høgslund et al., 2008), in the anoxic Santa Barbara Basin (California, USA) (Bernhard et al., 2012a) and in the seasonally hypoxic Gullmar Fjord (Sweden) (Risgaard-Petersen et al., 2006). Denitrifying foraminifera, e.g. *Bolivina subaenariensisi*, *Uvigerina phlegeri* and *Valvulineria bradyana*, can also be found in oxygenated areas such as the Bay of Biscay (France) or the Rhône delta (France) (Piña-Ochoa et al., (2010)). Recently, Xu et al. (2017) estimated the role of benthic foraminifera in the oxygenated bottom water sedimentary denitrification of the Yellow Sea and the East China Sea (based on the denitrifying rates of five abundant species) (Table 2).

Several foraminifera species can store intracellular nitrate (Risgaard-Petersen et al., 2006) with the highest intracellular nitrate concentrations for *Globobulimina* cf. *ovula* from Peru (375 ± 174 NO_3^- mM, Piña-Ochoa et al., 2010). Foraminiferal species able to concentrate intracellular nitrate seem to be able to respire it. Hence, several foraminiferal species may together represent an important reservoir of nitrate storage in sediments (Bernhard et al., 2012a), reaching 20 % of the nitrate pore water sediment in Gullmar Fjord (*G. turgida*) and 80 % in Sagami Bay (Risgaard-Petersen et al., 2006, Glud et al., 2009). Species that store intracellular nitrate and denitrify might be able to actively migrate into the sediment towards favourable micro niches for their food source and pore water environments (Koho et al., 2011;

Nomaki et al., 2015). For example, Koho et al. (2011) suggested that *Globobulimina turgida* is able to actively migrate into the sediment to find nitrate-containing strata and actively collect nitrate in the presence or absence of oxygen. Foraminifera can store intracellular nitrates that can be transported/produced in depth by bioirrigation or anoxic nitrification. The respiration of these nitrates by foraminifera could increase the loss of fixed nitrogen in suboxic/anoxic sediments (Prokopenko et al., 2011; Dale et al., 2016).

In addition to the ability of some benthic foraminiferal species to store nitrate for dissimilatory purposes, mixotrophic (*Haynesina germanica* and *Nonionellina labradorica*) and heterotrophic (*Ammonia tepida*) foraminiferal species are able to effectively assimilate ammonium, and integrate this nitrogen source in their biomass (LeKieffre et al., 2018; Jauffrais et al., 2019b; Bird et al., 2020). Ammonium assimilation was shown to be a suitable N source (as suggested for planktonic foraminifera; LeKieffre et al., 2018) for cell growth and development. Besides, Bird et al., (2020) and LeKieffre et al., (*in preparation*) suggested that nitrogen assimilation could be widespread among foraminifera. Moreover, benthic foraminifera might compete with MPB for NH_4^+ availability in a fast N-turnover environment (Eyre et al., 2016).

1.3.3 The preferential microhabitats/ microenvironments of benthic foraminifera

The TROX (TRophic conditions and OXygen concentration) model is a conceptual approach to explain the microhabitat preferences of benthic foraminifera (Jorissen et al., 1995) (Fig. 14 a). Briefly, under oligotrophic conditions, the depth of the microhabitat is controlled by the availability of metabolizable food particles in the sediment. Under more eutrophic conditions, the ecosystem is controlled by a critical level of oxygen concentration that determines downward flow. Under food-limited conditions, anaerobic degradation of organic matter may provide an additional food source around the redox front, which could explain the depth infaunal maxima reported in the literature (Jorissen et al., 1995). Since, the TROX model has been updated with for example the addition of some foraminifera species favoring nitrate respiration over oxygen (Glock et al., 2019). The concept of microhabitats was modified by indicating that denitrifying foraminifera migrate up or down through the depth of nitrate

penetration in sediments, which would provide a good tool for understanding nitrate transport by foraminifera in various marine environments (Fig. 14 b) (Xu et al., 2021).

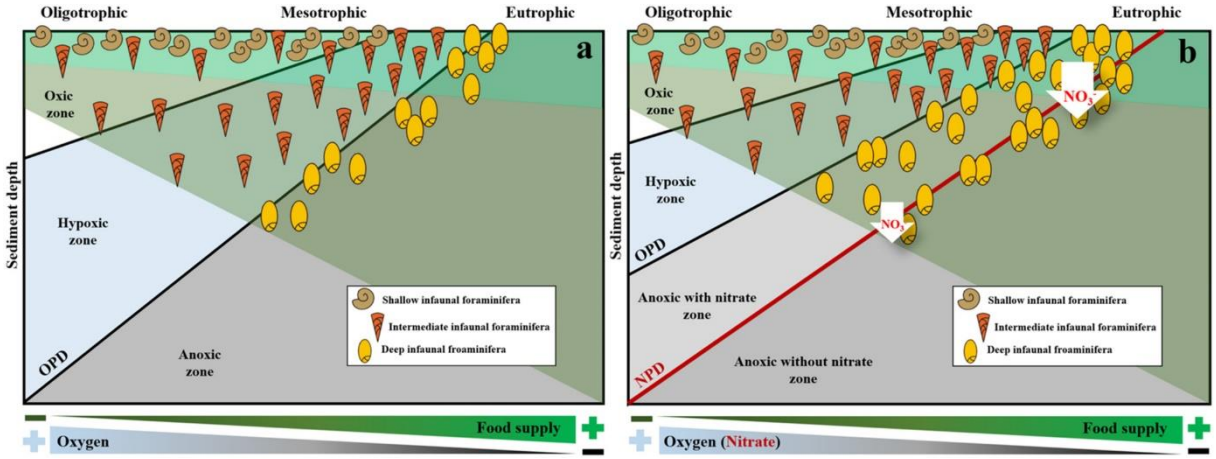

Figure14: Schematic diagram of the original (a) and modified (b) trophic oxygen model (Jorissen et al., 1995) illustrating the relationship between organic loading, oxygenation, pore water nitrate and their influence on foraminiferal vertical distribution and nitrate transport. From Xu et al., (2021).

The vertical distribution of foraminifera can also be explained by the downward transport of individuals by biomixing that introduces living foraminifera into the deeper sediments (Fig. 15; Thibault de Chanvalon et al., 2015). This burial of living individuals to the deeper sediment can be induced by biomixing (Alve and Bernhard, 1995; Goldstein et al., 1995; Moodley, et al., 1998; Alve and Murray, 2001; Jorissen, 2003; Bouchet et al., 2009) and/or by additional sediment deposition due to flood event. Three foraminiferal behaviors were suggested by Thibault de Chanvalon et al., (2015) to explain the typical vertical distribution of foraminifera in mudflats: 1) in the first ~ 3 cm depth, some individuals are able to migrate towards the oxygenated and organic-rich layer as soon as they detect redox gradients, 2) in deeper sediment ~ 8 cm depth, some individuals would no longer be able to ascend towards the superficial layers and remain blocked. Thus, after a prolonged presence in suboxic conditions foraminifera reduce their metabolism and become inactive (dormancy) or die (LeKieffre et al., 2017). 3). Moreover, foraminifera can be temporarily remobilized during

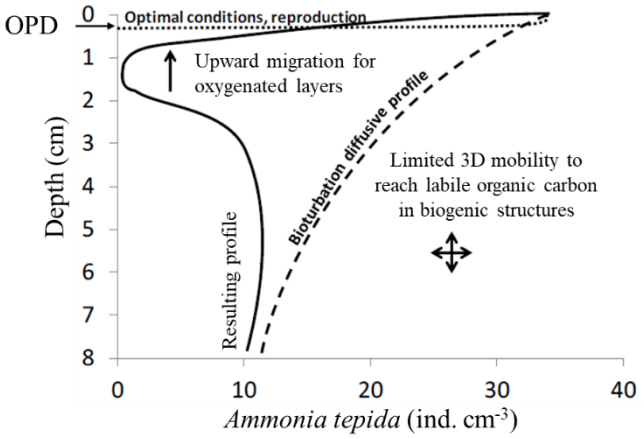

Figure 15: Putative mechanisms explaining the A. tepida density profile (OPD: oxygen penetration depth) in the "Les Brillantes" mudflat (Loire estuary). From Thibault de Chanvalon et al., (2015).

bioirrigation events, and could migrate towards organic-rich microenvironments in their vicinity (Thibault de Chanvalon et al., 2015). The choice of the method used to differentiate between living and dead foraminifera becomes crucial (Bernhard et al., 2006). Rose Bengal staining is recommended for biomonitoring of foraminifera contained in the first centimeter of the sediment (Schönfeld et al., 2012), whereas CellTracker Green labeled is recommended for the study of the foraminiferal vertical distribution in environments with high redox spatiotemporal variability (Nardelli et al., 2014; Langlet et al., 2014; Thibault de Chanvalon et al., 2015; Cesbron et al., 2016; LeKieffre et al., 2017; Charrieau et al., 2018; Richirt et al., 2019).

1.3.4 Foraminiferal preferential food source

Improving our knowledge on foraminiferal trophic interactions would allow to better understand their role in the ecosystem functioning and in the biogeochemical cycles. These interactions and nutrient transfers may drive mudflat ecosystems and biodiversity (LeKieffre et al., 2017). Benthic foraminifera have diverse trophic strategies: they can be mixotroph or heterotroph. Some species have shown omnivorous heterotrophic behaviors, feeding on various food sources: organic matter detritus, bacteria, fungi, microalgae and sometimes metazoans (Witte et al., 2003; Nomaki et al., 2005, 2006, 2008; Pascal et al., 2009; Dupuy et al., 2010; Enge et al., 2011; Mojtahid et al., 2011; Wukovits et al., 2017, 2018; Bird et al., 2018; Lintner et al., 2020). Some foraminiferal species are thought to display mixotrophic strategies. For example, some species harbor putative procaryote symbionts that could play a role in their host metabolism (Bernhard et al., 2003, 2012a; Bird et al., 2017; Prazeres et al., 2017). Another mixotrophic strategy involved kleptoplasts (i.e. stolen chloroplasts) (Lopez, 1979; Jauffrais et al., 2016; LeKieffre et al., 2018). Foraminiferal kleptoplasty is a symbiotic association whereby chloroplasts obtained from microalgal preys, are sequestered into the host cell (Clark et al., 1990). Some foraminiferal species from photic and aphotic zones have been found to perform kleptoplasty with diatom chloroplasts (Lopez, 1979; Bernhard and Bowser, 1999; Tsuchiya et al., 2015; Jauffrais et al., 2016, 2018). The kleptoplasts were proven to be functional (production of oxygen and inorganic carbon assimilation) only in species from photic environments (intertidal mudflats) (Lopez, 1979, Jauffrais et al. 2016, Lekieffre et al. 2018). In species from deeper aphotic environments such as *N. labradorica* sampled in the Gullmar fjord, the kleptoplasts were not photosynthetically active. Besides, kleptoplasts are also thought to play a role in nitrogen assimilation, accounting for another putative N assimilation pathway in the foraminiferal cell (Grzymski et al. 2002, LeKieffre et al. 2018).

In mudflats, four typical intertidal species are found with different trophic strategies. *Ammonia tepida* (Hayward et al., 2004; Richirt et al., 2019) is omnivorous, feeding on organic detritus, bacteria, microalgae and meiofauna (Dupuy et al., 2010; Mojtahid et al., 2011; Pascal et al., 2009; Wukovits et al., 2018). *Haynesina germanica* harbors kleptoplasts that were shown to be photosynthetically active (Jauffrais et al., 2016). Less is known about *Elphidium* species. *Elphidium oceanense* (d'Orbigny in Fornasini, 1904) and *Elphidium selseyense* (Heron-Allen and Earland, 1911) are kleptoplastic (Lopez, 1979; Pillet et al., 2011; Jauffrais et al., 2018, 2019b). Nevertheless, it has not been proven yet that the kleptoplasts are photosynthetically active in those two species.

Diatoms provide an important source of organic carbon and nutrients to benthic foraminifera (Moodley et al., 2000; Nomaki et al., 2005, 2006; LeKieffre et al., 2017, 2018; Lintner et al., 2020, 2021). Numerous experimental (Lee et al., 1966; Lopez, 1979; Gooday and Lambshead, 1989; Bernhard and Bowser, 1999; Heinz et al., 2002; Goldstein et al., 2004; Austin et al., 2005; LeKieffre et al., 2017) and metabarcoding (Pillet et al., 2011; Chronopoulou et al., 2019; Schweizer et al., *submitted*) studies suggest that foraminiferal-diatom trophic interactions are very specific. These foraminiferal-diatom trophic relationships would depend on the trophic regime of the foraminifera, how the foraminifera eat the diatoms (cracking of the frustule (Austin et al., (2005) or complete ingestion of the diatom (LeKieffre et al., (2017), Fig. 16) and the physicochemical conditions of the environment.

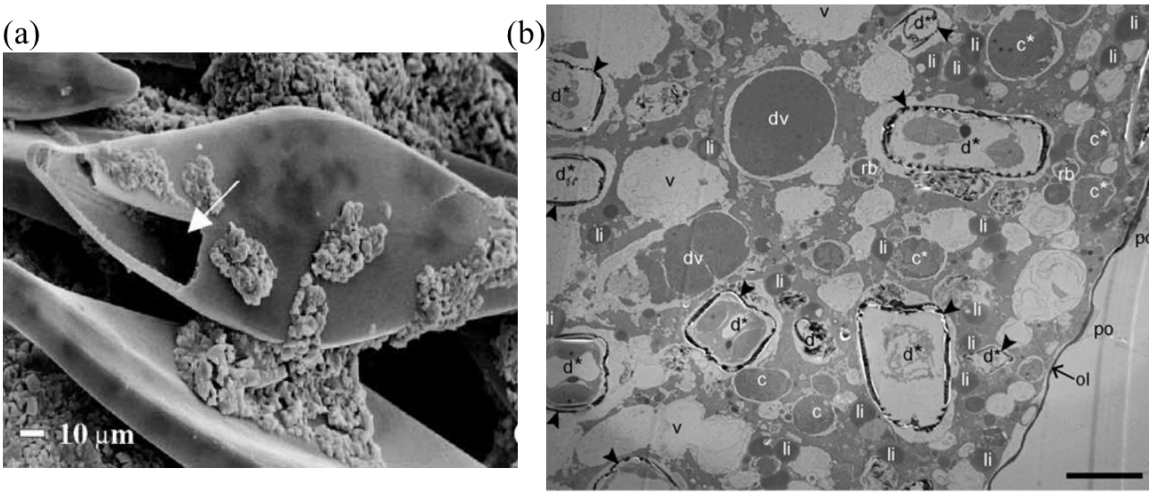

Figure 16: (a) Haynesina germanica cracking of captured Pleurosigma sp. (the arrow indicates the cracking of the diatom frustule), from Austin et al., (2005). (b) Transmission electron micrographs of different types of degradation vacuoles in Ammonia sp. T6. Cytoplasm of the antepenultimate chamber exhibiting numerous diatom frustules (arrowheads), in which the diatom cytoplasm is being digested (d) and diatom chloroplasts are in degradation (c*). c: chloroplasts, c*: chloroplasts in degradation, d*: diatom in degradation, dv: degradation vacuoles, fv: fibrillar vesicles, li: lipid droplets, m: mitochondria, ol: organic lining, po: pore, rb: residual bodies, v: vacuoles. Scale = 5 µm. From LeKieffre et al., (2017).*

1.4 Microphytobenthos

Beyond the trophic relations existing between foraminifera and diatoms, diatoms and foraminifera are two groups that can be used as bioindicators of marine ecosystems (Benito, 2020). Indeed, benthic foraminifera and diatoms respond rapidly and sensitively to environmental changes. Moreover, foraminiferal tests and diatom frustules can be preserved for a long time in the sediments. In coastal ecosystems such as intertidal mudflats, foraminiferal and diatom communities indicate the transition of the land-sea continuum. In land-sea transition systems, these bioindicators are valuable because spatiotemporal species dynamics are a means of determining species response to natural and/or human-induced environmental gradients (e.g., water physico-chemistry, substrate type, bathymetry, organic matter, and dissolved oxygen).

The microphytobenthos (MPB) is composed of an assemblage of benthic photosynthetic microalgae often dominated by diatoms (MacIntyre et al., 1996; Méléder et al., 2007). Thus, mudflats are highly productive coastal ecosystems (MacIntyre et al., 1996; Underwood and Kromkamp, 1999; Paterson et al., 2003). Diatoms have different "life forms" (e.g. epipelic, epipsammic, pelagic). Epipelic diatoms, are motile cells that move around sedimentary particles (mainly muddy sediment) (Round and Happey, 1965), showing upward and downward migrations according to the tidal cycle and photoperiod, modulated by light, temperature and nutrient availability (Round and Happey, 1965; Admiraal et al., 1984; Consalvey et al., 2004). These vertical migrations follow an endogenous circadian cycle synchronized with daily emersion periods whereby cells migrate to the sediment surface forming biofilms where they accumulate energy for metabolism (e.g. photosynthesis). Diatoms can make adjustments to their position in the sediment that can be interpreted as a photo-regulatory mechanism (Perkins et al., 2001; Jesus et al., 2006; Cartaxana et al., 2011; Serôdio et al., 2012; Prins et al., 2020). Thus when their energy quota is reached and/or when the tide rises, the cells down into the sediment where they can use nutrients and produce new biomass (Saburova and Polikarpov, 2003). Conversely, epipsammic diatoms (strongly associated to sandy grains) depend mainly on the thermal dissipation of excessive light energy to photo-regulate (Cartaxana et al., 2011; Barnett et al., 2015; Blommaert et al., 2018). At high tide, with tidal currents and waves, a part of the biofilm is resuspended in the water column (Fig. 17) and can contribute to the phytoplankton (pelagic) biomass (Guarini et al., 2004). The granulometry allows to explain the preferential life forms of diatoms in a mudflat (Méléder et al., 2007). Thus, mixed sediments (muddy and sandy) are mainly represented by epipsammic species. Conversely, a mudflat with finer particles is favourable to the development of epipelic species. Other life forms can be

found such as: epiphytic living attached to seagrass and sometimes pelagic species can settle on the sediment surface.

The spatial heterogeneity of intertidal mudflats is challenging to quantify accurately carbon stocks and flows in coastal areas (Legge et al., 2020). MPB spatiotemporal distribution is highly variable, as it is driven by physical (light photo-regulation, temperature, tides, and waves) and biological (grazing, biostabilization, and bioturbation) factors (Consalvey et al., 2004; Spilmont et al., 2007; Coelho et al., 2009, 2011; Serôdio et al., 2012; Savelli et al., 2018). To assess MPB biomass in tidal mudflat, measurements are often single-point sampling (Cartaxana et al., 2015; Pniewski et al., 2015). The normalized difference vegetation index (NDVI) (Tucker, 1979) was used as a proxy of MPB chlorophyll a, which itself is often used as a proxy for MPB biomass (Méléder et al., 2003b; Forster and Jesus, 2006; Benyoucef et al., 2014). Chlorophyll a is an ubiquitous pigment found in all MPB organisms. The development of remote sensing methods using NDVI are now more widely used for MPB studies on a large spatial scale (from one meter to several kilometers) (Méléder et al., 2003a; Brito et al., 2013; Benyoucef et al., 2014; Échappé et al., 2018; Launeau et al., 2018; Méléder et al., 2020).

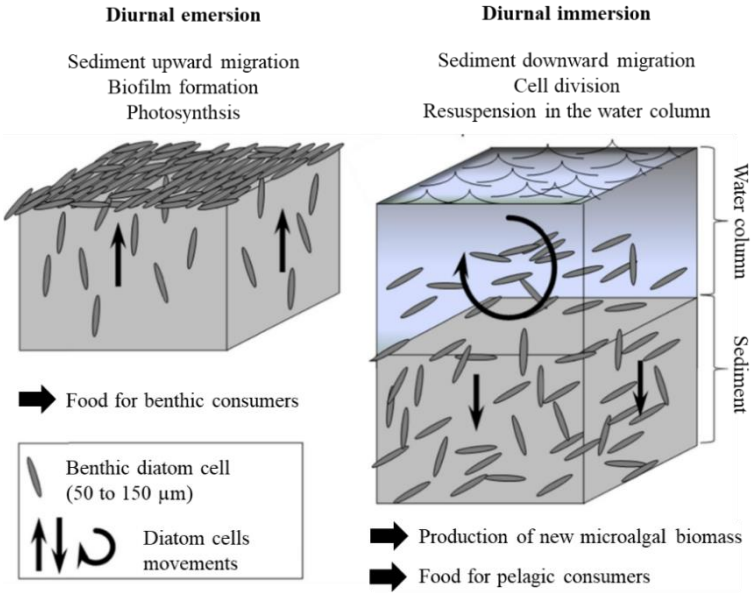

Figure 17: Conceptual diagram of the processes leading to microphytobenthos primary production on intertidal bare mudflats in relation with the alternance of tides: Upward migration of diatoms during low tide and process of suspension of benthic diatoms in the water column at high tide. From (Lebreton et al., 2019), modified from (Blanchard et al., 2006).

2. Objectives of the PhD thesis

The general aim of this PhD research was to better understand the benthic faunal and geochemical interactions from micro-scale to kilometer-scale in two contrasted coastal areas. This PhD thesis is divided into four chapters, each of them investigating different combined high resolution methods and multivariate analyses at different scales to reveal the interactions between benthic faunal and geochemical compartments.

Chapter 1: Denitrification by benthic foraminifera and their contribution to N-loss from a fjord environment

At the beginning of my PhD thesis in November 2017, a sampling cruise was performed at two oxygenated and nitrate contrasted stations in the Gullmar Fjord (Sweden). This **Chapter 1** investigated the contribution of denitrifying foraminifera to benthic nitrogen cycle in the oxygenated station near the entrance of the fjord and another station in the seasonal hypoxic deep basin. The benthic foraminifera *Nonionella* sp. T1 dominated in the oxygenated nitrate-rich station of the fjord which was discovered recently in this area (Polovodova Asteman and Schönfeld, 2015). The oxygenated station contained sediments with high pore-waters NO_3^- concentrations conversely to hypoxic station which was NO_3^- depleted. Thus, the NO_3^- were available to be respired by denitrifying species at the oxygenated station. Therefore, we investigated the nitrate respiration rate of the non-indigenous species (NIS) *Nonionella* sp. T1. The combined using of high resolution CTG-labeled, N_2O microsensors and NO_3^- 2D-DET gels methods allowed to estimate accurately the contribution of denitrifying foraminifera to the benthic nitrogen cycle. The general objectives of this **Chapter 1** were: (1) to characterize the density of the living benthic foraminifera at two contrasting stations in the Gullmar fjord: one with oxic bottom water and one with hypoxic bottom water. We focused on the relative abundance of the NIS *Nonionella* sp. T1 (2) to investigate if this NIS *Nonionella* sp. T1 can denitrify and (3) quantify its eventual contributions to benthic denitrification in the sediments. On the basis of the results we discussed the probable future impact of the NIS *Nonionella* sp. T1 on the foraminiferal fauna and the nitrogen cycle in the Gullmar Fjord.

Chapter 2: Impact of hypoxia and bioirrigation on benthic manganese release in the Gullmar Fjord using 2D high spatial resolution methods

The results of the **Chapter 2** benefited from samples obtained during the November 2017 cruise in the Gullmar Fjord. The two oxygenated contrasted stations were also contrasted in

dissolved and solid-phases manganese and impacted by macrofaunal activity. The Gullmar Fjord is rich in macrofauna (Austen and Widbom, 1991). Bioturbation and bioirrigation due to the macrofaunal burrowing disturb the early diagenesis redox fronts (Aller, 1982; Burdige, 2006). The Gullmar Fjord is Mn-rich in the sediments of the deep basin (Goldberg et al., 2012). However, no estimation of the Mn cycle and the impact of seasonal hypoxia and bioturbation on this cycle was previously established. In this **Chapter 2** we investigated an innovative approach to estimate the contribution of macrofaunal burrowing activity to Mn cycle in a seasonal hypoxic fjord. For this purpose, we combined the using of innovative and recent technical developments as: Mn_d 2D-DET gel method (Mouret et al., *in preparation*), embedded sediment slabs (Jauffrais et al., *in preparation*) and selective chemical extractions to visualise and quantify the contrasted dissolved and solid-phases Mn micro-distributions. Indeed, macrofaunal activity generates bioirrigation through burrows improving exchanges between anoxic deep sediments and the overlaying water. The objectives of this study were: 1) to describe the dissolved and solid-phases Mn micro-distribution of two oxygen contrasted stations in the Gullmar Fjord, 2) to calculate separately the diffusive and bioirrigational fluxes at both stations by the Savitsky-Golay Filter method (Thibault de Chanvalon et al., 2017) and 3) to estimate the benthic Mn cycle in the Gullmar Fjord based on oxygenated steady-state conditions and the impact of a hypoxic event on this cycle.

Chapter 3: Spatiotemporal dynamics of living benthic foraminifera revealed by hydrodynamics and *in situ* trophic model in intertidal mudflat (Bourgneuf Bay, France)

Three stations were selected for the MUDSURV project in early 2016, aiming to better understand the functioning of the "La Coupelasse" site in the Bourgneuf Bay mudflat (West coast of France). The Bourgneuf Bay is a semi-enclosed area located at the South of the Loire river estuary. The "La Coupelasse" sampling site is composed of three stations (A, B and C) spaced from 10 m apart (meso-scale/ decameter-scale) along a tidal channel near a path used by oyster farmers. The sampling effort in this study was high and benefited from a multi-parameter approach (geochemistry, microphytobenthos, benthic foraminifera). This **Chapter 3** benefited from a monthly then quarterly geochemical database from March 2016 to October 2019. Simultaneously a monthly benthic foraminiferal monitoring occurred in the 1st cm depth of the sediment, using Rose Bengal-staining and the adult size population of the dominant species (> 150 µm). The monthly microphytobenthos biomass was analyzed from April 2017 to July 2019 at the three stations. The MPB assemblages were analyzed at the station B.

Two research paths were explored in this Chapter 3. Firstly, we investigated the spatiotemporal dynamics of the dominant foraminiferal species through a multivariate analysis gathering 3 years of environmental dataset. The foraminiferal dynamics were characterized by: 1) hydrodynamism and meteorological parameters (discharge, rainfall, temperature, tidal coefficient, porosity, salinity, granulometry), 2) OM remineralization activity (alkalinity, OPD, DOU), 3) pore-waters nutrients (DRP, NH_4^+, NO_3^-, NO_2^-) and 4) proxy of the MPB biomass (NDVI). This analysis should allow to identify the environmental parameters inducing unfavourable *versus* favourable reproduction periods. Secondly, we investigated an *in situ* trophic model to find which diatom species were preferentially eaten by foraminiferal species and could explain their temporal variabilities. Finally, the aims of this study were: (1) to describe the spatial and temporal dynamics of the dominant foraminiferal species; (2) to characterize the main environmental parameters driving the spatiotemporal foraminiferal dynamics in a context of "confined waters" and (3) to discuss, *in situ* trophic model based on the temporal foraminiferal species–specific diatoms food preferences.

Chapter 4: Influence of the Loire river hydrodynamics on geochemical and benthic foraminiferal compartments in intertidal mudflat (Bourgneuf Bay, France)

This **Chapter 4** is a complementary approach of the Chapter 3. We investigated further the benthic faunal and geochemical compartments at two sampling time characterized by two hydrological and meteorological contrasted months. April 2019 was characterized by winter post-flooding period and October 2019 by summer low-water period. The aims of this Chapter 4 were: (1) to detail redox elements spatial variability at two hydrological and meteorological contrasted periods; (2) to investigate the role of the tidal pump and flood events on the dynamics of redox elements and the nutrient availability for benthic fauna; (3) to evaluate if the vertical foraminiferal micro-distribution (CTG-labeled) allow to characterize the late disturbed winter post-flooding and the stabilized late summer periods. To reach these objectives, we used high spatial resolution methods. The simultaneous deployment of Mn_d, Fe_d, NO_3^-, NH_4^+ and DRP 2D-DET gels was used to provide accurate redox elements and nutrients vertical and lateral variabilities at decimetric scale (within a station). Then, the using of dissolved and solid phases 1D profiles allowed us to capture the variability at decametric-scale (between the three stations). The description of the geochemical processes over a larger resolution window at two contrasted months could enable to understand the evolution of transient diagenesis driving especially the nutrients dynamics (Thibault de Chanvalon et al., 2015, 2016). Moreover, the *in situ* deployment of O_2 profiles through several hours during emersion time would provide

information about the MPB photosynthetic activity given indication on available oxygenated micro-environments for benthic foraminifera. The foraminiferal species densities should respond strongly to these contrasted months. We decided to explore the foraminiferal micro-distributions CTG-labeled up to 10 cm depth to identify if the species distributions reflect the state of sediment instability through unfavourable *versus* favourable periods.

3. Study areas

3.1 PART I: Gullmar Fjord

Fjords are characterized by a coastal geomorphology, formed by semi-enclosed marine basins. Fjords are located above the Northern Fjord Belt as the Gullmar Fjord (Sweden) (red star, Fig. 18) and under the Southern Fjord Belt (Bianchi et al., 2020).

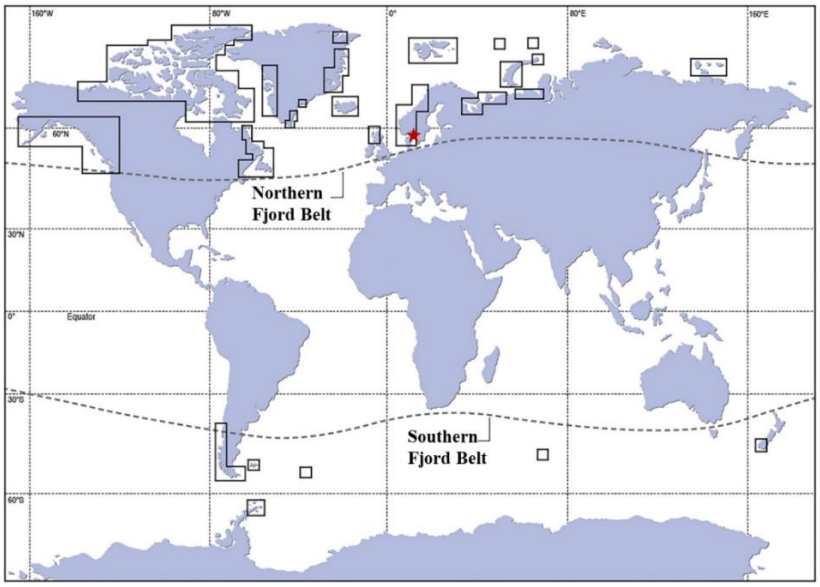

Figure 18: Global distribution of fjords. The red star indicates de Gullmar Fjord location. Modified from Bianchi et al., (2020).

Fjords are the result of glacial erosion, indeed the majority of the fjords had a glacier or still have one. The Gullmar fjord in Sweden, is an example of non-glaciated fjord. Non-glaciated fjords are transitional environments subjected to the exchange between open-ocean water masses and freshwater inputs from the land (Fig. 19). Generally, a sill located at the entrance of the fjords separates the adjacent coastal waters from the deep basin, limiting water exchange and circulation, and therefore the oxygen renewal (Howe et al., 2010). Limited water mass exchanges, high sedimentation rate, make fjords ideal environments to reconstruct climate change and anthropogenic impacts at high temporal resolution (Howe et al., 2010). Besides, fjords are considered as mini-oceans basin laboratories allowing to observe biogeochemical processes and typical benthic faunas (Skei, 1983; Howe et al., 2010). Sill fjords because of

organic inputs from land and insufficient deep-water renewal, could be seasonally hypoxic even anoxic (Filipsson and Nordberg, 2004b). The seasonal hypoxic Gullmar Fjord offers a high-resolution environmental archive (Filipsson and Nordberg, 2004a) allowing to investigate benthic geochemical processes and benthic faunal spatiotemporal variation.

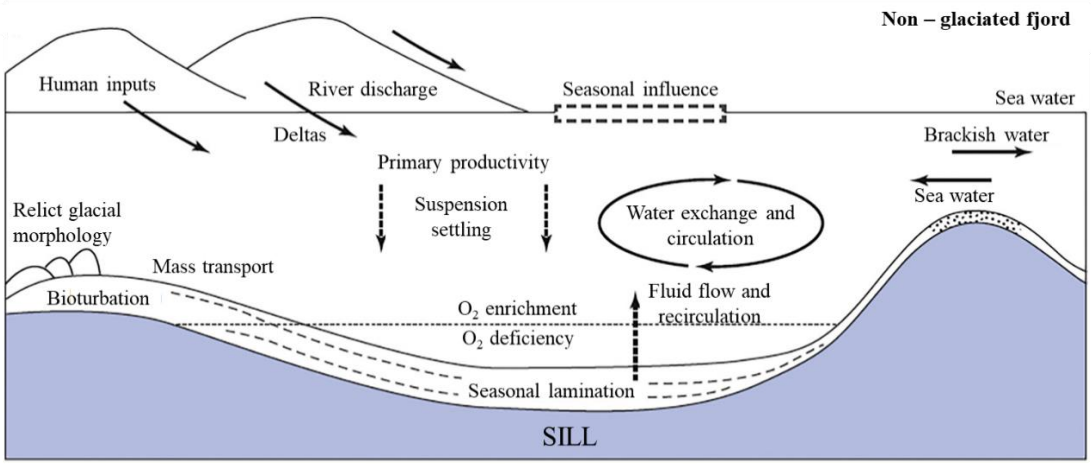

Figure 19: Principle physical processes within non-glaciated fjord (adapted from Howe, (2010) and Bianchi et al., (2020)).

The Gullmar Fjord is located on the Swedish west coast, oriented in the SW-NE direction (Fig. 20 a). The fjord fluctuates between cold and temperate climates and has a low tidal activity with a range of 20 cm in the Skagerrak-Kattegat region (Svansson, 1984; Nordberg, 1991). The hydrography of Gullmar Fjord depends on the waters of the adjacent Skagerrak an extension of the North Sea, and also on the waters from the Kattegat an extension of the Baltic Sea (Figure 20 b).

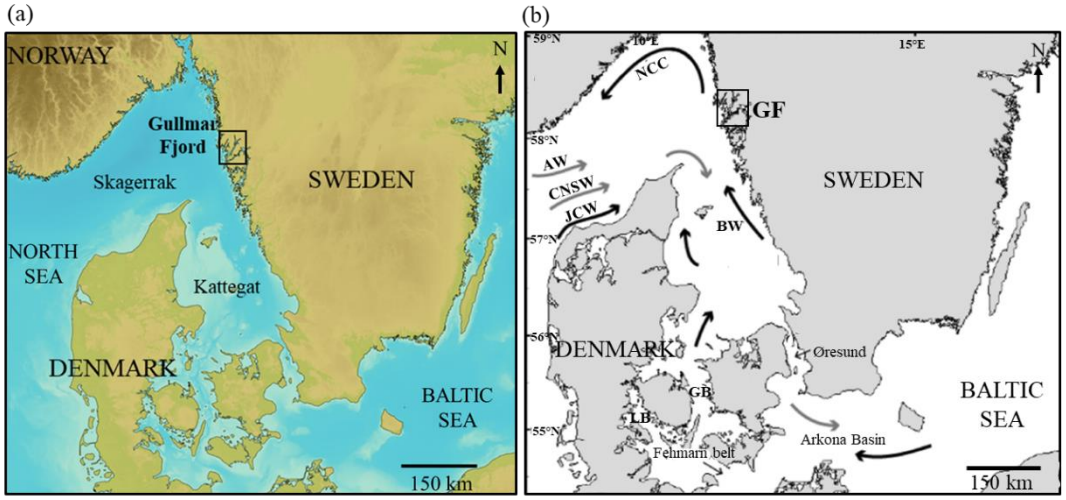

Figure 20: (a) Gullmar Fjord location (black framed) on the Swedish West coast (data from SHOM). (b) General water circulation: main surface currents (black arrows) and main deep currents (grey arrows). GB: Great Belt; LB: Little Belt; AW: Atlantic Water; CNSW: Central North Sea Water; JCW; Jutland Coastal Water; NCC; Norwegian Coastal Current; BW: Baltic Water. Modified form Charrieau et al., (2018).

Water exchanges occur during winter in the deepest part of the stagnant basin (near Alsbäck monitoring station, Fig. 21). The low mixing of deep basin waters in winter time are due to the 42 m deep sill (located between Släggö and GF17-3 stations, Fig. 21), reducing water exchanges. Fjord water masses are stratified (presence of haloclines) especially because of the deep sill located in the entrance (Arneborg, 2004). Surface waters (uppermost 1 m of the water column) are fresher than the underlying waters due to the inputs of the Örekilsälven river but without a significant impact on the fjord hydrography (Arneborg, 2004). The deeper water column layers are composed of the Baltic (1-18 m) and the Skagerrak (18-50 m) water masses. The deepest layer (> 50 m) corresponds to the stagnant basin (Svansson, 1984) which is influenced by both water exchanges and wind forcing during winter (Björk and Nordberg, 2003). Indeed, several scientific publications demonstrated the influence of NAO (North Atlantic Oscillation) on hypoxic events of the fjord (Hurrell, 1995; Nordberg et al., 2000; Björk and Nordberg, 2003; Filipsson and Nordberg, 2004b). From the late 1970s, the NAO is in positive phase. Westerly winds limit the renewal of bottom waters, favouring hypoxic events in the deepest part of the fjord. The first measured hypoxic event has been dated from February 1890 by Pettersson and Ekman (1891). Later several hypoxic events have been identified during the 20th century and at the beginning of the 21th century (Filipsson and Nordberg, 2004b; Polovodova Asteman and Nordberg, 2013). The recent hydrographic data used are obtained from the Swedish Meteorological and Hydrological Institute's (SMHI's) publicly available database SHARK (SMHI, 2020).

Different monitoring stations are located along the Gullmar Fjord (i.e. Släggö at 65 m, Björkholmen at 70 m, and Alsbäck at 117 m; SMHI, 2020). The monitoring of these stations is uneven. Björkholmen monitoring (white triangle, Fig. 21) started in 1968 and stopped from 1999 to 2014. Släggö monitoring (black dot, Fig. 21) started in 1986 and is still ongoing. Alsbäck monitoring (red square, Fig. 21), started in 1977 but stopped in July 2015. Since 2010, the hypoxia threshold ($[O_2] < 2$ mg L^{-1}, i.e., 63 μmol L^{-1}) in Alsbäck station is reached typically in late autumn and winter. As Alsbäck monitoring stopped in July 2015, Björkholmen station is used to estimate the hypoxic events after this date. The most external station Släggö, never became hypoxic (black dot, Fig 21) and it is used as reference station for the oxygenated part at the entrance of the fjord.

In the first part of this PhD thesis, two sampling cruises were conducted in the Gullmar Fjord. During November 2017 (cruise GF17) two stations were sampled. The first is the oxygenated station GF17-3 (50 m water depth) located near the entrance of the fjord (58°16'50.94"N/ 11°30'30.96"E, blue diamond, Fig. 21). The second is the hypoxic station GF17-1 (117 m water depth) located close to the deepest part of the fjord (58°19'41.40"N/11°33'8.40"E) near the Alsbäck monitoring station in the middle of the stagnant basin (red square, Fig. 21). Then, a second cruise conducted in September 2018, was focused on the sediment sampling at the oxygenated station (GF18-3).

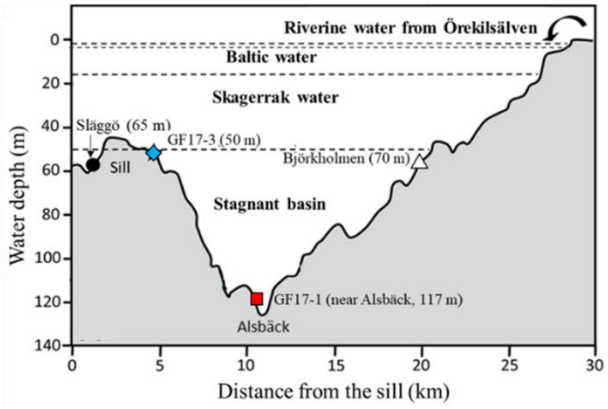

Figure 21: Transect from the sill with the four Gullmar Fjord water masses and the studied stations; blue diamond: GF17-3 oxic station (50 m water depth); red square: GF17-1 hypoxic station (117 m water depth); dark circles: monitoring stations Släggö (65 m water depth) and Björkholmen (70 m water depth) (modified from Arneborg et al., (2004) and Choquel et al., (2021)).

Focus on the main foraminiferal species of interest in the Gullmar Fjord

The denitrifying foraminifera *Globobulimina turgida* was found in the seasonal hypoxic Gullmar Fjord (Risgaard-Petersen et al., 2006). The genus *Nonionella* was described as denitrifying, such as *Nonionella* cf. *stella* (Risgaard-Petersen et al., 2006). Recently, *Nonionella* sp. T1 was described as a putative invasive species in the North Sea (Polovodova Asteman and Schönfeld, 2015; Charrieau et al., 2019; Deldicq et al., 2019). Some precisions are necessary to clarify *Nonionella* sp. T1 taxonomic ambiguity throughout literature. Briefly, its morphotype has been successively named: *Nonionella stella* (Polovodora Asteman and Schönfeld, 2015); *Nonionella* aff. *stella* by (Charrieau et al., 2018), *Nonionella* sp. by (LeKieffre et al., 2018) and finally *Nonionella* sp. T1 (Charrieau et al., 2019; Deldicq et al., 2019) to differentiate it from *Nonionella stella* T4 from Santa Barbara Basin. The genus *Nonionella* is denitrifying (Risgaard-Petersen et al., 2006; Pina-Ochoa et al., 2010), the species *Nonionella* sp. T1 is suspected to perform denitrification.

3.2 PART II: Bourgneuf Bay

Tidal mudflats are one of the most widespread coastal ecosystems, with a recent global area estimation of at least 127,921 km^2 (Murray et al., 2019). Indeed, intertidal mudflats are found all around the world in coastal areas as in estuaries, bays and fjords (Fig. 22). Intertidal mudflats play a major role in the ecosystem functioning due to their high biological productivity (Lebreton et al., 2019; Barillé et al., 2020). The location of intertidal mudflats supports the enrichment of adjacent terrestrial and marine ecosystems. Intertidal mudflats have high economic and ecological potential. Economic activities gathering: shellfish-farmers, fishermen, shellfish gatherers, tourists and birders are closely related to the ecological functions provided by intertidal bare mudflats (Atkins et al., 2011; Liquete et al., 2013). Intertidal mudflats with shellfish production (i.e. Bourgneuf Bay) are subject to regular sanitary monitoring including microbiological control of *Escherichia coli*, monitoring of toxins produced by microalgae, chemical contamination with heavy metals and the monitoring of oyster growth and mortality (Synthèse du rapport de l'Ifremer, 2014). The Water Framework Directive (WFD, 2000/60/EC) is the framework for community policy in the field of water management of aquatic environments, including coastal and transitional waters as the Bourgneuf Bay mudflat. The directive aims to achieve or maintain high ecological and chemical status of groundwater and surface water bodies. A final score is assigned to the ecological quality of the water masses. The score of the water mass of Bay of Bourgneuf in 2017 indicated a good quality (Bulletin de la surveillance 2018).

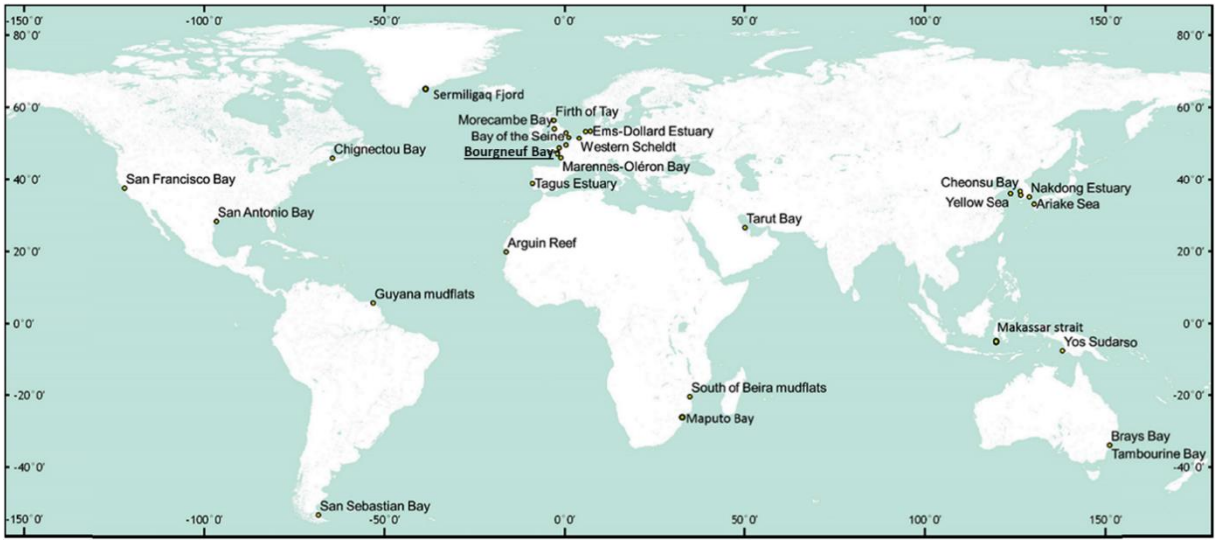

Figure 22: Examples of intertidal bare mudflats throughout tropical, temperate and polar zones illustrating their worldwide distribution. The Bourgneuf Bay location is indicated in bold underlined. Modified from Lebreton et al., (2019).

The Bourgneuf Bay (46°52′–47°08′ N, 1°58′–2°20′ W) is located in the south of the Loire river estuary on the West coast of France (Fig. 22 a). The Bourgneuf Bay is a semi-enclosed area over 340 km^2, constituted by a large intertidal mudflat of 100 km², opened to the Atlantic Ocean by 10 km wide passage between the North of the Noirmoutier Island and the "Pointe Saint Gildas" (Figure 22 b). A narrow second bay-ocean communication zone exists to the south of the bay located at the "goulet de Fromentine" (Debenay, 1978). The wide opening to the North-West of the bay is subject to the influence of the ocean but also of the Loire river estuary.

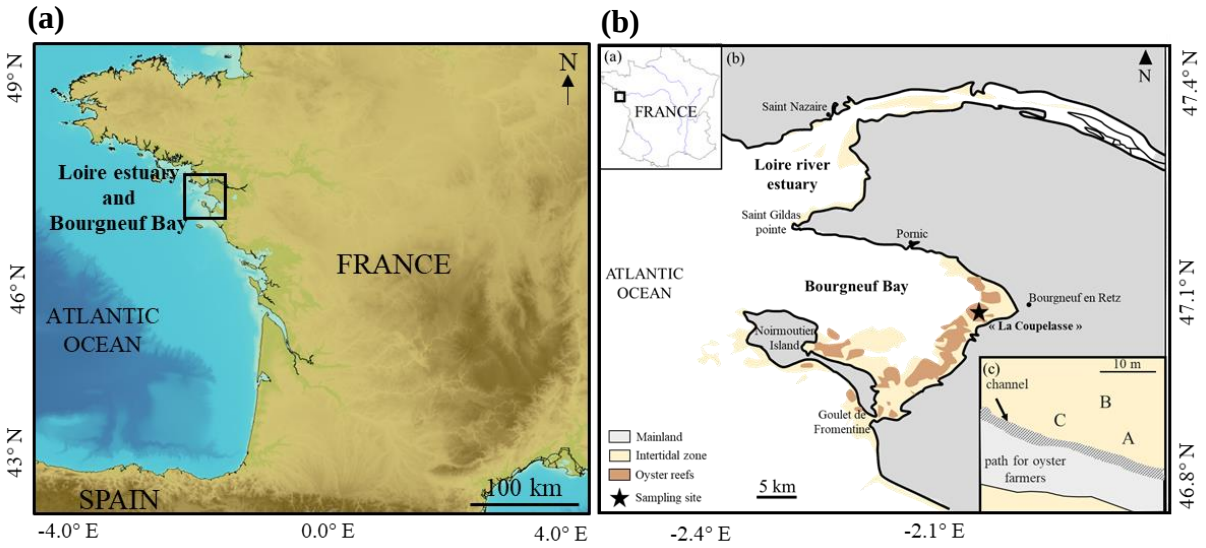

*Figure 22: **(a)** Bourgneuf Bay location (black frame) on the French West coast (data from SHOM). **(b)** (a) Bourgneuf Bay is located on the French Atlantic coast (b) on the South of the Loire Estuary, the sampling site "La Coupelasse" is symbolized with a star, and (c) is a zoom on the 3 sampling stations (A, B, C). Modified from Thomas et al., (2016).*

The Loire river mean discharge ranges from 120m^3 s^{-1} to 5200 m^3 s^{-1} (GIP, Loire Estuaire). The Loire estuary is hyper-synchronous: the estuary shows an increasing tidal range upstream (Le Floch, 1961), reaching a maximum tidal range of approximately 7 m. Due to strong hydrodynamics, the annual mean concentrations of suspended matter are higher in the northern part of the bay (154 mg L^{-1}) than in the southern part (34 mg L^{-1}) (Haure and Baud, 1995).

Oyster beds cover an area of 10 km^2, the Bourgneuf Bay is a site of extensive *Crassostrea gigas* aquaculture, with 5330 metric tons produced in 2012 (Agreste, 2015). Figure 23 provides general information on Bourgneuf Bay to present the details of the sampling site "La Coupelasse" (Fig; 22 b). The bathymetry (Fig. 23 a) indicates that the bay is shallow (max. -15 m, red color) and our sampling site is located on the foreshore at 0 m depth (grey zone, -

2.1°E; 47.1°N, Fig. 23 a). The surface of the sediments in the bay is diverse (Fig. 23 b), our study site is located in the sandy mud part (in green, -2.1°E; 47.1°N, Fig. 23 b). The Bourgneuf bay is an intertidal zone subject to tidal currents. Figures 23 c and d illustrate the strength and direction of the currents at (c) rising tide and at (d) ebb tide.

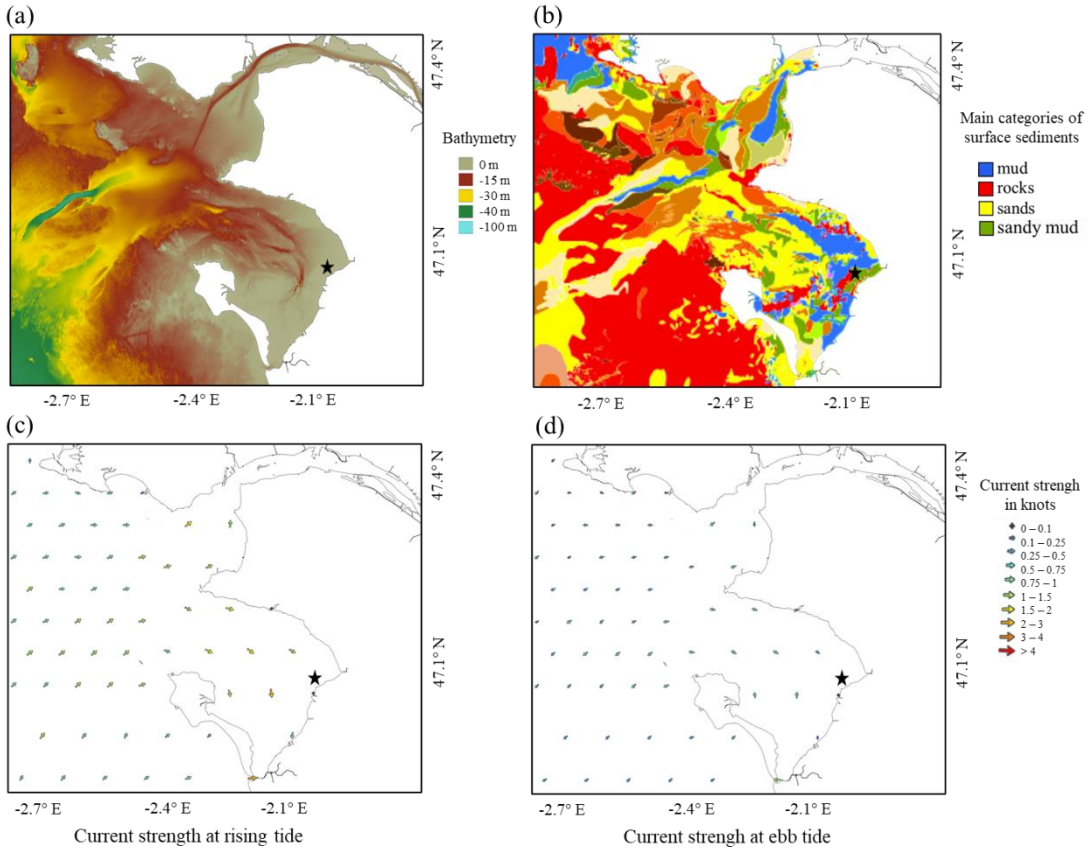

Figure 23: (a) Bathymetry, (b) sedimentology of the surface sediment, (c) current strength at the rising tide and (d) at ebb tide of the Bourgneuf Bay. The black star indicates the "La Coupelasse" site (data from SHOM).

Focus on the main foraminiferal species of interest in the Bourgneuf Bay mudflat

Numerous studies performed on benthic foraminifera of the Bourgneuf Bay are carried out since the PhD thesis of Debenay (Debenay, 1978) (e.g. Debenay and Guillou, 2002; Morvan et al., 2004; Ernst et al., 2006; Jauffrais et al., 2016; LeKieffre et al., 2017, 2018). Among the four main species found at the "La Coupelasse" site, some precisions are necessary to clarify the taxonomic ambiguity throughout previous studies. Briefly, *Ammonia tepida* (Debenay, 1978; Debenay, 1978; Debenay and Guillou, 2002; Morvan et al., 2004; Debenay et al., 2006) was since divided into pseudocryptic phylotypes, the main phylotype identified at our sampling site being *Ammonia* sp. T6 (Hayward et al., 2004; Richirt et al., 2019). Two phylotypes of the *"Elphidium excavatum*" species complex (Pillet et al., 2011; Darling et al., 2016) are found in

the Bourgneuf Bay: *Elphidium oceanense* (genetic type S3, Darling et al., 2016) and *Elphidium selseyense* (genetic type S5, Darling et al., 2016). *Elphidium oceanense* is previously named *Cribroelphidium gunteri* and *Elphidium selseyense* is named *Cribroelphidium excavatum* in Debenay, (1978) and Debenay and Guillou, (2002). No taxonomic precision is needed for *Haynesina germanica* (genetic type S16, Darling et al., 2016). These species are typical of transitional temperate Atlantic mesotidal to macrotidal environments. Their distributions are described according to the concept of "confined waters" in the Bourgneuf Bay (Debenay and Guillou, 2002). Thus, the distribution of these species depends both on a longitudinal marine-to-freshwater gradient and on a vertical water-to-land gradient. Thus in muddy sediments, the longitudinal distribution of these species indicates that *Cribroelphidium excavatum* dominates in the lower estuary (marine influence), passing upward to *Cribroelphidium gunteri* and *Ammonia tepida* and farther upstream in the bay to *Haynesina germanica*. The temporal dynamics of these species remains to be clarified at the La Coupelasse site which is located in intermediate position in the bay.

Bibliography

Abril, G., Etcheber, H., Hir, P. L., Bassoullet, P., Boutier, B., and Frankignoulle, M.: Oxic/anoxic oscillations and organic carbon mineralization in an estuarine maximum turbidity zone (The Gironde, France), 44, 1304–1315, https://doi.org/10.4319/lo.1999.44.5.1304, 1999.

Abril, G., Riou, S. A., Etcheber, H., Frankignoulle, M., de Wit, R., and Middelburg, J. J.: Transient, Tidal Time-scale, Nitrogen Transformations in an Estuarine Turbidity Maximum—Fluid Mud System (The Gironde, South-west France), Estuarine, Coastal and Shelf Science, 50, 703–715, https://doi.org/10.1006/ecss.1999.0598, 2000.

Abril, G., Commarieu, M.-V., Etcheber, H., Deborde, J., Deflandre, B., Živađinović, M. K., Chaillou, G., and Anschutz, P.: In vitro simulation of oxic/suboxic diagenesis in an estuarine fluid mud subjected to redox oscillations, Estuarine, Coastal and Shelf Science, 88, 279–291, https://doi.org/10.1016/j.ecss.2010.04.003, 2010.

Adl, S. M., Simpson, A. G. B., Lane, C. E., Lukeš, J., Bass, D., Bowser, S. S., Brown, M. W., Burki, F., Dunthorn, M., Hampl, V., Heiss, A., Hoppenrath, M., Lara, E., le Gall, L., Lynn, D. H., McManus, H., Mitchell, E. A. D., Mozley-Stanridge, S. E., Parfrey, L. W., Pawlowski, J., Rueckert, S., Shadwick, L., Schoch, C. L., Smirnov, A., and Spiegel, F. W.: The Revised Classification of Eukaryotes, J. Eukaryot. Microbiol., 59, 429–514, https://doi.org/10.1111/j.1550-7408.2012.00644.x, 2012.

Admiraal, W., Peletier, H., and Brouwer, T.: The Seasonal Succession Patterns of Diatom Species on an Intertidal Mudflat: An Experimental Analysis, Oikos, 42, 30–40, https://doi.org/10.2307/3544606, 1984.

Agreste. Recensement de la conchyliculture. http://agreste.agriculture.gouv.fr, 2015.

Aller, R. C.: Diagenetic Processes Near the Sediment-Water Interface of Long Island Sound. I.: Decomposition and Nutrient Element Geochemistry (S, N, P), in: Advances in Geophysics, vol. 22, edited by: Saltzman, B., Elsevier, 237–350, https://doi.org/10.1016/S0065-2687(08)60067-9, 1980.

Aller, R. C.: The Effects of Macrobenthos on Chemical Properties of Marine Sediment and Overlying Water, in: Animal-Sediment Relations: The Biogenic Alteration of Sediments, edited by: McCall, P. L. and Tevesz, M. J. S., Springer US, Boston, MA, 53–102, https://doi.org/10.1007/978-1-4757-1317-6_2, 1982.

Aller, R. C.: Benthic fauna and biogeochemical processes in marine sediment : the role of burrow structures, 1988.

Aller, R. C.: Bioturbation and Manganese Cycling in Hemipelagic Sediments, 331, 51–68, 1990.

Aller, R. C.: The sedimentary Mn cycle in Long Island Sound: Its role as intermediate oxidant and the influence of bioturbation, O*2*, and C*org* flux on diagenetic reaction balances, 1994.

Aller, R. C.: Transport and reactions in the bioirrigated zone, 269–301, 2001.

Aller, R. C.: Conceptual models of early diagenetic processes: The muddy seafloor as an unsteady, batch reactor, https://doi.org/info:doi/10.1357/0022240042880837, 2004.

Aller, R. C., Hall, P. O. J., Rude, P. D., and Aller, J. Y.: Biogeochemical heterogeneity and suboxic diagenesis in hemipelagic sediments of the Panama Basin, Deep Sea Research Part I: Oceanographic Research Papers, 45, 133–165, https://doi.org/10.1016/S0967-0637(97)00049-6, 1998.

Alve, E. and Bernhard, J. M.: Vertical migratory response of benthic foraminifera to controlled oxygen concentrations in an experimental mesocosm, Mar. Ecol. Prog. Ser., 116, 137–151, 1995.

Alve, E. and Goldstein, S. T.: Propagule transport as a key method of dispersal in benthic foraminifera (Protista), Limnol. Oceanogr., 48, 2163–2170, https://doi.org/10.4319/lo.2003.48.6.2163, 2003.

Alve, E. and Goldstein, S. T.: Dispersal, survival and delayed growth of benthic foraminiferal propagules, J. Sea Res., 63, 36–51, https://doi.org/10.1016/j.seares.2009.09.003, 2010.

Alve, E. and Murray, J.: Temporal variability in vertical distributions of live (stained) intertidal foraminifera, Southern England, J. Foraminifer. Res., 31, 12–24, https://doi.org/10.2113/0310012, 2001.

Anschutz, P., Zhong, S., Sundby, B., Mucci, A., and Gobeil, C.: Burial efficiency of phosphorus and the geochemistry of iron in continental margin sediments, 43, 53–64, https://doi.org/10.4319/lo.1998.43.1.0053, 1998.

Anschutz, P., Sundby, B., Lefrançois, L., Luther, G. W., and Mucci, A.: Interactions between metal oxides and species of nitrogen and iodine in bioturbated marine sediments, Geochimica et Cosmochimica Acta, 64, 2751–2763, https://doi.org/10.1016/S0016-7037(00)00400-2, 2000.

Anschutz, P., Dedieu, K., Desmazes, F., and Chaillou, G.: Speciation, oxidation state, and reactivity of particulate manganese in marine sediments - ScienceDirect, 2005.

Anschutz, P., Chaillou, G., and Lecroart, P.: Phosphorus diagenesis in sediment of the Thau Lagoon, Estuarine, Coastal and Shelf Science, 72, 447–456, https://doi.org/10.1016/j.ecss.2006.11.012, 2007.

Anschutz, P., Bouchet, S., Abril, G., Bridou, R., Tessier, E., and Amouroux, D.: In vitro simulation of oscillatory redox conditions in intertidal sediments: N, Mn, Fe, and P coupling, Continental Shelf Research, 177, 33–41, https://doi.org/10.1016/j.csr.2019.03.007, 2019.

Arneborg, L.: Turnover times for the water above sill level in Gullmar Fjord, Cont. Shelf Res., 24, 443–460, https://doi.org/10.1016/j.csr.2003.12.005, 2004.

Atkins, J. P., Burdon, D., Elliott, M., and Gregory, A. J.: Management of the marine environment: Integrating ecosystem services and societal benefits with the DPSIR framework in a systems approach, Mar. Pollut. Bull., 62, 215–226, https://doi.org/10.1016/j.marpolbul.2010.12.012, 2011.

Austin, H. A., Austin, W. E. N., and Paterson, D. M.: Extracellular cracking and content removal of the benthic diatom *Pleurosigma angulatum* (Quekett) by the benthic foraminifera *Haynesina germanica* (Ehrenberg), Mar. Micropaleontol., 57, 68–73, https://doi.org/10.1016/j.marmicro.2005.07.002, 2005.

Austen, M. C. and Wibdom, B.: Changes in and slow recovery of a meiobenthic nematode assemblage following a hypoxic period in the Gullmar Fjord basin, Sweden, Mar. Biol., 111, 139–145, https://doi.org/10.1007/BF01986355, 1991.

Barillé, L., Le Bris, A., Goulletquer, P., Thomas, Y., Glize, P., Kane, F., Falconer, L., Guillotreau, P., Trouillet, B., Palmer, S., and Gernez, P.: Biological, socio-economic, and administrative opportunities and challenges to moving aquaculture offshore for small French oyster-farming companies, Aquaculture, 521, 735045, https://doi.org/10.1016/j.aquaculture.2020.735045, 2020.

Barnett, A., Méléder, V., Blommaert, L., Lepetit, B., Gaudin, P., Vyverman, W., Sabbe, K., Dupuy, C., and Lavaud, J.: Growth form defines physiological photoprotective capacity in intertidal benthic diatoms, ISME J., 9, 32–45, https://doi.org/10.1038/ismej.2014.105, 2015.

Benito, X.: Benthic Foraminifera and Diatoms as Ecological Indicators, in: Modern Trends in Diatom Identification: Fundamentals and Applications, edited by: Cristóbal, G., Blanco, S., and Bueno, G., Springer International Publishing, Cham, 257–280, https://doi.org/10.1007/978-3-030-39212-3_15, 2020.

Bennett, W. W., Welsh, D. T., Serriere, A., Panther, J. G., and Teasdale, P. R.: A colorimetric DET technique for the high-resolution measurement of two-dimensional alkalinity distributions in sediment porewaters, Chemosphere, 119, 547–552, https://doi.org/10.1016/j.chemosphere.2014.07.042, 2015.

Benyoucef, I., Blandin, E., Lerouxel, A., Jesus, B., Rosa, P., Méléder, V., Launeau, P., and Barillé, L.: Microphytobenthos interannual variations in a north-European estuary (Loire estuary, France) detected by visible-infrared multispectral remote sensing, Estuar. Coast. Shelf Sci., 136, 43–52, https://doi.org/10.1016/j.ecss.2013.11.007, 2014.

Berg, P., Risgaard-Petersen, N., and Rysgaard, S.: Interpretation of measured concentration profiles in sediment pore water, 43, 1500–1510, https://doi.org/10.4319/lo.1998.43.7.1500, 1998.

Berner, R. A.: Early Diagenesis: A Theoretical Approach, Princeton University Press, 256 pp., 1980.

Bernhard, J. M. and Bowser, S. S.: Benthic foraminifera of dysoxic sediments: chloroplast sequestration and functional morphology, Earth-Sci. Rev., 46, 149–165, https://doi.org/10.1016/S0012-8252(99)00017-3, 1999.

Bernhard, J. M., Visscher, P. T., and Bowser, S. S.: Submillimeter life positions of bacteria, protists, and metazoans in laminated sediments of the Santa Barbara Basin, Limnol. Oceanogr., 48, 813–828, https://doi.org/10.4319/lo.2003.48.2.0813, 2003.

Bernhard, J. M., Ostermann, D. R., Williams, D. S., and Blanks, J. K.: Comparison of two methods to identify live benthic foraminifera: A test between Rose Bengal and CellTracker Green with implications for stable isotope paleoreconstructions: Foraminifera viability comparison method, Paleoceanography, 21, https://doi.org/10.1029/2006PA001290, 2006.

Bernhard, J. M., Edgcomb, V. P., Casciotti, K. L., McIlvin, M. R., and Beaudoin, D. J.: Denitrification likely catalyzed by endobionts in an allogromiid foraminifer, ISME J., 6, 951–960, https://doi.org/10.1038/ismej.2011.171, 2012a.

Bernhard, J. M., Casciotti, K. L., McIlvin, M. R., Beaudoin, D. J., Visscher, P. T., and Edgcomb, V. P.: Potential importance of physiologically diverse benthic foraminifera in sedimentary nitrate storage and respiration, J. Geophys. Res. Biogeosciences, 117, https://doi.org/10.1029/2012JG001949, 2012b.

Bianchi, T. S., Arndt, S., Austin, W. E. N., Benn, D. I., Bertrand, S., Cui, X., Faust, J. C., Koziorowska-Makuch, K., Moy, C. M., Savage, C., Smeaton, C., Smith, R. W., and Syvitski, J.: Fjords as Aquatic Critical Zones (ACZs), Earth-Sci. Rev., 203, 103145, https://doi.org/10.1016/j.earscirev.2020.103145, 2020.

Billerbeck, M., Werner, U., Polerecky, L., Walpersdorf, E., deBeer, D., and Huettel, M.: Surficial and deep pore water circulation governs spatial and temporal scales of nutrient recycling in intertidal sand flat sediment, 326, 61–76, https://doi.org/10.3354/meps326061, 2006.

Bird, C., Darling, K. F., Russell, A. D., Davis, C. V., Fehrenbacher, J., Free, A., Wyman, M., and Ngwenya, B. T.: Cyanobacterial endobionts within a major marine planktonic calcifier (*Globigerina bulloides*, Foraminifera) revealed by 16S rRNA metabarcoding, Biogeosciences, 14, https://doi.org/10.5194/bg-14-901-2017, 2017.

Bird, C., Darling, K. F., Russell, A. D., Fehrenbacher, J. S., Davis, C. V., Free, A., and Ngwenya, B. T.: 16S rRNA gene metabarcoding and TEM reveals different ecological strategies within the genus *Neogloboquadrina* (planktonic foraminifer), PLOS ONE, 13, e0191653, https://doi.org/10.1371/journal.pone.0191653, 2018.

Bird, C., LeKieffre, C., Jauffrais, T., Meibom, A., Geslin, E., Filipsson, H. L., Maire, O., Russell, A. D., and Fehrenbacher, J. S.: Heterotrophic Foraminifera Capable of Inorganic

Nitrogen Assimilation, Front. Microbiol., 11, https://doi.org/10.3389/fmicb.2020.604979, 2020.

Björk, G. and Nordberg, K.: Upwelling along the Swedish west coast during the 20th century, Cont. Shelf Res., 23, 1143–1159, https://doi.org/10.1016/S0278-4343(03)00081-5, 2003.

Blanchard, G. F., Agion, T., Guarini, J.-M., Herlory, O., and Richard, P.: Analysis of the short-term dynamics of microphytobenthos biomass on intertidal mudflats, 85–97, 2006.

Blommaert, L., Lavaud, J., Vyverman, W., and Sabbe, K.: Behavioural versus physiological photoprotection in epipelic and epipsammic benthic diatoms, Eur. J. Phycol., 53, 146–155, https://doi.org/10.1080/09670262.2017.1397197, 2018.

Borja, A., Elliott, M., Andersen, J. H., Berg, T., Carstensen, J., Halpern, B. S., Heiskanen, A.-S., Korpinen, S., Lowndes, J. S. S., Martin, G., and Rodriguez-Ezpeleta, N.: Overview of Integrative Assessment of Marine Systems: The Ecosystem Approach in Practice, Front. Mar. Sci., 3, https://doi.org/10.3389/fmars.2016.00020, 2016.

Bouchet, V. M. P., Sauriau, P.-G., Debenay, J.-P., Mermillod-Blondin, F., Schmidt, S., Amiard, J.-C., and Dupas, B.: Influence of the mode of macrofauna-mediated bioturbation on the vertical distribution of living benthic foraminifera: First insight from axial tomodensitometry, J. Exp. Mar. Biol. Ecol., 371, 20–33, https://doi.org/10.1016/j.jembe.2008.12.012, 2009.

Bouchet, V. M. P., Frontalini, F., Francescangeli, F., Sauriau, P.-G., Geslin, E., Martins, M. V. A., Almogi-Labin, A., Avnaim-Katav, S., Di Bella, L., Cearreta, A., Coccioni, R., Costelloe, A., Dimiza, M. D., Ferraro, L., Haynert, K., Martínez-Colón, M., Melis, R., Schweizer, M., Triantaphyllou, M. V., Tsujimoto, A., Wilson, B., and Armynot du Châtelet, E.: Indicative value of benthic foraminifera for biomonitoring: Assignment to ecological groups of sensitivity to total organic carbon of species from European intertidal areas and transitional waters, Mar. Pollut. Bull., 164, 112071, https://doi.org/10.1016/j.marpolbul.2021.112071, 2021.

Brandes, J. A., Devol, A. H., and Deutsch, C.: New Developments in the Marine Nitrogen Cycle, Chem. Rev., 107, 577–589, https://doi.org/10.1021/cr050377t, 2007.

Breitburg, D., Levin, L. A., Oschlies, A., Grégoire, M., Chavez, F. P., Conley, D. J., Garçon, V., Gilbert, D., Gutiérrez, D., Isensee, K., Jacinto, G. S., Limburg, K. E., Montes, I., Naqvi, S. W. A., Pitcher, G. C., Rabalais, N. N., Roman, M. R., Rose, K. A., Seibel, B. A., Telszewski, M., Yasuhara, M., and Zhang, J.: Declining oxygen in the global ocean and coastal waters, Science, 359, https://doi.org/10.1126/science.aam7240, 2018.

Brito, A. C., Benyoucef, I., Jesus, B., Brotas, V., Gernez, P., Mendes, C. R., Launeau, P., Dias, M. P., and Barillé, L.: Seasonality of microphytobenthos revealed by remote-sensing in a South European estuary, Cont. Shelf Res., 66, 83–91, https://doi.org/10.1016/j.csr.2013.07.004, 2013.

Brusseau, M. L.: Chapter 6 - Ecosystems and Ecosystem Services, in: Environmental and Pollution Science (Third Edition), edited by: Brusseau, M. L., Pepper, I. L., and Gerba, C. P., Academic Press, 89–102, https://doi.org/10.1016/B978-0-12-814719-1.00006-9, 2019.

Bulletin de la surveillance 2018- Qualité du Milieu Marin Littoral Départements de Loire-Atlantique et Vendée (Partie nord), Ifremer, 2019. https://archimer.ifremer.fr/doc/00510/62118/

Burdige, D. J.: The biogeochemistry of manganese and iron reduction in marine sediments, Earth-Science Reviews, 35, 249–284, https://doi.org/10.1016/0012-8252(93)90040-E, 1993.

Burdige, D. J.: Geochemistry of Marine Sediments, Princeton University Press, 629 pp., 2006.

Canfield, D. E., Jørgensen, B. B., Fossing, H., Glud, R., Gundersen, J., Ramsing, N. B., Thamdrup, B., Hansen, J. W., Nielsen, L. P., and Hall, P. O. J.: Pathways of organic carbon oxidation in three continental margin sediments, Marine Geology, 113, 27–40, https://doi.org/10.1016/0025-3227(93)90147-N, 1993.

Cartaxana, P., Ruivo, M., Hubas, C., Davidson, I., Serôdio, J., and Jesus, B.: Physiological versus behavioral photoprotection in intertidal epipelic and epipsammic benthic diatom communities, J. Exp. Mar. Biol. Ecol., 405, 120–127, https://doi.org/10.1016/j.jembe.2011.05.027, 2011.

Cartaxana, P., Vieira, S., Ribeiro, L., Rocha, R. J., Cruz, S., Calado, R., and da Silva, J. M.: Effects of elevated temperature and CO2 on intertidal microphytobenthos, BMC Ecol., 15, 10, https://doi.org/10.1186/s12898-015-0043-y, 2015.

Cesbron, F., Metzger, E., Launeau, P., Deflandre, B., Delgard, M.-L., Thibault de Chanvalon, A., Geslin, E., Anschutz, P., and Jézéquel, D.: Simultaneous 2D Imaging of Dissolved Iron and Reactive Phosphorus in Sediment Porewaters by Thin-Film and Hyperspectral Methods, 48, 2816–2826, https://doi.org/10.1021/es404724r, 2014.

Cesbron, F., Geslin, E., Jorissen, F. J., Delgard, M. L., Charrieau, L., Deflandre, B., Jézéquel, D., Anschutz, P., and Metzger, E.: Vertical distribution and respiration rates of benthic foraminifera: Contribution to aerobic remineralization in intertidal mudflats covered by *Zostera noltei* meadows, Estuar. Coast. Shelf Sci., 179, 23–38, https://doi.org/10.1016/j.ecss.2015.12.005, 2016.

Charrieau, L. M., Filipsson, H. L., Ljung, K., Chierici, M., Knudsen, K. L., and Kritzberg, E.: The effects of multiple stressors on the distribution of coastal benthic foraminifera: A case study from the Skagerrak-Baltic Sea region, Mar. Micropaleontol., 139, 42–56, https://doi.org/10.1016/j.marmicro.2017.11.004, 2018.

Charrieau, L. M., Ljung, K., Schenk, F., Daewel, U., Kritzberg, E., and Filipsson, H. L.: Rapid environmental responses to climate-induced hydrographic changes in the Baltic Sea entrance, Biogeosciences, 16, 3835–3852, https://doi.org/10.5194/bg-16-3835-2019, 2019.

Childs, C. R., Rabalais, N. N., Eugene, R., and Proctor, T. and L. M.: Sediment denitrification in the Gulf of Mexico zone of hypoxia, 2002.

Choquel, C., Geslin, E., Metzger, E., Filipsson, H. L., Risgaard-Petersen, N., Launeau, P., Giraud, M., Jauffrais, T., Jesus, B., & Mouret, A. Denitrification by benthic foraminifera and their contribution to N-loss from a fjord environment. Biogeosciences, 18(1), 327-341. https://doi.org/10.5194/bg-18-327-2021, 2021.

Christensen, P. B., Rysgaard, S., Sloth, N. P., Dalsgaard, T., and Schwærter, S.: Sediment mineralization, nutrient fluxes, denitrification and dissimilatory nitrate reduction to ammonium in an estuarine fjord with sea cage trout farms, 21, 73–84, https://doi.org/10.3354/ame021073, 2000.

Chronopoulou, P. M., Salonen, I., Bird, C., Reichart, G.-J., and Koho, K. A.: Metabarcoding insights into the trophic behaviour and identity of intertidal benthic foraminifera, Front. Microbiol., 10, https://doi.org/10.3389/fmicb.2019.01169, 2019.

Clark, K. B., Jensen, K. R., and Stirts, H. M.: Survey for functional kleptoplasty among west Atlantic Ascoglossa (= Sacoglossa) (Mollusca : Opisthobranchia), Surv. Funct. Kleptoplasty West Atl. Ascoglossa Sacoglossa Mollusca Opisthobranchia, 33, 339–345, 1990.

Coelho, H., Vieira, S., and Serôdio, J.: Effects of desiccation on the photosynthetic activity of intertidal microphytobenthos biofilms as studied by optical methods, J. Exp. Mar. Biol. Ecol., 381, 98–104, https://doi.org/10.1016/j.jembe.2009.09.013, 2009.

Coelho, H., Vieira, S., and Serôdio, J.: Endogenous versus environmental control of vertical migration by intertidal benthic microalgae, Eur. J. Phycol., 46, 271–281, https://doi.org/10.1080/09670262.2011.598242, 2011.

Conley, D. J., Carstensen, J., Ærtebjerg, G., Christensen, P. B., Dalsgaard, T., Hansen, J. L. S., and Josefson, A. B.: Long-Term Changes and Impacts of Hypoxia in Danish Coastal Waters, 17, S165–S184, https://doi.org/10.1890/05-0766.1, 2007.

Consalvey, M., Paterson, D. M., and Underwood, G. J. C.: The Ups and Downs of Life in a Benthic Biofilm: Migration of Benthic Diatoms, Diatom Res., 19, 181–202, https://doi.org/10.1080/0269249X.2004.9705870, 2004.

Costanza, R., d'Arge, R., de Groot, R., Farber, S., Grasso, M., Hannon, B., Limburg, K., Naeem, S., O'Neill, R. V., Paruelo, J., Raskin, R. G., Sutton, P., and van den Belt, M.: The value of the world's ecosystem services and natural capital, 387, 253–260, https://doi.org/10.1038/387253a0, 1997.

Dale, A. W., Sommer, S., Lomnitz, U., Bourbonnais, A., and Wallmann, K.: Biological nitrate transport in sediments on the Peruvian margin mitigates benthic sulfide emissions and drives pelagic N loss during stagnation events, Deep Sea Res. Part Oceanogr. Res. Pap., 112, 123–136, https://doi.org/10.1016/j.dsr.2016.02.013, 2016.

Dalsgaard, T. and Thamdrup, B.: Factors Controlling Anaerobic Ammonium Oxidation with Nitrite in Marine Sediments, Appl. Environ. Microbiol., 68, 3802–3808, https://doi.org/10.1128/AEM.68.8.3802-3808.2002, 2002.

Darling, K. F., Schweizer, M., Knudsen, K. L., Evans, K. M., Bird, C., Roberts, A., Filipsson, H. L., Kim, J.-H., Gudmundsson, G., Wade, C. M., Sayer, M. D. J., and Austin, W. E. N.: The genetic diversity, phylogeography and morphology of Elphidiidae (Foraminifera) in the Northeast Atlantic, Mar. Micropaleontol., 129, 1–23, https://doi.org/10.1016/j.marmicro.2016.09.001, 2016.

Davison, W., Grime, G. W., Morgan, J. a. W., and Clarke, K.: Distribution of dissolved iron in sediment pore waters at submillimetre resolution, Nature, 352, 323–325, https://doi.org/10.1038/352323a0, 1991.

Davison, W., Zhang, H., & Grime, G. (1994). Performance characteristics of gel probes used for measuring the chemistry of pore waters. Environmental Science & Technology, *28*(9), 1623-1632. https://doi.org/10.1021/es00058a015, 1994.

Debenay, J.-P.: Distribution des foraminifères vivants et des tests vides en Baie de Bourgneuf, PhD Thesis, 1978.

Debenay, J.-P. and Guillou, J.-J.: Ecological transitions indicated by foraminiferal assemblages in paralic environments, Estuaries, 25, 1107–1120, https://doi.org/10.1007/BF02692208, 2002.

Debenay, J.-P., Guillou, J.-J., Redois, F., and Geslin, E.: Distribution Trends of Foraminiferal Assemblages in Paralic Environments, in: Environmental Micropaleontology: The Application of Microfossils to Environmental Geology, edited by: Martin, R. E., Springer US, Boston, MA, 39–67, https://doi.org/10.1007/978-1-4615-4167-7_3, 2000.

Debenay, J.-P., Bicchi, E., Goubert, E., and Armynot du Châtelet, E.: Spatio-temporal distribution of benthic foraminifera in relation to estuarine dynamics (Vie estuary, Vendée, W France), Estuar. Coast. Shelf Sci., 67, 181–197, https://doi.org/10.1016/j.ecss.2005.11.014, 2006.

Deborde, J., Anschutz, P., Auby, I., Glé, C., Commarieu, M.-V., Maurer, D., Lecroart, P., and Abril, G.: Role of tidal pumping on nutrient cycling in a temperate lagoon (Arcachon Bay, France), Marine Chemistry, 109, 98–114, https://doi.org/10.1016/j.marchem.2007.12.007, 2008.

Deldicq, N., Alve, E., Schweizer, M., Asteman, I. P., Hess, S., Darling, K., and Bouchet, V. M. P.: History of the introduction of a species resembling the benthic foraminifera *Nonionella stella* in the Oslofjord (Norway): morphological, molecular and paleo-ecological evidences, https://doi.org/10.3391/ai.2019.14.2.03, 2019.

Delgard, M. L., Deflandre, B., Metzger, E., Nuzzio, D., Capo, S., Mouret, A., and Anschutz, P.: In situ study of short-term variations of redox species chemistry in intertidal permeable sediments of the Arcachon lagoon, Hydrobiologia, 699, 69–84, https://doi.org/10.1007/s10750-012-1154-5, 2012.

Denis, L. and Desreumaux, P.-E.: Short-term variability of intertidal microphytobenthic production using an oxygen microprofiling system, Mar. Freshwater Res., 60, 712–726, https://doi.org/10.1071/MF08070, 2009.

Diaz, R. J. and Rosenberg, R.: Marine benthic hypoxia: a review of its ecological effects and the behavioural responses of benthic macrofauna, 1995.

Diaz, R. J. and Rosenberg, R.: Spreading Dead Zones and Consequences for Marine Ecosystems, 321, 926–929, https://doi.org/10.1126/science.1156401, 2008.

Diaz, R. J., Eriksson-Hägg, H., and Rosenberg, R.: Hypoxia, 67–96, 2013.

Dijk, I. van, Mouret, A., Cotte, M., Houedec, S. L., Oron, S., Reichart, G.-J., Reyes-Herrera, J., Filipsson, H., and Barras, C.: Chemical Heterogeneity of Mg, Mn, Na, S, and Sr in Benthic Foraminiferal Calcite, Front. Earth Sci., 1, https://doi.org/10.3389/feart.2019.00281, 2019.

D'Orbigny, A. D.: Tableau méthodique de la classe des Céphalopodes, in Annales des sciences naturelles: comprenant La physiologie animale et végétale, l'anatomie comparée des deux règnes, la zoologie, la botanique, la minéralogie et la géologie., 1826.

Dujardin, F.: Annales des sciences naturelles, 1835.

Duport, E., Gilbert, F., Poggiale, J.-C., Dedieu, K., Rabouille, C., and Stora, G.: Benthic macrofauna and sediment reworking quantification in contrasted environments in the Thau Lagoon, Estuarine, Coastal and Shelf Science, 72, 522–533, https://doi.org/10.1016/j.ecss.2006.11.018, 2007.

Dupuy, C., Rossignol, L., Geslin, E., and Pascal, P.-Y.: Predation of mudflat meio-macrofaunal metazoans by a calcareous foraminifer, *Ammonia tepida* (Cushman, 1926), J. Foraminifer. Res., 40, 305–312, https://doi.org/10.2113/gsjfr.40.4.305, 2010.

Échappé, C., Gernez, P., Méléder, V., Jesus, B., Cognie, B., Decottignies, P., Sabbe, K., and Barillé, L.: Satellite remote sensing reveals a positive impact of living oyster reefs on microalgal biofilm development, Biogeosciences, 15, 905–918, https://doi.org/10.5194/bg-15-905-2018, 2018.

Enge, A. J., Nomaki, H., Ogawa, N. O., Witte, U., Moeseneder, M. M., Lavik, G., Ohkouchi, N., Kitazato, H., Kučera, M., and Heinz, P.: Response of the benthic foraminiferal community to a simulated short-term phytodetritus pulse in the abyssal North Pacific, Mar. Ecol. Prog. Ser., 438, 129–142, https://doi.org/10.3354/meps09298, 2011.

Ernst, S. R., Morvan, J., Geslin, E., Le Bihan, A., and Jorissen, F. J.: Benthic foraminiferal response to experimentally induced Erika oil pollution, Mar. Micropaleontol., 61, 76–93, https://doi.org/10.1016/j.marmicro.2006.05.005, 2006.

Eyre, B. D., Oakes, J. M., and Middelburg, J. J.: Fate of microphytobenthos nitrogen in subtropical subtidal sediments: A 15N pulse-chase study, Limnol. Oceanogr., 61, 2108–2121, https://doi.org/10.1002/lno.10356, 2016.

Filipsson, H.: Culturing of benthic foraminifera for improved paleoceanographic reconstructions, 23, https://doi.org/10.2110/palo.2008.S01, 2008.

Filipsson, H. L. and Nordberg, K.: A 200-year environmental record of a low-oxygen fjord, Sweden, elucidated by benthic foraminifera, sediment characteristics and hydrographic data, J. Foraminifer. Res., 34, 277–293, https://doi.org/10.2113/34.4.277, 2004a.

Filipsson, H. L. and Nordberg, K.: Climate variations, an overlooked factor influencing the recent marine environment. An example from Gullmar Fjord, Sweden, illustrated by benthic foraminifera and hydrographic data, Estuaries, 27, 867–881, https://doi.org/10.1007/BF02912048, 2004b.

Finlay, B. J., Span, A. S. W., and Harman, J. M. P.: Nitrate respiration in primitive eukaryotes, Nature, 303, 333–336, https://doi.org/10.1038/303333a0, 1983.

Fleming, L. E., Maycock, B., White, M. P., and Depledge, M. H.: Fostering human health through ocean sustainability in the 21st century, 1, People and Nature, 276–283, https://doi.org/10.1002/pan3.10038, 2019.

Fornasini, C.: Illustrazione di specie orbignyane di foraminiferi istituite nel 1826, Mem. R. Accad. Sci. Ist. Bologna, 1 (ser. 6) (1904), p. 17, 1904.

Forster, R. M. and Jesus, B.: Field spectroscopy of estuarine intertidal habitats, Int. J. Remote Sens., 27, 3657–3669, https://doi.org/10.1080/01431160500500367, 2006.

Franke, A., Blenckner, T., Duarte, C. M., Ott, K., Fleming, L. E., Antia, A., Reusch, T. B. H., Bertram, C., Hein, J., Kronfeld-Goharani, U., Dierking, J., Kuhn, A., Sato, C., van Doorn, E., Wall, M., Schartau, M., Karez, R., Crowder, L., Keller, D., Engel, A., Hentschel, U., and Prigge, E.: Operationalizing Ocean Health: Toward Integrated Research on Ocean Health and Recovery to Achieve Ocean Sustainability, One Earth, 2, 557–565, https://doi.org/10.1016/j.oneear.2020.05.013, 2020.

Friedman, G. M., Sanders, J. E., and 1926-: Principles of sedimentology, Wiley, 1978.

Froelich, P. N., Klinkhammer, G. P., Bender, M. L., Luedtke, N. A., Heath, G. R., Cullen, D., Dauphin, P., Hammond, D., Hartman, B., and Maynard, V.: Early oxidation of organic matter in pelagic sediments of the eastern equatorial Atlantic: suboxic diagenesis, Geochimica et Cosmochimica Acta, 43, 1075–1090, https://doi.org/10.1016/0016-7037(79)90095-4, 1979.

Galloway, J. N., Dentener, F. J., Capone, D. G., Boyer, E. W., Howarth, R. W., Seitzinger, S. P., Asner, G. P., Cleveland, C. C., Green, P. A., Holland, E. A., Karl, D. M., Michaels, A. F., Porter, J. H., Townsend, A. R., and Vöosmarty, C. J.: Nitrogen Cycles: Past, Present, and Future, Biogeochemistry, 70, 153–226, https://doi.org/10.1007/s10533-004-0370-0, 2004.

Gerino, M., Stora, G., François-Carcaillet, F., Gilbert, F., Poggiale, J.-C., Mermillod-Blondin, F., Desrosiers, G., and Vervier, P.: Macro-invertebrate functional groups in freshwater and marine sediments: a common mechanistic classification, 2003.

Geslin, E., Risgaard-Petersen, N., Lombard, F., Metzger, E., Langlet, D., and Jorissen, F.: Oxygen respiration rates of benthic foraminifera as measured with oxygen microsensors, J. Exp. Mar. Biol. Ecol., 396, 108–114, https://doi.org/10.1016/j.jembe.2010.10.011, 2011.

Gilbert, F., Aller, R. C., and Hulth, S.: The influence of macrofaunal burrow spacing and diffusive scaling on sedimentary nitrification and denitrification: An experimental simulation and model approach, Journal of Marine Research, 61, 101–125, https://doi.org/10.1357/002224003321586426, 2003.

Gilbert, F., Hulth, S., Grossi, V., Poggiale, J.-C., Desrosiers, G., Rosenberg, R., Gérino, M., François-Carcaillet, F., Michaud, E., and Stora, G.: Sediment reworking by marine benthic species from the Gullmar Fjord (Western Sweden): Importance of faunal biovolume, 348, 133–144, 2007.

GIP Loire estuaire. Groupement d'intérêt public Loire Estuaire. Last connexion 09/05/2021. https://www.loire-estuaire.org/accueil.

Glock, N.: Metabolic preference of nitrate over oxygen as an electron acceptor in Foraminifera from the Peruvian oxygen minimum zone, Pnas Proc. Natl. Acad. Sci. U. S. Am., 2019.

Glock, N., Schönfeld, J., Eisenhauer, A., Hensen, C., Mallon, J., and Sommer, S.: The role of benthic foraminifera in the benthic nitrogen cycle of the Peruvian oxygen minimum zone, Biogeosciences, 10, 4767–4783, https://doi.org/10.5194/bg-10-4767-2013, 2013.

Glock, N., Roy, A.-S., Romero, D., Wein, T., Weissenbach, J., Revsbech, N. P., Høgslund, S., Clemens, D., Sommer, S., and Dagan, T.: Metabolic preference of nitrate over oxygen as an electron acceptor in foraminifera from the Peruvian oxygen minimum zone, Proc. Natl. Acad. Sci., 116, 2860–2865, https://doi.org/10.1073/pnas.1813887116, 2019.

Glud, R. N., Thamdrup, B., Stahl, H., Wenzhoefer, F., Glud, A., Nomaki, H., Oguri, K., Revsbech, N. P., and Kitazato, H.: Nitrogen cycling in a deep ocean margin sediment (Sagami Bay, Japan), Limnol. Oceanogr., 54, 723–734, https://doi.org/10.4319/lo.2009.54.3.0723, 2009.

Glud, R. N., Ramsing, N. B., and Revsbech, N. P.: Photosynthesis and Photosynthesis-Coupled Respiration in Natural Biofilms Quantified with Oxygen Microsensors1, 28, 51–60, https://doi.org/10.1111/j.0022-3646.1992.00051.x, 1992.

Goldberg, T., Archer, C., Vance, D., Thamdrup, B., McAnena, A., and Poulton, S. W. Controls on Mo isotope fractionations in a Mn-rich anoxic marine sediment, Gullmar Fjord, Sweden. Chemical Geology, 296-297, 73-82. https://doi.org/10.1016/j.chemgeo.2011.12.020, 2012.

Goldstein, S. T.: Foraminifera: A biological overview, in: Modern Foraminifera, edited by: Sen Gupta, B. K., Springer Netherlands, Dordrecht, 37–55, https://doi.org/10.1007/0-306-48104-9_3, 1999.

Goldstein, S. T., Watkins, G. T., and Kuhn, R. M.: Microhabitats of salt marsh foraminifera: St. Catherines Island, Georgia, USA, Mar. Micropaleontol., 26, 17–29, https://doi.org/10.1016/0377-8398(95)00006-2, 1995.

Goldstein, S. T., Bernhard, J. M., and Richardson, E. A.: Chloroplast Sequestration in the Foraminifer Haynesina germanica: Application of High Pressure Freezing and Freeze Substitution, Microsc. Microanal., 10, 1458–1459, https://doi.org/10.1017/S1431927604885891, 2004.

Gooday, A. J. and Lambshead, P. J. D.: Influence of seasonally deposited phytodetritus on benthic foraminiferal populations in the bathyal northeast Atlantic: the species response, Mar. Ecol. Prog. Ser., 58, 53–67, 1989.

Goubert, E., Frenod, E., Peeters, P., Thuillier, P., Vested, H. J., and Bernard, N.: Utilisation de données altimétriques (Altus) dans la caractérisation de climats hydrodynamiques contrôlant le fonctionnement hydrosédimentaire d'une vasière intertidale : cas de l'estuaire de la Vilaine (Bretagne, France), 3, 6.1-6.15, https://doi.org/10.5150/revue-paralia.2010.006, 2010.

Grzymski, J., Schofield, O. M., Falkowski, P. G., and Bernhard, J. M.: The function of plastids in the deep-sea benthic foraminifer, *Nonionella stella*. *Limnology and Oceanography*, *47*(6), 1569-1580. https://doi.org/10.4319/lo.2002.47.6.1569, 2002.

Guarini, J.-M., Gros, P., Blanchard, G., Richard, P., and Fillon, A.: Benthic contribution to pelagic microalgal communities in two semi-enclosed, European-type littoral ecosystems (Marennes-Oléron Bay and Aiguillon Bay, France), J. Sea Res., 52, 241–258, https://doi.org/10.1016/j.seares.2004.04.003, 2004.

Halpern, B. S.: Building on a Decade of the Ocean Health Index, One Earth, 2, 30–33, https://doi.org/10.1016/j.oneear.2019.12.011, 2020.

Haslett, S. K.: Coastal Systems, University of Wales Press, 256 pp., 2016.

Haure, J. and Baud, J.-P.: Approche de la capacité trophique dans le bassin ostréicole (Baie de Bourgneuf), 1995.

Hayward, B. W., Holzmann, M., Grenfell, H. R., Pawlowski, J., and Triggs, C. M.: Morphological distinction of molecular types in Ammonia – towards a taxonomic revision of the world's most commonly misidentified foraminifera, Mar. Micropaleontol., 50, 237–271, https://doi.org/10.1016/S0377-8398(03)00074-4, 2004.

Heinz, P., Hemleben, C., and Kitazato, H.: Time-response of cultured deep-sea benthic foraminifera to different algal diets, Deep Sea Res. Part Oceanogr. Res. Pap., 49, 517–537, https://doi.org/10.1016/S0967-0637(01)00070-X, 2002.

Herbert, R. A.: Nitrogen cycling in coastal marine ecosystems, FEMS Microbiol Rev, 23, 563–590, https://doi.org/10.1111/j.1574-6976.1999.tb00414.x, 1999.

Høgslund, S., Revsbech, N. P., Cedhagen, T., Nielsen, L. P., and Gallardo, V. A.: Denitrification, nitrate turnover, and aerobic respiration by benthic foraminiferans in the oxygen minimum zone off Chile, J. Exp. Mar. Biol. Ecol., 359, 85–91, https://doi.org/10.1016/j.jembe.2008.02.015, 2008.

Howe, J. A., Austin, W. E. N., Forwick, M., Paetzel, M., Harland, R., and Cage, A. G.: Fjord systems and archives: a review, Geol. Soc. Lond. Spec. Publ., 344, 5–15, https://doi.org/10.1144/SP344.2, 2010.

Huettel, M. and Webster, I. T.: Porewater flow in permeable sediment, The Benthic Boundary Layer: Transport Processes and Biogeochemistry, 144–179, 2000.

Hurrell, J. W.: Decadal Trends in the North Atlantic Oscillation: Regional Temperatures and Precipitation, Science, 269, 676–679, https://doi.org/10.1126/science.269.5224.676, 1995.

Hyacinthe, C., Anschutz, P., Carbonel, P., Jouanneau, J.-M., and Jorissen, F. J.: Early diagenetic processes in the muddy sediments of the Bay of Biscay, Marine Geology, 177, 111–128, https://doi.org/10.1016/S0025-3227(01)00127-X, 2001.

Jauffrais, T., Jesus, B., Metzger, E., Mouget, J.-L., Jorissen, F., and Geslin, E.: Effect of light on photosynthetic efficiency of sequestered chloroplasts in intertidal benthic foraminifera (*Haynesina germanica* and *Ammonia tepida*), Biogeosciences, 13, 2715–2726, https://doi.org/10.5194/bg-13-2715-2016, 2016.

Jauffrais, T., LeKieffre, C., Schweizer, M., Geslin, E., Metzger, E., Bernhard, J. M., Jesus, B., Filipsson, H. L., Maire, O., and Meibom, A.: Kleptoplastidic benthic foraminifera from aphotic habitats: insights into assimilation of inorganic C, N and S studied with sub-cellular resolution, Environ. Microbiol., 21, 125–141, https://doi.org/10.1111/1462-2920.14433, 2018.

Jauffrais, T., LeKieffre, C., Schweizer, M., Geslin, E., Metzger, E., Bernhard, J. M., Jesus, B., Filipsson, H. L., Maire, O., and Meibom, A.: Kleptoplastidic benthic foraminifera from aphotic habitats: insights into assimilation of inorganic C, N and S studied with sub-cellular resolution, Environ. Microbiol., 21, 125–141, https://doi.org/10.1111/1462-2920.14433, 2019a.

Jauffrais, T., LeKieffre, C., Schweizer, M., Jesus, B., Metzger, E., and Geslin, E.: Response of a kleptoplastidic foraminifer to heterotrophic starvation: photosynthesis and lipid droplet biogenesis, FEMS Microbiol. Ecol., 95, https://doi.org/10.1093/femsec/fiz046, 2019b.

Jauffrais, T., Mouret, A., Metzger, E., Jesus, B., Jean-Soro, L., Bernhard, J. M., & Geslin, E. Combined characterization of fine-scale distributions and microenvironments of living protists in intertidal sediment. Journal of Experimental Biology and Ecology, *in preparation.*

Jauffrais, T., Mouret, A., Metzger, E., Jesus, B., Bernhard, J. M., & Geslin, E. Two-dimensional paired analyses of fine-scale sediment geochemistry and live benthic protists, and metazoans distributions in mudflat chemoclines. Environmental Sciences &Technology, *in preparation.*

Jesus, B., Mendes, C. R., Brotas, V., and Paterson, D. M.: Effect of sediment type on microphytobenthos vertical distribution: Modelling the productive biomass and improving ground truth measurements, J. Exp. Mar. Biol. Ecol., 332, 60–74, https://doi.org/10.1016/j.jembe.2005.11.005, 2006.

Jézéquel, D., Brayner, R., Metzger, E., Viollier, E., Prévot, F., and Fiévet, F.: Two-dimensional determination of dissolved iron and sulfur species in marine sediment pore-waters by thin-film based imaging. Thau lagoon (France), Estuarine, Coastal and Shelf Science, 72, 420–431, https://doi.org/10.1016/j.ecss.2006.11.031, 2007.

Jorissen, F., Nardelli, M. P., Almogi-Labin, A., Barras, C., Bergamin, L., Bicchi, E., El Kateb, A., Ferraro, L., McGann, M., Morigi, C., Romano, E., Sabbatini, A., Schweizer, M., and Spezzaferri, S.: Developing Foram-AMBI for biomonitoring in the Mediterranean: Species assignments to ecological categories, Mar. Micropaleontol., https://doi.org/10.1016/j.marmicro.2017.12.006, 2018.

Jorissen, F. J.: Benthic foraminiferal microhabitats below the sediment-water interface, in: Modern Foraminifera, edited by: Sen Gupta, B. K., Springer Netherlands, Dordrecht, 161–179, https://doi.org/10.1007/0-306-48104-9_10, 2003.

Jorissen, F. J., de Stigter, H. C., and Widmark, J. G. V.: A conceptual model explaining benthic foraminiferal microhabitats, Mar. Micropaleontol., 26, 3–15, https://doi.org/10.1016/0377-8398(95)00047-X, 1995.

Jouffray, J.-B., Blasiak, R., Norström, A. V., Österblom, H., and Nyström, M.: The Blue Acceleration: The Trajectory of Human Expansion into the Ocean, One Earth, 2, 43–54, https://doi.org/10.1016/j.oneear.2019.12.016, 2020.

Kamp, A., Beer, D. de, Nitsch, J. L., Lavik, G., and Stief, P.: Diatoms respire nitrate to survive dark and anoxic conditions, Proc. Natl. Acad. Sci., 108, 5649–5654, https://doi.org/10.1073/pnas.1015744108, 2011.

Kamp, A., Stief, P., Knappe, J., and Beer, D. de: Response of the Ubiquitous Pelagic Diatom Thalassiosira weissflogii to Darkness and Anoxia, PLOS ONE, 8, e82605, https://doi.org/10.1371/journal.pone.0082605, 2013.

Kamp, A., Høgslund, S., Risgaard-Petersen, N., and Stief, P.: Nitrate Storage and Dissimilatory Nitrate Reduction by Eukaryotic Microbes, Front. Microbiol., 6, https://doi.org/10.3389/fmicb.2015.01492, 2015.

Katsev, S., Chaillou, G., Sundby, B., and Mucci, A.: Effects of progressive oxygen depletion on sediment diagenesis and fluxes: A model for the lower St. Lawrence River Estuary, 52, 2555–2568, https://doi.org/10.4319/lo.2007.52.6.2555, 2007.

Katz, M. E., Cramer, B. S., Franzese, A., Hönisch, B., Miller, K. G., Rosenthal, Y., and Wright, J. D. Traditional and emerging geochemical proxies in Foraminifera, J. Foraminifer. Res., 40, 165–192, https://doi.org/10.2113/gsjfr.40.2.165, 2010.

Kemp, W. M., Sampou, P., Caffrey, J., Mayer, M., Henriksen, K., and Boynton, W. R.: Ammonium recycling versus denitrification in Chesapeake Bay sediments, 35, 1545–1563, https://doi.org/10.4319/lo.1990.35.7.1545, 1990.

Kemp, W. M., Boynton, W. R., Adolf, J. E., Boesch, D. F., Boicourt, W. C., Brush, G., Cornwell, J. C., Fisher, T. R., Glibert, P. M., Hagy, J. D., Harding, L. W., Houde, E. D., Kimmel, D. G., Miller, W. D., Newell, R. I. E., Roman, M. R., Smith, E. M., and Stevenson, J. C.: Eutrophication of Chesapeake Bay: historical trends and ecological interactions, 303, 1–29, https://doi.org/10.3354/meps303001, 2005.

Knowles, R.: Denitrification., Microbiol. Rev., 46, 43–70, 1982.

Koho, K. A., García, R., de Stigter, H. C., Epping, E., Koning, E., Kouwenhoven, T. J., and van der Zwaan, G. J.: Sedimentary labile organic carbon and pore water redox control on species distribution of benthic foraminifera: A case study from Lisbon–Setúbal Canyon (southern Portugal), Prog. Oceanogr., 79, 55–82, https://doi.org/10.1016/j.pocean.2008.07.004, 2008.

Koho, K. A., Pina-Ochoa, E., Geslin, E., and Risgaard-Petersen, N.: Vertical migration, nitrate uptake and denitrification: survival mechanisms of foraminifers (Globobulimina turgida) under low oxygen conditions, 2011.

Kristensen, E., Kristiansen, K. D., and Jensen, M. H.: Temporal behavior of manganese and iron in a sandy coastal sediment exposed to water column anoxia, Estuaries, 26, 690–699, https://doi.org/10.1007/BF02711980, 2003.

Kristensen, E., Penha-Lopes, G., Delefosse, M., Valdemarsen, T., Quintana, C. O., and Banta, G. T.: What is bioturbation? The need for a precise definition for fauna in aquatic sciences, 446, 285–302, https://doi.org/10.3354/meps09506, 2012.

Kristiansen, K. D., Kristensen, E., and Jensen, E. M. H.: The Influence of Water Column Hypoxia on the Behaviour of Manganese and Iron in Sandy Coastal Marine Sediment, Estuarine, Coastal and Shelf Science, 55, 645–654, https://doi.org/10.1006/ecss.2001.0934, 2002.

Krom, M. D. and Berner, R. A.: Adsorption of phosphate in anoxic marine sediments1, 25, 797–806, https://doi.org/10.4319/lo.1980.25.5.0797, 1980.

Krom, M. D., Davison, P., Zhang, H., and Davison, W.: High-resolution pore-water sampling with a gel sampler, 39, 1967–1972, https://doi.org/10.4319/lo.1994.39.8.1967, 1994.

Labrune, C., Grémare, A., Guizien, K., and Amouroux, J. M.: Long-term comparison of soft bottom macrobenthos in the Bay of Banyuls-sur-Mer (north-western Mediterranean Sea): A reappraisal, Journal of Sea Research, 58, 125–143, https://doi.org/10.1016/j.seares.2007.02.006, 2007.

Langlet, D., Baal, C., Geslin, E., Metzger, E., Zuschin, M., Riedel, B., Risgaard-Petersen, N., Stachowitsch, M., and Jorissen, F. J.: Foraminiferal species responses to in situ, experimentally

induced anoxia in the Adriatic Sea, Biogeosciences, 11, 1775–1797, https://doi.org/10.5194/bg-11-1775-2014, 2014.

Larsen, M., Thamdrup, B., Shimmield, T., and Glud, R. N.: Benthic mineralization and solute exchange on a Celtic Sea sand-bank (Jones Bank), Prog. Oceanogr., 117, 64–75, https://doi.org/10.1016/j.pocean.2013.06.010, 2013.

Launeau, P., Méléder, V., Verpoorter, C., Barillé, L., Kazemipour-Ricci, F., Giraud, M., Jesus, B., and Le Menn, E.: Microphytobenthos Biomass and Diversity Mapping at Different Spatial Scales with a Hyperspectral Optical Model, Remote Sens., 10, 716, https://doi.org/10.3390/rs10050716, 2018.

Le Floch, J. F.: Propagation de la marée dynamique dans l'estuaire de la Seine et en Seine maritime, Unpubl. PhD Diss. Univ. Paris Fr., 1961.

Lebreton, B., Rivaud, A., Picot, L., Prévost, B., Barillé, L., Sauzeau, T., Beseres Pollack, J., and Lavaud, J.: From ecological relevance of the ecosystem services concept to its socio-political use. The case study of intertidal bare mudflats in the Marennes-Oléron Bay, France, Ocean Coast. Manag., 172, 41–54, https://doi.org/10.1016/j.ocecoaman.2019.01.024, 2019.

Lee, J. J., McEnery, M., Pierce, S., Freudenthal, H. D., and Muller, W. A.: Tracer Experiments in Feeding Littoral Foraminifera, J. Protozool., 13, 659–670, https://doi.org/10.1111/j.1550-7408.1966.tb01978.x, 1966.

Legge, O., Johnson, M., Hicks, N., Jickells, T., Diesing, M., Aldridge, J., Andrews, J., Artioli, Y., Bakker, D. C. E., Burrows, M. T., Carr, N., Cripps, G., Felgate, S. L., Fernand, L., Greenwood, N., Hartman, S., Kröger, S., Lessin, G., Mahaffey, C., Mayor, D. J., Parker, R., Queirós, A. M., Shutler, J. D., Silva, T., Stahl, H., Tinker, J., Underwood, G. J. C., Van Der Molen, J., Wakelin, S., Weston, K., and Williamson, P.: Carbon on the Northwest European Shelf: Contemporary Budget and Future Influences, Front. Mar. Sci., 7, https://doi.org/10.3389/fmars.2020.00143, 2020.

LeKieffre, C., Spangenberg, J. E., Mabilleau, G., Escrig, S., Meibom, A., and Geslin, E.: Surviving anoxia in marine sediments: The metabolic response of ubiquitous benthic foraminifera (*Ammonia tepida*), PLOS ONE, 12, e0177604, https://doi.org/10.1371/journal.pone.0177604, 2017.

LeKieffre, C., Bernhard, J. M., Mabilleau, G., Filipsson, H. L., Meibom, A., and Geslin, E.: An overview of cellular ultrastructure in benthic foraminifera: New observations of rotalid species in the context of existing literature, Mar. Micropaleontol., 138, 12–32, https://doi.org/10.1016/j.marmicro.2017.10.005, 2018.

LeKieffre, C., Jauffrais, T., Geslin, E., Jesus, B., Bernhard, J. M., Giovani, M.-E., and Meibom, A. Inorganic carbon and nitrogen assimilation in cellular compartments of a benthic kleptoplastic foraminifer. Scientific Reports, 8(1), 10140. https://doi.org/10.1038/s41598-018-28455-1, 2018.

LeKieffre, C., Jauffrais, T., Bernhard, J. M., Filipsson, H. L., Roberge, H., Schmidt, C., Maire, O., Panieri, G., Geslin, E., & Meibom, A. Inorganic nitrogen and sulfur assimilation in benthic foraminifer, *in preparation.*

Lerman, A.: Geochemical processes. Water and sediment environments., 1979.

Levin, L. A., Rathburn, A. E., Gutiérrez, D., Muñoz, P., and Shankle, A.: Bioturbation by symbiont-bearing annelids in near-anoxic sediments: Implications for biofacies models and paleo-oxygen assessments, Palaeogeography, Palaeoclimatology, Palaeoecology, 199, 129–140, https://doi.org/10.1016/S0031-0182(03)00500-5, 2003.

Lintner, M., Biedrawa, B., Wukovits, J., Wanek, W., and Heinz, P.: Salinity-depending carbon and nitrogen uptake of two intertidal foraminifera (*Ammonia tepida* and *Haynesina germanica*), Biogeosciences Discuss., 1–17, https://doi.org/10.5194/bg-2019-359, 2019.

Lintner, M., Biedrawa, B., Wukovits, J., Wanek, W., and Heinz, P.: Reviews and syntheses: Salinity-dependent algae uptake and subsequent carbon and nitrogen metabolisms of two intertidal foraminifera (*Ammonia tepida* and *Haynesina germanica*), Biogeosciences, 17, 3723–3732, https://doi.org/10.5194/bg-17-3723-2020, 2020.

Lintner, M., Lintner, B., Wanek, W., Keul, N., and Heinz, P.: The effect of the salinity, light regime and food source on carbon and nitrogen uptake in a benthic foraminifer, Biogeosciences, 18, 1395–1406, https://doi.org/10.5194/bg-18-1395-2021, 2021.

Liquete, C., Piroddi, C., Drakou, E. G., Gurney, L., Katsanevakis, S., Charef, A., and Egoh, B.: Current Status and Future Prospects for the Assessment of Marine and Coastal Ecosystem Services: A Systematic Review, PLOS ONE, 8, e67737, https://doi.org/10.1371/journal.pone.0067737, 2013.

Lopez: Algal Chloroplasts in the Protoplasm of Three Species of Benthic Foraminifera: Taxonomic Affinity, Viability and Persistence, 1979.

Luther, G. W., Sundby, B., Lewis, B. L., Brendel, P. J., and Silverberg, N.: Interactions of manganese with the nitrogen cycle: Alternative pathways to dinitrogen, Geochimica et Cosmochimica Acta, 61, 4043–4052, https://doi.org/10.1016/S0016-7037(97)00239-1, 1997.

MacIntyre, H. L., Geider, R. J., and Miller, D. C.: Microphytobenthos: The ecological role of the "secret garden" of unvegetated, shallow-water marine habitats. I. Distribution, abundance and primary production, Estuaries, 19, 186–201, https://doi.org/10.2307/1352224, 1996.

McKee, B. A., Aller, R. C., Allison, M. A., Bianchi, T. S., and Kineke, G. C.: Transport and transformation of dissolved and particulate materials on continental margins influenced by major rivers: benthic boundary layer and seabed processes, Continental Shelf Research, 24, 899–926, https://doi.org/10.1016/j.csr.2004.02.009, 2004.

Meade, R. H.: Factors influencing the early stages of the compaction of clays and sands; review, Journal of Sedimentary Research, 36, 1085–1101, https://doi.org/10.1306/74D71604-2B21-11D7-8648000102C1865D, 1966.

Meile, C., Koretsky, C. M., and Cappellen, P. V.: Quantifying bioirrigation in aquatic sediments: An inverse modeling approach, 46, 164–177, https://doi.org/10.4319/lo.2001.46.1.0164, 2001.

Méléder, V., Launeau, P., Barillé, L., and Rincé, Y.: Cartographie des peuplements du microphytobenthos par télédétection spatiale visible-infrarouge dans un écosystème

conchylicole, C. R. Biol., 326, 377–389, https://doi.org/10.1016/S1631-0691(03)00125-2, 2003a.

Méléder, V., Barillé, L., Launeau, P., Carrère, V., and Rincé, Y.: Spectrometric constraint in analysis of benthic diatom biomass using monospecific cultures, Remote Sens. Environ., 88, 386–400, https://doi.org/10.1016/j.rse.2003.08.009, 2003b.

Méléder, V., Rincé, Y., Barillé, L., Gaudin, P., and Rosa, P.: Spatiotemporal changes in microphytobenthos assemblages in a macrotidal flat (Bourgneuf Bay,France)1, J. Phycol., 43, 1177–1190, https://doi.org/10.1111/j.1529-8817.2007.00423.x, 2007.

Méléder, V., Savelli, R., Barnett, A., Polsenaere, P., Gernez, P., Cugier, P., Lerouxel, A., LE BRIS, A., Dupuy, C., Le Fouest, V., and Lavaud, J.: Mapping the Intertidal Microphytobenthos Gross Primary Production Part I: Coupling Multispectral Remote Sensing and Physical Modeling, Front. Mar. Sci., https://doi.org/10.3389/fmars.2020.00520, 2020.

Metzger, E., Thibault de Chanvalon, A., Cesbron, F., Barbe, A., Launeau, P., Jézéquel, D., and Mouret, A.: Simultaneous Nitrite/Nitrate Imagery at Millimeter Scale through the Water–Sediment Interface, 50, 8188–8195, https://doi.org/10.1021/acs.est.6b00187, 2016.

Metzger, E., Barbe, A., Cesbron, F., Thibault de Chanvalon, A., Jauffrais, T., Jézéquel, D., and Mouret, A.: Two-dimensional ammonium distribution in sediment pore waters using a new colorimetric diffusive equilibration in thin-film technique, Water Research X, 2, 100023, https://doi.org/10.1016/j.wroa.2018.100023, 2019.

Middelburg, J. J. and Levin, L. A.: Coastal hypoxia and sediment biogeochemistry, Biogeosciences, 6, 1273–1293, https://doi.org/10.5194/bg-6-1273-2009, 2009.

Mojtahid, M., Zubkov, M. V., Hartmann, M., and Gooday, A. J.: Grazing of intertidal benthic foraminifera on bacteria: Assessment using pulse-chase radiotracing, J. Exp. Mar. Biol. Ecol., 399, 25–34, https://doi.org/10.1016/j.jembe.2011.01.011, 2011.

Moncelon, R., Gouazé, M., Pineau, P., Bénéteau, E., Bréret, M., Philippine, O., Robin, F.-X., Dupuy, C., and Metzger, E.: Coupling between sediment biogeochemistry and phytoplankton development in a temperate freshwater marsh (Charente-Maritime, France): Evidence of temporal pattern, Water Research, 189, 116567, https://doi.org/10.1016/j.watres.2020.116567, 2021.

Moodley, L., Schaub, B., Van der Zwaan, G.J., Herman, P.M.J., Ecosystems Studies, and Spatial Ecology: Tolerance of benthic foraminifera (Protista : Sarcodina) to hydrogen sulphide, Mar. Ecol. Prog. Ser., 169, 77–86, https://doi.org/10.3354/meps169077, 1998.

Moodley, L., Boschker, H. T. S., Middelburg, J. J., Pel, R., Herman, P. M. J., Deckere, E. de, and Heip, C. H. R.: Ecological significance of benthic foraminifera: 13C labelling experiments, Mar. Ecol. Prog. Ser., 202, 289–295, https://doi.org/10.3354/meps202289, 2000.

Mortimer, R. J. G., Harris, S. J., Krom, M. D., Freitag, T. E., Prosser, J. I., Barnes, J., Anschutz, P., Hayes, P. J., and Davies, I. M.: Anoxic nitrification in marine sediments, 276, 37–51, 2004.

Morvan, J., Cadre, V. L., Jorissen, F., and Debenay, J.-P.: Foraminifera as potential bio-indicators of the “Erika” oil spill in the Bay of Bourgneuf: Field and experimental studies, Aquat. Living Resour., 17, 317–322, https://doi.org/10.1051/alr:2004034, 2004.

Mouret, A., Barbe, A., Levrard, R., Charbonnier, C., Cesbron, F., Choquel, C., & Metzger, E. Two-dimensional determination of dissolved manganese in sediment porewaters. Frontiers in Chemistry, *in preparation.*

Murray, J. M. H., Meadows, A., and Meadows, P. S.: Biogeomorphological implications of microscale interactions between sediment geotechnics and marine benthos: a review, Geomorphology, 47, 15–30, https://doi.org/10.1016/S0169-555X(02)00138-1, 2002.

Murray, J. W.: Ecology and Applications of Benthic Foraminifera, Cambridge University Press, 320 pp., 2006.

Murray, N. J., Phinn, S. R., DeWitt, M., Ferrari, R., Johnston, R., Lyons, M. B., Clinton, N., Thau, D., and Fuller, R. A. The global distribution and trajectory of tidal flats. Nature, 565(7738), 222-225. https://doi.org/10.1038/s41586-018-0805-8, 2019.

Nardelli, M. P., Barras, C., Metzger, E., Mouret, A., Filipsson, H. L., Jorissen, F., and Geslin, E.: Experimental evidence for foraminiferal calcification under anoxia, Biogeosciences, 11, 4029–4038, https://doi.org/10.5194/bg-11-4029-2014, 2014.

Neubacher, E. C., Parker, R. E., and Trimmer, M.: The potential effect of sustained hypoxia on nitrogen cycling in sediment from the southern North Sea: a mesocosm experiment | SpringerLink, 2013.

Nomaki, H., Heinz, P., Nakatsuka, T., Shimanaga, M., and Kitazato, H.: Species-specific ingestion of organic carbon by deep-sea benthic foraminifera and meiobenthos: In situ tracer experiments, Limnol. Oceanogr., 50, 134–146, https://doi.org/10.4319/lo.2005.50.1.0134, 2005.

Nomaki, H., Heinz, P., Nakatsuka, T., Shimanaga, M., Ohkouchi, N., Ogawa, N. O., Kogure, K., Ikemoto, E., and Kitazato, H.: Different ingestion patterns of 13C-labeled bacteria and algae by deep-sea benthic foraminifera, Mar. Ecol. Prog. Ser., 310, 95–108, https://doi.org/10.3354/meps310095, 2006.

Nomaki, H., Ogawa, N., Ohkouchi, N., Suga, H., Toyofuku, T., Shimanaga, M., Nakatsuka, T., and Kitazato, H.: Benthic foraminifera as trophic links between phytodetritus and benthic metazoans: carbon and nitrogen isotopic evidence, Mar. Ecol. Prog. Ser., 357, 153–164, https://doi.org/10.3354/meps07309, 2008.

Nomaki, H., Chikaraishi, Y., Tsuchiya, M., Toyofuku, T., Ohkouchi, N., Uematsu, K., Tame, A., and Kitazato, H.: Nitrate uptake by foraminifera and use in conjunction with endobionts under anoxic conditions, Limnol. Oceanogr., 59, 1879–1888, https://doi.org/10.4319/lo.2014.59.6.1879, 2014.

Nomaki, H., Chikaraishi, Y., Tsuchiya, M., Toyofuku, T., Suga, H., Sasaki, Y., Uematsu, K., Tame, A., and Ohkouchi, N.: Variation in the nitrogen isotopic composition of amino acids in benthic foraminifera: Implications for their adaptation to oxygen-depleted environments, Limnol. Oceanogr., 60, 1906–1916, https://doi.org/10.1002/lno.10140, 2015.

Nordberg, K.: Oceanography in the Kattegat and Skagerrak Over the Past 8000 Years, Paleoceanography, 6, 461–484, https://doi.org/10.1029/91PA01132, 1991.

Nordberg, K., Gustafsson, M., and Krantz, A.-L.: Decreasing oxygen concentrations in the Gullmar Fjord, Sweden, as confirmed by benthic foraminifera, and the possible association with NAO, J. Mar. Syst., 23, 303–316, https://doi.org/10.1016/S0924-7963(99)00067-6, 2000.

Oakes, J. M., Riekenberg, P. M., and Eyre, B. D.: Assimilation and short-term processing of microphytobenthos nitrogen in intertidal sediments, 65, 2377–2389, https://doi.org/10.1002/lno.11459, 2020.

Pagès, A., Teasdale, P. R., Robertson, D., Bennett, W. W., Schäfer, J., and Welsh, D. T.: Representative measurement of two-dimensional reactive phosphate distributions and co-distributed iron(II) and sulfide in seagrass sediment porewaters, Chemosphere, 85, 1256–1261, https://doi.org/10.1016/j.chemosphere.2011.07.020, 2011.

Parent, B., Hyams-Kaphzan, O., Barras, C., Lubinevsky, H., and Jorissen, F.: Testing foraminiferal environmental quality indices along a well-defined organic matter gradient in the Eastern Mediterranean, Ecol. Indic., 125, 107498, https://doi.org/10.1016/j.ecolind.2021.107498, 2021.

Pascal, P.-Y., Dupuy, C., Richard, P., Mallet, C., Telet, E. A. du C., and Niquilb, N.: Seasonal variation in consumption of benthic bacteria by meio- and macrofauna in an intertidal mudflat, Limnol. Oceanogr., 54, 1048–1059, https://doi.org/10.4319/lo.2009.54.4.1048, 2009.

Paterson, D. M., Perkins, R., Consalvey, M., and Underwood, G. J. C.: Ecosystem Function, Cell Micro-Cycling and the Structure of Transient Biofilms, in: Fossil and Recent Biofilms: A Natural History of Life on Earth, edited by: Krumbein, W. E., Paterson, D. M., and Zavarzin, G. A., Springer Netherlands, Dordrecht, 47–63, https://doi.org/10.1007/978-94-017-0193-8_3, 2003.

Pawlowski, J., Holzmann, M., Berney, C., Fahrni, J., Gooday, A. J., Cedhagen, T., Habura, A., and Bowser, S. S.: The evolution of early Foraminifera, Proc. Natl. Acad. Sci., 100, 11494–11498, https://doi.org/10.1073/pnas.2035132100, 2003.

Perkins, R. G., Underwood, G. J. C., Brotas, V., Snow, G. C., Jesus, B., and Ribeiro, L.: Responses of microphytobenthos to light: primary production and carbohydrate allocation over an emersion period, Mar. Ecol. Prog. Ser., 223, 101–112, https://doi.org/10.3354/meps223101, 2001.

Petersen, J., Barras, C., Bézos, A., La, C., de Nooijer, L. J., Meysman, F. J. R., Mouret, A., Slomp, C. P., and Jorissen, F.: Mn⁄Ca intra- and inter-test variability in the benthic foraminifer Ammonia tepida, 2018.

Pettersson, O. and G. Ekman. Grunddragen af Skageracks och Kattegats hydrografi. Kongliga Svenska Vetenskaps-akademiens handlingar 24:13, 1891.

Pillet, L., de Vargas, C., and Pawlowski, J.: Molecular Identification of Sequestered Diatom Chloroplasts and Kleptoplastidy in Foraminifera, Protist, 162, 394–404, https://doi.org/10.1016/j.protis.2010.10.001, 2011.

Pina-Ochoa, E., Hogslund, S., Geslin, E., Cedhagen, T., Revsbech, N. P., Nielsen, L. P., Schweizer, M., Jorissen, F., Rysgaard, S., and Risgaard-Petersen, N.: Widespread occurrence of nitrate storage and denitrification among Foraminifera and Gromiida, Proc. Natl. Acad. Sci., 107, 1148–1153, https://doi.org/10.1073/pnas.0908440107, 2010.

Point, D., Monperrus, M., Tessier, E., Amouroux, D., Chauvaud, L., Thouzeau, G., Jean, F., Amice, E., Grall, J., Leynaert, A., Clavier, J., and Donard, O. F. X.: Biological control of trace metal and organometal benthic fluxes in a eutrophic lagoon (Thau Lagoon, Mediterranean Sea, France), Estuarine, Coastal and Shelf Science, 72, 457–471, https://doi.org/10.1016/j.ecss.2006.11.013, 2007.

Pniewski, F. F., Biskup, P., Bubak, I., Richard, P., Latała, A., and Blanchard, G.: Photo-regulation in microphytobenthos from intertidal mudflats and non-tidal coastal shallows, Estuar. Coast. Shelf Sci., 152, 153–161, https://doi.org/10.1016/j.ecss.2014.11.022, 2015.

Polovodova Asteman, I. and Nordberg, K.: Foraminiferal fauna from a deep basin in Gullmar Fjord: The influence of seasonal hypoxia and North Atlantic Oscillation, J. Sea Res., 79, 40–49, https://doi.org/10.1016/j.seares.2013.02.001, 2013.

Polovodova Asteman, I. and Schönfeld, J.: Recent invasion of the foraminifer Nonionella stella Cushman & Moyer, 1930 in northern European waters: evidence from the Skagerrak and its fjords, J. Micropalaeontology, 35, 20–25, https://doi.org/10.1144/jmpaleo2015-007, 2015.

Prazeres, M., Ainsworth, T., Roberts, T. E., Pandolfi, J. M., and Leggat, W.: Symbiosis and microbiome flexibility in calcifying benthic foraminifera of the Great Barrier Reef, Microbiome, 5, 38, https://doi.org/10.1186/s40168-017-0257-7, 2017.

Prazeres, M., Martínez-Colón, M., and Hallock, P.: Foraminifera as bioindicators of water quality: The FoRAM Index revisited, Environmental Pollution, 257, 113612, https://doi.org/10.1016/j.envpol.2019.113612, 2020.

Prins, A., Déléris, P., Hubas, C., and Jesus, B.: Effect of Light Intensity and Light Quality on Diatom Behavioral and Physiological Photoprotection, Front. Mar. Sci., 7, 203, https://doi.org/10.3389/fmars.2020.00203, 2020.

Prokopenko, M. G., Sigman, D. M., Berelson, W. M., Hammond, D. E., Barnett, B., Chong, L., and Townsend-Small, A.: Denitrification in anoxic sediments supported by biological nitrate transport, Geochim. Cosmochim. Acta, 75, 7180–7199, https://doi.org/10.1016/j.gca.2011.09.023, 2011.

Rabalais, N. N., Turner, R. E., Gupta, B. K. S., Platon, E., and Parsons, M. L.: Sediments the History of Eutrophication and Hypoxia in the Northern Gulf of Mexico, Ecol. Appl., 17, S129–S143, https://doi.org/10.1890/06-0644.1, 2007.

Rabalais, N. N., Turner, R. E., Díaz, R. J., & Justić, D. Global change and eutrophication of coastal waters. ICES Journal of Marine Science, 66(7), 1528-1537. https://doi.org/10.1093/icesjms/fsp047, 2009.

Rabalais, N. N., Díaz, R. J., Levin, L. A., Turner, R. E., Gilbert, D., and Zhang, J.: Dynamics and distribution of natural and human-caused hypoxia, Biogeosciences, 7, 585–619, https://doi.org/10.5194/bg-7-585-2010, 2010.

Redfield, A. C.: The influence of organisms on the composition of seawater, 2, 26–77, 1963.

Redzuan, N. S. and Underwood, G. J. C.: The importance of weather and tides on the resuspension and deposition of microphytobenthos (MPB) on intertidal mudflats, Estuarine, Coastal and Shelf Science, 251, 107190, https://doi.org/10.1016/j.ecss.2021.107190, 2021.

Reimers, C. E.: An in situ microprofiling instrument for measuring interfacial pore water gradients: methods and oxygen profiles from the North Pacific Ocean, Deep Sea Research Part A. Oceanographic Research Papers, 34, 2019–2035, https://doi.org/10.1016/0198-0149(87)90096-3, 1987.

Revsbech, N. P., Barker Jorgensen, B., and Blackburn, T. H.: Oxygen in the Sea Bottom Measured with a Microelectrode, Science, 207, 1355–1356, https://doi.org/10.1126/science.207.4437.1355, 1980.

Richirt, J.: Le genre *Ammonia* (Foraminifères) dans les écosystèmes côtiers de la façade Atlantique, PhD thesis, Angers, 2020.

Richirt, J., Riedel, B., Mouret, A., Schweizer, M., Langlet, D., Seitaj, D., Meysman, F., Slomp, C. P., and Jorissen, F.: Foraminiferal community response to seasonal anoxia in Lake Grevelingen (the Netherlands), Biogeosciences Discuss., https://doi.org/10.5194/bg-2019-382, 2020.

Richirt, J., Schweizer, M., Bouchet, V. M. P., Mouret, A., Quinchard, S., and Jorissen, F. J.: Morphological Distinction of Three *Ammonia* Phylotypes Occurring Along European Coasts | Journal of Foraminiferal Research | GeoScienceWorld, 2019.

Riedel, B., Diaz, R. J., Rosenberg, R., and Stachowitsch, M.: the ecological consequences of marine hypoxia: from behavioural to ecosystem responses, in Stressors in the marine enviroment: physiological responses and ecological implication, 2016.

Risgaard-Petersen, N., Nielsen, L. P., Rysgaard, S., Dalsgaard, T., and Meyer, R. L.: Application of the isotope pairing technique in sediments where anammox and denitrification coexist, 1, 63–73, https://doi.org/10.4319/lom.2003.1.63, 2003.

Risgaard-Petersen, N., Langezaal, A. M., Ingvardsen, S., Schmid, M. C., Jetten, M. S. M., Op den Camp, H. J. M., Derksen, J. W. M., Piña-Ochoa, E., Eriksson, S. P., Peter Nielsen, L., Peter Revsbech, N., Cedhagen, T., and van der Zwaan, G. J.: Evidence for complete denitrification in a benthic foraminifer, Nature, 443, 93–96, https://doi.org/10.1038/nature05070, 2006.

Robertson, D., Teasdale, P. R., and Welsh, D. T.: A novel gel-based technique for the high resolution, two-dimensional determination of iron (II) and sulfide in sediment, 6, 502–512, https://doi.org/10.4319/lom.2008.6.502, 2008.

Rosenberg, R., Hellman, B., and Johansson, B.: Hypoxic tolerance of marine benthic fauna, 79, 127–131, 1991.

Round, F. E. and Happey, C. M.: Persistent, vertical-migration rhythms in benthic microflora, Br. Phycol. Bull., 2, 463–471, https://doi.org/10.1080/00071616500650081, 1965.

Roy, M., McManus, J., Goñi, M. A., Chase, Z., Borgeld, J. C., Wheatcroft, R. A., Muratli, J. M., Megowan, M. R., and Mix, A.: Reactive iron and manganese distributions in seabed sediments near small mountainous rivers off Oregon and California (USA), Continental Shelf Research, 54, 67–79, https://doi.org/10.1016/j.csr.2012.12.012, 2013.

Rysgaard, S., Risgaard-Petersen, N., Peter, S. N., Kim, J., and Peter, N. L.: Oxygen regulation of nitrification and denitrification in sediments, 39, 1643–1652, https://doi.org/10.4319/lo.1994.39.7.1643, 1994.

Saburova, M. A. and Polikarpov, I. G.: Diatom activity within soft sediments: behavioural and physiological processes, Mar. Ecol. Prog. Ser., 251, 115–126, https://doi.org/10.3354/meps251115, 2003.

Santner, J., Larsen, M., Kreuzeder, A., and Glud, R. N.: Two decades of chemical imaging of solutes in sediments and soils – a review, Analytica Chimica Acta, 878, 9–42, https://doi.org/10.1016/j.aca.2015.02.006, 2015.

Santschi, P. H., Anderson, R. F., Fleisher, M. Q., and Bowles, W.: Measurements of diffusive sublayer thicknesses in the ocean by alabaster dissolution, and their implications for the measurements of benthic fluxes, 96, 10641–10657, https://doi.org/10.1029/91JC00488, 1991.

Savelli, R., Dupuy, C., Barillé, L., Lerouxel, A., Guizien, K., Philippe, A., Bocher, P., Polsenaere, P., and Le Fouest, V.: On biotic and abiotic drivers of the microphytobenthos seasonal cycle in a temperate intertidal mudflat: a modelling study, Biogeosciences, 15, 7243–7271, https://doi.org/10.5194/bg-15-7243-2018, 2018.

Schmidtko, S., Stramma, L., and Visbeck, M.: Decline in global oceanic oxygen content during the past five decades, 542, 335–339, https://doi.org/10.1038/nature21399, 2017.

Schönfeld, J., Alve, E., Geslin, E., Jorissen, F., Korsun, S., and Spezzaferri, S.: The FOBIMO (FOraminiferal BIo-MOnitoring) initiative—Towards a standardised protocol for soft-bottom benthic foraminiferal monitoring studies, Mar. Micropaleontol., 94–95, 1–13, https://doi.org/10.1016/j.marmicro.2012.06.001, 2012.

Schulz, H. D.: Quantification of Early Diagenesis: Dissolved Constituents in Pore Water and Signals in the Solid Phase, in: Marine Geochemistry, edited by: Schulz, H. D. and Zabel, M., Springer, Berlin, Heidelberg, 73–124, https://doi.org/10.1007/3-540-32144-6_3, 2006.

Schweizer, M., Jauffrais, T., Méléder, V., Quinchard, S., Choquel, C., and Geslin, E.: Trophic strategies of intertidal foraminifera explored with single-cell microbiome metabarcoding and morphological methods: what is on the menu?, Mol. Ecol., *submitted*.

Serôdio, J., Vieira, S., and Barroso, F.: Relationship of variable chlorophyll fluorescence indices to photosynthetic rates in microphytobenthos, 49, 71–85, https://doi.org/10.3354/ame01129, 2007.

Serôdio, J., Ezequiel, J., Barnett, A., Mouget, J.-L., Méléder, V., Laviale, M., and Lavaud, J.: Efficiency of photoprotection in microphytobenthos: role of vertical migration and the xanthophyll cycle against photoinhibition, Aquat. Microb. Ecol., 67, 161–175, https://doi.org/10.3354/ame01591, 2012.

Serôdio, J., Paterson, D. M., Meleder, V., and Vyverman, W.: Advances and Challenges in Microphytobenthos Research: From Cell Biology to Coastal Ecosystem Function, Frontiers Media SA, 311 pp., 2020.

Seuront, L. and Spilmont, N.: Self-organized criticality in intertidal microphytobenthos patch patterns, Physica A: Statistical Mechanics and its Applications, 313, 513–539, https://doi.org/10.1016/S0378-4371(02)00989-5, 2002.

Shoun, H. and Tanimoto, T.: Denitrification by the fungus Fusarium oxysporum and involvement of cytochrome P-450 in the respiratory nitrite reduction., J. Biol. Chem., 266, 11078–11082, 1991.

Shuttleworth, Sarah. M., Davison, W., and Hamilton-Taylor, J.: Two-Dimensional and Fine Structure in the Concentrations of Iron and Manganese in Sediment Pore-Waters, Environ. Sci. Technol., 33, 4169–4175, https://doi.org/10.1021/es990184l, 1999.

Sigman, D. M., Karsh, K. L., and Casciotti, K. L.: Nitrogen Isotopes in the Ocean, 40–54, https://doi.org/10.1016/B978-012374473-9.00632-9, 2009.

Skei, J.: Why sedimentologists are interested in Fjords, Sediment. Geol., 36, 75–80, https://doi.org/10.1016/0037-0738(83)90002-7, 1983.

Slomp, C. P., Malschaert, J. F. P., Lohse, L., and van Raaphorst, W.: Iron and manganese cycling in different sedimentary environments on the North Sea continental margin, 1997.

Spilmont, N., Migné, A., Seuront, L., and Davoult, D.: Short-term variability of intertidal benthic community production during emersion and the implication in annual budget calculation, Mar. Ecol. Prog. Ser., 333, 95–101, https://doi.org/10.3354/meps333095, 2007.

Stein, L. Y.: Eukaryotic Evolution: An Ancient Breath of Nitrate, Curr. Biol., 28, R875–R877, https://doi.org/10.1016/j.cub.2018.06.029, 2018.

Stockdale, A., Davison, W., and Zhang, H.: Micro-scale biogeochemical heterogeneity in sediments: A review of available technology and observed evidence, Earth-Science Reviews, 92, 81–97, https://doi.org/10.1016/j.earscirev.2008.11.003, 2009.

Stouff, V.: Interet des elevages de foraminiferes en laboratoire : etudes biologiques et ultrastructurales, These de doctorat, Angers, 1998.

Sundbäck, K. and Granéli, W.: Influence of microphytobenthos on the nutrient flux between sediment and water: a laboratory study, 43, 63–69, 1988.

Sundby, B.: Transient state diagenesis in continental margin muds, Marine Chemistry, 102, 2–12, https://doi.org/10.1016/j.marchem.2005.09.016, 2006.

Sundby, B. and Silverberg, N.: Manganese fluxes in the benthic boundary layer1: Manganese fluxes, 30, 372–381, https://doi.org/10.4319/lo.1985.30.2.0372, 1985.

Sundby, B., Anderson, L. G., Hall, P. O. J., Iverfeldt, Å., van der Loeff, M. M. R., and Westerlund, S. F. G.: The effect of oxygen on release and uptake of cobalt, manganese, iron and phosphate at the sediment-water interface, Geochimica et Cosmochimica Acta, 50, 1281–1288, https://doi.org/10.1016/0016-7037(86)90411-4, 1986.

Sundby, B., Gobeil, C., Silverberg, N., and Alfonso, M.: The phosphorus cycle in coastal marine sediments, 37, 1129–1145, https://doi.org/10.4319/lo.1992.37.6.1129, 1992.

Synthèse du rapport de l'Ifremer : « Bulletin de la surveillance de la qualité du milieu marin littoral 2013 Départements de Loire-Atlantique et Vendée (partie Nord) – Résultats acquis jusqu'en 2013» http://envlit.ifremer.fr/content/download/81951/580583/version/1/file/bull_tm_2014.pdf

Svansson, A.: Hydrography of the Gullmar Fjord, Medd. Fraan Havsfiskelab. Lysekil Swed., 1984.

Swedish Meteorological and Hydrological Institute's (SMHI): https://sharkweb.smhi.se/, last access: 13th of July 2020.

Taillefert, M., Neuhuber, S., and Bristow, G.: The effect of tidal forcing on biogeochemical processes in intertidal salt marsh sediments, Geochemical Transactions, 8, 6, https://doi.org/10.1186/1467-4866-8-6, 2007.

Takaya, N., Suzuki, S., Kuwazaki, S., Shoun, H., Maruo, F., Yamaguchi, M., and Takeo, K.: Cytochrome P450nor, a Novel Class of Mitochondrial Cytochrome P450 Involved in Nitrate Respiration in the Fungus Fusarium oxysporum, Arch. Biochem. Biophys., 372, 340–346, https://doi.org/10.1006/abbi.1999.1499, 1999.

Thamdrup, B.: Advances in Microbial Ecology, Springer Science & Business Media, 301 pp., 2000.

Thamdrup, B. and Dalsgaard, T.: Microbial Ecology of the Oceans, 1st ed., John Wiley & Sons, Ltd, https://doi.org/10.1002/9780470281840, 2008.

Thamdrup, B., Fossing, H., and Barker Jorgensen, B.: Manganese, iron, and sulfur cycling in a coastal marine sediment, Aarhus Bay, Denmark — University of Southern Denmark, 1994.

Thibault de Chanvalon, A.: Transformation de la phase solide à travers l'estuaire de la Loire en relation avec son environnement chimique et biologique, These de doctorat, Nantes, 2016.

Thibault de Chanvalon, A., Metzger, E., Mouret, A., Cesbron, F., Knoery, J., Rozuel, E., Launeau, P., Nardelli, M. P., Jorissen, F. J., and Geslin, E.: Two-dimensional distribution of living benthic foraminifera in anoxic sediment layers of an estuarine mudflat (Loire estuary, France), 12, 6219–6234, https://doi.org/10.5194/bg-12-6219-2015, 2015.

Thibault de Chanvalon, A., Mouret, A., Knoery, J., Geslin, E., Péron, O., and Metzger, E.: Manganese, iron and phosphorus cycling in an estuarine mudflat, Loire, France, Journal of Sea Research, 118, 92–102, https://doi.org/10.1016/j.seares.2016.10.004, 2016.

Thibault de Chanvalon, A., Metzger, E., Mouret, A., Knoery, J., Geslin, E., and Meysman, F. J. R.: Two dimensional mapping of iron release in marine sediments at submillimetre scale, 191, 34–49, https://doi.org/10.1016/j.marchem.2016.04.003, 2017.

Thomas, Y., Pouvreau, S., Alunno-Bruscia, M., Barillé, L., Gohin, F., Bryère, P., & Gernez, P. Global change and climate-driven invasion of the Pacific oyster (Crassostrea gigas) along European coasts : A bioenergetics modelling approach. *Journal of Biogeography*, *43*(3), 568-579. https://doi.org/10.1111/jbi.12665, 2016.

Tsuchiya, M., Toyofuku, T., Uematsu, K., Brüchert, V., Collen, J., Yamamoto, H., and Kitazato, H.: Cytologic and Genetic Characteristics of Endobiotic Bacteria and Kleptoplasts of Virgulinella fragilis (Foraminifera), J. Eukaryot. Microbiol., 62, 454–469, https://doi.org/10.1111/jeu.12200, 2015.

Tucker, C. J.: Red and photographic infrared linear combinations for monitoring vegetation, Remote Sens. Environ., 8, 127–150, https://doi.org/10.1016/0034-4257(79)90013-0, 1979.

Underwood, G. J. C. and Kromkamp: Primary production by phytoplankton and microphytobenthos in estuaries., 1999.

Visbeck, M.: Ocean science research is key for a sustainable future, Nature communications, 9, 690, https://doi.org/10.1038/s41467-018-03158-3, 2018.

Wang, Y. and Van Cappellen, P.: A multicomponent reactive transport model of early diagenesis: Application to redox cycling in coastal marine sediments, Geochimica et Cosmochimica Acta, 60, 2993–3014, https://doi.org/10.1016/0016-7037(96)00140-8, 1996.

Witte, U., Wenzhöfer, F., Sommer, S., Boetius, A., Heinz, P., Aberle, N., Sand, M., Cremer, A., Abraham, W.-R., Jørgensen, B. B., and Pfannkuche, O.: In situ experimental evidence of the fate of a phytodetritus pulse at the abyssal sea floor, Nature, 424, 763–766, https://doi.org/10.1038/nature01799, 2003.

Woehle, C., Roy, A.-S., Glock, N., Wein, T., Weissenbach, J., Rosenstiel, P., Hiebenthal, C., Michels, J., Schönfeld, J., and Dagan, T.: A Novel Eukaryotic Denitrification Pathway in Foraminifera, Curr. Biol., https://doi.org/10.1016/j.cub.2018.06.027, 2018.

Wong, P. P., Losada, I. J., Gattuso, J.-P., Hinkel, J., Khattibi, A., Mclnnes, K. L., Saito, Y., and Sallenger, A.: Coastal systems and low-lying areas. In: Climate Change 2014: Impacts,Adaptation, and Vulnerability. Part A: Global and Sectoral Aspects. Contribution of Working Group II to the Fifth Assessment Report of the Intergovernmental Panel on Climate Change. Cambridge University Press, Cambridge, pp. 361- 409., 2014.

Wukovits, J., Enge, A. J., Wanek, W., Watzka, M., and Heinz, P.: Increased temperature causes different carbon and nitrogen processing patterns in two common intertidal foraminifera (Ammonia tepida and Haynesina germanica), Biogeosciences, 14, 2815–2815, 2017.

Wukovits, J., Oberrauch, M., Enge, A. J., and Heinz, P.: The distinct roles of two intertidal foraminiferal species in phytodetrital carbon and nitrogen fluxes - results from laboratory feeding experiments, Biogeosciences, 15, 6185–6185, 2018.

Xu, Z., Liu, S., Xiang, R., and Song, G.: Live benthic foraminifera in the Yellow Sea and the East China Sea: vertical distribution, nitrate storage, and potential denitrification, Mar. Ecol. Prog. Ser., 571, 65–81, https://doi.org/10.3354/meps12135, 2017.

Xu, Z., Liu, S., and Ning, X.: Potential foraminiferal nitrate transport in sediments in contact with oxic overlying water, Limnol. Oceanogr., 66, 1510–1530, https://doi.org/10.1002/lno.11701, 2021.

.

CHAPTER 1

Denitrification by benthic foraminifera and their contribution to N-loss from a fjord environment

Chapter 1: Denitrification by benthic foraminifera and their contribution to N-loss from a fjord environment

Constance Choquel[1], Emmanuelle Geslin[1], Edouard Metzger[1], Helena L. Filipsson[2], Nils Risgaard-Petersen[3], Patrick Launeau[1], Manuel Giraud[1], Thierry Jauffrais[4,1], Bruno Jesus[5,6], and Aurélia Mouret[1]

1: UMR 6112 LPG BIAF, Univ. Angers, Univ. Nantes, CNRS, Angers, France
2: Department of Geology, Lund University, Lund, Sweden
3: Department of Biology, Aquatic Biology, Aarhus University, Aarhus, Denmark
4: Ifremer, IRD, Univ. Nouvelle-Calédonie, Univ. La Réunion, CNRS, UMR 9220 ENTROPIE, Noumea, New Caledonia
5: Université de Nantes, Mer Molécules Santé, EA 2160, Nantes, France
6: BioISI – Biosystems & Integrative Sciences Institute, Campo Grande, Faculty of Sciences, University of Lisbon, Lisbon, Portugal

Correspondence: Constance Choquel (constance.choquel@gmail.com) and Emmanuelle Geslin (emmanuelle.geslin@univ-angers.fr)

Published in Biogeosciences, 18, 327–341, 2021

Received: 23 July 2020 – Discussion started: 5 August 2020

Revised: 13 November 2020 – Accepted: 1 December 2020 – Published: 15 January 2021

Abstract

Oxygen and nitrate availabilities impact the marine nitrogen cycle at a range of spatial and temporal scales. Here, we demonstrate the impact of denitrifying foraminifera on the nitrogen cycle at two oxygen and nitrate contrasting stations in a fjord environment (Gullmar Fjord, Sweden). Denitrification by benthic foraminifera was determined through the combination of specific density counting per microhabitat and specific nitrate respiration rates obtained through incubation experiments using N_2O microsensors. Benthic nitrate removal was calculated from submillimeter chemical gradients extracted from 2D porewater images of the porewater nitrate concentration. These were acquired by combining the DET technique (diffusive equilibrium in thin film) with chemical colorimetry and hyperspectral imagery. Sediments with high nitrate concentrations in the porewater and oxygenated overlying water were dominated by the non-indigenous species (NIS) Nonionella sp. T1. Denitrification by this species could account for 50 %–100% of the nitrate loss estimated from the nitrate gradients. In contrast sediments below hypoxic bottom waters had low inventories of porewater nitrate, and denitrifying foraminifera were rare. Their contribution to benthic nitrate removal was negligible (<5 %). Our study showed that benthic foraminifera can be a major contributor to nitrogen mitigation in oxic coastal ecosystems and should be included in ecological and diagenetic models aiming to understand biogeochemical cycles coupled to nitrogen.

1. Introduction

Hypoxic water (i.e., [O2] < 63 μmol L^{-1}; (Diaz and Rosenberg, 2008a; Breitburg et al., 2018)) occurs frequently in bottom waters of shallow coastal seas, due to remineralization of organic matter and water stratification. Hypoxia may have large ecological effects (Levin et al., 2009; Rabalais et al., 2010; Zhang et al., 2010), such as an increase in fauna mortality (Stachowitsch, 1984; Diaz, 2001). However, certain microorganisms, e.g., bacteria and foraminifera, can perform denitrification by respiring nitrate (Risgaard-Petersen et al., 2006) and thereby survive in depleted oxygen environments. The effects of decreasing dissolved oxygen availability at spatial and temporal scales will impact biogeochemical cycles such as the nitrogen cycle (Childs et al., 2002; Kemp et al., 2005; Conley et al., 2007; Diaz and Rosenberg, 2008b; Neubacher et al., 2013; Breitburg et al., 2018). The nitrogen cycle in marine

sediments is a perpetual balance between nitrogen inputs (e.g., terrestrial runoff, atmospheric precipitations) and outputs (e.g., denitrification from sediment and water column) (Galloway et al., 2004; Sigman et al., 2009). In most semi-enclosed marine environments such as the Baltic Sea, the nitrogen loss through benthic denitrification exceeds the inputs of nitrogen through nitrogen fixation. These nitrogen sink regions of the ocean are mostly associated with anoxic regions (Gruber and Sarmiento, 1997).

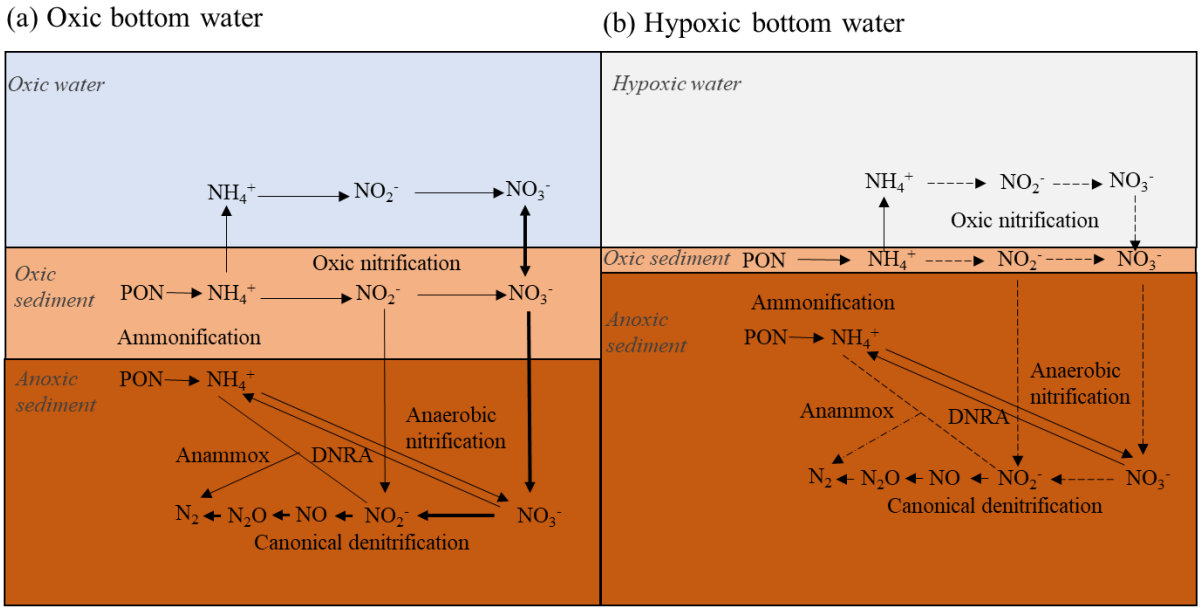

Figure 1. Simplified nitrogen cycling in marine sediments when the bottom water is oxic (a) and hypoxic (b). Chemical formulae: PON (particulate organic nitrogen), NH_4^+ (ammonium), NO_3^- (nitrate), NO_2^- (nitrite), NO (nitrogen oxide), N2O (nitrous oxide) and N_2 (nitrogen). The bold (dotted) arrows indicate reactions advantaged (reduced) by oxygen and nitrate presence (depletion). See text for more details. Modified from (Jäntti and Hietanen, 2012).

At oxic bottom water conditions (Fig. 1 a), ammonium (NH_4^+) produced from remineralization of particulate organic nitrogen (PON) in sediments, diffuses toward the oxic sediment-superficial layer and through the sediment-water interface (SWI). Nitrification is an aerobic process which converts NH_4^+ to nitrate (NO_3^-) in the oxic sediment and in the oxic water column (Rysgaard et al., 1994; Thamdrup and Dalsgaard, 2008). Total denitrification, the sum of "canonical denitrification" (NO_3^- → NO_2^- → NO → N_2O → N_2) and anammox is an anaerobic process, that converts NO_2^- or NO_3^- to N gasses, such as e.g. N_2 ((Brandes et al., 2007) and references within) generating N removal from the environment. The process typically occurs in sediment layers where oxygen is scarce (i.e. < 5 µmol L^{-1}, (Devol et al., 2008)) and is the dominant process of nitrate reduction in coastal marine sediments (Herbert, 1999;

Thamdrup and Dalsgaard, 2008). Denitrification depends on the nitrate transported from the water column and adjacent sedimentary nitrification zones. Nitrification and denitrification are thereby strongly coupled (Kemp et al., 1990; Cornwell et al., 1999). This dependency on nitrification can imply a reduction of denitrification rates as bottom water turns hypoxic, (Fig. 1 b) since nitrification rates are reduced as nitrification cannot proceed under low oxygen concentrations (~ 0 µmol L^{-1}; (Rysgaard et al., 1994; Mortimer et al., 2004)). The exception however is anoxic nitrification occurring through secondary reactions with NH_4^+ oxidation by Mn and Fe oxides (Luther et al., 1997; Mortimer et al., 2004). In reduced sediment, dissimilatory nitrate reduction to ammonium (DNRA) can also contribute to nitrate depletion leading to NO_3^- conversion into NH_4^+ instead of nitrogen (N_2) (Christensen et al., 2000) and compete denitrification.

Benthic foraminifera were the first marine eukaryotes found to perform complete denitrification (Risgaard-Petersen et al., 2006), but not all foraminifera species can denitrify (Pina-Ochoa et al., 2010). Denitrifying foraminifera species are defined in our study as species able to perform denitrification proved by denitrification rate measurements. The denitrifying species have a facultative anaerobic metabolism and store nitrate in their cells, which can be used for denitrification. *Nonionella* cf. *stella* (Charrieau et al., 2019) and references therein)) and *Globobulimina turgida* were identified as the first denitrifying foraminifera species (Risgaard-Petersen et al., 2006) but currently, nineteen denitrifying species within 9 genera are known (Glock et al., 2019). Their cell specific rate range from 7 ± 1 pmol N $indiv^{-1}$ d^{-1} to 2241 ± 1825 pmol N $indiv^{-1}$ d^{-1} (Glock et al., 2019), and the contribution of benthic foraminiferal communities to benthic denitrification lies in the range from 1 to 90 % (Kamp et al., 2015; Dale et al., 2016; Xu et al., 2017).

Recently, a non-indigenous and suspected invasive *Nonionella stella* morphotype: *Nonionella* sp. T1 was described in the North Sea region (Deldicq et al., 2019)and also reported from the Gullmar Fjord (Sweden) (< 5 %, (Polovodova Asteman and Schönfeld, 2015)). The genus *Nonionella* is potentially capable to denitrify as demonstrated for *Nonionella* cf. *stella* by Risgaard-Petersen et al. (2006). However, the NIS *Nonionella* sp. T1 morphotype, differs both morphologically and genetically from *Nonionella stella* specimens sampled previously at other localities, such as the Santa Barbara Basin (California USA) (Charrieau et al., 2018), the Kattegat and Oslo Fjord (Norway) (Deldicq et al., 2019). As a consequence, the denitrification capacity of the NIS *Nonionella* sp. T1 is unclear.

In the present study, we investigate if the suspected invasion of the NIS *Nonionella* sp. T1 has any implication for the nitrogen cycle in sections of the Gullmar Fjord (Sweden) that is subjected to hypoxic events. Several denitrifying foraminifera species are present in the Gullmar Fjord sediments: *Globobulimina turgida* (Risgaard-Petersen et al., 2006), *Globobulimina auriculata* (Woehle et al., 2018), *Stainforthia fusiformis* and *Bolivina pseudopunctata* (Gustafsson and Nordberg, 2001; Filipsson and Nordberg, 2004). The denitrification capacity of the latter two species in the Gullmar Fjord is indicative from direct measurement on affiliated species sampled at the coast of Peru, Bay of Biscay (France) and also Santa Barbara Basin (Glock et al. (2019); Piña-Ochoa et al. (2010) and (Bernhard et al., 2012)). Several species, which apparently lack the ability to denitrify, but are able to survive anoxia, are, however, also present in the sediments of the fjord. These include *Bulimina marginata*, *Cassidulina laevigata*, *Hyalinea balthica*, *Leptohalysis scotti*, *Liebusella goesi*, *Nonionellina labradorica* and *Textularia earlandi*. In the context of ecosystem function and service, it is therefore of interest if the NIS *Nonionella* sp. T1 can denitrify and thereby if its invasion into the Gullmar Fjord maintains (or elevates) the denitrification capacity of the overall foraminifera community and thus the sediment or, alternatively, if the organism share a metabolism similar to the non-denitrifying specimens above, with the possible consequence that the suspected invasion of NIS *Nonionella* sp. T1 implies reduced contribution of foraminifera based denitrification to the loss of N from the fjord.

Estimates of foraminifera contribution to benthic denitrification are limited by the high spatial and temporal variability of sediment geochemistry and distribution of denitrifying foraminifera. Marine sediments often include chemical micro-heterogeneities (Aller et al., 1998; Stockdale et al., 2009), which can be averaged out within the volume of a sediment slice. Moreover, sediment core slicing or centrifugation can induce cell lysis, which can lead to a bias in porewater nitrate concentrations (Risgaard-Petersen et al., 2006). To obtain better estimates of the chemical microenvironments at relevant submillimeter/ millimeter scales, new approaches have to be used. Recently, a 2D-DET (two Dimensions Diffusive Equilibrium in Thin-film) technique combined with colorimetry and hyperspectral imagery was developed to obtain the distribution of nitrite and nitrate in sediment porewater at millimeter resolution in two dimensions (Metzger et al., 2016). This method avoids mixing of intracellular nitrate and the nitrate contained in the sediment porewater. We will apply this technique here to get information about the distribution and concentration of nitrate at a scale relevant for modeling denitrification rates.

The general objectives of the study are (1) to characterize the density of the living benthic foraminifera at two contrasting stations in the Gullmar fjord: one with oxic bottom water and one with hypoxic bottom water. We will in particular focus on the relative abundance of the NIS *Nonionella* sp. T1 (2) to investigate if this NIS *Nonionella* sp. T1 can denitrify and (3) quantify its eventual contributions to benthic denitrification in the sediments. On the basis of the results we will discuss the probable future impact of the NIS *Nonionella* sp. T1 on the foraminifera fauna and the nitrogen cycle in the Gullmar Fjord.

2. Material and Methods

2.1 Site description and sampling conditions

The Gullmar Fjord is 28 km long, 1-2 km wide and located on the Swedish West coast (Fig. 2). The fjord undergoes fluctuations between cold and temperate climates (Svansson, 1975; Nordberg, 1991; Polovodova Asteman and Nordberg, 2013; Polovodova Asteman et al., 2018). The fjord is stratified (Fig. 2 d) in four water masses (Svansson, 1984; Arneborg, 2004). Hypoxia events in the fjord have been linked to the influence of the North Atlantic Oscillation (NAO) (Nordberg et al., 2000; Björk and Nordberg, 2003; Filipsson and Nordberg, 2004). Several monitoring stations are located in the fjord: Släggö (65 m water depth), Björkholmen (70 m water depth) and Alsbäck (117 m water depth), the hydrographic and nutrient data were obtained from the Swedish Meteorological and Hydrological Institute's (SMHI) publicly available data-base SHARK (SMHI, 2020). Since 2010, the threshold of hypoxia ($[O_2] < 2$ mg L^{-1}, i.e. 63 µmol L^{-1}) in Alsbäck station (red squares, Fig. 3) is reached typically in late autumn and winter. Deep-water exchanges usually occur in late winter-early spring. However, the duration of hypoxia varies between years and hypoxia events occurred in the summer 2014 and 2015, due to lack of deep-water exchange. The frequency of hypoxic events has increased in the fjord (Nordberg et al., 2000; Filipsson and Nordberg, 2004).

Two sampling cruises were conducted in the Gullmar Fjord on board R/V *Skagerak* and *Oscar von Sydow*, respectively. The 2017 cruise (GF17) took place between 14th and 15th November 2017 and two stations were sampled (GF17-3 and GF17-1, Fig. 2 c and d) to define the living foraminifera fauna and the sediment geochemistry at two contrasted stations. The 2018 cruise (GF18) took place on the 5th September 2018 with the focus to collect living

Nonionella sp. T1 for O_2 respiration and denitrification rates measurements. Only one station (at the same position as GF17-3) was sampled.

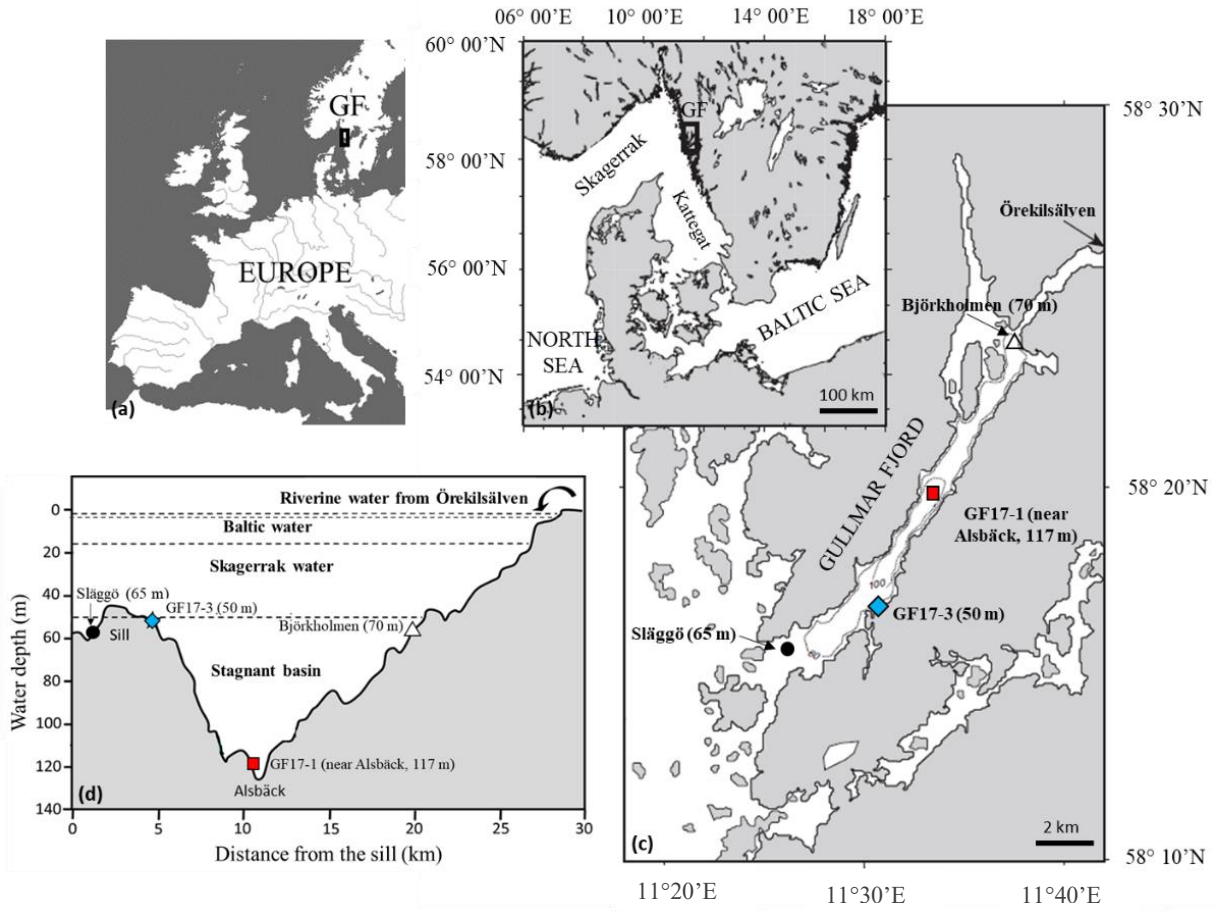

Figure 2. (a-c) Location of studied stations in the Gullmar Fjord (Sweden); blue diamond: GF17-3 oxic station (50 m water depth); red square: GF17-1 hypoxic station (117 m water depth); dark circles: monitoring stations Släggö (65 m water depth) and Björkholmen (70 m water depth). (d) Transect from the sill with the four Gullmar Fjord water masses and the studied stations (modified from Arneborg et al., 2004).

GF17-3 (50 m water depth) is located closest to the mouth of the fjord (58°16'50.94"N/ 11°30'30.96"E) with bottom waters from Skagerrak (blue diamond, Fig. 3) and GF17-1 (117 m water depth) close to the deepest part of the fjord (58°19'41.40"N/11°33'8.40"E) near Alsbäck monitoring station in the middle of the stagnant basin (red square, Fig. 3). In November 2017, CTD profiles indicated the water mass structures at both stations (Fig. S1). Bottom water at GF17-3 station was oxic with a dissolved oxygen content of 234 µmol L^{-1}. The dissolved oxygen content decreased strongly with depth at the GF17-1 station reaching 9 µmol L^{-1} at the seafloor, which is below the severe hypoxia threshold.

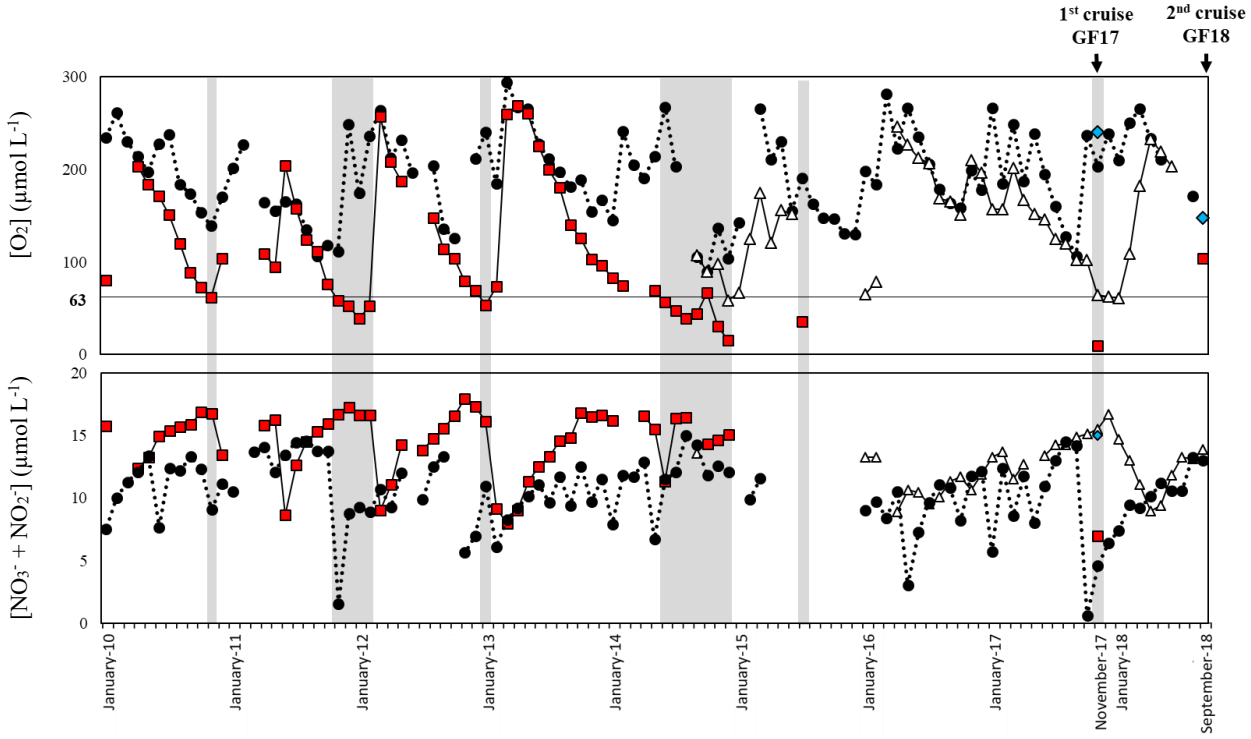

Figure 3. Record from January 2010 to September 2018 of bottom water oxygen ([O_2]) and nitrite + nitrate ([NO_3^- + NO_2^-]) measurements from the monitoring stations Släggö (65 m water depth; black dot), Björkholmen (70 m water depth; white triangle) and the sampling stations GF17-1 (Alsbäck, 117 m water depth; red square) and GF17-3 (50 m water depth; blue diamond). The arrows indicate the date of the two sampling cruises: the 2017 cruise (14th, 15th November 2017) and the 2018 cruise (5th September 2018). The grey zones indicate hypoxic periods with a threshold of [O_2] < 63 µmol L^{-1}.

2.2 Foraminifera sampling and processing

During the 2017 cruise, two sediment cores per station (1A, 1C and 3A, 3C for GF17-1 and GF17-3 stations respectively) were immediately subsampled with a smaller cylindrical core (Ø 8.2 cm) and sliced every 2 mm from the sediment surface to 2 cm depth and every 5 mm from 2 cm to 5 cm depth to study living foraminifera distribution. The samples were incubated without light for 10–19 hours in ambient seawater with Cell Tracker Green (CMFDA, 1 mM final concentration) at *in situ* temperature (Bernhard et al., 2006) and then fixed with ethanol 96°. Fixed samples were sieved (> 355, 150, 125 and 100 µm) and the > 100 µm fraction, the most commonly fraction used for foraminiferal analyses in the Gullmar Fjord (see Charrieau et al., 2018 and references therein) was examined using an epifluorescence microscope equipped for fluorescein detection (i.e., 470 nm excitation; Olympus SZX13). In the present study, the foraminifera distribution will be described highlighting the NIS *Nonionella* sp. T1.

2.3 Geochemical sampling and processing

One core from the shallow GF17-3 station was reserved for O_2 microelectrode profiling. Oxygen concentration was measured in the dark with a Clark electrode (50 µm tip diameter, Unisense ®, Denmark) within the first 5 mm depth at a 100 µm vertical resolution. Due to technical problems, no oxygen profiling was done at the GF17-1 station.

One core per station was dedicated for geochemical analyses; they were carefully brought to Lund University (Sweden) and stored at *in situ* temperature (10°C) until further analysis the next day. Overlaying water of the GF17-3 core was gently air bubbled to maintain the oxygenated conditions recorded at this station. Hypoxia in the overlaying water of the GF17-1 core was maintained by bubbling with N_2 gas passed through a solution of carbonate/bicarbonate to avoid pH rise due to degassing of CO_2.

Nitrite/Nitrate were analyzed using the 2D-DET method from Metzger et al. (2016). In brief, for each core, a DET (Diffusive Equilibrium in Thin films) gel probe (16 cm x 6.5 cm and 0.1 cm thickness) was hand-made prepared. The gel probe was inserted into the sediment and left for 5 hours to allow diffusive equilibration between the gel and porewaters. After equilibration, the gel was removed of the core and laid on a first NO_2^- reagent gel. After 15 minutes at ambient temperature a pink coloration must appear where nitrite is detected. A reflectance image of the nitrite gels was taken with a hyperspectral camera (HySpex VNIR 1600). The next step was to convert existing nitrate into nitrite with the addition of a reagent gel of vanadium chloride (VCl_3). After 20 minutes at 50°C, additional pink coloration is interpreted as porewater nitrate concentration. Followed by the acquisition of another hyperspectral image and the conversion into false colors through a calibrated scale of concentrations, the final gel images were cropped to avoid border effects. Each pixel (190 µm x 190 µm) was decomposed as a linear combination of the logarithm of the different end-member spectra using ENVI software (unmixing function) (Cesbron et al., 2014; Metzger et al., 2016). Nitrite and nitrate detection limits are 1.7 µmol L^{-1} (Metzger et al., 2016).

2.4 Oxygen and nitrate respiration rate measurements of the NIS *Nonionella* sp. T1

The two cores sampled during the 2018 cruise (GF18) at the shallower GF17-3 station were carefully transported and stored at *in situ* temperature (8 °C) for three days at the

Department of Geosciences, Aarhus University (Denmark). *Nonionella* sp. T1 specimens were picked at *in situ* temperature and collected in a Petri dish, containing a thin layer of sediment (32 µm) to check their vitality. Only living, active *Nonionella* sp. T1 specimens were picked using a brush and cleaned several times with micro-filtered, nitrate-free artificial seawater.

Oxygen respiration rates were measured, following the method developed by (Høgslund et al., 2008) using a Clark type oxygen microsensors (50 µm tip diameter, Unisense ®, Denmark) (Revsbech, 1989). The O_2 sensor was calibrated at *in situ* temperature (8 °C) in 0.7 M alkaline ascorbate solution (zero O_2) and air-saturated sea water. Then, a pool of five living *Nonionella* sp. T1 was transferred into a glass microtube (inner diameter 0.5 mm, height 7.5 mm), that was fixed inside a 20 ml test tube mounted in a glass-cooling bath (8 °C). A motorized micromanipulator was used to measure O_2 concentration profiles along a distance gradient that ranged from 200 µm of the foraminifera to 1200 µm using 100 µm steps. Seven O_2 concentration profiles were generated with one incubation containing the pool of *Nonionella* sp. T1. Negative controls were done by measuring O_2 rates from microtube with empty foraminifera shells and blanks with empty microtube. Oxygen respiration rates were calculated with Fick's first law of diffusion, J = -D * dC/dx, where J is the flux, dC/dx is the concentration gradient obtained by profiles and D is the free diffusion coefficient of oxygen at 8 °C for a salinity of 34 (1.382×10^{-5} cm^{-2} s^{-1}, Ramsing and Gundersen, 1994). The seven O_2 respiration rates were calculated as the product of the flux by the cross section area of the microtube (0.196 mm^2). Then, the average O_2 respiration rate was divided by number (n = 5) of *Nonionella* sp. T1 present in the microtubes to obtain the respiration rate per individual.

The same pool of *Nonionella* sp. T1 specimens as for the O_2 respiration measurements was used for denitrification measurements. These measurements were performed in the microtubes as described in (Høgslund et al., 2017). A N_2O microprobe (Andersen et al., 2001) with a 50 µm tip diameter was used to measure the N_2O concentration profile, that developed in the chamber after acetylene inhibition of the final step in the denitrification process ($N_2O \rightarrow N_2$). Calibration of the sensor was performed using the standard addition method by successive injections of a N_2O saturated solution in order to have 14 µM steps of final concentration. The cell specific N_2O production rate was calculated from the N_2O flux (estimated from the concentration gradient and Fick's first law), the surface area of the microtube (0.25 mm^2) and the number of *Nonionella* sp. T1 in the tubes (n=5) as described above. Rates are reported with the unit pmol N $indiv^{-1}$ d^{-1}.

Since O_2 respiration and denitrification rates are linked to cytoplasmic volumes or biovolumes (BV) (Geslin et al., 2011; Glock et al., 2019), the specimens from the pool of *Nonionella* sp. T1 were measured (width (a) and length (b), Fig. 4) using a micrometer mounted on a Leica stereomicroscope (MZ 12.5) to estimate the average BV. The volume of each shell was estimated by using the best resembling geometric shape, a spheroid prolate ($V = \frac{4}{3}\pi\left(\frac{a}{2}\right)^2\left(\frac{b}{2}\right)$). Then, according to (Hannah et al., 1994), 75 % of the measured entire volume of the shell was used as the estimated cytoplasmic volume. Five *Nonionella* sp. T1 specimens sampled during the 2017 cruise (GF17, study of the fauna) were also measured to compare their average size with the size of the specimens sampled during the 2018 cruise (GF18, denitrification rate measurements).

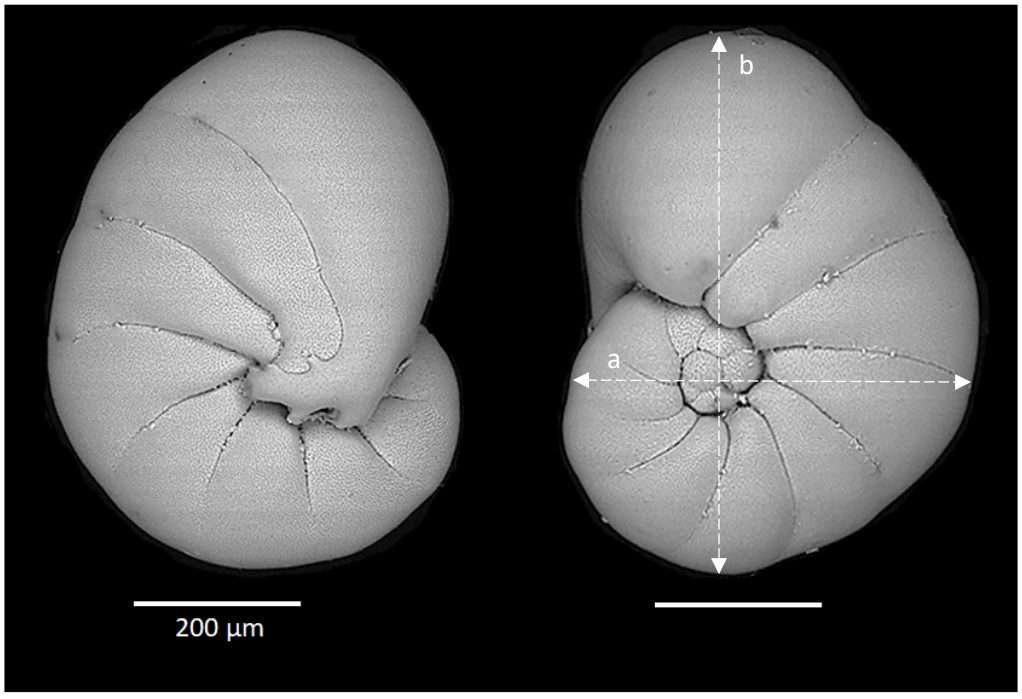

Figure 4. Scanning Electronic Microscope images of a Nonionella sp. T1 from the GF17-3 oxic station in the Gullmar Fjord. White lines (a, b) correspond to measured distances serving for a spheroid prolate volume model.

2.5 Contributions of the NIS *Nonionella* sp. T1 to benthic denitrification

Benthic denitrification was estimated using the 2D nitrate concentrations obtained with the DET technique. An average 1D nitrate profile was obtained by calculating the mean of 290 vertical profiles ((5.5 cm width x 1 pixel) / 0.019 cm for 1-pixel size) extracted from the 2D concentration image. Then, nitrate production and consumption zones were calculated with

PROFILE software (Berg et al., 1998). With the assumption that nitrate consumption was equivalent to denitrification, the benthic denitrification rate was calculated by integrating nitrate consumption over the depth.

The denitrification activity of the NIS *Nonionella* sp. T1 population was calculated using the specimen abundances in the nitrate consumption zones and their cell specific activity. The size of the *Nonionella* sp. T1 specimens sampled during the two cruises, however, differed markedly (Table 1). The cell specific denitrification rate of denitrifying foraminifera is correlated with their size according to the model: ln (y) = 0.68 ln (x) – 5.57, where y is the denitrification rate (pmol ind^{-1} d^{-1}) and x is the shell BV (μm^3) (Geslin et al., 2011; Glock et al., 2019; Equation S1) and we therefore used this model to correct the denitrification estimates for size specific variations.

A maximum estimate of the contribution of the NIS *Nonionella* sp. T1 population to benthic denitrification was obtained from the ratio of the denitrification activity of *Nonionella* sp. T1 population and the benthic denitrification rate estimated from the porewater nitrate concentration profiles. This presumes that *Nonionella* sp. T1 exclusively use nitrate dissolved in the sediment porewater as source for denitrification (calculation approach A). A minimum estimate of the contribution of *Nonionella* sp. T1 population to benthic denitrification was obtained from the ratio between the denitrification activity of *Nonionella* sp. T1 population and the benthic denitrification rate estimated from porewater nitrate concentration profiles plus the denitrification activity of *Nonionella* sp. T1 population. This presumes that *Nonionella* sp. T1 exclusively use intracellular nitrate as source for denitrification (calculation approach B).

Table 1. Total shell volume (μm^3) and the biovolume (BV, μm^3) corresponding to 75 % of the total shell volume measured on the pool of five Nonionella sp. T1 from the 2017 and the 2018 cruises in the Gullmar Fjord. Abbreviations: sd (standard deviation), ind. (individual).

Nonionella sp. T1	1st cruise total shell volume	1st cruise BV	2nd cruise total shell volume	2nd cruise BV
ind. 1	6.7 10^{+06}	5.0 10^{+06}	3.1 10^{+06}	2.3 10^{+06}
ind. 2	4.5 10^{+06}	3.4 10^{+06}	2.4 10^{+06}	1.8 10^{+06}
ind. 3	5.1 10^{+06}	3.8 10^{+06}	1.4 10^{+06}	1.0 10^{+06}
ind. 4	4.9 10^{+06}	3.7 10^{+06}	9.2 10^{+05}	6.9 10^{+05}
ind. 5	5.8 10^{+06}	4.4 10^{+06}	6.2 10^{+05}	4.7 10^{+05}
Average (μm^3)	5.4 10^{+06}	4.0 10^{+06}	1.7 10^{+06}	1.3 10^{+06}
sd (μm^3)	0.8 10^{+06}	0.6 10^{+06}	1.0 10^{+06}	0.7 10^{+06}

3. Results

3.1 The NIS *Nonionella sp.* T1 oxygen and nitrate respiration rates in the Gullmar Fjord

The O_2 respiration rate measured from the pool of *Nonionella* sp. T1 specimens collected during the 2018 cruise (GF18) was 169 ± 11 pmol O_2 indiv.$^{-1}$ d^{-1} with an average BV of 1.3 ± 0.7 10^{+06} µm^3 (BV details, Table 1). The denitrification rate measured from the same pool of specimens was 21 ± 9 pmol N indiv^{-1} d^{-1}.

The *Nonionella* sp. T1 average BV of the specimens collected during the 2017 cruise (GF17-3) was 4.0 ± 0.6 10^{+06} µm^3, i.e. more than three times the *Nonionella* sp. T1 average BV of the 2018 samples (1.3 ± 0.7 10^{+06} µm^3). As denitrification rates and foraminifera BV are related (see method), the measured denitrification rate was corrected using the BV of *Nonionella* sp. T1 from the 2017 cruise. Hence, the *Nonionella* sp. T1 corrected denitrification rate was 38 ± 8 pmol N indiv.$^{-1}$ d^{-1} (Equation S1).

3.2 The NIS *Nonionella* sp. T1 and foraminifera fauna regarding porewater nitrate micro-distribution

The bottom water at GF17-3 station was oxic (Fig. S1, [O_2] = 234 µmol L^{-1}) and the measured oxygen penetration depth (OPD) in the sediment was 4.7 ± 0.2 mm (n = 3). No nitrite was revealed on the gel (< 1.7 µmol L^{-1}), only nitrate was detected. Bottom water average NO_3^- concentration was 14.6 ± 2.3 µmol L^{-1} and nitrate concentration decreased with depth in the sediment (Fig. 5 c, d). Nitrate concentrations ranged between 13.1 ± 3.2 to 11.7 ± 3.4 µmol L^{-1}, from the SWI to the OPD. Nitrate concentrations decreased strongly under the OPD from 11.7 ± 3.4 to 2.8 ± 0.9 µmol L^{-1} at 4.0 cm depth. From 4.0 to 5.0 cm depth, NO_3^- concentration was very low with an average value of 2.7 ± 0.9 µmol L^{-1} (Fig. 5 c, d). The PROFILE parameters (Berg et al., 1998) used on laterally averaged nitrate porewater vertical distribution of both stations are available in Table S1. Thus, the PROFILE modelling of the averaged nitrate porewater profile revealed one nitrification zone from 0 to 1.2 cm depth and two denitrifying zones (red line, Fig. 5 d). The first denitrification zone occurred between 1.2 to 3.5 cm depth with a nitrate consumption of 3.92 E^{-05} nmol cm^{-3} s^{-1} and the second smaller consumption zone was from 3.5 to 5 cm depth (1.53 E^{-06} nmol cm^{-3} s^{-1}). The total denitrification rate from 1.2 to 5 cm depth was 4.07 E^{-05} nmol cm^{-3} s^{-1} (Fig. 5 d).

The total densities of living foraminifera were similar between the cores GF17-3A and 3C (Ø 8.2 cm, 5 cm depth) with 1256 individuals and 1428 individuals, respectively (Fig. 5 a and b; Table S2, GF17-3A and 3C). *Nonionella* sp. T1 was the main denitrifying species, accounting for 34 % of the total living fauna in the core GF17-3A and 74 % in GF17-3C (Fig. 5 a, b; Table S3). One other candidate for denitrification, *Stainforthia fusiformis*, was in minority: 1 % of the total fauna in both cores (Fig. 5 a, b; Table S3, GF17-3A and 3C). The other known denitrifying species previously reported in the Gullmar Fjord, *Globobulimina turgida* (Risgaard-Petersen et al., 2006) and *Globobulimina auriculata* (Woehle et al., 2018) were absent. Three non-denitrifying species (Pina-Ochoa et al., 2010; Xu et al., 2017; Glock et al., 2019) were dominant in the cores GF17-3A and 3C: *Bulimina marginata* (37 and 5 %, respectively), *Cassidulina laevigata* (9 and 5 %) and *Leptohalysis scotti* (11 and 9 %).

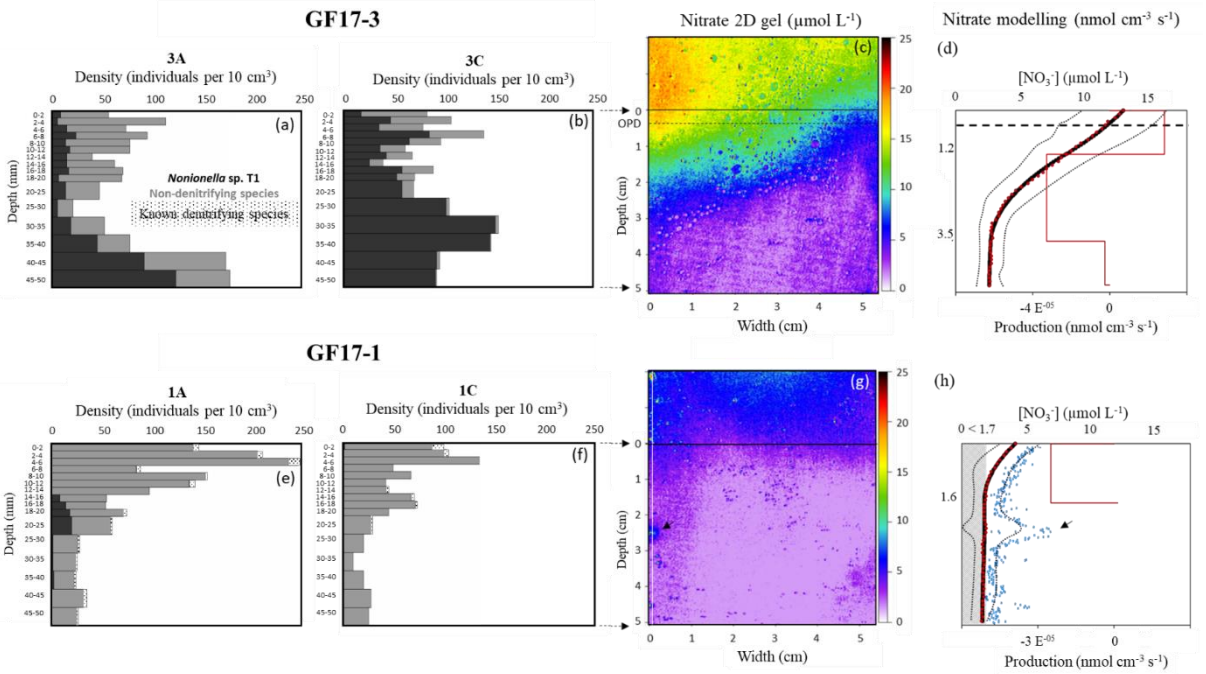

Figure 5. Micro-distributions of living foraminifera densities in GF17-3 oxic station (a, b) and in GF17-1 hypoxic station (e, f). Nonionella sp. T1 specimens are in black, the sum of the non-denitrifying species in grey and the small dots (e, f) show the other denitrifying species (known and potential candidates). The maps of porewater nitrate 2D gels are presented for the stations GF17-3 (c) and GF17-1 (g). The SWI is represented by a black line at 0 cm depth (c, g) and the OPD is represented by the dashed line in bold at 4.7 ± 0.2 mm depth (c). Nitrate 1D profiles (d and h, black dots) are calculated using the average value of each pixel line of the nitrate distribution image (290 pixels wide), the standard deviation is represented by two fine dotted lines. The corresponding best-fitting concentration profiles (red dots, d and h) and the production zones (red line) are modelled with PROFILE software. The 1D profile corresponding to x = 1 mm (white line, g) is represented with a blue square profile (h) and the deep nitrate spot is indicated by a black arrow. The hatched grey zone (h) represents the detection limit of the nitrate 2D gel (<1.7 µmol L^{-1}).

The density and the micro-distribution of *Nonionella* sp. T1 differed between the two cores (Fig. 5 a and b; Table S2, GF17-3A and 3C)..*Nonionella* sp. T1 relative abundance accounted for 18 % and 50 % of the fauna in the nitrification zone (from the SWI to 1.2 cm depth) for the cores GF17-3A and 3C respectively (Table S3). In the main denitrifying zone (from 1.2 cm to 3.5 cm), the *Nonionella* sp. T1 relative abundance represented 27 % of the fauna for the core GF17-3A and 78 % for the core GF17-3C. In the second denitrifying zone, the *Nonionella* sp. T1 relative abundance increased from 3.5 to 5 cm depth and dominated the fauna with relative abundances of 60 % and 98 % (GF17-3A and 3C respectively). The relative abundance of the denitrifying candidate, *Stainforthia fusiformis*, was a minor component in each zones of both cores and did not exceed 2 % (Table S3, GF17-3A and 3C). The three non-denitrifying species (e.g. *B. marginata*, *C. laevigata* and *L. scotti*) also dominated the fauna of both cores (Table S2 and S4). From the SWI to 1.2 cm depth, *B. marginata* accounted for 42 % and 12 %, *C. laevigata* 16 % and 13 % and *L. scotti* 6 % and 11 %, for the cores GF17-3A and 3C respectively. In the first denitrifying zone (1.2-3.5 cm depth), *B. marginata* accounted for 34 % and 2 %, *C. laevigata* for 7 % and 2 % and *L. scotti* for 25 % and 13 % (GF17-3A and 3C respectively). In the second denitrifying zone (3.5-5 cm depth), *B. marginata* accounted for 34 % and 0 %, *C. laevigata* was absent and *L. scotti* 5 % and 1 % (GF17-3A and 3C respectively).

Due to severe hypoxia at the GF17-1 station, oxygen was assumed to be below detection limit within the sediment. No nitrite was detected at this station (< 1.7 µmol L^{-1}). Average NO_3^- concentration in the bottom water reached 5.7 ± 1.0 µmol L^{-1} (Fig. 5 g and h). Nitrate concentrations decreased from the SWI (4.2 ± 1.0 µmol L^{-1}) to 1.6 cm depth (1.8 ± 0.6 µmol L^{-1}) and then average nitrate concentration remained below the detection limit (1.7 µmol L^{-1}). However, a micro-environment with higher nitrate concentration was visible on the left part of the gel between 2.0 and 3.0 cm depth. A 1D vertical profile passing through this micro-environment (white line, Fig. 5 g) was extracted from the 2D image and the maximal nitrate concentration of this patch was above the detection limit with a value of 6.5 µmol L^{-1} at 2.3 cm depth (blue square profile, Fig. 5 h). The PROFILE modelling (Table S1) of the laterally averaged nitrate vertical distribution revealed at the sampling time one denitrifying zone from the SWI to 1.6 cm depth with a nitrate consumption of 2.71 E^{-05} nmol cm^{-3} s^{-1} (red line, Fig. 5 h). No PROFILE modelling was done under 1.6 cm depth, because nitrate concentration was below the detection limit (hatched grey zone, Fig. 5 h).

Living foraminifera showed a large difference in both species distribution and total densities between the two cores GF17-1A and 1C (Fig. 5 e, f; Table S2) with 1457 individuals and 786 individuals respectively (Ø 8.2, 5 cm depth). *Nonionella* sp. T1 represented a low relative abundance of the total fauna with 5 % for the core GF17-1A and was almost absent (1 %) for the core GF17-1 C (Table S3). The known denitrifying *G. auriculata* was minor in the fauna with relative abundances of 1 % and 2% (GF17-1A and 1C respectively). The denitrifying candidate *S. fusiformis* was also found in both cores reaching only 3% of the total fauna (Figure 5 e, f; Table S3). The other denitrifying candidate *B. pseudopunctata,* was almost absent of the total fauna with relative abundances of 0 % and 2 % for the cores GF17-1A and GF17-1C respectively (Table S3). The same three non-denitrifying species observed in oxic station were also dominant for both cores GF17-1A and 1C: *B. marginata* (64 and 30 %), *C. laevigata* (16 and 15 %) and *L. scotti* (4 and 36 %).

In the denitrifying zone (0-1.6 cm), *Nonionella* sp. T1 relative abundance was rare (2 %) for the core GF17-1A) and almost absent from the fauna for the core GF17-1C. For the core GF17-1A, *Nonionella* sp. T1 relative abundance reached 26 % of the fauna between 1.6 and 2.5 cm depth (Fig. 5 e, GF17-1A), whereas it was almost absent from the rest of the core GF17-1A and it was absent from the core GF17-1C (Table S3). For the cores GF17-1A and 1C, *S. fusiformis* reached respectively 2 % and 3 % in the denitrifying zone (0-1.6 cm). Under the denitrifying zone (1.6-5 cm), *S. fusiformis* represented 4 and 1 % of the fauna (GF17-1A and 1C respectively). The three other non-denitrifying species dominated both cores in the denitrifying zone (0-1.6 cm): *B. marginata* accounted for 66 % and 35 %, *C. laevigata* 19 % and 19 % and *L. scotti* 4 % and 24 % for the cores GF17-1A and 1C respectively. From 1.6 to 5 cm depth, *B. marginata* accounted for 61 % and 11 %, *C. laevigata*for 5 % and 2 % and *L. scotti* for 6 % and 75 % (GF17-1A and 1C respectively).

4. Discussion

4.1 The NIS *Nonionella* sp. T1 density in comparison with other species from the Gullmar Fjord

The presence and relative abundance of the NIS *Nonionella* sp. T1 in the Gullmar Fjord and in the Skagerrak-Kattegat strait have been documented during the last decades. The earliest SEM observations of specimens resembling *Nonionella* sp. T1 morphotype in the deepest part

of the fjord date back to summer 1993 (identified as *Nonionella turgida*, (Gustafsson and Nordberg, 2001)). The invasive characteristics of *Nonionella stella* were firstly revealed by Polovodova Asteman and Schönfeld, (2015). Then, *Nonionella stella* was identified as *Nonionella* sp. T1 morphotype also described as a NIS and potentially invasive species in the Oslofjord by Deldicq et al. (2019). The estimated introduction date of *Nonionella* sp. T1 into the deepest part of the Gullmar Fjord is 1985 according to Polovodova Asteman and Schönfeld, (2015). The relative abundance of *Nonionella* sp. T1 in the deepest fjord station was less than 5 % between 1985 and 2007 (Polovodova Asteman and Schönfeld, 2015 and references within). At the GF17-1 hypoxic station, the *Nonionella* sp. T1 relative abundance was between 1-5 % (Table S3, GF17-1A and 1C). Thus, the *Nonionella* sp. T1 relative abundance in the deepest part of the fjord seems to remain stable. In contrast to GF17-1 station, the GF17-3 oxic station was sampled for the first time in this study. In this station closer to the mouth of the fjord than GF17-1, the relative abundance of *Nonionella* sp. T1 varied between 34 and 74 % (Table S3, GF17-3A and 3C). Previous studies showed an increase in the relative abundance of *Nonionella* sp. T1 morphotype in the Skagerrak-Kattegat region (near the entrance of the Gullmar Fjord). The *Nonionella* sp. T1 represented 10 % of the fauna in June 2013 (Polovodova Asteman and Schönfeld, 2015). The Öresund strait linking the North Skagerrak, the Kattegat and the Baltic Sea showed an increase in *Nonionella* sp. T1 relative abundance from 1 % to 14 % observed between 1998 and 2009 (Charrieau et al., 2019). The foraminifera fauna in the Gullmar Fjord changed over the last decades and *Nonionella* sp. T1 seems to become an invasive species in the Gullmar Fjord oxic shallow water area.

The foraminifera fauna found at the GF17-1 station in the deepest part of the fjord differed from previous studies (Nordberg et al., 2000; Filipsson and Nordberg, 2004; Risgaard-Petersen et al., 2006; Polovodova Asteman and Nordberg, 2013; Polovodova Asteman and Schönfeld, 2015). Indeed, until the early 1980s, the foraminifera fauna in the deepest part of the fjord was dominated by a typical Skagerrak – Kattegat fauna (*Bulimina marginata, Cassidulina laevigata, Hyalinea balthica, Liebusella goësi, Nonionellina labradorica* and *Textularia earlandi*) (Nordberg et al., 2000). However, the fauna changed. *S. fusiformis* and *B. pseudopunctata* became the major species (Nordberg et al., 2000; Filipsson and Nordberg, 2004). Further studies by Polovodova Asteman and Nordberg (2013) demonstrated that at least until 2011 *S. fusiformis, B. pseudopunctata* and *T. earlandi* dominated the fauna. Foraminifera fauna described in the present study differs. In November 2017 *S. fusiformis* did not exceed 3 % of the fauna (Table S3, GF17-1A and 1C), *B. pseudopunctata* reached only 2 % in the core GF17-

1C (Table S3, GF17-1C) and *T. earlandi* was a minor species < 1 %. Then, in November 2017, *B. marginata, C. laevigata* and *L. scotti* were the dominant species in the fjord. The *Elphidium clavatum-selseyensis* species complex (following the definition from Charrieau et al., 2018), *H. baltica*, *N. labradorica*, and *T. earlandi* were present with a low relative abundance (< 5 %, Table S3). Namely, *G. turgida* reached 37 % of the foraminifera fauna in August 2005 at the deepest station (Risgaard-Petersen et al., 2006); whereas in November 2017 this species relative abundance decreased to become a minor species of the assemblage. However, such trend for *S. fusiformis* and *B. pseudopunctata* must be interpreted with caution since our study used the > 100 µm fraction whereas some of the previous studies used the > 63 µm fraction. We also wet picked the specimens and used Cell Tracker Green to identify living foraminifera, which might affect the results compared to Rose Bengal studies of dry sediment residuals.

The relative abundance of the potential invasive *Nonionella* sp. T1 in 2017increased compared to the study of Polovodova Asteman and Schönfeld (2015) in the oxic part of the fjord. It is also noteworthy that the two non-denitrifying species *B. marginata* and *C. laevigata* described as typical species of the Skagerrak-Kattegat fauna (Filipsson and Nordberg, 2004) increased markedly in the fjord as well. It is evident that the foraminifera fauna in the Gullmar Fjord is presently very dynamic with considerable species composition shifts probably following seasonal water body stratification and consecutive oxygen depletion occurring in the fjord (Fig. 3).

4.2 Foraminifera ecology considering porewater nitrate micro-distribution

For the first time a core sampled in the Gullmar fjord shows *Nonionella* sp. T1 as a dominant species. This observation was made under oxic conditions at GF17-3 station (50 m depth) during November 2017 (Fig. 5 a, b; Table S2; S4). *Nonionella* sp. T1 density increased with sediment depth below the sedimentary oxic zone (Fig. 5 a – d; Table S2), which could be explained by its preference to respire nitrate rather than oxygen. This would be in agreement with the hypothesis of using nitrate as the preferred electron acceptor suggested by Glock et al. (2019). *Nonionella* sp. T1 distribution could be explained by its capacity to store nitrate intracellularly before porewater nitrate is denitrified by other organisms such as bacteria. In detail, in the upper part of the sediment, within the oxic zone, *Nonionella* sp. T1 would respire oxygen at the rate of 169 ± 11 pmol O_2 $indiv^{-1}$ d^{-1}(Fig. 5 c and d). Below the oxygen penetration

depth (from 4.7 ± 0.2 mm to 3.5 cm), *Nonionella* sp. T1 could store and respire the ambient nitrate at the rate of 38 ± 8 pmol N $indiv^{-1}$ d^{-1}. Further down, where the nitrate porewater is depleted (Fig. 5 c, d; from 3.5 to 5 cm depth), *Nonionella* sp. T1 would respire on its intracellular nitrate reserves to survive (Fig. 5 a, b; from 3.5 to 5 cm depth). When the intracellular nitrate reserve runs out, *Nonionella* sp. T1 would be able to migrate to an upper zone where nitrate is still present in the sediment to regenerate its intracellular nitrate reserve (Fig. 5 a, b; from 1.2 to 3.5 cm depth).

Hypoxia occurred approximately at least one month before the sampling cruise in the deepest part of the fjord (Fig. 3). When hypoxia is extended to the water column, nitrification both in the water column and the sediment is reduced or even stopped, as oxygen is almost absent (Fig. 1 b; Childs et al., 2002; Kemp et al., 2005; Conley et al., 2007; Jäntti and Hietanen, 2012). Under this condition, the coupled nitrification-denitrification processes are strongly reduced (Kemp et al., 1990). At the GF17-1 station, no nitrification in superficial sediment was showed by our data and nitrate was low but still detectable in the bottom water. Nitrate can diffuse from the water column into the sediment, and thereby generate the denitrification zone as modelled by PROFILE between the SWI and 1.6 cm depth (Fig. 5 h).

The rare presence of the NIS *Nonionella* sp. T1 and other denitrifying species as *Globobulimina auriculata, Bolivina pseudopunctata* and *Stainforthia fusiformis* in the hypoxic station indicates that sediment chemical conditions turned unfavorable towards denitrification during prolonged hypoxia. Instead, the non-denitrifying species *Bulimina marginata, Cassidulina laevigata,* and *Leptohalysis scotti* dominated in this hypoxic environment. Their survival could be due to seasonal dormancy (Ross and Hallock, 2016; LeKieffre et al., 2017) and their ability to release propagules which can disperse and grow when environmental conditions turn favorable again (Alve and Goldstein, 2003). The suspected deep nitrification zone (blue square profile, Fig. 5 h) could indicate the presence of nitrate micro-niches deeper in the sediment and might explain the patchy distribution of *Nonionella* sp. T1 also at the hypoxic site (see Fig. 5 e; Table S2, GF17-1A). Therefore, deep nitrate production in these micro-environments could favor the presence of *Nonionella* sp. T1, which can be attracted by this nitrate source of electron acceptor to respire (Nomaki et al., 2015; Koho et al., 2011). This deep nitrification zone could be the result of macrofaunal activity (burrowing activity) that introduce some oxygen deeper into anoxic sediment (Aller, 1982; Karlson et al., 2007; Nizzoli et al., 2007; Stief, 2013; Maire et al., 2016). This nitrification zone could also be due to an

anaerobic process. The Gullmar Fjord is Mn-rich (Goldberg et al., 2012) and metal-rich particles can be bio-transported into the anoxic sediment, thus allowing ammonium oxidation into NO_3^- by Mn and Fe-oxides in the absence of oxygen deeper in the sediment (Aller, 1994; Luther et al., 1997).

Table 2. Summary of the NIS Nonionella sp. T1 contributions to benthic denitrification in the Gullmar Fjord. The porewater denitrification zones come from PROFILE modelling (Fig. 5 d, h). To estimate the contributions of Nonionella sp. T1 the number of counted specimens per zones was used. Two different approaches were used to estimate the contribution of Nonionella sp. T1: (A) Nonionella sp. T1 denitrification rate divided by nitrate porewater denitrification rate; (B) Nonionella sp. T1 denitrification rate divided by nitrate porewater denitrification rate plus Nonionella sp. T1 denitrification rate. The calculations are detailed in Equation S2.

Stations	Sediment depth interval of denitrification (cm)	*Nonionella* sp. T1 (counted specimens per zone)	Nitrate porewater denitrification rates (nmol cm^{-3} s^{-1})	*Nonionella* sp. T1 denitrification rates (nmol cm^{-3} s^{-1})	*Nonionella* sp. T1 contribution (%), approach A	*Nonionella* sp. T1 contribution (%), approach B
GF17-3A	1.2 to 5	841	4.07 E^{-07}	1.90 E^{-05}	47	32
GF17-3C	1.2 to 5	1807	4.07 E^{-07}	4.06 E^{-05}	100	50
GF17-1A	0 to 1.6	3	2.71 E^{-05}	6.72 E^{-08}	0	0
GF17-1C	0 to 1.6	12	2.71 E^{-05}	2.69 E^{-07}	1	0

4.3 Contributions and potential impacts of the NIS *Nonionella* sp. T1 to benthic denitrification in the Gullmar Fjord

Considering that *Nonionella* sp. T1 is denitrifying the nitrate from sediment porewater (approach A, Table 2; see method 2.5), its contribution to benthic denitrification in the oxic station would be 47 % in the core GF17-3A and would reach 100 % in the core GF17-3C. If we consider that *Nonionella* sp. T1 uses its intracellular nitrate pool for denitrification (approach B), its contribution to benthic denitrification would be 32 % in the core GF17-3A and would reach 50 % in the core GF17-3C (Table 2). These two calculation approaches highlight the difficulties and the importance of knowing the concentration of environmental nitrate and foraminifera intracellular nitrate at the same time to estimate the contributions of foraminifera to benthic denitrification. Moreover, in this study there is no data on anammox process which contributes also to the total denitrification (Brandes et al., 2007). The results reported in previous studies as (Engström et al., 2005) do not allow us to extrapolate their data at our oxic station, located at the entrance of the fjord. Thus, we assume that our estimate of denitrification is conservative since the possible contribution of anammox is not included in the calculation. However, despite these uncertainties *Nonionella* sp. T1 contribution to benthic denitrification

supports the hypothesis that this non-indigenous denitrifying foraminifer plays a major role in the benthic nitrogen cycle.

At the hypoxic station, the opposite was shown where the estimated contribution of *Nonionella* sp. T1 to benthic denitrification was below 1 % whatever the calculation approach. The estimated contributions of the other denitrifying foraminifera found in this station were low. Foraminifera contributed to almost 5 % of benthic denitrification. Compared to the oxic station, the NIS *Nonionella* sp. T1 and the other denitrifying species contributions to benthic denitrification were weak in a prolonged hypoxic station of the Gullmar Fjord.

Overall, the Gullmar Fjord is well oxygenated except for the deepest basin where oxygen goes down when there is no deep water exchange (Fig. 3 c). Therefore, the GF17-3 oxic station could be considered representative of the Gullmar Fjord benthic ecosystem. *Nonionella* sp. T1 is not the most efficient denitrifying species compared to *Globobulimina turgida* (42 pmol N ind^{-1} d^{-1}, with BV = 1.3 10^{+06} μm^3) and also less efficient than *Nonionella* cf. *stella* from Perú. However, *Nonionella* sp. T1 high density could accelerate sediment denitrification and participate to increase the contrast between the two hydrographic conditions. Indeed, the increasing discrepancy of bottom water oxygenation between stations induces a gap in the availability of nitrate for anaerobic facultative metabolisms in the sediment. In the oxygenated part of the fjord, high contribution to benthic denitrification (estimated between 50 and 100%) by *Nonionella* sp. T1 could take part to a potential de-eutrophication of the system by increasing the nitrogen loss. Primary production (PP) in the Gullmar Fjord is dominated by diatom blooms in spring and autumn (Lindahl and Hernroth, 1983). Since the 1990s, (Lindahl et al., 2009) observed an increase in PP in the Gullmar Fjord, potentially changing its trophic status towards eutrophic. This increase in PP also shown in the adjacent Kattegat could be related to the nitrogen input loading from the land and atmosphere (Carstensen et al., 2003). Lindahl et al. (2003) argued that the PP in the Gullmar Fjord was due to climatic forces resulting from a strong positive North Atlantic Oscillation (NAO) index, which increased the availability of deep-water nutrients (Kattegat nitrate-rich) through changes in the thermocline. The benthic denitrification of the Gullmar Fjord produces nitrogen unassimilable by primary producers. Moreover, foraminiferal nitrate uptake and intracellular storage act as an additional sink through bio-transportation and permanent sequestration in sediments (Glock et al., 2013; Prokopenko et al., 2011). Thus, denitrifying foraminifera including *Nonionella* sp. T1 could

help counterbalance a potential eutrophication of the system via nitrogen loss (Seitzinger, 1988).

Contrastingly, in the hypoxic part of the fjord, nitrate and nitrite rapidly exhausted become scarce, resulting in a decrease in benthic denitrification including foraminifera contribution. As a consequence of oxygen and nitrate scarcity, nitrification, denitrification and anammox processes are less intense resulting in a decrease of nitrogen mitigation and accumulation of ammonium in the deeper part of the fjord subjected to prolonged severe hypoxia (Fig. 1). Moreover, the low availability of nitrate in the sediment would possibly increase the benthic transfer towards the water column of reduced compounds such as manganese and iron produced deeper in the sedimentary column by other anaerobic metabolisms (Hulth et al., 1999). These new results demonstrate that the role of denitrifying foraminifera is underestimated in the nitrogen cycle and that overlooking this part of the meiofauna may lead to a misunderstanding of environments subject to hydrographic changes.

5. Conclusion

This study revealed a drastic change in living foraminifera fauna due to several hypoxic events that occurred in the last decades in the Gullmar Fjord. For the first time, the non-indigenous species (NIS) *Nonionella* sp. T1 dominated up to 74 % the foraminifera fauna at a station with oxygenated bottom waters and high nitrate content in sediment porewater. This NIS can denitrify up to 50-100 % of the nitrate porewater sediment under oxic conditions in the fjord. Whereas, under prolonged hypoxia, nitrate depletion turns environmental conditions unfavorable for foraminifera denitrification, resulting in a low density of *Nonionella* sp. T1 and other denitrifying species. Foraminifera contribution to benthic denitrification was negligible (~ 5 %) during prolonged seasonal hypoxia in the fjord. Moreover, the potential invasive denitrifying *Nonionella* sp. T1 could impact the nitrogen cycle under oxic conditions by increasing the sediment denitrification and could counterbalance potential eutrophication of the Gullmar Fjord. Our study demonstrated that the role of denitrifying foraminifera is underestimated in the nitrogen cycle especially in oxic environments.

Author contributions

C.C. participated in the sampling cruise, did the foraminifera taxonomy, contributed to 2D gel experiments and analyses by hyperspectral camera. C.C. did the nitrate and oxygen respiration measurements and wrote the present manuscript. E.G. participated in the sampling cruise, contributed to foraminifera analysis, scientific discussions. E.M. participated in the sampling cruise, managed with A.M. the 2D gels experiments, and contributed to hyperspectral camera treatments and scientific discussions and manuscript rewriting. H.L.F managed with A.M the sampling cruise and contributed to foraminifera taxonomy and scientific discussions and manuscript rewriting. N.R.P. managed the oxygen and nitrate respiration measurements and contributed to the scientific discussions. P.L. managed hyperspectral treatments for 2D gels and contributed to scientific discussion. M.G. participated in the 2D gel lab experiments and hyperspectral treatments. T.J. participated to the sampling cruise, contributed to 2D gels experiments and scientific discussions and manuscript rewriting. B.J. contributed to scientific discussion and manuscript rewriting. A.M. managed the sampling cruise and 2D gels experiments and contributed to hyperspectral camera treatments and scientific discussions and manuscript rewriting.

Acknowledgements

The authors gratefully acknowledge the crews of the R/V Skagerak and Oscar von Sydow and the Kristineberg Marine Research Station, the hydrographic data used in the project are from SMHI's database – SHARK. The collection of data for SHARK is organized by the Swedish environmental monitoring program and funded by the Swedish Agency for Marine and Water Management (SWAM). Thanks to Charlotte LeKieffre who helped during the sampling cruise, the SCIAM (Service Commun d'Imagerie et d'Analyses Microscopiques) of Angers University for the SEM images. HLF acknowledges funding from the Swedish Research Council VR (grant number 2017-04190). This project was funded by the French National Program MANGA-2D (CNRS-INSU) and by the FRESCO project supported by the Region Pays de la Loire and by University of Angers.

Bibliography

Aller, R. C.: The Effects of Macrobenthos on Chemical Properties of Marine Sediment and Overlying Water, in: Animal-Sediment Relations: The Biogenic Alteration of Sediments, edited by: McCall, P. L. and Tevesz, M. J. S., Springer US, Boston, MA, 53–102, https://doi.org/10.1007/978-1-4757-1317-6_2, 1982.

Aller, R. C., Hall, P. O. J., Rude, P. D., and Aller, J. Y.: Biogeochemical heterogeneity and suboxic diagenesis in hemipelagic sediments of the Panama Basin, Deep Sea Res. Part Oceanogr. Res. Pap., 45, 133–165, https://doi.org/10.1016/S0967-0637(97)00049-6, 1998.

Alve, E. and Goldstein, S. T.: Propagule transport as a key method of dispersal in benthic foraminifera (Protista), Limnol. Oceanogr., 48, 2163–2170, https://doi.org/10.4319/lo.2003.48.6.2163, 2003.

Andersen, K., Kjær, T., and Revsbech, N. P.: An oxygen insensitive microsensor for nitrous oxide, Sens. Actuators B Chem., 81, 42–48, https://doi.org/10.1016/S0925-4005(01)00924-8, 2001.

Arneborg, L.: Turnover times for the water above sill level in Gullmar Fjord, Cont. Shelf Res., 24, 443–460, https://doi.org/10.1016/j.csr.2003.12.005, 2004.

Berg, P., Risgaard-Petersen, N., and Rysgaard, S.: Interpretation of measured concentration profiles in sediment pore water, Limnol. Oceanogr., 43, 1500–1510, https://doi.org/10.4319/lo.1998.43.7.1500, 1998.

Bernhard, J. M., Ostermann, D. R., Williams, D. S., and Blanks, J. K.: Comparison of two methods to identify live benthic foraminifera: A test between Rose Bengal and CellTracker Green with implications for stable isotope paleoreconstructions: Foraminifera viability method comparison, Paleoceanography, 21, https://doi.org/10.1029/2006PA001290, 2006.

Bernhard, J. M., Edgcomb, V. P., Casciotti, K. L., McIlvin, M. R., and Beaudoin, D. J.: Denitrification likely catalyzed by endobionts in an allogromiid foraminifer, ISME J., 6, 951–960, https://doi.org/10.1038/ismej.2011.171, 2012.

Björk, G. and Nordberg, K.: Upwelling along the Swedish west coast during the 20th century, Cont. Shelf Res., 23, 1143–1159, https://doi.org/10.1016/S0278-4343(03)00081-5, 2003.

Brandes, J. A., Devol, A. H., and Deutsch, C.: New Developments in the Marine Nitrogen Cycle, Chem. Rev., 107, 577–589, https://doi.org/10.1021/cr050377t, 2007.

Breitburg, D., Levin, L. A., Oschlies, A., Grégoire, M., Chavez, F. P., Conley, D. J., Garçon, V., Gilbert, D., Gutiérrez, D., Isensee, K., Jacinto, G. S., Limburg, K. E., Montes, I., Naqvi, S. W. A., Pitcher, G. C., Rabalais, N. N., Roman, M. R., Rose, K. A., Seibel, B. A., Telszewski, M., Yasuhara, M., and Zhang, J.: Declining oxygen in the global ocean and coastal waters, Science, 359, https://doi.org/10.1126/science.aam7240, 2018.

Carstensen, J., Conley, D., and Müller-Karulis, B.: Spatial and temporal resolution of carbon fluxes in a shallow coastal ecosystem, the Kattegat, Mar. Ecol. Prog. Ser., 252, 35–50, https://doi.org/10.3354/meps252035, 2003.

Cesbron, F., Metzger, E., Launeau, P., Deflandre, B., Delgard, M.-L., Thibault de Chanvalon, A., Geslin, E., Anschutz, P., and Jézéquel, D.: Simultaneous 2D Imaging of Dissolved Iron and Reactive Phosphorus in Sediment Porewaters by Thin-Film and Hyperspectral Methods, Environ. Sci. Technol., 48, 2816–2826, https://doi.org/10.1021/es404724r, 2014.

Charrieau, L. M., Filipsson, H. L., Ljung, K., Chierici, M., Knudsen, K. L., and Kritzberg, E.: The effects of multiple stressors on the distribution of coastal benthic foraminifera: A case study from the Skagerrak-Baltic Sea region, Mar. Micropaleontol., 139, 42–56, https://doi.org/10.1016/j.marmicro.2017.11.004, 2018.

Charrieau, L. M., Ljung, K., Schenk, F., Daewel, U., Kritzberg, E., and Filipsson, H. L.: Rapid environmental responses to climate-induced hydrographic changes in the Baltic Sea entrance, Biogeosciences, 16, 3835–3852, https://doi.org/10.5194/bg-16-3835-2019, 2019.

Childs, C. R., Rabalais, N. N., Eugene, R., and Proctor, T. and L. M.: Sediment denitrification in the Gulf of Mexico zone of hypoxia, 2002.

Christensen, P. B., Rysgaard, S., Sloth, N. P., Dalsgaard, T., and Schwærter, S.: Sediment mineralization, nutrient fluxes, denitrification and dissimilatory nitrate reduction to ammonium in an estuarine fjord with sea cage trout farms, Aquat. Microb. Ecol., 21, 73–84, https://doi.org/10.3354/ame021073, 2000.

Conley, D. J., Carstensen, J., Ærtebjerg, G., Christensen, P. B., Dalsgaard, T., Hansen, J. L. S., and Josefson, A. B.: Long-Term Changes and Impacts of Hypoxia in Danish Coastal Waters, Ecol. Appl., 17, S165–S184, https://doi.org/10.1890/05-0766.1, 2007.

Cornwell, J. C., Kemp, W. M., and Kana, T. M.: Denitrification in coastal ecosystems: methods, environmental controls, and ecosystem level controls, a review, Aquat. Ecol., 33, 41–54, https://doi.org/10.1023/A:1009921414151, 1999.

Dale, A. W., Sommer, S., Lomnitz, U., Bourbonnais, A., and Wallmann, K.: Biological nitrate transport in sediments on the Peruvian margin mitigates benthic sulfide emissions and drives pelagic N loss during stagnation events, Deep Sea Res. Part Oceanogr. Res. Pap., 112, 123–136, https://doi.org/10.1016/j.dsr.2016.02.013, 2016.

Deldicq, N., Alve, E., Schweizer, M., Asteman, I. P., Hess, S., Darling, K., and Bouchet, V. M. P.: History of the introduction of a species resembling the benthic foraminifera *Nonionella stella* in the Oslofjord (Norway): morphological, molecular and paleo-ecological evidences, 2019.

Devol, A., Ruef, W., Newton, J., and Richey, J.: Anthropogenic Contributions to Hypoxia in Lower Hood Canal, Washington State, AGU Fall Meet. Abstr., 43, OS43C-1309, 2008.

Diaz, R. J.: Overview of Hypoxia around the World, J. Environ. Qual., 30, 275–281, https://doi.org/10.2134/jeq2001.302275x, 2001.

Diaz, R. J. and Rosenberg, R.: Spreading Dead Zones and Consequences for Marine Ecosystems, Science, 321, 926–929, https://doi.org/10.1126/science.1156401, 2008a.

Engström, P., Dalsgaard, T., Hulth, S., and Aller, R. C.: Anaerobic ammonium oxidation by nitrite (anammox): Implications for N2 production in coastal marine sediments, Geochim. Cosmochim. Acta, 69, 2057–2065, https://doi.org/10.1016/j.gca.2004.09.032, 2005.

Filipsson, H. L. and Nordberg, K.: Climate variations, an overlooked factor influencing the recent marine environment. An example from Gullmar Fjord, Sweden, illustrated by benthic foraminifera and hydrographic data, Estuaries, 27, 867–881, https://doi.org/10.1007/BF02912048, 2004.

Galloway, J. N., Dentener, F. J., Capone, D. G., Boyer, E. W., Howarth, R. W., Seitzinger, S. P., Asner, G. P., Cleveland, C. C., Green, P. A., Holland, E. A., Karl, D. M., Michaels, A. F., Porter, J. H., Townsend, A. R., and Vöosmarty, C. J.: Nitrogen Cycles: Past, Present, and Future, Biogeochemistry, 70, 153–226, https://doi.org/10.1007/s10533-004-0370-0, 2004.

Geslin, E., Risgaard-Petersen, N., Lombard, F., Metzger, E., Langlet, D., and Jorissen, F.: Oxygen respiration rates of benthic foraminifera as measured with oxygen microsensors, J. Exp. Mar. Biol. Ecol., 396, 108–114, https://doi.org/10.1016/j.jembe.2010.10.011, 2011.

Glock, N., Schönfeld, J., Eisenhauer, A., Hensen, C., Mallon, J., and Sommer, S.: The role of benthic foraminifera in the benthic nitrogen cycle of the Peruvian oxygen minimum zone, Biogeosciences, 10, 4767–4783, https://doi.org/10.5194/bg-10-4767-2013, 2013.

Glock, N., Roy, A.-S., Romero, D., Wein, T., Weissenbach, J., Revsbech, N. P., Høgslund, S., Clemens, D., Sommer, S., and Dagan, T.: Metabolic preference of nitrate over oxygen as an electron acceptor in foraminifera from the Peruvian oxygen minimum zone, Proc. Natl. Acad. Sci., 116, 2860–2865, https://doi.org/10.1073/pnas.1813887116, 2019.

Goldberg, T., Archer, C., Vance, D., Thamdrup, B., McAnena, A., and Poulton, S. W.: Controls on Mo isotope fractionations in a Mn-rich anoxic marine sediment, Gullmar Fjord, Sweden, Chem. Geol., 296–297, 73–82, https://doi.org/10.1016/j.chemgeo.2011.12.020, 2012.

Gruber, N. and Sarmiento, J. L.: Global patterns of marine nitrogen fixation and denitrification, Glob. Biogeochem. Cycles, 11, 235–266, https://doi.org/10.1029/97GB00077, 1997.

Gustafsson, M. and Nordberg, K.: Living (stained) Benthic Foraminiferal Response to Primary Production and Hydrography in the Deepest Part of the Gullmar Fjord, Swedish West Coast, with Comparisons to Höglund's 1927 Material, J. Foraminifer. Res., 31, 2–11, https://doi.org/10.2113/0310002, 2001.

Hannah, F., Rogerson, R., and Laybourn-Parry, J.: Respiration rates and biovolumes of common benthic Foraminifera (Protozoa), J. Mar. Biol. Assoc. U. K., 74, 301–312, https://doi.org/10.1017/S0025315400039345, 1994.

Herbert, R. A.: Nitrogen cycling in coastal marine ecosystems, FEMS Microbiol. Rev., 23, 563–590, https://doi.org/10.1111/j.1574-6976.1999.tb00414.x, 1999.

Høgslund, S., Revsbech, N. P., Cedhagen, T., Nielsen, L. P., and Gallardo, V. A.: Denitrification, nitrate turnover, and aerobic respiration by benthic foraminiferans in the oxygen minimum zone off Chile, J. Exp. Mar. Biol. Ecol., 359, 85–91, https://doi.org/10.1016/j.jembe.2008.02.015, 2008.

Høgslund, S., Cedhagen, T., Bowser, S. S., and Risgaard-Petersen, N.: Sinks and Sources of Intracellular Nitrate in Gromiids, Front. Microbiol., 8, https://doi.org/10.3389/fmicb.2017.00617, 2017.

Hulth, S., Aller, R. C., and Gilbert, F.: Coupled anoxic nitrification/manganese reduction in marine sediments, Geochim. Cosmochim. Acta, 63, 49–66, https://doi.org/10.1016/S0016-7037(98)00285-3, 1999.

Jäntti, H. and Hietanen, S.: The Effects of Hypoxia on Sediment Nitrogen Cycling in the Baltic Sea, AMBIO, 41, 161–169, https://doi.org/10.1007/s13280-011-0233-6, 2012.

Kamp, A., Høgslund, S., Risgaard-Petersen, N., and Stief, P.: Nitrate Storage and Dissimilatory Nitrate Reduction by Eukaryotic Microbes, Front. Microbiol., 6, https://doi.org/10.3389/fmicb.2015.01492, 2015.

Karlson, K., Bonsdorff, E., and Rosenberg, R.: The Impact of Benthic Macrofauna for Nutrient Fluxes from Baltic Sea Sediments, AMBIO J. Hum. Environ., 36, 161–167, https://doi.org/10.1579/0044-7447(2007)36[161:TIOBMF]2.0.CO;2, 2007.

Kemp, W. M., Sampou, P., Caffrey, J., Mayer, M., Henriksen, K., and Boynton, W. R.: Ammonium recycling versus denitrification in Chesapeake Bay sediments, Limnol. Oceanogr., 35, 1545–1563, https://doi.org/10.4319/lo.1990.35.7.1545, 1990.

Kemp, W. M., Boynton, W. R., Adolf, J. E., Boesch, D. F., Boicourt, W. C., Brush, G., Cornwell, J. C., Fisher, T. R., Glibert, P. M., Hagy, J. D., Harding, L. W., Houde, E. D., Kimmel, D. G., Miller, W. D., Newell, R. I. E., Roman, M. R., Smith, E. M., and Stevenson, J. C.: Eutrophication of Chesapeake Bay: historical trends and ecological interactions, Mar. Ecol. Prog. Ser., 303, 1–29, https://doi.org/10.3354/meps303001, 2005.

Koho, K. A., Pina-Ochoa, E., Geslin, E., and Risgaard-Petersen, N.: Vertical migration, nitrate uptake and denitrification: survival mechanisms of foraminifers (*Globobulimina turgida*) under low oxygen conditions, 2011.

LeKieffre, C., Spangenberg, J. E., Mabilleau, G., Escrig, S., Meibom, A., and Geslin, E.: Surviving anoxia in marine sediments: The metabolic response of ubiquitous benthic foraminifera (*Ammonia tepida*), PLOS ONE, 12, e0177604, https://doi.org/10.1371/journal.pone.0177604, 2017.

Levin, L. A., Ekau, W., Gooday, A. J., Jorissen, F., Middelburg, J. J., Naqvi, S. W. A., Neira, C., Rabalais, N. N., and Zhang, J.: Effects of natural and human-induced hypoxia on coastal benthos, 2009.

Lindahl, Andersson, and Belgrano: Primary phytoplankton productivity in the Gullmar Fjord, Sweden, 2009.

Lindahl, O. and Hernroth, L.: Phyto-Zooplankton Community in Coastal Waters of Western Sweden -An Ecosystem Off Balance?, Mar. Ecol. Prog. Ser., 10, 119–126, https://doi.org/10.3354/meps010119, 1983.

Luther, G. W., Sundby, B., Lewis, B. L., Brendel, P. J., and Silverberg, N.: Interactions of manganese with the nitrogen cycle: Alternative pathways to dinitrogen, Geochim. Cosmochim. Acta, 61, 4043–4052, https://doi.org/10.1016/S0016-7037(97)00239-1, 1997.

Maire, O., Barras, C., Gestin, T., Nardelli, M., Romero-Ramirez, A., Duchêne, J., and Geslin, E.: How does macrofaunal bioturbation influence the vertical distribution of living benthic foraminifera?, Mar. Ecol. Prog. Ser., 561, 83–97, https://doi.org/10.3354/meps11929, 2016.

Metzger, E., Thibault de Chanvalon, A., Cesbron, F., Barbe, A., Launeau, P., Jézéquel, D., and Mouret, A.: Simultaneous Nitrite/Nitrate Imagery at Millimeter Scale through the Water–Sediment Interface, Environ. Sci. Technol., 50, 8188–8195, https://doi.org/10.1021/acs.est.6b00187, 2016.

Mortimer, R. J. G., Harris, S. J., Krom, M. D., Freitag, T. E., Prosser, J. I., Barnes, J., Anschutz, P., Hayes, P. J., and Davies, I. M.: Anoxic nitrification in marine sediments, Mar. Ecol. Prog. Ser., 276, 37–51, 2004.

Neubacher, E. C., Parker, R. E., and Trimmer, M.: The potential effect of sustained hypoxia on nitrogen cycling in sediment from the southern North Sea: a mesocosm experiment | SpringerLink, Biogeochemistry, 2013.

Nizzoli, D., Bartoli, M., Cooper, M., Welsh, D. T., Underwood, G. J. C., and Viaroli, P.: Implications for oxygen, nutrient fluxes and denitrification rates during the early stage of sediment colonisation by the polychaete *Nereis* spp. in four estuaries, Estuar. Coast. Shelf Sci., 75, 125–134, https://doi.org/10.1016/j.ecss.2007.03.035, 2007.

Nomaki, H., Chikaraishi, Y., Tsuchiya, M., Toyofuku, T., Suga, H., Sasaki, Y., Uematsu, K., Tame, A., and Ohkouchi, N.: Variation in the nitrogen isotopic composition of amino acids in benthic foraminifera: Implications for their adaptation to oxygen-depleted environments, Limnol. Oceanogr., 60, 1906–1916, https://doi.org/10.1002/lno.10140, 2015.

Nordberg, K.: Oceanography in the Kattegat and Skagerrak Over the Past 8000 Years, Paleoceanography, 6, 461–484, https://doi.org/10.1029/91PA01132, 1991.

Nordberg, K., Gustafsson, M., and Krantz, A.-L.: Decreasing oxygen concentrations in the Gullmar Fjord, Sweden, as confirmed by benthic foraminifera, and the possible association with NAO, J. Mar. Syst., 23, 303–316, https://doi.org/10.1016/S0924-7963(99)00067-6, 2000.

Pina-Ochoa, E., Hogslund, S., Geslin, E., Cedhagen, T., Revsbech, N. P., Nielsen, L. P., Schweizer, M., Jorissen, F., Rysgaard, S., and Risgaard-Petersen, N.: Widespread occurrence of nitrate storage and denitrification among Foraminifera and Gromiida, Proc. Natl. Acad. Sci., 107, 1148–1153, https://doi.org/10.1073/pnas.0908440107, 2010.

Polovodova Asteman, Filipsson, H. L., and Nordberg, K.: Tracing winter temperatures over the last two millennia using a north-east Atlantic coastal record, 2018.

Polovodova Asteman, I. and Nordberg, K.: Foraminiferal fauna from a deep basin in Gullmar Fjord: The influence of seasonal hypoxia and North Atlantic Oscillation, J. Sea Res., 79, 40–49, https://doi.org/10.1016/j.seares.2013.02.001, 2013.

Polovodova Asteman, I. and Schönfeld, J.: Recent invasion of the foraminifer *Nonionella stella* Cushman & Moyer, 1930 in northern European waters: evidence from the Skagerrak and its fjords, J. Micropalaeontology, 35, 20–25, https://doi.org/10.1144/jmpaleo2015-007, 2015.

Prokopenko, M. G., Sigman, D. M., Berelson, W. M., Hammond, D. E., Barnett, B., Chong, L., and Townsend-Small, A.: Denitrification in anoxic sediments supported by biological nitrate transport, Geochim. Cosmochim. Acta, 75, 7180–7199, https://doi.org/10.1016/j.gca.2011.09.023, 2011.

Rabalais, N. N., Díaz, R. J., Levin, L. A., Turner, R. E., Gilbert, D., and Zhang, J.: Dynamics and distribution of natural and human-caused hypoxia, Biogeosciences, 7, 585–619, https://doi.org/10.5194/bg-7-585-2010, 2010.

Ramsing, N. and J. Gundersen Seawater and Gases-Tabulated Physical Parameters of Interest to People Working with Microsensors in Marine Systems. Version 2.0. Unisense Internal Report, 1994.

Revsbech, N. P.: An oxygen microsensor with a guard cathode, Limnol. Oceanogr., 34, 474–478, https://doi.org/10.4319/lo.1989.34.2.0474, 1989.

Risgaard-Petersen, N., Langezaal, A. M., Ingvardsen, S., Schmid, M. C., Jetten, M. S. M., Op den Camp, H. J. M., Derksen, J. W. M., Piña-Ochoa, E., Eriksson, S. P., Peter Nielsen, L., Peter Revsbech, N., Cedhagen, T., and van der Zwaan, G. J.: Evidence for complete denitrification in a benthic foraminifer, Nature, 443, 93–96, https://doi.org/10.1038/nature05070, 2006.

Ross, B. J. and Hallock, P.: Dormancy in the Foraminifera: a review, J. Foraminifer. Res., 46, 358–368, https://doi.org/10.2113/gsjfr.46.4.358, 2016.

Rysgaard, S., Risgaard-Petersen, N., Peter, S. N., Kim, J., and Peter, N. L.: Oxygen regulation of nitrification and denitrification in sediments, Limnol. Oceanogr., 39, 1643–1652, https://doi.org/10.4319/lo.1994.39.7.1643, 1994.

Seitzinger, S. P.: Denitrification in freshwater and coastal marine ecosystems: Ecological and geochemical significance, Limnol. Oceanogr., 33, 702–724, https://doi.org/10.4319/lo.1988.33.4part2.0702, 1988.

Sigman, D. M., Karsh, K. L., and Casciotti, K. L.: Nitrogen Isotopes in the Ocean, Encycl. Ocean Sci., 40–54, https://doi.org/10.1016/B978-012374473-9.00632-9, 2009.

Stachowitsch, M.: Mass Mortality in the Gulf of Trieste: The Course of Community Destruction, Mar. Ecol., 5, 243–264, https://doi.org/10.1111/j.1439-0485.1984.tb00124.x, 1984.

Stief, P.: Stimulation of microbial nitrogen cycling in aquatic ecosystems by benthic macrofauna: mechanisms and environmental implications, Biogeosciences, 10, 7829–7846, https://doi.org/10.5194/bg-10-7829-2013, 2013.

Stockdale, A., Davison, W., and Zhang, H.: Micro-scale biogeochemical heterogeneity in sediments: A review of available technology and observed evidence, Earth-Sci. Rev., 92, 81–97, https://doi.org/10.1016/j.earscirev.2008.11.003, 2009.

Svansson, A.: Physical and chemical oceanography of the Skagerrak and the Kattegat., 1975.

Svansson, A.: Hydrography of the Gullmar Fjord, Medd. Fraan Havsfiskelab. Lysekil Swed., 1984.

Swedish Meteorological and Hydrological Institute's (SMHI): https://sharkweb.smhi.se/, last access: 13th of July 2020.

Thamdrup, B. and Dalsgaard, T.: Microbial Ecology of the Oceans, 1st ed., John Wiley & Sons, Ltd, https://doi.org/10.1002/9780470281840, 2008.

Woehle, C., Roy, A.-S., Glock, N., Wein, T., Weissenbach, J., Rosenstiel, P., Hiebenthal, C., Michels, J., Schönfeld, J., and Dagan, T.: A Novel Eukaryotic Denitrification Pathway in Foraminifera, Curr. Biol., https://doi.org/10.1016/j.cub.2018.06.027, 2018.

Xu, Z., Liu, S., Xiang, R., and Song, G.: Live benthic foraminifera in the Yellow Sea and the East China Sea: vertical distribution, nitrate storage, and potential denitrification, Mar. Ecol. Prog. Ser., 571, 65–81, https://doi.org/10.3354/meps12135, 2017.

Zhang, J., Gilbert, D., Gooday, A., Levin, L., Naqvi, S. W. A., Middelburg, J. J., Scranton, M., Ekau, W., Pena, A., Dewitte, B., Oguz, T., Monteiro, P. M. S., Urbán, E., Rabalais, N. N., Ittekkot, V., Kemp, W. M., Ulloa, O., Elmgren, R., Escobar-Briones, E., and Van Der Plas, A. K.: Natural and human-induced hypoxia and consequences for coastal areas: synthesis and future development, Biogeosciences, 7, 1443–1467, https://doi.org/10.5194/bg-7-1443-2010, 2010.

Supplementary material

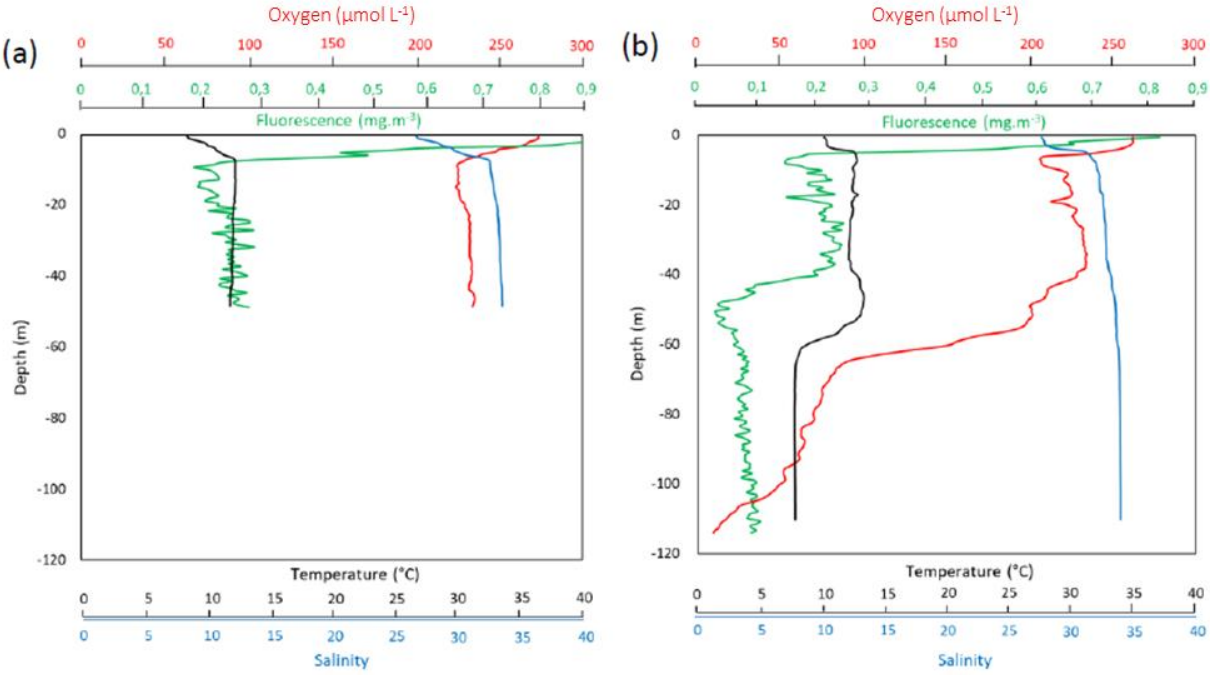

Figure S1. CTD profiles of temperature, salinity, fluorescence and oxygen concentration in the water column of the both stations: (a) GF17-3 oxic station (50 m water depth) and (b) GF17-1 hypoxic station (near Alsbäck, 117 m water depth).

Equation S1. Detailed calculation for biovolume correction for the denitrification rate of the NIS Nonionella sp. T1 from the November 2017 cruise. Equation used according to Geslin et al. (2011) and Glock et al. (2019).

ln(denitrification rate 2018 cruise) * (0.68 * ln (BV 2017 cruise) – 5.57) / (0.68 * ln (BV 2018 cruise) – 5.57) = ln(corrected denitrification rate 2017 cruise)

Example: ln(21) * (0.68 * ln (1.3 10^{+06}) – 5.57) / (0.68 * ln (4.0 10^{+06}) – 5.57) = ln(38).

Table S1: PROFILE software parameters used to generate the porewater nitrate modelling in both stations GF17-3 and GF17-1 in the Gullmar Fjord (see details in Berg et al., 1998).

PROFILE parameters	GF17-3	GF17-1
Depth at top of calculation domain (cm)	0	0
Depth at bottom of calculation domain (cm)	4.8	4.8
Max number of equally spaced zones in interpretation (1 to 12)	8	8
Type of boundary conditions (4:t=C b=F)	4	4
First boundary condition (µmol L^{-1})	13.1	4.2
Second boundary condition	0	0
Nitrate diffusion coefficient (cm^{-2} s^{-1}) in water	1.4 10^{-05}	1.4 10^{-05}
Expression for sediment diffusivity (Ds) (2: Ds=FI^2*D)	2	2
Concentration in water column (µmol L^{-1})	14.6	5.7
Minimum for production rate	-1.0 10^{+20}	-1.0 10^{+20}
Maximum for production rate	1.0 10^{+20}	1.0 10^{+20}
Maximum deviation (in %) when accepting a calculated minimum	0.001	0.001
Level of significance in the F statistics	0.01	0.01

Table S2. Total densities (individuals per slice of 10 cm^3) and relative abundances (%) of the foraminiferal fauna from the GF17-3A and 3C cores and from the GF17-1A and 1C cores of the Gullmar Fjord (GF). The cores were sliced every 2 mm from the SWI to 20 mm depth and every 5 mm from 20 to 50 mm depth. The foraminiferal sections are divided as: the NIS and potential invasive Nonionella sp. T1 species in the GF according to Polovodova Asteman and Schönfeld (2015) and Deldicq et al. (2019), the known denitrifying species in the GF according to Risgaard-Petersen et al. (2006) and Woehle et al. (2018), the non-denitrying species according to Pina-Ochoa et al. (2010) and the minor other species of the fauna.

GF17-3A	Species	0-2	2-4	4-6	6-8	8-10	10-12	12-14	14-16	16-18	18-20	20-25	25-30	30-35	35-40	40-45	45-50	Total density per species	Relative abundance (%)
invasive species	*Nonionella* sp.T1 (Deldicq and al., 2019)	9	6	15	24	14	18	15	15	17	7	14	6	19	45	91	122	436	34
known denitrifying species in GF	*Globobulimina turgida* (Bailey)	0	0	0	0	0	0	0	0	0	0	0	0	0	0	0	0	0	0
	Globobulimina auricula (Höglund)	0	0	0	0	0	0	0	0	0	0	0	0	0	0	0	0	0	0
candidate denitrifying species	*Bolivina pseudopunctata* (Höglund)	1	1	0	0	1	1	0	0	0	0	0	0	0	0	0	0	4	0
	Stainforthia fusiformis (Williamson)	2	0	0	1	3	1	0	0	2	0	1	0	0	0	0	0	10	1
non-denitrifyng species	*Bulimina marginata* (d'Orbigny)	22	48	37	32	30	35	12	14	26	26	15	6	25	26	73	43	471	37
	Cassidulina laevigata (d'Orbigny)	10	41	4	19	9	2	2	24	3	1	0	0	0	0	0	0	114	9
	Leptohalysis scotti (Chaster)	2	1	6	6	4	9	9	6	17	29	13	8	6	5	5	9	134	11
minor other species	*Ammonia falsobeccari* (Rouvillois)	0	0	0	0	0	0	1	0	1	0	0	0	1	0	0	0	3	0
	Bolivina skagerrakensis (Qvale and Nigam)	0	0	3	0	0	0	0	0	3	0	0	0	0	0	0	0	6	1
	Bolivina spathulata (Williamson)	0	0	0	0	0	0	0	0	0	0	0	0	0	0	0	0	0	0
	Bolivina sp.	0	0	0	0	0	0	0	0	0	0	0	0	0	0	0	0	0	0
	Cribrostomoides nitida (Goës)	0	0	0	0	0	0	0	0	0	0	0	0	0	0	0	0	0	0
	Eggerella scabra (Williamson)	0	0	0	0	0	0	0	0	0	0	0	0	0	0	0	0	0	0
	Elphidium clavatum-selseyensis (d'Orbigny)	0	0	0	1	0	0	0	0	0	0	0	0	0	0	0	0	1	0
	Hyalinea balthica (Schroeter)	0	0	0	0	0	0	0	1	0	0	0	0	0	0	0	0	1	0
	Lenticulina sp.	0	0	0	0	0	0	0	0	0	0	0	0	0	0	0	0	0	0
	Liebusella goesi (Höglund)	0	0	0	0	0	0	0	0	0	0	0	0	0	0	0	0	0	0
	Nonionella labradorica (Dawson)	0	0	4	0	3	0	0	0	0	3	0	0	0	0	0	0	10	1
	Nonionella turgida (Williamson)	1	0	1	1	6	9	0	0	0	0	2	0	0	0	0	0	20	2
	Pyrgo williamsoni (Silvestry)	4	9	0	5	1	0	0	0	0	0	0	0	0	0	0	0	19	2
	Quinqueloculina bosciana (d'Orbigny)	0	0	0	1	1	0	0	0	0	0	0	0	0	0	0	0	2	0
	Quinqueloculina seminulum (Linné)	1	5	0	0	1	0	0	0	0	0	0	0	0	0	0	0	7	1
	Quinqueloculina stalkeri (Loeblich and Tappan)	1	0	0	0	0	0	0	0	0	0	0	0	0	0	0	0	1	0
	Reophax subfusiformis (Earland)	0	0	0	0	0	0	0	0	0	0	0	0	0	0	0	0	0	0
	Scutulons sp.	0	0	0	0	0	0	0	0	0	0	0	0	0	0	0	0	0	0
	Stainforthia loeblichi (Feyling-Hanssen)	1	0	3	2	1	0	0	2	0	1	0	0	0	0	0	0	11	1
	Textularia earlandi (Parker)	0	0	0	0	0	0	0	0	0	0	0	0	0	0	0	0	0	0
	Textularia sagittula (Defrance)	0	0	0	0	0	0	0	0	0	0	0	0	0	0	0	0	0	0
	other species	0	0	1	2	0	0	0	1	0	2	0	1	0	1	0	0	7	1
	Total density per slice	53	111	73	93	73	75	40	63	68	68	45	22	52	77	170	175	1256	100

GF17-3C	Species	0-2	2-4	4-6	6-8	8-10	10-12	12-14	14-16	16-18	18-20	20-25	25-30	30-35	35-40	40-45	45-50	Total density per species	Relative abundance (%)
invasive species	*Nonionella* sp.T1 (Deldicq and al., 2019)	17	45	34	82	63	35	41	25	56	51	56	98	145	140	89	88	1063	74
known denitrifying species in GF	*Globobulimina turgida* (Bailey)	0	0	0	0	0	0	0	0	0	0	0	0	0	0	0	0	0	0
	Globobulimina auricula (Höglund)	0	0	0	0	0	0	0	0	0	0	0	0	0	0	0	0	0	0
candidate denitrifying species	*Bolivina pseudopunctata* (Höglund)	0	0	0	0	0	0	0	0	0	0	0	0	0	0	0	0	0	0
	Stainforthia fusiformis (Williamson)	0	2	2	0	2	1	0	0	1	0	0	0	0	0	0	0	8	1
non-denitrifyng species	*Bulimina marginata* (d'Orbigny)	18	9	9	16	11	2	2	2	1	2	0	0	1	0	0	1	75	5
	Cassidulina laevigata (d'Orbigny)	15	14	15	12	9	5	9	0	0	0	0	0	0	0	0	0	79	5
	Leptohalysis scotti (Chaster)	15	9	8	16	7	7	12	5	21	11	9	3	2	1	3	0	128	9
minor other species	*Ammonia falsobeccari* (Rouvillois)	0	0	0	0	0	0	0	0	0	0	0	0	0	0	0	0	0	0
	Bolivina skagerrakensis (Qvale and Nigam)	1	3	3	0	0	0	0	0	0	0	0	0	0	0	0	0	7	0
	Bolivina spathulata (Williamson)	0	0	0	0	0	0	0	0	0	0	0	0	0	0	0	0	0	0
	Bolivina sp.	0	0	0	0	0	0	0	0	0	0	0	0	0	0	0	0	0	0
	Cribrostomoides nitida (Goës)	0	0	0	0	0	0	0	0	0	0	0	0	0	0	0	0	0	0
	Eggerella scabra (Williamson)	4	0	0	0	0	0	0	0	0	0	0	0	0	0	0	0	4	0
	Elphidium clavatum-selseyensis (d'Orbigny)	0	2	0	0	0	0	0	0	0	0	0	0	0	0	0	0	2	0
	Hyalinea balthica (Schroeter)	0	0	0	0	0	0	0	0	0	0	0	0	0	0	0	0	0	0
	Lenticulina sp.	0	0	0	0	0	0	0	0	0	0	0	0	0	0	0	0	0	0
	Liebusella goesi (Höglund)	0	0	0	0	0	0	0	0	0	0	0	0	0	0	0	0	0	0
	Nonionella labradorica (Dawson)	0	5	1	3	0	4	1	7	7	4	1	0	0	0	0	0	31	2
	Nonionella turgida (Williamson)	0	0	0	0	0	0	0	0	0	0	0	0	0	0	0	0	0	0
	Pyrgo williamsoni (Silvestry)	0	2	0	0	0	1	0	0	0	0	0	0	0	0	0	0	3	0
	Quinqueloculina bosciana (d'Orbigny)	0	0	0	0	0	0	0	0	0	0	0	0	0	0	0	0	0	0
	Quinqueloculina seminulum (Linné)	3	2	0	3	0	0	0	0	0	0	0	0	0	0	0	0	8	1
	Quinqueloculina stalkeri (Loeblich and Tappan)	0	0	0	0	0	0	0	0	0	0	0	0	0	0	0	0	0	0
	Reophax subfusiformis (Earland)	0	0	0	0	0	0	0	0	0	0	0	0	0	0	0	0	0	0
	Scutulons sp.	0	0	0	0	0	0	0	0	0	0	0	0	0	0	0	0	0	0
	Stainforthia loeblichi (Feyling-Hanssen)	0	0	1	0	0	0	1	0	0	0	0	0	0	0	0	0	2	0
	Textularia earlandi (Parker)	1	0	1	0	0	0	0	0	0	0	0	0	0	0	0	0	2	0
	Textularia sagittula (Defrance)	6	7	1	2	0	3	0	0	0	0	0	0	0	0	0	0	18	1
	other species	0	0	0	0	0	0	0	0	0	0	0	0	0		0	0	0	0
	Total density per slice	80	98	74	134	91	57	65	38	85	68	66	101	148	141	92	88	1428	100

GF17-1A	Species	0-2	2-4	4-6	6-8	8-10	10-12	12-14	14-16	16-18	18-20	20-25	25-30	30-35	35-40	40-45	45-50	Total density per species	Relative abundance (%)
invasive species	*Nonionella* sp.T1 (Deldicq and al., 2019)	0	1	0	1	1	0	0	9	15	19	21	2	2	3	1	1	74	5
known denitrifying species in GF	*Globobulimina turgida* (Bailey)	0	1	1	0	0	0	0	1	0	1	0	0	0	1	0	0	5	0
	Globobulimina auricula (Höglund)	0	0	1	0	0	0	1	0	1	0	1	2	0	0	1	2	8	1
candidate denitrifying species	*Bolivina pseudopunctata* (Höglund)	1	1	0	0	0	0	0	0	0	0	0	0	0	0	0	0	2	0
	Stainforthia fusiformis (Williamson)	8	4	13	3	1	5	0	0	0	2	0	1	1	1	3	2	43	3
non-denitrifyng species	*Bulimina marginata* (d'Orbigny)	83	130	165	63	115	112	51	36	32	38	23	19	16	14	24	17	937	64
	Cassidulina laevigata (d'Orbigny)	27	47	46	13	30	12	38	4	4	5	2	2	1	0	2	1	234	16
	Leptohalysis scotti (Chaster)	19	10	6	3	5	2	4	0	0	2	5	0	3	4	1	1	65	4
minor other species	*Ammonia falsobeccari* (Rouvillois)	0	0	0	0	0	0	0	0	1	0	0	0	0	0	0	0	1	0
	Bolivina skagerrakensis (Qvale and Nigam)	0	0	5	1	0	1	0	0	0	1	0	0	0	0	0	0	8	1
	Bolivina spathulata (Williamson)	0	0	0	0	0	0	0	0	0	0	0	0	0	0	0	0	0	0
	Bolivina sp.	0	0	0	0	1	0	0	0	0	0	0	0	0	0	0	0	1	0
	Cribrostomoides nitida (Goës)	0	0	0	0	0	0	0	0	0	0	0	0	0	0	0	0	0	0
	Eggerella scabra (Williamson)	0	0	0	0	0	0	0	0	0	0	0	0	0	0	0	0	0	0
	Elphidium clavatum-selseyensis (d'Orbigny)	0	1	1	0	0	1	1	0	0	0	1	0	0	0	0	1	6	0
	Hyalinea balthica (Schroeter)	1	4	2	1	1	0	1	0	0	0	0	0	0	0	0	0	11	1
	Lenticulina sp.	0	0	0	0	0	0	0	0	0	0	0	0	0	0	0	0	0	0
	Liebusella goesi (Höglund)	0	0	0	0	0	0	0	0	0	0	0	0	0	0	0	0	0	0
	Nonionella labradorica (Dawson)	2	2	2	0	0	7	3	4	0	0	2	0	0	0	0	0	20	1
	Nonionella turgida (Williamson)	0	0	1	0	1	0	1	2	2	6	2	0	0	0	0	0	15	1
	Pyrgo williamsoni (Silvestry)	0	1	0	0	0	0	0	0	0	0	1	2	0	0	0	0	4	0
	Quinqueloculina bosciana (d'Orbigny)	0	0	0	0	0	0	0	0	0	0	0	0	0	0	0	0	0	0
	Quinqueloculina seminulum (Linné)	3	2	7	1	2	0	0	1	0	0	0	0	0	0	0	0	16	1
	Quinqueloculina stalkeri (Loeblich and Tappan)	0	0	0	0	0	0	0	0	0	0	0	0	0	0	0	0	0	0
	Reophax subfusiformis (Earland)	0	1	0	0	0	0	0	0	0	0	0	0	0	0	0	0	1	0
	Scutulons sp.	0	0	0	0	0	0	0	0	0	0	0	0	0	0	0	0	0	0
	Stainforthia loeblichi (Feyling-Hanssen)	0	3	0	0	0	0	0	0	0	0	0	0	0	0	0	0	3	0
	Textularia earlandi (Parker)	0	0	0	0	0	0	0	0	0	0	0	0	0	0	0	0	0	0
	Textularia sagittula (Defrance)	0	0	0	0	0	0	0	0	0	0	0	0	0	0	0	0	0	0
	other species	0	0	0	1	0	0	0	0	0	0	0	0	0	0	0	0	1	0
	Total density per slice	143	207	249	86	156	139	99	56	55	73	59	27	24	24	33	26	1457	100

GF17-1C	Species	0-2	2-4	4-6	6-8	8-10	10-12	12-14	14-16	16-18	18-20	20-25	25-30	30-35	35-40	40-45	45-50	Total density per species	Relative abundance (%)
invasive species	*Nonionella* sp.T1 (Deldicq and al., 2019)	2	1	0	0	0	0	0	0	1	0	0	0	0	0	0	0	4	1
known denitrifying species in GF	*Globobulimina turgida* (Bailey)	0	0	0	0	0	0	0	0	0	0	0	0	0	0	0	0	0	0
	Globobulimina auricula (Höglund)	0	0	0	0	0	0	0	11	1	1	1	0	0	0	0	0	14	2
candidate denitrifying species	*Bolivina pseudopunctata* (Höglund)	2	1	1	1	1	1	5	2	1	4	0	0	0	0	0	0	18	2
	Stainforthia fusiformis (Williamson)	11	8	0	0	0	0	1	1	1	0	1	0	0	0	0	0	23	3
non-denitrifyng species	*Bulimina marginata* (d'Orbigny)	31	38	66	17	31	9	11	12	12	1	3	1	2	2	2	4	244	30
	Cassidulina laevigata (d'Orbigny)	9	24	26	20	11	7	5	9	6	3	0	0	0	0	0	0	119	15
	Leptohalysis scotti (Chaster)	21	12	17	8	17	14	17	18	35	31	18	18	6	17	24	19	293	36
minor other species	*Ammonia falsobeccari* (Rouvillois)	0	0	0	0	0	0	0	0	0	0	0	0	0	0	0	0	0	0
	Bolivina skagerrakensis (Qvale and Nigam)	0	0	0	0	0	0	0	0	0	0	0	0	0	0	0	0	0	0
	Bolivina spathulata (Williamson)	0	2	2	0	0	1	0	0	0	0	0	0	0	0	0	0	5	1
	Bolivina sp.	0	2	0	0	0	0	0	0	0	0	0	0	0	0	0	0	2	0
	Cribrostomoides nitida (Goës)	0	0	0	0	0	0	0	0	0	0	0	0	0	0	0	0	0	0
	Eggerella scabra (Williamson)	0	0	0	0	0	0	0	0	0	0	0	0	0	0	0	0	0	0
	Elphidium clavatum-selseyensis (d'Orbigny)	0	0	0	0	0	0	0	0	0	0	0	0	0	0	0	0	1	0
	Hyalinea balthica (Schroeter)	1	0	0	0	0	0	0	2	0	0	0	0	0	0	0	0	3	0
	Lenticulina sp.	0	2	0	0	1	0	0	0	0	0	0	0	0	0	0	0	3	0
	Liebusella goesi (Höglund)	0	0	0	0	0	0	0	0	0	0	0	0	0	0	0	0	0	0
	Nonionella labradorica (Dawson)	1	0	1	0	0	2	0	0	3	0	0	0	0	0	0	0	7	1
	Nonionella turgida (Williamson)	0	0	0	0	0	0	0	0	0	1	3	0	0	0	0	0	4	0
	Pyrgo williamsoni (Silvestry)	2	2	6	1	2	1	1	5	3	1	0	0	0	0	0	0	24	3
	Quinqueloculina bosciana (d'Orbigny)	0	0	2	0	0	0	0	0	0	0	0	0	0	0	0	0	2	0
	Quinqueloculina seminulum (Linné)	3	3	1	0	0	1	0	0	0	0	0	0	0	0	0	0	8	1
	Quinqueloculina stalkeri (Loeblich and Tappan)	0	0	0	0	0	0	0	0	0	0	0	0	0	0	0	0	0	0
	Reophax subfusiformis (Earland)	1	0	0	0	0	0	0	0	0	0	0	0	0	0	0	0	1	0
	Scutulons sp.	0	1	0	0	0	0	0	0	0	0	0	0	0	0	0	0	1	0
	Stainforthia loeblichi (Feyling-Hanssen)	1	1	0	0	0	1	1	0	0	1	0	0	0	0	0	0	5	1
	Textularia earlandi (Parker)	0	0	1	0	0	0	0	0	0	0	0	0	0	0	0	0	1	0
	Textularia sagittula (Defrance)	0	0	0	0	0	0	0	0	0	0	0	0	0	0	0	0	0	0
	other species	0	0	1	1	0	1	0	1	0	0	0	0	0	0	0	0	4	1
	Total density per slice	85	96	123	47	63	38	41	61	63	43	27	20	9	20	26	24	786	100

Table S3: Relative abundance (%) of the main foraminiferal species of the Gullmar Fjord per zones defined by porewater nitrate modelling profiles. In the GF17-3 oxic station, three zones are delimited: the nitrification zone from 0 to 12 mm depth, the 1st denitrification zone from 12 to 35 mm depth and the 2nd denitrification zone from 35 to 50 mm depth, then the foraminiferal relative abundance of the total core from 0 to 50 mm depth. In the GF17-1 hypoxic station, one zone is delimited by the porewater nitrate modelling profile: the nitrification zone from 0 to 16 mm depth. Then, the rest of the core corresponded to the undetected nitrate zone from 16 to 50 mm depth. The foraminiferal sections are divided as: the invasive Nonionella sp. T1 species according to Polovodova Asteman and Schönfeld (2015) and Deldicq et al. (2019), the known denitrifying species in the GF according to Risgaard-Petersen et al. (2006) and Woehle et al. (2018), the non-denitrying species according to Pina-Ochoa et al. (2010) and the minor other species of the fauna.

GF17-3A	Species	Relative percentage from 0-12 mm depth zone	Relative percentage from 12-35 mm depth zone	Relative percentage from 35-50 mm depth zone	Total Relative percentage from 0-50 mm depth zone
invasive species	*Nonionella* sp.T1	18	27	60	34
known denitrifying species in GF	*Globobulimina turgida*	0	0	0	0
	Globobulimina auricula	0	0	0	0
candidate denitrifying species	*Bolivina pseudopunctata*	1	0	0	0
	Stainforthia fusiformis	2	1	0	1
non-denitrifying species	*Bulimina marginata*	42	34	34	37
	Cassidulina laevigata	16	7	0	9
	Leptohalysis scotti	6	25	5	11
minor other species	other species (<5%)	16	6	1	8
	% by zone	100	100	100	100

GF17-3C	Species	Relative percentage from 0-12 mm depth zone	Relative percentage from 12-35 mm depth zone	Relative percentage from 35-50 mm depth zone	Total Relative percentage from 0-50 mm depth zone
invasive species	*Nonionella* sp.T1	50	78	98	74
known denitrifying species in GF	*Globobulimina turgida*	0	0	0	0
	Globobulimina auricula	0	0	0	0
candidate denitrifying species	*Bolivina pseudopunctata*	0	0	0	0
	Stainforthia fusiformis	1	0	0	1
non-denitrifying species	*Bulimina marginata*	12	2	0	5
	Cassidulina laevigata	13	2	0	5
	Leptohalysis scotti	11	13	1	9
minor other species	other species (<5%)	13	5	0	6
	% by zone	100	100	100	100

GF17-1A	Species	Relative percentage from 0-16 mm depth zone	Relative percentage from 16-50 mm depth zone	Total average from 0-50 mm depth zone
invasive species	*Nonionella* sp.T1	2	15	5
known denitrifying species in GF	*Globobulimina turgida*	0	0	0
	Globobulimina auriculata	0	2	1
candidate denitrifying species	*Bolivina pseudopunctata*	0	0	0
	Stainforthia fusiformis	2	4	3
non-denitrifying species	*Bulimina marginata*	66	61	64
	Cassidulina laevigata	19	5	16
	Leptohalysis scotti	4	6	4
minor other species	other species (<5%)	7	7	6
	% by zone	100	100	100

GF17-1C	Species	Relative percentage from 0-16 mm depth zone	Relative percentage from 16-50 mm depth zone	Total average from 0-50 mm depth zone
invasive species	*Nonionella* sp.T1	0	0	1
known denitrifying species in GF	*Globobulimina turgida*	0	0	0
	Globobulimina auricula	0	0	0
candidate denitrifying species	*Bolivina pseudopunctata*	3	1	2
	Stainforthia fusiformis	3	1	3
non-denitrifying species	*Bulimina marginata*	35	11	30
	Cassidulina laevigata	19	2	15
	Leptohalysis scotti	24	75	36
minor other species	other species (<5%)	13	10	14
	% by zone	100	100	100

Equation S2. Calculation example of the Nonionella sp. T1 denitrification rate (nmol cm^{-3} d^{-1}) and the contributions (%) of Nonionella sp. T1 to nitrogen cycle (GF17-3A).

Conversion of *Nonionella* sp. T1 denitrification rate in nmol cm^{-3} s^{-1}

Corrected *Nonionella* sp. T1 denitrification rate = 38 pmol ind^{-1} d^{-1}

38 pmol ind^{-1} d^{-1}/ 1000/ 86400 = 4.4 nmol ind^{-1} s^{-1}

4.4 nmol ind^{-1} s^{-1} * 841 (number of *Nonionella* sp. T1)/ (PI * 25/4) (cross section area of the microtube) = 1.90 E $^{-05}$ nmol cm^{-3} s^{-1}

Contribution of *Nonionella* sp. T1 to benthic denitrification

Contribution A (%) = Foraminifera denitrification / Denitrification estimated by PROFILE from nitrate porewater.

Contribution A (%) from GF17-3A= (1.90 E $^{-05}$ nmol cm^{-3} s^{-1} * 100) / 4.07 E $^{-05}$ nmol cm^{-3} s^{-1} (sum of the two porewater denitrifying zones, Fig. 5 d, Table 1) = 47%.

Contribution B (%) = Foraminifera denitrification / (Foraminifera denitrification + Denitrification estimated by PROFILE from nitrate porewater).

Contribution B (%) from GF17-3A= (1.90 E $^{-05}$ nmol cm^{-3} s^{-1} * 100) / (1.90 E $^{-05}$ nmol cm^{-3} s^{-1} + 4.07 E $^{-05}$ nmol cm^{-3} s^{-1}) sum of the two porewater denitrifying zones, Fig. 5 d, Table 1) = 32%.

CHAPTER 2

Impact of hypoxia and bioirrigation on benthic manganese release in the Gullmar Fjord using 2D high spatial resolution methods

Chapter 2: Impact of hypoxia and bioirrigation on benthic manganese release in the Gullmar Fjord using 2D high spatial resolution methods

C. Choquel[1]*, E. Meztger[1], E. Geslin[1], T. Jauffrais[2], A. Thibault de Chanvalon[3], H.L. Filipsson[4], P. Launeau[1], L. Jean-Soro[5], N. Risgaard-Petersen[6], B. Jesus[7,8] and A. Mouret[1]

Correspondance to: Constance Choquel (constance.choquel@gmail.com) and Aurélia Mouret (aurelia.mouret@univ-angers.fr)

1: UMR 6112 LPG BIAF, Univ. Angers, Univ. Nantes, CNRS, France
2: Ifremer, IRD, Univ. Nouvelle-Calédonie, Univ. La Réunion, CNRS, UMR 9220 ENTROPIE, New Caledonia
3: IPREM UMR 5254 CNRS-UPPA, Pau university, France
4: Department of Geology, Lund University, Sweden
5: IFSTTAR, GERS, EE, Nantes, France
6: Department of Biology, Aquatic Biology, Aarhus University, Denmark

1. Introduction

In natural environments, the most common oxidation states of manganese (Mn) are Mn(II), Mn(III) and Mn(IV). In marine and freshwaters, the Mn oxidation states are coupled to reactions affecting the biogeochemical cycles as carbon, nitrogen, sulfur, oxygen, and iron (Burdige, 1993; Aller, 1994b; Hulth et al., 1999). Two redox phases of Mn are commonly described in sediments: the dissolved and reduced Mn(II) phase and the solid-phase Mn(III, IV) oxides/oxyhydroxides. Mn(IV) oxides result from the aging of Mn(III) during sediment burial (Anschutz et al., 2005). Soluble Mn(III) complexed with a ligand has long been underestimated in the dissolved Mn phase of the sediments due to methodological limitations (Madison et al., 2013; Thibault de Chanvalon and Luther, 2019). Soluble Mn(III) can be both electron acceptor or donor. Soluble Mn(III) results mainly from the oxidation of the reduced Mn(II) (Madison et al., 2013).

The Mn is involved in the recycling of organic matter (OM) and many secondary reactions through redox reactions which mobilize oxidized and reduced forms (Froelich et al., 1979; Burdige, 1993). In the absence of oxygen, Mn oxides can be reduced by ammonia (NH_4^+), dissolved iron (Fe(II)), iron sulphide (FeS) and hydrogen sulphide (H_2S) (Froelich et al., 1979; Aller and Rude, 1988; Luther et al., 1997; Hulth et al., 1999; Thamdrup and Dalsgaard, 2000; Madison et al., 2013). The dissolved Mn(III) mainly comes from the oxidation of reduced Mn(II) by oxygen and also from Mn oxides reduction by dissolved iron (Madison et al., 2013). The reduced Mn(II) can be oxidized by oxygen (O_2), nitrate (NO_3^-) and iodate (IO_3^-) (Hulth et al., 1999; Anschutz et al., 2000). In marine oxygenated environment, at steady-state, the surface sediment is constituted of a layer enriched in solid-phase oxidized Mn with Mn(IV) oxides and Mn(III) oxyhydroxides (both forms are referred as Mn oxides) (Canfield et al., 1993; Burdige, 1993). Deeper in anoxic sediments, Mn oxides are reduced to dissolved Mn(II) (Burdige, 1993). Due to the concentration gradient of Mn(II), a part of the benthic flux of dissolved Mn(II) escapes from the anoxic sediment and can be reoxidized at the sediment surface. The presence of a superficial Mn oxides layer creates a cap preventing Mn(II) escape from sediment (Canfield 1993). However, exchanges exist across the sediment oxic-anoxic boundary and across the SWI by diffusion of Mn(II) in the bottom waters and its precipitation in solid phase (Sundby and Silverberg, 1985; Anschutz et al., 2005). In anoxic sediments, Mn(II) can be buried when it precipitates as a carbonate phase.

Hypoxia (< 63 µmol L^{-1} O_2; (Levin et al., 2009; Breitburg et al., 2018)) leads to a transient state of redox boundaries impacting Mn biogeochemical cycle (Burdige, 1993; Aller, 1994b;

Anschutz et al., 2000; Kristensen et al., 2003; Sundby, 2006). A decrease in the O_2 bottom water concentration decreases the reoxidation efficiency of the dissolved Mn (Mn(II) and Mn(III)) which, in well oxygenated bottom water conditions, builds the enrichment in Mn oxides in the oxic sediment layer. The fluxes of reduced compounds as dissolved manganese (Mn_d) from the anoxic sediment to the water column increase (Aller, 1994; Kristiansen et al., 2002; Katsev et al., 2007). The increase of the Mn_d fluxes coincides with the decrease of the oxic sediment layer. Indeed, the impermeability of the oxic layer containing the major part of Mn oxides is exhausted by O_2 depletion and the Mn_d can more easily cross the SWI (Thamdrup et al., 1994). The Mn_d flux released to the water column varies in intensity during hypoxia (Sundby et al., 1986; Thamdrup et al., 1994; Aller, 1994; Kristiansen et al., 2002; Katsev et al., 2007). At the beginning of a hypoxia event, the Mn_d flux increases rapidly until a maximal Mn_d concentration reached in anoxia. Then, the Mn_d flux decreases progressively corresponding to the depletion of the reservoir (or stock) of Mn_d combined with the low reoxidation of Mn oxides (Sundby et al., 1986).

Since 1950, an increase of oxygen consumption of about 50% was observed in the deep water basin of the Gullmar Fjord, located on the Swedish West Coast (Erlandsson et al., 2006). Seasonal hypoxia events occurred in the deep basin of the Gullmar Fjord between early autumn to late winter and sometimes in summer (Nordberg et al., 2000; Filipsson and Nordberg, 2004; Arneborg, 2004; Erlandsson et al., 2006; Polovodova Asteman and Nordberg, 2013; Choquel et al., 2021). The deep basin of the Gullmar Fjord is one of the known Mn oxide-rich environments worldwide (Sundby et al., 1986; Thamdrup, 2000; Engström et al., 2005; Vandieken et al., 2012; Goldberg et al., 2012) with a high organic carbon content (~ 3 %, (Engström et al., 2005)). The reduction of Mn oxides in the Gullmar Fjord was identified as a significant anaerobic carbon oxidation pathway (Engström et al., 2005; Vandieken et al., 2012, 2014).

The Gullmar Fjord sediments are rich in macro and meiofauna (Austen and Wibdom, 1991). Bioturbation is induced in the sediment by infauna as; biodiffusors (e.g. bivalve, echinoderma) which randomly rearranged sediment particles and gallery-diffusors (e.g. polychaeta) which dig galleries, tubes and burrows (Austen and Wibdom, 1991; Gerino et al., 2003; Gilbert et al., 2007). Bioturbation creates a three-dimensional mosaic of sediment oxic-anoxic boundaries (Middelburg and Levin, 2009). Bioturbation contributes to disturb the vertical distribution of redox species, inducing a transient state (Aller, 1982; Berner, 1980; Anschutz et al., 2000). Indeed, benthic infaunal activity impacts solute transport through the passive or active flushing of burrow, generating a network between SWI and deeper sediment, namely bioirrigation

(Meile et al., 2001). Bioirrigation may increase Mn_d fluxes across the SWI to the point that the measured benthic fluxes may be mainly due to bioirrigation rather than diffusion. Bioturbation and bioirrigation impact strongly Mn cycle; metal oxides are conveyed downwards in reduced zones and reduced forms are mixed upwards to reoxidation zones (Canfield et al., 1993; Aller, 1994; Thamdrup, 2000; Burdige, 2006). Early hypoxia may enhance infaunal activity due to biological stress (Point et al., 2007), inducing an increase of bioirrigational Mn_d fluxes to the overlying water (Sundby and Silverberg, 1985). Mn redox transformations occur at millimetre scales, often localized at the SWI and near active flushed (i.e. ventilated) burrows. To better estimates the Mn_d micro-environments, 2D-DET (two-dimensional diffusive equilibrium in thin film) recent technique have to be used to obtain the distribution of Mn_d in sediment porewater at millimeter resolution in two dimensions (Mouret et al., *in preparation*).

Few previous studies reported dissolved and solid-phase Mn measurements in the Gullmar Fjord (Sundby et al., 1986; Engström et al., 2005; Goldberg et al., 2012). No estimation of the Mn cycle and the impact of seasonal hypoxia on this cycle has been established. The present study aimed to fill this gap investigating an innovative modelling approach combining 2D- DET gels (Mn dissolved-phase), embedded sediment (solid-phase Mn) and selective chemical extractions from core samples to quantify the solid-phase Mn. The 2D-DET gels method is a new approach to target manganese micro-environments at millimeter scales combining colorimetry and scanner imagery (Mouret et al., *in preparation*). The mathematical approach developed by Thibault de Chanvalon et al., (2017) to quantify iron fluxes from 2D-DET gels and estimate the SWI diffusive flux and the bioirrigational flux was adapted to calculate Mn dissolved fluxes.

The objectives of this study were: 1) to describe the dissolved and solid-phase Mn micro-distribution of two oxygen contrasted stations in the Gullmar Fjord, 2) to calculate the diffusive and bioirrigational fluxes at both stations and 3) to estimate the benthic Mn cycle in the Gullmar Fjord based on oxygenated steady-state conditions and the impact of a hypoxic event on this cycle.

2. Material and methods

2.1 Site description

The Gullmar Fjord is 28 km long, 1-2 km wide and located on the Swedish West coast (Fig. 1). The fjord climate fluctuates between cold and temperate conditions (Svansson, 1975; Nordberg, 1991; Polovodova Asteman and Nordberg, 2013; Polovodova Asteman et al., 2018).

The Gullmar Fjord is stratified in four water masses (Svansson, 1984; Arneborg, 2004). Hypoxic events in the fjord have been linked to the influence of the North Atlantic Oscillation (Nordberg et al., 2000; Björk and Nordberg, 2003; Filipsson and Nordberg, 2004). In the deepest basin, the sediment accumulation rates were estimated between 0.7 to 0.9 cm/ y^{-1} (Filipsson and Nordberg, 2004; Nordberg et al., 2009). The monitoring from January 2010 to September 2018 of oxygen bottom water concentrations of several stations located in the Gullmar Fjord (Släggö (65 m depth), Björkholmen (70 m) and Alsbäck (117 m)) was presented in Choquel et al., (2021), data were obtained from the Swedish Meteorological and Hydrological Institute's (SMHI's) publicly available database SHARK (SMHI, 2020). Since 2010, the threshold of hypoxia (< 63 µmol L^{-1} O_2) in Alsbäck station (117 m water depth) is reached typically in late autumn and winter. Deep-water exchanges usually occur in late winter to early spring. However, the duration of hypoxia varies between years and hypoxia events occurred in the summers 2014 and 2015, due to a lack of deep-water exchange. The frequency of hypoxic events has increased in the Gullmar Fjord (Nordberg et al., 2000; Filipsson and Nordberg, 2004).

2.2 Sampling

2.2.1 Sediment core sampling

The sampling cruise was conducted in the Gullmar Fjord with R/V Skagerak and took place the 14th and 15th November 2017 (Choquel et al., 2021). Two stations were sampled. GF17-3 station (50 m water depth) was located closest to the mouth of the fjord (58°16'50.94"N/ 11°30'30.96"E) with bottom waters from the Skagerrak (blue diamond, Fig. 1) and GF17-1 station (117 m water depth) was located close to the deepest part of the fjord (58°19'41.40"N/11°33'8.40"E) near Alsbäck monitoring station in the middle of the stagnant basin (red square, Fig. 1). CTD profiles (Choquel et al., 2021) allowed to determine bottom water oxygenation at both stations, with [O_2] = 234 µmol L^{-1} for the GF17-3 station and [O_2] = 9 µmol L^{-1} for the GF17-1 station. Two cores (Ø 9 cm and max length 80 cm) per station were sampled with a Ge-Max corer for geochemical analyses. The first core was dedicated for two-dimensional analyses and the second to O_2 microelectrode profiling and solid-phase Mn analyses. Temperature and salinity were measured in the core supernatant water immediately after their recovery on the deck using a WTW Series 3110 conductivity meter.

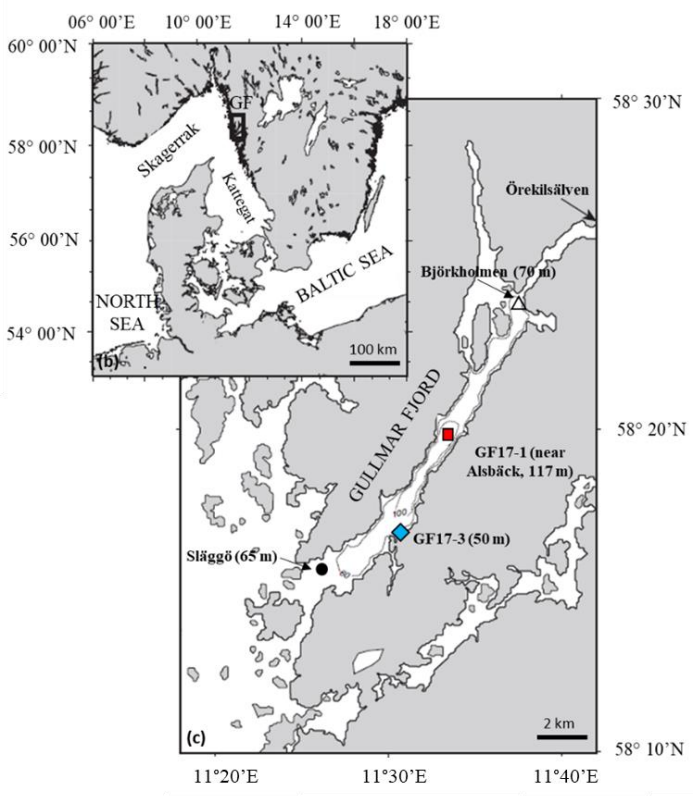

Figure 1: Location of studied stations in the Gullmar Fjord (modified from Choquel et al., (2021)). (a) Location of the Gullmar Fjord (Sweden). (b) Location of the sampling stations: blue diamond for GF17-3 oxic station (50 m water depth) and red square for GF17-1 hypoxic station (117 m water depth). The dark circle and white triangle indicate the monitoring stations Släggö (65 m water depth) and Björkholmen (70 m water depth), respectively.

2.2.2 Sampling and treatment for two-dimensional analyses

One core per station was carefully brought to Lund University (Sweden) and stored at *in situ* temperature (10°C) until further analyses the next day. Overlaying water of the GF17-3 core was gently air bubbled to maintain the oxygenated conditions recorded at this station. Hypoxia in the overlaying water of the GF17-1 core was maintained by bubbling with N_2 gas passed through a solution of carbonate/ bicarbonate to avoid pH rise due to degassing of carbon dioxide (CO_2). A schematic of sampling and treatment for the Mn_d 2D-DET gel and the sediment slab associated is presented in Figure 2. For each core, a 2D-DET (Diffusive Equilibrium in Thin films) gel probe (16 cm x 6.5 cm and 0.5 mm thickness, Fig. 2) was handmade-prepared and mounted on a Plexiglas plate and protected from particles by a PVDF membrane (0.2 µm). Then, the DET gel probes were mounted on stainless-steel boxes. These boxes were cut to have an opening of the size of the 2D-DET gel. This opening was covered with a PVDF membrane (0.2 µm) to allow diffusive transport between sediment into the box and 2D-DET gel and latter solution exchanges during embedding of the slab. The device was

inserted in the two sampled cores GF17-3 and GF17-1 respectively (see Fig. 2, b1) for 5h of diffusive equilibration time. Once the devices recovered, the stainless steel boxes were disassembled to realize the different treatments and analyses: 1) the dissolved Mn phase with 2D-DET gels analyses (see details part 3.1) and 2) the solid-phase Mn analyses (see details part 3.2).

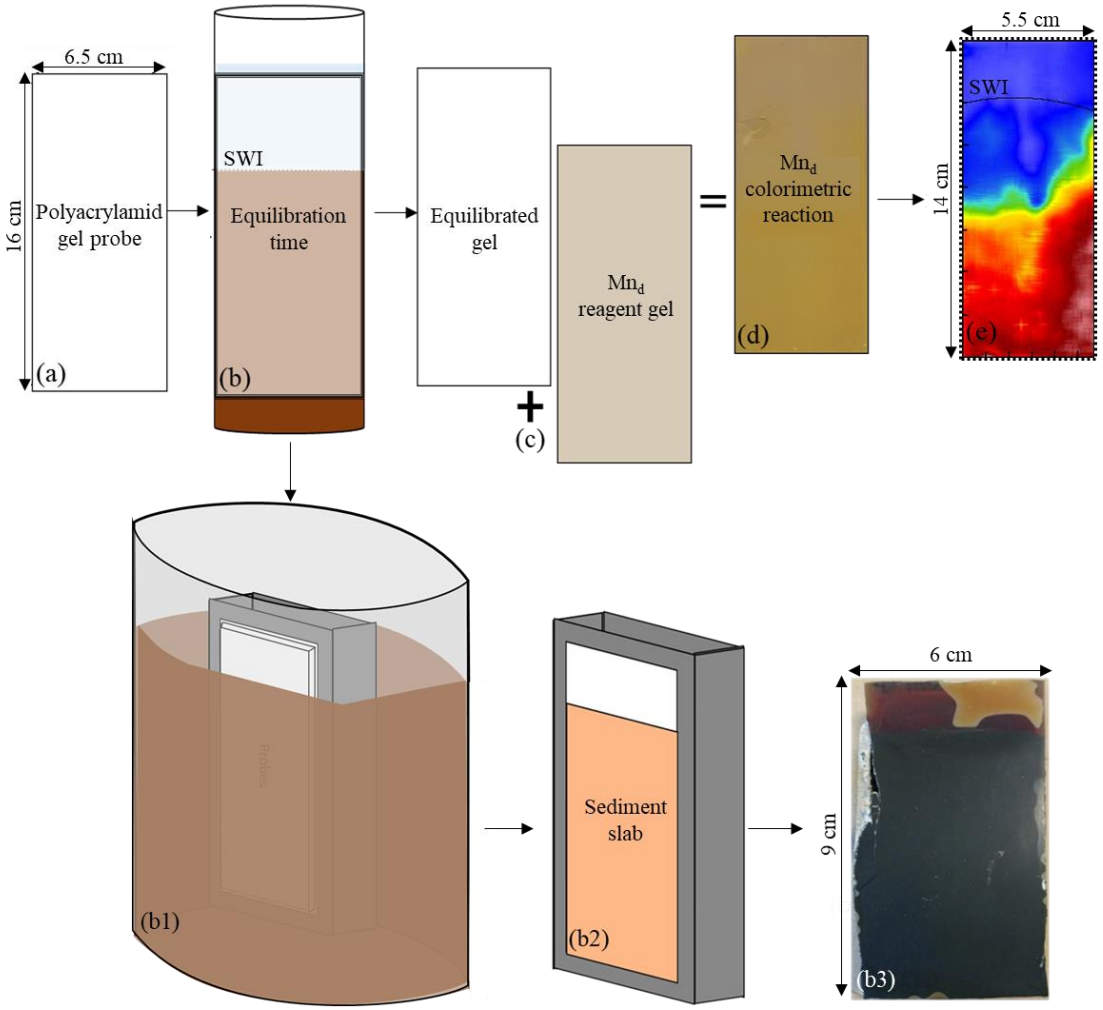

Figure 2: Schematic of the deployment of 2D device for sampling the Mn_d 2D-DET gel and the sediment slab associated and the treatment of the 2D-DET gel. (a) Gel probe dimensions, then (b and b1) the probe was inserted into the sediment core and left for 5 hours of diffusive equilibration time. (c) The equilibrated gel was removed of the core and was laid on a Mn_d reagent gel, the reaction happened in the dark. (d) A yellowish coloration appeared revealing porewater manganese. (e) The gels were scanned and converted into concentrations thanks to a calibrated scale of concentrations. The final image was cut to avoid border effects. (b2) Once the Mn_d step was completed, the sediment slab into the stainless steel box was (b3) embedded to allow Mn solid phase analyses.

The sediment slabs contained in the steel boxes (Fig. 2 b2) were placed in a bigger box to realize the embedding process. No picture of the raw sediment slabs was done due to the PVDF membranes on each side of stainless steel boxes covering the sediment slabs. The embedded

process was described in (Jauffrais et al., *in preparation*, *in preparation* a). The treatment consisted into a series of chemical baths allowing exchanges between the sediment slabs and the bath solutions through the PVDF membrane. The box containing the slabs and the solutions were placed inside a vacuum chamber initially saturated with nitrogen to avoid oxygen contamination of the anoxic sediment and was put under vacuum to promote infiltration into pore spaces. Then, the box containing the embedded slabs was dried in an oven (50°C) until the resin hardens. Once the resin hardened, the epoxy-embedded sediment slabs were cut and the surfaces were polished before to be analysed. The final size of the embedded slabs was 9 x 6 cm (Fig. 2 b3). During the embedding process, a vertical sediment compaction of ~ 1.5 cm was observed.

2.3 Analyses

2.3.1 Dissolved Mn phase analyses with 2D-DET gels

A summary of the Mn_d 2D gel method was presented in Fig. 2 (a – e). This method allowed to determine in 2D the dissolved manganese concentration of sediment porewaters (Mouret et al., *in preparation*). Briefly, in the presence of imidazole, the dissolved manganese (Mn(II) and Mn(III)) of the gel probe reacts with the cadmium-TCPP (4,4′,4″,4‴-(Porphine-5,10,15,20-tetrayl) tetrakis (benzoic acid)) complex and forms a Mn-TCPP complex via a substitution of Cd by Mn. The reagent gel was equilibrated in the dark during 30 minutes with the reactive solution (Fig. 2). Then, a photograph of the gel assemblage was taken with a scanner (CanoScan LiDE 600F). The manganese 2D-DET images were processed with ImageJ® software. Images were cropped at the edges (5 mm omitted from analysis), to remove boundary effects. The final size of the gels was 5.5 cm width by 14 cm long. Then, the images were split into primary colour intensities (red, green and blue), and converted into 16-bit grey-scale images. The blue colour intensity was found to give the most sensitive response for manganese. The pixel values of the manganese gel were calibrated using the pixel values of the manganese standards and plotted with R software (package plot3D). The detection limit of the Mn_d 2D-DET gel used was 19 µmol L^{-1} (Mouret et al. *in prep*).

2.3.2 Solid-phase Mn analyses

Micro-X-ray fluorescence (µ-XRF) analyses

Once the sediment slabs were polished, the surfaces of sides associated to the Mn_d 2D gel faces were analysed with micro-X-ray fluorescence (µ-XRF) to characterize solid-phase Mn

distribution. A Bruker M4 TORNADO laboratory instrument equipped with a Rh X-ray tube operated at 50 kV and 300 µA was used. The X-ray fluorescence was measured using a silicon drift detector with a spot size of 25 µm and a distance of 40 µm between the centre of two spots. The maps were recorded in vacuum with an acquisition time of 50 ms/pixel. The images obtained were assembled on ImageJ® software. All the surface of the embedded sediment was not analyzed (too long acquisition time). Color scaling of images was based on the count intensity range within the mapped area and adjusted for brightness and contrast to optimize the visualization of features with ImageJ® software. The signal intensity transformed into color intensity of the GF17-1 image was low and was multiplied by 11 to be as visible as the GF17-3 image.

Selective chemical extractions

The same cores dedicated to O_2 microelectrode profiling (internal diameter = 8.2 cm) were sliced, frozen and freeze-dried for the determination of reactive solid-phase Mn analyses. An aliquot (~100 mg) was used for the extraction of reactive manganese. Aliquots were exposed to 10 mL of an ascorbate solution (buffered at pH 8) over 24 h (Anschutz et al., 1998; Hyacinthe et al., 2001) to dissolve the reactive Mn oxides and oxyhydroxides referred as Mn(III, IV) (Anschutz et al., 2005). A second aliquot (~100 mg) was exposed to 10 mL of a solution of HCl over 24 h to extract the reactive Mn(III, IV) and the Mn(II) of carbonate phases. Manganese was measured with an ICP-OES ICAP 6300 Thermo-Fischer, using an external aqueous standard for calibration. The results of the extraction by ascorbate are noted Mn-Asc and those of the extraction by HCl, Mn-HCl.

The granulometry of the sediment was performed on the same core used for O_2 microelectrode profiling and solid-phase Mn analyses (Annex 1). The granulometry scale comes from (Blott and Pye, 2001).

2.3.3 Production rate estimates, fluxes and stock calculations

Both fluxes and production rates of dissolved manganese were determined from the measured 2D distributions of Mn_d concentrations. The detailed method was described in Thibault de Chanvalon et al., (2017) for 2D distributions of dissolved iron. Briefly, the procedure was based on the polynomial interpolation of data by the Savitsky-Golay Filter (SGF) procedure on R software. The diffusive Mn_d flux was obtained by applying Fick's first law across the SWI. The uncertainty for SWI positioning using SGF procedure was estimated at ±

1 mm and the diffusive Mn_d flux standard deviation was estimated at 20 % (Thibault de Chanvalon et al., 2017). Bioirrigation is generated by the flushing of ventilated burrow networks (Aller, 2001). Burrows that showed a clear depletion (consumption) of Mn_d (discolouration) were considered as active. The delimitation of the depletion named "burrow lining" was shown by a black line in the 2D image of the sediment. The bioirrigational flux (J_{irr}) was normalized per unit of sediment surface area according to the equation $J_{irr} = (\sum F_{burrow})/ (d_{sed} L_{sed})$ where F_{burrow} was the burrow removal rate, the width (L_{sed}) and the thickness (d_{sed}) of the 2D gel analysed. The uncertainty of the bioirrigational Mn_d flux was estimated at 52 % (i.e. sum of standard deviations from numerical reconstruction and parameter sensitivity, see details in Thibault de Chanvalon et al., 2017). In a steady-state situation, the total efflux of Mn_d across the SWI should be matched by an equal input of manganese (hydr)oxides into the sediment, thus the total Mn_d efflux across the SWI was calculated as the sum of the diffusive and the bioirrigational Mn_d fluxes. The uncertainty of the total Mn_d flux was the sum of the uncertainties of the diffusive Mn_d flux and the bioirrigational Mn_d flux.

The production rate (expressed in µmol L^{-1} d^{-1}) was calculated using the first and the second derivatives of the polynomial at each pixel (Thibault de Chanvalon et al., 2017). The production rate calculation was based on four assumptions: (1) the steady state of diagenesis reactions, (2) the absence of advection, (3) the occurrence of only negligible lateral exchanges and (4) the absence of solute exchange at a lower scale than the sampling resolution. The negative production rate in the 2D image characterised Mn_d consumption zones and the positive production rate showed Mn_d production zones. According to Thibault de Chanvalon et al., (2017), only burrows detected on the basis of a combination of the manganese depletion onto the 2D gels and consumption areas were identified as actively flushed burrows. The "apparent recycling rate" (ARR) was defined as the transfer of manganese from the dissolved phase back to the solid phase of the sediment, expressed for 1 m^2 of the surface of sediment. The ARR was calculated by integrating the production rate for all pixels that show a negative production rate (i.e. manganese consumption) over the whole sediment domain (5.5 cm × 14 cm), dividing this quantity by the domain width (L_{sed} = 5.5 cm) and subtracting the bioirrigational flux. The validity and consequences of these assumptions were abundantly discussed in Thibault de Chanvalon et al., (2017) and references within. The transfer of the solid phase to the dissolved phase was the sum of the ARR and the total Mn_d fluxes. The solid-phase Mn flux was calculated using the Mn-Asc concentrations, the average sedimentation rate of 0.8 cm. y^{-1} (Filipsson and Nordberg, 2004) and a standard porosity of 0.8 and a standard volumic mass of 2560 kg. m^{-3}. The solid-phase Mn stock corresponding to the quantity of Mn oxides (mmol m^{-2}) at the

sediment surface was estimated using the Mn-Asc profiles, the standard porosity, the standard volumic mass and the thickness of the Mn oxides layer.

3. Results

3.1 2D porewater distributions of Mn_d concentrations

Figure 3 shows the two-dimensional data set for the distribution of Mn_d obtained with the 2D gels at the well oxygenated GF17-3 station (Fig. 3a) and at the hypoxic GF17-1 station (Fig. 3b). At the GF17-3 station (Fig. 3a), the Mn_d was almost absent in the bottom water (~ 0 µmol L^{-1}) and increased in a Mn_d accumulation zone from SWI to 8 cm depth (see average profile, Fig. 3c), the maximal peak value reached 50 µmol L^{-1} (Fig. 3a) with an average value of 21 ± 6 µmol L^{-1} in this zone (Fig. 3c), then decreased rapidly near 0 µmol L^{-1} from 8 to 12 cm depth. In the Mn_d accumulation zone (i.e. from SWI to 8 cm depth) the lateral variability was heterogeneous. In the middle of the image (Fig. 3a), a green zone is visible from the SWI to 5 cm depth and presents lower concentrations near 15 µmol L^{-1}, (red 1D profile; Annex 2a, b) compared to concentrations around (yellowish zone, Fig. 3a) reaching until 40 µmol L^{-1} (black 1D profile; Annex 2a, b). This manganese depletion zone (Fig. 3a) is characterized by a decreasing Mn_d concentration towards a potential active burrow lining due to flushed ventilation through burrows to the water column (Fig. 3a).

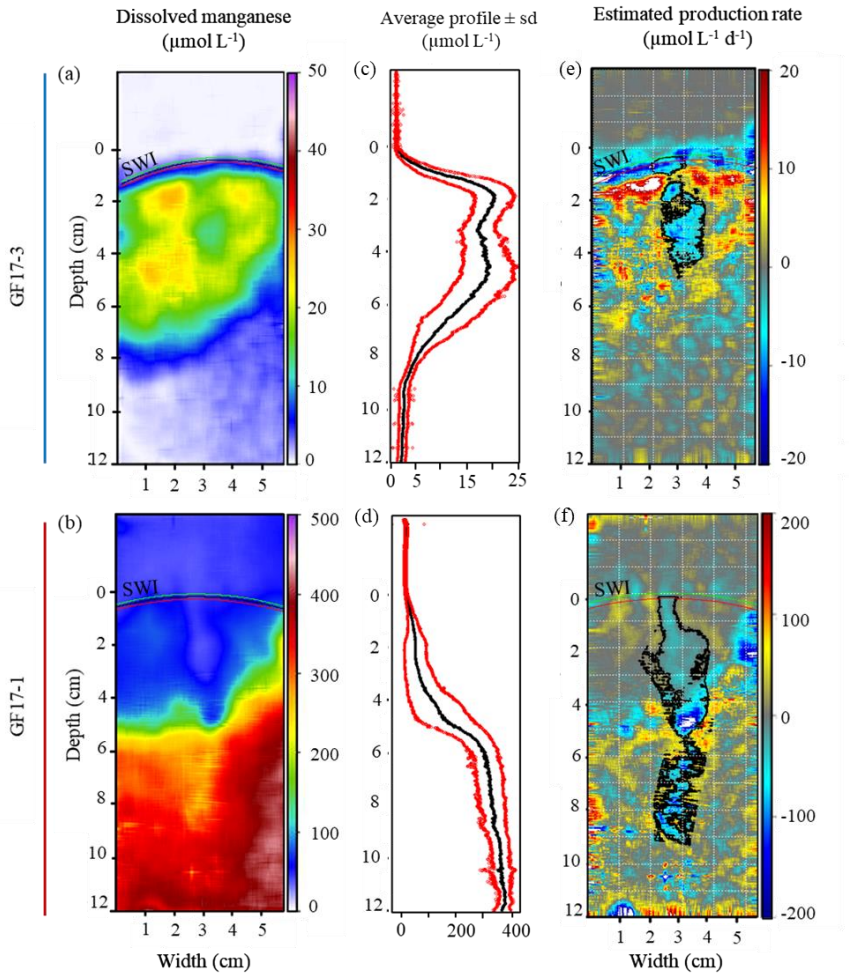

Figure 3: (a, b) Concentrations (µmol L^{-1}) of Mn_d converted in false colour. The SWI is represented by the black line and the uncertainty of ± 1mm on SWI position was represented by the red and green lines. For the hypoxic GF17-1 station, the scale of the concentrations of dissolved manganese was ten time higher than for GF17-3 station. (c, d) Average concentration profiles of the 2D gels (µmol L^{-1}) in black ± standard deviation in red. (e, f) Mn_d production rates (µmol L^{-1} d^{-1}) estimated by SGF procedure. The consumption zones are in blue and the production zones in red. The lining of active burrows is in black.

The 2D Mn_d distributions were highly contrasted between the two stations (Fig. 3a, b). In the hypoxic station, the Mn_d (Fig. 3b) concentration in the bottom water reached 43 ± 5 µmol L^{-1}. In the sediment, the lateral and vertical gradients of Mn_d differed. From the SWI to 5.5 cm depth, the average concentration increased from 41 ± 4 to 228 ± 76 µmol L^{-1} then from 5.5 cm to 12 cm depth the average concentration remained stable 372 ± 31 µmol L^{-1} (average profile, Fig. 3d). In the middle of the image (Fig. 3b), the manganese depleted zone from the SWI to 4 cm depth has concentration similar to bottom water concentrations (red 1D profile, Annex 2c, d). Then, the manganese depleted zone extends deeper from 4 cm to almost 9 cm depth (yellowish zone, Fig. 3b; red 1D profile, Annex 2c, d). This manganese depletion zone from the SWI to 9 cm depth was also related to an active burrow. On the right of the manganese

depleted zone, the concentration gradient was higher from the SWI to 5.5 cm depth (blue 1D profile, Annex 2c, d) and the maximal concentration of 500 µmol L^{-1} was reached at the bottom right of the image (purplish area, Fig. 3b).

Figure 3e and f showed the calculated production rates resulting of the SGF procedure. For the oxygenated GF17-3 station, below the SWI, the main consumption zone was observed at 1cm depth (dark blue zone, Fig. 3e). A production zone, matching with the Mn_d maxima around 2 cm depth (reddish orange zone, Fig. 3e), was located below this consumption zone. Different fragmented patterns were visible with a vertical alternation of production and consumption zones. The lining of the active burrow was delimited by a black line (from SWI to 5 cm depth), corresponding to the boundary between a consumption area and flanked by zones of production. The main consumption zone was inside the burrow (Fig. 3e) and corresponding to the Mn_d green front (15 µmol L^{-1} d^{-1}, Fig. 3a). The production rate was lower and more diffuse (near 0 µmol L^{-1} d^{-1}, Fig. 3e) below the burrow lining from 5 cm depth to the deeper sediment. At the GF17-1 station (Fig. 3f), no clear production and consumption zones were present below the SWI. In the middle of the image, from SWI to 9 cm depth, a consumption zone (blue zone) corresponding to the manganese depletion created by the active burrow (Fig. 3b) was observed. A production zone (orangish zone, Fig. 3f) was visible flanked to the consumption zone. The edge of the active burrow located between these consumption and production zones is delimited by a black line. Around the burrow structure, the production rate was almost 0 µmol L^{-1} d^{-1} without clearly other defined vertical structure.

The SGF procedure allowed to calculate separately the diffusive Mn_d flux from the bioirrigational Mn_d flux across the SWI. Thus, the diffusive Mn_d flux at the oxygenated GF17-3 station was 38 ± 8 µmol m^{-2} d^{-1} and the bioirrigational Mn_d flux was 37 ± 19 µmol m^{-2} d^{-1}. At the hypoxic GF17-1 station, the diffusive Mn_d flux was 83 ± 17 µmol m^{-2} d^{-1} and the bioirrigational Mn_d flux was 555 ± 289 µmol m^{-2} d^{-1}.

3.2 2D distributions of solid-phase Mn

The granulometry of the sediment from the both stations were similarly composed of 80% of coarse silt (16- 31 µm) (Annex 1). The solid-phase Mn micro-distribution was obtained by µ-XRF analyses from the embedded sediment slabs (Fig. 4a, c). The quantification of the solid-phase Mn distribution was obtained by selective chemical extractions (Mn-Asc and Mn-HCl; Fig. 4b, d). At the oxygenated GF17-3 station (Fig. 4a), the solid-phase Mn micro-distribution was scattered (orange patchiness) and decreased from 4 cm to 9 cm depth (less signal intensity

with darker colouration). At SWI, the Mn concentrations were lower than the GF17-1 station with 9 µmol g^{-1} Mn-Asc and 15 µmol g^{-1} Mn-HCl (Fig. 4b). Then, the concentrations decreased from 0.2 to 8 cm depth with 1 ± 1 µmol g^{-1} Mn-Asc and 5 ± 1 µmol g^{-1} Mn-HCl. At the hypoxic GF17-1 station, the solid-phase Mn micro-distribution showed a front enriched in solid-phase Mn below the SWI (Fig. 4c). A vertical structure (targeted by a white arrow, Fig.4c) probably corresponds to a burrow structure. The profiles of Mn-Asc and Mn-HCl (Fig. 4d) showed high concentrations at SWI with 293 µmol g^{-1} for Mn-Asc and 489 µmol g^{-1} for Mn-HCl to 1.2 cm depth with a maximum of 464 µmol g^{-1} and 589 µmol g^{-1}, respectively. Then, the concentration decreased rapidly from 3 cm to 9 cm depth with 11 ± 2 µmol g^{-1} Mn-Asc and 27 ± 5 µmol g^{-1} Mn-HCl. At the bottom (from 8 to 9 cm depth) on the left side of the Figure 4c, the intensity of the signal increased (orange patch), however no increase of the Mn-Asc and Mn-HCl was observed (Fig 4d).

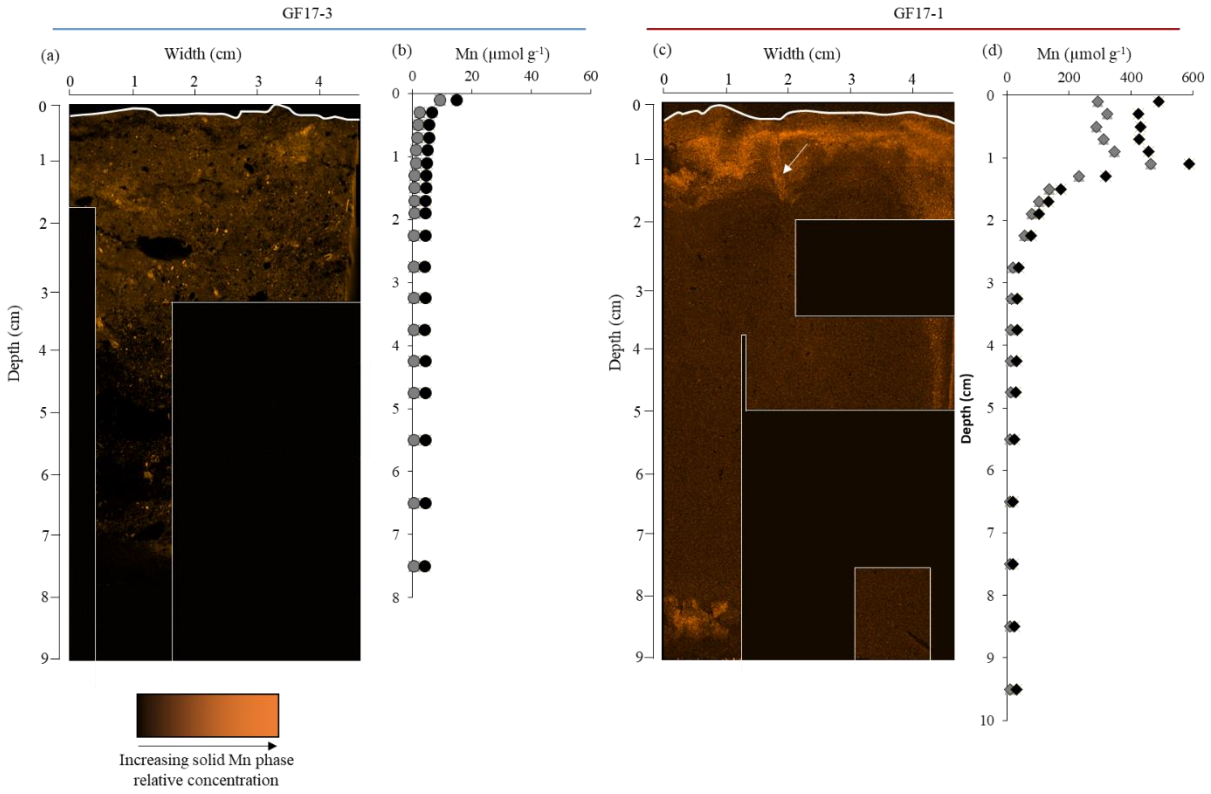

Figure 4: (a, c) Maps of the solid-phase Mn determined with µ-XRF analyses. The white line represents the sediment-water interface and the outlines of the analysed zones. The black parts were the not-analysed zones. Colour scaling from black (the lowest relative concentration) to orange (the highest relative concentration) is based on the count intensity range within the mapped zone and adjusted for brightness and contrast to optimize the visualisation of features. (c) The signal intensity transformed into color intensity of the GF17-1 image was low and was multiplied by 11 to be as visible as the GF17-3 image. (a). The white arrow (c) targets an enriched burrow in solid-phase Mn. (b, d) Vertical distributions of selective chemical extractions; Mn-Asc (µmol. g^{-1}, in grey) and Mn-HCl (µmol. g^{-1}, in black).

4. Discussion

4.1 Comparison with previous studies

To compare the Mn concentrations obtained in this study with the existing literature, the Table 1 summarises a non-exhaustive references list from different places worldwide where Mn concentrations were available.

The Mn_d concentrations at the oxygenated GF17-3 station was not investigated previously. However, a similar maximal Mn_d concentration of 50 µmol L^{-1} was found by (Sundby et al., 1986) at a very shallow station near Kristineberg marine station where bottom waters are well oxygenated (Table 1). When bottom waters are oxygenated, Mn oxides are present in the oxic surface layer. However, no clear solid-phase Mn layer enrichment was visible for the station GF17-3 and the Mn micro-distribution was relatively homogeneous in the four first centimetres on the Mn µXRF map (Fig. 4a). The selective chemical extractions revealed that the first centimeter of sediment was slightly enriched in Mn (Fig. 4b). The low Mn-Asc concentrations are equivalent to Mn oxides data (extraction by hydroxylamine and acetic acid) of Engström et al., (2005) for a station at 70 m water depth located further inside the Gullmar Fjord (Table 1). Maximal solid-phase Mn concentrations were 33 times higher for the hypoxic GF17-1 station and the Mn µXRF map shows an enrichment in the first centimetre of sediment. The Mn-Asc concentrations at the GF17-1 station were slightly higher than the previous Mn oxides (extraction by hydroxylamine and acetic acid) measurements reported in the Alsbäck deep basin by Engström et al., (2005) who sampled in February 2001, one month after the beginning of a hypoxic event (Table 1). Goldberg et al., (2012) sampled the Alsbäck station in January 2009, one month after the beginning of a hypoxic event and found almost twice lower Mn-HCl concentrations and twice lower maximal Mn_d concentrations (Table 1). But in general, our data are consistent with data previously published for the Gullmar Fjord.

Table 1: An overview of the Mnd concentration (µmol L^{-1}) and fluxes (µmol m^{-2} day^{-1}) and the Mn solid phase of the surface sediment (Mn-Asc, µmol. g^{-1}).

References	Water depth (m)	Oxygenation conditions of bottom waters	Methods for Mn_d	Methods for Mn-oxides	Maximal Mn_d (µmol L^{-1})	Maximum Mn-oxides (µmol. g^{-1})	Maximum Mn-HCl (µmol.g^{-1})	Diffusive Mn_d flux (µmol m^{-2} d^{-1})	Total Mn_d flux (µmol m^{-2} d^{-1})
Gullmar Fjord									
This study	50 m	oxic	2D gels	extraction by ascorbate	40	9	15	38	75
This study	117 m	hypoxic	2D gels	extraction by ascorbate	500	293	589	83	638
Sundby et al., 1986	6 m	oxic (begining of the experiment)	porewater extracted by centrifugation/ benthic chamber	-	50	-	-	93	66
Engström et al., 2005	116 m	hypoxic	-	extraction by hydroxylamine and acetic acid	-	250	-	-	-
Engström et al., 2005	70 m	oxic	-	extraction by hydroxylamine and acetic acid		5.7	-	-	-
Goldberg et al., 2012	119 m	hypoxic	porewater extracted by rhizons	-	246	-	~300		-
Skagerrak									
Rajendran et al., 1992	200-600 m	oxic	porewater extracted with a squeezer	extraction by hydrolamine and citrate	45-60	~27-320	~27-320	533-877	-
Bakker et Helder, 1993	35-677 m	oxic	porewater extracted with a squeezer	-	10- 100	-	-	20- 180	-
Canfield et al., 1993	190-695 m	oxic	porewater extracted by centrifugation	extraction by oxalate and dithionite	45- 450	5-330	-		-
Slomp et al., 1997	19-330 m	oxic	porewater extracted by centrifugation	extraction by citrate-dithinite-bicarbonate	2- 220	7	-	-	-
Thamdrup and Dalsgaard, 2000	700 m	oxic	porewater extracted with a squeezer	extraction by oxalate	250	528	-	-	-
Engström et al., 2005	90 and 700 m	oxic		extraction by hydrolamine and acetic acid		3 to 325	-	-	-
Baltic Sea									
Pakhomova et al., 2007	55 m (Gulf of Finland)	oxic	sediment core/ benthic chamber		350			1750	4400
Pakhomova et al., 2007	79 m (Gulf of Finland)	hypoxic	sediment core/ benthic chamber		70			300	1300
Lenz et al., 2015	67 m (Northern Gotland Basin)	oxic	porewater extracted by centrifugation		~10			115	
Lenz et al., 2015	89 m (Bornholm Basin)	hypoxic	porewater extracted by centrifugation		250			236	
Lenz et al., 2015	169 m (Northern Gotland Basin)	anoxic/euxinic	porewater extracted by centrifugation		200			81	
Lenz et al., 2015	191 m (Faro Deep)	anoxic/euxinic	porewater extracted by centrifugation		300			84	
Lenz et al., 2015	238 m (Gotland Deep)	anoxic/euxinic	porewater extracted by centrifugation		250			98	
Lenz et al., 2015	416 m (Landsort Deep)	anoxic/euxinic	porewater extracted by centrifugation		1200			220	
Hermans et al., 2019	238 m (Gotland Deep)	Reoxygenated	porewater extracted by centrifugation	extraction by citrate-dithinite-bicarbonate	411	500		4400	
Hermans et al., 2019	65 m to 200 m (Gotland Basin)	hypoxic	porewater extracted by centrifugation	extraction by citrate-dithinite-bicarbonate	7 to 506	~0 to 400		0 to 6520	
Lenstra et al,, 2021	60 m to 80 m (Gulf of Finland)	seasonally hypoxic	porewater extracted by centrifugation		40 to 350			90 to 4200	3700 to 6600
Lenstra et al,, 2021	67 m (Gotland area)	seasonally hypoxic	porewater extracted by centrifugation		18			80	170
Lenstra et al,, 2021	237 m (Goatland area)	Reoxygenated	porewater extracted by centrifugation		415			4500	15300
Lenstra et al,, 2021	173 m (Gotland area)	euxinic	porewater extracted by centrifugation		80			30	0
Lenstra et al,, 2021	87 m (Bornholm basin)	Reoxygenated	porewater extracted by centrifugation		70			580	2000
Lenstra et al,, 2021	47 m (Arkona basin)	seasonally hypoxic	porewater extracted by centrifugation		22			900	100
Panama basin									
Aller, 1990		oxic	porewater extracted by a squeezer	extraction by hydrolamine and acetic acid	150- 350	21			
Aarhus Bay									
Thamdrup et al., 1994	Aarhus Bay (Denmark)	oxic/ hypoxic	porewater extracted by a squeezer/ benthic chamber		75-110		20	410-1200	330-420
Long Island Sound									
Aller, 1994	Long Island Sound (USA)	oxic-hypoxic	core extractions/ incubations	extraction by hydrolamine and citrate	50-300	4- 30		-10-4590	-6- 3800
Laurentian trough									
Katsev et al., 2007	St Lawrence	hypoxic	porewater extracted by a squeezer/incubations		200			$7\ 10^{-6}$ - $7\ 10^{-5}$	120-419
Madison et al., 2013	St Lawrence	hypoxic	porewater extracted by a squeezer	extraction by ascorbate	50-200	14-140			

The deep basin of the Gullmar Fjord is one of the known Mn oxide-rich environments worldwide (Sundby et al., 1986; Thamdrup, 2000; Engström et al., 2005; Vandieken et al., 2012; Goldberg et al., 2012) with a high organic carbon content (~ 3 %, Engström et al., 2005). In the Skagerrak and in the Baltic sea, the maximal Mn oxides concentrations and the maximal Mn_d concentrations showed ranges of values similar to our results for the Gullmar Fjord (Table 1 and references within). Strong surface enrichments in Mn oxides occur in areas where the flux of metal oxides from the overlying water is large and/or as a result of long-term internal cycling of Mn. A large flux of metal oxides to sediment can be supported by a high input from nearby riverine sources (e.g. on the Amazon shelf; (Aller et al., 1986)), by redeposition of metal oxide rich material eroded from other areas (e.g. in coastal environments; Aller, 1994; Thamdrup et al., 1994), or by "Mn-refluxing", i.e. remobilization of Mn_d from sediment pore water, formation of Mn oxides in the water column and redeposition of the Mn oxides (Adelson et al., 2001; Sulu-Gambari et al., 2017). The dominance of microbial manganese reduction in anaerobic carbon oxidation for Mn oxides rich environments like the Gullmar Fjord was previously shown or suggested (Aller, 1990; Canfield et al., 1993; Engström et al., 2005; Vandieken et al., 2012, 2014; Hyun et al., 2017).

4.2 Impact of hypoxia

Production of dissolved Mn in sediments through reductive dissolution of Mn oxides is driven by the degradation of organic matter (Burdige, 2006). Part of the dissolved Mn can be released to the overlying water and this release is most pronounced for sediments under oxygen-depleted waters (Pakhomova et al., 2007; Homoky et al., 2011). Deeper water in the Gullmar Fjord gets renewed once a year usually during late winter/early spring. Oxygen concentrations decrease during the rest of the year, being lower than 63 µmol L^{-1} during autumn and winter. The low oxygen concentration (9 µmol L^{-1}) of bottom waters at the deep station at the sampling time favour the reductive dissolution of Mn oxides (Burdige, 1993). Maximal Mn_d concentrations are 10 times higher at the GF17-1 station impacted by hypoxia than at the oxic GF17-3 station. They are also twice higher than maximal concentrations measured by Goldberg et al., (2012) who sampled the Alsbäck station in January 2009 during a hypoxic event (Table 1). Mn_d fluxes were calculated from the 2D gels and modelled using the SGF method (Thibault de Chanvalon et al., 2017). Table 2 summarises all Mn_d fluxes calculated from the 2D gels: diffusive flux, bioirrigational flux and total sediment-water flux which corresponds to the sum of diffusive flux and bioirrigational flux. The diffusive Mn_d flux for the oxic GF17-3 station was twice lower than the diffusive flux for the hypoxic GF17-1 station (Table 2). When hypoxia

occurred in the bottom waters, Mn oxides reduction into dissolved manganese increase. Thus, a larger part of the Mn_d can diffuse toward the SWI, increasing the diffusive Mn_d flux. Previous laboratory experiments and studies for other coastal areas found highest benthic release rates of Mn at sites with low bottom water oxygen (Table 1, e.g. (Sundby et al., 1986; Thamdrup et al., 1994; Katsev et al., 2007; Lenz et al., 2015; Hermans et al., 2019)). The Mn_d diffusive flux of the GF17-1 station was not as high compared to other hypoxic Mn-rich places worldwide which can reach higher Mn_d flux values ranging from 370 to 6500 µmol m^{-2} d^{-1} (Table 1; Thamdrup et al., 1994; Aller, 1994; Pakhomova et al., 2007; Hermans et al., 2019; (Lenstra et al., 2021)).

Low Mn oxide concentrations were observed at the oxic station GF17-3 located at 50 m water depth and also at another station located at 70 m water depth sampled by Engström et al., (2005). Contrastingly, the deep station GF17-1 was enriched in Mn oxides (e.g., our study and Engström et al, 2005). The both stations sampled for our study present non negligible Mn_d effluxes towards overlying bottom waters, even the oxic GF17-3 station (Tables 1 and 2). Dissolved Mn released from sediments into oxic overlying waters may precipitate as Mn oxides (Emerson et al., 1982; Millero et al., 1987). They can remain suspended or can settle to the seafloor, often resulting to a cycle of deposition at the SWI, mobilization in dissolved form in the sediment, escape to the overlying water and oxidation upon contact with oxygen followed by redeposition (Aller, 1994). This recycling including the water column is called “refluxing” (Adelson et al., 2001). Additionally, in the presence of dissolved organic matter, a part of dissolved Mn(II) can be oxidized to Mn(III) and complexed with organic ligands and stay in solution (Oldham et al., 2017). Some of the Mn in the water column might be transported laterally and might be precipitated/ be deposited in the deepest part of the fjord leading to Mn sediment focussing. Moreover, during seasonal hypoxic events, remobilization of dissolved Mn from sediments in the deep part of the Gullmar Fjord likely can likely contribute to high dissolved Mn concentrations in the water column as shown by Lenstra et al., (2021) in the Baltic Sea. After the annual inflow of oxygenated water in the deep basin, part of the Mn_d may precipitate as Mn oxides that can be rapidly redeposited due to gravity-driven settling (e.g., Adelson et al., 2001; Sulu-Gambari et al., 2017; Lenstra et al., 2021) and due to the rapid reduction of Mn oxides in the sediment, dissolved Mn could be released back into the water column. In the Baltic Sea, the resulting strong refluxing is responsible for the surface sediment enrichments in Mn and high benthic release fluxes. The refluxing rate would also benefit from a thin hypoxic layer, as this would reduce the time required for upward diffusive and turbulent transfer of dissolved Mn into the oxic waters and downward, gravity-driven settling of Mn oxides (Lenstra et al., 2021). However, to assess the contribution of potential Mn refluxing to

Mn enrichment in the Gullmar Fjord, a combination of pore water profiles, benthic flux determinations and dissolved and particulate Mn analyses in the water column would be required.

Table 2: Summary of different manganese fluxes calculated from the 2D gels by the SGF method and the solid Mn stock from Mn-Asc extractions.

	Oxic GF17-3 station	**Hypoxic GF17-1 station**
Average sedimentation rate (cm. y^{-1})	0.7	0.7
Porosity	0.8	0.8
Volumic mass (kg. m^{-3})	2650	2650
Average [Mn-HCl]-[Mn-Asc] below the Mn oxide peak (µmol. g^{-1})	3.8	18.8
Mn carbonate flux (µmol m^{-2} d^{-1})	39	191
diffusive Mn_d flux (µmol m^{-2} d^{-1}) ± 20%	38 ± 8	83 ± 17
bioirrigational Mn_d flux (µmol m^{-2} d^{-1}) ± 52 %	37 ± 19	555 ± 289
Total SWI Mn_d flux (µmol m^{-2} d^{-1})	75 ± 27	638 ± 306
Apparent Recycling Rate (ARR) (µmol m^{-2} d^{-1}) ± 37 %	131 ± 48	1254 ± 464
Apparent Production Rate (APR) (µmol m^{-2} d^{-1}) ± 37 %	191 ± 71	1800 ± 666
Mn oxide inventory (mmol m^{-2})	16	2200
Number of recycling before burial	1.9	2.4
Residence time	84 days	3.3 years
Time to deplete Mn oxide inventory	213 days	9.4 years

4.3 Impacts of bioirrigation

The macrofauna in the deepest part of the Gullmar Fjord (e.g., mainly Polychaeta, Mollusca, Crustacea) was dense until 3000 ind. m^{-2} in 1978. However, macrofauna disappeared due to a high mortality episode after a severe hypoxic event in the winter 1979/1980 (Josefson and Widbom, 1988). A recolonization followed but the density reached 700 ind. m^{-2}. In July 2001, macrofauna was sampled during oxic conditions at the Alsbäck station for sediment reworking experiments and density values were similar with 795 ind. m^{-2} (Gilbert et al., 2007). (Josefson et al., 2002) sampled a station at 40 m water depth in the innermost part of the Gullmar Fjord in 1999 and found a macrofaunal density of 1300 ind. m^{-2}.

These highly inhabited sediments are perforated with tubes and burrows formed by bottom-dwelling animals such as polychaetes, crustaceans and bivalves. These structures influence the geometry of reaction rates and solute distribution in the sediment creating a mosaic of microenvironments (Kristensen, 2000). During "burrow ventilation," macrofauna flush their burrows with overlying water, meanwhile causing "bioirrigation," which describes the

enhanced solute transport through bulk sediments around the burrow (Kristensen et al., 2012). Macrofaunal water renewal is likely to bring oxic water into the burrows, which consumes reduced dissolved Mn and replenishes the stock of Mn oxide. In the hypoxic GF17-1 station, a Mn-rich structure on the µXRF map (white arrow, Fig. 4c) was identified as a burrow enriched in Mn oxides. This structure could correspond to the burrow identified on the Mn_d 2D gel (Fig. 3b). In the oxic GF17-3 station, no Mn-rich burrow or superficial layer below the SWI was visible on the µXRF map (Fig. 4a). This is probably due to the low concentrations of Mn-oxide (Mn-Asc data). Nevertheless, a burrow structure was identified on the Mn_d 2D gel (Fig. 3a). It is also possible that the burrow was not inside the sediment slab as Mn gel was on the external side of the sampling device (Fig. 2 b1).

Dissolved manganese concentrations decreased towards the interior of the burrows (consumption zones, Fig. 3 c, d). These consumption zones were also observed for 2D dissolved iron distribution in coastal sediments with a high density of macrofaunal burrows (Thibault de Chanvalon et al., 2015, 2017). Thus, the pore-waters with high Mn_d concentrations accumulated in the reduced sediment could be intensively ventilated by burrows and released in the water column. The bioirrigationnal Mn_d flux of the oxic GF17-3 station was equivalent to the diffusive Mn_d flux (Table 2). Conversely at the hypoxic station, the bioirrigationnal Mn_d flux was 7 times higher than the diffusive Mn_d flux (Table 2). Bioirrigationnal fluxes contributed to 49 % and 87 % of the total Mn_d flux for the oxic GF17-3 and the hypoxic GF17-1 stations, respectively. Other studies in environments rich in macrofauna used the comparison between diffusive fluxes calculated using 1D Mn_d profiles and total fluxes measured with *in-situ* benthic chambers or core incubation measurements to estimate the contribution of bioirrigation. In this way, (Warnken et al., 2001) found in the oxic environment of Trinity Bay region in Galveston Bay a contribution of biorrigational Mn_d fluxes of 62-95%. In Gulf of Finland, Pakhomova et al., (2007) obtained a contribution of bioirrigation to total Mn fluxes of 60% and 77% for the oxic and hypoxic stations, respectively. Our estimated contributions are similar to the evaluations of these studies.

Although macrofauna density is probably lower in the deepest part of the Gullmar Fjord, the release of Mn into the water column by bioirrigation is extremely high. The bioirrigational Mn_d flux is lower in the shallow station (Table 2) probably because the Mn-oxide enrichment of the deep station leads to the building of higher Mn_d concentrations in porewater. Nevertheless, these very high pore-water Mn_d concentrations are probably increased with the hypoxic conditions established in the deep part of the fjord one month before sampling.

Hypoxia already had large consequences for the functioning of benthic ecosystems in the Gullmar Fjord as showed by the high decrease of macrofauna density after a severe hypoxia event (Josefson et Widbom, 1988). In severe cases of hypoxia or anoxia, macrofauna density may decrease or disappear. Depending on species resistance to low oxygen conditions/anoxia, bioirrigation may be affected and the total Mn flux to overlying water may strongly decrease (Middelburg and Levin, 2009). However, some macrofauna species can compensate for low oxygen content of the overlying water by increased pumping activity (Gamble, 1970; Kristensen, 1983; Forster et al., 1995). In this case, Mn_d bioirrigational fluxes would be increased.

4.4 Estimated manganese budget of the Gullmar Fjord

A manganese budget is suggested in the Figure 5 for both stations. The oxic GF17-3 station was assumed to be at steady-state; however, the GF17-1 station encountering a hypoxic event was in a transient state. Nevertheless, for the calculations, the steady-state was also assumed at the GF17-1 station. The solid-phase Mn oxides inventories were 2200 mmol m^{-2} and 16 mmol m^{-2} in the hypoxic GF17-1 station and the oxic GF17-3 station respectively (Table 2; Figure 5). The apparent recycling rate (ARR), defined by Thibault de Chanvalon et al. (2017) as the transfer of Mn from the dissolved phase back to the solid phase of the sediment, was calculated for both stations. ARR was 131 ± 48 µmol m^{-2} d^{-1} for the oxic station and 1254 ± 464 µmol m^{-2} d^{-1} for the hypoxic station. An equivalent estimation can be done with the apparent production rate (APR) based on the production of Mn_d from Mn oxides. APR was 191 ± 71 µmol m^{-2} d^{-1} for the oxic station and 1800 ± 666 µmol m^{-2} d^{-1} for the hypoxic station. In steady state conditions, the APR should correspond to the sum of the ARR with the diffusive flux across the SWI and the bioirrigational flux. Accordingly, the Mn budget estimated here shows only a small deficit between 5 and 8 % for oxic and hypoxic stations respectively, which remains within the uncertainty of the estimated fluxes.

Mouret et al., (2009) showed in the Bay of Biscay that when the difference between Mn-HCl and Mn-Asc concentrations was constant at depth, it could be in majority attributed to the precipitation of mixed Ca-Mn carbonates (Middelburg et al., 1987; Mucci, 1988, 2004; Jakobsen and Postma, 1989). Using a sediment accumulation rate of 0.7 cm y^{-1} determined for the deep station (Filipsson and Nordberg, 2004) and average Mn-HCl-Mn-Asc contents of 3.8 µmol g^{-1} and 18.8 µmol g^{-1} below the Mn oxides peaks for the oxic and hypoxic stations respectively, burial fluxes of Mn as carbonate phase can be estimated. Mn burial fluxes of 39 and 191 µmol m^{-2} d^{-1} were found for the oxic and hypoxic stations respectively. Assuming that

Mn inventory in sediment is stable, these estimated Mn carbonate fluxes allow to infer the portion of the ARR reoxidized as Mn oxides (ARR – Mn carbonate flux). These calculations show that 45% and 56% of the Mn_d produced by Mn oxides dissolution are reoxidized in sediment for the oxic and hypoxic stations respectively, 36% and 34% are released to the overlying water and 19% and 10% are buried in sediments as carbonate phase. Based on steady state conditions, this Mn budget allows to estimate the settling Mn oxide fluxes to be 99 µmol m^{-2} d^{-1} for the oxic station and 737 µmol m^{-2} d^{-1} for the hypoxic station. These Mn budget estimations show that 39% and 26% of the settling Mn oxides fluxes for GF17-3 and GF17-1 stations are ultimately buried in sediments. For the hypoxic station, these estimations are more indicative than quantitatively reliable due to the transient state at the time of sampling, with hypoxic conditions likely increasing the APR and decreasing the Mn_d re-oxidation rate in sediments.

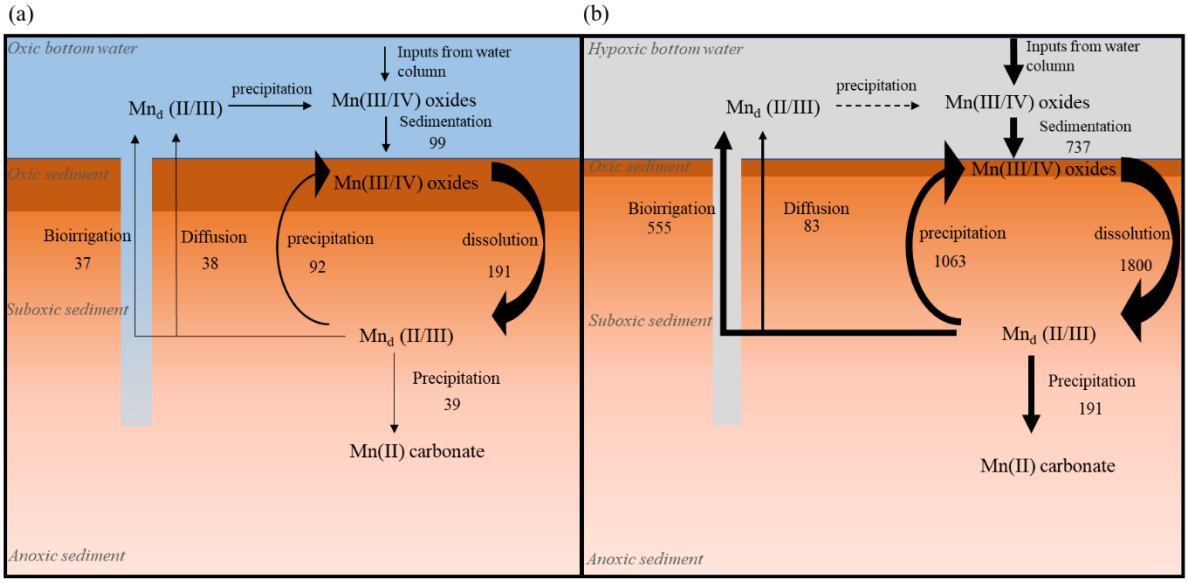

Figure 5: Estimated Mn cycle from the two contrasted O_2 stations in the Gullmar Fjord, (a) oxygenated GF17-3 station (50 m) and (b) hypoxic GF17-1 station (117 m). The black values indicated the Mn_d budget in µmol m^{-2} d^{-1} from the 2D gels modelling. The white values indicated the solid Mn(III/ IV) oxides flux (µmol m^{-2} d^{-1}) from the bottom water to the oxic sediment and the solid Mn(III/ IV) oxides stock in mmol m^{-2} in the oxic sediment layer. Abbreviations; Apparent Recycling Rate (ARR).

The residence time of Mn oxides was calculated from the Mn oxides inventory divided by the APR (Figure 5 and Annex 3 calculation details). The residence time was 84 days and 3.3 years for the GF17-3 station and the GF17-1 station respectively (Table 2). Canfield et al., (1993) obtained a residence time of 250 days in the Skagerrak indicating a rapid recycling of Mn that is of the same order of magnitude as the value obtained for the oxic station. Metal

recycling in sediments allows one metal molecule to be used in organic matter degradation a number of times before burial (Aller, 1990). Solid phase metal oxide is reduced in the metal oxide reduction zone in the anoxic sediment. The reduced metal, which is dissolved in the pore water, can be reoxidized after diffusion into the oxic layer or by reaction with a reoxidizing agent. A subsequent mixing event, such as bioturbation, mixes the newly formed particulate metal oxide into the reducing layer where the metal can be re-used. As long as no metal escape this cycle, metal oxide reduction continued. The ratio of APR to Mn oxides input to sediment reveals that a Mn atom is recycled 1.9 times for the oxic station and 2.4 times for the hypoxic station before finally being buried. These values are very low compared to other estimates in the Skagerrak by (Canfield et al., 1993) (130-260 times) or in the Ulleung Basin by (Hyun et al., 2017) (3800 times). This very low recycling is likely due to high Mn_d effluxes with a high contribution of bioirrigation at both stations.

Oxygen concentration in the waters of the Gullmar Fjord continues to decrease annually due to enhanced oxygen consumption in the deep water (Erlandsson et al., 2006). The sill depth is 42 m and the basin water below the sill level constitutes the part of the basin affected by hypoxia/anoxia due to the annual stagnation of water for 9 months (Erlandsson et al., 2006). The time required to deplete Mn-oxides inventories was estimated by dividing the Mn-oxide inventory by the total Mn_d flux (Figure 5 and Annex 3 calculation details). This time was 9.4 years for the GF17-1 station and 213 days for the GF17-3 station. The oxic GF17-3 station could be affected by hypoxic conditions during severe hypoxia/anoxia periods due to its location below the sill level. Prolonged hypoxic conditions will induce a higher Mn oxides reduction rate and a lower Mn_d re-oxidation rate leading to higher Mn_d efflux and depletion of Mn oxides inventory.

5. Conclusion

This study revealed an innovative approach to estimate the contribution of macrofaunal burrowing activity to manganese (Mn) cycle in the seasonal hypoxic Gullmar Fjord. We combined the using of Mn_d 2D-DET gel method with embedded sediment slabs and selective chemical extractions to visualise and quantify the contrasted dissolved and solid-phases Mn micro-distributions, in oxic station and another impacted by hypoxia event. The deep station GF17-1 impacted by hypoxia revealed a high Mn dissolved and solid-phases. Below the surface a Mn oxides enriched layer and an enriched macrofaunal burrow were visible on the 2D µXRF map. Conversely, the shallower oxic station GF17-3 indicated lower Mn dissolved and solid-

phases. The Mn micro-distribution indicated a homogenous zone with the 2D µXRF map. The dissolved manganese (Mn_d) was 10 times higher in the hypoxic station (reaching up to 500 µmol L^{-1}) than in the oxic station. A burrow lining was detected on the Mn_d 2D gel at the two stations, allowing to calculate separately the diffusive and bioirrigational Mn_d fluxes with the Savitsky-Golay Filter method (Thibault de Chanvalon et al., 2017). In the oxic station, the bioirrigational and diffusive Mn_d fluxes were equivalent. The bioirrigational flux contributed up to 49 % of the total Mn_d flux (sum of the diffusive and bioirrigational Mn_d fluxes, 75 µmol m^{-2} d^{-1}). Conversely, in the hypoxic station the bioirrigational Mn_d flux was 7 times higher than the diffusive flux. This high Mn-rich station was fueled by the intense ventilation of burrows and refluxing (enrichment of the water column and then redeposition linked to focusing). The bioirrigational flux should contribute up to 87 % of the total Mn_d flux (sum of the diffusive and bioirrigational Mn_d fluxes, 638 µmol m^{-2} d^{-1}). Hypoxia can lead to a harsh decrease in macrofaunal density. However, the contribution of bioirrigation to Mn cycle in hypoxia remained high. This would be due to the high amount of Mn_d found in deep sediments. Then, despite the decrease in macrofaunal density, some species of the macrofauna can compensate the lack of oxygen by increasing their pumping activity (more flushing). This study highlighted the high contribution of macrofaunal burrowing activity to the Mn cycle. Finally, we suggested an estimation of the Mn budget in the two contrasted stations. These estimates allowed to quantify (suggesting the steady state) the fluxes between the different states of Mn (e.g. dissolved phase, solid phase, burial) and to reveal how important the bioirrigation part is in the contribution of this cycle.

Bibliography

Adelson, J. M., Helz, G. R., and Miller, C. V.: Reconstructing the rise of recent coastal anoxia; molybdenum in Chesapeake Bay sediments11Associate editor:R. H. Byrne, Geochim. Cosmochim. Acta, 65, 237–252, https://doi.org/10.1016/S0016-7037(00)00539-1, 2001.

Aller, R. C.: The Effects of Macrobenthos on Chemical Properties of Marine Sediment and Overlying Water, in: Animal-Sediment Relations: The Biogenic Alteration of Sediments, edited by: McCall, P. L. and Tevesz, M. J. S., Springer US, Boston, MA, 53–102, https://doi.org/10.1007/978-1-4757-1317-6_2, 1982.

Aller, R. C.: Bioturbation and Manganese Cycling in Hemipelagic Sediments, Philos. Trans. R. Soc. Lond. Ser. Math. Phys. Sci., 331, 51–68, 1990.

Aller, R. C.: The sedimentary Mn cycle in Long Island Sound: Its role as intermediate oxidant and the influence of bioturbation, O2, and Corg flux on diagenetic reaction balances, J. Mar. Res., 52, 259–295, https://doi.org/10.1357/0022240943077091, 1994.

Aller, R. C.: Transport and reactions in the bioirrigated zone, 269–301, 2001.

Aller, R. C. and Rude, P. D.: Complete oxidation of solid phase sulfides by manganese and bacteria in anoxic marine sediments, Geochim. Cosmochim. Acta, 52, 751–765, https://doi.org/10.1016/0016-7037(88)90335-3, 1988.

Aller, R. C., Mackin, J. E., and Cox, R. T.: Diagenesis of Fe and S in Amazon inner shelf muds: apparent dominance of Fe reduction and implications for the genesis of ironstones, Cont. Shelf Res., 6, 263–289, https://doi.org/10.1016/0278-4343(86)90064-6, 1986.

Anschutz, P., Zhong, S., Sundby, B., Mucci, A., and Gobeil, C.: Burial efficiency of phosphorus and the geochemistry of iron in continental margin sediments, Limnol. Oceanogr., 43, 53–64, https://doi.org/10.4319/lo.1998.43.1.0053, 1998.

Anschutz, P., Sundby, B., Lefrançois, L., Luther, G. W., and Mucci, A.: Interactions between metal oxides and species of nitrogen and iodine in bioturbated marine sediments, Geochim. Cosmochim. Acta, 64, 2751–2763, https://doi.org/10.1016/S0016-7037(00)00400-2, 2000.

Anschutz, P., Dedieu, K., Desmazes, F., and Chaillou, G.: Speciation, oxidation state, and reactivity of particulate manganese in marine sediments - ScienceDirect, Chem. Geol., 2005.

Arneborg, L.: Turnover times for the water above sill level in Gullmar Fjord, Cont. Shelf Res., 24, 443–460, https://doi.org/10.1016/j.csr.2003.12.005, 2004.

Austen, M. C. and Wibdom, B.: Changes in and slow recovery of a meiobenthic nematode assemblage following a hypoxic period in the Gullmar Fjord basin, Sweden, Mar. Biol., 111, 139–145, https://doi.org/10.1007/BF01986355, 1991.

Berner, R. A.: Early Diagenesis: A Theoretical Approach, Princeton University Press, 256 pp., 1980.

Björk, G. and Nordberg, K.: Upwelling along the Swedish west coast during the 20th century, Cont. Shelf Res., 23, 1143–1159, https://doi.org/10.1016/S0278-4343(03)00081-5, 2003.

Blott, S. J. and Pye, K.: GRADISTAT: a grain size distribution and statistics package for the analysis of unconsolidated sediments, Earth Surf. Process. Landf., 26, 1237–1248, https://doi.org/10.1002/esp.261, 2001.

Breitburg, D., Levin, L. A., Oschlies, A., Grégoire, M., Chavez, F. P., Conley, D. J., Garçon, V., Gilbert, D., Gutiérrez, D., Isensee, K., Jacinto, G. S., Limburg, K. E., Montes, I., Naqvi, S. W. A., Pitcher, G. C., Rabalais, N. N., Roman, M. R., Rose, K. A., Seibel, B. A., Telszewski, M., Yasuhara, M., and Zhang, J.: Declining oxygen in the global ocean and coastal waters, Science, 359, https://doi.org/10.1126/science.aam7240, 2018.

Burdige, D. J.: The biogeochemistry of manganese and iron reduction in marine sediments, Earth-Sci. Rev., 35, 249–284, https://doi.org/10.1016/0012-8252(93)90040-E, 1993.

Burdige, D. J.: Geochemistry of Marine Sediments, Princeton University Press, 629 pp., 2006.

Canfield, D. E., Jørgensen, B. B., Fossing, H., Glud, R., Gundersen, J., Ramsing, N. B., Thamdrup, B., Hansen, J. W., Nielsen, L. P., and Hall, P. O. J.: Pathways of organic carbon

oxidation in three continental margin sediments, Mar. Geol., 113, 27–40, https://doi.org/10.1016/0025-3227(93)90147-N, 1993.

Choquel, C., Geslin, E., Metzger, E., Filipsson, H. L., Risgaard-Petersen, N., Launeau, P., Giraud, M., Jauffrais, T., Jesus, B., and Mouret, A.: Denitrification by benthic foraminifera and their contribution to N-loss from a fjord environment, Biogeosciences, 18, 327–341, https://doi.org/10.5194/bg-18-327-2021, 2021.

Emerson, S., Kalhorn, S., Jacobs, L., Tebo, B. M., Nealson, K. H., and Rosson, R. A.: Environmental oxidation rate of manganese(II): bacterial catalysis, Geochim. Cosmochim. Acta, 46, 1073–1079, https://doi.org/10.1016/0016-7037(82)90060-6, 1982.

Engström, P., Dalsgaard, T., Hulth, S., and Aller, R. C.: Anaerobic ammonium oxidation by nitrite (anammox): Implications for N2 production in coastal marine sediments, Geochim. Cosmochim. Acta, 69, 2057–2065, https://doi.org/10.1016/j.gca.2004.09.032, 2005.

Erlandsson, C. P., Stigebrandt, A., and Arneborg, L.: The sensitivity of minimum oxygen concentrations in a fjord to changes in biotic and abiotic external forcing, Limnol. Oceanogr., 51, 631–638, https://doi.org/10.4319/lo.2006.51.1_part_2.0631, 2006.

Filipsson, H. L. and Nordberg, K.: Climate variations, an overlooked factor influencing the recent marine environment. An example from Gullmar Fjord, Sweden, illustrated by benthic foraminifera and hydrographic data, Estuaries, 27, 867–881, https://doi.org/10.1007/BF02912048, 2004.

Forster, S., Graf, G., Kitlar, J., and Powilleit, M.: Effects of bioturbation in oxic and hypoxic conditions: a microcosm experiment with a North Sea sediment community, Mar. Ecol. Prog. Ser., 116, 153–161, 1995.

Froelich, P. N., Klinkhammer, G. P., Bender, M. L., Luedtke, N. A., Heath, G. R., Cullen, D., Dauphin, P., Hammond, D., Hartman, B., and Maynard, V.: Early oxidation of organic matter in pelagic sediments of the eastern equatorial Atlantic: suboxic diagenesis, Geochim. Cosmochim. Acta, 43, 1075–1090, https://doi.org/10.1016/0016-7037(79)90095-4, 1979.

Gamble, J. C.: Effect of low dissolved oxygen concentrations on the ventilation rhythm of three tubicolous crustaceans, with special reference to the phenomenon of intermittent ventilation, Mar. Biol., 6, 121–127, https://doi.org/10.1007/BF00347241, 1970.

Gerino, M., Stora, G., François-Carcaillet, F., Gilbert, F., Poggiale, J.-C., Mermillod-Blondin, F., Desrosiers, G., and Vervier, P.: Macro-invertebrate functional groups in freshwater and marine sediments: a common mechanistic classification, 2003.

Gilbert, F., Hulth, S., Grossi, V., Poggiale, J.-C., Desrosiers, G., Rosenberg, R., Gérino, M., François-Carcaillet, F., Michaud, E., and Stora, G.: Sediment reworking by marine benthic species from the Gullmar Fjord (Western Sweden): Importance of faunal biovolume, J. Exp. Mar. Biol. Ecol., 348, 133–144, 2007.

Goldberg, T., Archer, C., Vance, D., Thamdrup, B., McAnena, A., and Poulton, S. W.: Controls on Mo isotope fractionations in a Mn-rich anoxic marine sediment, Gullmar Fjord, Sweden, Chem. Geol., 296–297, 73–82, https://doi.org/10.1016/j.chemgeo.2011.12.020, 2012.

Hermans, M., Lenstra, W. K., van Helmond, N. A. G. M., Behrends, T., Egger, M., Séguret, M. J. M., Gustafsson, E., Gustafsson, B. G., and Slomp, C. P.: Impact of natural re-oxygenation on the sediment dynamics of manganese, iron and phosphorus in a euxinic Baltic Sea basin, Geochim. Cosmochim. Acta, 246, 174–196, https://doi.org/10.1016/j.gca.2018.11.033, 2019.

Homoky, W. B., Hembury, D. J., Hepburn, L. E., Mills, R. A., Statham, P. J., Fones, G. R., and Palmer, M. R.: Iron and manganese diagenesis in deep sea volcanogenic sediments and the origins of pore water colloids, Geochim. Cosmochim. Acta, 75, 5032–5048, https://doi.org/10.1016/j.gca.2011.06.019, 2011.

Hulth, S., Aller, R. C., and Gilbert, F.: Coupled anoxic nitrification/manganese reduction in marine sediments, Geochim. Cosmochim. Acta, 63, 49–66, https://doi.org/10.1016/S0016-7037(98)00285-3, 1999.

Hyacinthe, C., Anschutz, P., Carbonel, P., Jouanneau, J.-M., and Jorissen, F. J.: Early diagenetic processes in the muddy sediments of the Bay of Biscay, Mar. Geol., 177, 111–128, https://doi.org/10.1016/S0025-3227(01)00127-X, 2001.

Hyun, J.-H., Kim, S.-H., Mok, J.-S., Cho, H., Lee, T., Vandieken, V., and Thamdrup, B.: Manganese and iron reduction dominate organic carbon oxidation in surface sediments of the deep Ulleung Basin, East Sea, Biogeosciences, 14, 941–958, https://doi.org/10.5194/bg-14-941-2017, 2017.

Jakobsen, R. and Postma, D.: Formation and solid solution behavior of Ca-rhodochrosites in marine muds of the Baltic deeps, Geochim. Cosmochim. Acta, 53, 2639–2648, https://doi.org/10.1016/0016-7037(89)90135-X, 1989.

Jauffrais, T., Mouret, A., Metzger, E., Jesus, B., Jean-Soro, L., Bernhard, J. M., and Geslin, E.: Combined characterization of fine-scale distributions and microenvironments of living protists in intertidal sediment., J. Exp. Biol. Ecol., in preparation.

Jauffrais, T., Mouret, A., Metzger, E., Jesus, B., Bernhard, J. M., and Geslin, E.: Two-dimensional paired analyses of fine-scale sediment geochemistry and live benthic protists, and metazoans distributions in mudflat chemoclines., Environ. Sci. Technol., in preparation.

Josefson, A. B. and Widbom, B.: Differential response of benthic macrofauna and meiofauna to hypoxia in the Gullmar Fjord basin, Mar. Biol., 100, 31–40, https://doi.org/10.1007/BF00392952, 1988.

Josefson, A. B., Forbes, T. L., and Rosenberg, R.: Fate of phytodetritus in marine sediments: functional importance of macrofaunal community, Mar. Ecol. Prog. Ser., 230, 71–85, https://doi.org/10.3354/meps230071, 2002.

Katsev, S., Chaillou, G., Sundby, B., and Mucci, A.: Effects of progressive oxygen depletion on sediment diagenesis and fluxes: A model for the lower St. Lawrence River Estuary, Limnol. Oceanogr., 52, 2555–2568, https://doi.org/10.4319/lo.2007.52.6.2555, 2007.

Kristensen, E.: Ventilation and oxygen uptake by three species of Nereis (Annelida: Polychaeta). I. Effects of hypoxia, Mar. Ecol. Prog. Ser., 12, 289–297, 1983.

Kristensen, E.: Organic matter diagenesis at the oxic/anoxic interface in coastal marine sediments, with emphasis on the role of burrowing animals, in: Life at Interfaces and Under Extreme Conditions, Dordrecht, 1–24, https://doi.org/10.1007/978-94-011-4148-2_1, 2000.

Kristensen, E., Kristiansen, K. D., and Jensen, M. H.: Temporal behavior of manganese and iron in a sandy coastal sediment exposed to water column anoxia, Estuaries, 26, 690–699, https://doi.org/10.1007/BF02711980, 2003.

Kristensen, E., Penha-Lopes, G., Delefosse, M., Valdemarsen, T., Quintana, C. O., and Banta, G. T.: What is bioturbation? The need for a precise definition for fauna in aquatic sciences, Mar. Ecol. Prog. Ser., 446, 285–302, https://doi.org/10.3354/meps09506, 2012.

Kristiansen, K. D., Kristensen, E., and Jensen, E. M. H.: The Influence of Water Column Hypoxia on the Behaviour of Manganese and Iron in Sandy Coastal Marine Sediment, Estuar. Coast. Shelf Sci., 55, 645–654, https://doi.org/10.1006/ecss.2001.0934, 2002.

Lenstra, W. K., Hermans, M., Séguret, M. J. M., Witbaard, R., Severmann, S., Behrends, T., and Slomp, C. P.: Coastal hypoxia and eutrophication as key controls on benthic release and water column dynamics of iron and manganese, Limnol. Oceanogr., 66, 807–826, https://doi.org/10.1002/lno.11644, 2021.

Lenz, C., Jilbert, T., Conley, D. J., Wolthers, M., and Slomp, C. P.: Are recent changes in sediment manganese sequestration in the euxinic basins of the Baltic Sea linked to the expansion of hypoxia?, Biogeosciences, 12, 4875–4894, https://doi.org/10.5194/bg-12-4875-2015, 2015.

Levin, L. A., Ekau, W., Gooday, A. J., Jorissen, F., Middelburg, J. J., Naqvi, S. W. A., Neira, C., Rabalais, N. N., and Zhang, J.: Effects of natural and human-induced hypoxia on coastal benthos, 2009.

Luther, G. W., Sundby, B., Lewis, B. L., Brendel, P. J., and Silverberg, N.: Interactions of manganese with the nitrogen cycle: Alternative pathways to dinitrogen, Geochim. Cosmochim. Acta, 61, 4043–4052, https://doi.org/10.1016/S0016-7037(97)00239-1, 1997.

Madison, A. S., Tebo, B. M., Mucci, A., Sundby, B., and Luther, G. W.: Abundant Porewater Mn(III) Is a Major Component of the Sedimentary Redox System, Science, 341, 875–878, https://doi.org/10.1126/science.1241396, 2013.

Meile, C., Koretsky, C. M., and Cappellen, P. V.: Quantifying bioirrigation in aquatic sediments: An inverse modeling approach, Limnol. Oceanogr., 46, 164–177, https://doi.org/10.4319/lo.2001.46.1.0164, 2001.

Middelburg, J. J. and Levin, L. A.: Coastal hypoxia and sediment biogeochemistry, Biogeosciences, 6, 1273–1293, https://doi.org/10.5194/bg-6-1273-2009, 2009.

Middelburg, J. J., De Lange, G. J., and van Der Weijden, C. H.: Manganese solubility control in marine pore waters, Geochim. Cosmochim. Acta, 51, 759–763, https://doi.org/10.1016/0016-7037(87)90086-X, 1987.

Millero, F. J., Sotolongo, S., and Izaguirre, M.: The oxidation kinetics of Fe(II) in seawater, Geochim. Cosmochim. Acta, 51, 793–801, https://doi.org/10.1016/0016-7037(87)90093-7, 1987.

Mouret, A., Barbe, A., Levrard, R., Charbonnier, C., Cesbron, F., Choquel, C., and Metzger, E.: Two-dimensional determination of dissolved manganese in sediment porewaters, Front. Chem., in preparation.

Mouret, A., Anschutz, P., Lecroart, P., Chaillou, G., Hyacinthe, C., Deborde, J., Jorissen, F. J., Deflandre, B., Schmidt, S., and Jouanneau, J.-M.: Benthic geochemistry of manganese in the Bay of Biscay, and sediment mass accumulation rate, Geo-Mar. Lett., 29, 133–149, https://doi.org/10.1007/s00367-008-0130-6, 2009.

Mucci, A.: Manganese uptake during calcite precipitation from seawater: Conditions leading to the formation of a pseudokutnahorite, Geochim. Cosmochim. Acta, 52, 1859–1868, https://doi.org/10.1016/0016-7037(88)90009-9, 1988.

Mucci, A.: The Behavior of Mixed Ca–Mn Carbonates in Water and Seawater: Controls of Manganese Concentrations in Marine Porewaters, Aquat. Geochem., 10, 139–169, https://doi.org/10.1023/B:AQUA.0000038958.56221.b4, 2004.

Nordberg, K.: Oceanography in the Kattegat and Skagerrak Over the Past 8000 Years, Paleoceanography, 6, 461–484, https://doi.org/10.1029/91PA01132, 1991.

Nordberg, K., Gustafsson, M., and Krantz, A.-L.: Decreasing oxygen concentrations in the Gullmar Fjord, Sweden, as confirmed by benthic foraminifera, and the possible association with NAO, J. Mar. Syst., 23, 303–316, https://doi.org/10.1016/S0924-7963(99)00067-6, 2000.

Nordberg, K., Filipsson, H. L., Linné, P., and Gustafsson, M.: Stable oxygen and carbon isotope information on the establishment of a new, opportunistic foraminiferal fauna in a Swedish Skagerrak fjord basin, in 1979/1980, Mar. Micropaleontol., 73, 117–128, https://doi.org/10.1016/j.marmicro.2009.07.006, 2009.

Oldham, V. E., Mucci, A., Tebo, B. M., and Luther III, G. W.: Soluble Mn(III)–L complexes are abundant in oxygenated waters and stabilized by humic ligands - ScienceDirect, Geochim. Cosmochim. Acta, 2017.

Pakhomova, S. V., Hall, P. O. J., Kononets, M. Yu., Rozanov, A. G., Tengberg, A., and Vershinin, A. V.: Fluxes of iron and manganese across the sediment–water interface under various redox conditions, Mar. Chem., 107, 319–331, https://doi.org/10.1016/j.marchem.2007.06.001, 2007.

Point, D., Monperrus, M., Tessier, E., Amouroux, D., Chauvaud, L., Thouzeau, G., Jean, F., Amice, E., Grall, J., Leynaert, A., Clavier, J., and Donard, O. F. X.: Biological control of trace metal and organometal benthic fluxes in a eutrophic lagoon (Thau Lagoon, Mediterranean Sea, France), Estuar. Coast. Shelf Sci., 72, 457–471, https://doi.org/10.1016/j.ecss.2006.11.013, 2007.

Polovodova Asteman, Filipsson, H. L., and Nordberg, K.: Tracing winter temperatures over the last two millennia using a north-east Atlantic coastal record, 2018.

Polovodova Asteman, I. and Nordberg, K.: Foraminiferal fauna from a deep basin in Gullmar Fjord: The influence of seasonal hypoxia and North Atlantic Oscillation, J. Sea Res., 79, 40–49, https://doi.org/10.1016/j.seares.2013.02.001, 2013.

Sulu-Gambari, F., Roepert, A., Jilbert, T., Hagens, M., Meysman, F. J. R., and Slomp, C. P.: Molybdenum dynamics in sediments of a seasonally-hypoxic coastal marine basin, Chem. Geol., 466, 627–640, https://doi.org/10.1016/j.chemgeo.2017.07.015, 2017.

Sundby, B.: Transient state diagenesis in continental margin muds, Mar. Chem., 102, 2–12, https://doi.org/10.1016/j.marchem.2005.09.016, 2006.

Sundby, B. and Silverberg, N.: Manganese fluxes in the benthic boundary layer1: Manganese fluxes, Limnol. Oceanogr., 30, 372–381, https://doi.org/10.4319/lo.1985.30.2.0372, 1985.

Sundby, B., Anderson, L. G., Hall, P. O. J., Iverfeldt, Å., van der Loeff, M. M. R., and Westerlund, S. F. G.: The effect of oxygen on release and uptake of cobalt, manganese, iron and phosphate at the sediment-water interface, Geochim. Cosmochim. Acta, 50, 1281–1288, https://doi.org/10.1016/0016-7037(86)90411-4, 1986.

Svansson, A.: Physical and chemical oceanography of the Skagerrak and the Kattegat., 1975.

Svansson, A.: Hydrography of the Gullmar Fjord, Medd. Fraan Havsfiskelab. Lysekil Swed., 1984.

Swedish Meteorological and Hydrological Institute's (SMHI): https://sharkweb.smhi.se/, last access: 13th of July 2020

Thamdrup, B.: Advances in Microbial Ecology, Springer Science & Business Media, 301 pp., 2000.

Thamdrup, B. and Dalsgaard, T.: The fate of ammonium in anoxic manganese oxide-rich marine sediment, Geochim. Cosmochim. Acta, 64, 4157–4164, https://doi.org/10.1016/S0016-7037(00)00496-8, 2000.

Thamdrup, B., Fossing, H., and Barker Jorgensen, B.: Manganese, iron, and sulfur cycling in a coastal marine sediment, Aarhus Bay, Denmark — University of Southern Denmark, Geochim. Cosmochim. Acta, 1994.

Thibault de Chanvalon, A. and Luther, G. W.: Mn speciation at nanomolar concentrations with a porphyrin competitive ligand and UV–vis measurements, Talanta, 200, 15–21, https://doi.org/10.1016/j.talanta.2019.02.069, 2019.

Thibault de Chanvalon, A., Metzger, E., Mouret, A., Cesbron, F., Knoery, J., Rozuel, E., Launeau, P., Nardelli, M. P., Jorissen, F. J., and Geslin, E.: Two-dimensional distribution of living benthic foraminifera in anoxic sediment layers of an estuarine mudflat (Loire estuary, France), Biogeosciences, 12, 6219–6234, https://doi.org/10.5194/bg-12-6219-2015, 2015.

Thibault de Chanvalon, A., Metzger, E., Mouret, A., Knoery, J., Geslin, E., and Meysman, F. J. R.: Two dimensional mapping of iron release in marine sediments at submillimetre scale, Mar. Chem., 191, 34–49, https://doi.org/10.1016/j.marchem.2016.04.003, 2017.

Vandieken, V., Pester, M., Finke, N., Hyun, J.-H., Friedrich, M. W., Loy, A., and Thamdrup, B.: Three manganese oxide-rich marine sediments harbor similar communities of acetate-oxidizing manganese-reducing bacteria, ISME J., 6, 2078–2090, https://doi.org/10.1038/ismej.2012.41, 2012.

Vandieken, V., Finke, N., and Thamdrup, B.: Hydrogen, acetate, and lactate as electron donors for microbial manganese reduction in a manganese-rich coastal marine sediment, FEMS Microbiol. Ecol., 87, 733–745, https://doi.org/10.1111/1574-6941.12259, 2014.

Warnken, K. W., Gill, G. A., Griffin, L. L., and Santschi, P. H.: Sediment-water exchange of Mn, Fe, Ni and Zn in Galveston Bay, Texas, Mar. Chem., 73, 215–231, https://doi.org/10.1016/S0304-4203(00)00108-0, 2001.

Supplementary material

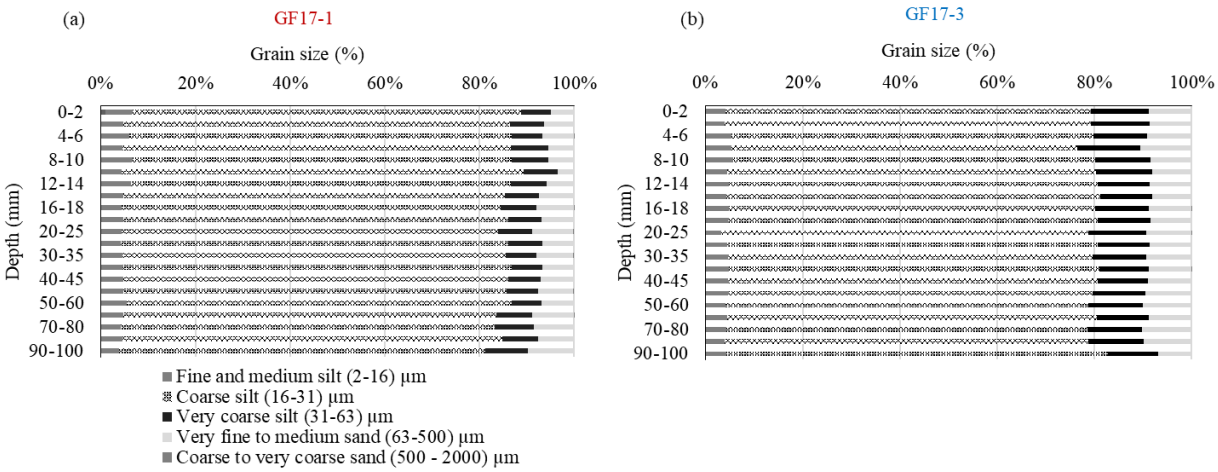

Annex 1: Gullmar Fjord grain size analyses (%) (a) hypoxic GF17-1 station and (b) oxygenated GF17-3 station. Five size fractions were detailed; in grey fine, and medium silt (2-16) µm, in dotted line, coarse silt (16-31) µm, in black very, coarse silt (31-63) µm, in light grey, very fine to medium sand (63-500) µm, in dark grey, coarse to very coarse sand (500-2000) µm. The granulometry scale came from Blott and Pye, (2001).

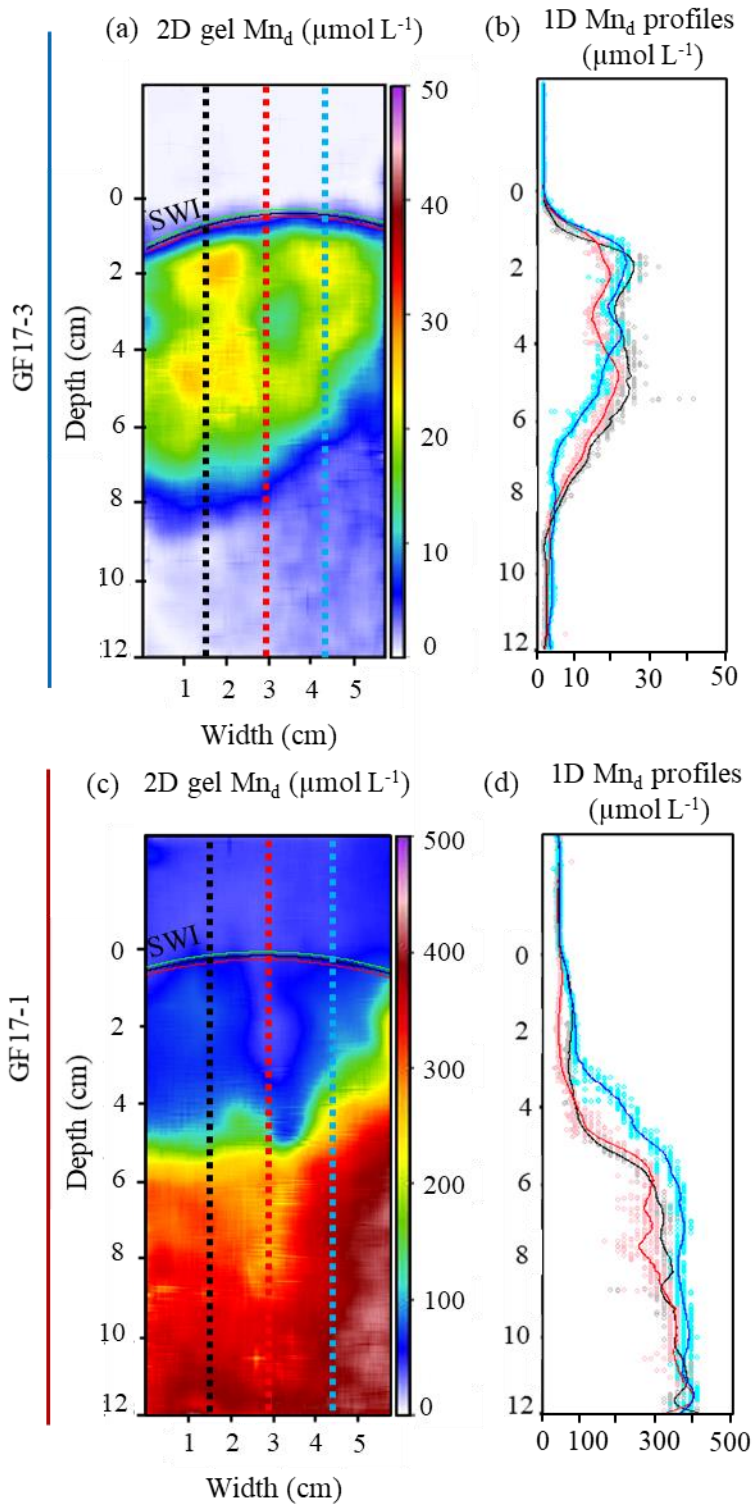

Annex 2: (a-b) Oxygenated GF17-3 station and (c-d) hypoxic GF17-1 station. (a, c) 2D gels Mn$_d$, the dotted vertical lines were the location of the 1D profiles visible in figure b and d, respectively. Abbreviations; sediment-water interface (SWI).

Annex 3 calculation details of the Table 2:

Mn carbonate flux
Sediment flux = [Sediment rate ($cm.y^{-1}$)/ 100] x 0.2 x Volumic mass ($kg.m^{-3}$) = (0.7/ 100) x 0.2 x 2650 = 3.71 kg m^{-2} y^{-1}

Mn carbonate flux= [Solid flux (kg m^{-2} y^{-} 1) x average [MnHCl]-[MnAsc] (µmol g^{-1}) x 1000]/ number of days per year= (4.24 x 3.8 x 1000)/ 365.25 days = 38 µmol m^{-2} d^{-1}

Mn oxide inventory (mmol m^{-2})
For a sediment slice:
Mn-Asc (µmol g^{-1}) x (1- porosity) x Volumic mass ($kg.m^{-3}$) x thickness of the slice (m)

Inventories are calculated as the sum of all sediment slices belonging to the Mn-rich peak in the MnAsc profile.

Number of recycling before burial:
APR (µmol m^{-2} d^{-1}) /settling Mn oxide flux (µmol m^{-2} d^{-1}) = 191 / 99 = 1.9

Residence time (days):
[Mn oxide inventory (mmol m^{-2}) x 1000/ APR (µmol m^{-2} d^{-1})] = 16 x 1000 / 191= 84 days

Time to deplete Mn oxide inventory (days):
[Mn oxide inventory (mmol m^{-2}) x 1000/ Total SWI Mn_d flux (µmol m^{-2} d^{-1})] = 16 x 1000 / 75 = 213 days

CHAPTER 3

Spatiotemporal dynamics of living benthic foraminifera revealed by multiple environmental parameters and *in situ* trophic model in intertidal mudflat (Bourgneuf Bay, France)

Chapter 3: Spatiotemporal dynamics of living benthic foraminifera revealed by multiple environmental parameters and *in situ* trophic model in intertidal mudflat (Bourgneuf Bay, France)

C. Choquel[1]*, E. Geslin[1], E. Metzger[1], E. Houliez[4], B. Jesus[3], A. Prins[3], T. Jauffrais[2], E. Bénéteau[1], A. Mouret[1]

1: UMR 6112 LPG BIAF, Univ. Angers, Univ. Nantes, CNRS, France

2: Ifremer, IRD, Univ. Nouvelle-Calédonie, Univ. La Réunion, CNRS, UMR 9220 ENTROPIE, New Caledonia

3: Université de Nantes, Mer Molécules Santé, EA 2160, France

4: Université de Lille, CNRS, Université du Littoral Côte d'Opale, UMR 8187, LOG, Laboratoire d'Océanologie et de Géosciences, F 62930 Wimereux, France

(*correspondance: Constance Choquel (constance.choquel@gmail.com) and Emmanuelle Geslin (emmanuelle.geslin@univ-angers.fr))

1. Introduction

Intertidal environments occur at the transition between the marine and continental realms, as semi-enclosed bays subjected to fluctuating fresh water supply from a river discharge. In these areas, the intertidal sediments are in a transient state and the sediment stability is rarely achieved due to the variation of various environmental parameters. Indeed, several hydrological (river discharges, tidal cycles, waves and currents), meteorological (rainfall, temperature, wind-storms), and biological (benthic fauna) factors occur at different spatial and temporal scales. Large scale disturbances, such as flood events in a semi-enclosed area, can strongly affect the sediment properties. The "confine waters" concept has been previously described as the time of renewal with marine-originated (dissolved) elements in each given point, driving the organisms' distribution, assemblage composition and longitudinal geochemical gradients (Guelorget and Perthuisot, 1992; Debenay et al., 2000; Debenay and Guillou, 2002; Whitfield et al., 2012). The complexity of that concept makes it challenging to evaluate the average environmental characteristics at a given point and the *in situ* response time of benthic fauna to these environmental changes (Debenay et al., 2000, 2006). After a winter flood event, three different stages: 1) during the flood, 2) post-flooding period and 3) stabilized period have been identified (Thibault de Chanvalon et al., 2016). These three stages in the context of "confine waters" require a multi-parameters approach to target the high variability of physicochemical parameters and sediment deposit and/or resuspension on benthic meiofauna (foraminifera).

Intertidal mudflats are highly productive ecosystems, mainly due to the presence of communities of benthic microalgae and photosynthetic bacteria, communally known as microphytobenthos (MPB). MPB forms transient biofilms at the surface sediment during emersion periods. Measuring the MPB biomass is challenging due to its high spatiotemporal variability (Méléder et al., 2005; Jesus et al., 2005, 2006; Brito et al., 2009; Benyoucef et al., 2014; Serôdio et al., 2020). Nevertheless, some non-destructive techniques (e.g. normalized difference vegetation index (NDVI)), are now routinely used to increase the amount of measured biofilm surface. These photosynthetic organisms have a key role in coastal ecosystems; they drive biogeochemical cycles through their nutrients uptakes, carbon sequestration and primary organic matter (OM) production, further supporting marine and coastal food-webs (MacIntyre et al., 1996; Echappé et al., 2018). Microphytobenthos from muddy sediments is often dominated by diatoms (class Bacillariophyceae, (Dangeard, 1933) (Underwood and Smith, 1998)), which form dense golden-brown biofilms in the first millimeters of mudflat sediments (Méléder et al., 2003a, 2005; Benyoucef et al., 2014; Launeau et al., 2018) and they are characterized by many cell sizes and shapes (Hillebrand et al., 1999;

Sun and Liu, 2003; Olenina et al., 2006). Their biomass and relative abundance (diatoms assemblage) vary based on the fluctuations of different parameters (e.g. hydrodynamism, tides, light exposure, temperature, nutrients availability), therefore they can be used as bioindicators of environmental conditions (De Jonge and Van Beusekom, 1996; Guarini et al., 1997; Seuront and Spilmont, 2002; Méléder et al., 2005; Jesus et al., 2006; Échappé et al., 2018; Oakes et al., 2020; Benito, 2020). Moreover, diatoms are significant food source for benthic meiofauna as foraminifera (Nomaki et al., 2006; Pascal et al., 2009; Mojtahid et al., 2011).

Foraminifera are ubiquitous marine single-cell protists, protected by a calcareous, agglutinated or organic external shell. Like diatoms, foraminifera are bioindicators of the environmental variability of their habitats (e.g. hydrodynamism, tides, temperature, oxygen availability, food source) (e.g. (Bradshaw, 1961; Jorissen et al., 1995; Debenay et al., 2000; Debenay and Guillou, 2002; Debenay et al., 2006; Schönfeld et al., 2012; Mojtahid et al., 2016; Jauffrais et al., 2017; Benito, 2020; Bouchet et al., 2021). Moreover, benthic foraminifera have diverse trophic strategies. In mudflats, a part of foraminiferal species has shown omnivorous heterotrophic behaviors feeding on various food sources (OM detritus, bacteria, fungi, microalgae and metazoans) (Nomaki et al., 2008; Pascal et al., 2009; Dupuy et al., 2010; Mojtahid et al., 2011; Wukovits et al., 2018). Others are mixotrophic and use chloroplasts from their preys to perform active photosynthesis (i.e. kleptochloroplasts; (Lopez, 1979)) (Pillet et al., 2011; Jauffrais et al., 2016; Cesbron et al., 2017; LeKieffre et al., 2017; Lintner et al., 2020, 2021). Diatoms are an important source of organic carbon and nutrients to benthic foraminifera (Moodley et al., 2000; Nomaki et al., 2005, 2006; LeKieffre et al., 2017; Lintner et al., 2020, 2021). Experimental (Lee et al., 1966; Lopez, 1979; Gooday, 1988; Bernhard and Bowser, 1999; Heinz et al., 2002; Goldstein et al., 2004; Austin et al., 2005; LeKieffre et al., 2018b) and metabarcoding (Pillet et al., 2011; Chronopoulou et al., 2019; Schweizer et al., *submitted*) approaches have shown that benthic foraminiferal species might feed on specific diatoms. However, there is a lack of *in situ* evidences of foraminiferal species–specific diatoms as food source due to the technical issues of studying ecological relationships between benthic foraminifera and diatoms.

The Bourgneuf Bay mudflat (West coast of France) is a semi-enclosed area under the influence of the Loire river discharge when flood events combined with currents and tides push particles towards the interior of the bay (GIP Loire Estuaire). The surface of intertidal sediments is subjected to the alternance between instability and stable periods. These sedimentary changes generate a highly variable environment influencing the dynamics and relationships of benthic meiofauna. Thus, before using foraminiferal dynamics as bioindicators in intertidal

environments, there is a need to understand foraminiferal responses to environmental parameters. Through a 3-years monthly/quarterly monitoring of environmental and biological parameters, the aims of the present study are: (1) to describe the spatial and temporal dynamics of the dominant foraminiferal species; (2) to characterize the main environmental parameters driving the spatio-temporal foraminiferal dynamics in a context of "confined waters" and (3) to present, *in situ* trophic model based on the temporal foraminiferal species–specific diatoms food preferences.

2. Material and Methods

2.1 Site description

The Bourgneuf Bay (46°52′–47°08′N, 1°58′–2°20′W) is located on the French Atlantic coast in the south of the Loire river estuary (Figure 1). The Bourgneuf Bay is a semi-enclosed area of 340 km^2, with a large intertidal mudflat area of 100 km^2, connected with the Atlantic Ocean by a 10 km wide passage between the North of the Noirmoutier Island and the "Saint Gildas pointe". A narrow second bay-ocean communication zone named "goulet de Fromentine" exists to the south of the bay (Debenay, 1978). The wide north west opening allows a connection with the ocean and the Loire estuary. The Loire estuary shows an increasing tidal range upstream, reaching a maximum tidal range of approximately seven meter (Le Floch, 1961). The sediments rejected by the Loire estuary are largely pushed towards the interior of the Bourgneuf Bay through saltation processes (Debenay, 1978).

The sampling site was located at "La Coupelasse" (Fig. 1b). Three stations A (47°0'56.49'N, 2°1'26.72'W), B (47°0'56.83'N, 2°1'26.80'W) and C (47°0'56.67'N, 2°1'27.16'W) were sampled along a small tidal channel near a path used by oyster farmers to access to a large tidal channel located at the middle of the mudflat (500 m of distance from shore) (Fig. 1c). The three stations were located ten meter apart. The stations A and C were the closest to the tidal channel and the station B was the more distant from the channel. These three stations were sampled monthly since March 2016 for the MUDSURV monitoring survey (OSUNA, Pays de la Loire).

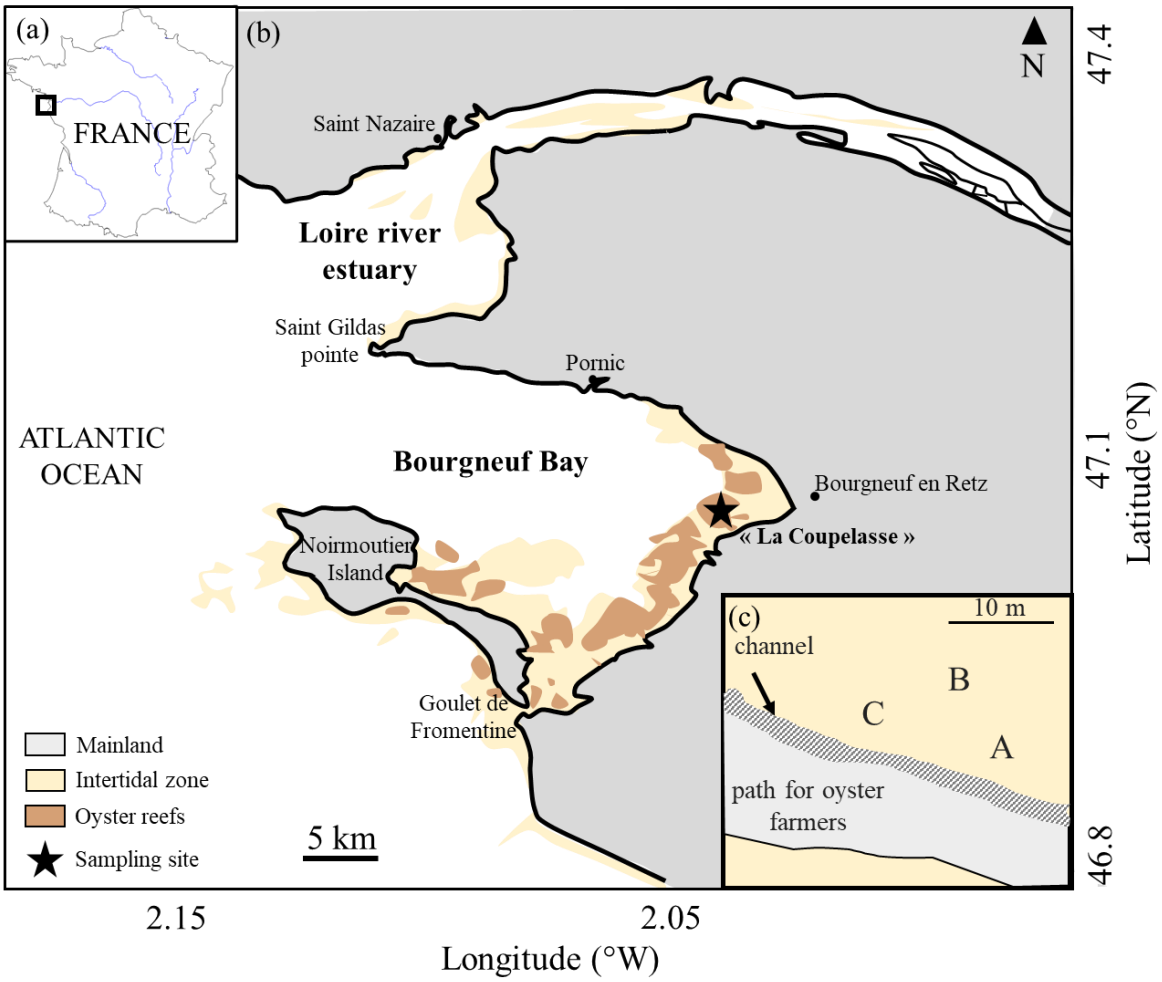

Figure 1: (a) Bourgneuf Bay is located on the French Atlantic coast (b) on the South of the Loire river estuary, the sampling site "La Coupelasse" is indicated with a star, and (c) is a zoom on the 3 sampling stations (A, B, C). Modified from (Thomas et al., 2016).

2.2 Sampling strategy

MUDSURV survey includes a large dataset of fourteen environmental parameters and two biological parameters (sampling strategy summarized in Table 1).

Table 1: Sampling strategy of the MUDSURV monitoring.

	Parameters used	Sampling dates	Sampling location	Analyses location
Environmental parameters				
Global hydrological and meteorological parameters	Loire river discharge monthly air temperature monthly rainfall tidal coefficient	monthly from Marsh 2016 to April 2017 then quaternaly until July 2019	Weather station of Bourgneuf en retz and Montjean sur Loire hydrological station	Angers
Pore-waters geochemical parameters	alkalinity, dissolved reactive phosphorus (DRP), ammonium (NH_4^+), nitrite (NO_2^-), nitrate (NO_3^-), salinity, diffusive oxygen uptake (DOU)	monthly from Marsh 2016 to April 2017 then quaternaly until July 2019	Stations A, B, C	Angers
Sedimentary physical parameters	porosity	monthly from Marsh 2016 to April 2017 then quaternaly until July 2019	Stations A, B, C	Angers
	granulometry	monthly from April 2017 to July 2019	Stations A, B, C	Nantes
Organic matter mineralization activity	oxygen penetration depth (OPD) dissolved oxygen uptake (DOU)	monthly from Marsh 2016 to April 2017 then quaternaly until July 2019	Station C	Angers
MPB Chla proxy	NDVI (Normalized difference vegetation index)	monthly from April 2017 to July 2019	Stations A, B, C	Nantes
Biological parameters				
Benthic foraminiferal species	> 5 % of the assemblage (1st cm depth)	monthly from Marsh 2016 to April 2017 then quaternaly until July 2019	Stations A, B, C	Angers
MPB diatom species	> 5 % of the assemblage (2 mm depth)	monthly from April 2017 to July 2019	Station B	Nantes

2.3 Hydrological and meteorological parameters

The tidal coefficients reported at each sampling months, came from Pornic (http://www.maree.info). The monthly Loire river discharge (m^3 s^{-1}) was monitored at the Montjean-sur-Loire station, located ~ 120 km upstream from the estuary (http://www.hydro.eaufrance.fr/). The monthly air temperature (T°C), the monthly rainfall (mm) and wind-storm events (> 70 km h^{-1}) were retrieved from the weather station of Bourgneuf-en-Retz (Fig. 2 b) (47,04°N | 1,95°W) using the information from SHOM (https://www.shom.fr). The wind-storm events were punctual and were not included in further data analyses.

2.4 Geochemical and physical sampling

2.4.1 Geochemical sampling and processing

One core per sampling for each station was used for pore-waters and solid-phases analyses. The cores (internal diameter = 8.2 cm) were carefully brought back to the Angers laboratory and stored at *in situ* temperature until further analyses the next day. The cores were sliced in a bag filled with nitrogen (N_2) to avoid oxygen contamination of the reduced sediments. The cores were sliced every 2 mm down to 2 cm depth, then 5 mm down to 5 cm and 1 cm down to 11 cm depth. For the aims of this study, only the concentrations of the 1st cm

(the average of the first 5 slices of 2 mm depth) were used for the nutrients, alkalinity and salinity analyses. Each sediment slice was weighed and centrifuged (3500 rpm) for 15 min and the supernatant was filtered using a 0.2 µl filter (RC25, Sartorius ©). One aliquot was used for nutrient colorimetric analyses (ammonium (NH_4^+), nitrite (NO_2^-), and nitrate (NO_3^-)), a second aliquot was used for alkalinity analysis. All spectrophotometric analyses were performed using a Genesys 20 from Thermo-Fischer. Ammonium was analyzed using a phenol-hypochlorite method (Harwood and Kühn, 1970). Nitrite was analyzed using the Griess reagent (Griess, 1879), a second reagent was prepared using vanadium chloride (VCl_3) to reduce nitrate into nitrite, allowing nitrate determination (Cecchini and Rocchina Caputo, 2012). Alkalinity was measured using the colorimetric bromophenol blue/formic acid method (Sarazin et al., 1999). A third pore-water aliquot was acidified with HNO_3 and analyzed by ICP-AES (Thermo Scientific iCAP 6300 Radial) to measure sodium (Na), dissolved Mn, Fe and P for further analyses. The salinity was calculated from the Na measurements (Thibault de Chanvalon et al., 2015).

2.4.2 Physical sampling and processing

The sediment resulting from the centrifugation was frozen for solid-phases analyses. Within one week, samples were freeze-dried, weighed again to calculate the porosity. Aliquots were kept for ascorbate-extraction of the reactive solid-phases for further studies.

Granulometry analysis was carried out on the first centimeter of the sediment from April 2017 to March 2019 for the three sampling stations. The analyses were conducted using a laser granulometer MalvernTM Mastersizer 3000 (MMS, Nantes) and data were processed with the RYSGRAN package in R (R core team). The median grain size (D50) was the main parameter considered for the analyses in this study.

2.5 Oxygen profiling and modeling in dark conditions

One extra core from the station C was used to perform profiles of O_2 using a microelectrode to quantify oxygen penetration depth (OPD, mm) and dissolved oxygen uptake (DOU, nmol cm^{-2} s^{-1}). Sediment oxygen profiles were measured in Angers laboratory the day after sampling, in dark conditions (i.e. aerobic mineralization) with a Clark electrode (50 µm tip diameter, Unisense ®, Denmark). A motorized micromanipulator was used to measure O_2 concentration profiles along the sediment core using 100 µm steps. Each oxygen profile was repeated 5 to 10 times (with 5 minutes intervals) to confirm the stability of the O_2 gradient. The average of ~ 10 profiles was used to calculate the OPD and DOU, using PROFILE software

(Berg et al., 1998). The two boundary conditions used for the calculations corresponded to the overlying water oxygen concentration and the zero flux at the bottom of the oxic zone. The bulk sediment molecular diffusion coefficient (Ds) was estimated according to DS = φ2D0 (Ullman and Aller, 1982) where ϕ was the sediment porosity and D0 was the diffusion coefficient in water at *in situ* temperature (Li and Gregory, 1974).

2.6 NDVI sampling and processing

Microphytobenthos (MPB) was monitored from April 2017 to July 2019. The NDVI (Tucker, 1979) was used as a proxy of MPB chlorophyll *a*, which itself is often used as a proxy for MPB biomass (Méléder et al., 2003b; Forster and Jesus, 2006; Benyoucef et al., 2014). Chlorophyll *a* is an ubiquitous pigment found in all MPB organisms. The NDVI is calculated using the following formula:

$$NDVI = (R_{750} - R_{673}) / (R_{750} + R_{673})$$

R_{750} is the reflectance at 750 nm in the near infrared (NIR) and R_{673} is red reflectance of chlorophyll *a* at 673 nm (Bargain et al., 2012). The sediment surface was sampled at each station and brought back to Nantes laboratory to be analyzed the day after to avoid potential migration effects. Finally, from 5 to 8 punctual measurements where performed on the sediment surface of the 3 stations with a spectroradiometer in the range of 400 nm to 900 nm (Flame 3 spectroradiometer (OceanOptics)).

2.7 Biological parameters

2.7.1 Microphytobenthos species sampling and processing

Microphytobenthos biodiversity was analyzed monthly at the station B from April 2017 to July 2019. The topmost 2-mm of sediment (where the majority of the MPB was present) was frozen using liquid nitrogen according to the contact–coring method (Ford and Honeywill, 2002). Samples were brought back to the laboratory and stored at -80 °C before taxonomic identification and cells counting. Diatom cells were prepared following a protocol adapted from (Ribeiro, 2010). Diatom cells identification and counting were performed by microscopic observations at a 200x or 400x magnification (Zeiss Axioskop 50 microscope) based on morphological criteria (Hillebrand et al., 1999; Méléder et al., 2003b; Ribeiro, 2010; Harrison et al., 2015). A minimum of 100 frustules was counted per sample. The occurrence (relative abundance) per diatom species was used. The temporal variability of diatom species was designed using different shape and size classes (Hillebrand et al., 1999; Ribeiro, 2010; Harrison et al., 2015). Diatom shape and size seem to be important factors influencing the predation by

the foraminifera (Lopez, 1979; Austin et al., 2005; LeKieffre et al., 2018a). The dominant diatom species (> 5 % of the assemblage) was selectionned to perform predator (foraminifera)-prey (diatoms) temporal relationships analyses. The life-forms (epipelic (moving cells), epipsammic (sand-fixed cells), pelagic (planktonic) and epiphytic (attached on seagrass)) of each diatom species were determined according to (Méléder et al., 2007; Ribeiro, 2010).

2.7.2 Foraminiferal sampling and processing

Foraminiferal specimens were sampled monthly from March 2016 to October 2019 (38 sampling date). One sediment core per station was collected each month, excepted in: August, November and December 2017, and in February, August and September 2019, where the sampling campaigns could not be carried out. The uppermost centimeter of the sediment core (diameter 8.2 cm) was used to analyze foraminiferal assemblage composition. Then, the foraminiferal densities (i.e absolute abundances) were standardized and expressed as individuals per 50 cm^{-3} (Schönfeld et al., 2012). Directly after collection, the first centimeter of the cores was sliced and stored in bottles with 95% ethanol containing 2 g L^{-1} of Rose Bengal stain. The sediment slices were then washed and sieved (using a 350, 150, 125 and 63 µm meshes). The > 150 µm fraction was examined under a stereomicroscope (Leica S9i, 10x magnification). Only specimens colored in pink (with the exception of the last chamber) were considered as living cell at the sampling date. Foraminifera were placed in micropaleontological slides and identified using morphological criteria. The 125 µm and 63 µm fractions were not analyzed, thus this study did not include juvenile forms, which are rarely found in the 150 µm fraction. This limitation should be considered when interpreting temporal dynamics (Murray and Alve, 2000; Richirt et al., 2020). All living specimens were taxonomically assigned with the exception of high density samples (i.e. > 300 individuals), which were micro–split with an Otto Microsplitter. The micro splitter allows to reduce equitably the amount of individual to a manageable numbers of cells and therefore save time for the identification (Alve and Murray, 2001). Scanning electron microscopy (SEM) images of the dominant species were taken with a Zeiss EVO LS10 at low vacuum (50Pa).

2.8 Data analyses

2.8.1 Permutational multivariate analysis of variance (PERMANOVA)

The NDVI values and the foraminiferal densities were subjected to a 3 factors mixed model PERMANOVA (stations, months and years) with a Monte Carlo test (Anderson et al., 2008). This analysis will test whether NDVI values and foraminiferal species density

significantly differed spatially (i.e. among stations) and temporally (i.e. months and years). The Bray-Curtis distance was used for foraminifera and the Euclidean distance for the environmental parameter NDVI. The PERMANOVA model was performed with the VEGAN package on R version 4.0.2 (R core team).

2.8.2) Canonical Correspondence Analysis (CCA)

A canonical correspondence analysis (CCA) was performed to characterize the preferential ecological environments of the foraminiferal species. The analysis was conducted with the PAST software (paleontological statistics, 3.08, (Hammer, 2001)) To determine the foraminiferal spatiotemporal dynamics, dominant foraminiferal species (with relative abundance > 5 %) and 14 environmental parameters were considered. The environmental dataset includes: 1) hydrodynamism and meteorological parameters (discharge, rainfall, temperature, tidal coefficient, porosity, salinity, granulometry), 2) OM remineralization activity (alkalinity, OPD, DOU), 3) pore-waters nutrients (DRP, NH_4^+, NO_3^-, NO_2^-), 4) proxy of the MPB biomass (NDVI). To perform the analysis, the foraminiferal densities were square root transformed, whereas environmental parameters were centred and standardized per station as follow: (x - mean x)/ sd. In which x is the value of the variable in one station, mean x is the mean of the same variable among each station and sd is the corresponding standard deviation. The center and the standardization of the parameters allowed to obtain a dataset of independent variables having the same mean and dispersion and therefore the same weight in the ordination.

2.8.3 Distance-based linear model (DistLM)

The distance-based linear model (DistLM) routine was conducted using the software PRIMER v.6.0.2 (Clarke and Gorley, 2006) with the PERMANOVA add-on (Anderson et al., 2008). The DistLM model was used to determine which diatom species predict the temporal variation of foraminiferal species. In other words, we used the DistLM model to investigate which diatom species were preferentially feed by foraminiferal species and could explain their temporal variability. The foraminiferal species densities were square root transformed followed by the generation of a Bray-Curtis similarity matrix. The Akaike Information Criterion (AIC) and significant p-value (< 0.05) were used to select the "best fit" subset of diatom species. Two test were generated with the DistLM model: the marginal and the sequential tests. The Marginal tests analyzed individually the "best fit" subset of diatom species for each foraminiferal species. The sequential tests analyzed the "best fit" combinations of diatom species for each

foraminiferal species. Thus, the diatom species selected by the sequential test and not by the individual test were considered in this study as occasional species.

3. Results

3.1 Spatial and temporal variations of environmental parameters

3.1.1 Physicochemical sediment properties related to the hydrodynamism of the bay

The tidal coefficient registered at each sampling date varied between 50 and 114 (Fig. 2 a). To increase sampling time during the emersion period, the sampling was performed during high tidal coefficients. Five wind-storm events (> 70 km h^{-1}) were recorded by the weather station during the sampling period; in January, February and March 2017, January 2018 and March 2019 (black arrows, Fig. 2 a). The Loire river discharge showed large seasonal fluctuations with an average of 666 ± 599 m^3 s^{-1} (n=46 months) (black line and diamonds; Fig. 3 b). The discharge was characterized by flood events above > 1000 m^3 s^{-1} (Fig. 2 b) observed in February and June 2016, in January, February and March 2018. Below < 500 m^3 s^{-1} the discharge was in low waters especially from early summer to late autumn (Fig. 2 b). Namely, the low waters periods occurred from July to December 2016, May to November 17, July to November 2018 and April to October 2019. The rainfall (grey triangles and dotted line; Fig. 2 b) followed the Loire river discharge fluctuations. The temperature showed a clear seasonal trend every year (Fig. 2 c) with an annual average of 13.5 ± 4.8°C (n=46 months). The higher temperatures were reached from late summer to early autumn (Fig. 2 c) coinciding with the low waters periods and a lower rainfall (Fig. 2 b). The data of the tidal coefficient, Loire river discharge, rainfall and temperature are available in Annex 1.

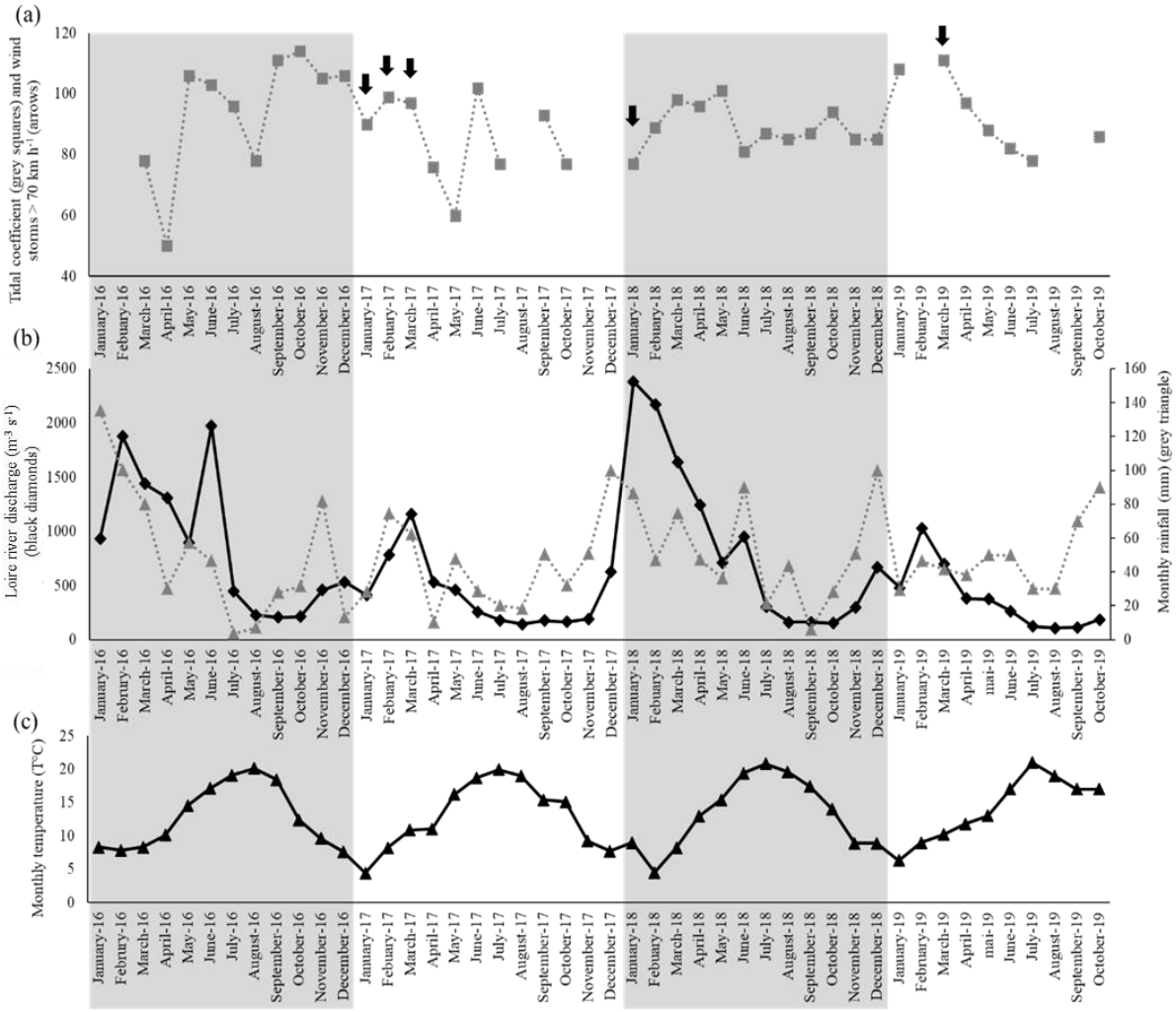

Figure 2: Hydrological and meteorological parameters: (a) the tidal coefficient (grey squares and grey dotted line) with wind-storm events > 70 km h^{-1} occurring before sampling crop (black arrows), then (b) the Loire river discharge (m^3 s^{-1}) (black diamonds and black line) with the monthly rainfall (mm) (grey triangles and grey dotted line) and (c) the monthly air temperature (T°C) (black triangles). The two large grey squares indicated the separation between years.

The salinity calculated using the 1st cm at each station was: 35.73 ± 3.19 (n= 26 months) at the station A, 35.76 ± 2.99 (n= 25 months) at the station C and 36.51 ± 2.83 (n= 23 months). The salinity fluctuated insignificantly among stations, the higher salinity values were observed from spring to early autumn (Annex 2). The porosity calculated per station indicated: 0.86 ± 0.04 (n= 20 months) at the stations A, 0.86 ± 0.03 (n= 20 months) at the stations B and 0.84 ± 0.09 (n= 20 months) at the stations C. No significant trends were observed, but lower porosity values were sometimes observed in spring mostly at the station C (Annex 2). The median grain-size (D50) measured at each station were: 28.18 ± 12.46 µm (n=21) at the station A, 25.82 ± 3.13 µm (n= 19) at the station B and 25.01 ± 3.30 µm (n=13) at the station C. The granulometry was stable and sometimes showed higher values in winter and spring at the station A. In Annex

2 are detailed the values of environmental parameters per station (salinity, porosity, D50, alkalinity, NH_4^+, NO_2^-, DRP).

3.1.2 Temporal variation of OM remineralization activity

The OM mineralization activity was followed with OPD and DOU measurements performed in dark conditions. A temporal plot for OPD and DOU is available in Annex 3. The OPD measured at the station C was 1.52 ± 0.44 mm (n= 22 months) and the calculated DOU was 36.24 ± 15.45 mmol m^{-2} d^{-1}. The OPD and DOU widely fluctuated temporally and may tend to show negative trends (Annex 3). Then, alkalinity measured between stations was: 5.50 ± 1.12 mmol kg^{-1} (n= 21 months) at the station A, 5.18 ± 0.94 mmol kg^{-1} (n=19 months) at the station B and 5.61 ± 0.89 mmol kg^{-1} (n= 19) at the station C. The alkalinity concentrations poorly fluctuated between stations. Overall, the higher alkalinity values seemed to be reached from spring to early autumn (Annex 3).

3.1.3 Spatiotemporal variations of pore-waters nutrients

The pore-waters nutrients measured from the 1st cm depth, widely fluctuated spatially and temporally. A spatiotemporal plot for each parameter is available in Annex 3. At this stage it remained difficult to detect spatiotemporal trends. Overall, NO_2^- concentrations measured per station were: 0.40 ± 0.47 µmol L^{-1} (n= 21) at the station A, 0.59 ± 0.83 µmol L^{-1} (n= 20) at the station B and 0.56 ± 0.64 µmol L^{-1} (n= 20) at the station C. The NO_2^- concentrations were low and closed to the limit of detection, no clear seasonal trend was observed (Annex 3). No NO_3^- concentration (~ 0 µmol L^{-1}) was detected (data not shown). Ammonium concentrations measured per station were: 25.38 ± 33.19 µmol L^{-1} (n= 23) at the station A, 31.12 ± 44.06 µmol L^{-1} (n= 22) at the station B and 24.68 ± 32.95 µmol L^{-1} (n= 23) at the station C. The NH_4^+ concentrations strongly fluctuated spatially and temporally. Higher NH_4^+ concentrations were observed mostly in autumn and winter (Annex 3). The dissolved reactive phosphorus concentrations measured per station were: 7.66 ± 10.20 µmol L^{-1} (n= 24) at the station A, 7.00 ± 10.88 µmol L^{-1} (n= 24) at the station B and 6.98 ± 10.20 µmol L^{-1} (n= 24) at the station C. The DRP concentrations also strongly fluctuated. Higher DRP concentrations were observed mostly in summer and early autumn (Annex 3).

3.1.4 Spatiotemporal variations of MPB biomass

The NDVI values did not show a clear seasonal trend. The NDVI values highly fluctuated spatially (details in Annex 4). Average NDVI values at the station A was 0.26 ± 0.10

(n=24 months), 0.33 ± 0.15 (n= 24 months) at station B and 0.31 ± 0.04 (n= 24 months) at station C. The PERMANOVA test applied on the NDVI values between stations and months were no-significant (p-value = 0.29 and 0.12, respectively). However, the inter-annual variations differed, supported by a significant PERMANOVA test between years (p-value = 0.001).

3.2 Spatial and temporal dynamics of biological parameters

3.2.1 Temporal dynamics of the diatom species shapes

At the station B, 29 diatom dominant species (> 5 % of the assemblage) were identified (details in Annex 5). These diatoms showed seven different shapes according to Hillebrand et al., (1999), presented in Figure 4. Frustules shape were elongated, "prism on elliptic base" (Fig. 4 a), "prism on parallelogram base" (Fig. 4 b), "cylinder" (Fig. 4 c), "half elliptic prism" (Fig. 4 d) and "cymbelloid" (Fig. 4 e). Two other complex shapes were found: "cylinder + 2 half spheres" (Fig. 4 f) and "prolate spheroid + 2 cylinders" (Fig. 4 g).

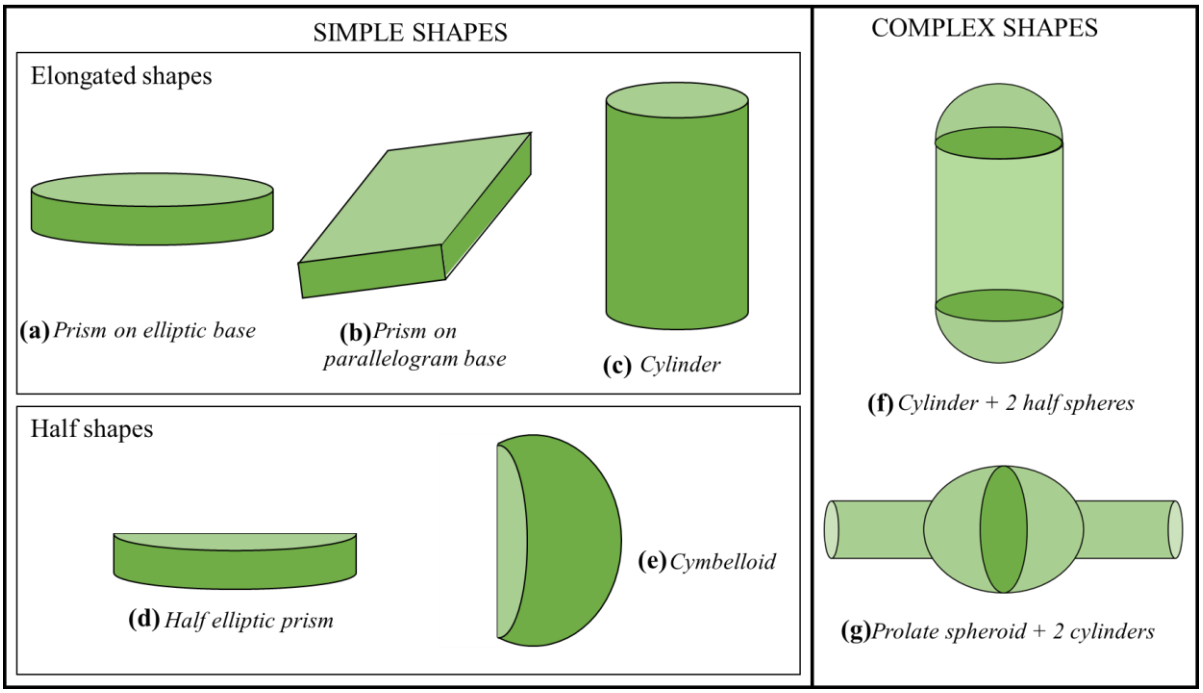

Figure 4: Summary of the seven diatoms shapes identified in the assemblage. According to Hillebrand et al., 1999.

Figure 5 shows the temporal dynamics of the seven diatom shapes. The details of the diatom species per shape is available in Annex 5. Two shapes dominated the diatoms assemblage: the "prisms on elliptic base" (grey, Fig. 5) and the "prisms on parallelogram base" (dark blue). The "prisms on elliptic base" (grey, Fig. 5) were composed of *Navicula*

meuleumansii (Bory de Saint-Vincent), *Plagiogrammopsis vanheurckii* ((Grunow) Hasle, Stosch et Syvertsen), *Navicula spartinetensis* (M. J. Sullivan et Reimer), *Navicula abscondita* (Hustedt), *Chaetoceros* sp. (Ehrenberg), *Staurophora salina* ((W.Smith) Mereschkowsky), *Psammodictyion* sp. (Kelly), *Plagiotropis seriata* ((Cleve) Kuntze), *Entomoneis paludosa* ((W. Smith) Reimer), *Planothidium septentrionalis* ((Østrup) Round & Bukhtiyarova), *Navicula* cf *flagellifera* (Hustedt) and *Plagiotropis vanheurckii* (Grunow in Van Heurck). The occurrence of the "prisms on elliptic base" shape fluctuated temporally, reaching up to 70% of the assemblage in spring and summer and seemed to be less representative in autumn and winter. The "prisms on parallelogram base" (dark blue, Fig. 5) were composed of *Gyrosigma limosum* (Sterrenburg & Underwood), *Gyrosigma fasciola* ((Ehrenberg) J.W.Griffith & Henfrey), *Gyrosigma wansbeckii* ((Donkin) Cleve), *Pleurosigma formosum* (W.Smith), *Pleurosigma angulatum* ((Queckett) W. Smith), *Nitzschia* cf *distans* (W.Gregory), *Nitzschia* cf *aequorea* (Hustedt), *Nitzschia maxima* (Grunow) and *Cymatosira belgica* (Grunow). The occurrence of the "prisms on parallelogram base" shape seemed to alternate with the previous shape (Fig. 5). Thus, the "prisms on parallelogram base" shape was more representative of the assemblage (up to 80 %) in autumn and winter. Then, other shapes were less representative of the diatom assemblage. The "cylinder" shape (green, Fig. 5) was composed of two species: *Thalassiosira* sp. (Cleve) and *Melosira* sp. (C.Agardh). This shape was observed mainly in spring and autumn reaching up to 20% of the assemblage. The "half elliptic prism" shape (orange, Fig. 5) was composed of *Eutonogramma dubium* (Hust) reaching until 6 % of the shape assemblage. This shape was not observed in winter. The "cymbelloid" shape was composed of *Halamphora* sp. ((Cleve) Mereschkowsky). This shape was poorly represented on the assemblage, reaching the 6 % in spring. Overall, this shape was not observed in autumn and winter. The "cylinder + 2 half spheres" shape (light blue, Fig. 5) was composed of *Podosira stelligera* ((Bailey) A. Mann) and *Skeletonema* sp. (Greville). This shape was poorly represented in the assemblage, reaching up to 8 % in late autumn and spring. Overall, this shape was not observed in winter. Then, the "prolate spheroid + 2 cylinders" (pink, Fig. 5) shape was composed of *Cylindrotheca* sp. (Rabenhorst). This shape did not show clear trend, it composed the 11% of the shape assemblage in spring 2018, and was also observed in early autumn.

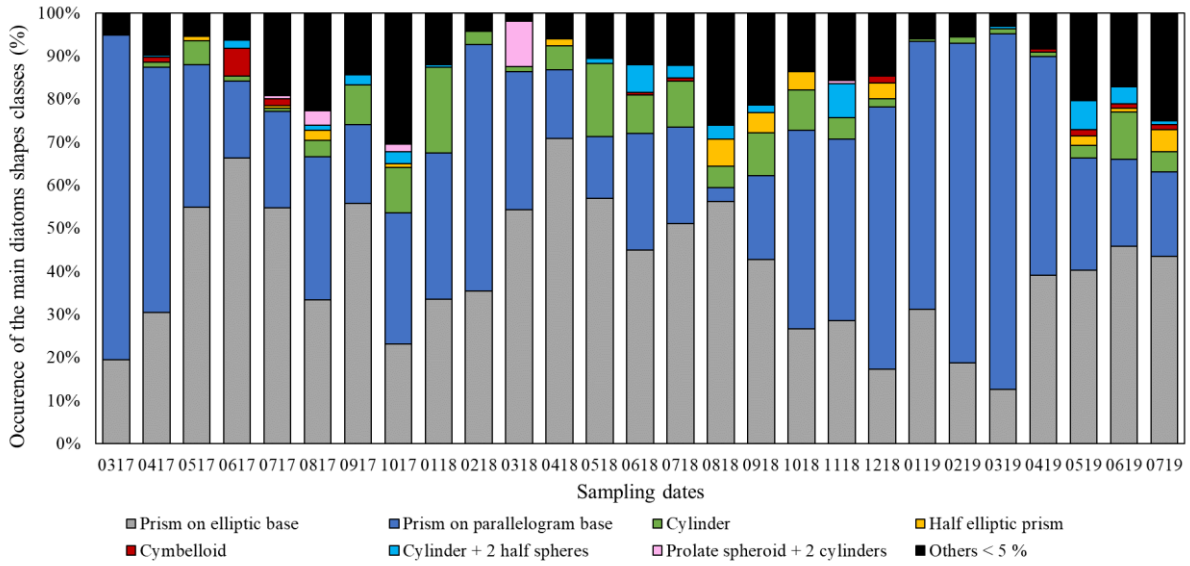

Figure 5: Temporal variations of the seven diatoms shapes obtained from the species (abundance > 5 % of the assemblage) at the station B.

3.2.2 Spatiotemporal dynamics of foraminiferal species density

The dominant foraminifera identified were *Ammonia* sp. T6. (Hayward et al., 2004; Richirt et al., 2019), *Haynesina germanica* (Ehrenberg, 1840), *Elphidium oceanense* (D' Orbigny in Fornasini, 1904), "*Elphidium excavatum*" complex species from Darling et al., (2016) and *Elphidium selseyense* (Heron-Allen and Earland, 1911, "*Elphidium excavatum*" complex species from (Darling et al., 2016)) (Figure 6).

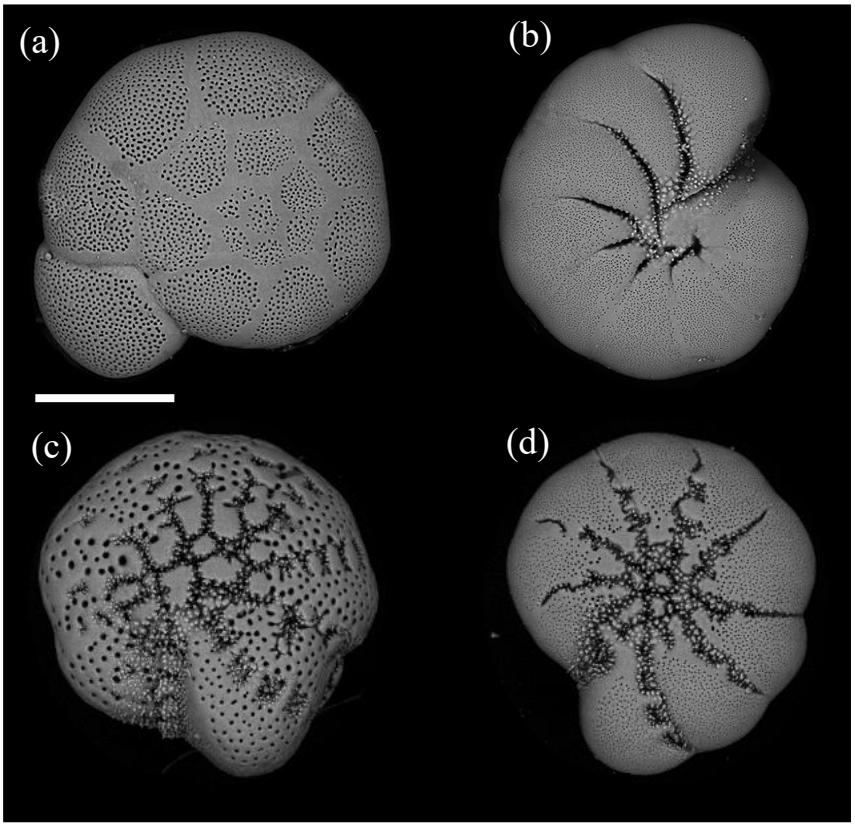

Figure 6: Scanning Electronic Microscope images of the dominant foraminiferal species(a) Ammonia sp. T6, (b) Haynesina germanica, (c) Elphidium oceanense and (d) Elphidium selseyense found at "La Coupelasse" in the Bourgneuf Bay mudflat (France) (> 150 µm). The scale bar indicates 100 µm.

The spatial variation of the foraminiferal species densities between station was not supported by a significant PERMANOVA test (*Ammonia* sp. T6 (p-value = 0.08), *Haynesina germanica* (p-value = 0.94), *Elphidium oceanense* (p-value = 0.27) and *Elphidium selseyense* (p-value = 0.19)). Nevertheless, these species densities showed significant temporal variation per month and year. Significantly fluctuations were observed for *Ammonia* sp. T6 (p-value = 0.001 for both parameters) and *Elphidium oceanense* (p-value = 0.001 and 0.001 for month and year, respectively) as well as for *Elphidium selseyense* (p-value = 0.002 and 0.001 for month and year, respectively), but not for *Haynesina germanica* which varied only monthly (p-value = 0.001) not yearly (p-value = 0.71).

Ammonia sp. T6 spatiotemporal dynamics (Fig. 7 a) indicated high density events > 600 ind. 50 cm^{-3} (indicated by black arrows in Fig. 7 a). In 2016 two high density events were observed: in spring 2016 (March and May) and in autumn 2016 (October and November)). In 2017 one high density event was observed in autumn (September and October). In 2018 two high density events were observed: in winter (February) and in late summer 2018 (August).

However, no high density event was observed in 2019. Also *Haynesina germanica* spatiotemporal dynamics (Fig. 7 b) indicated high density events > 600 ind. 50 cm^{-3} (indicated by black arrows in Fig. 7 b). *Haynesina germanica* showed the same high density events than *Ammonia* sp. T6. In spring 2016 two high density events were observed: in spring (March) and autumn (November). Similarly, in 2017 one high density event was observed in autumn (September). In winter 2018 two high density events were observed: in winter (February) and late summer (August) 2018. However, in 2019 one high density event was observed in summer (July). *Elphidium oceanense* spatiotemporal dynamics indicated globally low density (Fig. 7 c). One high density event (> 600 ind. 50 cm^{-3}, Fig. 7 c) was observed each year in autumn: in September 2017, in late August 2018, in October 2019, however, in autumn 2016 no high density event was observed. *Elphidium selseyense* density was very low (< 100 ind. 50 cm^{-3}, Fig. 7 d) compared to the other species (see the lower scale, Fig. 8 d). *Elphidium selseyense* spatiotemporal dynamics indicated density events (> 100 ind. 50 cm^{-3}, Fig. 7 d) each year in spring and summer: in May, July and August 2016, from May to July 2017, from May to August 2018, however no density event was observed in 2019. Annex 6 presents the dominant foraminiferal species density (ind. 50 cm^{-3} > 150 µm) from March 2016 to October 2019 sampled at the three station.

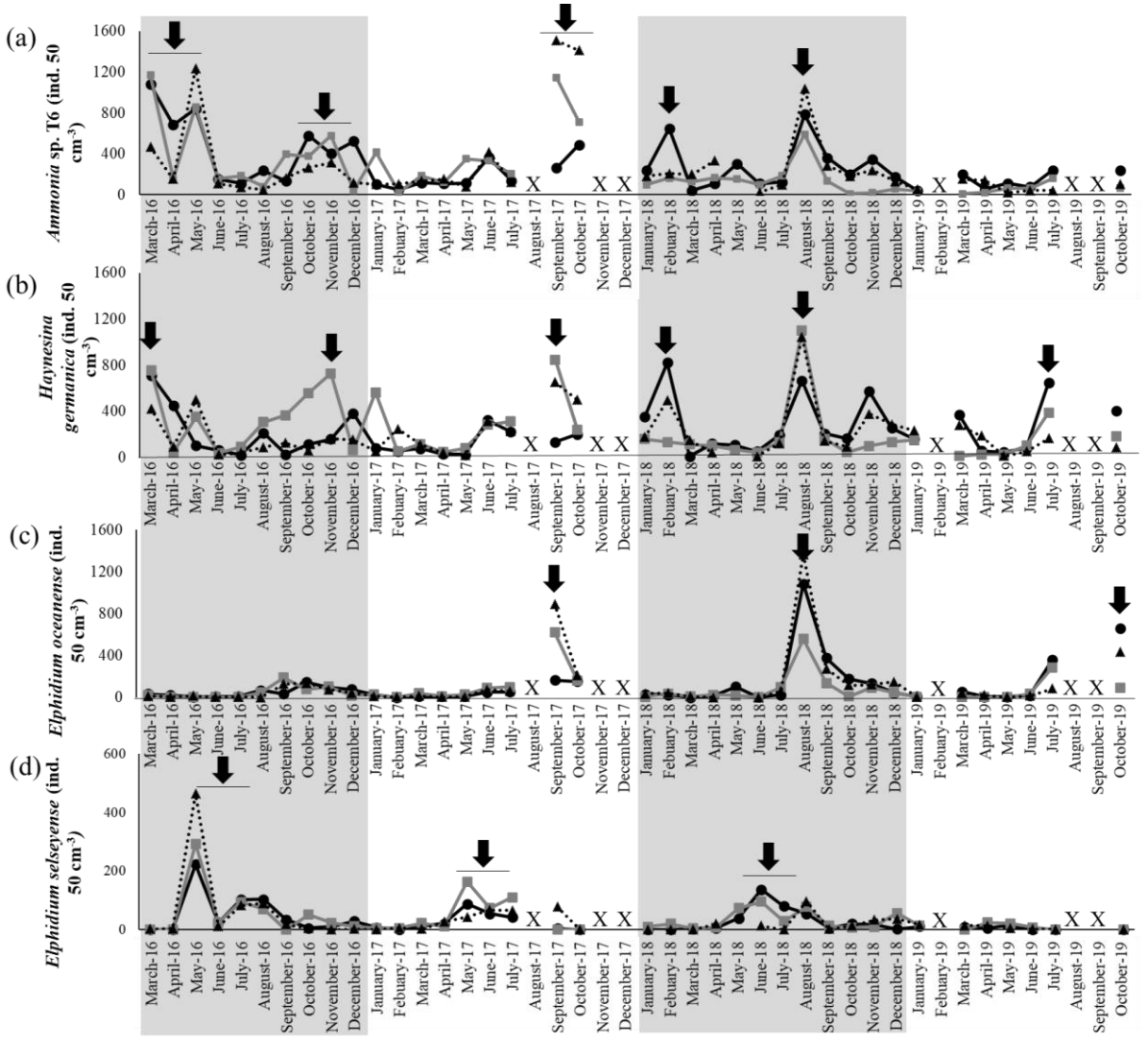

Figure 7: Spatiotemporal dynamics of the four dominant foraminiferal species (ind. per 50 cm^{-3}, > 150 µm) Ammonia sp. T6 (a), Haynesina germanica (b), Elphidium oceanense (c) and Elphidium selseyense (d). Different line patterns represent the three sampling stations: stations A (in black with black circles), B (in grey with a grey squares) and C (in black dotted line with black triangles). The black arrows indicate the high density events > 600 ind. cm^{-3} for Ammonia sp. T6, Haynesina germanica, Elphidium oceanense and > 100 ind. 50 cm^{-3} for Elphidium selseyense. Note that the density scale of Elphidium selseyense is lower than the scales of the other species. The cross indicates no available data. The grey boxes separate the different years.

3.3 Ecological preferences of the foraminiferal species

3.3.1 Environmental parameters driving the spatiotemporal foraminiferal dynamics

The canonical correspondence analysis (Fig. 8, database in Annex 7) provided information on the spatiotemporal dynamics of foraminiferal species in relation with the

environmental parameters. The factorial plan of the CCA axes used the scale type 1 of Legendre and Legendre (1998), gathers 93 % of the total variance (axis 1, eigenvalue = 0.04, variance = 51 %; axis 2, eigenvalue = 0.03, variance = 42 %). The significance of both axes using the Monte Carlo permutation test (n = 999) for both axes was significant ($p < 0.001$). The CCA discriminated clearly the environmental variables (vector arrows) (Fig. 8). The sampling dates of the three stations (A (black circle), B (grey square) and C (white triangle)) were not separate but indicated a single set. Three main foraminiferal preferential environments were identified. *Ammonia* sp. T6 and *Haynesina germanica* were negatively correlated with both axes, *Elphidium oceanense* was correlated negatively with the axis 1 and positively with the axis 2, whereas *Elphidium selseyense* was correlated positively with both axes. Firstly, the spatiotemporal dynamics of *Ammonia* sp. T6 and *Haynesina germanica* were mainly related to parameters linked to the hydrodynamism of the bay and winter conditions (i.e. discharge, rainfall, D50) and a higher OPD. Secondly, the spatiotemporal dynamics of *Elphidium oceanense* was mainly related to high salinity, then by high NH_4^+ concentrations and higher NDVI values. Thirdly, the spatiotemporal dynamics of *Elphidium selseyense* was mainly related to high temperature then by parameters reflecting OM remineralization activity (i.e. alkalinity and DOU).

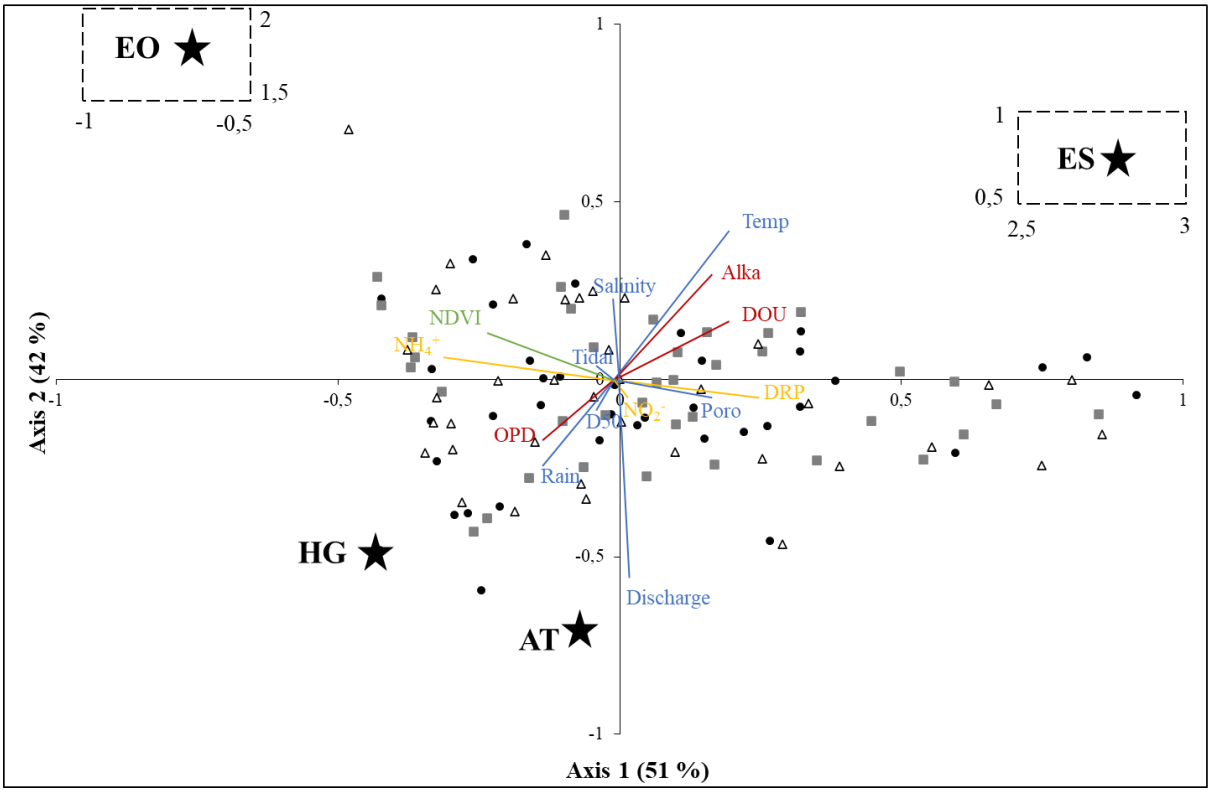

Figure 8: Canonical correspondence analysis (CCA) biplot summarizing the effects of the environmental parameters on the foraminiferal spatiotemporal dynamics (sqrt ind. 50 cm^{-3}). The environmental parameters are composed of: 1) parameters linked to the hydrodynamism and meteorology in blue (discharge, rainfall, temperature, tidal coefficient, porosity, salinity, granulometry), 2) OM remineralization activity in red (alkalinity, OPD, DOU), 3) pore-waters nutrients in orange (DRP, NH_4^+, NO_3^-, NO_2^-), 4) proxy of the MPB biomass in green (NDVI). The sampling dates were represented for the three stations: station A (black circle), station B (grey square) and station C (white triangle). The foraminiferal species are indicated with a star; Ammonia sp. T6 *(AT), Haynesina germanica (HG), Elphidium oceanense* (EO) and *Elphidium selseyense* (ES). *The first two axes support 51 % (axis 1) and 42 % (axis 2) of the variables information. To facilitate the reading of the CCA dotted frames show the coordinates of the CCA axes for Elphidium selseyense* (ES) *and Elphidium oceanense* (EO). *The details of the CCA with sampling dates is available in Annex 7.*

3.3.2 *In situ* temporal variability of the foraminiferal species–specific diatoms food preferences

Foraminiferal species density responded specifically to the changing environmental parameters of the Bourgneuf Bay (Fig. 8). The results of the DistLM model were presented in Figure 9 (detailed in Annex 8). The "best fit" explanatory diatom species were designed with their shapes (see Figure 5). Their size classes were also represented according to Ribeiro et al., (2010): "small" (< 250 µm), "medium" (250-1000 µm) and "large" (> 1000 µm).

The DistLM analysis highlighted 16 "best fit" diatom species explaining foraminiferal temporal dynamics (Figure 9). Most of these "best fit" diatom species were represented by two

shapes “prism on elliptic base” and “prism on parallelogram base”, the most common shapes found in the diatoms assemblage (Fig. 5). The temporal dynamics of these 16 “best fit” diatom species are available in Annex 8. *Ammonia* sp. T6 (Fig. 9 a) was characterized by 6 “best fit” diatom species (*Navicula spartinetensis*, *Pleurosigma formosum*, *Gyrosigma Fasciola*, *Pleurosigma angulatum*, *Cymatosira belgica* and *Thalassiosira* sp.), showing various simple elongated shapes “prism on elliptic base”, “prism on parallelogram base”, “cylinder” and all size classes “small, medium and large”. *Haynesina germanica* (Fig. 9 b), was characterized by 3 “best fit” diatom species (*Pleurosigma formosum*, *Navicula* cf *flagellifera* and *Plagiotropis vanheurckii*), showing specifically two simple elongated shapes “prism on elliptic base”, “prism on parallelogram base” and only large size class. One occasional large “prism on parallelogram base” species was found (*Nitzschia* cf *distans*; in grey, Fig. 9 b). Conversely, *Elphidium oceanense* (Fig. 9 c) was characterized by 8 “best fit” diatom species (*Thalassiosira* sp., *Skeletonema* sp., *Plagiotropis vanheurckii*, *Eutonogramma dubium*, *Navicula* cf *flagellifera*, *Podosira stelligera*, *Gyrosigma wansbeckii* and *Plagiogrammopsis vanheurckii*) showing the most various shapes: simple elongated shapes “prism on elliptic base”, “prism on parallelogram base”, “cylinder”, “half elliptic shape” and a complex shape “cylinder + 2 half spheres”. Moreover, all sizes classes were represented. Two occasional large “prism on elliptic base” species were found (*Navicula spartinetensis* and *Entomoneis paludosa*; in grey, Fig. 9 c). *Elphidium selseyense* (Fig. 9 d) was not characterized by a “best fit” diatom species, any species was significant. However, one occasional large “prism on elliptic base” species (*Navicula abscondita*) was found. Some “best fit” diatom species were not exclusive and were shared by two foraminiferal species as: *Pleurosigma formosum* shared by *Ammonia* sp. T6 and *Haynesina germanica*, *Thalassiosira* sp. and *Navicula spartinetensis* shared by *Ammonia* sp. T6 and *Elphidium oceanense*, finally *Plagiotropis vanheurckii* and *Navicula* cf *flagellifera* were shared by *Haynesina germanica* and *Elphidium oceanense*. The temporal dynamics of the 16 diatom species is detailed in Annex 9.

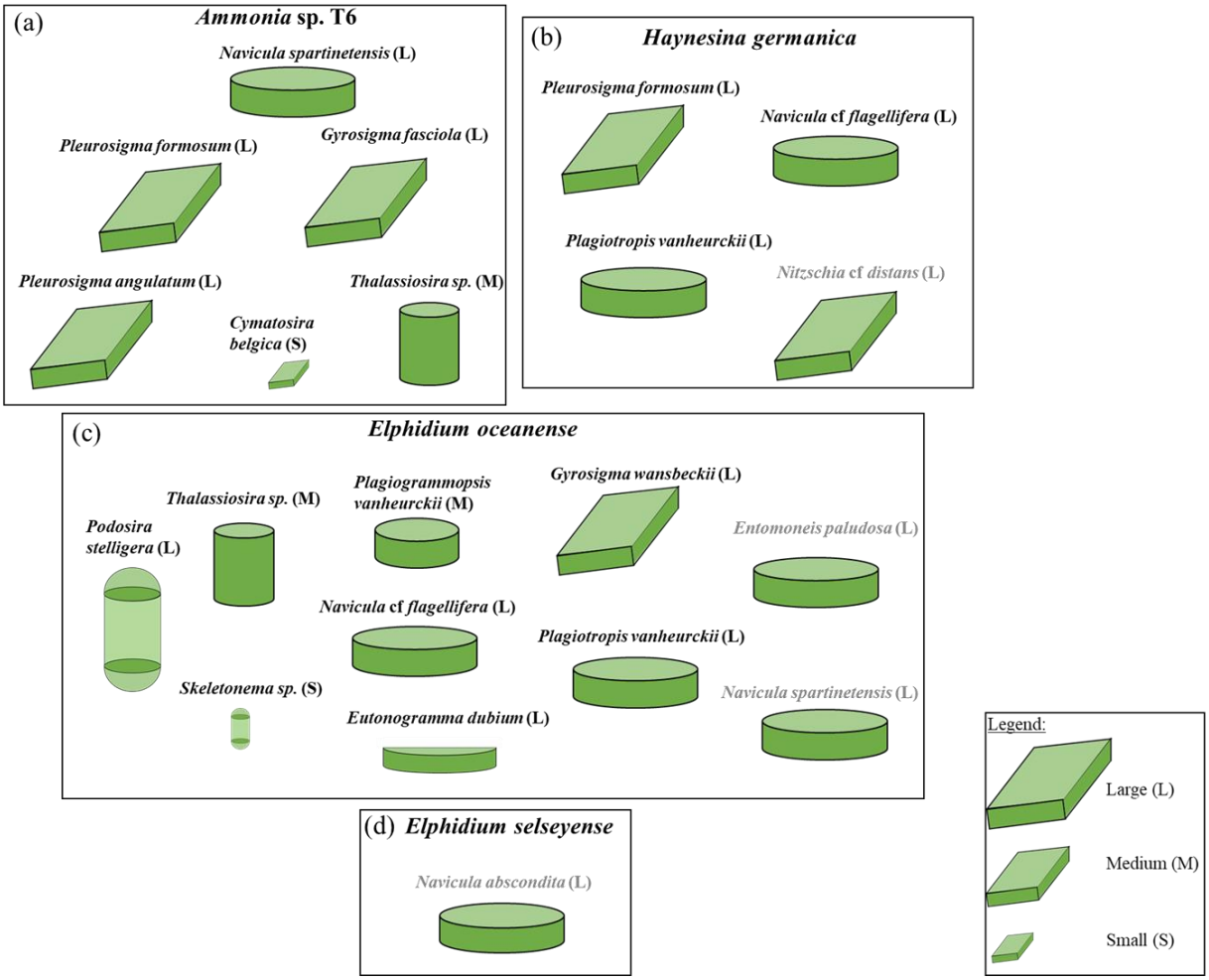

Figure 9: The foraminiferal species–specific diatoms food preferences found by the DistLM model; (a) Ammonia sp. T6, (b) Haynesina germanica, (c) Elphidium oceanense and (d) Elphidium selseyense. The "best fit" diatom species (in bold) were designed according to their shape (details in Figure 5) and their size (S= small, M= medium and L= large). The species indicated in grey are considered occasional species.

4. Discussion

4.1 Taxonomy of the dominant foraminiferal species in the Bourgneuf Bay

The dominant foraminiferal species identified at the sampling stations were *Ammonia* sp. T6, *Haynesina germanica*, *Elphidium oceanense* and *Elphidium selseyense* (Fig. 6). The morphospecies *Ammonia tepida* previously identified in the Bourgneuf Bay (Debenay, 1978; Debenay and Guillou, 2002; Morvan et al., 2004; Debenay et al., 2006) is composed of 3 different phylotypes which are not closely related genetically and can be considered as three pseudocryptic species. These common phylotypes in the French Atlantic coast are *Ammonia* sp. T1, T2 and T6 (Hayward et al., 2004; Schweizer et al., 2011; Richirt et al., 2019; Bird et al., 2020). *Ammonia* sp. T6 dominates in the Loire estuary with 90 % relative abundance and

Ammonia sp. T1 represent the remaining 10 % (Richirt, 2020). Two important morphological criteria distinguish T1 from T6; the average pore diameters and the suture elevation (Richirt et al., 2019). *Ammonia* sp. T1 is described with intermediate pores and raised sutures whereas *Ammonia* sp. T6 (Fig. 6a) has large pores and flush sutures (Richirt et al., 2019). The two phylotypes were not discriminated systematically in the current study, even if some samples were punctually observed at the different sampling sites to assess the general ratio between the two phylotypes. It was estimated that *Ammonia* sp. T1 represented less than < 5 % in the samples and can be considered as a minor species and therefore can be included in the *Ammonia* sp. T6 counts. *Ammonia* sp. T6 is a typical intertidal species (e.g. mudflat, marshes and brackish lakes) present in Europe and East Asia (Hayward et al., 2004; Schweizer et al., 2011; Lintner et al., 2019; Richirt et al., 2020; Bird et al., 2020).

Haynesina germanica (Ehrenberg, 1840; genetic type S16; Darling et al., 2016) is described with a rounded test, with slightly lobate periphery, densely scattered pores, without sutural bridges, and an umbilical area covered by irregular papillae (see Fig. 6b). *Haynesina germanica* is a typical intertidal species, abundant in transitional environments at temperate latitudes as in the Bourgneuf Bay mudflat (Ellison, 1984; Cearreta, 1988; Alve and Murray, 2001; Debenay, 1978; Debenay and Guillou, 2002; Debenay et al., 2006; Armynot du Châtelet et al., 2004; Morvan et al., 2006; Cesbron et al., 2016; Mojtahid et al., 2016; Saad and Wade, 2017).

Two phylotypes of the *"Elphidium excavatum*" species complex (Pillet et al., 2011; Darling et al., 2016) are found in the Bourgneuf Bay: *Elphidium oceanense* (genetic type S3, Darling et al., 2016) and *Elphidium selseyense* (genetic type S5, Darling et al., 2016). *Elphidium oceanense* (d'Orbigny in Fornasini, 1904) has an inflated test with coarse pores, long and irregular sutural bridges, a large umbilical area covered by irregular and coarse bosses (see Fig. 6c). This morphospecies was identified in the Bourgneuf Bay by LeKieffre et al., (2017), Jauffrais et al., (2018), and in the Loire estuary by Durand (2017). In previous studies, *Elphidium oceanense* does not appear in the foraminiferal assemblages of the bay and near areas (Debenay, 1978; Debenay and Guillou, 2002, Morvan et al., 2004; Debenay et al., 2006; Mojtahid et al., 2016). Indeed, this morphospecies have been identified with the species name *Elphidium gunteri*, as shown by the SEM image in Debenay, (1978). *Elphidium gunteri* was first described in Florida (Cole, 1931), and it is therefore preferable to use the name *E. oceanense* which was described in Europe (d'Orbigny in Fornasini, 1904) and encountered in shallow intertidal to subtidal waters (Darling et al., 2016; Jauffrais et al., 2018).

Elphidium selseyense (Heron-Allen and Earland, 1911; genetic type S5 in Darling et al., 2016) has a moderately inflated test with relatively coarse and densely scattered pores, depressed sutures and an umbilical region covered by a few umbilical knobs (see Fig. 6d). This species was identified in the Bourgneuf Bay by LeKieffre et al., (2017) and Jauffrais et al., (2018). In previous publications, *Elphidium selseyense* did not appear in the foraminiferal assemblages of the bay and near areas. Before the study of Darling et al., (2016), *Elphidium selseyense* was referred as *Elphidium excavatum* forma *selseyensis* (Feyling-Hanssen, 1972; Pillet et al., 2013). *Elphidium excavatum* also known as *Cribroelphidium excavatum* (Terquem, 1875) was identified in the Loire estuary (Mojtahid et al., 2016; SEM image available in Durand, 2017), Gulf of Morbihan (Redois, 1996), Vie estuary (Debenay et al., 2006), Bourgneuf Bay (Debenay and Guillou, 2002; Morvan et al., 2004). SEM images for each study are required to harmonize the species assignments and avoid species confusion according to the different authors. *Elphidium seleyense* is a widespread and opportunistic species found in shallow intertidal waters in temperate latitudes (Darling et al., 2016; Jauffrais et al., 2018).

4.2 Spatial distribution and population dynamics of foraminiferal species in the "confined waters" concept

4.2.1 Spatial distribution of foraminiferal species

The spatial distribution of benthic foraminifera species in the Bourgneuf Bay has been subject of several previous studies, especially by Debenay (Debenay, 1978; Debenay et al., 2000; Debenay and Guillou, 2002). The assemblage at the "La Coupelasse" site was composed of four dominant species. These species are typical of "confined" transitional environments. Indeed, their distributions depend both on a longitudinal marine-to-freshwater gradient and on a vertical water-to-land gradient (Debenay and Guillou, 2002). The "La Coupelasse" site was characterized by muddy (coarse silt) sediments (Annex 3) and located in the upper middle part of the bay (Fig. 1b; Fig. 10). *Ammonia tepida* and *Haynesina germanica* were the two dominant species during the monthly survey, showing one or two high density events at contrasting hydrological and meteorological periods (Fig. 7). Therefore, these two species would be present at an optimal site where they could develop at two different seasons: in a winter period (characterized by high hydrodynamism and continental freshwater inputs) and in early autumnal period (characterized by lower hydrodynamism and more marine influence) (Fig. 7). Conversely, *Elphidium selseyense* and *Elphidium oceanense* indicated one event or short period of high density, in spring and autumn, respectively (Fig. 7). The hypothesis established by Debenay and Guillou, (2002) suggests that the *Elphidium* are species indicating a marine

influence (Fig. 10). Therefore, these two *Elphidium* species would be located at a site where they could be less privileged, explaining their almost absence during periods under the influence of the Loire river discharge (e.g. decreasing the salinity of the bay).

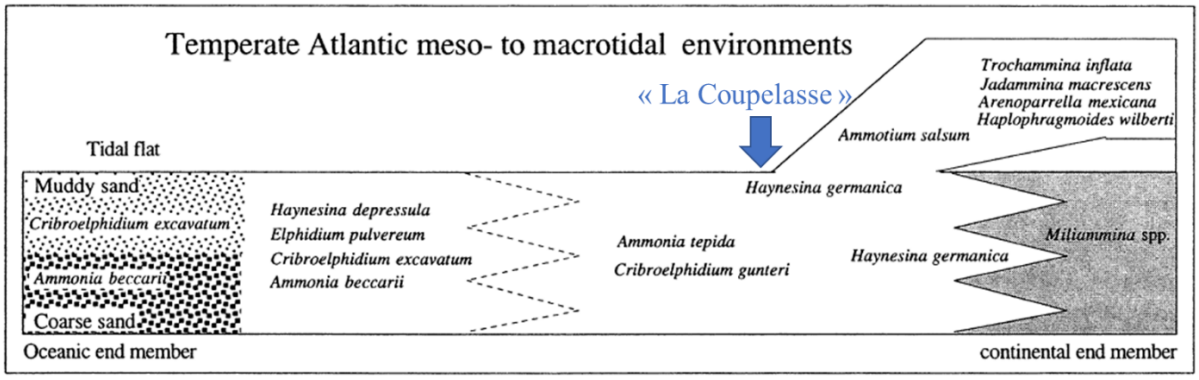

Figure 10: Distribution of the dominant species in the Bourgneuf Bay mudflat and the hypothetical location of the "La Coupelasse" site dominated by Ammonia tepida, Cribroelphidium gunteri and Haynesina germanica according to Debenay and Guillou, (2002). According to the new taxonomy Cribroelphidium excavatum is the previous name of Elphidium selseyense, then Cribroelphidium gunteri is the previous name of Elphidium oceanense. Modified from Debenay and Guillou, (2002).

In ecological studies it is crucial to assess the patchiness of benthic foraminifera at decameter scale (~ 10 m) to characterize correctly the intra variation of the sampling site (Valiela, 1995; Murray and Alve, 2000; Buzas, 2015; Debenay et al., 2000, 2006; Armynot du Châtelet et al., 2017). A low spatial variability was observed at decameter scale (surface area ~ 43 m^2 (area = ($\sqrt{3}/4$) x 10^2), Fig. 1 c) for foraminiferal species density between the three sampling stations (see Results section 3.2.2, Fig. 7). The patchiness observed at some sampling dates as September and October 2017 (Fig. 6) might be promoted by sediment surface heterogeneity (e.g. grazing, mud ripples, MPB biomass, bioturbation). The spatial distribution of benthic foraminiferal species allowed to contextualize the study site through the concept of "confine waters". However, the population dynamics of these species remain unclear.

4.2.3 Population dynamics

The increase of peaks in foraminiferal species densities observed in this study (Fig. 7) was interpreted as reproductive events, whereas the decrease in density was interpreted as mortality of specimens (Alve and Murray, 2000). The observation of population dynamics was limited to the adult stage > 150 µm. Therefore, a time lag potentially occurred between the reproductive event and the observed adult stage. This time lag is challenging to determine *in situ* and experimentally because foraminiferal life cycle (i.e. propagules, juveniles, adult stages)

is species-specific and several environmental factors can impact reproduction events (i.e. food source, hydrodynamism, pollution; (Walton, 1955; Ellison, 1984; Erskian and Lipps, 1987; Alve and Murray, 1994; Murray and Alve, 2000; Langezaal et al., 2003; Alve and Goldstein, 2003; Ernst et al., 2006). In this study we considered adult specimens, and consequently a complete view of the growth cohorts was not possible. Besides, previous population dynamics studies using growth cohorts, reported difficulties in following accurately species life cycle (Myers, 1943; Murray and Alve, 2000; Richirt, 2020). A possible way would be to study the ontogenetic rate of a species under controlled experimental conditions. The ontogenetic rate of *Ammonia tepida* is studied experimentally by (Stouff, 1998). The multiplication of loges is rapid at the beginning of ontogeny: in less than two weeks it grows from the proloculus stage (1 loge) to the juvenile stage (~ 8-9 loges) at which stage the test size can reach up to 100 µm. However, the adult stage with maximal size is reached in 3 months (~ 14-20 loges). Consequently, a reproductive event with specimens > 150 µm would be possible within a month. Moreover, in intertidal environments an increased density response of adult foraminifera is supposed to be around 1 month (Boltovskoy and Lena, 1969; Morvan et al., 2006; Debenay et al., 2006). Consequently, we hypothesized that the high density events observed in this study (Fig. 7) were rapid responses to a reproductive event that occurred from 1 to 3 month before the observation.

Ammonia sp. T6 and *Haynesina germanica* were the two main species of the assemblage (Fig. 7). Other studies, have previously reported the presence of these two species all year round (e.g. (Jones and Ross, 1979; Cearreta, 1988; Basson and Murray, 1995; Gustafsson and Nordberg, 1999; Murray and Alve, 2000). At our sampling site, *Ammonia* sp. T6 and *Haynesina germanica* showed similar spatiotemporal dynamics (Fig. 7). However, they did not show a clear yearly cyclicity of high density events. This was observed in several intertidal areas for *Ammonia tepida* (Murray and Alve 2000, 2001; Alve and Murray, 1994; Morvan et al., 2006, Debenay et al., 2006; Saad and Wade, 2017), and *Haynesina germanica* (Ellison 1984; Santoña estuary, Cearreta, 1988; Alve and Murray, 2001; Morvan et al., 2006, Debenay et al., 2006; Saad and Wade, 2017; Cesbron et al., 2016). At “La Coupelasse” site, these species indicated one or two high density events at contrasting hydrological and meteorological periods (Fig.7). The late winter/early spring high density events did not occur each year. We hypothesized that there was a dual response to high hydrodynamism and winter meteorological conditions: foraminiferal faunas might respond with strongly increased mortality (2017 and 2019, Fig. 7), and/or with accelerated reproduction (2016 and 2018, Fig. 7). This dual response was also suggested in relation to oil-induced pollution in the Bourgneuf Bay by Ernst et al., (2006). Then,

we suggest that the high-density events were due to reproduction (asexual or sexual) of the specimens *in situ* but instead due to a contribution of propagules transported by the currents from the Loire estuary, where these species are also present (Mojtahid et al., 2016). It is possible that the propagules could find more suitable conditions for their development in the bay (Alve and Goldstein, 2003). Another explanation could be the lower sampling frequency during the year 2019 with a consequent miss out of the reproductive event (Fig. 7). In late summer/early autumn, the hydrodynamism was lower, indicating a period more favorable for the reproduction of specimens and also for the development of dormant propagules. Conversely, *Elphidium selseyense* and *Elphidium oceanense* indicated one event or short period of high density, in lower hydrodynamism and summer conditions periods (Fig. 7), indicating a higher marine influence (Debenay and Guillou, 2002; Fig. 10). The temporal dynamics of *Elphidium oceanense* is poorly known. The reproductive event of *Elphidium oceanense* was almost synchronous with those shown by *Ammonia* sp. T6 and *Haynesina germanica*. However, we noticed the absence of reproduction event in autumn 2016 (Fig. 7), suggesting that *Elphidium oceanense* could be linked to other environmental parameters. *Elphidium selseyense* was not synchronous with the three previous species (Fig. 7), showing lower densities and reproduction event in spring. As for *Elphidium oceanense*, the temporal dynamics of *Elphidium selseyense* in intertidal areas is poorly known. Jones and Ross, (1979) described the same seasonal reproduction events in spring/early summer at the Samish Bay (Washington). In the Grevelingen lake submitted to anoxic events (the Netherlands, Richirt et al., 2020), *Elphidium selseyense* shows a complex spatiotemporal distribution and the dominance of *Elphidium selseyense* over *Ammonia* sp. T6 would not come from its ability to withstand anoxia but it rather be linked to the availability of food source.

4.3 Environmental parameters driving the spatiotemporal foraminiferal dynamics at « La Coupelasse » site

4.3.1 Environmental parameters influencing the spatiotemporal variability of the MPB biomass

The average NDVI values found at the three sampling stations matched with typical values (~ 0.30) found in the Bourgneuf Bay (Méléder et al., 2005; Beyoucef et al., 2014). At decimeter scale, the spatial heterogeneity of the MPB biomass fluctuated widely at each station (result part 3.1.4), as observed in previous studies (Méléder et al., 2005; Benyoucef et al., 2014; Echappé et al., 2018). Indeed, the MPB biomass is influenced by biotic parameters not included in this study: aggregation of cells (Decho, 2000), vertical migrations of cells (Jesus et al., 2006)

and grazing (Gooday, 1996; Seuront and Spilmont, 2002). Consequently, the spatial heterogeneity indicated no significant difference at decameter scale between the three stations (result part 3.1.4). Indeed, no clear seasonal trend was identified for the MPB biomass (Annex 4), as observed by Méléder et al., (2005).

The multivariate analysis allowed to contextualize the spatiotemporal variability of the MPB biomass in parallel to other environmental parameters (NDVI, Fig. 8). Previous studies, indicate that the spatiotemporal variability of the MPB biomass is mainly driven by temperature, tidal height and sediment structure variations (Seuront and Spilmont, 2002; Jesus et al., 2005, 2006, 2009; Méléder et al., 2003a, 2005; Brito et al., 2009; Spilmont et al., 2011). At the "La Coupelasse" site, a high hydrodynamism (i.e. discharge, rainfall, higher mean grain size, sand events and wind-storms) seemed to reduce NDVI values (Fig. 8). Indeed, a high hydrodynamism induces adverse conditions, for instance the potential destruction of the sediment surface by deposition and resuspension (De Jonge and Van Beusekom, 1996; Benyoucef et al., 2014). Moreover, high temperatures did not impact the development of MPB biomass (Fig. 8). Indeed, protracted high temperature combined with longer light exposure can lead to MPB photo–inhibition and a consequent decrease in the total biomass (Jesus et al., 2006; Cartaxana et al., 2015). Finally, desiccation of the sediment surface (inducing lower porosity, and higher salinity) might also limit the MPB biomass development, as shown previously (Guarini et al., 1997; Blanchard et al., 1997; Benyoucef et al., 2014).

The nitrogen uptake is crucial for MPB biomass, especially NO_3^- and NH_4^+ (Underwood and Kromkamp, 1999; Seuront and Spilmont, 2002; Méléder et al., 2007; Oakes et al., 2020). At the sampling site, NO_2^- and NO_3^- concentrations were closed to the detection limit or undetected during the entire sampling period. This would suggest that denitrification was very high and that NO_3^- was rapidly used by MPB and bacteria (Dalsgaard and Thamdrup, 2002; Risgaard-Petersen et al., 2003). Ammonium was clearly correlated with the NDVI contrary to phosphorus (Fig. 8). Ammonium and phosphorus are essential nutrients for benthic primary producers (Sundbäck and Granéli, 1988; Feuillet-Girard et al., 1997; Deborde et al., 2008; Oakes et al., 2020). However, this study was limited in the interpretation of these nutrients which are dependent on diagenetic processes occurring deeper in the sediment.

4.3.2 Synthesis of the environmental parameters driving the spatiotemporal foraminiferal species dynamics

The Bourgneuf Bay is a semi-enclosed area under marine and fresh waters influences (Debenay, 1978; Debenay and Guillou, 2002). The multivariate analysis presented in Figure 8

confirmed the characterization of the parameters related to the hydrodynamism and the meteorology of the Bourgneuf Bay. The late winter/early spring periods were characterized by a high winter hydrodynamism, cumulating flood events (high discharge) and a higher rainfall (Fig. 8). These parameters would induce sediment mixing showed by a higher mean grain size and punctual sand inputs (Annex 3). The porosity also seemed to be lower (Fig. 8), likely due to particles mixing (resuspension/deposit). The particles mixing occurring at the sediment surface could have induced a higher oxygenation and consequent deeper OPD. Then, the river discharge generated a lower salinity in the surface sediments. These parameters suggested a sediment instability period, characterizing the dual response of *Ammonia* sp. T6 and *Haynesina germanica* reproductive events previously discussed. The early autumn period was characterized by a lower hydrodynamism and summer conditions, suitable for MPB biomass development and the favorable reproductive period for the marine species *Elphidium oceanense*, and for *Ammonia* sp. T6 and *Haynesina germanica*. *Elphidium selseyense* reproductive period differed from the three other species. Late spring/early summer period was characterized by higher temperature, matching with a higher organic matter aerobic (DOU) and anaerobic (alkalinity, increasing DRP) processes. Foraminiferal species show diverse behavioral and alternative metabolisms. However, in this study the foraminiferal sampling (1st cm depth) did not allow to go further in the interpretations. A vertical micro-distribution study at contrasted seasons would estimate the foraminiferal species contributions to OM remineralization and would allow exploration of potential micro-niches deeper in the sediments.

4.4 *In situ* trophic model based on the temporal foraminiferal species–specific diatoms food preferences

4.4.1 Temporal variations of the diatom shapes assemblage

The MPB assemblage at the station B, was composed of 29 dominant diatom species showing seven diatom shapes (see Results section 3.2.1). The occurrence of these diatom shape classes fluctuated temporally (Fig. 5). Each shape class was constituted of a set of species indicating various life-forms (e.g. epipelic, epipsammic, epiphytic, pelagic).

The main diatom life-form found in muddy sediment was epipelic. These moving cells, located at the sediment surface, are able to perform vertical migration that supports intense gradients of environmental parameters. Moreover, these cells are localized where the nitrogen food source is easily assimilated compared to sandy sites (Underwood and Krompkamp, 1999; Méléder et al., 2007).

Episammic diatoms species correspond mainly to mixed and sandy sediment. These sediments are characterize by grains providing greater surface area for epipsammic cells attachment (Paterson and Hagerthey, 2001). Then, these sediments are related to high physical stress and various nutrients levels (Underwood and Krompkamp, 1999; Paterson and Hagerthey, 2001; Méléder et al., 2007). Moreover, epipsammic species could indicate a decreasing photosynthetic active biomass (Méléder et al., 2005; Jesus et al., 2009). Rarely observed in the assemblage, pelagic species (settling from the water column to the sediment surface) were identified in the "prism on elliptic base" shape (*Chaetoceros* sp.), and the complex shape "cylinder + 2 half spheres" (e.g. *Skeletonema* sp., *Podosira stelligera*). Namely, *Podosira stelligera* can be also considered as pelagic species (Continuous Plankton Recorder Survey teams, 2004). Then, the epiphytic life-form was identified in the "cylinder" shape (*Melosira* sp.). The pelagic and epiphytic life-forms identified punctually might transported by currents from another area of the bay.

Diatom life-forms are explained by the hydrodynamism of the Bourgneuf Bay, especially the granulometry of the sediments (Méléder et al., 2007). A further analysis in progress could provide additional information on the diatoms assemblage in the view of physicochemical parameters.

4.4.2 Foraminiferal species-specific diatoms food preferences

The theoretical trophic model suggested in this study aimed to establish possible preferential temporal relationships between prey (diatoms) and predators (foraminifera). *Haynesina germanica* feed preferentially on large "prism on elliptic base" and "prism on parallelogram base" shapes. These shapes are also commonly named "pennate" diatoms. The broad and elongated simple "pointed tip" diatoms might be easier to feed on. Indeed, the ornamented aperture of *Haynesina germanica* allows to fracture (i.e. cracking) the diatom frustule to empty the diatom cellular content towards the foraminiferal cytoplasm (Austin et al., 2005; LeKieffre et al., 2017). Thus, the four identified diatom species eaten by *Haynesina germanica* (*Pleurosigma formosum*, *Plagiotropis vanheurckii*, *Navicula* cf *flagellifera* and *Nitzschia* cf *distans*) were only epipelic forms. We hypothesized that the diatom life-forms might influence the diet of *Haynesina germanica* and the other foraminiferal species. The trophic model did not suggest that *Haynesina germanica* feeds only on these four species, other species with the same shape and size could be eaten. As suggested by the metabarcoding study of (Schweizer et al., *submitted*), other diatom forms are identified in the *Haynesina germanica* microbiome such as: *Pleurosigma* spp., *Gyrosigma* spp. but also unknow diatom sequences.

Ammonia sp. T6 would prefer to feed on other diatom species such as *Navicula spartinetensis*, *Pleurosigma formosum*, *Gyrosigma fasciola*, *Pleurosigma angulatum*, and *Thalassiosira* sp. These species showed various sizes (small, medium and large), and elongated shape with a "pointed tip" but also cylindrical. *Ammonia* sp. T6 does not break the diatom frustule, it rather incorporates the entire diatom cell (LeKieffre et al., 2017). The study of (Schweizer et al., *submitted*) also identified sequences of *Thalassiosira* spp. and *Gyrosigma* spp. in the *Ammonia* sp. T6 microbiome as well as unknown diatom species. *Ammonia* sp. T6 would feed on both epipelic and epipsammic species. This more diverse trophic regime could indicate that there would be no competition between *Ammonia* sp. T6 and *Haynesina germanica* for the diatom species preferentially eaten.

The consumption of diatoms by *Elphidium* spp. is poorly known. *Elphidium oceanense* and *Elphidium selseyense* also share ornamentation on the aperture that might function to break diatom frustules (Austin et al., 2005). *Elphidium oceanense* shown the most diverse diet, preferring to feed on species of various sizes and shapes: simple elongated shape with a "pointed tip", cylindrical, and also complex shapes. Moreover, the diatom life-forms were diverse: epipelic (*Gyrosigma wansbeckii*, *Entomoneis paludosa*, *Navicula spartinetensis*, *Plagiotropis vanheurckii*, *Navicula* cf *flagellifera*), epipsammic (*Plagiogrammopsis vanheurckii*, *Eutonogramma dubium*, *Thalassiosira* sp., *Podosira stelligera*) but also pelagic species such as *Skeletonema* sp. and *Podosira stelligera*. This preference for pelagic forms could be explained by the preferred marine influence of *Elphidium oceanense*. Some of these diatom species are identified in the *Elphidium oceanense* microbiome as *Navicula* spp., *Thalassiosira* spp., *Entomoneis* spp. but also other species present in the bay, such as *Nitzschia* spp. and *Odontella* spp. (Schweizer et al., *submitted*).

No clear diatom species would explain the temporal dynamics of *Elphidium selseyense,* with the only exception of the large pennate form *Navicula abscondita*. No previous studies using a metabarcoding approach, inducing a lack of knowledge on this species. A recent study from (Lintner et al., 2021) analyzed *Elphidium excavatum* (related to *Elphidium selseyense*) in controlled conditions and suggested that this species would prefer to feed on Chlorophyceae rather than diatoms (soft shell would be easier to feed). In the Bourgneuf Bay, Méléder et al., (2007) suggested that Euglenophyceae (soft shell) could be a component of summer diatom assemblages. The presence of *Elphidium selseyense* in late spring/early summer period could corroborate that this species feed preferentially on other microalgae as food source.

5. Conclusion

This study investigated the monthly spatiotemporal dynamics of the dominant foraminiferal species in the “La Coupelasse” muddy site of the Bourgneuf Bay (West coast of France). Four typical intertidal foraminifera dominated: *Ammonia* sp. T6, *Haynesina germanica*, *Elphidium oceanense* and *Elphidium selseyense*. No spatial variability at decameter scale was found. *Ammonia* sp. T6 and *Haynesina germanica* showed one or two density events per year. The winter/early spring period was characterized by a combination of high hydrodynamism and winter meteorological parameters (i.e. Loire river discharge, wind-storm events, high rainfall, higher granulometry and lower porosity). The sediment instability would generate a dual response for *Ammonia* sp. T6 and *Haynesina germanica*: mortality *versus* accelerating reproduction. Conversely, the density events observed in early autumn were characterized by a lower hydrodynamism and summer conditions (i.e. low waters of the Loire river, higher temperature and MPB biomass). This more favourable period for benthic fauna indicated reproductive events for *Ammonia* sp. T6, *Haynesina germanica* and *Elphidium oceanense*. *Elphidium selseyense* reproduced only in spring, suggesting to be driven by other environmental parameters. Finally, the foraminiferal spatiotemporal dynamics provided accurate information on the "confined waters" concept. The foraminiferal temporal dynamics are also driven by their food source. The ecological *in situ* trophic model allowed to confirm and complete the prey (diatoms) – predator (foraminifera) relationships. *Haynesina germanica* showed a restrictive diet, feeding on few large elongated epipelic diatom species. *Ammonia* sp. T6 showed a wider diatoms diet, feeding on different sizes, elongated shapes and life-forms (epipelic and epipsammic). *Elphidium oceanense* presented the most various diet, feeding on different sizes, simple and complex shapes, and life-forms (epipelic, epipsammic and pelagic). No diatom species indicated clearly the temporal variability of *Elphidium selseyense*. Besides, this trophic model would suggest that foraminiferal species feed preferential on their own diatom species, inducing no competition for diatom food source.

Bibliography

Alve, E. and Goldstein, S. T.: Propagule transport as a key method of dispersal in benthic foraminifera (Protista), Limnol. Oceanogr., 48, 2163–2170, https://doi.org/10.4319/lo.2003.48.6.2163, 2003.

Alve, E. and Murray, J.: Temporal variability in vertical distributions of live (stained) intertidal foraminifera, Southern England, J. Foraminifer. Res., 31, 12–24, https://doi.org/10.2113/0310012, 2001.

Alve, E. and Murray, J. W.: Ecology and taphonomy of benthic foraminifera in a temperate mesotidal inlet, Ecology and taphonomy of benthic foraminifera in a temperate mesotidal inlet Journal of Foraminiferal Research, 24 (1). pp. 18-27. DOI 10.2113/gsjfr.24.1.18 http://dx.doi.org/10.2113/gsjfr.24.1.18., 1994.

Anderson M.J., Gorley R.N. and Clarke K.R. PERMANOVA+ for *PRIMER: Guide to Software and Statistical Methods.* PRIMER-E: Plymouth, UK, 2008.

Armynot du Châtelet, Frontalini, and Francescangeli: Significance of replicates: Environmental and paleoenvironmental studies on benthic foraminifera and testate amoebae, 2017.

Armynot du Châtelet, E., Debenay, J.-P., and Soulard, R.: Foraminiferal proxies for pollution monitoring in moderately polluted harbors, Environ. Pollut., 127, 27–40, https://doi.org/10.1016/S0269-7491(03)00256-2, 2004.

Austin, H. A., Austin, W. E. N., and Paterson, D. M.: Extracellular cracking and content removal of the benthic diatom *Pleurosigma angulatum* (Quekett) by the benthic foraminifera *Haynesina germanica* (Ehrenberg), Mar. Micropaleontol., 57, 68–73, https://doi.org/10.1016/j.marmicro.2005.07.002, 2005.

Bargain, A., Robin, M., Le Men, E., Huete, A., and Barillé, L.: Spectral response of the seagrass Zostera noltii with different sediment backgrounds, Aquat. Bot., 98, 45–56, https://doi.org/10.1016/j.aquabot.2011.12.009, 2012.

Basson, P. W. and Murray, J. W.: Temporal variations in four species of intertidal foraminifera, Bahrain, Arabian Gulf, Micropaleontology, 41, 69–76, 1995.

Benito, X.: Benthic Foraminifera and Diatoms as Ecological Indicators, in: Modern Trends in Diatom Identification: Fundamentals and Applications, edited by: Cristóbal, G., Blanco, S., and Bueno, G., Springer International Publishing, Cham, 257–280, https://doi.org/10.1007/978-3-030-39212-3_15, 2020.

Benyoucef, I., Blandin, E., Lerouxel, A., Jesus, B., Rosa, P., Méléder, V., Launeau, P., and Barillé, L.: Microphytobenthos interannual variations in a north-European estuary (Loire estuary, France) detected by visible-infrared multispectral remote sensing, Estuar. Coast. Shelf Sci., 136, 43–52, https://doi.org/10.1016/j.ecss.2013.11.007, 2014.

Berg, P., Risgaard-Petersen, N., and Rysgaard, S.: Interpretation of measured concentration profiles in sediment pore water, Limnol. Oceanogr., 43, 1500–1510, https://doi.org/10.4319/lo.1998.43.7.1500, 1998.

Bernhard, J. M. and Bowser, S. S.: Benthic foraminifera of dysoxic sediments: chloroplast sequestration and functional morphology, Earth-Sci. Rev., 46, 149–165, https://doi.org/10.1016/S0012-8252(99)00017-3, 1999.

Bird, C., LeKieffre, C., Jauffrais, T., Meibom, A., Geslin, E., Filipsson, H. L., Maire, O., Russell, A. D., and Fehrenbacher, J. S.: Heterotrophic Foraminifera Capable of Inorganic Nitrogen Assimilation, Front. Microbiol., 11, https://doi.org/10.3389/fmicb.2020.604979, 2020.

Blanchard, G. F., Guarini, J.-M., Gros, P., and Richard, P.: Seasonal Effect on the Relationship Between the Photosynthetic Capacity of Intertidal Microphytobenthos and Temperature1, J. Phycol., 33, 723–728, https://doi.org/10.1111/j.0022-3646.1997.00723.x, 1997.

Boltovskoy, E. and Lena, H.: Seasonal occurences, standing crop and production in benthic foraminifera of Puerto Deseado, Contrib. Cushman Found. Foraminifer. Res., 20, 87–95, 1969.

Bouchet, V. M. P., Frontalini, F., Francescangeli, F., Sauriau, P.-G., Geslin, E., Martins, M. V. A., Almogi-Labin, A., Avnaim-Katav, S., Di Bella, L., Cearreta, A., Coccioni, R., Costelloe, A., Dimiza, M. D., Ferraro, L., Haynert, K., Martínez-Colón, M., Melis, R., Schweizer, M., Triantaphyllou, M. V., Tsujimoto, A., Wilson, B., and Armynot du Châtelet, E.: Indicative value of benthic foraminifera for biomonitoring: Assignment to ecological groups of sensitivity to total organic carbon of species from European intertidal areas and transitional waters, Mar. Pollut. Bull., 164, 112071, https://doi.org/10.1016/j.marpolbul.2021.112071, 2021.

Bradshaw, J. S.: Laboratory experiments on the ecology of foraminifera., Cushman Found Foram Res Contr, 12, 87–106, 1961.

Brito, A., Newton, A., Tett, P., and Fernandes, T. F.: Temporal and spatial variability of microphytobenthos in a shallow lagoon: Ria Formosa (Portugal), Estuar. Coast. Shelf Sci., 83, 67–76, https://doi.org/10.1016/j.ecss.2009.03.023, 2009.

Buzas, M. A.: Pulsating Patches: History and Analyses of Spatial, Seasonal, and Yearly Distribution of Living Benthic Foraminifera, https://doi.org/10.5479/si.19436688.97, 2015.

Cartaxana, P., Vieira, S., Ribeiro, L., Rocha, R. J., Cruz, S., Calado, R., and da Silva, J. M.: Effects of elevated temperature and CO_2 on intertidal microphytobenthos, BMC Ecol., 15, 10, https://doi.org/10.1186/s12898-015-0043-y, 2015.

Cearreta, A.: Population dynamics of benthic foraminifera in the Santona estuary, Spain, Rev. Paléobiol., 721–724, 1988.

Cecchini, S. and Rocchina Caputo, A.: A Direct Spectrophotometric Assay for Evaluating Nitrate-Nitrogen in Intensive Aquaculture Systems, 2012.

Cesbron, F., Geslin, E., Jorissen, F. J., Delgard, M. L., Charrieau, L., Deflandre, B., Jézéquel, D., Anschutz, P., and Metzger, E.: Vertical distribution and respiration rates of benthic foraminifera: Contribution to aerobic remineralization in intertidal mudflats covered by *Zostera noltei* meadows, Estuar. Coast. Shelf Sci., 179, 23–38, https://doi.org/10.1016/j.ecss.2015.12.005, 2016.

Cesbron, F., Geslin, E., Lekieffre, C. M. N., Jauffrais, T., Nardelli, M. P., Langlet, D., Mabilleau, G., Jorissen, F. J., Jezequel, D., and Metzger, E.: Sequestered Chloroplasts In The

Benthic Foraminifer Haynesina Germanica: Cellular Organization, Oxygen Fluxes And Potential Ecological Implications, J. Foraminifer. Res., 47, 268–278, https://doi.org/10.2113/gsjfr.47.3.268, 2017.

Chronopoulou, P. M., Salonen, I., Bird, C., Reichart, G.-J., and Koho, K. A.: Metabarcoding insights into the trophic behaviour and identity of intertidal benthic foraminifera, Front. Microbiol., 10, https://doi.org/10.3389/fmicb.2019.01169, 2019.

Clarke, K.R., and Gorley, R.N. Getting started with PRIMER v 6 PRIMER-E: Plymouth, 2006.

Dalsgaard, T. and Thamdrup, B.: Factors Controlling Anaerobic Ammonium Oxidation with Nitrite in Marine Sediments, Appl. Environ. Microbiol., 68, 3802–3808, https://doi.org/10.1128/AEM.68.8.3802-3808.2002, 2002.

Darling, K. F., Schweizer, M., Knudsen, K. L., Evans, K. M., Bird, C., Roberts, A., Filipsson, H. L., Kim, J.-H., Gudmundsson, G., Wade, C. M., Sayer, M. D. J., and Austin, W. E. N.: The genetic diversity, phylogeography and morphology of *Elphidiidae* (Foraminifera) in the Northeast Atlantic, Mar. Micropaleontol., 129, 1–23, https://doi.org/10.1016/j.marmicro.2016.09.001, 2016.

Debenay, J.-P.: Distribution des foraminifères vivants et des tests vides en Baie de Bourgneuf, PhD Thesis, 1978.

Debenay, J.-P. and Guillou, J.-J.: Ecological transitions indicated by foraminiferal assemblages in paralic environments, Estuaries, 25, 1107–1120, https://doi.org/10.1007/BF02692208, 2002.

Debenay, J.-P., Guillou, J.-J., Redois, F., and Geslin, E.: Distribution Trends of Foraminiferal Assemblages in Paralic Environments, in: Environmental Micropaleontology: The Application of Microfossils to Environmental Geology, edited by: Martin, R. E., Springer US, Boston, MA, 39–67, https://doi.org/10.1007/978-1-4615-4167-7_3, 2000.

Debenay, J.-P., Bicchi, E., Goubert, E., and Armynot du Châtelet, E.: Spatio-temporal distribution of benthic foraminifera in relation to estuarine dynamics (Vie estuary, Vendée, W France), Estuar. Coast. Shelf Sci., 67, 181–197, https://doi.org/10.1016/j.ecss.2005.11.014, 2006.

Deborde, J., Anschutz, P., Auby, I., Glé, C., Commarieu, M.-V., Maurer, D., Lecroart, P., and Abril, G.: Role of tidal pumping on nutrient cycling in a temperate lagoon (Arcachon Bay, France), Mar. Chem., 109, 98–114, https://doi.org/10.1016/j.marchem.2007.12.007, 2008.

Decho, A. W.: Microbial biofilms in intertidal systems: an overview, Cont. Shelf Res., 20, 1257–1273, https://doi.org/10.1016/S0278-4343(00)00022-4, 2000.

Dupuy, C., Rossignol, L., Geslin, E., and Pascal, P.-Y. Predation of mudflat meio-macrofaunal metazoans by a calcareous foraminifer, *Ammonia tepida* (Cushman, 1926), J. Foraminifer. Res., 40, 305–312, https://doi.org/10.2113/gsjfr.40.4.305, 2010.

Echappé, C., Gernez, P., Méléder, V., Jesus, B., Cognie, B., Decottignies, P., Sabbe, K., and Barillé, L.: Satellite remote sensing reveals a positive impact of living oyster reefs on microalgal biofilm development, Biogeosciences, 15, 905–918, https://doi.org/10.5194/bg-15-905-2018, 2018.

Échappé, C., Gernez, P., Méléder, V., Jesus, B., Cognie, B., Decottignies, P., Sabbe, K., and Barillé, L.: Satellite remote sensing reveals a positive impact of living oyster reefs on microalgal biofilm development, Biogeosciences, 15, 905–918, https://doi.org/10.5194/bg-15-905-2018, 2018.

Ellison, R. L.: Foraminifera and meiofauna on an intertidal mudflat, Cornwall, England: Populations; respiration and secondary production; and energy budget, Hydrobiologia, 109, 131–148, https://doi.org/10.1007/BF00011572, 1984.

Ernst, S. R., Morvan, J., Geslin, E., Le Bihan, A., and Jorissen, F. J.: Benthic foraminiferal response to experimentally induced Erika oil pollution, Mar. Micropaleontol., 61, 76–93, https://doi.org/10.1016/j.marmicro.2006.05.005, 2006.

Erskian, M. G. and Lipps, J. H.: Population dynamics of the foraminiferan *Glabratella ornatissima* (Cushman) in Northern California, J. Foraminifer. Res., 17, 240–256, https://doi.org/10.2113/gsjfr.17.3.240, 1987.

Feuillet-Girard, M., Gouleau, D., Blanchard, G., and Joassard, L.: Nutrient fluxes on an intertidal mudflat in Marennes-Oléron Bay, and influence of the emersion period, Aquat. Living Resour., 10, 49–58, https://doi.org/10.1051/alr:1997005, 1997.

Feyling-Hanssen, R. W.: The foraminifer *Elphidium excavatum* (Terquem) and its variant forms, Micropaleontology, 18, 337–354, 1972.

Ford, R. B. and Honeywill, C.: Grazing on intertidal microphytobenthos by macrofauna: is pheophorbide a a useful marker?, Mar. Ecol. Prog. Ser., 229, 33–42, https://doi.org/10.3354/meps229033, 2002.

Forster, R. M. and Jesus, B.: Field spectroscopy of estuarine intertidal habitats, Int. J. Remote Sens., 27, 3657–3669, https://doi.org/10.1080/01431160500500367, 2006.

Goldstein, S. T., Bernhard, J. M., and Richardson, E. A.: Chloroplast Sequestration in the Foraminifer *Haynesina germanica*: Application of High Pressure Freezing and Freeze Substitution, Microsc. Microanal., 10, 1458–1459, https://doi.org/10.1017/S1431927604885891, 2004.

Gooday, A. J.: A response by benthic Foraminifera to the deposition of phytodetritus in the deep sea, Nature, 332, 70–73, https://doi.org/10.1038/332070a0, 1988.

Gooday, A. J.: Epifaunal and shallow infaunal foraminiferal communities at three abyssal NE Atlantic sites subject to differing phytodetritus input regimes, Deep Sea Res. Part Oceanogr. Res. Pap., 43, 1395–1421, https://doi.org/10.1016/S0967-0637(96)00072-6, 1996.

Griess, P.: Bemerkungen zu der Abhandlung der HH. Weselsky und Benedikt „Ueber einige Azoverbindungen", Berichte Dtsch. Chem. Ges., 12, 426–428, https://doi.org/10.1002/cber.187901201117, 1879.

Guarini, J., Blanchard, G., Gros, P., and Harrisson, S.: Modelling the mud surface temperature on intertidal flats to investigate the spatio-temporal dynamics of the benthic microalgal photosynthetic capacity, Mar. Ecol. Prog. Ser., 153, 25–36, https://doi.org/10.3354/meps153025, 1997.

Guelorget, O. and Perthuisot, J. P.: Paralic ecosystems. Biological organization and functionning, Paralic Ecosyst. Biol. Organ. Funct., 42, 215–251, 1992.

Gustafsson, M. and Nordberg, K.: Benthic foraminifera and their response to hydrography, periodic hypoxic conditions and primary production in the Koljö fjord on the Swedish west coast, J. Sea Res., 41, 163–178, https://doi.org/10.1016/S1385-1101(99)00002-7, 1999.

Hammer, O.: PAST : Paleontological Statistics Software Package for Education and Data Analysis, Palaeontol. Electron., 4, 2001.

Harrison, P. J., Zingone, A., Mickelson, M. J., Lehtinen, S., Ramaiah, N., Kraberg, A. C., Sun, J., McQuatters-Gollop, A., and Jakobsen, H. H.: Cell volumes of marine phytoplankton from globally distributed coastal data sets, Estuar. Coast. Shelf Sci., 162, 130–142, https://doi.org/10.1016/j.ecss.2015.05.026, 2015.

Harwood, J. E. and Kühn, A. L.: A colorimetric method for ammonia in natural waters, Water Res., 4, 805–811, https://doi.org/10.1016/0043-1354(70)90037-0, 1970.

Hayward, B. W., Holzmann, M., Grenfell, H. R., Pawlowski, J., and Triggs, C. M.: Morphological distinction of molecular types in Ammonia – towards a taxonomic revision of the world's most commonly misidentified foraminifera, Mar. Micropaleontol., 50, 237–271, https://doi.org/10.1016/S0377-8398(03)00074-4, 2004.

Heinz, P., Hemleben, C., and Kitazato, H.: Time-response of cultured deep-sea benthic foraminifera to different algal diets, Deep Sea Res. Part Oceanogr. Res. Pap., 49, 517–537, https://doi.org/10.1016/S0967-0637(01)00070-X, 2002.

Hillebrand, H., Dürselen, C.-D., Kirschtel, D., Pollingher, U., and Zohary, T.: Biovolume Calculation for Pelagic and Benthic Microalgae, J. Phycol., 35, 403–424, https://doi.org/10.1046/j.1529-8817.1999.3520403.x, 1999.

Jauffrais, T., Jesus, B., Metzger, E., Mouget, J.-L., Jorissen, F., and Geslin, E.: Effect of light on photosynthetic efficiency of sequestered chloroplasts in intertidal benthic foraminifera (*Haynesina germanica* and *Ammonia tepida*), Biogeosciences, 13, 2715–2726, https://doi.org/10.5194/bg-13-2715-2016, 2016.

Jauffrais, T., LeKieffre, C., Koho, K. A., Tsuchiya, M., Schweizer, M., Bernhard, J. M., Meibom, A., and Geslin, E.: Ultrastructure and distribution of kleptoplasts in benthic foraminifera from shallow-water (photic) habitats, Mar. Micropaleontol., https://doi.org/10.1016/j.marmicro.2017.10.003, 2017.

Jesus, B., Brotas, V., Marani, M., and Paterson, D. M.: Spatial dynamics of microphytobenthos determined by PAM fluorescence, Estuar. Coast. Shelf Sci., 65, 30–42, https://doi.org/10.1016/j.ecss.2005.05.005, 2005.

Jesus, B., Mendes, C. R., Brotas, V., and Paterson, D. M.: Effect of sediment type on microphytobenthos vertical distribution: Modelling the productive biomass and improving ground truth measurements, J. Exp. Mar. Biol. Ecol., 332, 60–74, https://doi.org/10.1016/j.jembe.2005.11.005, 2006.

Jesus, B., Brotas, V., Ribeiro, L., Mendes, C. R., Cartaxana, P., and Paterson, D. M.: Adaptations of microphytobenthos assemblages to sediment type and tidal position, Cont. Shelf Res., 29, 1624–1634, https://doi.org/10.1016/j.csr.2009.05.006, 2009.

Jones, G. D. and Ross, C. A.: Seasonal Distribution of Foraminifera in Samish Bay, Washington, J. Paleontol., 53, 245–257, 1979.

Jonge, V. N. D. and Beusekom, J. E. E. V.: Wind- and tide-induced resuspension of sediment and microphytobenthos from tidal flats in the Ems Estuary, Oceanogr. Lit. Rev., 3, 250, 1996.

Jorissen, F. J., de Stigter, H. C., and Widmark, J. G. V.: A conceptual model explaining benthic foraminiferal microhabitats, Mar. Micropaleontol., 26, 3–15, https://doi.org/10.1016/0377-8398(95)00047-X, 1995.

Langezaal, A. M., Ernst, S. R., Haese, R. R., van Bergen, P. F., and van der Zwaan, G. J.: Disturbance of intertidal sediments: the response of bacteria and foraminifera, Estuar. Coast. Shelf Sci., 58, 249–264, https://doi.org/10.1016/S0272-7714(03)00078-7, 2003.

Launeau, P., Méléder, V., Verpoorter, C., Barillé, L., Kazemipour-Ricci, F., Giraud, M., Jesus, B., and Le Menn, E.: Microphytobenthos Biomass and Diversity Mapping at Different Spatial Scales with a Hyperspectral Optical Model, Remote Sens., 10, 716, https://doi.org/10.3390/rs10050716, 2018.

Le Floch, J. F.: Propagation de la marée dynamique dans l'estuaire de la Seine et en Seine maritime, Unpubl. PhD Diss. Univ. Paris Fr., 1961.

Lee, J. J., McEnery, M., Pierce, S., Freudenthal, H. D., and Muller, W. A.: Tracer Experiments in Feeding Littoral Foraminifera, J. Protozool., 13, 659–670, https://doi.org/10.1111/j.1550-7408.1966.tb01978.x, 1966.

LeKieffre, C., Spangenberg, J. E., Mabilleau, G., Escrig, S., Meibom, A., and Geslin, E.: Surviving anoxia in marine sediments: The metabolic response of ubiquitous benthic foraminifera (*Ammonia tepida*), PLOS ONE, 12, e0177604, https://doi.org/10.1371/journal.pone.0177604, 2017.

LeKieffre, C., Bernhard, J. M., Mabilleau, G., Filipsson, H. L., Meibom, A., and Geslin, E.: An overview of cellular ultrastructure in benthic foraminifera: New observations of rotalid species in the context of existing literature, Mar. Micropaleontol., 138, 12–32, https://doi.org/10.1016/j.marmicro.2017.10.005, 2018a.

LeKieffre, C., Spero, H. J., Russell, A. D., Fehrenbacher, J. S., Geslin, E., and Meibom, A.: Assimilation, translocation, and utilization of carbon between photosynthetic symbiotic dinoflagellates and their planktic foraminifera host, Mar. Biol., 165, 104, https://doi.org/10.1007/s00227-018-3362-7, 2018b.

Li, Y.-H. and Gregory, S.: Diffusion of ions in sea water and in deep-sea sediments, 1974.

Lintner, M., Biedrawa, B., Wukovits, J., Wanek, W., and Heinz, P.: Reviews and syntheses: Salinity-dependent algae uptake and subsequent carbon and nitrogen metabolisms of two intertidal foraminifera (*Ammonia tepida* and *Haynesina germanica*), Biogeosciences, 17, 3723–3732, https://doi.org/10.5194/bg-17-3723-2020, 2020.

Lintner, M., Lintner, B., Wanek, W., Keul, N., and Heinz, P.: The effect of the salinity, light regime and food source on carbon and nitrogen uptake in a benthic foraminifer, Biogeosciences, 18, 1395–1406, https://doi.org/10.5194/bg-18-1395-2021, 2021.

Lopez, E.: Algal chloroplasts in the protoplasm of three species of benthic foraminifera: taxonomic affinity, viability and persistence, Mar. Biol., 53, 201–211, https://doi.org/10.1007/BF00952427, 1979.

MacIntyre, H. L., Geider, R. J., and Miller, D. C.: Microphytobenthos: The ecological role of the "secret garden" of unvegetated, shallow-water marine habitats. I. Distribution, abundance and primary production, Estuaries, 19, 186–201, https://doi.org/10.2307/1352224, 1996.

Méléder, V., Launeau, P., Barillé, L., and Rincé, Y.: Cartographie des peuplements du microphytobenthos par télédétection spatiale visible-infrarouge dans un écosystème conchylicole, C. R. Biol., 326, 377–389, https://doi.org/10.1016/S1631-0691(03)00125-2, 2003a.

Méléder, V., Barillé, L., Launeau, P., Carrère, V., and Rincé, Y.: Spectrometric constraint in analysis of benthic diatom biomass using monospecific cultures, Remote Sens. Environ., 88, 386–400, https://doi.org/10.1016/j.rse.2003.08.009, 2003b.

Méléder, V., Barillé, L., Rincé, Y., Morançais, M., Rosa, P., and Gaudin, P.: Spatio-temporal changes in microphytobenthos structure analysed by pigment composition in a macrotidal flat (Bourgneuf Bay, France), Mar. Ecol. Prog. Ser., 297, 83–99, https://doi.org/10.3354/meps297083, 2005.

Méléder, V., Rincé, Y., Barillé, L., Gaudin, P., and Rosa, P.: Spatiotemporal changes in microphytobenthos assemblages in a macrotidal flat (Bourgneuf Bay,France)1, J. Phycol., 43, 1177–1190, https://doi.org/10.1111/j.1529-8817.2007.00423.x, 2007.

Mojtahid, M., Zubkov, M. V., Hartmann, M., and Gooday, A. J.: Grazing of intertidal benthic foraminifera on bacteria: Assessment using pulse-chase radiotracing, J. Exp. Mar. Biol. Ecol., 399, 25–34, https://doi.org/10.1016/j.jembe.2011.01.011, 2011.

Mojtahid, M., Geslin, E., Coynel, A., Gorse, L., Vella, C., Davranche, A., Zozzolo, L., Blanchet, L., Bénéteau, E., and Maillet, G.: Spatial distribution of living (Rose Bengal stained) benthic foraminifera in the Loire estuary (western France), J. Sea Res., 118, 1–16, https://doi.org/10.1016/j.seares.2016.02.003, 2016.

Moodley, L., Boschker, H. T. S., Middelburg, J. J., Pel, R., Herman, P. M. J., Deckere, E. de, and Heip, C. H. R.: Ecological significance of benthic foraminifera: 13C labelling experiments, Mar. Ecol. Prog. Ser., 202, 289–295, https://doi.org/10.3354/meps202289, 2000.

Morvan, J., Cadre, V. L., Jorissen, F., and Debenay, J.-P.: Foraminifera as potential bio-indicators of the "Erika" oil spill in the Bay of Bourgneuf: Field and experimental studies, Aquat. Living Resour., 17, 317–322, https://doi.org/10.1051/alr:2004034, 2004.

Morvan, J., Debenay, J.-P., Jorissen, F., Redois, F., Bénéteau, E., Delplancke, M., and Amato, A.-S.: Patchiness and life cycle of intertidal foraminifera: Implication for environmental and paleoenvironmental interpretation, Mar. Micropaleontol., 61, 131–154, https://doi.org/10.1016/j.marmicro.2006.05.009, 2006.

Murray, J. W. and Alve, E.: Major aspects of foraminiferal variability (standing crop and biomass) on a monthly scale in an intertidal zone, J. Foraminifer. Res., 30, 177–191, https://doi.org/10.2113/0300177, 2000.

Myers, E. H.: Life Activities of Foraminifera in Relation to Marine Ecology, Proc. Am. Philos. Soc., 86, 439–458, 1943.

Nomaki, H., Heinz, P., Nakatsuka, T., Shimanaga, M., and Kitazato, H.: Species-specific ingestion of organic carbon by deep-sea benthic foraminifera and meiobenthos: In situ tracer experiments, Limnol. Oceanogr., 50, 134–146, https://doi.org/10.4319/lo.2005.50.1.0134, 2005.

Nomaki, H., Heinz, P., Nakatsuka, T., Shimanaga, M., Ohkouchi, N., Ogawa, N. O., Kogure, K., Ikemoto, E., and Kitazato, H.: Different ingestion patterns of 13C-labeled bacteria and algae by deep-sea benthic foraminifera, Mar. Ecol. Prog. Ser., 310, 95–108, https://doi.org/10.3354/meps310095, 2006.

Nomaki, H., Ogawa, N., Ohkouchi, N., Suga, H., Toyofuku, T., Shimanaga, M., Nakatsuka, T., and Kitazato, H.: Benthic foraminifera as trophic links between phytodetritus and benthic metazoans: carbon and nitrogen isotopic evidence, Mar. Ecol. Prog. Ser., 357, 153–164, https://doi.org/10.3354/meps07309, 2008.

Oakes, J. M., Riekenberg, P. M., and Eyre, B. D.: Assimilation and short-term processing of microphytobenthos nitrogen in intertidal sediments, Limnol. Oceanogr., 65, 2377–2389, https://doi.org/10.1002/lno.11459, 2020.

Olenina, I., Hajdu, S., Edler, L., Andersson, A., Wasmund, N., Göbel, J., Huttunen, M., Jaanus, A., Ledaine, I., Huseby, S., and Niemkiewicz, E.: Biovolumes and size-classes of phytoplankton in the Baltic Sea, Balt. Sea Environ. Proc., 2006.

Pascal, P.-Y., Dupuy, C., Richard, P., Mallet, C., Telet, E. A. du C., and Niquilb, N.: Seasonal variation in consumption of benthic bacteria by meio- and macrofauna in an intertidal mudflat, Limnol. Oceanogr., 54, 1048–1059, https://doi.org/10.4319/lo.2009.54.4.1048, 2009.

Paterson, D. M. and Hagerthey, S. E.: Microphytobenthos in Constrasting Coastal Ecosystems: Biology and Dynamics, in: Ecological Comparisons of Sedimentary Shores, edited by: Reise, K., Springer, Berlin, Heidelberg, 105–125, https://doi.org/10.1007/978-3-642-56557-1_6, 2001.

Pillet, L., de Vargas, C., and Pawlowski, J.: Molecular Identification of Sequestered Diatom Chloroplasts and Kleptoplastidy in Foraminifera, Protist, 162, 394–404, https://doi.org/10.1016/j.protis.2010.10.001, 2011.

Pillet, L., Voltski, I., Korsun, S., and Pawlowski, J.: Molecular phylogeny of *Elphidiidae* (foraminifera), Mar. Micropaleontol., 103, 1–14, https://doi.org/10.1016/j.marmicro.2013.07.001, 2013.

Ribeiro, L. L. C. S.: Intertidal benthic diatoms of the Tagus estuary : taxonomic composition and spatial-temporal variation, 2010.

Richirt, J.: Le genre *Ammonia* (Foraminifères) dans les écosystèmes côtiers de la façade Atlantique, PhD thesis, Angers, 2020.

Richirt, J., Schweizer, M., Bouchet, V. M. P., Mouret, A., Quinchard, S., and Jorissen, F. J.: Morphological Distinction of Three *Ammonia* Phylotypes Occurring Along European Coasts | Journal of Foraminiferal Research | GeoScienceWorld, 2019.

Richirt, J., Riedel, B., Mouret, A., Schweizer, M., Langlet, D., Seitaj, D., Meysman, F. J. R., Slomp, C. P., and Jorissen, F.: Foraminiferal community response to seasonal anoxia in Lake Grevelingen (the Netherlands), Biogeosciences, 2020.

Risgaard-Petersen, N., Nielsen, L. P., Rysgaard, S., Dalsgaard, T., and Meyer, R. L.: Application of the isotope pairing technique in sediments where anammox and denitrification coexist, Limnol. Oceanogr. Methods, 1, 63–73, https://doi.org/10.4319/lom.2003.1.63, 2003.

Saad, S. A. and Wade, C. M.: Seasonal and Spatial Variations of Saltmarsh Benthic Foraminiferal Communities from North Norfolk, England, Microb. Ecol., 73, 539–555, https://doi.org/10.1007/s00248-016-0895-5, 2017.

Sarazin, G., Michard, G., and Prevot, F.: A rapid and accurate spectroscopic method for alkalinity measurements in sea water samples, Water Res., 33, 290–294, https://doi.org/10.1016/S0043-1354(98)00168-7, 1999.

Schönfeld, J., Alve, E., Geslin, E., Jorissen, F., Korsun, S., and Spezzaferri, S.: The FOBIMO (FOraminiferal BIo-MOnitoring) initiative—Towards a standardised protocol for soft-bottom benthic foraminiferal monitoring studies, Mar. Micropaleontol., 94–95, 1–13, https://doi.org/10.1016/j.marmicro.2012.06.001, 2012.

Schweizer, M., Jauffrais, T., Méléder, V., Quinchard, S., Choquel, C., and Geslin, E.: Trophic strategies of intertidal foraminifera explored with single-cell microbiome metabarcoding and morphological methods: what is on the menu?, Mol. Ecol., *submitted*.

Schweizer, M., Polovodova, I., Nikulina, A., and Schönfeld, J.: Molecular identification of *Ammonia* and *Elphidium* species (Foraminifera, Rotaliida) from the Kiel Fjord (SW Baltic Sea) with rDNA sequences, Helgol. Mar. Res., 65, 1–10, https://doi.org/10.1007/s10152-010-0194-3, 2011.

Serôdio, J., Paterson, D. M., Meleder, V., and Vyverman, W.: Advances and Challenges in Microphytobenthos Research: From Cell Biology to Coastal Ecosystem Function, Frontiers Media SA, 311 pp., 2020.

Seuront, L. and Spilmont, N.: Self-organized criticality in intertidal microphytobenthos patch patterns, Phys. Stat. Mech. Its Appl., 313, 513–539, https://doi.org/10.1016/S0378-4371(02)00989-5, 2002.

Spilmont, N., Seuront, L., Meziane, T., and Welsh, D. T.: There's more to the picture than meets the eye: Sampling microphytobenthos in a heterogeneous environment, Estuar. Coast. Shelf Sci., 95, 470–476, https://doi.org/10.1016/j.ecss.2011.10.021, 2011.

Stouff, V.: Interet des elevages de foraminiferes en laboratoire : etudes biologiques et ultrastructurales, These de doctorat, Angers, 1998.

Sun, J. and Liu, D.: Geometric models for calculating cell biovolume and surface area for phytoplankton, J. Plankton Res., 25, 1331–1346, https://doi.org/10.1093/plankt/fbg096, 2003.

Sundbäck, K. and Granéli, W.: Influence of microphytobenthos on the nutrient flux between sediment and water: a laboratory study, Mar. Ecol. Prog. Ser., 43, 63–69, 1988.

Thibault de Chanvalon, A., Metzger, E., Mouret, A., Cesbron, F., Knoery, J., Rozuel, E., Launeau, P., Nardelli, M. P., Jorissen, F. J., and Geslin, E.: Two-dimensional distribution of living benthic foraminifera in anoxic sediment layers of an estuarine mudflat (Loire estuary, France), Biogeosciences, 12, 6219–6234, https://doi.org/10.5194/bg-12-6219-2015, 2015.

Thibault de Chanvalon, A., Mouret, A., Knoery, J., Geslin, E., Péron, O., and Metzger, E.: Manganese, iron and phosphorus cycling in an estuarine mudflat, Loire, France, J. Sea Res., 118, 92–102, https://doi.org/10.1016/j.seares.2016.10.004, 2016.

Thomas, Y., Pouvreau, S., Alunno-Bruscia, M., Barillé, L., Gohin, F., Bryère, P., and Gernez, P.: Global change and climate-driven invasion of the Pacific oyster (*Crassostrea gigas*) along European coasts: a bioenergetics modelling approach, J. Biogeogr., 43, 568–579, https://doi.org/10.1111/jbi.12665, 2016.

Tucker, C. J.: Red and photographic infrared linear combinations for monitoring vegetation, Remote Sens. Environ., 8, 127–150, https://doi.org/10.1016/0034-4257(79)90013-0, 1979.

Ullman, W. J. and Aller, R. C.: Diffusion coefficients in nearshore marine sediments1, Limnol. Oceanogr., 27, 552–556, https://doi.org/10.4319/lo.1982.27.3.0552, 1982.

Underwood, G. J. C. and Kromkamp: Primary production by phytoplankton and microphytobenthos in estuaries., 1999.

Underwood, G. J. C. and Smith, D. J.: Predicting Epipelic Diatom Exopolymer Concentrations in Intertidal Sediments from Sediment Chlorophyll a, Microb. Ecol., 2, 116–125, 1998.

Valiela, I.: Spatial Structure: Patchiness, in: Marine Ecological Processes, edited by: Valiela, I., Springer, New York, NY, 325–353, https://doi.org/10.1007/978-1-4757-4125-4_11, 1995.

Walton, W. R.: Ecology of Living Benthonic Foraminifera, Todos Santos Bay, Baja California, J. Paleontol., 29, 952–1018, 1955.

Whitfield, A. K., Elliott, M., Basset, A., Blaber, S. J. M., and West, R. J.: Paradigms in estuarine ecology – A review of the Remane diagram with a suggested revised model for estuaries, Estuar. Coast. Shelf Sci., 97, 78–90, https://doi.org/10.1016/j.ecss.2011.11.026, 2012.

Wukovits, J., Oberrauch, M., Enge, A. J., and Heinz, P.: The distinct roles of two intertidal foraminiferal species in phytodetrital carbon and nitrogen fluxes - results from laboratory feeding experiments, Biogeosciences, 15, 6185–6185, 2018.

Supplementary material

Annex 1: Environmental parameters: Tidal (tidal coefficient at the sampling dates), Rainfall (monthly rainfall (mm)), Discharge (monthly average Loire river discharge (m^3 s^{-1})), temperature (monthly air temperature (T°C)).

Months	Tidal	Rainfall	Discharge	Temperature
0116		135	934	8
0216		100	1880	8
0316	78	80	1440	8
0416	50	30	1310	10
0516	106	57	893	15
0616	103	47	1970	17
0716	96	4	444	19
0816	78	7	227	20
0916	111	28	206	18
1016	114	32	212	12
1116	105	82	457	10
1216	106	13	531	8
0117	90	28	409	4
0217	99	74	783	8
0317	97	62	1160	11
0417	76	10	529	11
0517	60	48	457	16
0617	102	29	257	19
0717	77	20	178	20
0817		18	143	19
0917	93	51	177	15
1017	77	32	165	15
1117		51	191	9
1217		100	625	8
0118	77	86	2380	9
0218	89	47	2170	5
0318	98	74	1640	8
0418	96	47	1240	13
0518	101	36	713	15
0618	81	90	951	19
0718	87	21	302	21
0818	85	44	161	20
0918	87	6	161	17
1018	94	28	153	14
1118	85	51	297	9
1218	85	100	670	9

0119	108	29	478	6
0219		47	1030	9
0319	111	42	698	10
0419	97	38	379	12
0519	88	50	373	13
0619	82	50	264	17
0719	78	30	121	21
0819		30	106	19
0919		70	113	17
1019	86	90	185	17

Annex 2: Environmental data for the stations A, B and C. Porosity, Salinity, Alkalinity (mmol kg^{-1}), NH_4^+ (µmol L^{-1}), DRP (µmol L^{-1}), NO_2^- (µmol L^{-1}) and D50 (µm).

Station A

Months	Porosity	Salinity	Alkalinity	NH_4^+	DRP	NO_2^-	D50
0316_A	0.88	28.84	4.83	21.45	14.17	0.33	
0416_A	0.84	30.87	4.97	6.08			
0516_A	0.84	31.32	6.06	5.73			
0616_A		32.41	6.23	5.04	44.74		
0716_A		33.14	8.22		13.08		
0816_A		35.32	4.89	55.64	6.22	0.25	
0916_A		36.00	6.97	32.08	5.21	0.03	
1016_A	0.87	37.13	4.92		4.12	0.06	
1116_A	0.88	36.76	4.40	57.02	3.43	0.02	
1216_A	0.91	35.13	4.55	2.08	0.00	0.06	
0117_A	0.89	35.52	3.85	0.00	1.72	0.00	
0217_A	0.86	33.18	3.81	33.01	1.62	0.11	
0317_A	0.85	32.06	6.28	10.98	5.34	0.89	24.61
0417_A	0.87	43.86	5.05	11.29	1.92	0.59	28.35
0517_A	0.94	35.13			20.72		23.18
0617_A	0.84	38.53		19.34	2.01	0.39	20.64
0717_A	0.85	34.79		13.10	20.55	1.22	26.75
0917_A							23.83
1017_A	0.86	38.10	5.43	150.98	0.92	1.92	23.66
0118_A	0.79	38.10	4.99	71.10	0.92	0.32	23.12
0218_A							26.14
0318_A							79.39
0418_A	0.83	37.41	5.01	12.19	1.53	0.42	32.05
0518_A							23.12
0618_A							26.14
0718_A		39.11	7.03	25.94	0.89	0.11	25.31

0818_A							27.06
0918_A							21.57
1018_A		37.26		13.38	0.68	0.45	24.61
1118_A							23.02
1218_A							26.32
0119_A	0.89	35.00	5.10	4.62	4.03	0.07	40.20
0319_A							22.59
0419_A	0.86	36.76		12.10	9.08	0.72	
0519_A							
0619_A							
0719_A	0.80	39.19	6.48	8.99	2.84	0.18	
1019_A	0.82	38.11	6.41	11.60	18.07	0.24	

Station B

Months	**Porosity**	**Salinity**	**Alkalinity**	**NH_4^+**	**DRP**	**NO_2^-**	**D50**
0316_B	0.87	28.63	4.66	13.25	9.55	0.60	
0416_B	0.86	30.06	5.05	0.88			
0516_B	0.90	32.30	5.98	6.34			
0616_B		33.40	6.06	13.96	51.75		
0716_B		33.31	6.23		20.36		
0816_B					3.48		
0916_B		35.69	5.23	181.05	3.48	0.62	
1016_B	0.83	34.49	4.39		3.42	0.91	
1116_B	0.83	36.26	4.60	55.16	3.43	0.38	
1216_B	0.88	34.85	4.30	3.21	0.00	0.91	
0117_B	0.84	35.28	3.34	0.00	4.03	0.64	
0217_B	0.93	36.13	3.37	32.32	2.56	0.07	
0317_B	0.83	31.70	5.51	33.78	3.19	0.47	25.78
0417_B	0.84	40.85	5.43	8.78	1.98	0.33	29.48
0517_B	0.86	36.30			19.73		21.03
0617_B	0.82	37.25		12.26	3.20	0.22	22.96
0717_B	0.84	39.21		15.93	5.53	0.87	24.00
0917_B							25.02
1017_B	0.85	36.99	5.82	134.50	0.91	3.82	25.48
0118_B	0.82	36.99	4.82	49.02	0.91	0.20	24.56
0218_B							30.95
0318_B							34.59
0418_B	0.86	38.37	5.07	21.69	1.96	0.26	24.79
0518_B							23.50
0618_B							
0718_B		36.41	6.22	34.61	2.11	0.13	24.73
0818_B							27.32
0918_B							22.59

1018_B		37.28		12.42	1.31	1.14	24.90
1118_B							
1218_B							25.43
0119_B	0.91	36.03	4.63	13.13	4.57	0.14	26.94
0319_B							26.51
0419_B	0.91	40.82		19.91	10.06	0.16	
0519_B							
0619_B							
0719_B	0.82	38.84	6.77	7.51	2.94	0.00	
1019_B	0.86	36.54	6.08	15.01	7.46	0.00	

Station C

Months	**Porosity**	**Salinity**	**Alkalinity**	**NH_4^+**	**DRP**	**NO_2^-**	**D50**
0316_C	0.50			4.89	8.62		
0416_C	0.84		4.34	36.64		0.36	
0516_C	0.90	34.02	6.38	7.77			
0616_C		33.77	6.94	1.87	32.65		
0716_C		32.20	6.80		27.48		
0816_C					21.59		
0916_C		35.69	5.78	32.04	21.59	0.72	
1016_C	0.87	36.88	5.73	4.75	2.31	0.12	
1116_C	0.87	36.72	4.39	48.75	2.25	0.11	
1216_C	0.90	35.73	4.90	1.87	0.00	0.12	
0117_C	0.91	36.86	4.02	0.00	0.00	0.18	
0217_C	0.93	33.06	4.49	29.94	6.05	0.08	
0317_C	0.86	31.86	5.58	4.26	1.57	0.33	20.36
0417_C	0.86	43.66	5.64	10.31	1.72	0.60	29.21
0517_C	0.86	36.50			3.06		
0617_C	0.81	38.60		19.34	5.02	1.75	21.98
0717_C	0.85	41.58		23.35	4.73	0.52	21.42
0917_C							
1017_C	0.85	37.63	5.52	156.09	0.00	1.87	
0118_C	0.78	37.63	5.45	56.82	0.00	0.32	26.88
0218_C							28.88
0318_C							
0418_C	0.87	38.63	5.63	8.75	0.90	0.41	24.16
0518_C							22.91
0618_C							
0718_C		37.86	5.92	40.60	3.01	0.09	31.53
0818_C							
0918_C							
1018_C		37.11		14.95	0.14	0.35	
1118_C							24.96

1218_C							23.28
0119_C	0.84	36.23	5.45	6.83	4.95	1.24	24.96
0319_C							24.61
0419_C	0.76	37.41		35.18	9.59	2.05	
0519_C							
0619_C							
0719_C	0.81	32.51	6.54	9.38	3.25	0.00	
1019_C	0.83	37.64	7.00	13.23	7.13	0.06	

Annex 3: Spatiotemporal plot for each physicochemical parameter: Salinity. Porosity. D50 (µm). OPD (mm) and DOU (mmol m^{-2} d^{-1}). Alkalinity (mmol kg^{-1}). NO_2^- (µmol L^{-1}). NH_4^+ (µmol L^{-1}). and DRP (µmol L^{-1}).

Salinity

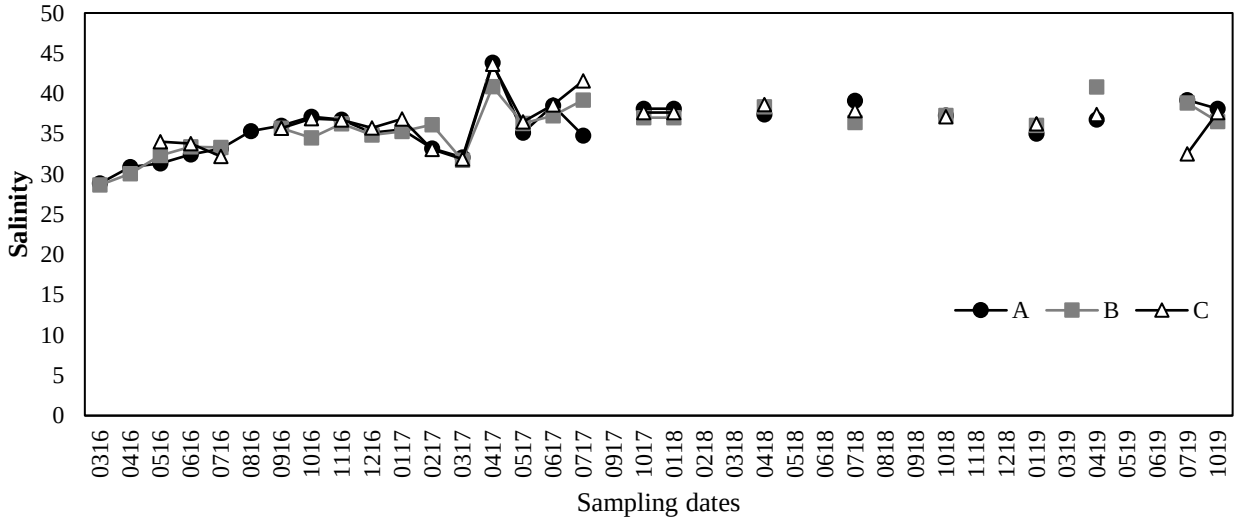

Porosity

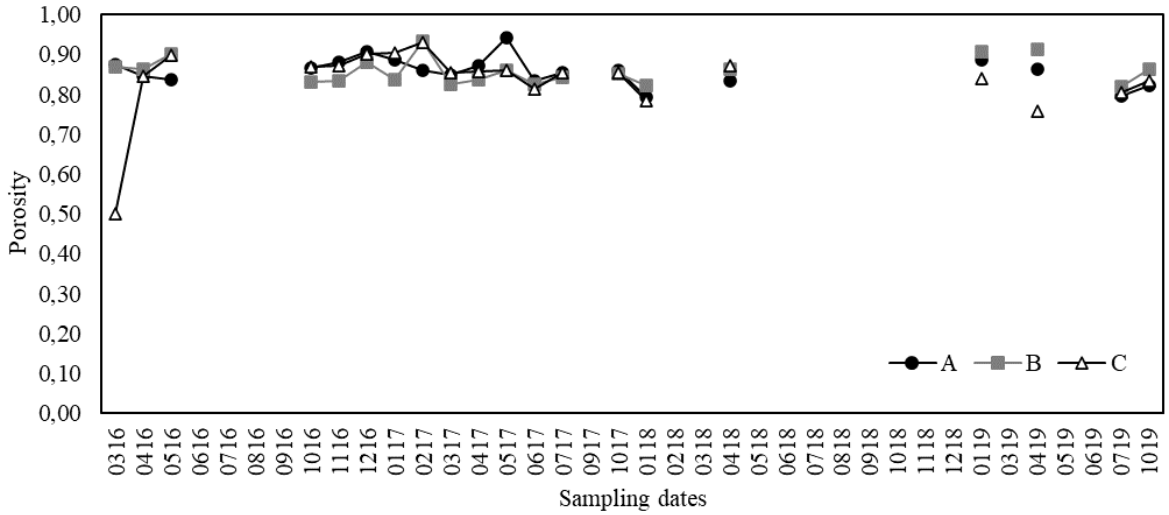

D50 (µm)

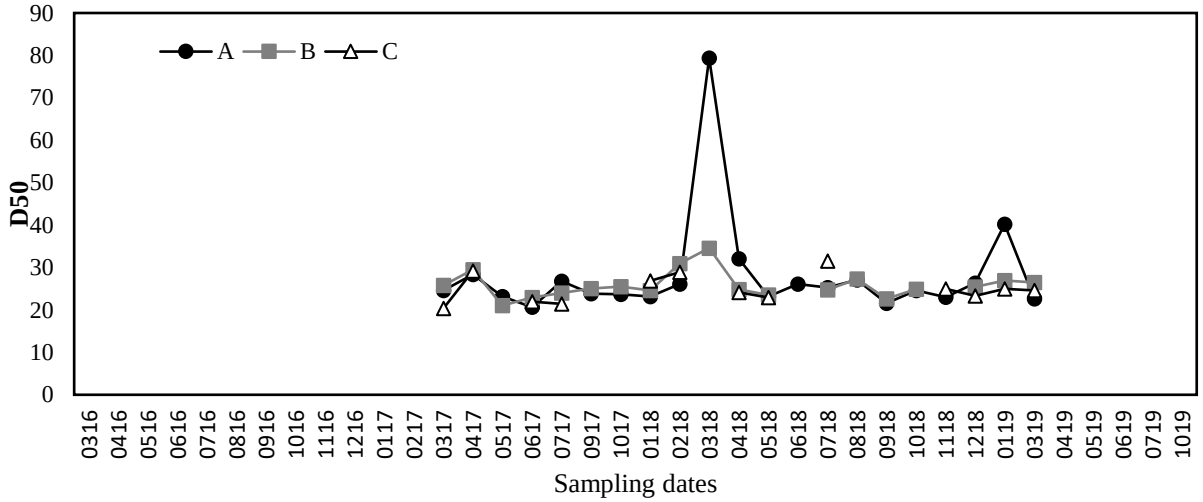

OPD (mm) and DOU (mmol m^{-2} d^{-1})

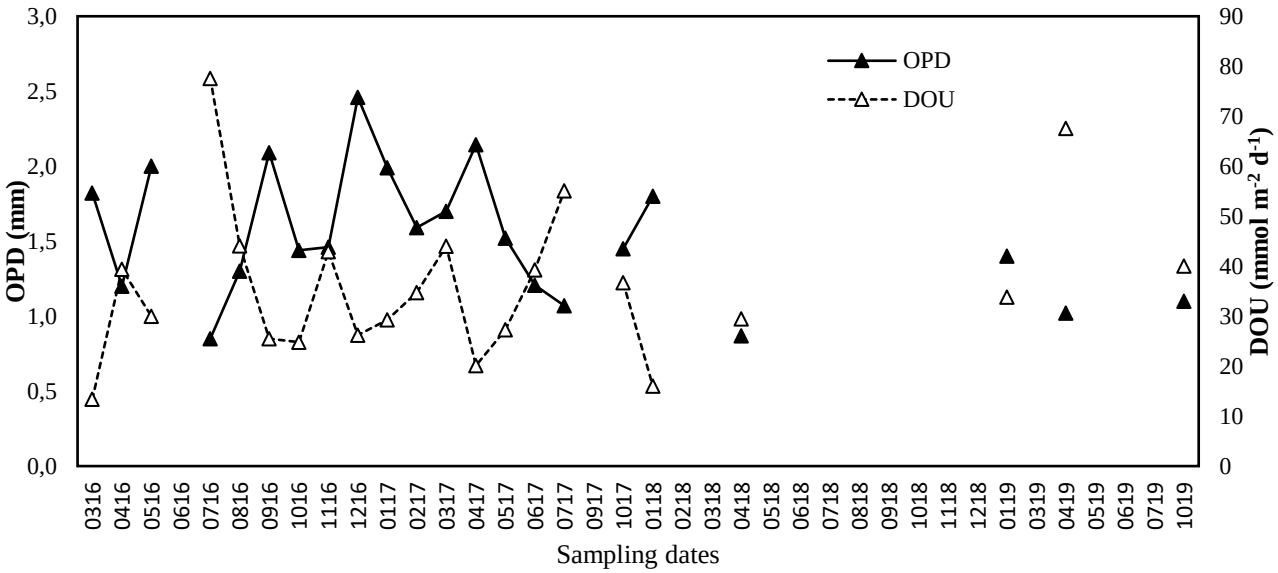

Alkalinity (mmol kg^{-1})

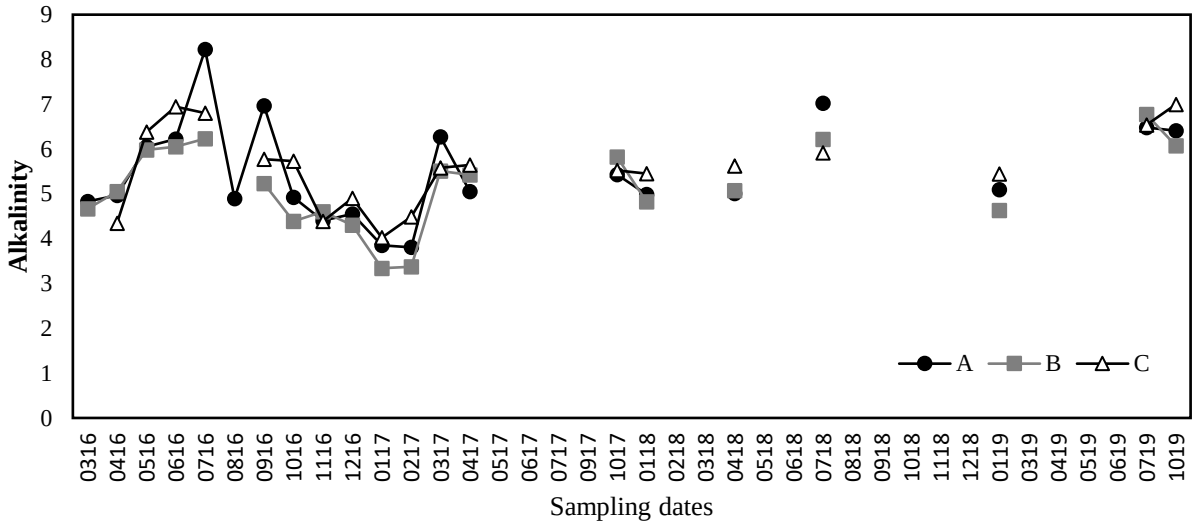

NO_2^- (µmol L^{-1})

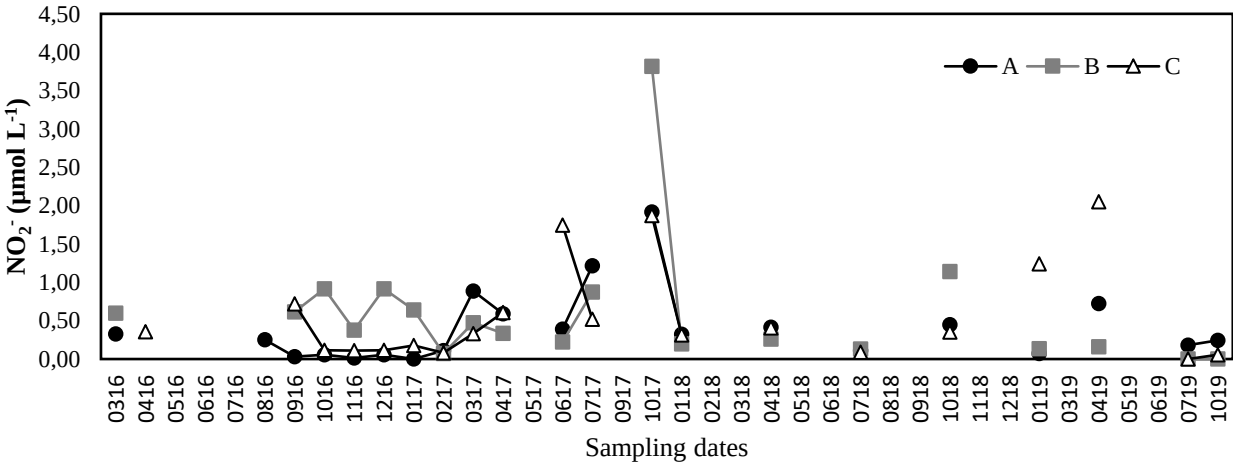

NH_4^+ (µmol L^{-1})

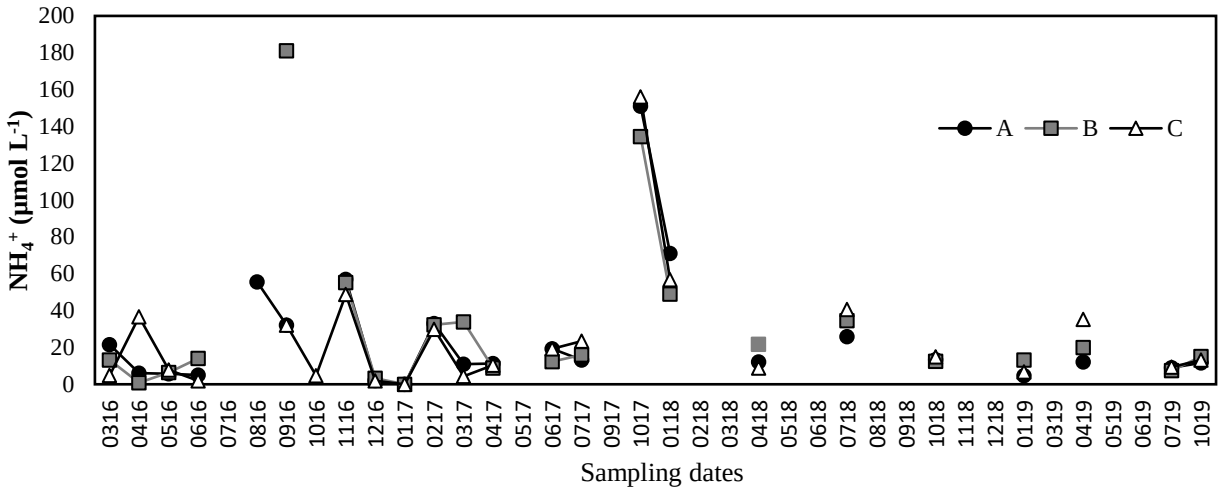

DRP (µmol L^{-1})

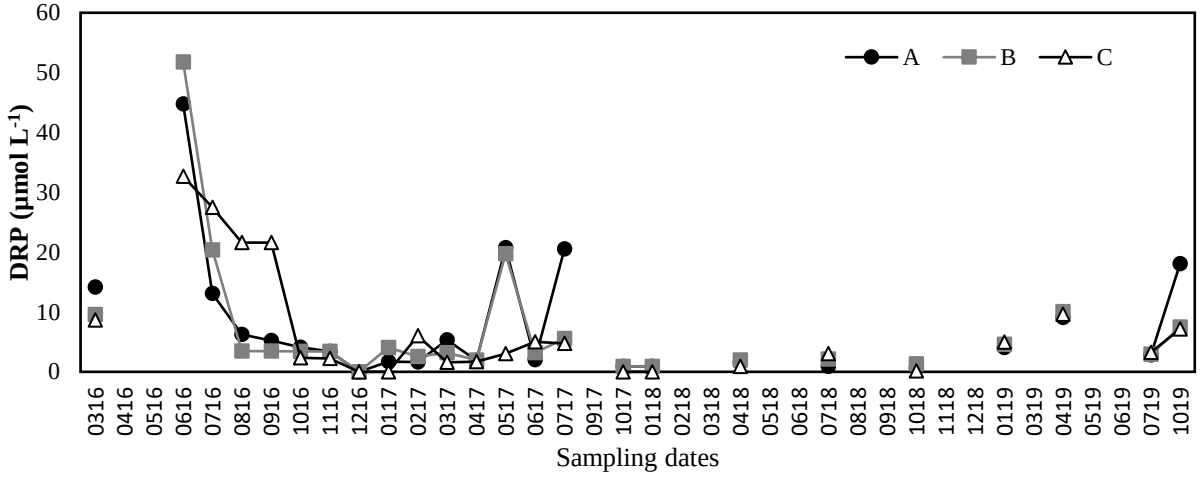

Annex 4: Spatiotemporal variations of the NDVI values at the 3 sampling stations A (black line. black circles). B (grey line. grey diamonds) and C (dotted line. black squares). The two large grey squares indicate the separation between the years.

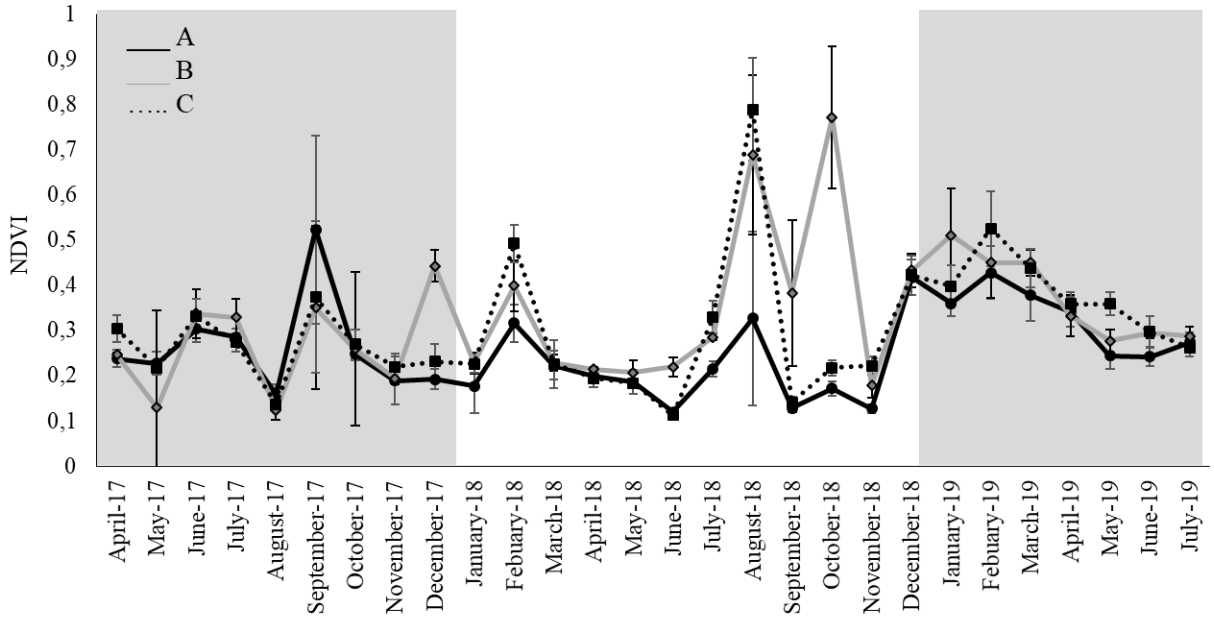

Annex 5: The 29 diatom dominant species (> 5 % of the assemblage) identified at the station B of "La Coupelasse" site. The shape of each diatom species is indicated.

Occurrences > 5 %	Shapes	0317	0417	0517	0617	0717	0817	0917	1017
Navicula meulemansii	prism on elliptic base	11	3	11	9	13	17	45	0
Gyrosigma limosum	prism on parallelogram base	1	3	26	3	15	1	2	3
Pleurosigma formosum	prism on parallelogram base	54	36	0	2	0	0	2	1
Pleurosigma angulatum	prism on parallelogram base	12	3	1	1	0	8	3	3
Plagiogrammopsis vanheurckii	prism on elliptic prism	1	2	2	3	5	5	4	5
Navicula spartinetensis	prism on elliptic prism	1	4	0	4	6	2	1	0
Gyrosigma wansbeckii	prism on parallelogram base	1	3	7	4	1	6	2	0
Navicula abscondita	prism on elliptic base	0	2	40	4	1	0	1	0
Thalassiosira sp.	cylinder	1	4	1	1	3	9	9	22
Chaetoceros sp.	prism on elliptic base	0	15	1	0	0	0	0	0
Staurophora salina	prism on elliptic base	0	0	0	40	1	1	0	0
Psammodictyion sp.	prism on elliptic base	1	1	2	1	3	3	2	10
Pleurosigma formosum	prism on parallelogram base	0	0	0	4	1	15	1	0
Nitzschia cf *aequorea*	prism on parallelogram base	5	6	0	0	1	2	1	10
Melosira sp.	cylinder	0	2	1	0	1	0	0	2
Plagiotropis seriata	prism on elliptic base	0	0	0	3	0	0	2	0
Gyrosigma fasciola	prism on parallelogram base	0	1	0	0	0	0	0	1
Nitzschia cf *distans*	prism on parallelogram base	0	2	0	3	0	0	5	1
Nitschia maxima	prism on parallelogram base	0	0	1	0	0	1	0	0
Entomoneis paludosa	prism on elliptic base	0	0	2	0	19	1	0	0
Cymatosira belgica	prism on parallelogram base	2	1	1	1	0	1	2	8
Planothidium septentrionalis	prism on elliptic base	0	0	0	0	0	0	0	6
Podosira stelligera	cylinder + 2 half spheres	0	1	0	2	0	1	2	2
Navicula cf *flagellifera*	prism on elliptic base	0	0	0	2	0	5	1	0
Cylindrotheca sp.	prolate spheroid + 2 cylinders	0	0	0	1	3	0	2	0
Eutonogramma dubium	half heliptic prism	0	1	0	1	2	0	1	0
Plagiotropis vanheurckii	prism on elliptic base	5	3	0	0	0	1	0	0
Halamphora sp.	cymbelloid	0	1	0	6	1	0	0	0
Skeletonema sp.	cylinder + 2 half spheres	0	0	0	0	0	0	0	0
others < 5 %		5	9	6	6	18	23	14	27
total %		100	100	100	100	100	100	100	100

Occurrences > 5 %	Shapes	0118	0218	0318	0418	0518	0618	0718	0818	0918	1018	1118	1218
Navicula meulemansii	prism on elliptic base	18	28	41	33	9	13	0	2	0	4	4	2
Gyrosigma limosum	prism on parallelogram base	6	48	22	7	7	6	7	0	1	1	0	3
Pleurosigma formosum	prism on parallelogram base	1	0	0	0	0	5	1	0	0	0	26	24
Pleurosigma angulatum	prism on parallelogram base	13	1	0	2	1	2	1	0	18	41	0	15
Plagiogrammopsis vanheurckii	prism on elliptic prism	2	0	1	1	7	6	19	24	28	9	13	2
Navicula spartinetensis	prism on elliptic prism	2	2	6	3	16	6	4	0	2	8	1	7
Gyrosigma wansbeckii	prism on parallelogram base	1	2	11	4	7	11	4	0	0	1	0	4
Navicula abscondita	prism on elliptic base	1	1	7	4	7	2	9	0	1	5	2	2
Thalassiosira sp.	cylinder	3	1	5	0	8	4	5	10	10	5	1	1
Chaetoceros sp.	prism on elliptic base	0	0	1	20	19	10	1	1	2	0	3	1
Staurophora salina	prism on elliptic base	0	0	1	0	1	1	10	0	2	1	0	0
Psammodictyion sp.	prism on elliptic base	1	1	2	1	2	4	0	6	3	1	2	2
Pleurosigma formosum	prism on parallelogram base	1	0	0	0	0	1	1	0	0	4	7	2
Nitzschia cf *aequorea*	prism on parallelogram base	13	0	0	0	0	1	4	0	0	1	1	0
Melosira sp.	cylinder	0	0	0	19	1	7	0	0	0	0	1	0
Plagiotropis seriata	prism on elliptic base	0	0	0	0	0	1	7	11	2	1	1	0
Gyrosigma fasciola	prism on parallelogram base	0	0	0	0	0	0	0	0	0	2	2	11
Nitzschia cf *distans*	prism on parallelogram base	3	1	0	1	0	0	2	0	0	1	1	1
Nitschia maxima	prism on parallelogram base	2	0	0	0	0	1	1	0	0	0	5	4
Entomoneis paludosa	prism on elliptic base	0	0	0	0	0	0	0	1	1	0	0	0
Cymatosira belgica	prism on parallelogram base	1	0	1	1	0	1	2	3	1	0	0	1
Planothidium septentrionalis	prism on elliptic base	15	1	0	0	0	0	0	2	0	0	0	0
Podosira stelligera	cylinder + 2 half spheres	1	0	0	0	1	1	3	3	2	0	6	0
Navicula cf *flagellifera*	prism on elliptic base	0	1	0	0	0	0	0	8	3	1	3	3
Cylindrotheca sp.	prolate spheroid + 2 cylinders	0	11	0	0	0	0	0	0	0	1	0	0
Eutonogramma dubium	half heliptic prism	0	0	1	0	0	0	6	5	5	0	4	0
Plagiotropis vanheurckii	prism on elliptic base	1	0	0	0	0	2	1	0	0	1	0	0
Halamphora sp.	cymbelloid	0	0	0	0	0	1	1	0	0	0	0	2
Skeletonema sp.	cylinder + 2 half spheres	0	0	0	0	0	6	0	0	0	0	2	0
others < 5 %		15	4	2	5	12	12	12	25	21	15	16	16
total %		100	100	100	100	100	100	100	100	100	100	100	100

Occurrences > 5 %	Shapes	0119	0219	0319	0419	0519	0619	0719
Navicula meulemansii	prism on elliptic base	12	9	6	19	9	0	8
Gyrosigma limosum	prism on parallelogram base	9	2	2	7	6	5	10
Pleurosigma formosum	prism on parallelogram base	6	55	59	30	4	2	1
Pleurosigma angulatum	prism on parallelogram base	12	7	7	3	2	1	0
Plagiogrammopsis vanheurckii	prism on elliptic prism	0	1	0	2	5	13	4
Navicula spartinetensis	prism on elliptic prism	9	9	6	8	4	5	6
Gyrosigma wansbeckii	prism on parallelogram base	17	2	3	2	7	4	1
Navicula abscondita	prism on elliptic base	7	0	0	2	2	7	1
Thalassiosira sp.	cylinder	1	1	1	1	4	5	4
Chaetoceros sp.	prism on elliptic base	0	0	0	0	9	1	1
Staurophora salina	prism on elliptic base	1	0	0	1	1	9	2
Psammodictyion sp.	prism on elliptic base	1	1	0	3	3	1	3
Pleurosigma formosum	prism on parallelogram base	0	1	3	0	1	1	2
Nitzschia cf *aequorea*	prism on parallelogram base	0	0	0	3	1	3	2
Melosira sp.	cylinder	0	0	0	2	7	0	1
Plagiotropis seriata	prism on elliptic base	1	1	1	0	1	7	1
Gyrosigma fasciola	prism on parallelogram base	7	5	5	0	0	1	0
Nitzschia cf *distans*	prism on parallelogram base	1	1	3	2	1	2	0
Nitschia maxima	prism on parallelogram base	10	1	0	0	0	1	1
Entomoneis paludosa	prism on elliptic base	0	0	0	0	1	1	15
Cymatosira belgica	prism on parallelogram base	0	1	1	2	1	2	1
Planothidium septentrionalis	prism on elliptic base	0	0	0	0	0	1	1
Podosira stelligera	cylinder + 2 half spheres	0	0	1	0	1	3	1
Navicula cf *flagellifera*	prism on elliptic base	0	0	0	3	0	0	1
Cylindrotheca sp.	prolate spheroid + 2 cylinders	0	0	0	0	0	0	3
Eutonogramma dubium	half heliptic prism	0	0	0	2	1	5	3
Plagiotropis vanheurckii	prism on elliptic base	0	0	0	0	3	2	0
Halamphora sp.	cymbelloid	0	0	0	1	1	1	1
Skeletonema sp.	cylinder + 2 half spheres	0	0	0	0	5	1	0
others < 5 %		6	6	3	8	19	18	25
total %		100	100	100	100	100	100	100

Annex 6: Dominant foraminifera species densities (ind. 50 cm^{-3} > 150 µm) from March 2016 to October 2019 sampled at "La Coulepesse" (France). AT (Ammonia sp. T6). HG (Haynesina germanica). EO (Elphidium oceanense). ES (Elphidium selseyense).

Months	AT	HG	EO	ES	total
0316_A	1081	711	35	0	1826
0416_A	684	451	22	1	1159
0516_A	841	105	7	222	1175
0616_A	155	63	10	24	252
0716_A	113	22	9	102	246
0816_A	237	214	67	103	620
0916_A	136	28	34	34	232
1016_A	579	115	145	6	844
1116_A	402	160	94	10	666
1216_A	524	383	77	29	1013
0117_A	103	83	24	8	218
0217_A	53	54	0	0	108
0317_A	117	78	8	14	217
0417_A	111	31	9	20	171
0517_A	117	28	9	88	242
0617_A	366	323	50	54	794
0717_A	137	224	51	42	454
0917_A	261	136	165	4	566
1017_A	489	202	151	0	843
0118_A	241	355	31	0	627
0218_A	649	823	23	0	1495
0318_A	44	10	0	3	56
0418_A	111	120	12	6	249
0518_A	303	109	101	39	551
0618_A	109	51	2	137	299
0718_A	124	198	23	80	425
0818_A	784	668	1087	54	2594
0918_A	361	208	377	6	951
1018_A	202	167	178	19	566
1118_A	348	573	134	17	1072
1218_A	178	256	42	2	478
0119_A	42	161	10	11	223
0319_A	202	372	55	9	638
0419_A	55	57	7	5	124
0519_A	112	48	7	15	181
0619_A	79	84	17	0	181
0719_A	241	649	361	0	1250
1019_A	241	408	660	0	1309

0316_B	1167	753	21	0	1942
0416_B	159	43	4	0	206
0516_B	860	353	6	293	1513
0616_B	158	39	3	23	223
0716_B	185	91	3	94	374
0816_B	82	307	47	70	505
0916_B	396	367	188	0	951
1016_B	377	555	78	50	1060
1116_B	579	730	101	23	1433
1216_B	43	65	18	11	137
0117_B	415	565	27	6	1013
0217_B	25	53	1	6	85
0317_B	185	117	39	22	363
0417_B	122	46	12	11	190
0517_B	352	82	26	163	623
0617_B	331	285	88	74	779
0717_B	204	313	100	110	726
0917_B	1142	847	621	0	2610
1017_B	713	241	159	0	1113
0118_B	101	160	4	10	275
0218_B	163	134	37	19	353
0318_B	128	114	8	4	253
0418_B	167	105	23	8	303
0518_B	155	66	19	74	315
0618_B	100	45	1	96	242
0718_B	186	134	95	29	445
0818_B	590	1099	559	78	2326
0918_B	135	163	136	14	448
1018_B	10	48	10	8	75
1118_B	19	100	93	10	222
1218_B	59	135	46	56	296
0119_B	37	152	7	13	209
0319_B	10	14	5	0	28
0419_B	22	27	1	24	75
0519_B	63	28	3	20	115
0619_B	66	103	35	8	212
0719_B	161	390	285	0	837
1019_B	63	186	93	0	343
0316_C	467	423	13	2	905
0416_C	153	91	6	3	253
0516_C	1231	502	15	463	2211
0616_C	108	25	3	11	147
0716_C	73	41	4	83	200

0816_C	50	88	0	90	228
0916_C	165	125	127	17	435
1016_C	266	60	137	4	467
1116_C	313	162	74	0	549
1216_C	120	153	44	2	319
0117_C	104	54	12	0	170
0217_C	105	249	3	6	362
0317_C	135	113	16	2	265
0417_C	154	41	2	26	223
0517_C	78	20	5	44	147
0617_C	418	317	75	67	877
0717_C	125	227	57	66	476
0917_C	1507	652	893	78	3130
1017_C	1410	501	210	0	2120
0118_C	183	176	38	0	396
0218_C	210	497	39	0	746
0318_C	200	150	9	0	358
0418_C	334	43	0	19	396
0518_C	NA	NA	NA	NA	NA
0618_C	22	9	0	13	44
0718_C	99	124	58	0	282
0818_C	1033	1045	1367	97	3542
0918_C	283	142	274	2	701
1018_C	183	95	116	13	406
1118_C	241	379	120	33	773
1218_C	132	287	148	37	604
0119_C	53	234	5	17	309
0319_C	155	279	43	15	491
0419_C	142	188	21	13	364
0519_C	20	13	2	6	41
0619_C	41	51	14	2	108
0719_C	42	165	83	1	290
1019_C	107	87	433	0	627

Annex 7: Inputs data for the CCA analysis. Environmental parameters are centred and standardized per station: (x - mean x)/ sd. in which x is the value of the variable in one station. mean x is the mean of the same variable among a station and sd is the corresponding standard deviation. The foraminifera species densities (> 150 µm. 50 cm^{-3}) are square-root transformed.

Months	Discharge	Temperature	Tidal	Rainfall	Porosity	D50	Salinity
0316_A	1.30	-1.07	-0.89	1.39	0.47		-2.16
0416_A	1.08	-0.70	-2.90	-0.56	-0.39		-1.53
0516_A	0.39	0.21	1.12	0.50	-0.58		-1.38
0616_A	2.19	0.75	0.91	0.08			-1.04
0716_A	-0.36	1.16	0.41	-1.61			-0.81
0816_A	-0.73	1.36	-0.89	-1.47			-0.13
0916_A	-0.76	1.01	1.48	-0.66			0.08
1016_A	-0.75	-0.22	1.70	-0.51	0.18		0.44
1116_A	-0.34	-0.80	1.05	1.47	0.66		0.32
1216_A	-0.22	-1.21	1.12	-1.22	1.41		-0.19
0117_A	-0.42	-1.87	-0.02	-0.63	0.82		-0.07
0217_A	0.20	-1.09	0.62	1.17	0.07		-0.80
0317_A	0.83	-0.53	0.48	0.70	-0.27	-0.29	-1.15
0417_A	-0.22	-0.51	-1.03	-1.35	0.41	0.01	2.55
0517_A	-0.34	0.56	-2.18	0.12	2.39	-0.40	-0.19
0617_A	-0.68	1.08	0.84	-0.63	-0.66	-0.60	0.88
0717_A	-0.81	1.32	-0.96	-0.96	-0.15	-0.11	-0.29
0917_A	-0.81	0.40	0.19	0.24		-0.35	
1017_A	-0.83	0.33	-0.96	-0.49	0.07	-0.36	0.74
0118_A	2.87	-0.92	-0.96	1.64	-1.84	-0.41	0.74
0218_A	2.52	-1.85	-0.10	0.09		-0.16	
0318_A	1.63	-1.09	0.55	1.17		4.11	
0418_A	0.97	-0.12	0.41	0.10	-0.70	0.31	0.53
0518_A	0.09	0.40	0.76	-0.32		-0.41	
0618_A	0.48	1.22	-0.67	1.77			
0718_A	-0.60	1.51	-0.24	-0.92		-0.23	1.06
0818_A	-0.84	1.26	-0.38	-0.04		-0.09	
0918_A	-0.84	0.81	-0.24	-1.51		-0.53	
1018_A	-0.85	0.11	0.26	-0.63		-0.29	0.48
1118_A	-0.61	-0.94	-0.38	0.24			
1218_A	0.01	-0.94	-0.38	2.18		-0.15	
0119_A	-0.31	-1.48	1.27	-0.60	0.77	0.97	-0.23
0319_A	0.06	-0.68	1.48	-0.12		-0.45	
0419_A	-0.47	-0.35	0.48	-0.25	0.12		0.32
0519_A	-0.48	-0.10	-0.17	0.21			
0619_A	-0.66	0.73	-0.60	0.21			
0719_A	-0.90	1.55	-0.89	-0.57	-1.80		1.08
1019_A	-0.80	0.73	-0.31	1.78	-1.01		0.75
0316_B	1.30	-1.07	-0.89	1.39	0.34		-2.38

0416_B	1.08	-0.70	-2.90	-0.56	0.10		-1.90
0516_B	0.39	0.21	1.12	0.50	1.31		-1.16
0616_B	2.19	0.75	0.91	0.08			-0.79
0716_B	-0.36	1.16	0.41	-1.61			-0.82
0816_B	-0.73	1.36	-0.89	-1.47			
0916_B	-0.76	1.01	1.48	-0.66			-0.02
1016_B	-0.75	-0.22	1.70	-0.51	-0.83		-0.43
1116_B	-0.34	-0.80	1.05	1.47	-0.78		0.17
1216_B	-0.22	-1.21	1.12	-1.22	0.65		-0.31
0117_B	-0.42	-1.87	-0.02	-0.63	-0.69		-0.16
0217_B	0.20	-1.09	0.62	1.17	2.21		0.12
0317_B	0.83	-0.53	0.48	0.70	-0.97	-0.01	-1.35
0417_B	-0.22	-0.51	-1.03	-1.35	-0.68	1.17	1.70
0517_B	-0.34	0.56	-2.18	0.12	0.08	-1.53	0.18
0617_B	-0.68	1.08	0.84	-0.63	-1.03	-0.91	0.50
0717_B	-0.81	1.32	-0.96	-0.96	-0.47	-0.58	1.15
0917_B	-0.81	0.40	0.19	0.24		-0.26	
1017_B	-0.83	0.33	-0.96	-0.49	-0.22	-0.11	0.41
0118_B	2.87	-0.92	-0.96	1.64	-1.14	-0.40	0.41
0218_B	2.52	-1.85	-0.10	0.09		1.64	
0318_B	1.63	-1.09	0.55	1.17		2.80	
0418_B	0.97	-0.12	0.41	0.10	0.16	-0.33	0.87
0518_B	0.09	0.40	0.76	-0.32		-0.74	
0618_B	0.48	1.22	-0.67	1.77			
0718_B	-0.60	1.51	-0.24	-0.92		-0.35	0.22
0818_B	-0.84	1.26	-0.38	-0.04		0.48	
0918_B	-0.84	0.81	-0.24	-1.51		-1.03	
1018_B	-0.85	0.11	0.26	-0.63		-0.29	0.51
1118_B	-0.61	-0.94	-0.38	0.24			
1218_B	0.01	-0.94	-0.38	2.18		-0.13	
0119_B	-0.31	-1.48	1.27	-0.60	1.42	0.36	0.09
0319_B	0.06	-0.68	1.48	-0.12		0.22	
0419_B	-0.47	-0.35	0.48	-0.25	1.61		1.69
0519_B	-0.48	-0.10	-0.17	0.21			
0619_B	-0.66	0.73	-0.60	0.21			
0719_B	-0.90	1.55	-0.89	-0.57	-1.19		1.03
1019_B	-0.80	0.73	-0.31	1.78	0.11		0.26
0316_C	1.30	-1.07	-0.89	1.39	-3.77		
0416_C	1.08	-0.70	-2.90	-0.56	0.10		
0516_C	0.39	0.21	1.12	0.50	0.71		-0.88
0616_C	2.19	0.75	0.91	0.08			-0.97
0716_C	-0.36	1.16	0.41	-1.61			-1.52
0816_C	-0.73	1.36	-0.89	-1.47			
0916_C	-0.76	1.01	1.48	-0.66			-0.29
1016_C	-0.75	-0.22	1.70	-0.51	0.39		0.13

1116_C	-0.34	-0.80	1.05	1.47	0.42		0.07
1216_C	-0.22	-1.21	1.12	-1.22	0.73		-0.28
0117_C	-0.42	-1.87	-0.02	-0.63	0.78		0.12
0217_C	0.20	-1.09	0.62	1.17	1.05		-1.22
0317_C	0.83	-0.53	0.48	0.70	0.22	-1.41	-1.65
0417_C	-0.22	-0.51	-1.03	-1.35	0.26	1.27	2.53
0517_C	-0.34	0.56	-2.18	0.12	0.28		0.00
0617_C	-0.68	1.08	0.84	-0.63	-0.25	-0.92	0.74
0717_C	-0.81	1.32	-0.96	-0.96	0.21	-1.09	1.79
0917_C	-0.81	0.40	0.19	0.24			
1017_C	-0.83	0.33	-0.96	-0.49	0.20		0.39
0118_C	2.87	-0.92	-0.96	1.64	-0.59	0.57	0.39
0218_C	2.52	-1.85	-0.10	0.09		1.17	
0318_C	1.63	-1.09	0.55	1.17			
0418_C	0.97	-0.12	0.41	0.10	0.42	-0.26	0.75
0518_C	0.09	0.40	0.76	-0.32		-0.64	
0618_C	0.48	1.22	-0.67	1.77			
0718_C	-0.60	1.51	-0.24	-0.92		1.98	0.48
0818_C	-0.84	1.26	-0.38	-0.04			
0918_C	-0.84	0.81	-0.24	-1.51			
1018_C	-0.85	0.11	0.26	-0.63			0.21
1118_C	-0.61	-0.94	-0.38	0.24		-0.02	
1218_C	0.01	-0.94	-0.38	2.18		-0.52	
0119_C	-0.31	-1.48	1.27	-0.60	0.06	-0.02	
0319_C	0.06	-0.68	1.48	-0.12		-0.12	
0419_C	-0.47	-0.35	0.48	-0.25	-0.87	-7.58	0.32
0519_C	-0.48	-0.10	-0.17	0.21			
0619_C	-0.66	0.73	-0.60	0.21			
0719_C	-0.90	1.55	-0.89	-0.57	-0.33		-1.42
1019_C	-0.80	0.73	-0.31	1.78	-0.03		0.40

Months	**NO_2^-**	**NH_4^+**	**DRP**	**NDVI**	**Alkalinity**	**OPD_C**	**DOU_C**
0316_A	-0.15	-0.12	0.64		-0.60	0.68	-1.48
0416_A		-0.58			-0.47	-0.73	0.20
0516_A		-0.59			0.50	1.09	-0.40
0616_A		-0.61	3.64		0.65		
0716_A			0.53		2.43	-1.53	2.68
0816_A	-0.31	0.91	-0.14		-0.54	-0.51	0.51
0916_A	-0.78	0.20	-0.24		1.31	1.30	-0.70
1016_A	-0.73		-0.35		-0.52	-0.19	-0.74
1116_A	-0.81	0.95	-0.41		-0.98	-0.14	0.43
1216_A	-0.73	-0.70	-0.75		-0.85	2.14	-0.65
0117_A	-0.85	-0.76	-0.58		-1.47	1.07	-0.45
0217_A	-0.61	0.23	-0.59		-1.51	0.16	-0.10
0317_A	1.04	-0.43	-0.23		0.69	0.41	0.50

0417_A	0.41	-0.42	-0.56	-0.24	-0.40	1.42	-1.04
0517_A			1.28	-0.35		0.00	-0.58
0617_A	-0.02	-0.18	-0.55	0.43		-0.72	0.20
0717_A	1.74	-0.37	1.26	0.25		-1.03	1.22
0917_A				2.68			
1017_A	3.23	3.78	-0.66	-0.13	-0.06	-0.16	0.03
0118_A	-0.16	1.38	-0.66	-0.86	-0.45	0.63	-1.31
0218_A				0.56			
0318_A				-0.39			
0418_A	0.04	-0.40	-0.60	-0.63	-0.43	-1.49	-0.44
0518_A				-0.77			
0618_A				-1.45			
0718_A	-0.62	0.02	-0.66	-0.47	1.36		
0818_A				0.67			
0918_A				-1.37			
1018_A	0.10	-0.36	-0.68	-0.92			
1118_A				-1.37			
1218_A				1.60			
0119_A	-0.69	-0.63	-0.36	1.01	-0.36	-0.28	-0.16
0319_A				1.20			
0419_A	0.69	-0.40	0.14	0.82		-1.15	2.03
0519_A				-0.18			
0619_A				-0.20			
0719_A	-0.46	-0.49	-0.47	0.13	0.88		
1019_A	-0.33	-0.42	1.02	-2.68	0.82	-0.96	0.24
0316_B	0.01	-0.41	0.23		-0.55	0.68	-1.48
0416_B		-0.69			-0.14	-0.73	0.20
0516_B		-0.56			0.86	1.09	-0.40
0616_B		-0.39	4.11		0.94		
0716_B			1.23		1.13	-1.53	2.68
0816_B			-0.32			-0.51	0.51
0916_B	0.03	3.40	-0.32		0.06	1.30	-0.70
1016_B	0.39		-0.33		-0.85	-0.19	-0.74
1116_B	-0.26	0.55	-0.33		-0.62	-0.14	0.43
1216_B	0.39	-0.63	-0.64		-0.94	2.14	-0.65
0117_B	0.06	-0.71	-0.27		-1.97	1.07	-0.45
0217_B	-0.63	0.03	-0.41		-1.93	0.16	-0.10
0317_B	-0.14	0.06	-0.35		0.36	0.41	0.50
0417_B	-0.31	-0.51	-0.46	-0.58	0.26	1.42	-1.04
0517_B			1.17	-1.35		0.00	-0.58
0617_B	-0.45	-0.43	-0.35	0.01		-0.72	0.20
0717_B	0.34	-0.34	-0.14	-0.04		-1.03	1.22
0917_B				0.10			
1017_B	3.88	2.35	-0.56	-0.50	0.69	-0.16	0.03
0118_B	-0.48	0.41	-0.56	-0.70	-0.38	0.63	-1.31

0218_B				0.42			
0318_B				-0.70			
0418_B	-0.40	-0.21	-0.46	-0.79	-0.11	-1.49	-0.44
0518_B				-0.84			
0618_B				-0.76			
0718_B	-0.56	0.08	-0.45	-0.32	1.11		
0818_B				2.32			
0918_B				0.31			
1018_B	0.66	-0.42	-0.52	2.87			
1118_B				-1.03			
1218_B				0.65			
0119_B	-0.55	-0.41	-0.22	1.15	-0.59	-0.28	-0.16
0319_B				0.75			
0419_B	-0.52	-0.25	0.28	-0.02		-1.15	2.03
0519_B				-0.38			
0619_B				-0.26			
0719_B	-0.72	-0.54	-0.37	-0.31	1.70		
1019_B	-0.72	-0.37	0.04		0.96	-0.96	0.24
0316_C		-0.60	0.18			0.68	-1.48
0416_C	-0.32	0.36			-1.42	-0.73	0.20
0516_C		-0.51			0.87	1.09	-0.40
0616_C		-0.69	2.78		1.51		
0716_C			2.22		1.35	-1.53	2.68
0816_C			1.58			-0.51	0.51
0916_C	0.24	0.22	1.58		0.19	1.30	-0.70
1016_C	-0.70	-0.61	-0.51		0.14	-0.19	-0.74
1116_C	-0.71	0.73	-0.51		-1.37	-0.14	0.43
1216_C	-0.70	-0.69	-0.76		-0.79	2.14	-0.65
0117_C	-0.60	-0.75	-0.76		-1.78	1.07	-0.45
0217_C	-0.75	0.16	-0.10		-1.26	0.16	-0.10
0317_C	-0.36	-0.62	-0.59		-0.02	0.41	0.50
0417_C	0.07	-0.44	-0.57	-0.05	0.04	1.42	-1.04
0517_C			-0.43	-0.66		0.00	-0.58
0617_C	1.84	-0.16	-0.21	0.16		-0.72	0.20
0717_C	-0.07	-0.04	-0.24	-0.26		-1.03	1.22
0917_C				0.46			
1017_C	2.04	3.99	-0.76	-0.29	-0.09	-0.16	0.03
0118_C	-0.39	0.98	-0.76	-0.60	-0.17	0.63	-1.31
0218_C				1.30			
0318_C				-0.60			
0418_C	-0.24	-0.48	-0.66	-0.83	0.02	-1.49	-0.44
0518_C				-0.90			
0618_C				-1.41			
0718_C	-0.74	0.48	-0.43	0.14	0.35		
0818_C				3.42			

0918_C				-1.21			
1018_C	-0.33	-0.30	-0.74	-0.66			
1118_C				-0.63			
1218_C				0.80			
0119_C	1.06	-0.54	-0.22	0.63	-0.18	-0.28	-0.16
0319_C				0.91			
0419_C	2.32	0.32	0.28	0.35		-1.15	2.03
0519_C				0.35			
0619_C				-0.09			
0719_C	-0.88	-0.46	-0.41	-0.34	1.05		
1019_C	-0.79	-0.35	0.02		1.57	-0.96	0.24

Months	**AT**	**HG**	**EO**	**ES**
0316_A	32.87	26.66	5.91	0.00
0416_A	26.16	21.25	4.73	0.99
0516_A	29.00	10.24	2.61	14.91
0616_A	12.46	7.94	3.12	4.93
0716_A	10.61	4.73	2.96	10.10
0816_A	15.39	14.61	8.18	10.14
0916_A	11.66	5.31	5.83	5.83
1016_A	24.05	10.70	12.03	2.41
1116_A	20.05	12.66	9.70	3.12
1216_A	22.90	19.56	8.76	5.40
0117_A	10.14	9.14	4.93	2.79
0217_A	7.31	7.37	0.00	0.00
0317_A	10.84	8.81	2.79	3.69
0417_A	10.52	5.57	2.96	4.52
0517_A	10.79	5.31	2.96	9.40
0617_A	19.13	17.98	7.11	7.37
0717_A	11.70	14.98	7.17	6.46
0917_A	16.16	11.66	12.85	1.97
1017_A	22.12	14.21	12.31	0.00
0118_A	15.52	18.85	5.57	0.00
0218_A	25.47	28.69	4.83	0.00
0318_A	6.61	3.12	0.00	1.71
0418_A	10.52	10.97	3.41	2.41
0518_A	17.40	10.43	10.05	6.23
0618_A	10.43	7.17	1.39	11.70
0718_A	11.15	14.07	4.83	8.92
0818_A	28.01	25.84	32.98	7.37
0918_A	19.00	14.41	19.41	2.41
1018_A	14.21	12.92	13.33	4.41
1118_A	18.64	23.93	11.57	4.18
1218_A	13.33	16.01	6.46	1.39
0119_A	6.46	12.70	3.12	3.27

0319_A	14.21	19.28	7.44	2.96
0419_A	7.44	7.57	2.61	2.20
0519_A	10.57	6.90	2.61	3.82
0619_A	8.87	9.19	4.18	0.00
0719_A	15.52	25.47	19.00	0.00
1019_A	15.52	20.19	25.69	0.00
0316_B	34.16	27.45	4.62	0.00
0416_B	12.62	6.54	1.97	0.00
0516_B	29.33	18.80	2.41	17.12
0616_B	12.58	6.23	1.71	4.83
0716_B	13.62	9.55	1.71	9.70
0816_B	9.03	17.52	6.83	8.36
0916_B	19.90	19.16	13.72	0.00
1016_B	19.41	23.57	8.81	7.11
1116_B	24.05	27.02	10.05	4.83
1216_B	6.54	8.07	4.29	3.27
0117_B	20.36	23.77	5.21	2.41
0217_B	5.02	7.31	0.99	2.41
0317_B	13.62	10.79	6.23	4.73
0417_B	11.06	6.76	3.41	3.27
0517_B	18.77	9.03	5.12	12.77
0617_B	18.20	16.89	9.40	8.59
0717_B	14.28	17.68	10.00	10.47
0917_B	33.79	29.10	24.93	0.00
1017_B	26.69	15.52	12.62	0.00
0118_B	10.05	12.66	1.97	3.12
0218_B	12.77	11.57	6.07	4.41
0318_B	11.32	10.66	2.79	1.97
0418_B	12.92	10.24	4.83	2.79
0518_B	12.46	8.13	4.41	8.59
0618_B	10.00	6.68	0.99	9.80
0718_B	13.65	11.57	9.75	5.40
0818_B	24.30	33.15	23.65	8.81
0918_B	11.62	12.77	11.66	3.69
1018_B	3.12	6.90	3.12	2.79
1118_B	4.41	10.00	9.65	3.12
1218_B	7.70	11.62	6.76	7.50
0119_B	6.07	12.35	2.61	3.55
0319_B	3.12	3.69	2.20	0.00
0419_B	4.73	5.21	0.99	4.93
0519_B	7.94	5.31	1.71	4.52
0619_B	8.13	10.14	5.91	2.79
0719_B	12.70	19.76	16.89	0.00
1019_B	7.94	13.65	9.65	0.00
0316_C	21.61	20.57	3.55	1.39

0416_C	12.39	9.55	2.41	1.71
0516_C	35.09	22.40	3.82	21.52
0616_C	10.38	5.02	1.71	3.27
0716_C	8.53	6.39	1.97	9.08
0816_C	7.04	9.40	0.00	9.50
0916_C	12.85	11.19	11.28	4.18
1016_C	16.31	7.76	11.70	1.97
1116_C	17.68	12.73	8.59	0.00
1216_C	10.97	12.39	6.61	1.39
0117_C	10.19	7.37	3.41	0.00
0217_C	10.24	15.77	1.71	2.41
0317_C	11.62	10.61	3.94	1.39
0417_C	12.42	6.39	1.39	5.12
0517_C	8.81	4.52	2.20	6.61
0617_C	20.46	17.79	8.65	8.18
0717_C	11.19	15.07	7.57	8.13
0917_C	38.82	25.54	29.89	8.81
1017_C	37.55	22.38	14.48	0.00
0118_C	13.51	13.26	6.15	0.00
0218_C	14.48	22.30	6.23	0.00
0318_C	14.14	12.23	2.96	0.00
0418_C	18.28	6.54	0.00	4.41
0518_C				
0618_C	4.73	2.96	0.00	3.55
0718_C	9.95	11.15	7.63	0.00
0818_C	32.14	32.32	36.97	9.85
0918_C	16.84	11.91	16.55	1.39
1018_C	13.51	9.75	10.75	3.55
1118_C	15.52	19.46	10.97	5.75
1218_C	11.49	16.95	12.15	6.07
0119_C	7.31	15.30	2.20	4.06
0319_C	12.46	16.69	6.54	3.82
0419_C	11.91	13.72	4.62	3.55
0519_C	4.52	3.55	1.39	2.41
0619_C	6.39	7.17	3.69	1.39
0719_C	6.46	12.85	9.08	0.99
1019_C	10.33	9.35	20.81	0.00

Annex 8: Results of the DistLM analysis used to explore the relationship between foraminiferal species and diatoms species. p-values are obtained using 999 permutations of residuals under the best fit model. The occasional species were selected based on AIC test and p-value. AIC (Akaike information criterion).

***Ammonia* sp. T6**		
Species	***p-values***	***AIC***
Pleurosigma formosum	0.004	
Pleurosigma angulatum	0.026	
Navicula spartinetensis	0.04	
Thalassiosira sp.	0.014	
Gyrosigma fasciola	0.017	
Cymatosira belgica	0.046	
Haynesina germanica		
Species	***p-values***	***AIC***
Pleurosigma formosum	0.003	
Navicula cf *flagellifera*	0.048	
Plagiotropis vanheurckii	0.041	
Nitzschia cf *distans*	0.028	139.61
Elphidium oceanense		
Species	***p-values***	***AIC***
Plagiotropis vanheurckii	0.014	
Gyrosigma wansbeckii	0.008	
Thalassiosira sp.	0.048	
Podosira stelligera	0.011	
Navicula cf *flagellifera*	0.027	
Eutonogramma dubium	0.016	
Plagiogrammopsis vanheurckii	0.023	
Skeletonema sp.	0.049	
Entomoneis paludosa	0.014	160.64
Navicula spartinetensis	0.045	151.11
Elphidium selseyense		
Species	***p-values***	***AIC***
Navicula abscondita	0.018	120.53

Annex 9: Occurrence (%) of the selected diatom species by the DistLM analysis.

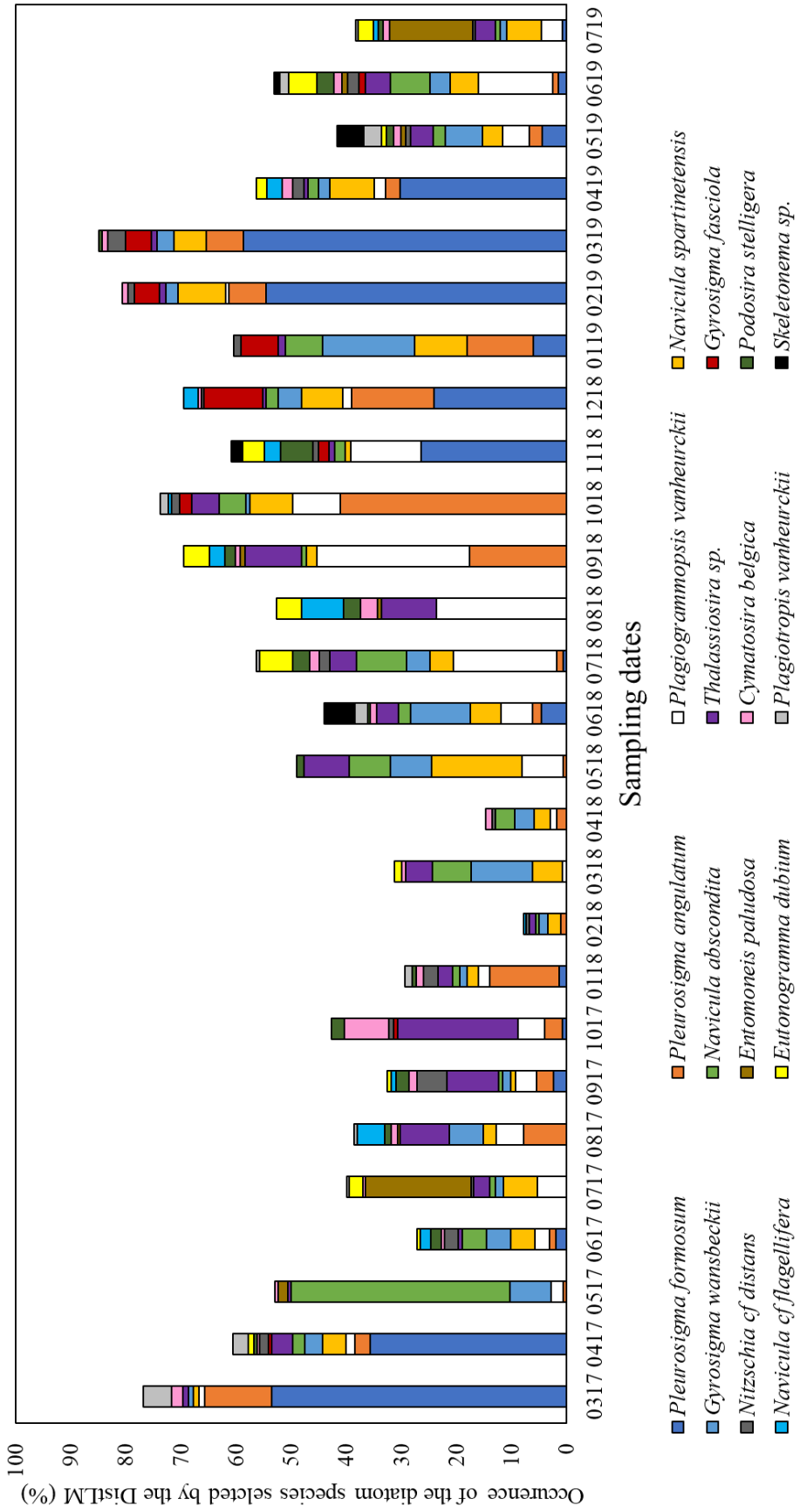

CHAPTER 4

Influence of the Loire river hydrodynamics on geochemical and benthic foraminiferal compartments in intertidal mudflat (Bourgneuf Bay, France)

Chapter 4: Influence of the Loire river hydrodynamics on geochemical and benthic foraminiferal compartments in intertidal mudflat (Bourgneuf Bay, France)

C. Choquel[1]*, E. Metzger[1], E. Geslin[1], P. Launeau[1], B. Jesus[2], A. Mouret[1]

1: UMR CNRS 6112 LPG BIAF, Univ. Angers, Univ. Nantes, France

2: Mer Molécules Santé, EA 2160, Université de Nantes, France

(*correspondence: constance.choquel@gmail.com)

1. Introduction

Intertidal sediments are in transient state. The stability of the sediment is influenced by various environmental parameters combining: hydrological (river discharge, tidal cycles, waves and currents), meteorological (rainfall, temperature, wind-storms), and biological (benthic fauna) factors occurring at different spatial (from micro to kilometers) and temporal (from day to years) scales. A flood event can significantly affect the sediment properties over a large scale. To evaluate the impacts of such disturbance, spatiotemporal geochemical and biological sediment instability markers (combination of redox chemical elements and benthic fauna distributions) are used.

River floods have significant physical sedimentary effects on nearshore areas like the deposition and resuspension of sediment (Aller, 2004; McKee et al., 2004; Sundby, 2006; Roy et al., 2013; Thibault de Chanvalon et al., 2016). The frequent remobilization of muddy sediments affects the porosity and destructures the redox fronts established during diagenesis processes (Froelich et al., 1979; McKee et al., 2004). Different redox stages have been previously described in the intertidal mudflat of Loire estuary following a flood event during the winter flood, the about 1 month later for the post-flooding period and finally the stabilized summer period (~ 6 months later) (Thibault de Chanvalon et al., 2016). Namely, in the winter flood period, no manganese (Mn), iron (Fe) and phosphorus (P) are released into pore waters within the flood-deposited layer. In post-flooding period, a high Mn-Fe-P oxidized phases are consumed while the dissolved phases smoothly increased. In stabilized period, the oxides are strongly dissolved. The increase of nutrients as ammonium (NH_4^+) and dissolved reactive phosphorus (DRP) are favored by: the higher anaerobic organic matter (OM) remineralization (higher alkalinity, sulfato-reduction process). A high P/ Fe ratio allow the release of phosphorus to feed primary producers at the sediment surface (Thibault de Chanvalon et al., 2016).

Tidal cycles, rain and flood events, participate to the microphytobenthos (MPB) biofilm resuspension (Dupuy et al., 2014; Ha et al., 2018; Redzuan and Underwood, 2021). MPB biomass as well as the diversity and photosynthetic activity are influenced by the availability of light modulated by the deposit and/ or resuspension of sediment (Bartoli Marco et al., 2003; Méléder et al., 2005, 2007; Jesus et al., 2006, 2009; Brito et al., 2009; Delgard et al., 2012). Therefore, decreasing O_2 availability influences the microhabitats of benthic meiofauna as foraminifera (Jorissen et al., 1995; Geslin et al., 2011; Koho and Piña-Ochoa, 2012; Thibault de Chanvalon et al., 2015; Jauffrais et al., 2016). Benthic foraminifera react to physicochemical disturbances by a fluctuating density and specific richness (Culver and Buzas, 1995; Ernst et al., 2006; Armynot du Châtelet and Debenay, 2010; Nardelli et al., 2014; Thibault de Chanvalon

et al., 2015; Cesbron et al., 2016; Mojtahid et al., 2016; Richirt et al., 2020). One the one hand, during a stabilized period, the vertical micro-distribution patterns of living foraminifera reflect species micro-environment preferences, indicated by a higher density in the oxygenized zone (Cesbron et al., 2016). On the other hand, the physicochemical disturbances increase the patchiness due to the variety of foraminiferal response to stress conditions (Murray and Alve, 2000; Ernst et al., 2006). Thus, the dormant specimens and propagules wait for favorable conditions to recolonize the sediment (Alve, 1999; Alve and Goldstein, 2003, 2010; Ross and Hallock, 2016; LeKieffre et al., 2017). The challenge remains the identification of the time lag between the flood event and the response of foraminifera. This lag depends on the sediment stabilization as well as food supply and O_2 availability and can range from several days to several months (Morvan et al., 2004; Ernst et al., 2006; Debenay et al., 2006; Koho et al., 2007; Hess and Jorissen, 2009; Papaspyrou et al., 2013).

At microenvironment scale, the complex interactions between geochemical and biological compartments can be difficult to observe with conventional technics. Moreover, the resolution is generally limited by the dimensions of the sampling windows (Stockdale et al., 2009). To overcome this limitation, new methods and multiple sampling time point are required to evaluate the spatial and temporal variability with sufficient confident level. Developments of two-dimensional diffusive equilibrium in thin film gels (2D-DET) coupled with colorimetric methods, allow a high resolution at mm and sub-millimeter scales of dissolved elements like Fe/ DRP (Cesbron et al., 2014), NO_2^-/ NO_3^- (Metzger et al., 2016), NH_4^+ (Metzger et al., 2019), Mn (Mouret et al., *in prep*). The advantage of 2D gels is to provide the characterization of microenvironments about biogeochemical processes in both horizontal and vertical dimensions simultaneously (e.g. diffusive fluxes, production/ consumptions zones) (Jézéquel et al., 2007; Santner et al., 2015; Thibault de Chanvalon et al., 2017; Choquel et al., 2021; Moncelon et al., 2021). Oxygen microsensors are commonly used to evaluate aerobic mineralization (O_2 consumption, in dark conditions) and photosynthetic activity (O_2 production, in light conditions) (Revsbech, 1989; Glud et al., 2005; Delgard et al., 2012). Repeated O_2 profiling during low tide, allow to observe the O_2 dynamics impacting both redox zonations and O_2 availability for benthic meiofauna as foraminifera (Papaspyrou et al., 2013). Namely, a drastic instability of pore waters O_2 gradients can be lethal for some foraminiferal species that cannot withstand sub-to anoxic sediment conditions and not able to migrate to preferential oxygenation zones (Moodley, L. et al., 1998; Jorissen et al., 1995; Ernst et al., 2002; Geslin et al., 2011).

In this study, we focused on the Loire river estuary seasonal discharge impacting nearshore areas as the Bourgneuf Bay mudflat, when flood events combined to currents and tides pushed

particles by the river plume towards the interior of the bay (GIP Loire Estuaire). Intertidal sediments, where diagenetic processes are transient may be fueled by sediment deposit and/ or resuspension in post-flooding period, generating higher instability of redox chemical elements and benthic faunal compartments. The aims of this chapter are: (1) to detail redox elements spatial variability at two hydrological and meteorological contrasted periods; (2) to investigate the role of the tidal pump and flood events on the dynamics of redox elements and the nutrient availability for benthic fauna; (3) to evaluate if the vertical foraminiferal micro-distribution (CTG-labeled) allow to characterize the late disturbed winter post-flooding and the stabilized late summer periods.

2. Materials and Methods

2.1 Site description

The Bourgneuf Bay (46°52′–47°08′N, 1°58′–2°20′W) is located on the French Atlantic coast in the South of the Loire river estuary (West Atlantic coast, France; Chapter 4). The Bourgneuf Bay is a semi-enclosed area of 340 km^2, with a large intertidal mudflat area of 100 km^2, connected with the Atlantic Ocean by 10 km wide passage between the North of the Noirmoutier Island and the “Pointe Saint Gildas”. A narrow second bay-ocean communication zone named "goulet de Fromentine" exists to the south of the bay (Debenay, 1978). The wide North West opening allows a connection with the ocean and the Loire estuary. The sediments rejected by the Loire estuary are largely pushed towards the interior of the Bourgneuf Bay generating siltation (Debenay, 1978).

The sampling site was located at “La Coupelasse” (Chapter 3). Three stations A (47°0’56.49’N, 2°1’26.72’W), B (47°0’56.83’N, 2°1’26.80’W) and C (47°0’56.67’N, 2°1’27.16’W) were sampled along a tidal channel near a path used by oyster farmers to access at the middle of the mudflat (500 m of distance from shore). The three stations were 10 m apart. The stations A and C were the closest to the tidal channel and the station B was the more distant from the channel.

2.2 Sampling strategy

In this study, sampling was focused on two contrasted hydrologically situations during the year 2019: in April and October 2019. The Loire river flood event occurred in February 2019. April corresponded to a period of post-flooding of the Loire river (2 months after the flood) and October to a period of low water level (8 months after the flood). The three stations were sampled for 1D geochemical analyses until 11 cm depth and living foraminiferal species

densities (Rose Bengal staining) in the first centimeter of sediment. In this study, the station C was sampled for additional analyses: foraminiferal vertical micro-distributions (CTG-labelling) until 10 cm depth and 2D geochemical analyses.

2.3 Tidal, hydrological and meteorological data

The tidal coefficients reported at each sampling months, came from Pornic (http://www.maree.info). The monthly Loire river discharge (m^3 s^{-1}) was monitored at the Montjean-sur-Loire station, located ~ 120 km upstream from the estuary (http://www.hydro.eaufrance.fr/). The monthly air temperature (T°C), the monthly rainfall (mm) and wind-storm events (> 70 km h^{-1}) were retrieved from the weather station of Bourgneuf-en-Retz (Chapter 3) (47,04°N | 1,95°W) using the information from SHOM (https://www.shom.fr). The wind-storm events were punctual events and not included in the further data analyses.

2.4 Geochemical sampling and processing

2.4.1 1D sampling and processing

One core per sampling time was used for pore water and solid-phase analyses. The core (internal diameter = 9.4 cm) was brought to the Angers laboratory and stored at *in situ* temperature (15 and 18°C, respectively for April and October) until further analysis the next day. The core was sliced in a glove bag filled with nitrogen (N_2) to avoid oxygen contamination of the reduced sediments. The core was sliced every 2 mm up to 2 cm depth, then 5 mm up to 5 cm and 1 cm up to 11 cm depth. Each sediment slice was weighed then centrifuged (3500 rpm) for 15 min and the supernatant was filtered using a 0.2 µm filter (RC25, Sartorius ©). An aliquot was used for nutrient colorimetric analyses (ammonium (NH_4^+), nitrite (NO_2^-), and nitrate (NO_3^-)), a second was used for alkalinity analysis. All spectrophotometric analyses were performed using a Genesys 20 from Thermo-Fischer. Ammonium was analyzed using a phenol-hypochlorite method (Harwood and Kühn, 1970). Nitrite was analyzed using the Griess reagent (Griess, 1879), a second reagent was prepared using vanadium chloride (VCl_3) to reduce nitrate into nitrite, allowing nitrate determination. Alkalinity was measured using the colorimetric bromophenol blue/ formic acid method (Sarazin et al., 1999). A third pore water aliquot was acidified with HNO_3 and analyzed by ICP-AES (Thermo Scientific iCAP 6300 Radial) to measure sodium (Na), dissolved iron (Fe_d), dissolved manganese (Mn_d) and dissolved reactive phosphorus (DRP) (uncertainty is 5% for Fe_d and Mn_d and 25% for DRP). The salinity was

calculated from the Na measurements ((*Na x 35)/ 469*, Thibault de Chanvalon et al., 2015). The precision of the salinity values was of the order of 1 or 2 units.

Centrifuged sediment plugs were frozen for solid-phases analyses. Within one week, samples were freeze-dried, weighed again to determine the porosity and manually ground using an agate mortar. About 100 mg were used for the extraction of reactive manganese (Mn_{asc}), iron (Fe_{asc}), and associated phosphorus (P_{asc}). Aliquots were exposed to 10 mL of ascorbate solution (buffered at pH 8) over 24 h (Anschutz et al., 1998, 2005; Hyacinthe et al., 2001). Measurements were performed after a 50-fold dilution with a 1% ultrapure nitric acid with an ICP-AES ICAP 6300 Thermo-Fischer.

2.4.2 2D sampling and processing

The principle of the 2D-DET methods (Jézéquel et al., 2007; Robertson et al., 2008; Pagès et al., 2011; Cesbron et al., 2014; Bennett et al., 2015; Metzger et al., 2016, 2019) is to adapt existing colorimetric reaction for solutions to the hydrogel 2D samples. The principle is to superimpose one or two reagent gels over a sample gel that was previously equilibrated in the sediment. The 2D-DET gels methods used in this study were: NO_2^-/ NO_3^- (detailed method in Metzger et al., 2016, summarized in Choquel et al., 2021), Mn_d (detailed method in Mouret et al., *in prep*; summarized in Chapter 3), NH_4^+ (detailed method in Metzger et al., 2019) and Fe_d/ DRP (detailed method in Cesbron et al., 2014 and summarized in Thibault de Chanvalon et al., 2015). For the 2D sampling deployment, we used a "stainless steel support" to simultaneously sample a sediment slab and the pore waters with the 2D-DET gels (Fig. 1). Two 2D-DET gel probes for sampling Mn_d and NO_2^-/ NO_3^- were placed on each side of a Plexiglas plate and on a second Plexiglas plate were placed a combination of two 2D-DET gel probes for sampling Fe_d/ DRP and NH_4^+. The two Plexiglas plates with the four gels were mounted on a "stainless-steel support" allowing to sample the sediment slab.

For each chemistry: NO_2^-/ NO_3^- , Mn_d, Fe_d/ DRP and NH_4^+ (Metzger et al., 2016, Mouret et al., *in prep*, Metzger et al., 2019, Cesbron et al., 2014), a DET gel probe was -prepared and protected from particles by a PVDF membrane (0.2 µm) when mounted on the Plexiglas plates (Fig. 1 a). Then, the DET gel probes were assembled with the "stainless-steel support" forming the sampling device. This 2D sampling device was deployed *in situ* at the station C in April and October 2019 at low tide. Because of the equilibration time of 5 hours, a large mud core (glass walls, size 30 x 30 x 25 cm, ~ 0.02 m^3) was sampled around the sampling device, transported to the lab and maintained at *in situ* temperature (15 and 18°C, respectively for April and October) (Fig. 1 b-e). Once the 2D sampling device removed, the 2D-DET gel probes were

disassembled (Fig. 1 f) and laid on specific colorimetric reagent gels in order to obtain the coloration development for each chemical species. Photographs (reflectance analysis) of the gel assemblages for NO_2^-/ NO_3^- and Fe_d/ DRP were taken with a hyperspectral camera (HySpex VNIR 1600). These hyperspectral images were converted into false colors through calibrated scales of concentrations corresponding to each chemistry. Each pixel was decomposed as a linear combination of the logarithm of the different endmember spectra using ENVI software (unmixing function) (Cesbron et al., 2014; Metzger et al., 2016). Photographs of the gel assemblages for Mn_d and NH_4^+ were taken with a scanner (CanoScan LiDE 600F). These images were processed with ImageJ® software, split into primary color intensities (red, green and blue) and converted into 16-bit grey-scale images. The blue color intensity was found to give the most sensitive response for manganese concentration (Mouret et al., *in prep*; Chapter 2). The red color intensity was found to give the most sensitive response for NH_4^+ concentrations (Metzger et al., 2019). The grey values of each pixel of the Mn_d and NH_4^+ images were converted into concentrations using calibrated scales of concentrations for Mn_d and NH_4^+). The final concentration images were plotted with R software (package plot3D) and cropped to avoid border effects. The final size of the images was 5 cm width by 10 cm long. The detection limits are 1.7 µmol $^{L-1}$ for the NO_2^-/ NO_3^- 2D-gels (Metzger et al., 2016), 19 µmol L^{-1} for Mn_d (Mouret et al. *in prep*), about 1 µmol L^{-1} for Fe_d, 2 µmol L^{-1} for DRP (Cesbron et al., 2014) and about 20 µmol L^{-1} for NH_4^+ (Metzger et al., 2019). The sediment slab into the "stainless-steel support" (Fig. 1 f) was embedded for further solid-phase analyses (see Chapter 2).

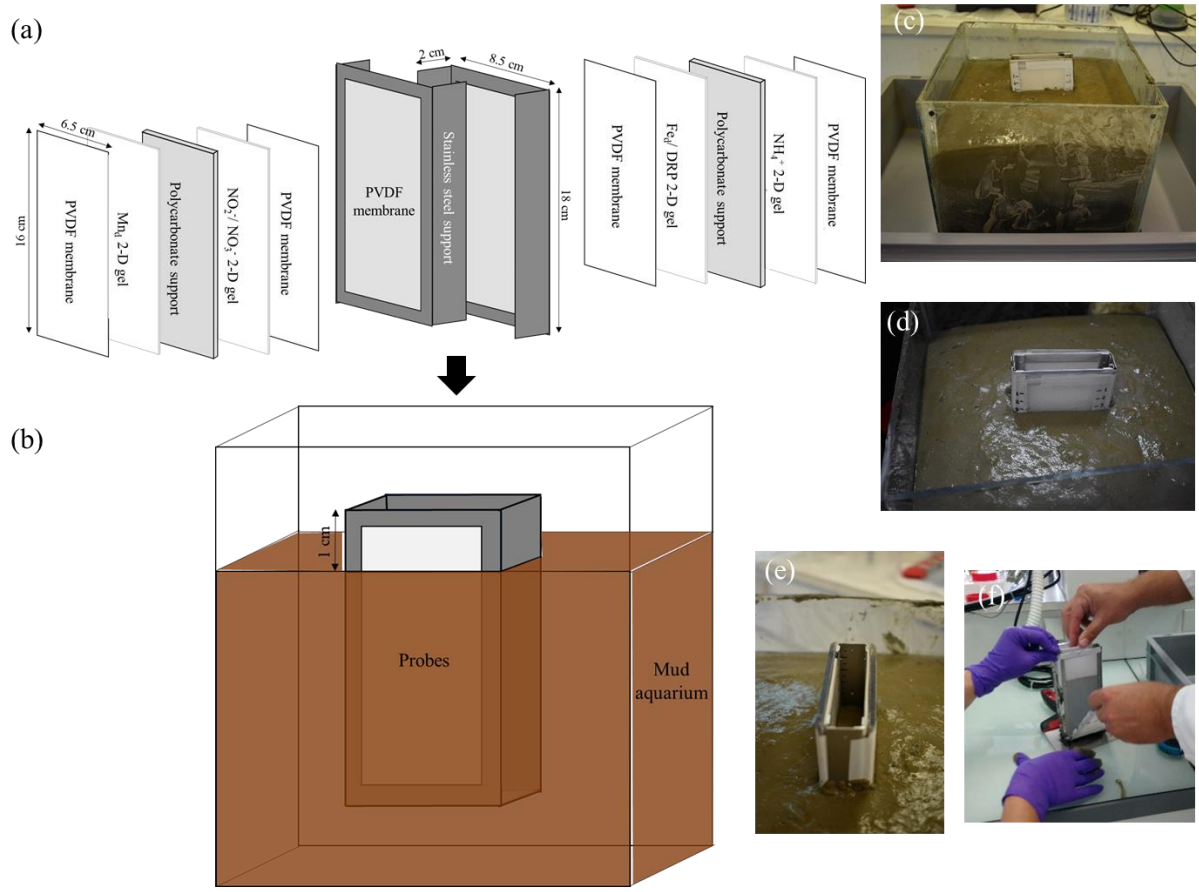

Figure 1: Schematic view of the sampling device, (a) the different 2D-DET gel probes were mounted on a "stainless steel support", then (b) the 2D sampling deployment was assembled and inserted in a" mud aquarium" for 5 h equilibration time. The "mud aquarium" was sampled at the station C in the Bourgneuf Bay mudflat in April and October 2019. (c- e) Photography of the 2D sampling deployment and the large mud core. (f) The 2D-DET gel probes were disassembled to be analyzed and the sediment slab into the "stainless steel support" was embedded for further solid-phase analyses.

2.5 *In situ* oxygen profiling and modelling in light and dark conditions

During the sampling days, *in situ* O_2 profiling was performed at low tide during 4 hours (~ 2 h before and after the low tide hour). Sampling was carried out at low tide at 11h 07 on 18 April 2019 and at 15h06 on 3 October 2019. Sediment O_2 profiles were measured in the light with a Clark electrode (50 µm tip diameter, Unisense ®, Denmark) to determine MPB photosynthetic activity. A motorized micromanipulator was used to realize O_2 concentration profiles within the first 5mm depth at a 100 µm vertical resolution. Oxygen profiling was continuously repeated in order to evaluate the intensity variations of the MPB photosynthesis activity. The average oxygen penetration depth (OPD) was used with standard deviation (n = 12 in April, n= 11 in October). The profile (n=1) showing the higher O_2 production was selected for modelling dissolved oxygen uptake (DOU) (µmol m^{-2} d^{-1}) and O_2 production/ consumption (nmol cm^{-3} s^{-1}) zones. During O_2 profiling a black plastic bag was wrapped around the profiling

device (~ 1 hour) to measure aerobic mineralization (O_2 consumption without photosynthesis activity).

2.6 Pore water concentration modelling

The 1D profiles and the average profiles obtained from 2D concentration images were modeled using PROFILE software (Berg et al., 1998). The two boundary conditions used for the calculations corresponded to the first solute concentration at the top and the last solute concentration at the bottom. The bulk sediment molecular diffusion coefficient (Ds) was estimated according to $DS = \varphi 2D0$ (Ullman and Aller, 1982) where ϕ was the sediment porosity acquired along the sediment depth and D0 was the diffusion coefficient in water ($1.7079E^{-05}$ cm^2 s^{-1} in April and $1.8575E^{-05}$ cm^2 s^{-1} in October) at *in situ* temperature (15 and 18°C, respectively) and salinity (Li and Gregory, 1974).

2.7 Foraminiferal sampling and processing

The foraminiferal vertical distributions were performed in April and October 2019. One core per date was collected with a cylindrical core (Ø 8.2 cm) and sliced every 2 mm up to 2 cm, 5 mm up to 5 cm and 1 cm up to 10 cm depth. The samples were incubated without light for 10–19 hours in ambient seawater with CellTracker Green (CMFDA, 1 mM final concentration) at *in situ* temperatures (Bernhard et al., 2006) and then fixed with ethanol 96°. Fixed samples were sieved (> 355, 150, 125 and 63 µm) and the > 125 µm fraction was analyzed, using an epifluorescence microscope equipped for fluorescein detection (i.e., 470 nm excitation; Olympus SZX13). All foraminifera that fluoresced continuously and brightly were wet-picked, air-dried, identified and counted. Scanning Electron Microscopy (SEM) images of the dominant foraminifera species (> 5 % of the assemblage) are available in Chapter 4. These foraminiferal vertical distributions were performed in addition to the classic sampling used for foraminiferal MUDSURV biomonitoring (> 1 cm depth, 150 µm fraction, Rose Bengal staining) (see Chapter 3).

3. Results

3.1 Sediment biogeochemistry

3.1.1 Environmental context and physico-biogeochemical sediment properties

The Loire river discharge widely fluctuated from October 2018 to October 2019 (Fig. 2 a). The winter flood event (1030 m^{-3} s^{-1}) occurred in February 2019. The sampling in April (379 m^{-3} s^{-1}) occurred two months after the flood and one month after the last wind-storm event (>

70 km h^{-1}). The second sampling in October was in a period of low water level (< 200 m^{-3} s^{-1}) since July. The average monthly rainfall indicated a sharp increase in early autumn reaching 90 mm in October (Fig. 2 a). The biogeochemical sediment properties differed between the two months. In April the OPD (measured in the dark) was 1.02 ± 0.003 mm (n=2) and it was higher in October reaching 1.89 ± 0.06 mm (n=6). One O_2 profile per sampling event was shown in Fig. 2 b. In April, the porosity profile was disturbed showing a lower value in the 1st cm depth (0.76 ± 0.02) and fluctuated deeper (Fig. 2 c). In October, the sediment showed a higher porosity in the 1st cm depth (0.83 ± 0.03), then the porosity stayed stable deeper. The surface alkalinity was similar until 6 cm depth, then the alkalinity increased in October until 16 mmol kg^{-1} (Fig. 2 d). The sediment surface salinity in April was 39.7 and 37.7 in October, then the two profiles decreased and stayed similar (Fig. 2 e).

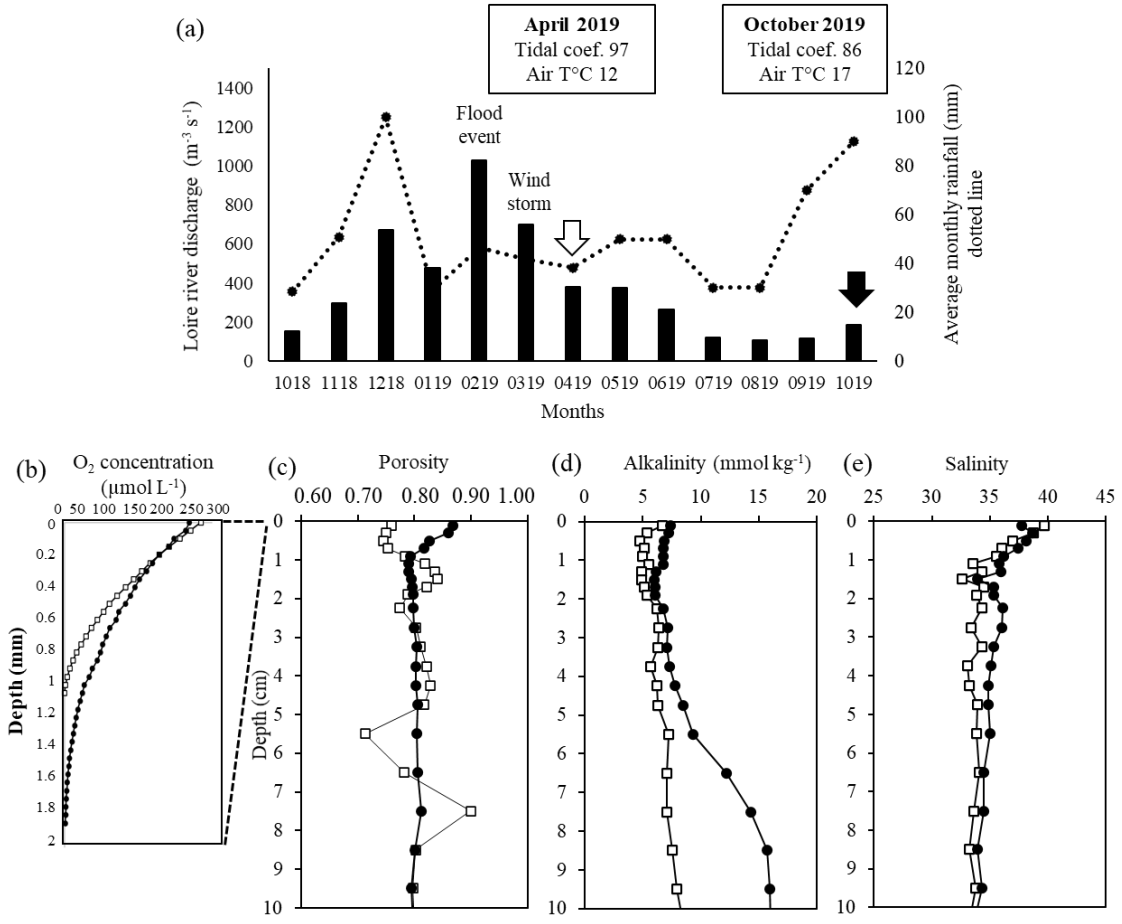

Figure 2: (a) Loire river discharge (m^{-3} s^{-1}) from October 2018 to October 2019 (black histogram), a flood event (1030 m^{-3} s^{-1}) occurred in February and a wind-storm event (> 70 km h^{-1}) in March. The average monthly rainfall (mm) is shown by a dotted line (38 mm in April) and (90 mm in October). The white and black arrows indicate the sampling months. The tidal coefficients of the sampling days were 97 in April and 86 in October. The average monthly air temperature was 12°C in April and 17°C in October. (b) OPD (depth scale in mm), (c) porosity, (d) alkalinity and (e) salinity profiles for the station C were reported for April (white square) and October (black circle).

3.1.2 1D profiles of Mn, Fe and P

Figure 3 presents the 1D profiles of ascorbate-extracted and dissolved Mn, Fe and P in April (a-c) and October (d-f) 2019. In the 1st cm of sediment, the reactive Mn oxides (Mn_{asc}, white symbols; Fig. 3 a, d) decreased from 4.1 µmol g^{-1} to 2.1 µmol g^{-1} in April and from 6.2 µmol g^{-1} to 2.1 µmol g^{-1} in October. Mn_{asc} showed a constant concentration below the 1st cm of 2.4 ± 0.2 µmol g^{-1} in April and 1.6 ± 0.4 µmol g^{-1} in October. In April, the associated 1D Mn_d (dark square; Fig. 3 a) increased from 9.2 µmol L^{-1} to 108.5 µmol L^{-1} in the two first cm of sediment and stayed quite stable deeper (101.1 ± 11.6 µmol L^{-1}). In October, the Mn_d (dark circle; Fig. 3 d) indicated a bimodal 1D profile, with an increase from 2.0 µmol L^{-1} to 158.9 µmol L^{-1} in the 1st cm depth, then a second peak deeper reaching 183.6 µmol L^{-1} at 7.5 cm depth.

The reactive Fe oxides (Fe_{asc}, white symbols; Fig. 3 b, e) decreased with sediment depth. In April the Fe_{asc} decreased from 77.2 µmol g^{-1} to 30.2 µmol g^{-1} in the 1st cm depth, then stayed stable deeper (32.8 ± 4.9 µmol g^{-1}) (white square; Fig. 3 b). In October, the sediment surface showed a lower concentration of 42.2 µmol g^{-1} to 29.0 µmol g^{-1} in the 1st cm, then Fe_{asc} was stable with 28.6 ± 7.5 µmol g^{-1} (white circle; Fig. 3 e). The associated 1D Fe_d profile increased with depth until a maximal value of 903.0 µmol L^{-1} reached at 2.5 cm depth in April (dark square; Fig. 3 b) and 1694.6 µmol L^{-1} reached at 5.5 cm depth in October (dark circle; Fig. 3 e).

Fe-bound phosphorus (P_{asc}, white symbol; Fig. 3 c, f) had similar pattern to $Fe_{asc.}$ In April, the P_{asc} increased from 7.1 µmol g^{-1} to 10.3 µmol g^{-1} in the 1st cm of sediment and decreased continuously deeper (7.9 ± 1.5 µmol g^{-1}) (white square; Fig. 3 c). In October, the P_{asc} decreased from 9.4 µmol g^{-1} to 6.0 µmol g^{-1} in 1st cm depth, then stayed stable deeper with 6.5 ± 1.2 µmol g^{-1} (white circle; Fig. 3 f). In April, the associated 1D DRP profile (dark symbol; Fig. 5 b, e) continuously increased until 50.1 µmol L^{-1} at 10.5 cm depth (dark square; Fig. c). In October, the DRP was stable until 3 cm depth then increased until 172.8 µmol L^{-1} at 10.5 cm depth (dark circle; Fig. 4 f).

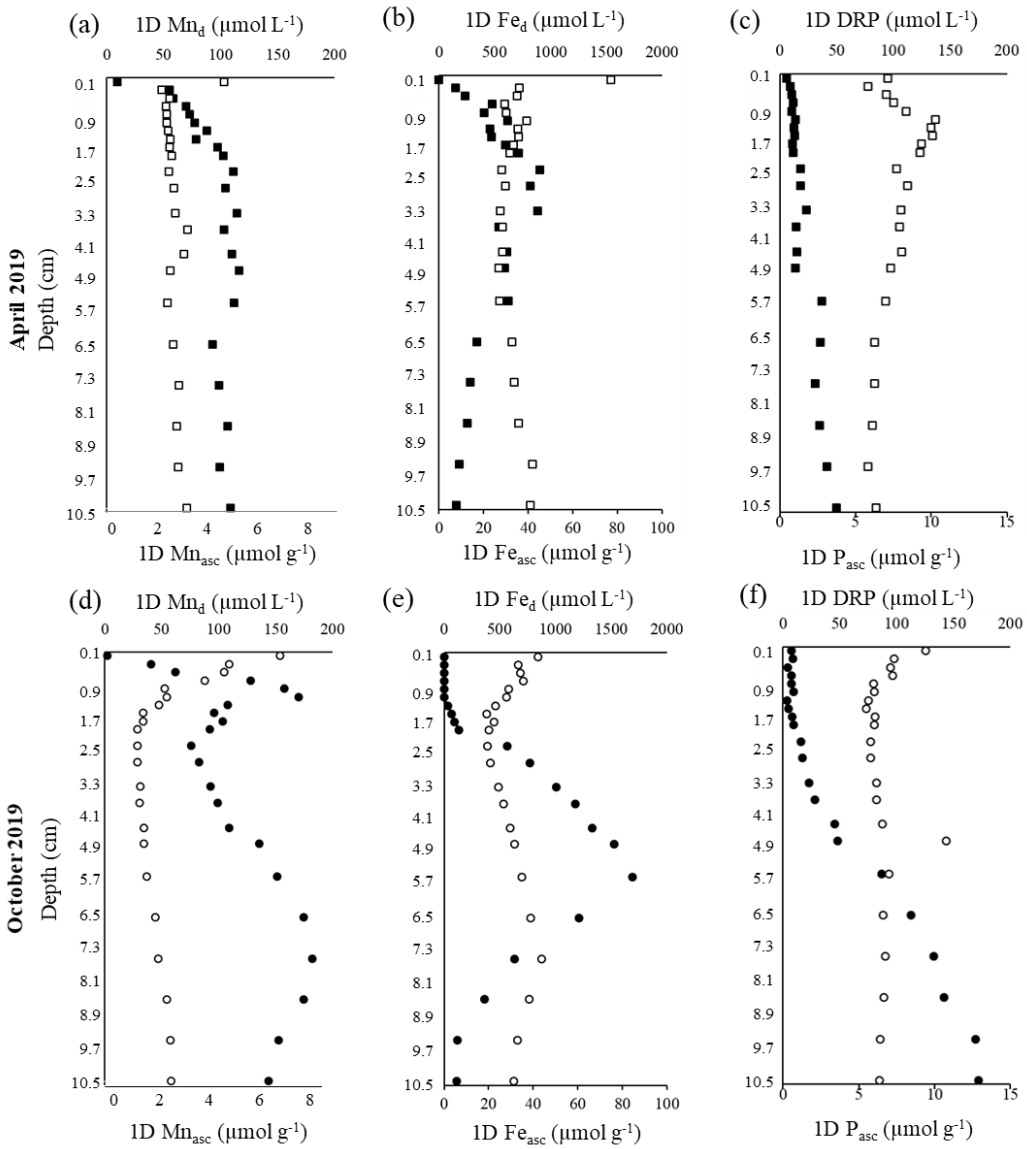

Figure 3: Ascorbate-extracted (white symbol) and dissolved manganese, iron and phosphorus (dark symbol) from (a-c) April and (d-f) October. A single 1D ascorbate-extracted and dissolved profile was reported for each chemical element from the station C.

3.1.3 1D and 2D Mn_d distribution and modelling

Figure 4 illustrates the spatial variability of the Mn_d concentration and modelling using 1D (dark symbol) and 2D (white symbol) methods in April (Fig. 4 a-d) and October (Fig. 4 e-h). In April, the difference between the 1D and the 2D profiles was high (Fig. 4 a). The average 2D profile showed high Mn_d concentrations between 106.0 ± 88.9 µmol L^{-1} and 410.6 ± 120.0 µmol L^{-1} in the 1st cm of sediment. Below the Mn_d increased until a maximum (corresponding to the reddish color zone of the 2D gel; Fig. 4 b) between 3 and 7 cm depth (741.9 ± 12.0 µmol L^{-1}) and then decreased deeper. The modelling indicated negative (i.e. from the sediment to the overlaying water) Mn_d top fluxes: 1D -1.61E^{-04} µmol m^{-2} d^{-1} and 2D -7.53E^{-04} µmol m^{-2} d^{-1}.

One main production zone was found from the surface to ~ 4 cm depth with the 1D ($2.13E^{-04}$ nmol cm^{-3} s^{-1}; Fig. 4 d) and 2D modelling ($1.28E^{-03}$ nmol cm^{-3} s^{-1}; Fig. 4 c). One main consumption zone was found below 4 cm depth with the 1D ($-4.76E^{-05}$ nmol cm^{-3} s^{-1}; Fig. 5 d) and 2D modelling ($-3.06E^{-04}$ nmol cm^{-3} s^{-1}; Fig. 5 c).

In October (Fig. 4 e-h), the 1D and 2D profiles indicated a similar pattern (Fig. 4 e). The average 2D profile showed higher Mn_d values between 85.6 ± 52.8 µmol L^{-1} and 220.2 ± 43.6 µmol L^{-1} in the 1st cm of sediment, slightly fluctuated deeper (238.9 ± 22.1 µmol L^{-1}) (homogeneous color zone visible with the 2D gel, Fig. 4 f). The modelling indicated similar negative Mn_d top fluxes; 1D $-7.33E^{-04}$ µmol m^{-2} d^{-1} and 2D $-8.62E^{-04}$ µmol m^{-2} d^{-1}. One main production zone was found from the surface to ~ 1.5 cm depth with the 1D ($1.36E^{-04}$ nmol cm^{-3} s^{-1}) and 2D ($1.31E^{-03}$ nmol cm^{-3} s^{-1}) modelling. Below 1.5 cm depth the Mn_d showed a main consumption zone between 1.5 to 2.5 cm depth with the 1D ($-4.34E^{-04}$ nmol cm^{-3} s^{-1}) and 2D ($-3.61E^{-04}$ nmol cm^{-3} s^{-1}) modelling. Deeper, the production zones detected were very low.

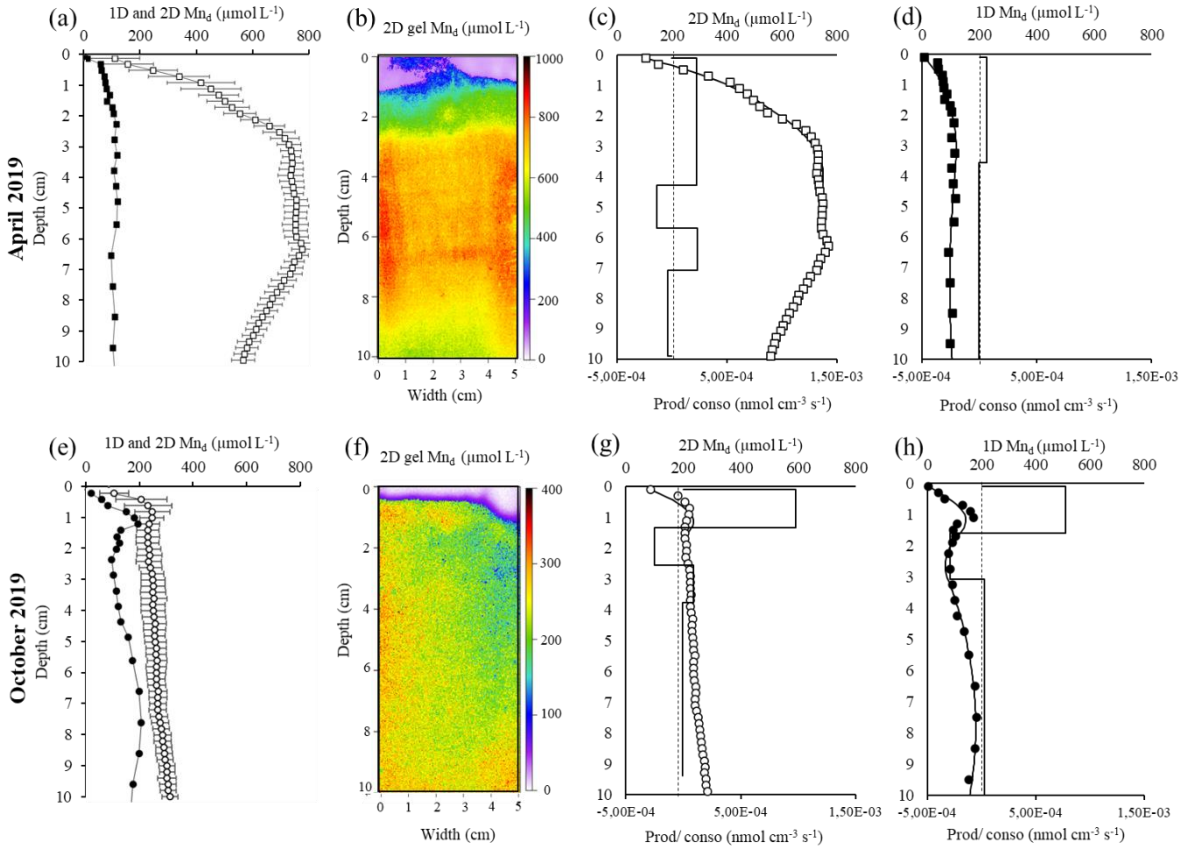

Figure 4: 1D and average 2D Mn_d profiles and associated modelling in (a-d) April and (e-h) October. (a, e) 1D profiles (dark symbol) and 2D profiles (white symbol). The average ± standard deviation of the 2D profiles were extracted from the 2D gels b and f, respectively. The production and consumption zones of the 2D profiles were in c and g, respectively and the production and consumption zones of the 1D profiles were in d and h, respectively. The dotted

line (c, d, g, h) represents the limit (zero) between production (positive values) and consumption (negative values).

3.1.4 1D and 2D Fe_d distribution and modelling

Figure 5 illustrates the spatial variability of the Fe_d concentration and modelling using 1D (dark symbol) and 2D (white symbol) methods in April (Fig. 5 a-d) and October (Fig. 5 e-h). In April the difference between the 1D and the 2D profiles was high (Fig. 5 a). The 1D profile showed higher maximum concentrations than the average 2D profile. The average 2D profile increased between 7.8 ± 2.9 µmol L^{-1} to 188.9 ± 79.2 µmol L^{-1} in the 1st cm, then slightly decreased deeper (292.05 ± 45.37 µmol L^{-1}). The modelling indicated negative Fe_d top fluxes; 1D -1.33E^{-03} µmol m^{-2} d^{-1} and 2D -5.51E^{-04} µmol m^{-2} d^{-1}. Globally, one main production zone was found from the surface to ~ 3 cm depth with the 1D (1.94E^{-03} nmol cm^{-3} s^{-1}; Fig. 5 d) 2D (7.65E^{-04} nmol cm^{-3} s^{-1}; Fig. 6 c) modelling. One main consumption zone was found from 4 cm depth to 10 cm depth with the 1D modelling (-3.33E^{-04} nmol cm^{-3} s^{-1}; Fig. 5 c).

Conversely in October, the 1D and 2D profiles presented a similar pattern (Fig. 5 e) but appeared vertically shifted. The surface concentrations were higher with the 2D method, from 14.9 ± 3.5 µmol L^{-1} to 285.94 ± 98.1 µmol L^{-1} in the 1st cm depth whereas no Fe_d was detected with the 1D profile. The maximal Fe_d peak of 1695.6 µmol L^{-1} was reached at 6 cm depth with the 1D method (Fig. 5 e) and 1562.3 ± 132.2 µmol L^{-1} reached at 4 cm depth with 2D method (high concentrated zone from the surface to 6 cm depth, the black arrow indicated a potential macrofaunal burrow trace; Fig. 5 f, Thibault de Chanvalon et al., 2015). The modelling indicated a negative Fe_d top flux 2D -8.12E^{-04} µmol m^{-2} d^{-1}. No estimate of the Fe_d 1D top flux was suggested due to the absence of Fe_d concentration in the first cm depth. One main consumption zone was found from the surface to ~ 2 cm depth with the 1D (-4.21E^{-03} nmol cm^{-3} s^{-1}) and 2D (-2.42E^{-03} nmol cm^{-3} s^{-1}) modelling. The production zone was deeper from 2 to 6 cm depth with the 1D (3.50E^{-03} nmol cm^{-3} s^{-1}) and the 2D (3.37E^{-03} nmol cm^{-3} s^{-1}) modelling. Deeper, a second lower consumption zone was detected.

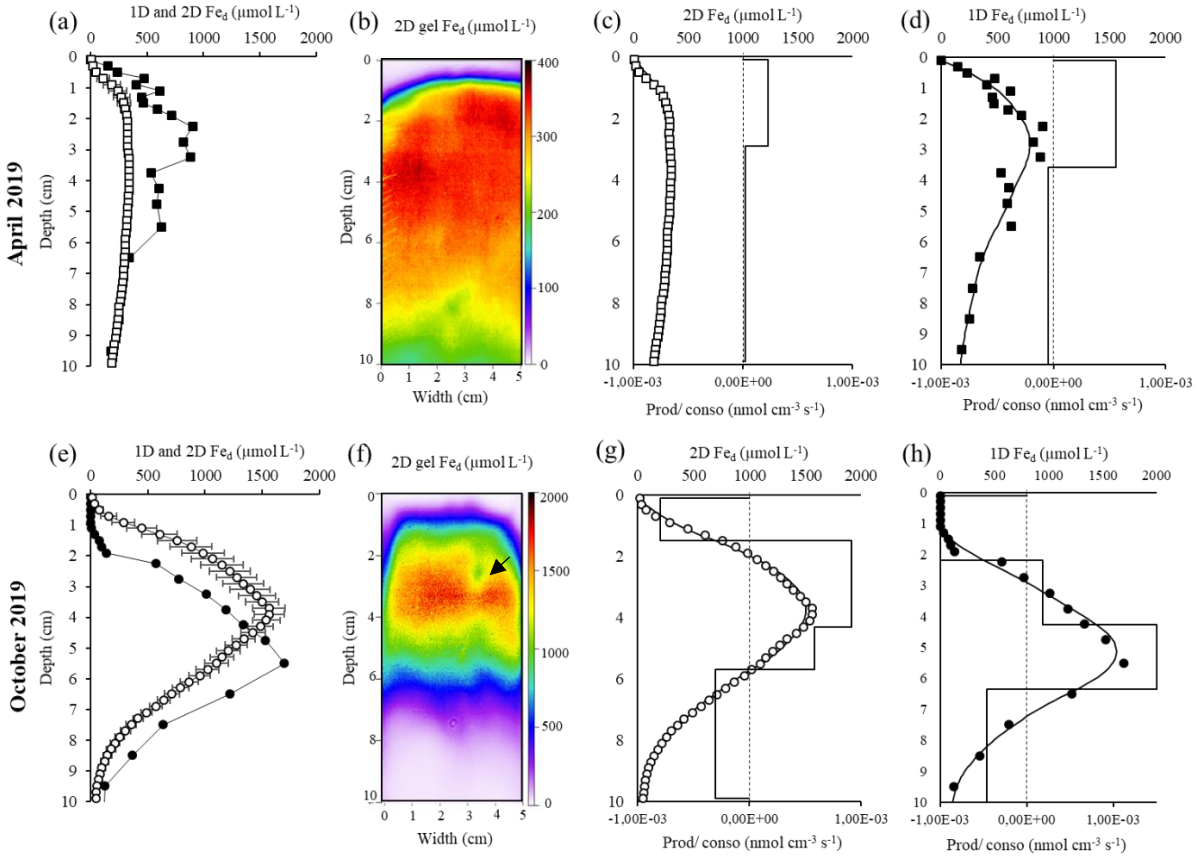

Figure 5: 1D and average 2D Fe$_d$ profiles and associated modelling from (a-d) April and (e-h) October. (a, e) 1D profiles (dark symbol) and 2D profiles (white symbol). The average ± standard deviation of the 2D profiles were extracted from the 2D gels b and f, respectively. The production and consumption zones of the 2D profiles were in c and g, respectively and the production and consumption zones of the 1D profiles were in d and h, respectively. The dotted line (c, d, g, h) represents the limit (zero) between production (positive values) and consumption (negative values). The black arrow on the October 2D Fe$_d$ gel indicated a potential macrofaunal burrow trace.

3.1.5 Pore water NO_3^- and NO_2^- availability

The 2D gels performed to analyze the spatial variability of NO_2^- and NO_3^- showed no detected concentrations in April and in October. No NO_3^- was also detected in pore waters of the 1D sediment cores. The 1D NO_2^- profile indicated concentrations closed to the detection limit in April with concentration of 2.1 ± 1.4 µmol L^{-1} in the 1st cm of sediment and a maximal concentration of 5.03 µmol L^{-1} reached at 3 cm depth. In October, the NO_2^- was not detected. No robust modelling was performed with NO_2^- (data not shown).

3.1.6 1D and 2D NH_4^+ distribution and modelling

Figure 6 illustrates the spatial variability of the NH_4^+ concentration and modelling using 1D (dark symbol) and 2D (white symbol) methods in April (Fig. 6 a-d) and October (Fig. 6 e-

h) 2019. In April the difference between the 1D and the 2D profiles was low (Fig. 6 a). The 1D profile decreased from 29.0 µmol L^{-1} to 18.6 µmol L^{-1} at 0.5 cm depth, then increased until 58.3 µmol L^{-1} in the 1st cm depth. Deeper the NH_4^+ concentration increased gradually until 386.6 µmol L^{-1} at 10.5 cm depth. The average 2D profile increased almost with the same range of concentration in the 1st cm of sediment, and increased deeper until 426.9 ± 12.6 µmol L^{-1} at 10 cm depth. The modelling indicated negative NH_4^+ top fluxes; 1D -1.61E^{-04} µmol m^{-2} d^{-1} and 2D -7.49E^{-05} µmol m^{-2} d^{-1}. Globally, one main consumption zone was found from the surface to ~ 1.5 cm depth with the 1D modelling (-1.21E^{-03} nmol cm^{-3} s^{-1}; Fig. 6 d) and from the surface to 3 cm depth with the 2D modelling (-4.09E^{-04} nmol cm^{-3} s^{-1}; Fig. 6 c). Globally, one main production zone was found below 1.5 cm depth with the 1D modelling (1.22E^{-03} nmol cm^{-3} s^{-1}; Fig. 6 c) and below 3 cm with the 2D modelling (3.01E^{-04} nmol cm^{-3} s^{-1}; Fig. 6 c).

In October, the 1D profile increased between 6.7 µmol L^{-1} to 56.2 µmol L^{-1} in the first 2.25 cm depth, then increased strongly deeper until 648.7 µmol L^{-1} at 7.5 cm depth then decreased (515.3 µmol L^{-1}) and increased again until 644.3 µmol L^{-1} at 10.5 cm depth (Fig. 6 e). The average 2D profile increased almost with the same range of NH_4^+ concentration in the two first centimeters, then increased until 589.6 ± 22.3 µmol L^{-1} at 10 cm depth. The modelling indicated negative 1D NH_4^+ top fluxes; 1D -7.15E^{-05} µmol m^{-2} d^{-1}. No 2D NH_4^+ top flux was suggested due to the uncertainty of the positioning of the interface. One main consumption zone was found from the surface to ~ 4 cm depth with the 1D (-7.65E^{-03} nmol cm^{-3} s^{-1}) and 2D (-1.09E^{-03} nmol cm^{-3} s^{-1}) modelling. The production zone was below 4 cm depth with the 1D modelling (5.47E^{-03} nmol cm^{-3} s^{-1}) and below 5 cm depth with the 2D modelling (7.19E^{-04} nmol cm^{-3} s^{-1}).

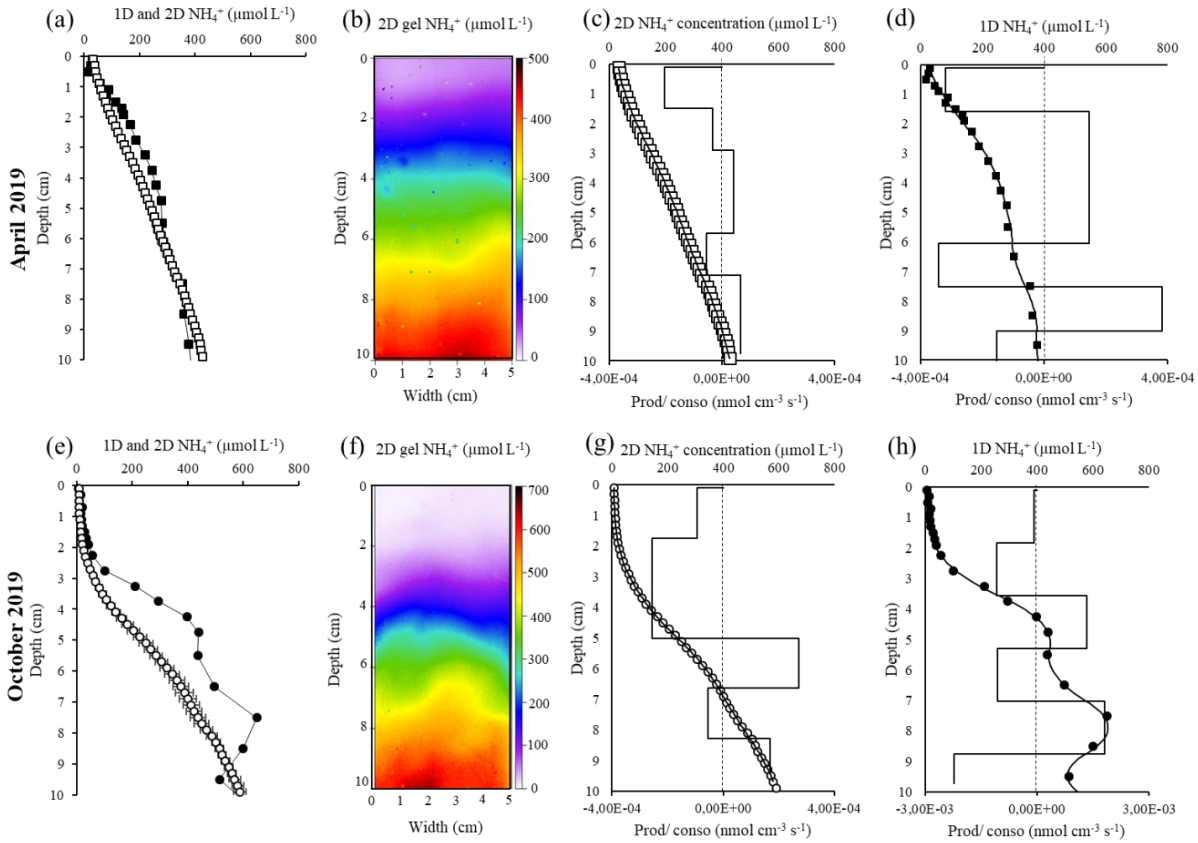

Figure 6: 1D and 2D NH_4^+ profiles and associated modelling from (a-d) April and (e-h) October. (a, e) 1D profiles (dark symbol) and 2D profiles (white symbol). The average ± standard deviation of the 2D profiles were extracted from the 2D gels b and f, respectively. The production and consumption zones of the 2D profiles were in c and g, respectively and the production and consumption zones of the 1D profiles were in d and h, respectively. The dotted line (c, d, g, h) represents the limit (zero) between production (positive values) and consumption (negative values).

3.1.7 1D and 2D DRP distribution and modelling

Figure 7 illustrates the spatial variability of the DRP concentration and modelling using 1D (white symbol) and 2D (black symbol) methods in April (Fig. 7 a-d) and October (Fig. 7 e-h) 2019. In April the difference between the 1D and the 2D profiles was high (Fig. 7 a). The average 2D profile stayed stable between 1.2 ± 0.1 µmol L^{-1} to 6.6 ± 0.5 µmol L^{-1} in the first 4 cm depth, then slightly increased 6.1 ± 0.2 µmol L^{-1} at 10 cm depth. The modelling indicated a positive DRP top flux 2D 5.51E^{-07} µmol m^{-2} d^{-1}. No estimate of the 1D DRP top flux was suggested. Globally, a low consumption zone was found all along the 1D profile modelling (-6.14E^{-06} nmol cm^{-3} s^{-1}; Fig. 7 d) and from the surface to 2 cm depth with the 2D modelling (-9.67E^{-06} nmol cm^{-3} s^{-1}; Fig. 7 c). One main production zone was found from 2 to 4 cm depth with the 2D modelling (9.37E^{-06} nmol cm^{-3} s^{-1}; Fig. 7 c).

In October, the 1D and 2D profiles showed again a high difference (Fig. 7 e). The average 2D profile was stable between 2.6 ± 0.1 µmol L^{-1} to 5.0 ± 0.9 µmol L^{-1} in the first 2 cm, below the DRP increased until 125.8 ± 9.5 µmol L^{-1} at 10 cm depth (higher DRP concentrations visible on the 2D gel, the black arrow indicates a potential macrofaunal burrow trace; Fig. 7 f). The modelling indicated positive DRP top fluxes; 1D 2.12E^{-05} µmol m^{-2} d^{-1} and 2D 2.80E^{-07} µmol m^{-2} d^{-1}. One main consumption zone was found from the surface to ~ 5.5 cm depth with the 1D (-1.43^{-04} nmol cm^{-3} s^{-1}) and 2D (-9.83E^{-05} nmol cm^{-3} s^{-1}) modelling. The production zone was below 5.5 cm depth with the 1D (9.71E^{-05} nmol cm^{-3} s^{-1}) and the 2D (5.80E^{-05} nmol cm^{-3} s^{-1}) modelling.

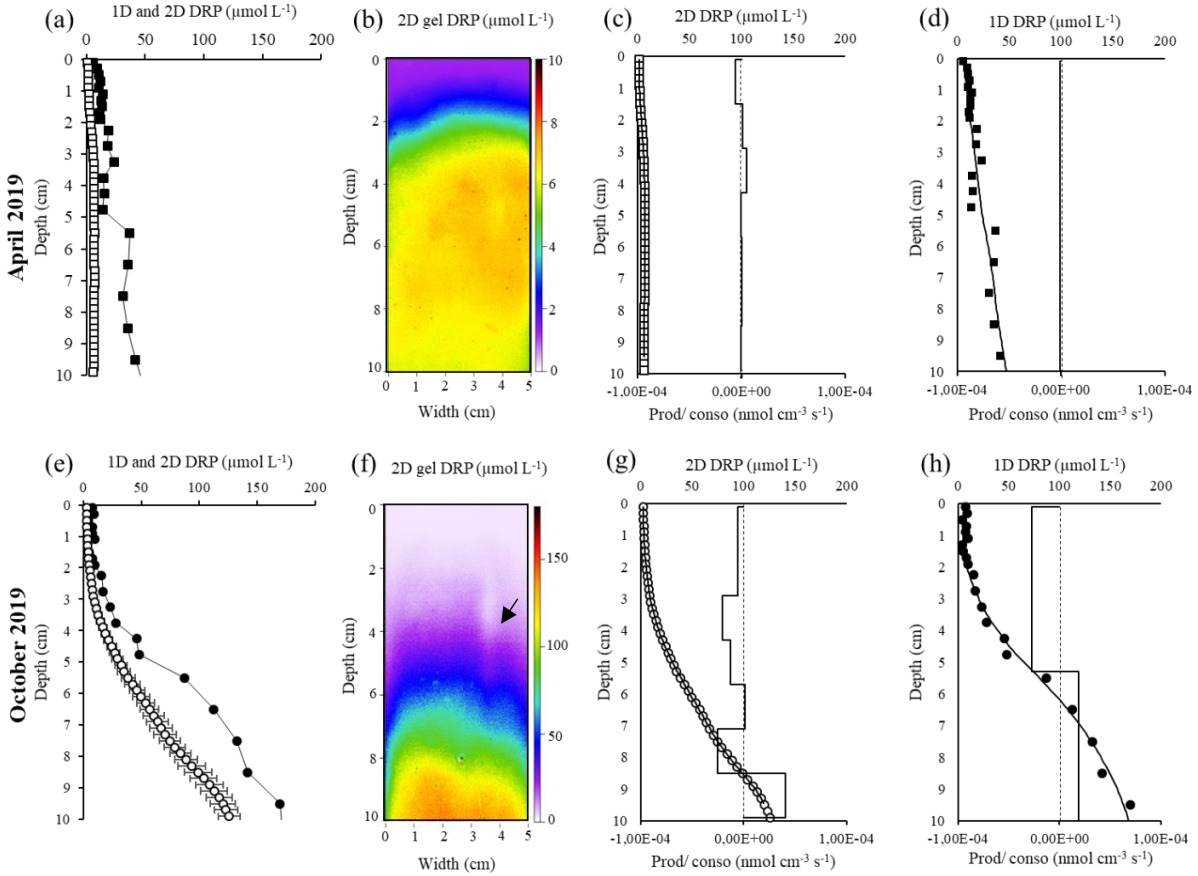

Figure 7: 1D and 2D dissolved reactive phosphorus profiles and associated modelling from (a-d) April 2019 and (e-h) October 2019. (a, e) 1D profiles (dark symbol) and 2D profiles (white symbol). The 2D profiles are the average DRP profile extracted from the 2D gels b and f, respectively. The average ± standard deviation of the 2D profiles were extracted from the 2D gels b and f, respectively. The production and consumption zones of the 2D profiles were in c and g, respectively and the production and consumption zones of the 1D profiles were in d and h, respectively. The dotted line (c, d, g, h) represents the limit (zero) between production (positive values) and consumption (negative values). The black arrow on the October 2D DRP gel indicated a potential macrofaunal burrow trace.

3.2 Microphytobenthos photosynthetic activity

3.2.1 *In situ* temporal photosynthetic activity dynamics

In April the maximal photosynthetic activity (yellowish profiles; Fig. 8 a) measured before the low tide hour produced until [O_2] 559 µmol L^{-1} (OPD = 1650 µm depth). The deeper OPD reached 1800 µm. The profiles measured closer to the low tide hour indicated a decreasing OPD. A profile was measured in dark condition (OPD = 1050 µm; dark profile, Fig. 8 b). The profiles measured after the low tide hour (blue profiles) indicated a lower oxygen concentration (until 390 µmol L^{-1}). In October the O_2 production was twice as high (Fig. 8 a, b). The maximal photosynthetic activity (yellowish profiles) measured before the low time hour produced until [O_2] 880 µmolL^{-1} (OPD = 2450 µm depth; Fig. 8 b). The deeper OPD reached 4000 µm. The profiles measured closer to the low tide hour indicated also a decreasing OPD. A profile was also measured in dark condition (OPD = 1800 µm; dark profile, Fig. 8 b). The profiles measured after the low tide hour (blue profiles) indicated a lower O_2 concentration (until 470 µmol L^{-1}).

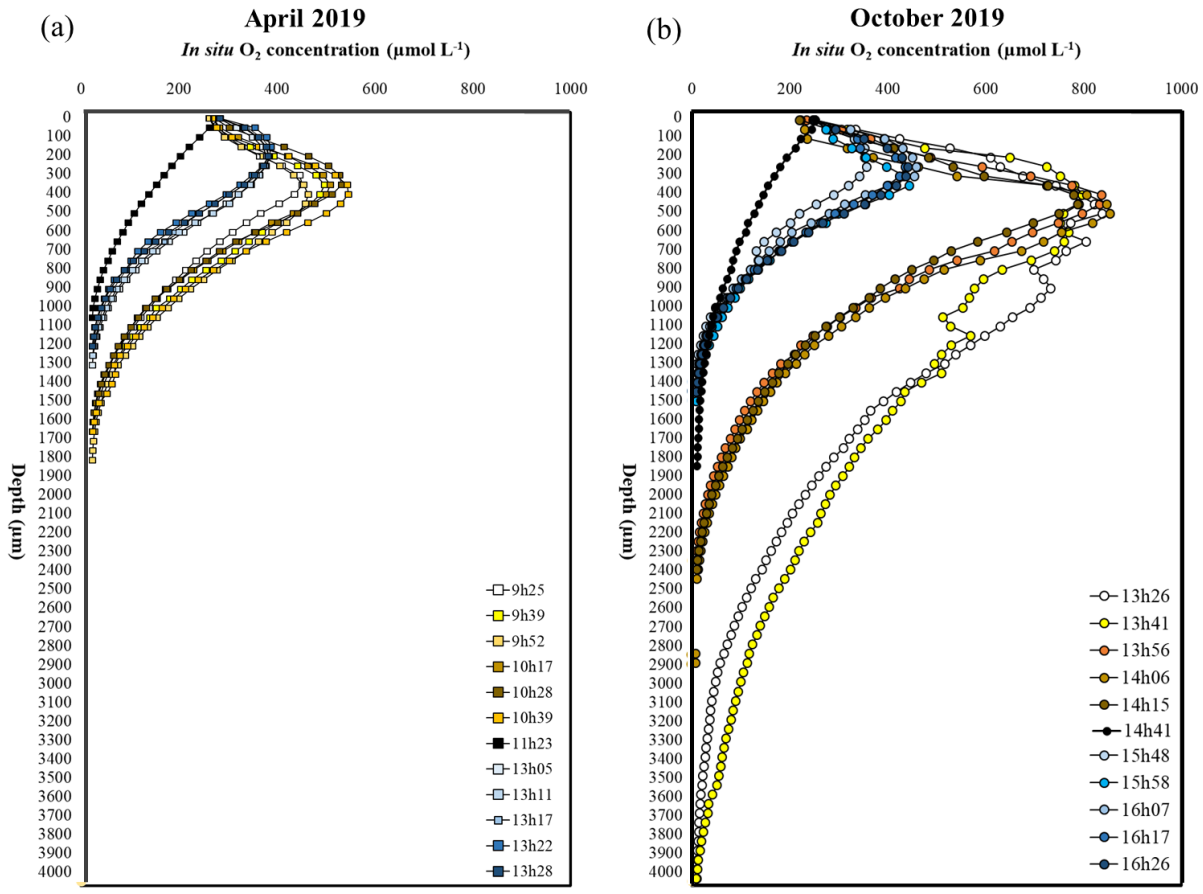

Figure 8: In situ temporal dynamics of MPB photosynthetic activity before and after low time hour in (a) April and in (b) October. The dark profiles were realized in situ in the dark. The yellowish profiles were performed before low time hour (10h 28 and 14h 15, respectively). The blue profiles were performed after low time hour. The vertical scale was in µm.

3.2.2 DOU and maximal photosynthetic production modelling

The DOU fluxes measured *in situ* in dark conditions (Table 1) were positive fluxes whereas the DOU fluxes measured *in situ* at light conditions were negative (Table 1). The DOU fluxes measured in the dark were similar in April and October. The DOU fluxes measured at light had a value three times higher in October. The same order of magnitude was observed for O_2 consumption zones. The O_2 production zones modeled with the maximal photosynthetic activity profile, showed a value twice higher in October.

Table 1: Modelling performed on two in situ profiles in light and dark conditions in April and October. The low tide hour, in situ profiling hour and in situ temperature for O_2 profiling were indicated. One profile performed in the dark and one profile showing the maximal photosynthetic activity were selected for DOU fluxes, production and consumption zones modelling.

	April		October	
Light conditions	Light	Dark	Light	Dark
Low tide time	11h 07		15h 06	
In situ profiling time	10h 39		14h 06	
In situ T°C	15	15	18	18
OPD (mm)	1.45 ± 0.02 (n=12)	1.03 ± 0.003 (n=2)	2.31 ± 1.03 (n=11)	1.89 ± 0.06 (n=6)
Profile used	(n = 1; OPD = 1.65 mm)	(n = 1; OPD = 1.00 mm)	(n = 1; OPD = 2.45 mm)	(n = 1; OPD = 1.10 mm)
DOU (µmol m^{-2} d^{-1})	$-2.28E^{-02}$	$2.98E^{-02}$	$-7.63E^{-02}$	$3.53E^{-02}$
O_2 consumption (nmol cm^{-3} s^{-1})	$-1.40E^{-01}$	$-3.45E^{-02}$	$-3.83E^{-01}$	$-4.08E^{-02}$
O_2 production (nmol cm^{-3} s^{-1})	$1.66E^{-01}$		$4.72E^{-01}$	
Maximal [O_2] (µmol L^{-1})	559		880	

3.3 Benthic foraminiferal fauna

3.3.1 Foraminiferal vertical micro-distributions

The benthic foraminiferal vertical micro-distribution (CTG-labelling) showed drastic contrasted densities and a changing *Elphidium* species between April and October (Fig. 9). In April, the total density was very low reaching 92 individuals in the 1st cm depth (50 cm^{-3}). Three dominant species were identified: *Ammonia* sp. T6 (white, Fig. 9 a), *Haynesina germanica* (light grey, Fig. 9 a) and *Elphidium selseyense* (dark grey, Fig. 9 a). The vertical foraminiferal micro-distribution showed a bimodal trend with two peaks of density; in the 1st cm depth and from 5 to 10 cm depth, however the density remains low. In October, the total density was

higher in the 1st cm depth reaching 752 ind. 50 cm^{-3} (Fig. 9 b). Three species were also identified: *Ammonia* sp. T6, (white, Fig. 9 b), *Haynesina germanica* (light grey, Fig. 9 b) and *Elphidium oceanense* (dark grey, Fig. 9 b).The foraminiferal densities decreased with depth.

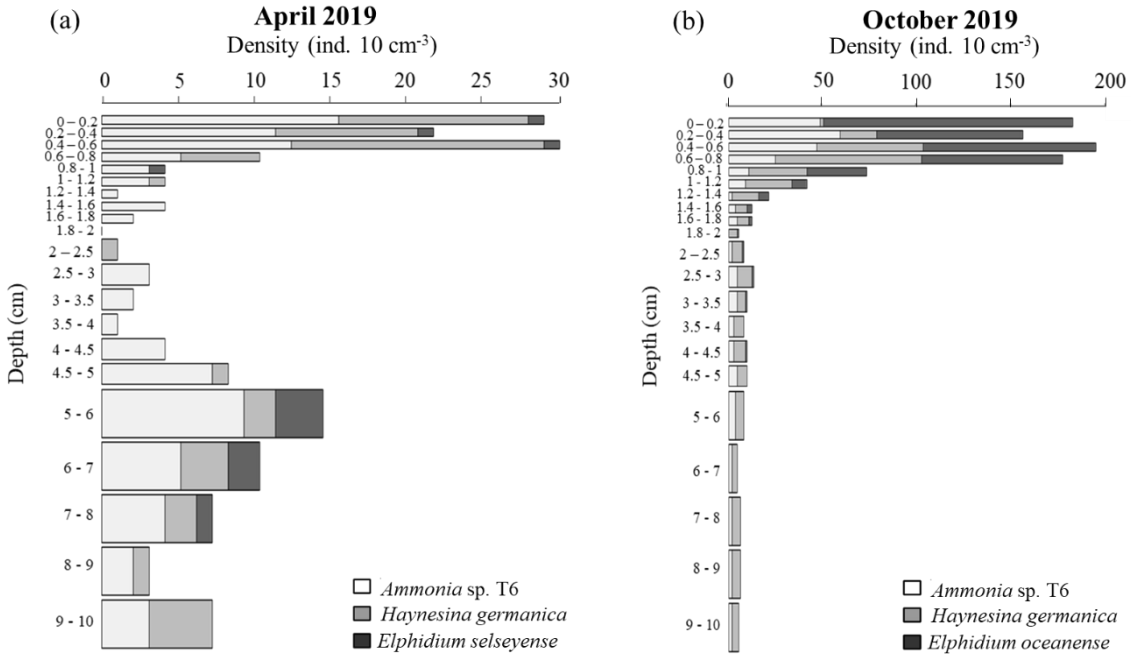

Figure 9: Living foraminiferal vertical micro-distribution (individuals per 10 cm^{-3}) in (a) April 2019 and in (b) October 2019 (CTG-labelling). The density scale was lower in April (30 ind. 10 cm^{-3}) than in October (200 ind. 10 cm^{-3}). Four dominant species were found (>150 µm fraction); Ammonia sp. T6 *(white), Haynesina germanica (light grey), Elphidium selseyense was found only in April (dark grey) and Elphidium Oceanense was found in October (dark grey).*

3.3.2 CellTracker-Green *versus* Rose Bengal methods

In this study the CellTracker-Green (CTG) was used for foraminiferal micro-distribution (Fig. 9). However, the MUDSURV biomonitoring survey at the three sampling stations uses Rose Bengal staining (RB). Table 2 indicated the densities of the living foraminifera counted in the 1st cm core with the two methods. In April, the counted living foraminifera differed between the two methods. Four times more living individuals were counted with the Rose Bengal method (92 *versus* 364 ind. 50 cm^{-3}). Living *Ammonia* sp. T6, *Haynesina germanica* and *Elphidium selseyense* were 3 to 4 times more abundant with RB., some individuals of *Elphidium oceanense* were counted in April with RB. In October, the difference between the two methods was lower (Table 2). The total density of counted living foraminifera in the 1st cm depth was similar (752 *versus* 627 ind. 50 cm^{-3}), however some differences were observed between species. *Ammonia* sp. T6 and *Haynesina germanica* were

1.5 to 2 times less abundant with the RB. There was no living *Elphidium selseyense* specimen and the number of living *Elphidium oceanense* was similar between the two methods.

Table 2: Comparison of foraminiferal individuals per 50 cm^{-3} of the 1st cm sediment from the station C (> 150 µm) by two staining methods; CellTracker Green (CTG) and Rose Bengal (RB). The Rose Bengal data of the stations A and B were added for meso-scale variability discussion.

	Staining methods	*Ammonia* sp. T6	*Haynesina germanica*	*Elphidium selseyense*	*Elphidium oceanense*	Total (ind. 50 cm^{-3})
April-C	CTG	46	42	4	0	92
	RB	142	188	13	21	364
October-C	CTG	168	171	0	413	752
	RB	107	87	0	433	627

4. Discussion

4.1 Multiple deployments to provide detailed spatiotemporal variability of redox elements and nutrients

4.1.1 Vertical distribution of redox species

Sediments of the intertidal Bourgneuf Bay mudflat are characterized by a high anaerobic OM remineralization. According to Froelich et al. (1979), anaerobic processes like the reduction of Mn oxides and Fe oxides take place below a thin oxic layer. However, in this study the depth of the Mn_d and Fe_d, production and consumption zones differed between the two sampling periods (Fig. 4 and 5). A summary of the calculated fluxes and production/ consumption zones is available in Annex 1 a and b, respectively. In April, the dissolved Mn_d and Fe_d shared the same production depths between the sediment surface to 4 cm depth with consumption zones deeper (Fig. 4 and 5). Whereas in October, the Mn_d production was constrained from the surface to 2 cm depth and the Fe_d production zone was from 2 to 6 cm depth. Therefore, a decoupling of the Mn_d and Fe_d production zones was observed in October. It could be explained by the expected succession of available terminal electron acceptors yielding the maximum energy as predicted by the theory (Froelich et al., 1979) which was well established in October but not in April. The mudflat topography and sedimentation rate were not measured in our study, however a flood deposit of a layer with a thickness of 5 to 10 cm on mudflats has frequently been reported for the French Atlantic coast (Goubert et al., 2010; Thibault de Chanvalon et al., 2016). In February, the flood deposition could represent an important stock of oxidants that are likely to fuel transient diagenesis for several months

(Thibault de Chanvalon et al., 2016). In October, the maximal Fe_d concentration and the production zone (2-6 cm depth; Fig 5 f, g) would be limited by the increasing of sulfato-reduction process taking place from ~ 7 cm depth (Annex 2 b) (Taillefert et al., 2007). The increase in anaerobic processes was also shown by the higher alkalinity values at these depths in October (Fig. 1 d; Annex 3 c). In April, the Fe_d concentration zone was deeper (Fig. 5 f), might suggesting that the sulfato-reduction zone was almost absent in the 10 first centimeters of sediment and was probably deeper (Annex 2 a).

4.1.2 Spatial variability of redox elements at decametric and decimetric scales

The used of the combination of 1D and 2D methods revealed the spatial heterogeneity of the Mn_d and Fe_d at decimetric-scale (within the same station) (Fig. 4 and 5). At decametric scale (~ 10 m), the 1D profiles performed at the stations A (blue triangle), B (green square) and C (grey circle) are available in Annex 3. In April, the 1D and average 2D Mn_d concentration profiles and fluxes highly differed (Fig. 4 a-d; Annex 1 b). At decametric scale, the 1D Mn_d profile at the station B (Annex 3 c) was similar to the average 2D Mn_d profile at the station C. This observation might suggest a higher spatial heterogeneity at decimetric scale. Indeed, the difference observed between the 1D profile of the C core and the average profile obtained from the 2D Mn_d gels (spaced a few tens of centimeters apart) was as large as the difference observed between the 1D profiles from A, B and C cores (spaced from 10 m apart). Therefore, there was no larger heterogeneity at the decametric scale. Moreover, heterogeneity could occur on a smaller scale than the decimetric scale. The presence of macrofaunal burrows (only visible on the 2D Fe_d and DRP gels (Fig. 5 f and Fig. 7 f) can generated an average concentration profile and an associated standard deviation showing less variability at the 2D gel-scale compared to the difference between the 1D profiles at decametric scale. This would suggest that the heterogeneity occurred mainly at the decimetric scale. Conversely in low water period (October), the Mn_d profiles showed similar trend and concentrations, suggesting homogeneous benthic properties for Mn (Fig. 4 e-h; Annex 1 b).

The 1D and average 2D Fe_d concentration profiles at the station C and fluxes differed laterally in April (Fig. 5) and vertically in October as discussed previously. Moreover, a vertical discoloration on the 2D Fe_d gel in October (black arrow; Fig. 5 f) targets a potential trace of macrofaunal burrow (as observed on other gel images in Thibault de Chanvalon et al., 2015) increasing the sediment heterogeneity at decimetric scale. In April, the 1D Fe_d profiles at decametric scale (Annex 3 f) showed shifted concentration peaks conversely to the average 2D profile showing lower Fe_d concentrations (Fig. 5 b). In October, the 1D Fe_d profiles at

decametric scale also present contrasted vertical distributions (Annex 3 f). Finally, the vertical heterogeneity of the Fe_d distributions was very high in both April and October at decametric scale (depth of appearance of the Fe_d, position of the peak, and maximal concentrations). The spatial variability of 1D SO_4^{2-} profiles at decametric scale indicated similar trend profiles in April, excepted at the station B showing larger vertical fluctuations (Annex 3 k, l). In October, the 1D SO_4^{2-} profiles at decametric scale indicated similar trend profiles with an increased concentration at ~ 7 cm depth (Annex 3 l).

4.1.3 Spatial variability of nutrients (NH_4^+ and DRP)

The used of the combination of 1D and 2D methods revealed the spatial heterogeneity of the NH_4^+ at decimetric and decametric scales (Fig. 6; Annex 3 g-h). In April, the 1D and average 2D NH_4^+ concentration profiles were similar (Fig. 6 a-d), whereas in October the decimetric scale was higher (Fig. 6 e-h). In April, the 1D concentration profiles where lower at the stations A and B compared to the station C, whereas in October, the 1D concentration profiles of the stations A and B where similar to the 2D average profile. These observations might suggest that the spatial heterogeneity was higher at decametric scale in post-flooding period and the spatial heterogeneity was higher at decimetric scale in stabilized summer period. The NH_4^+ spatial variability was also visible through fluxes, especially in October where the 1D profile was negative and the average 2D profile was positive. Moreover, the NH_4^+ production was higher (Annex 1 a-b).

The used of the combined 1D and 2D methods also revealed the spatial heterogeneity of the DRP at decimetric and decametric scales (Fig. 7; Annex 3 i-j). In April and October, the 1D DRP profiles were higher than the 2D average profiles, this would suggest a high spatial heterogeneity at decimetric scale at the two periods. Moreover, as the 2D Fe_d average concentration profile, a macrofaunal burrow (black arrow; Fig. 7 f) was visible on the 2D DRP image. In the same way, the DRP average concentration profile and associated standard deviation showed less variability at the 2D gel-scale compared to the difference between the 1D profiles at decametric scale. This would suggest that the heterogeneity occurred mainly at the decimetric scale. However, in April the spatial heterogeneity at decametric scale was low, indeed the three 1D DRP profiles were similar (Annex 3 i). In October, the spatial heterogeneity at decametric scale was higher as the 1D profile of the station B was similar to the 2D average profile from the station C (Fig. 7 f; Annex 3 j).

Finally, the redox spatial variability differed between the two hydrological contrasted periods. Indeed, the spatial variability of redox elements Mn, Fe and SO_4^{2-} seemed higher at decametric scale in April, whereas in October Mn and SO_4^{2-} would indicate lower variability excepted Fe showing high vertical distribution variability. At decimetric scale, the spatial variability of Mn and Fe were higher in April and lower in October. Concerning nutrients, the spatial variability at decimetric and decametric scales was high in October. Conversely in April, NH_4^+ concentration profiles were homogeneous at decimetric scale and heterogeneous at decametric scale, the reverse was observed for DRP.

4.2 Combined influence of the tidal pump fueled by contrasted hydrological periods

4.2.1 Linking tidal dynamics of O_2 with the MPB photosynthetic activity

Micro-scale variations of O_2 concentration at the sediment surface are linked to the tidal cycles (Delgard et al., 2012). During low tide, the O_2 concentration and production fluctuated with the MPB photosynthetic activity in the uppermost millimeters of the sediment surface in ~ 4 hours (Fig. 8 a, b; Table 1). At ebb tide, the benthic O_2 concentration and production increased deeper by approximately 500 µm in sediments until low tide time. At rising time, the peak of O_2 concentration decreased (~ divided by a factor 2) and increase towards the surface by approximately 200 µm (Fig 8; Table 1). In this study, irradiance was not measured during O_2 profiling. According to previous literacy, the fluctuation in photosynthetic activity is linked to the endogenous vertical migratory movement of diatom cells (epipelic life-form) impacted by irradiance (Serôdio et al., 1997; Guarini et al., 2000; Bartoli Marco et al., 2003; Brotas et al., 2003; Jesus et al., 2009; Walpersdorf et al., 2017; Pniewski et al., 2015; Prins et al., 2020). Namely, the cells migrate upward to the surface at ebb tide, then the cell migrate deeper in sediment before incoming tide (Easley et al., 2005; Jesus et al., 2006, 2009; Brito et al., 2009; Serôdio et al., 2020). However, some previous studies showed that cells can migrate deeper in the sediment due to light stress, inducing photo-regulation response and an optimal depth (Jesus et al., 2006; Prins et al., 2020). Thus, our results (Fig. 8; Table 1) would suggest that at ebb tide the maximum photosynthetic activity occurred deeper in the sediment, to avoid inhibition of irradiation. Then with incoming tide, photosynthetic activity decreased and occurred closer to the surface. The study of Delgard et al., (2012) describes that at rising tide the O_2 concentration decreases in the oxic zone greater more than an hour before the arrival of the water (decreasing OPD) and illumination does not change.

4.2.2 The dynamics of reduced species and nutrient availability

The tidal pump generates hydrostatic pressure gradients at low tide inducing a seeping (negative fluxes) of anoxic pore waters and advection of pore waters through macrofaunal burrows and permeable sediments. This process is a major contributor of solute export from the sediment to the tidal channels (Billerbeck et al., 2006; Taillefert et al., 2007; Deborde et al., 2008; Abril et al., 2010; Delgard et al., 2012; Anschutz et al., 2019). The contrasted hydrological context fueled the dynamics in oscillatory redox elements generated by tidal pump. In this study the permeability of the sediment was not measured, however it is possible to suggest hypotheses about the permeability from the mean grained size measurements of the sediment (Burdige, 2006). In April, the flood deposit/ resuspension decreased the porosity at the sediment surface and deeper until 10 cm depth (Fig. 1 b). Some very coarse silt and very fine sand inputs were observed at the "La Coupelasse" site in post flooding period (see D50 in annex Chapter 3). This would indicate a higher permeability of the sediment. These coarser grained could suggest that pore water containing the dissolved chemical elements could circulate by advection in response to pressure gradients in the sediments (Janssen et al., 2005). On the contrary, the higher porosity at the sediment surface in October can indicate a more compacted sediment and constituted mainly of coarse silt (see D50 in annex Chapter 3). The finer gained sediment could induce a lower permeability. Thus in stabilized period, the pore water transport processes would be dominated by molecular diffusion, bioturbation and bioirrigation (Berner, 1980; Aller, 1982). Besides, macrofaunal activity could be higher in October (macrofaunal burrow trace; 2D Fe_d, DRP gels in October; Fig. 5 f; Fig. 6 f). It would be interesting to estimate the contribution of Fe_d and DRP bioirrigational fluxes to diffusive fluxes by the Savitsky-Golay Filter method (Thibault de Chanvalon et al., 2017) in further analyses (as presented in Chapter 3). The redox elements and nutrients fluxes calculated in this study were based on transport by molecular diffusion and not by transport by advection. Advective pore water fluxes provide a transport mechanism faster than diffusion (Huettel et al., 1998; McKee et al., 2004). We hypothesized that the advection process should play a minor role at "La Coupelasse" site, further analyses based on the calculation of sediment permeability and advection are required.

Ammonium and DRP are essential nutrients for benthic primary producers (Sundbäck and Granéli, 1988; Feuillet-Girard et al., 1997; Deborde et al., 2008; Oakes et al., 2020). In marine environments rich in OM, the production of DRP and NH_4^+ by sulfato-reduction is important because sulfato-reduction is a major process of OM degradation in depth. Moreover, DRP can be release in pore water by desorption when Fe oxides are reductively dissolved (Krom and Berner, 1980; Sundby et al., 1992; Anschutz et al., 1998, 2019). The general correlation between $[P]_{asc}$ and $[Fe]_{asc}$ ($R^2 > 0.6$) in April show a similar trend in October 2019 ($R^2 = 0.56$). This result confirm that P_{asc} was bound to Fe oxides, contrary to April that did not show significant linear correlation due to a bimodal distribution (Annex 4). Nevertheless, we observed a higher quantity of P_{asc} adsorbed on Fe_{asc} in April (for the group of points from 1 to 5.5 cm deep) than in October. This observation could indicate that different processes are involved than those observed by Thibault de Chanvalon et al., (2016) in the Les Brillantes mudflat after the flooding. This same trend was observed at the station A but not at station B (data not shown). In October, DRP increased with depth independently of Fe_d (decoupling of zones; Fig. 5 f and Fig. 7 f), which suggests the increasing contribution of the organic P source from OM remineralization according to depth (increasing sulfato-reduction, Annex 2 c). In April, the DRP concentration was very low and Fe_d remained high. Figure 10 shows the pattern of $[P]_{asc}/[Fe]_{asc}$, at the surface: $[P]_{asc}/[Fe]_{asc}$ ~ 0.1 in April and ~ 0.2 in October, indicating a progressive P enrichment of Fe oxides at the sediment surface in post-flooding period. Deeper in sediment the $[P]_{asc}/[Fe]_{asc}$ ratios were high (~ 0.3) compared to the previous studies summarized in Thibault de Chanvalon et al., (2016). These high ratios indicated that Fe oxides were saturated in P in April and October. Moreover, in case of redox oscillations the kinetics of Fe oxidation was higher than P adsorption (Thibault de Chanvalon et al., 2016). As a consequence, DRP produced in the deep sediment by the OM remineralization diffused towards the sediment surface, without to be retained by Fe oxides, to feed benthic primary producers. The low DRP concentrations observed in April (Fig. 8 (a-d); Annex 3 i) might suggest the DRP exhaustion by the tidal pump and primary producers.

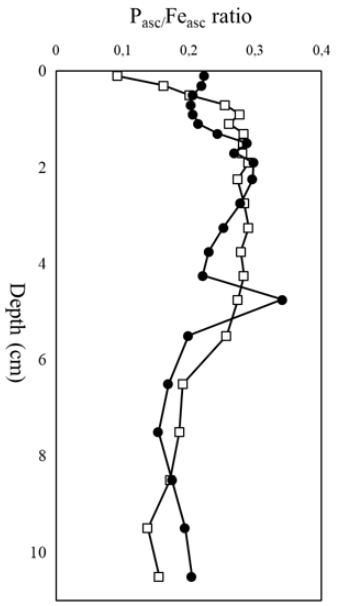

Figure 10: $[P]_{asc}/[Fe]_{asc}$ ratio according to depth in April (white square) and in October (black circle).

At the Bourgneuf Bay sampling site, NO_2^- and NO_3^- concentrations were closed to the detection limit or undetected during the year (see part 3.3.1). This would suggest that

denitrification is very high and NO_3^- rapidly consume by MPB and bacteria (Dalsgaard and Thamdrup, 2002; Risgaard-Petersen et al., 2003). Ammonium was more concentrated in deep sediment in April and was higher in October (Fig. 6; Annex 3 g, h). The linear correlations between NH_4^+ and DRP concentrations were good (R^2= 0.74 and R^2=0.85, respectively; Fig. 11 a). However, the slopes differed, especially lower in October. The NH_4^+ consumption could be more efficient in October, which could correspond to the increase in the MPB biomass observed during the stabilized late summer period (see Chapter 4). The N/P ratios (Fig. 11 b) indicated lower values than the Redfield ratio (16:1), excepted in April from ~ 4 to 6 cm depth. This would imply that nitrogen was mainly limiting at the sampling site and phosphorus in excess (Hillebrand and Sommer, 1997), excepted in April where DRP was very low.

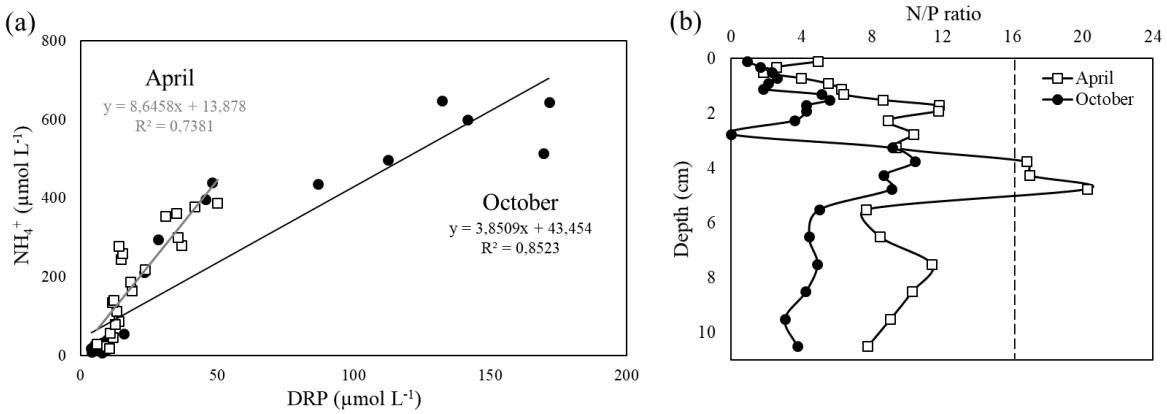

Figure 11: (a) Pore water concentration of NH_4^+ versus DRP (µmol L^{-1}) in April (white square) and in October (black circle), respectively with the equations and R^2 of their associated linear regressions. (b) The N/P ratio function of depth in April (white square) and in October (black) circle. The dotted line indicates the N/P Redfield ratio (16:1).

4.3 Foraminiferal micro-distribution (CTG); good bioindicators of the sediment stability in two hydrological contrasted periods

4.3.1 The vertical micro-distributions of living benthic foraminifera

The foraminiferal density and vertical micro-distribution profiles differed between the disturbed post-flooding and stabilized late summer periods (Fig. 9). In April, the foraminiferal density was low suggesting unfavorable conditions for foraminiferal development (e.g; discharge, rain, high tidal coefficient, lower porosity, currents, wind-storms). In these conditions only the two typical species inhabiting transitional environment were observed *Ammonia* sp. T6 and *Haynesina germanica* with some exception of few specimens of *Elphidium oceanense*. The vertical distribution in April showed a bimodal trend probably due to the sediment deposit/ resuspension of specimens after the flooding (Fig. 9 a). The same bimodal trend was shown in *Ammonia tepida* vertical distribution at Les Brillantes mudflat (Loire

estuary) explained partly by the impact of intense macrofaunal bioturbation (Thibault de Chanvalon et al., 2015). This explanation cannot be used in the present case, where the macrofaunal bioturbation existed but remained rare (few burrows were observed during slicing cores, personal observations). Thibault de Chanvalon et al., (2015) suggest an alternative mechanism that can explain our case. Along the first 3 cm depth, foraminifera are capable to migrate up to the oxygenated, organic-rich surface layers once they detect redox gradients, whereas in deeper sediment layers, they are no longer capable to reach the superficial oxygenated layer and remained blocked in depth. The vertical micro-distribution observed in April might reflect mixed residuals individuals in disturbed sediments. In October, the sedimentary conditions were stable, favored by several months of lower hydrodynamism and summer conditions (Fig. 1 a). Higher foraminiferal densities were observed in the 1st cm depth and then decreased strongly with depth (Fig. 9 b). The high density found at the sediment surface suggests favorable conditions for the development of living foraminiferal specimens particularly for *Elphidium oceanense*.

The time lag between the propagules and the adult stages depends on the growth rate which can take from 1 to 3 months (for *Ammonia tepida* in (Stouff, 1998)). In previous studies, two reproductive event triggers were reported: 1) reproductive events occurs under favorable conditions (stable sediments, high O_2 concentration and food availability) (Debenay et al., 2006; Alve and Goldstein, 2003; Hess and Jorissen, 2009; Mojtahid et al., 2016; LeKieffre et al., 2017), reproductive events occurs under stress conditions (unstable geochemical gradients, sub-anoxia, anthropogenic pollution) inducing a fast reproduction in the following days (Morvan et al., 2004; Ernst et al., 2006) leading to high densities. In this study, the April foraminiferal vertical distribution occurred two months after the Loire river flood and one month after the last wind-storm event (Fig. 2). Therefore, the sediment underwent strong physicochemical disturbances. The early spring 2019 was not described by a rapid reproduction event but by the increased mortality of the specimens (no reproduction, no juvenile observed in fraction 125 µm). In October, the stabilized sedimentary conditions induced a favorable reproductive period for three species, *Ammonia* sp. T6, *Haynesina germanica* and *Elphidium oceanense*. However, *Ammonia* sp. T6 and *Haynesina germanica* did not show a high reproduction event as already observed in previous years with densities exceeding 1000 ind. 50 cm^{-3} per species (see Chapter 3). The maximal reproduction event could have been reached in the previous months (August and September) or following months (November, December) as observed in previous years (see Chapter 3).

4.3.2 Comparison between Rose Bengal *versus* CellTracker Green methods

Rose Bengal was the first method used as a means to distinguish living from dead foraminifera in the 1950s. The principle consists to bound specific proteins to living cells to produce a magenta coloration of the specimen (Walton, 1952; Bernhard et al., 2006). CellTracker Green (CTG) probe forms a fluorescent compound when hydrolyzed with non-specific esterase, making accurate identification of living organisms under an epifluorescent microscope (Bernard et al., 2006). CTG is often used in ecological and experimental studies to differentiate living from dead benthic foraminifera (Bernhard et al., 2006; Nardelli et al., 2014; Langlet et al., 2014; Thibault de Chanvalon et al., 2015; Cesbron et al., 2016; Charrieau et al., 2018; Richirt et al., 2020; Choquel et al., 2021). The advantage of CTG in comparison with Rose Bengal is the efficiency on short time scales and therefore the limitation of false positives crucial to describe population dynamics in highly transient environments (Bernhard et al., 2006; Figueira et al., 2012; Pucci et al., 2009; Ross and Hallock, 2016; Melaniuk, 2021).

In this study, the difference in live staining and fluorescent specimens counted in the 1st cm depth with the two methods was striking (Table 2). The Rose Bengal staining overestimated the living specimens in April. However, the live specimens counted in October with both methods were in the same range. The difference of both methods in the determination of "live" specimens in the 1st cm depth in April can indicate that a part of foraminiferal specimens stained with Rose Bengal were actually dead. In October sediments indicated stable conditions, high foraminiferal densities at the surface are the result of the presence of abundant labile OM and oxygenated layer (Jorissen et al., 1995; Cesbron et al., 2016). Moreover, in October, smaller individuals were counted in the 125 µm fraction of the 1st cm depth: 37 ind. 50 cm^{-3} for *Ammonia tepida*, 34 ind. 50 cm^{-3} for *Haynesina germanica* and 28 ind. 50 cm^{-3} for *Elphidium oceanense*, no specimen of this fraction was observed below 1 cm depth. This suggests that a reproduction event occurred on the sediment surface. Some individuals were found in deep at the two months, this would be induced by downward transport by macrofaunal biomixing introducing living foraminifera into deeper sediment layers (Thibault de Chanvalon et al., 2015). Then, some specimens could be dormant after a prolonged presence in sub-oxic conditions, reducing their metabolism but still detected with CTG (Thibault de Chanvalon et al., 2015; LeKieffre et al., 2017).

The spatial variability (patchiness) observed with Rose Bengal specimens at decametric scale (between the three stations) in April was high (Annex 5), however the patchiness observed at decimetric-scale at the station C was higher between Rose Bengal and CTG specimens. Despite this spatial variability and the use of the two methods, we can observe a significant

distinction between the two *Elphidium* species. *Elphidium selseyense* was only present in Spring (Chapter 3). *Elphidium oceanense* was less represented but show a peak of reproduction in autumn (Chapter 3).

Previous studies insist to compare the two staining methods at each sampling site (Bernhard et al., 2006; Pucci et al., 2009; Figueira et al., 2012; Melaniuk et al., 2021). The offset between living and dead specimens can lead to inaccurate population turnover, complicating ecological interpretations in transient environments. Therefore, ecological and experimental studies are performed only with CTG labelling (Nardelli et al., 2014; Langlet et al., 2014; Thibault de Chanvalon et al., 2015; Cesbron et al., 2016; Charrieau et al., 2018; Richirt et al., 2020; Choquel et al., 2021).

4.3.3 O_2 respiration rates and alternative metabolisms

The foraminiferal O_2 respiration rate method is detailed in Annex 6 a, and the O_2 respiration rate per species is available in Annex 6 b. The contribution of foraminifera to benthic aerobic mineralization is detailed in Annex 7 a. The contribution of foraminifera to benthic aerobic mineralization was considered low (< 1 %) in the Bourgneuf Bay at the station C (Annex 7 b), as previously shown in coastal sediments (Geslin et al., 2011; Cesbron et al., 2016). In suboxic zones, some foraminifera species can survive with alternative respiration pathways as denitrification (Risgaard-Petersen et al., 2006). However, not all species (i.e. *Ammonia tepida*) are able to store intracellular nitrate to perform the denitrification (Pina-Ochoa et al., 2010; Glock, 2019). To our knowledge, no evidences of measured denitrification rate is available for *Haynesina germanica* and the two *Elphidium* species. According to the low seasonal availability of pore waters nitrate, denitrification would not be a preferential metabolic pathway in this environment conversely to other coastal environments where denitrification by foraminifera affects significantly the N cycle (Pina-Ochoa et al., 2010; Glock, 2019; Choquel et al., 2021).

Other alternative metabolisms pathways are suggested in previous studies allowing some species to benefit from alternative O_2 and nutrient sources. *Haynesina germanica* is known to performed active kleptoplastidy, producing O_2 by the functional sequester chloroplasts during several days (Jauffrais et al., 2016). Thus, *Haynesina germanica* would benefit from seasonal oxygenated and nutrient-rich micro-niches. NH_4^+ assimilation by mixotrophic (*Haynesina germanica*) and heterotrophic (*Ammonia tepida*) foraminiferal species was revealed (LeKieffre et al., 2018a; Jauffrais et al., 2019; Chronopoulou et al., 2019). The intracellular NH_4^+ pool in benthic foraminifera was never quantified, however NH_4^+ assimilation could be a favorable N

source (as suggested for planktonic foraminifera; (LeKieffre et al., 2018b)) for cell growth and development (Bird et al., 2020). Benthic foraminifera might compete with MPB for NH_4^+ availability in a fast N-turnover environment (Eyre et al., 2016). As NH_4^+, DRP can be assimilated by some species to build their cell membranes. Moreover, some foraminiferal species can concentrate intracellular DRP pool up to three orders-of-magnitude higher than in the ambient pore water in Peruvian oxygen minimum zone (Glock et al., 2020). This hypothesis suggests that foraminifera may play a role in the global phosphorus cycle and need to be further explored, particularly in intertidal environments.

5. Conclusion

The recycling of redox elements and nutrients in the Bourgneuf Bay mudflat appears to be influencing by the high winter hydrodynamism fueling transient diagenesis over contrasted months: in post-flooding and low water level periods. The 2D gel methods provide detailed vertical and lateral distributions of solute elements at decimetric scale showing homogeneous and heterogeneous zones. To capture the decametric heterogeneity complementary analyses using 1D profiles on different cores were performed. In post-flooding period, Mn and Fe share the same redox front due to recent sediment deposit/ resuspension. Conversely, in low water level period, the stabilized sediment shows the decoupling of the Mn and Fe redox fronts. Fe oxides are saturated with phosphorus at the two periods, inducing that phosphorus dynamics is mainly linked to the increase of deep anaerobic OM mineralization as sulfato-reduction process and less to the P release by the reductive dissolution of Fe oxides. The nitrogen turnover is high, overall NO_3^- and NH_4^+ are limiting nutrients for benthic primary producers. Ammonium and DRP are actively consumed at the sediment surface, excepted in post-flooding period where the DRP is depleted. The O_2 redox front is highly dynamic and influenced by tidal cycles. The increase of O_2 availability deeper in the sediment as in low water level period, allows more favorable oxygenated micro-environments for benthic foraminifera. Furthermore, the foraminifera responded strongly to these contrasted conditions. The CTG-labelling foraminiferal micro-distributions indicate the state of sediment instability through unfavorable *versus* favorable periods.

Bibliography

Abril, G., Commarieu, M.-V., Etcheber, H., Deborde, J., Deflandre, B., Živađinović, M. K., Chaillou, G., and Anschutz, P.: In vitro simulation of oxic/suboxic diagenesis in an estuarine fluid mud subjected to redox oscillations, Estuar. Coast. Shelf Sci., 88, 279–291, https://doi.org/10.1016/j.ecss.2010.04.003, 2010.

Aller, R. C.: The Effects of Macrobenthos on Chemical Properties of Marine Sediment and Overlying Water, in: Animal-Sediment Relations: The Biogenic Alteration of Sediments, edited by: McCall, P. L. and Tevesz, M. J. S., Springer US, Boston, MA, 53–102, https://doi.org/10.1007/978-1-4757-1317-6_2, 1982.

Aller, R. C.: Conceptual models of early diagenetic processes: The muddy seafloor as an unsteady, batch reactor, https://doi.org/info:doi/10.1357/0022240042880837, 2004.

Alve, E.: Colonization of new habitats by benthic foraminifera: a review, Earth-Sci. Rev., 46, 167–185, https://doi.org/10.1016/S0012-8252(99)00016-1, 1999.

Alve, E. and Goldstein, S. T.: Propagule transport as a key method of dispersal in benthic foraminifera (Protista), Limnol. Oceanogr., 48, 2163–2170, https://doi.org/10.4319/lo.2003.48.6.2163, 2003.

Alve, E. and Goldstein, S. T.: Dispersal, survival and delayed growth of benthic foraminiferal propagules, J. Sea Res., 63, 36–51, https://doi.org/10.1016/j.seares.2009.09.003, 2010.

Anschutz, P., Zhong, S., Sundby, B., Mucci, A., and Gobeil, C.: Burial efficiency of phosphorus and the geochemistry of iron in continental margin sediments, Limnol. Oceanogr., 43, 53–64, https://doi.org/10.4319/lo.1998.43.1.0053, 1998.

Anschutz, P., Dedieu, K., Desmazes, F., and Chaillou, G.: Speciation, oxidation state, and reactivity of particulate manganese in marine sediments - ScienceDirect, Chem. Geol., 2005.

Anschutz, P., Bouchet, S., Abril, G., Bridou, R., Tessier, E., and Amouroux, D.: In vitro simulation of oscillatory redox conditions in intertidal sediments: N, Mn, Fe, and P coupling, Cont. Shelf Res., 177, 33–41, https://doi.org/10.1016/j.csr.2019.03.007, 2019.

Armynot du Châtelet, É. and Debenay, J.-P.: The anthropogenic impact on the western French coasts as revealed by foraminifera: A review, Rev. Micropaléontologie, 53, 129–137, https://doi.org/10.1016/j.revmic.2009.11.002, 2010.

Bartoli Marco, Nizzoli Daniele, and Viaroli Pierluigi: Microphytobenthos activity and fluxes at the sediment-water interface: interactions and spatial variability, Aquat. Ecol., 37, 2003.

Bennett, W. W., Welsh, D. T., Serriere, A., Panther, J. G., and Teasdale, P. R.: A colorimetric DET technique for the high-resolution measurement of two-dimensional alkalinity distributions in sediment porewaters, Chemosphere, 119, 547–552, https://doi.org/10.1016/j.chemosphere.2014.07.042, 2015.

Berg, P., Risgaard-Petersen, N., and Rysgaard, S.: Interpretation of measured concentration profiles in sediment pore water, Limnol. Oceanogr., 43, 1500–1510, https://doi.org/10.4319/lo.1998.43.7.1500, 1998.

Berner, R. A.: Early Diagenesis: A Theoretical Approach, Princeton University Press, 256 pp., 1980.

Bernhard, J. M., Ostermann, D. R., Williams, D. S., and Blanks, J. K.: Comparison of two methods to identify live benthic foraminifera: A test between Rose Bengal and CellTracker Green with implications for stable isotope paleoreconstructions: Foraminifera viability method comparison, Paleoceanography, 21, https://doi.org/10.1029/2006PA001290, 2006.

Billerbeck, M., Werner, U., Polerecky, L., Walpersdorf, E., deBeer, D., and Huettel, M.: Surficial and deep pore water circulation governs spatial and temporal scales of nutrient recycling in intertidal sand flat sediment, Mar. Ecol. Prog. Ser., 326, 61–76, https://doi.org/10.3354/meps326061, 2006.

Brito, A., Newton, A., Tett, P., and Fernandes, T. F.: Temporal and spatial variability of microphytobenthos in a shallow lagoon: Ria Formosa (Portugal), Estuar. Coast. Shelf Sci., 83, 67–76, https://doi.org/10.1016/j.ecss.2009.03.023, 2009.

Brotas, V., Risgaard-Petersen, N., Serôdio, J., Ottosen, L., Dalsgaard, T., and Ribeiro, L.: In situ measurements of photosynthetic activity and respiration of intertidal benthic microalgal communities undergoing vertical migration, Ophelia, 57, 13–26, https://doi.org/10.1080/00785236.2003.10409502, 2003.

Burdige, D. J.: Geochemistry of Marine Sediments, Princeton University Press, 629 pp., 2006.

Cesbron, F., Metzger, E., Launeau, P., Deflandre, B., Delgard, M.-L., Thibault de Chanvalon, A., Geslin, E., Anschutz, P., and Jézéquel, D.: Simultaneous 2D Imaging of Dissolved Iron and Reactive Phosphorus in Sediment Porewaters by Thin-Film and Hyperspectral Methods, Environ. Sci. Technol., 48, 2816–2826, https://doi.org/10.1021/es404724r, 2014.

Cesbron, F., Geslin, E., Jorissen, F. J., Delgard, M. L., Charrieau, L., Deflandre, B., Jézéquel, D., Anschutz, P., and Metzger, E.: Vertical distribution and respiration rates of benthic foraminifera: Contribution to aerobic remineralization in intertidal mudflats covered by *Zostera noltei* meadows, Estuar. Coast. Shelf Sci., 179, 23–38, https://doi.org/10.1016/j.ecss.2015.12.005, 2016.

Charrieau, L. M., Filipsson, H. L., Ljung, K., Chierici, M., Knudsen, K. L., and Kritzberg, E.: The effects of multiple stressors on the distribution of coastal benthic foraminifera: A case study from the Skagerrak-Baltic Sea region, Mar. Micropaleontol., 139, 42–56, https://doi.org/10.1016/j.marmicro.2017.11.004, 2018.

Choquel, C., Geslin, E., Metzger, E., Filipsson, H. L., Risgaard-Petersen, N., Launeau, P., Giraud, M., Jauffrais, T., Jesus, B., and Mouret, A.: Denitrification by benthic foraminifera and their contribution to N-loss from a fjord environment, Biogeosciences, 18, 327–341, https://doi.org/10.5194/bg-18-327-2021, 2021.

Chronopoulou, P. M., Salonen, I., Bird, C., Reichart, G.-J., and Koho, K. A.: Metabarcoding insights into the trophic behaviour and identity of intertidal benthic foraminifera, Front. Microbiol., 10, https://doi.org/10.3389/fmicb.2019.01169, 2019.

Culver, S. J. and Buzas, M. A.: The effects of anthropogenic habitat disturbance, habitat destruction, and global warming on shallow marine benthic foraminifera, J. Foraminifer. Res., 25, 204–211, https://doi.org/10.2113/gsjfr.25.3.204, 1995.

Dalsgaard, T. and Thamdrup, B.: Factors Controlling Anaerobic Ammonium Oxidation with Nitrite in Marine Sediments, Appl. Environ. Microbiol., 68, 3802–3808, https://doi.org/10.1128/AEM.68.8.3802-3808.2002, 2002.

Debenay, J.-P.: Distribution des foraminifères vivants et des tests vides en Baie de Bourgneuf, PhD Thesis, 1978.

Debenay, J.-P., Bicchi, E., Goubert, E., and Armynot du Châtelet, E.: Spatio-temporal distribution of benthic foraminifera in relation to estuarine dynamics (Vie estuary, Vendée, W France), Estuar. Coast. Shelf Sci., 67, 181–197, https://doi.org/10.1016/j.ecss.2005.11.014, 2006.

Deborde, J., Anschutz, P., Auby, I., Glé, C., Commarieu, M.-V., Maurer, D., Lecroart, P., and Abril, G.: Role of tidal pumping on nutrient cycling in a temperate lagoon (Arcachon Bay, France), Mar. Chem., 109, 98–114, https://doi.org/10.1016/j.marchem.2007.12.007, 2008.

Delgard, M. L., Deflandre, B., Metzger, E., Nuzzio, D., Capo, S., Mouret, A., and Anschutz, P.: *In situ* study of short-term variations of redox species chemistry in intertidal permeable sediments of the Arcachon lagoon, Hydrobiologia, 699, 69–84, https://doi.org/10.1007/s10750-012-1154-5, 2012.

Dupuy, C., Mallet, C., Guizien, K., Montanié, H., Bréret, M., Mornet, F., Fontaine, C., Nérot, C., and Orvain, F.: Sequential resuspension of biofilm components (viruses, prokaryotes and protists) as measured by erodimetry experiments in the Brouage mudflat (French Atlantic coast), J. Sea Res., 92, 56–65, https://doi.org/10.1016/j.seares.2013.12.002, 2014.

Easley, J. T., Hymel, S. N., and Plante, C. J.: Temporal patterns of benthic microalgal migration on a semi-protected beach, Estuar. Coast. Shelf Sci., 64, 486–496, https://doi.org/10.1016/j.ecss.2005.03.013, 2005.

Ernst, S., Duijnstee, I., and van der Zwaan, B.: The dynamics of the benthic foraminiferal microhabitat: recovery after experimental disturbance, Mar. Micropaleontol., 46, 343–361, https://doi.org/10.1016/S0377-8398(02)00080-4, 2002.

Ernst, S. R., Morvan, J., Geslin, E., Le Bihan, A., and Jorissen, F. J.: Benthic foraminiferal response to experimentally induced Erika oil pollution, Mar. Micropaleontol., 61, 76–93, https://doi.org/10.1016/j.marmicro.2006.05.005, 2006.

Eyre, B. D., Oakes, J. M., and Middelburg, J. J.: Fate of microphytobenthos nitrogen in subtropical subtidal sediments: A 15N pulse-chase study, Limnol. Oceanogr., 61, 2108–2121, https://doi.org/10.1002/lno.10356, 2016.

Feuillet-Girard, M., Gouleau, D., Blanchard, G., and Joassard, L.: Nutrient fluxes on an intertidal mudflat in Marennes-Oléron Bay, and influence of the emersion period, Aquat. Living Resour., 10, 49–58, https://doi.org/10.1051/alr:1997005, 1997.

Figueira, B. O., Grenfell, H. R., Hayward, B. W., and Alfaro, A. C. Comparison of Rose Bengal and CellTracker Green staining for identification of live saltmarsh foraminifera, J. Foraminifer. Res., 42, 206–215, https://doi.org/10.2113/gsjfr.42.3.206, 2012.

Froelich, P. N., Klinkhammer, G. P., Bender, M. L., Luedtke, N. A., Heath, G. R., Cullen, D., Dauphin, P., Hammond, D., Hartman, B., and Maynard, V.: Early oxidation of organic matter

in pelagic sediments of the eastern equatorial Atlantic: suboxic diagenesis, Geochim. Cosmochim. Acta, 43, 1075–1090, https://doi.org/10.1016/0016-7037(79)90095-4, 1979.

Geslin, E., Risgaard-Petersen, N., Lombard, F., Metzger, E., Langlet, D., and Jorissen, F.: Oxygen respiration rates of benthic foraminifera as measured with oxygen microsensors, J. Exp. Mar. Biol. Ecol., 396, 108–114, https://doi.org/10.1016/j.jembe.2010.10.011, 2011.

Glock, N.: Metabolic preference of nitrate over oxygen as an electron acceptor in Foraminifera from the Peruvian oxygen minimum zone, Pnas Proc. Natl. Acad. Sci. U. S. Am., 2019.

Glock, N., Romero, D., Roy, A. S., Woehle, C., Dale, A. W., Schönfeld, J., Wein, T., Weissenbach, J., and Dagan, T.: A hidden sedimentary phosphate pool inside benthic foraminifera from the Peruvian upwelling region might nucleate phosphogenesis, Geochim. Cosmochim. Acta, https://doi.org/10.1016/j.gca.2020.08.002, 2020.

Glud, R. N., Wenzhöfer, F., Tengberg, A., Middelboe, M., Oguri, K., and Kitazato, H.: Distribution of oxygen in surface sediments from central Sagami Bay, Japan: In situ measurements by microelectrodes and planar optodes, Deep Sea Res. Part Oceanogr. Res. Pap., 52, 1974–1987, https://doi.org/10.1016/j.dsr.2005.05.004, 2005.

Goubert, E., Frenod, E., Peeters, P., Thuillier, P., Vested, H. J., and Bernard, N.: Utilisation de données altimétriques (Altus) dans la caractérisation de climats hydrodynamiques contrôlant le fonctionnement hydrosédimentaire d'une vasière intertidale : cas de l'estuaire de la Vilaine (Bretagne, France), Rev. Paralia, 3, 6.1-6.15, https://doi.org/10.5150/revue-paralia.2010.006, 2010.

Griess, P.: Bemerkungen zu der Abhandlung der HH. Weselsky und Benedikt „Ueber einige Azoverbindungen", Berichte Dtsch. Chem. Ges., 12, 426–428, https://doi.org/10.1002/cber.187901201117, 1879.

Guarini, J.-M., Blanchard, G. F., Gros, P., Gouleau, D., and Bacher, C.: Dynamic model of the short-term variability of microphytobenthic biomass on temperate intertidal mudflats, Mar. Ecol. Prog. Ser., 195, 291–303, https://doi.org/10.3354/meps195291, 2000.

Ha, H. J., Kim, H., Noh, J., Ha, H. K., and Khim, J. S.: Rainfall effects on the erodibility of sediment and microphytobenthos in the intertidal flat, Environ. Pollut., 242, 2051–2058, https://doi.org/10.1016/j.envpol.2018.06.079, 2018.

Harwood, J. E. and Kühn, A. L.: A colorimetric method for ammonia in natural waters, Water Res., 4, 805–811, https://doi.org/10.1016/0043-1354(70)90037-0, 1970.

Hess, S. and Jorissen, F. J.: Distribution patterns of living benthic foraminifera from Cap Breton canyon, Bay of Biscay: Faunal response to sediment instability, Deep Sea Res. Part Oceanogr. Res. Pap., 56, 1555–1578, https://doi.org/10.1016/j.dsr.2009.04.003, 2009.

Hillebrand, H. and Sommer, U.: Response of epilithic microphytobenthos of the Western Baltic Sea to *in situ* experiments with nutrient enrichment, Mar. Ecol. Prog. Ser., 160, 35–46, https://doi.org/10.3354/meps160035, 1997.

Huettel, M., Ziebis, W., Forster, S., and Luther, G. W.: Advective Transport Affecting Metal and Nutrient Distributions and Interfacial Fluxes in Permeable Sediments, Geochim. Cosmochim. Acta, 62, 613–631, https://doi.org/10.1016/S0016-7037(97)00371-2, 1998.

Hyacinthe, C., Anschutz, P., Carbonel, P., Jouanneau, J.-M., and Jorissen, F. J.: Early diagenetic processes in the muddy sediments of the Bay of Biscay, Mar. Geol., 177, 111–128, https://doi.org/10.1016/S0025-3227(01)00127-X, 2001.

Janssen, F., Huettel, M., and Witte, U.: Pore-water advection and solute fluxes in permeable marine sediments (II): Benthic respiration at three sandy sites with different permeabilities (German Bight, North Sea), Limnol. Oceanogr., 50, 779–792, https://doi.org/10.4319/lo.2005.50.3.0779, 2005.

Jauffrais, T., Jesus, B., Metzger, E., Mouget, J.-L., Jorissen, F., and Geslin, E.: Effect of light on photosynthetic efficiency of sequestered chloroplasts in intertidal benthic foraminifera (*Haynesina germanica* and *Ammonia tepida*), Biogeosciences, 13, 2715–2726, https://doi.org/10.5194/bg-13-2715-2016, 2016.

Jauffrais, T., LeKieffre, C., Schweizer, M., Jesus, B., Metzger, E., and Geslin, E.: Response of a kleptoplastidic foraminifer to heterotrophic starvation: photosynthesis and lipid droplet biogenesis, FEMS Microbiol. Ecol., 95, https://doi.org/10.1093/femsec/fiz046, 2019.

Jesus, B., Mendes, C. R., Brotas, V., and Paterson, D. M.: Effect of sediment type on microphytobenthos vertical distribution: Modelling the productive biomass and improving ground truth measurements, J. Exp. Mar. Biol. Ecol., 332, 60–74, https://doi.org/10.1016/j.jembe.2005.11.005, 2006.

Jesus, B., Brotas, V., Ribeiro, L., Mendes, C. R., Cartaxana, P., and Paterson, D. M.: Adaptations of microphytobenthos assemblages to sediment type and tidal position, Cont. Shelf Res., 29, 1624–1634, https://doi.org/10.1016/j.csr.2009.05.006, 2009.

Jézéquel, D., Brayner, R., Metzger, E., Viollier, E., Prévot, F., and Fiévet, F.: Two-dimensional determination of dissolved iron and sulfur species in marine sediment pore-waters by thin-film based imaging. Thau lagoon (France), Estuar. Coast. Shelf Sci., 72, 420–431, https://doi.org/10.1016/j.ecss.2006.11.031, 2007.

Jorissen, F. J., de Stigter, H. C., and Widmark, J. G. V.: A conceptual model explaining benthic foraminiferal microhabitats, Mar. Micropaleontol., 26, 3–15, https://doi.org/10.1016/0377-8398(95)00047-X, 1995.

Koho, K. A. and Piña-Ochoa, E.: Benthic Foraminifera: Inhabitants of Low-Oxygen Environments, in: Anoxia: Evidence for Eukaryote Survival and Paleontological Strategies, edited by: Altenbach, A. V., Bernhard, J. M., and Seckbach, J., Springer Netherlands, Dordrecht, 249–285, https://doi.org/10.1007/978-94-007-1896-8_14, 2012.

Koho, K. A., Kouwenhoven, T. J., de Stigter, H. C., and van der Zwaan, G. J.: Benthic foraminifera in the Nazaré Canyon, Portuguese continental margin: Sedimentary environments and disturbance, Mar. Micropaleontol., 66, 27–51, https://doi.org/10.1016/j.marmicro.2007.07.005, 2007.

Krom, M. D. and Berner, R. A.: Adsorption of phosphate in anoxic marine sediments1, Limnol. Oceanogr., 25, 797–806, https://doi.org/10.4319/lo.1980.25.5.0797, 1980.

Langlet, D., Baal, C., Geslin, E., Metzger, E., Zuschin, M., Riedel, B., Risgaard-Petersen, N., Stachowitsch, M., and Jorissen, F. J.: Foraminiferal species responses to in situ, experimentally

induced anoxia in the Adriatic Sea, Biogeosciences, 11, 1775–1797, https://doi.org/10.5194/bg-11-1775-2014, 2014.

LeKieffre, C., Spangenberg, J. E., Mabilleau, G., Escrig, S., Meibom, A., and Geslin, E.: Surviving anoxia in marine sediments: The metabolic response of ubiquitous benthic foraminifera (*Ammonia tepida*), PLOS ONE, 12, e0177604, https://doi.org/10.1371/journal.pone.0177604, 2017.

LeKieffre, C., Bernhard, J. M., Mabilleau, G., Filipsson, H. L., Meibom, A., and Geslin, E.: An overview of cellular ultrastructure in benthic foraminifera: New observations of rotalid species in the context of existing literature, Mar. Micropaleontol., 138, 12–32, https://doi.org/10.1016/j.marmicro.2017.10.005, 2018a.

LeKieffre, C., Jauffrais, T., Geslin, E., Jesus, B., Bernhard, J. M., Giovani, M.-E., and Meibom, A.: Inorganic carbon and nitrogen assimilation in cellular compartments of a benthic kleptoplastic foraminifer, Sci. Rep., 8, 10140, https://doi.org/10.1038/s41598-018-28455-1, 2018b.

Li, Y.-H. and Gregory, S.: Diffusion of ions in sea water and in deep-sea sediments, 1974.

McKee, B. A., Aller, R. C., Allison, M. A., Bianchi, T. S., and Kineke, G. C.: Transport and transformation of dissolved and particulate materials on continental margins influenced by major rivers: benthic boundary layer and seabed processes, Cont. Shelf Res., 24, 899–926, https://doi.org/10.1016/j.csr.2004.02.009, 2004.

Melaniuk, K.: Effectiveness of Fluorescent Viability Assays in Studies of Arctic Cold Seep Foraminifera, Frontiers in Marine Science, https://doi.org/DOI:10.3389/fmars.2021.587748, 2021.

Méléder, V., Barillé, L., Rincé, Y., Morançais, M., Rosa, P., and Gaudin, P.: Spatio-temporal changes in microphytobenthos structure analysed by pigment composition in a macrotidal flat (Bourgneuf Bay, France), Mar. Ecol. Prog. Ser., 297, 83–99, https://doi.org/10.3354/meps297083, 2005.

Méléder, V., Rincé, Y., Barillé, L., Gaudin, P., and Rosa, P.: Spatiotemporal changes in microphytobenthos assemblages in a macrotidal flat (Bourgneuf Bay,France)1, J. Phycol., 43, 1177–1190, https://doi.org/10.1111/j.1529-8817.2007.00423.x, 2007.

Metzger, E., Thibault de Chanvalon, A., Cesbron, F., Barbe, A., Launeau, P., Jézéquel, D., and Mouret, A.: Simultaneous Nitrite/Nitrate Imagery at Millimeter Scale through the Water–Sediment Interface, Environ. Sci. Technol., 50, 8188–8195, https://doi.org/10.1021/acs.est.6b00187, 2016.

Metzger, E., Barbe, A., Cesbron, F., Thibault de Chanvalon, A., Jauffrais, T., Jézéquel, D., and Mouret, A.: Two-dimensional ammonium distribution in sediment pore waters using a new colorimetric diffusive equilibration in thin-film technique, Water Res. X, 2, 100023, https://doi.org/10.1016/j.wroa.2018.100023, 2019.

Mojtahid, M., Geslin, E., Coynel, A., Gorse, L., Vella, C., Davranche, A., Zozzolo, L., Blanchet, L., Bénéteau, E., and Maillet, G.: Spatial distribution of living (Rose Bengal stained) benthic foraminifera in the Loire estuary (western France), J. Sea Res., 118, 1–16, https://doi.org/10.1016/j.seares.2016.02.003, 2016.

Moncelon, R., Gouazé, M., Pineau, P., Bénéteau, E., Bréret, M., Philippine, O., Robin, F.-X., Dupuy, C., and Metzger, E.: Coupling between sediment biogeochemistry and phytoplankton development in a temperate freshwater marsh (Charente-Maritime, France): Evidence of temporal pattern, Water Res., 189, 116567, https://doi.org/10.1016/j.watres.2020.116567, 2021.

Moodley, L., Schaub, B., Van der Zwaan, G.J., Herman, P.M.J., Ecosystems Studies, and Spatial Ecology: Tolerance of benthic foraminifera (Protista : Sarcodina) to hydrogen sulphide, Mar. Ecol. Prog. Ser., 169, 77–86, https://doi.org/10.3354/meps169077, 1998.

Morvan, J., Cadre, V. L., Jorissen, F., and Debenay, J.-P.: Foraminifera as potential bio-indicators of the "Erika" oil spill in the Bay of Bourgneuf: Field and experimental studies, Aquat. Living Resour., 17, 317–322, https://doi.org/10.1051/alr:2004034, 2004.

Murray, J. W. and Alve, E.: Major aspects of formainiferal variability (standing crop and biomass) on a monthly scale in an intertidal zone, Journal of Foraminiferal Research, 2000.

Nardelli, M. P., Barras, C., Metzger, E., Mouret, A., Filipsson, H. L., Jorissen, F., and Geslin, E.: Experimental evidence for foraminiferal calcification under anoxia, Biogeosciences, 11, 4029–4038, https://doi.org/10.5194/bg-11-4029-2014, 2014.

Oakes, J. M., Riekenberg, P. M., and Eyre, B. D.: Assimilation and short-term processing of microphytobenthos nitrogen in intertidal sediments, Limnol. Oceanogr., 65, 2377–2389, https://doi.org/10.1002/lno.11459, 2020.

Pagès, A., Teasdale, P. R., Robertson, D., Bennett, W. W., Schäfer, J., and Welsh, D. T.: Representative measurement of two-dimensional reactive phosphate distributions and co-distributed iron(II) and sulfide in seagrass sediment porewaters, Chemosphere, 85, 1256–1261, https://doi.org/10.1016/j.chemosphere.2011.07.020, 2011.

Papaspyrou, S., Diz, P., García-Robledo, E., Corzo, A., and Jimenez-Arias, J.-L.: Benthic foraminiferal community changes and their relationship to environmental dynamics in intertidal muddy sediments (Bay of Cádiz, SW Spain), Mar. Ecol. Prog. Ser., 490, 121–135, https://doi.org/10.3354/meps10447, 2013.

Pina-Ochoa, E., Hogslund, S., Geslin, E., Cedhagen, T., Revsbech, N. P., Nielsen, L. P., Schweizer, M., Jorissen, F., Rysgaard, S., and Risgaard-Petersen, N.: Widespread occurrence of nitrate storage and denitrification among Foraminifera and Gromiida, Proc. Natl. Acad. Sci., 107, 1148–1153, https://doi.org/10.1073/pnas.0908440107, 2010.

Pniewski, F. F., Biskup, P., Bubak, I., Richard, P., Latała, A., and Blanchard, G.: Photo-regulation in microphytobenthos from intertidal mudflats and non-tidal coastal shallows, Estuar. Coast. Shelf Sci., 152, 153–161, https://doi.org/10.1016/j.ecss.2014.11.022, 2015.

Prins, A., Déléris, P., Hubas, C., and Jesus, B.: Effect of Light Intensity and Light Quality on Diatom Behavioral and Physiological Photoprotection, Front. Mar. Sci., 7, 203, https://doi.org/10.3389/fmars.2020.00203, 2020.

Pucci, F., Geslin, E., Barras, C., Morigi, C., Sabbatini, A., Negri, A., and Jorissen, F. J.: Survival of benthic foraminifera under hypoxic conditions: Results of an experimental study using the CellTracker Green method, Mar. Pollut. Bull., 59, 336–351, https://doi.org/10.1016/j.marpolbul.2009.08.015, 2009.

Redzuan, N. S. and Underwood, G. J. C.: The importance of weather and tides on the resuspension and deposition of microphytobenthos (MPB) on intertidal mudflats, Estuar. Coast. Shelf Sci., 251, 107190, https://doi.org/10.1016/j.ecss.2021.107190, 2021.

Revsbech, N. P.: An oxygen microsensor with a guard cathode, Limnol. Oceanogr., 34, 474–478, https://doi.org/10.4319/lo.1989.34.2.0474, 1989.

Richirt, J., Riedel, B., Mouret, A., Schweizer, M., Langlet, D., Seitaj, D., Meysman, F. J. R., Slomp, C. P., and Jorissen, F.: Foraminiferal community response to seasonal anoxia in Lake Grevelingen (the Netherlands), Biogeosciences, 2020.

Risgaard-Petersen, N., Nielsen, L. P., Rysgaard, S., Dalsgaard, T., and Meyer, R. L.: Application of the isotope pairing technique in sediments where anammox and denitrification coexist, Limnol. Oceanogr. Methods, 1, 63–73, https://doi.org/10.4319/lom.2003.1.63, 2003.

Risgaard-Petersen, N., Langezaal, A. M., Ingvardsen, S., Schmid, M. C., Jetten, M. S. M., Op den Camp, H. J. M., Derksen, J. W. M., Piña-Ochoa, E., Eriksson, S. P., Peter Nielsen, L., Peter Revsbech, N., Cedhagen, T., and van der Zwaan, G. J.: Evidence for complete denitrification in a benthic foraminifer, Nature, 443, 93–96, https://doi.org/10.1038/nature05070, 2006.

Robertson, D., Teasdale, P. R., and Welsh, D. T.: A novel gel-based technique for the high resolution, two-dimensional determination of iron (II) and sulfide in sediment, Limnol. Oceanogr. Methods, 6, 502–512, https://doi.org/10.4319/lom.2008.6.502, 2008.

Ross, B. J. and Hallock, P.: Dormancy in the Foraminifera: a review, J. Foraminifer. Res., 46, 358–368, https://doi.org/10.2113/gsjfr.46.4.358, 2016.

Roy, M., McManus, J., Goñi, M. A., Chase, Z., Borgeld, J. C., Wheatcroft, R. A., Muratli, J. M., Megowan, M. R., and Mix, A.: Reactive iron and manganese distributions in seabed sediments near small mountainous rivers off Oregon and California (USA), Cont. Shelf Res., 54, 67–79, https://doi.org/10.1016/j.csr.2012.12.012, 2013.

Santner, J., Larsen, M., Kreuzeder, A., and Glud, R. N.: Two decades of chemical imaging of solutes in sediments and soils – a review, Anal. Chim. Acta, 878, 9–42, https://doi.org/10.1016/j.aca.2015.02.006, 2015.

Sarazin, G., Michard, G., and Prevot, F.: A rapid and accurate spectroscopic method for alkalinity measurements in sea water samples, Water Res., 33, 290–294, https://doi.org/10.1016/S0043-1354(98)00168-7, 1999.

Serôdio, J., Silva, J. M. da, and Catarino, F.: Nondestructive Tracing of Migratory Rhythms of Intertidal Benthic Microalgae Using in Vivo Chlorophyll a Fluorescence1,2, J. Phycol., 33, 542–553, https://doi.org/10.1111/j.0022-3646.1997.00542.x, 1997.

Serôdio, J., Paterson, D. M., Meleder, V., and Vyverman, W.: Advances and Challenges in Microphytobenthos Research: From Cell Biology to Coastal Ecosystem Function, Frontiers Media SA, 311 pp., 2020.

Stockdale, A., Davison, W., and Zhang, H.: Micro-scale biogeochemical heterogeneity in sediments: A review of available technology and observed evidence, Earth-Sci. Rev., 92, 81–97, https://doi.org/10.1016/j.earscirev.2008.11.003, 2009.

Stouff, V.: Interet des elevages de foraminiferes en laboratoire : etudes biologiques et ultrastructurales, These de doctorat, Angers, 1998.

Sundbäck, K. and Granéli, W.: Influence of microphytobenthos on the nutrient flux between sediment and water: a laboratory study, Mar. Ecol. Prog. Ser., 43, 63–69, 1988.

Sundby, B.: Transient state diagenesis in continental margin muds, Mar. Chem., 102, 2–12, https://doi.org/10.1016/j.marchem.2005.09.016, 2006.

Sundby, B., Gobeil, C., Silverberg, N., and Alfonso, M.: The phosphorus cycle in coastal marine sediments, Limnol. Oceanogr., 37, 1129–1145, https://doi.org/10.4319/lo.1992.37.6.1129, 1992.

Taillefert, M., Neuhuber, S., and Bristow, G.: The effect of tidal forcing on biogeochemical processes in intertidal salt marsh sediments, Geochem. Trans., 8, 6, https://doi.org/10.1186/1467-4866-8-6, 2007.

Thibault de Chanvalon, A., Metzger, E., Mouret, A., Cesbron, F., Knoery, J., Rozuel, E., Launeau, P., Nardelli, M. P., Jorissen, F. J., and Geslin, E.: Two-dimensional distribution of living benthic foraminifera in anoxic sediment layers of an estuarine mudflat (Loire estuary, France), Biogeosciences, 12, 6219–6234, https://doi.org/10.5194/bg-12-6219-2015, 2015.

Thibault de Chanvalon, A., Mouret, A., Knoery, J., Geslin, E., Péron, O., and Metzger, E.: Manganese, iron and phosphorus cycling in an estuarine mudflat, Loire, France, J. Sea Res., 118, 92–102, https://doi.org/10.1016/j.seares.2016.10.004, 2016.

Thibault de Chanvalon, A., Metzger, E., Mouret, A., Knoery, J., Geslin, E., and Meysman, F. J. R.: Two dimensional mapping of iron release in marine sediments at submillimetre scale, Mar. Chem., 191, 34–49, https://doi.org/10.1016/j.marchem.2016.04.003, 2017.

Ullman, W. J. and Aller, R. C.: Diffusion coefficients in nearshore marine sediments1, Limnol. Oceanogr., 27, 552–556, https://doi.org/10.4319/lo.1982.27.3.0552, 1982.

Walpersdorf, E., Kühl, M., Elberling, B., Andersen, T. J., Hansen, B. U., Pejrup, M., and Glud, R. N.: In situ oxygen dynamics and carbon turnover in an intertidal sediment (Skallingen, Denmark), Mar. Ecol. Prog. Ser., 566, 49–65, https://doi.org/10.3354/meps12016, 2017.

Walton, W. R.: Techniques for recognition of living foraminifera, Cushman Found Foram Res Contr, 3, 56–60, 1952.

Supplementary information

Annex 1 a: Calculated fluxes from PROFILE modeling at the air-sediment interface (µmol m^{-2} d^{-1}).

	Fluxes at the air-sediment interface (µmol m^{-2} d^{-1})	
	April	October
DOU in dark	$3.37E^{-02}$	$5.87E^{-02}$
DOU in light (Max. PA profile)	$-2.28E^{-02}$	$-7.63E^{-02}$
2D NH_4^+	$-7.49E^{-05}$	No estimate
1D NH_4^+	$-1.61E^{-04}$	$-7.15E^{-05}$
2D DRP	$5.51E^{-07}$	$2.80E^{-07}$
1D DRP	No estimate	$2.12E^{-05}$
2D Mn_d	$-7.53E^{-04}$	$-8.62E^{-04}$
1D Mn_d	$-1.61E^{-04}$	$-7.33E^{-04}$
2D Fe_d	$-5.51E^{-04}$	$-8.12E^{-04}$
1D Fe_d	$-1.33E^{-03}$	No estimate

Annex 1 b: Calculated global production/ consumption zones from PROFILE modeling of the 1D and 2D profiles (nmol cm^{-3} s^{-1}).

		Global production/ consumption (nmol cm^{-3} s^{-1})	
		April	October
O_2 in dark	production	-	-
	consumption	$-3.45E^{-02}$	$-4.08E^{-02}$
O_2 in light (Max. PA profile)	production	$1.66E^{-01}$	$4.72E^{-01}$
	consumption	$-1.10E^{-01}$	$-3.83E^{-01}$
2D NH_4^+	production	$3.01E^{-04}$	$7.19E^{-04}$
	consumption	$-4.09E^{-04}$	$-1.09E^{-03}$
1D NH_4^+	production	$1.22E^{-03}$	$5.47E^{-03}$
	consumption	$-1.21E^{-03}$	$-7.65E^{-03}$
2D DRP	production	$9.37E^{-06}$	$5.80E^{-05}$
	consumption	$-9.67E^{-06}$	$-9.83E^{-05}$
1D DRP	production	-	$9.71E^{-05}$
	consumption	$-6.14E^{-06}$	$-1.43E^{-04}$
2D Mn_d	production	$1.28E^{-03}$	$1.31E^{-03}$
	consumption	$-3.06E^{-04}$	$-3.61E^{-04}$
1D Mn_d	production	$2.13E^{-04}$	$1.36E^{-03}$
	consumption	$-4.76E^{-05}$	$-4.34E^{-04}$
2D Fe_d	production	$7.65E^{-04}$	$3.37E^{-03}$
	consumption	-	$-2.42E^{-03}$
1D Fe_d	production	$1.94E^{-03}$	$3.50E^{-03}$
	consumption	$-3.33E^{-04}$	$-4.21E^{-03}$

Annex 2: S/Na ratio (a) April and (b) October. The corresponding fluxes and production/ consumption zones are not exploitable but these profiles modelling allow to localize in sediment depth the zones of production/consumption of sulphates.

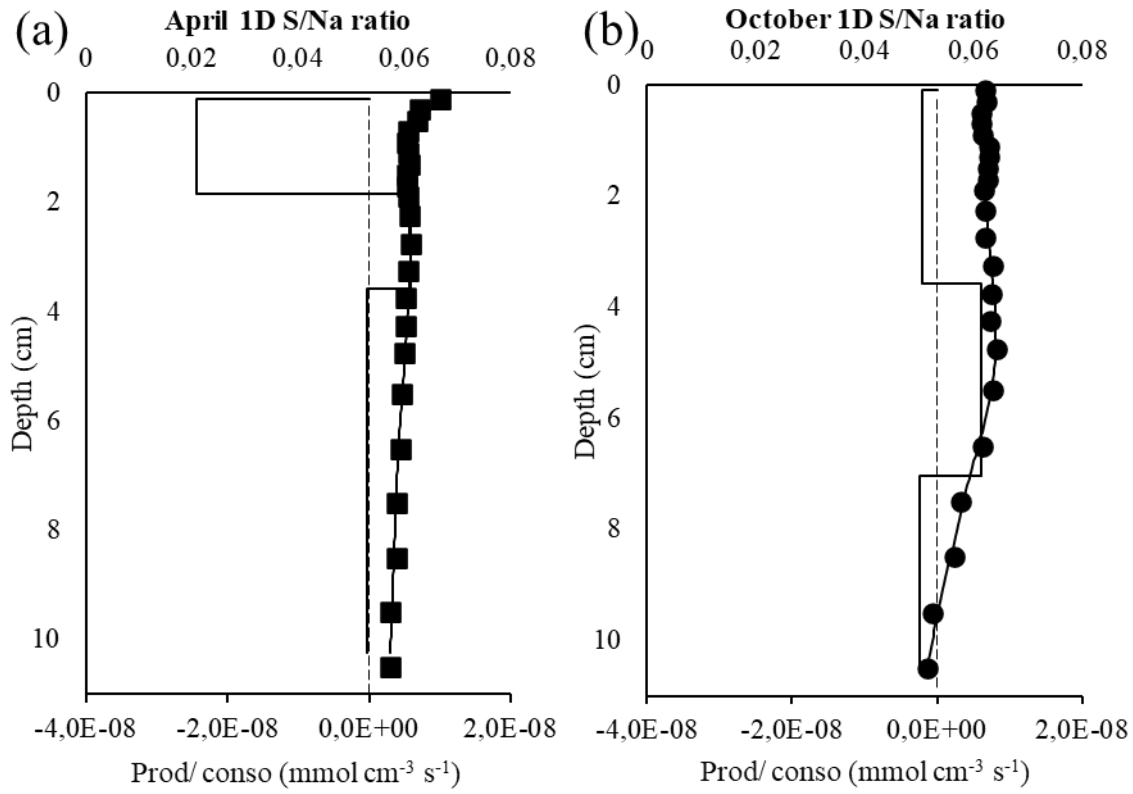

Annex 3: 1D profiles of alkalinity, Mn_d, Fe_d, NH_4^+ and DRP at the 3 sampling stations A (blue triangle), B (green square) and C (grey circle) in April and October 2019.

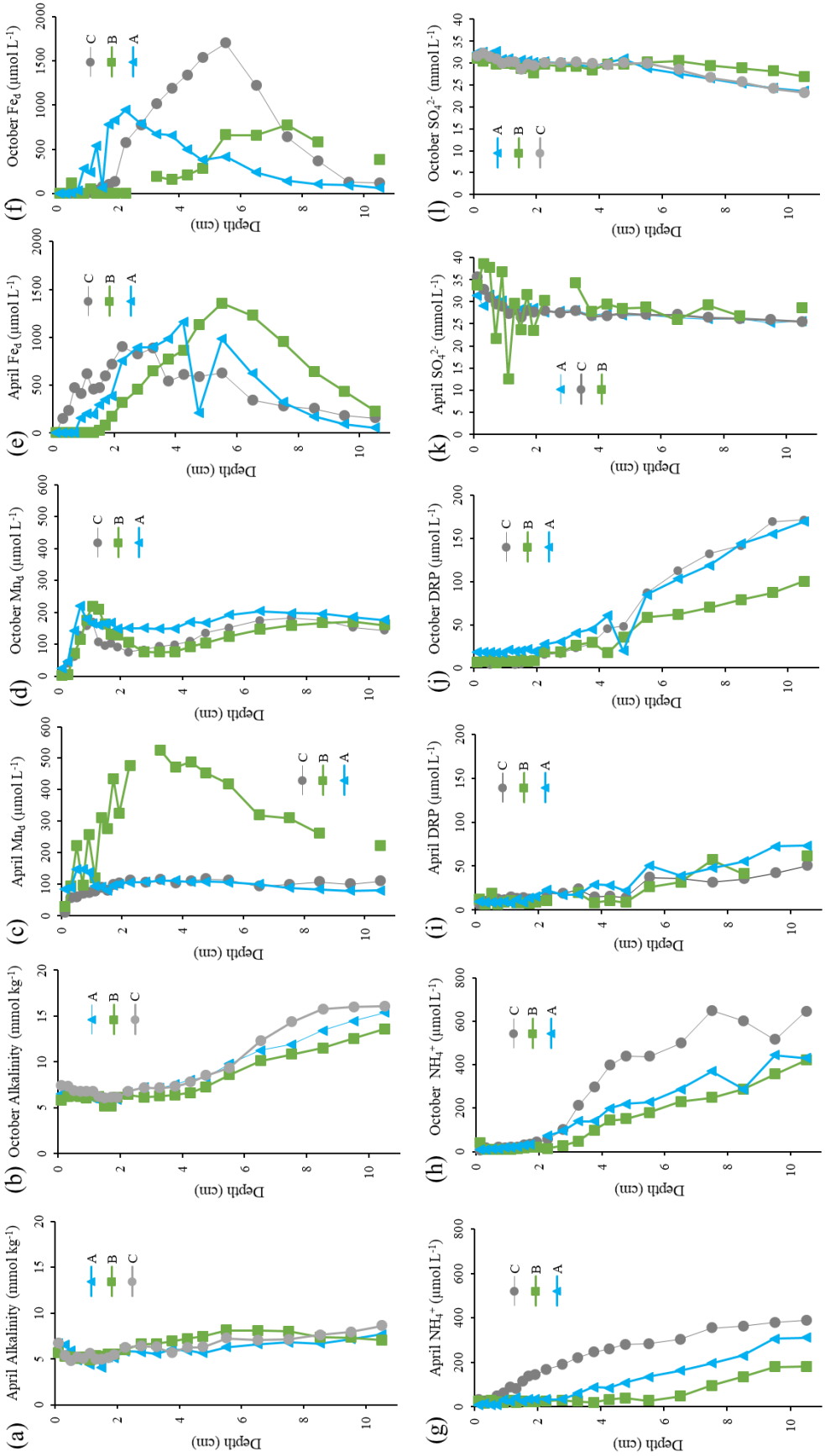

Annex 4: Ascorbate extracted $[P]_{asc}$ versus $[Fe]_{asc}$ in April (white square) and in October (black circle) at the station C (the P_{asc} at 4.75 cm deep was removed for October).

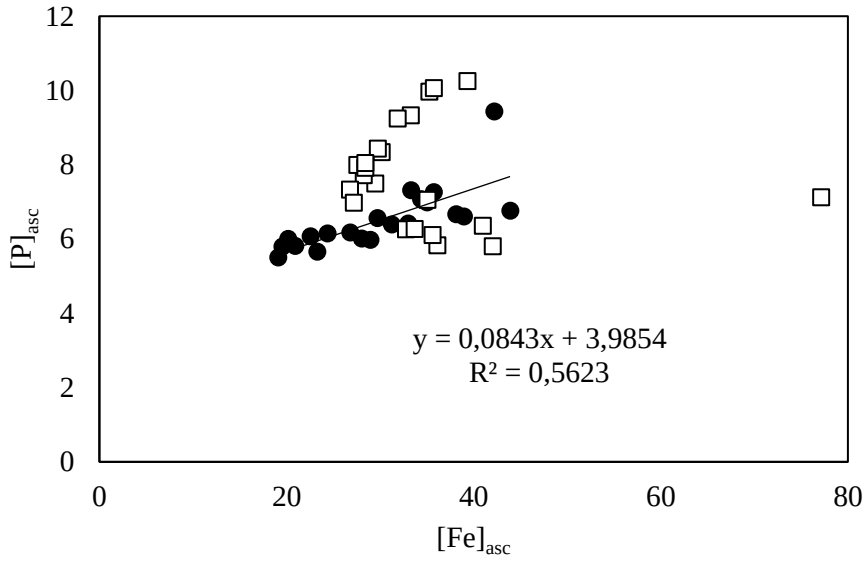

Annex 5: Number of foraminiferal specimens counted with the Rose Bengal-staining method in the 1st cm depth at the three stations A, B and C (> 150 µm). In bold the specimens counted at the station C used to compare with CTG-labelling method in Table 2.

	Staining methods	*Ammonia* sp. T6	*Haynesina germanica*	*Elphidium selseyense*	*Elphidium oceanense*	Total (ind. 50 cm^3)
April	RB-A	55	57	5	1	124
	RB-B	22	27	24	1	75
	RB-C	**142**	**188**	**13**	**21**	**364**
October	RB-A	241	408	0	660	1309
	RB-B	63	186	0	93	343
	RB-C	**107**	**87**	**0**	**433**	**627**

Annex 6 a: Foraminiferal oxygen respiration rate measurements

The first centimeter of one core dedicated to foraminiferal oxygen respiration rate measurements was sampled in April and October 2019. The cores were carefully transported at *in situ* temperature in Angers university to be analyzed the next day. The dominant foraminifera specimens were picked under *in situ* temperature and collected in a Petri dish, containing a thin layer of sediment (32 µm) to check their vitality. Only living, active specimens were picked and cleaned several times using a brush with micro-filtered artificial seawater.

Oxygen respiration rates were measured, following the method developed by Geslin et al. (2011) using a Clark type oxygen microsensors (50 µm tip diameter, Unisense ®, Denmark) (Revsbech, 1989) calibrated by a two-point calibration using air-saturated water at *in situ*

temperature and sodium ascorbate solution (to strip O_2 out of the system) as zero. Then, a pool of 4 or 5 living foraminifera was transferred into a glass microtube (inner diameter 0.5 mm, height 7.5 mm) that was fixed inside a 20 ml test tube mounted in a glass-cooling bath. A motorized micromanipulator was used to measure O_2 concentration profiles along a distance gradient that ranged from 200 µm of the foraminifera to 1200 µm using 100 µm steps. Each oxygen profile is repeated 5 to 10 times (with 5 minute intervals) in order to confirm the stability of the oxygen gradient. The last profile is selected to calculate the oxygen O_2 flux. Negative controls were done by measuring O_2 rates from microtube with empty foraminifera shells and blanks with empty microtube. Oxygen respiration rates were calculated with Fick's first law of diffusion, J = -D * dC/dx, where J is the flux, dC/dx is the concentration gradient obtained by profiles and D is the free diffusion coefficient of oxygen at in situ temperature and salinity (Ramsing and Gundersen, 1994). The O_2 respiration rates were calculated as the product of the flux by the cross section area of the microtube (0.196 mm^2). Then, the average O_2 respiration rate was divided by the number of foraminifera presented in the microtube to obtain the respiration rate per individual.

For every species, the total foraminiferal volume was estimated by using the best resembling geometric shape, a half sphere where the maximum (Dmax) and minimum (Dmin) diameters of each shell were measured (shell volume = $\frac{1}{2} x \frac{4}{3} x \pi x \left(\frac{Dmax+Dmin}{2}\right)^3$. The cytoplasmic volume (or biovolume) was estimated by assuming that the internal test volume corresponds to 75% of the total foraminiferal test volume (Hannah et al., 1994) and that the internal test volume of the shell was entirely filled with cytoplasm. The measurements were performed using a micrometer mounted on a Leica stereomicroscope (Leica MZ 12).

Annex 6 b: Foraminiferal O_2 respiration rates.

	species	Biovolume (μm^3) mean	Biovolume (μm^3) sd	respiration rates µmol L^{-1} mean	respiration rates µmol L^{-1} sd	Number of profiles	Number of specimens
April 2019	*Ammonia* sp. T6	6,98 E^{+05}	5,22 E^{+03}	1456	59	6	5
	Haynesina germanica	1,53E^{+06}	1,37 E^{+06}	1463	38	11	5
	Elphidium oceanense						
	Elphidium selseyense	6,52 E^{+05}	4.53 E^{+05}	670	18	10	5
October 2019	*Ammonia* sp. T6	2,42 E^{+05}	1.73 E^{+05}	1246	46	7	5
	Haynesina germanica	6,46 E^{+05}	3.52 E^{+05}	1218	83	11	5
	Elphidium oceanense	2,78 E^{+05}	1.85 E^{+05}	738	65	10	5
	Elphidium selseyense						

Annex 7 a: Contribution of the dominant foraminifera species to the local diffusive oxygen uptake

Total foraminiferal respiration was calculated as the product of the number of individuals of the various taxa in the oxic sediment layer and their respective oxygen respiration rates, extrapolated to the total fauna by multiplying with (100/cumulative percentage of the considered species). In order to estimate the foraminiferal contribution to benthic ecosystem respiration, the total foraminiferal oxygen respiration was compared with the diffusive oxygen uptake (DOU) estimated from vertical oxygen profiles obtained in the dedicated core to microprofiling. Diffusive oxygen uptake of the sediments was calculated from oxygen profiles using PROFILE software (Berg et al., 1998). The two boundary conditions used for the calculations correspond to the overlying water oxygen concentration and the zero flux at the bottom of the oxic zone. The bulk sediment molecular diffusion coefficient (Ds) is estimated according to DS = φ2D0 (Ullman and Aller, 1982) where ϕ is the sediment porosity and D0 is the diffusion coefficient in water at in situ temperature (Li and Gregory, 1974). Sediment oxygen profiles were determined using Clark-type electrodes (Revsbech, 1989) with tip diameters of 100 μm and measured in the dedicated core.

Annex 7 b: Contribution of foraminifera to O_2 consumption (%).

	species	Number of O_2 profiles	Individuals counted 0-2	Contribution 0-2	Individiuals counted 0-1 cm	Contribution 0-1 cm
April	*Ammonia* sp. T6	6	16	0,04	46	0,12
	Haynesina germanica	11	13	0,03	42	0,1
	Elphidium selseyense	10	1	0,001	4	0,004
October	*Ammonia* sp. T6	7	55	0,1	178	0,32
	Haynesina germanica	11	2	0,003	177	0,31
	Elphidium oceanense	10	15	0,16	435	0,46

Synthesis and perspectives

1. General synthesis with summary diagram

The general aim of this PhD research was to better understand the benthic faunal and geochemical interactions from micro-scale to kilometer-scale in two contrasted coastal areas. This PhD thesis was divided into four chapters, each of them investigating different combined high-resolution methods and multivariate analyses at different scales to reveal the interactions between benthic faunal and geochemical compartments. The articulations between the topics and the main conclusions of the four chapters are summarised in Figure 1.

Chapter 1 investigated the contribution of denitrifying foraminifera to benthic nitrogen cycle at two oxygen and nitrate contrasting stations in the Gullmar Fjord. The combination of high spatial resolution methods as CTG-labeled, N_2O microsensors and NO_3^- 2D-DET gels allowed to estimate accurately the contribution of denitrifying foraminifera to the benthic N cycle. This new ecological approach opened the possibility to estimate meiofaunal and geochemical benthic processes occurring at millimetric scale to ecosystem scale. **Chapter 2** presented an original and innovative approach to study the contribution of macrofaunal bioirrigation to the benthic Mn cycle at two oxygen-contrasting stations in the Gullmar Fjord. A 2D modelling approach was applied on the Mn_d 2D-DET gels, revealing the high contribution of bioirrigationnal fluxes to Mn cycle in the hypoxic Mn oxides-rich station. The 2D gels were combined with embedded sediment slabs labeled with CTG providing a complementary way to identify Mn micro-environments in 2D. **Chapter 3** explored the spatiotemporal dynamics of Rose Bengal-stained foraminifera in the semi-enclosed Bourgneuf Bay mudflat. The using of multivariate analysis performed on a large environmental dataset, revealed that foraminiferal dynamics were mainly driven by the Loire river hydrodynamics. Moreover, this work suggested a trophic model showing that temporal dynamics of foraminiferal species would correspond to specific diatom food source preferences. The results of this *in situ* ecological work validate and complement the previous published experimental and metabarcoding studies. Finally, complementing the previous chapter, **Chapter 4** investigated in more detail two contrasting hydrological situations in post-flooding and low water level periods. The use of O_2 microsensors and Mn_d, Fe_d, NH_4^+, DRP 2D-DET gel methods provided detailed information of redox species and nutrients behaviour in transient diagenetic conditions fueled by winter flood. Then, the micro-distribution of CTG-labeled foraminifera revealed the state of sediment instability through unfavourable *versus* favourable periods. The CTG-labeled appeared necessary to follow accurately the short-term foraminiferal dynamics.

General synthesis of the PhD thesis « Benthic foraminifera ecology, geochemical and biological interactions; multi-disciplinary approach at different scales »

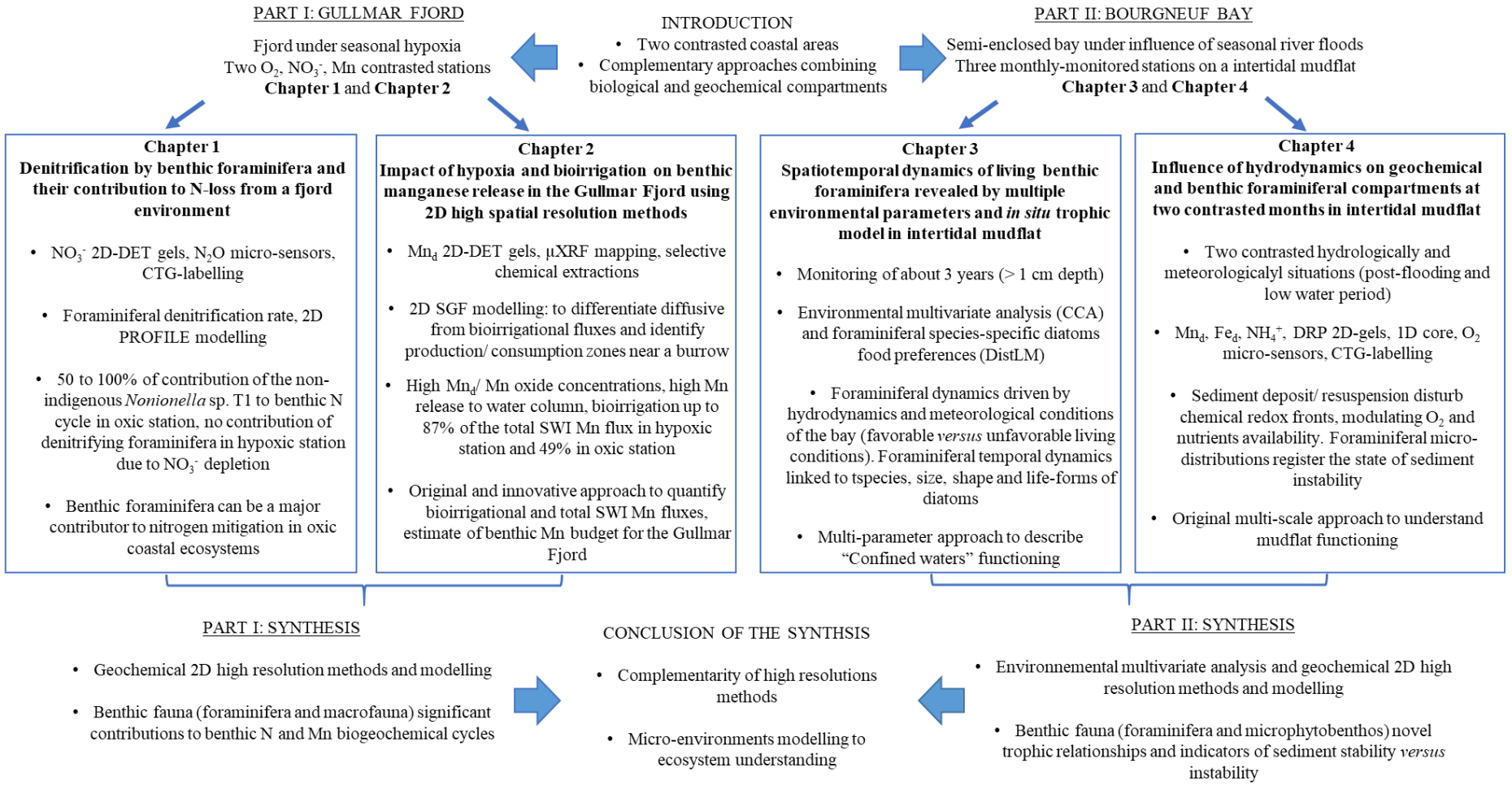

2. Chapter synthesis

2.1 PART 1: GULLMAR FJORD

2.1.1 Denitrification by benthic foraminifera and their contribution to N-loss from a fjord environment

In **Chapter 1**, an innovative approach was used to estimate the contribution of denitrifying benthic foraminifera to nitrogen (N) cycle in the seasonal hypoxic Gullmar Fjord. Benthic nitrate (NO_3^-) removal was calculated from submillimetre chemical gradients extracted from 2D images of the pore-water NO_3^- concentrations. These were acquired by combining the 2D-DET (two-dimensional-diffusive equilibrium in thin film) gel with chemical colorimetry and hyperspectral imagery. The using of 2D high resolution methods provided a novel approach for benthic geochemical interpretations. Initially, we expected to find many denitrifying foraminifera as *Globobulimina turgida* in the hypoxic station as previously found by Risgaard-Petersen et al. (2006) and few denitrifying species in the oxygenated station. Unexpectedly, very few *Globobulimina* specimens were found at the two sampled stations. The species *Nonionella* sp. T1, reported for the first time in this area by Polovodova Asteman and Schönfeld, (2015), dominated in the oxic part of the fjord. Actually, this station contained sediments with high pore-water NO_3^- concentrations. Thus, NO_3^- was available for respiration by denitrifying species. Therefore, we investigated the nitrate respiration rate of the non-indigenous species (NIS) *Nonionella* sp. T1 which was able to respire 38 ± 8 pmol N indiv.$^{-1}$ d^{-1}. Finally, the contribution of this species to nitrate loss through benthic denitrification estimated from pore-water nitrate gradients was high, ranging from 50%–100%. Contrastingly, at the hypoxic station, sediments had low pore-waters NO_3^-. Consequently, few NO_3^- were available and denitrifying foraminifera were rare and their contribution to N cycle (benthic denitrification) negligible (< 5 %). This first chapter, emphasized that denitrifying foraminifera can be a major contributor to N mitigation in oxic coastal ecosystems and their contribution is required to understand accurately biogeochemical cycles coupled to N. This chapter is published in Biogeosciences (Choquel et al., 2021).

2.1.2 Benthic manganese cycle in the Gullmar Fjord using 2D high spatial resolution methods

In **Chapter 2**, we investigated the benthic manganese (Mn) cycle using an innovative approach to quantify in 2D at high spatial resolution Mn distribution in pore waters and estimate the sediment water interface (SWI) Mn fluxes with the contribution of bioirrigation in the seasonal hypoxic Gullmar Fjord. For this purpose, we combined Mn_d 2D-DET gel method with embedded sediment slabs and selective chemical extractions to visualise and quantify the contrasted dissolved and solid phases Mn micro-distributions. Our results showed that macrofaunal burrows create visual structures on the 2D gels and on the µXRF map. These structures were generated by the Mn consumption inside the burrow due to flushing, as previously found on the Fe_d 2D gels by Thibault de Chanvalon et al., (2015, 2017). Burrow linings were detected on the Mn_d 2D gel for both stations, allowing to calculate separately the diffusive and bioirrigational Mn_d fluxes with the Savitsky-Golay Filter method (Thibault de Chanvalon et al., 2017). The oxic shallow station contained sediments with low dissolved and solid phases Mn. For this station, bioirrigational flux contributed up to 49 % of the total SWI Mn_d flux. No enrichment in Mn oxides could be observed on the embedded sediment. Conversely, Mn enrichment in the dissolved and solid phases was present at the hypoxic deep station. Pore-waters sediments contained 10 times higher Mn_d concentrations. As a consequence, the bioirrigational Mn_d flux was high (7 times higher than diffusive flux). At this hypoxic deep station, the bioirrigational flux contributed up to 87 % of the total SWI Mn_d flux. Severe hypoxia/anoxia can lead to a decrease in macrofaunal density and thus a decrease in the bioirrigational Mn_d flux leading to a lower Mn release to the overlying water. However, in response to low oxygen conditions, some macrofaunal species can compensate the lack of oxygen by increasing their pumping activity that would lead to increase the bioirrigational fluxes. Finally, this second chapter highlighted the high contribution of macrofaunal bioirrigation in the Mn cycle.

2.1.3 Synthesis PART 1

Chapter 1 and **Chapter 2** linked two interdependent compartments: the benthic faunal compartment (represented by the denitrifying foraminifera and the macrofaunal activity through burrow analyses) and the geochemical compartment. The aims were to visualize and quantify the micro-environments in which the fauna evolved and the impact of fauna on the

geochemical cycles. The elaborate geochemical sampling device deployed at the GF17-3 (oxic) and GF17-1 (hypoxic) stations allowed to combine two dissolved chemical species; NO_3^- (Chapter 1) and Mn_d (Chapter 2). In addition, the sampling device allowed the simultaneous sampling of a sediment slab which was subsequently embedded for 2D high resolution Mn solid-phase analyses. From the 2D gels, different approaches to model fluxes and production/consumption were used. 1D profiles averaged from NO_3^- 2D gels were modelled with PROFILE software to dissociate the pore-water NO_3^- consumption and production zones. This analysis was favoured due to the relative homogeneous lateral variability and the visible absence of a burrow structure. This method combining a submillimetre resolution and a window size at centimetric scale was appropriate for meiofaunal ecological questioning as benthic foraminifera. Concerning the second chapter, the Mn_d 2D gel method was used and the modelling approach differed. Indeed, the presence of macrofaunal burrow structures generated strong lateral and vertical heterogeneities of Mn_d gradients. 1D profiles averaged from Mn_d 2D gels and the "classic" PROFILE modelling seemed less appropriate to take into account these structures. The Savitsky-Golay Filter procedure (from Thibault de Chanvalon et al., 2017) allowed to differentiate in 2D the gradients, revealing the Mn_d production and consumption zones around the burrow lining. Burrow modelling allowed to differentiate bioirrigational fluxes and SWI diffusive fluxes, revealing the high contribution of macrofaunal activity to the Mn_d fluxes towards the water column. The embedded sediment was used to visualize burrows enriched in Mn solid-phase. Despite sediment compaction, linked to the fluffy surface sediments, the embedded sediment gave promising analytical perspectives. Thus, we detected living benthic foraminifera CTG-labeled on the slabs, and µCT-scan imagery revealed a 3D visualization of burrows and benthic foraminifera inside the sediment slabs. Finally, this first part of the PhD thesis highlighted the complementary of geochemical 2D high-resolution methods to accurately estimate the contribution of benthic fauna to biogeochemical cycles on a larger scale. Furthermore, this work highlighted the importance of non-bacterial benthic fauna in the N and Mn biogeochemical cycles.

2.2 PART 2: BOURGNEUF BAY

2.2.1 Spatiotemporal dynamics of living benthic foraminifera revealed by hydrodynamics and *in situ* trophic model in intertidal mudflat (Bourgneuf Bay, France)

In **Chapter 3,** we investigated with a multi-parameter approach (e.g. environmental and biological) the spatiotemporal dynamics of the dominant foraminiferal species in the Bourgneuf Bay mudflat (West Atlantic coast, France). Three stations spaced from 10 m apart (meso-scale or decameter-scale) were sampled at "La Coupelasse" site. The sampling effort in this study was high and benefited from a monthly then quarterly geochemical database from March 2016 to October 2019. Simultaneously a monthly benthic foraminiferal monitoring occurred in the 1st cm depth of the sediment, using Rose Bengal to stain living individuals and the adult size population of the dominant species (> 150 µm). The monthly microphytobenthos biomass was analysed from April 2017 to July 2019 at the three stations. The MPB assemblage was analysed at one station. No significant foraminiferal spatial variability between stations was found. Four typical intertidal living foraminiferal species dominated the fauna throughout the entire monitoring: *Ammonia* sp. T6, *Haynesina germanica*, *Elphidium oceanense* and *Elphidium selseyense*. Temporal dynamics were punctuated by high density events and periods of lower densities. We applied a multivariate analysis (CCA) to try to understand foraminiferal temporal dynamics depending on many environmental parameters: 1) hydrodynamics and meteorological parameters (discharge, rainfall, temperature, tidal coefficient, porosity, salinity, granulometry), 2) OM remineralization activity (alkalinity, OPD, DOU), 3) pore-water nutrients (DRP, NH_4^+, NO_3^-, NO_2^-) and 4) proxy of the MPB biomass (NDVI). *Ammonia* sp. T6 and *Haynesina germanica* were present all the year showing one or two density events per year in late winter and in early autumn. The winter/early spring period was characterized by a combination of high hydrodynamics and winter meteorological parameters (i.e. Loire river discharge, wind-storm events, high rainfall, higher granulometry, lower porosity and occasional fine sand inputs). The intensity of sedimentary disturbances may increase during these periods with consequences for benthic fauna (foraminiferal density and MPB biomass). The sediment instability would generate a dual response for *Ammonia* sp. T6 and *Haynesina germanica*: mortality *versus* accelerating reproduction. Conversely, the density events observed in early autumn were characterized by a lower hydrodynamics and summer conditions (i.e. low water level of the Loire river, higher temperature, higher MPB biomass, porosity and alkalinity). This more favourable period for benthic fauna favored reproductive events for *Ammonia* sp. T6, *Haynesina germanica* and *Elphidium oceanense*. Foraminiferal high densities may lead to

individual reproduction or development of numerous propagules. The present foraminiferal analysis was limited to adult population (> 150 µm), the exact time lag between the trigger for reproduction event or propagule development and the density peaks remains to be clarified. *Elphidium oceanense* and *Elphidium selseyense* were almost absent along the year with only one density event in autumn and in spring, respectively. The contrasted responses between the two dominant species and the two *Elphidium* species could be explained in the view of "confined waters" conceptual model of the foraminiferal distribution from transitional environments (Debenay and Guillou, 2002). Thus, *Ammonia* sp. T6 and *Haynesina germanica* would be located within their preferential distribution zone in the bay, whereas the two *Elphidium* species could be located at the limit of their preferential distribution zone.

Secondly, we hypothesized that foraminiferal species would select diatom species based on their shape and size. The ecological *in situ* trophic model suggested in this chapter confirmed and completed the previous results of published studies on prey (diatoms) – predator (foraminifera) relationships. The foraminiferal temporal dynamics was also driven by their diatom food source. *Haynesina germanica* showed a restrictive diet, feeding on few large elongated epipelic diatom species. *Ammonia* sp. T6 showed a wider diatoms diet, feeding on different sizes, elongated shapes and life-forms (epipelic and epipsammic). *Elphidium oceanense* presented the most various diet, feeding on different sizes, simple and complex shapes, and life-forms (epipelic, epipsammic and pelagic). No diatom species indicated clearly the temporal variability of *Elphidium selseyense*. Maybe this species could feed on another preferential food source such as soft microalgae (e.g. euglenas). This hypothesis can be supported by future metabarcoding analyses. Besides, this trophic model would suggest that foraminiferal species preferentially feed on their own diatom species, inducing no competition for diatom food source.

2.2.2 Influence of the Loire river hydrodynamics on geochemical and benthic foraminiferal compartments in intertidal mudflat (Bourgneuf Bay, France)

Chapter 4 is a complementary study of the previous Chapter 3. We further investigated the benthic faunal and geochemical compartments at two hydrological and meteorological contrasted situations: post-flooding (April 2019) and low water level (October 2019). We combined the simultaneous deployment of Mn_d, Fe_d, NO_3^-, NH_4^+ and DRP 2D-DET gels. These 2D gels provided information on vertical and lateral variability of redox elements and nutrients

at decimeter-scale (within a station). The use of "classic" 1D profiles from core slicing allowed to capture the decameter-scale variability (between the three stations). The 2D images of the different chemistries indicated strong vertical gradients and low lateral variability for both months. The modelling of the fluxes at the sediment-air interface and the characterization of the production/consumption zones were performed with PROFILE modelling (as in Chapter 1). The macrofaunal bioturbation at "La Coupelasse" site seems to be low (very few burrows observed). However, a small macrofaunal burrow lining was observed on the Fe_d/ DRP 2D gel in October. Another modelling could be applied as in Chapter 2. In addition, in this chapter the distribution of foraminifera (CTG-labeled) was performed at high vertical resolution (micro and centimetric scales).

The distribution of redox elements (Mn and Fe) and nutrients (NH_4^+ and DRP) in the Bourgneuf Bay mudflat seemed influenced by the high winter hydrodynamics fueling transient diagenesis in the post-flooding period. The 2D gel methods provided detailed vertical and lateral distributions of solute elements at millimetric scale. To capture decametric heterogeneity, complementary analyses using 1D profiles on sediment cores were performed. In post-flooding period, Mn and Fe shared the same redox front due to recent sediment deposit/ resuspension. Conversely, in low water level period, the stabilized sediment showed the decoupling of the Mn and Fe redox fronts as conventionally descripted for early diagenesis (Froelich et al., 1979). The behaviour of redox elements impacts the nutrient cycling. Fe oxides were saturated with phosphorus at the two periods, which could induce that phosphorus found at the sediment surface available for the benthic fauna was mainly linked to the increase of deep anaerobic organic matter mineralization as sulfato-reduction process. The nitrogen turnover was high. No NO_3^- was detected but low NO_2^- was measured indicating nitrification/denitrification activity. Overall, NO_3^- and NH_4^+ were limiting nutrients for benthic primary producers. Ammonium and DRP were actively consumed at the sediment surface, excepted in post-flooding period where the DRP was depleted. This study clarified the behaviour of redox species and nutrients over two contrasting time periods.

Intertidal sediments are continuously subjected to transient dynamics (tides, day/night cycles, meteorological conditions…) making the O_2 redox front highly variable. Profiling with O_2 microsensors during the emersion time reflected the MPB photosynthetic activity at micrometer-scale. Increased O_2 availability deeper in the sediment such as during low water level periods, could allow more favorable oxygenated micro-environments for benthic foraminifera. Furthermore, foraminiferal species responded strongly to these contrasted

periods. Foraminiferal micro-distributions (analyzed until 10 cm depth) appeared to indicate the state of instability of the sediments resulting in unfavorable *versus* favorable periods. Micro-distributions of CTG-labeled living foraminifera clearly showed low densities and bimodal distributions during unfavorable periods *versus* higher densities at the sediment surface and juvenile specimens identified during favorable periods. However, in this study, the difference between the staining of live specimens with Rose Bengal and fluorescent specimens with CellTracker Green was striking. Some clarification is still needed on this discrepancy found between the two methods.

2.2.3 Synthesis PART 2

Chapter 3 and **Chapter 4** provided complementarity approaches to understand the complex functioning of the Bourgneuf Bay mudflat through interactions between environmental parameters and benthic fauna. The intertidal mudflat is subject to hydrological, meteorological and tidal influences. These forcing generate sediment instability and modulate the geochemical and benthic faunal compartments. The sediment instability was followed by the spatiotemporal dynamics of benthic fauna and associated environmental parameters (physicochemical and biological). Thus, two contrasting hydrological and meteorological periods alternated: the winter flood/post-flooding period opposed to the summer conditions/ low-water period. The winter period was driven by a combination of high hydrodynamics and winter meteorological parameters (i.e. Loire river discharge, wind-storm events, high rainfall, higher granulometry, lower porosity and occasional fine sand inputs) leading to sedimentary instability (sediment deposit/ resuspension, sand deposits). The intertidal sediments were continuously undergoing transient diagenesis. This period is characterized by a destructuring of redox fronts, impacting nutrient turnover and oxygen availability for benthic fauna (Chapter 4). This period of sediment instability impacted the benthic microalgae/fauna showing low to moderate NDVI values (Chapter 3) and low density of benthic foraminifera (Chapter 3 and 4). However, the species *Ammonia* sp. T6 and *Haynesina germanica* showed a dual response indicating either a rapid reproductive event or high mortality (Chapter 3). During summer conditions and low-water period, sediment properties were stabilized (Chapter 3 and 4). The redox fronts showed a typical diagenetic profile with successive use of oxidants. The OM anaerobic remineralization activity increased inducing higher DOU at the SWI (Chapter 3 and 4) and sulfato-reduction process in depth (Chapter 4). The beginning of spring/ early summer

low-water period was characterized by the presence of *Elphidium selseyense*. MPB biomass was relatively moderate (the impact of high temperatures and photoperiod intensity can limit algal production). In late summer/ early fall, reproductive events were observed for *Ammonia* sp. T6, *Haynesina germanica* and *Elphidium oceanense*. These reproductive events occurred during a more favourable period (i.e. low water level of the Loire river, moderate temperature, higher MPB biomass, sediment stability). Indeed, the MPB biomass was higher showing a more important photosynthetic activity, fueled by the inputs of nutrients as NH_4^+ (Chapter 3) and DRP (Chapter 4). The foraminiferal temporal dynamics were also driven by diatom species dynamics. Indeed, this thesis work highlighted an *in situ* trophic model suggesting that foraminiferal species preferentially feed on preferential diatom species selected by their shape, size and life-forms.

3. Perspectives

This PhD thesis work emphasized and completed studies concerning the benthic fauna and geochemical interactions of two coastal areas. Some aspects of the PhD thesis were not developed. This section presents the main perspectives to be carried out in future research.

3.1 Denitrifying foraminifera and other alternative metabolisms

This PhD thesis emphasized the crucial role of denitrifying foraminifera in the benthic nitrogen cycle in the oxic part of the Gullmar Fjord. However, denitrifying foraminifera are still underestimated due to the lack of denitrification rate measurements for several species constituting the assemblages (e.g. *Stainforthia fusiformis, Bolivina pseudopunctata*; *Nonionellina labradorica*). Moreover, the seasonal dynamics of denitrifying species such as *Nonionella* sp. T1 and other species such as *Globobulimina turgida* is not known. However, nitrate concentrations in the overlying water at the deep station (GF17-1) vary within a year (Chapter 1). These changes in nitrate concentrations could induce variations in the density of denitrifying foraminifera and consequently modify their contribution to the N cycle during a year. Then, to better understand the micro-environments of *Nonionella* sp. T1 and other denitrifying species, consideration should be given to measuring intracellular nitrate in specimens from sediment layers identified as nitrate production and consumption zones. A better understanding of these denitrifying foraminifera in coastal ecosystems with high pore-

water NO_3^- concentration could allow to determine their role in benthic N mitigation, such as in areas subject to eutrophication.

Conversely to the Gullmar Fjord area, the Bourgneuf Bay mudflat presents very low seasonal NO_3^- availability in pore waters, probably due to a high nitrate consumption by microphytobenthos and bacteria (Risgaard-Petersen et al., 2003). Foraminiferal species showed reproduction events above the 1st cm depth in the oxic zone (Chapter 3 and 4). However, some living specimens were found deeper (in suboxic and anoxic zones). Nitrate respiration by the four dominant foraminiferal species would not be a preferential metabolic pathway. To confirm that these species do not denitrify, it would be interesting to measure denitrification rate on intertidal species as *Elphidium oceanense, Elphidium selseyense* and *Haynesina germanica*.

Besides denitrification, other alternative metabolisms can be suggested to explain the presence of these deeper living specimens capable of surviving complete anoxia for weeks to months. Dormancy was demonstrated in *Ammonia tepida*, resulting in a state of highly reduced metabolism (LeKieffre et al., 2017). Moreover, some benthic foraminiferal species such as *Haynesina germanica* are known to sequester chloroplasts from their food source and store them in their cytoplasm. The sequestered chloroplasts remain active in *Haynesina germanica* and may play a role in the assimilation of inorganic nitrogen, even in the absence of light. It has also been hypothesized that chloroplast retention may play a major role in the survival of foraminifera to cope with periods of starvation or in anoxic environments (Jauffrais et al., 2016). Recent *in situ* observations tend to show seasonality in kleptoplasty performed by *Haynesina germanica*. The ecological role of this particular metabolism is thought to be closely related to changes in environmental conditions, including unfavorable hydrological and meteorological conditions (Courtial et al., *in preparation*).

Recent studies showed NH_4^+ assimilation by mixotrophic (*Haynesina germanica*) and heterotrophic (*Ammonia tepida*) foraminiferal species (LeKieffre et al., 2018b; Bird et al., 2020). However, no quantification of the intracellular NH_4^+ pool in benthic foraminifera was demonstrated at this time. It would be possible to quantify the intracellular NH_4^+ pool by crushing living specimens and measuring NH_4^+. It would be possible to calculate the contribution of foraminiferal species to the consumption of pore water ammonium. Indeed, ammonium assimilation could be a favourable source of N (as suggested for planktonic foraminifera; (LeKieffre et al., 2018a) for cell growth and development (Bird et al., 2020). It

could be that benthic foraminifera compete with microphytobenthos for NH_4^+ in a fast N-turnover environment as intertidal areas (Eyre et al., 2016).

Similarly, dissolved reactive phosphorus (DRP) may be assimilated by some foraminiferal species to build their cell membranes. Foraminifera from the Peruvian oxygen minimum zone showed up to three orders-of-magnitude higher intracellular DRP than concentrations in pore-waters (Glock et al., 2020). This suggests that foraminifera may play role in phosphorus cycle that needs to be further explored, particularly in intertidal environments where DRP is highly dynamic (Chapter 4).

3.2 New challenges of technical developments

The FLEC "Fluorescently Labeled Embedded Core" method (Bernhard and Bowser, 1996; Bernhard and Richardson, 2014) was recently adapted into FLEP "Fluorescently Labelled Embedded Plate" method. This FLEP method was applied for the first time in Les Brillantes mudflat (Loire estuary) to embed a sediment slab. Articles are *in preparation* by Jauffrais et al. to present this method and the results of the sediment slab analyses (Jauffrais et al., *in preparation, in preparation b)*. The Mn_d 2D-DET gel method was also recently developed, the manuscript is *in preparation* by Mouret et al. (Mouret et al., *in preparation*) Chapters 2 and 4 of this PhD thesis use these new methods.

The process to embed the sediment plates is very long (about 3 to 4 months to obtain the plates from which analyses can be done) which limited the number of analyses that could be carried out in this PhD thesis. This PhD thesis presents some of the results obtained from the embedded sediment slabs. Indeed, the two embedded sediments slabs from the Gullmar Fjord were used in Chapter 2 to visualize the Mn solid-phase micro-distribution, especially around the burrows. The size of the sediment slab is quite large (6 x 9 cm) inducing a long data acquisition time for microscale analyses such as µXRF, therefore the entire surface was not analysed. Several micro-maps generated with µXRF focused on visible foraminifera specimens (CTG-labeled) in the Gullmar Fjord slabs. Figure 1 is an example of *Cassidulina laevigata* found in the GF17-3 slab, showing solid-phases maps for calcium (Ca), manganese (Mn), phosphorus (P) and iron (Fe). This work remains to be done with the embedded slabs from the Bourgneuf Bay.

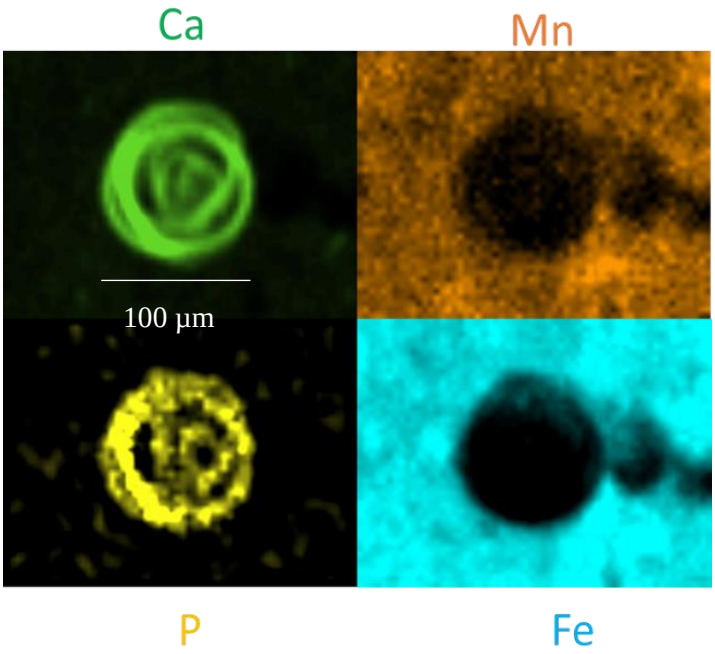

Figure 1: µXRF micro-maps of the foraminifera Cassidulina laevigata in the GF17-3 sediment slab. Calcium (Ca, in green), Manganese (Mn, in orange), Phosphorus (P, in yellow) and Iron (Fe, in blue). (Resolution 25 µm).

This previous work could help to select preferential zones for foraminiferal test analyses. For example, Mn/Ca is used as a proxy to reconstruct the oxygenation conditions in which foraminifera lived (Barras et al., 2018; Groeneveld and Filipsson, 2013; Dijk et al., 2019). Indeed, the combination of 2D-DET gel images, µXRF micro-distribution maps and additional laser ablation analyses on living foraminiferal tests (CTG-labeled) could provide a new perspective to better understand foraminiferal micro-environments. Another example, it would be possible to select foraminifera to be analysed that would be found in areas enriched in Mn in the first millimeters below the interface or specimens found around burrows and see if the same Mn concentrations would be found.

To go further in the characterization of solid phase chemical species, a project will be submitted to request analysis time at the Lucia beamline at the Synchrotron Soleil This project aims to co-locate Mn, Fe and P distribution at high spatial resolution and in 2D in some selected zones (including foraminiferal tests) of the embedded sediment slabs and to identify with XAS (X-ray absorption spectroscopy) the redox state of Fe, Mn and P and the mineral phases to better interpret diagenetic redox transformations. Calcareous tests of some living foraminiferal

specimens located in these selected zones can also be analyzed to document the geochemical links between foraminiferal calcite and their microhabitat.

MicroCTscan analyses were realized to investigate burrow structures and foraminiferal distribution. The analysis of embedded sediment slabs with µCTscan is challenging. Acquisition of high resolution images required to study meiofauna (foraminiferal test) and macrofauna (burrow structure) is time consuming and requires a large image processing capacity necessitating suitable computer hardware (software and image storage capacity) and imaging skills (engineers specialized in imaging). This technical development benefited from the imaging skills of two engineers: Helene Roberge and Dr. Aurelie Pace (Angers university) with the collaboration of Dr. Ronan Ledevin (Bordeaux university) and Dr. Helene Libouban (Angers university). Figure 2 shows the embedded sediment slab from GF17-1 station in 3D, emphasizing a macrofaunal burrow (vertical structure) and Figure 3 shows foraminiferal tests into the sediment slab. This work is still under development. A project will be submitted to request analysis time at the Anatomix beamline at the Synchrotron Soleil in order to improve the identification of foraminiferal tests with a higher spatial resolution (< 5µm).

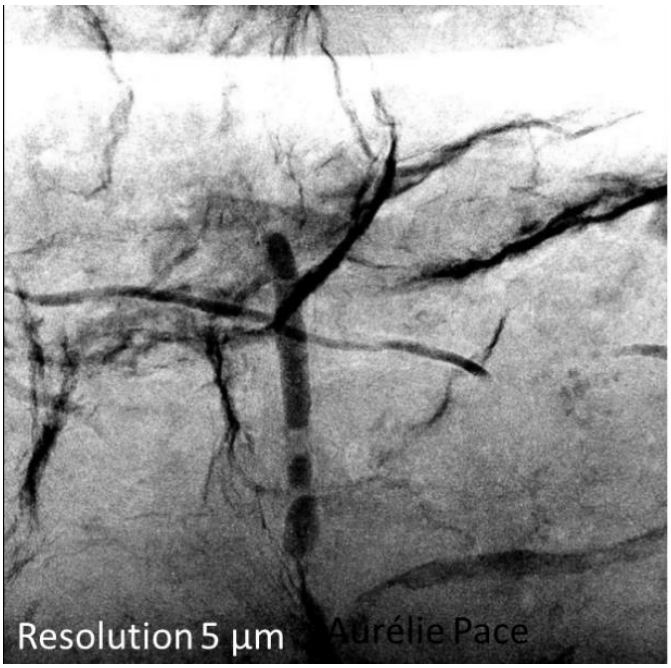

Figure 2: Micro-CTscan images of embedded sediment slab from GF17-1 station allowing to target a macrofaunal burrow structure in 3D (vertical structure). (Resolution 5 µm).

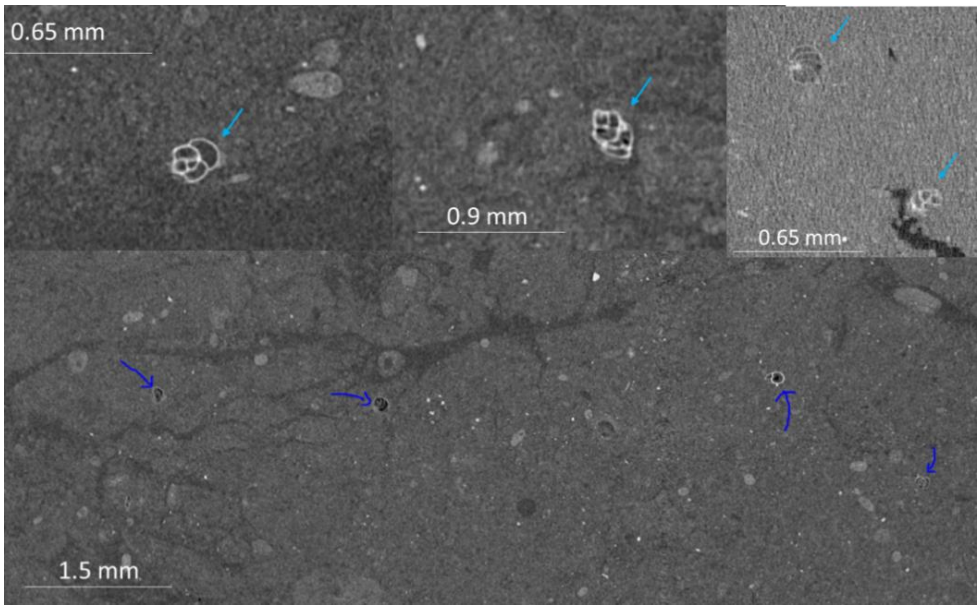

Figure 3: Micro-CTscan images of the embedded sediment slab of the GF17-1 station showing foraminiferal tests within the sediment slab. The blue arrows indicate the foraminiferal tests inside the embedded sediment. (Resolution 5 µm).

3.3 To overcome the lack of knowledge on the foraminiferal reproduction events

This thesis was based only on the analysis of the adult foraminiferal population (mainly > 150 µm). Due to time constraints, the other size fractions of foraminiferal assemblages, in particular the fractions < 125 µm, to study the dynamics of juveniles (< 63 µm) and propagules (< 32 µm) were not studied. The implementation of a sampling strategy to assess the time lag between an event of foraminiferal reproduction and the event triggering this reproduction (unfavourable or favourable conditions) is not obvious. A monthly study of the micro-distribution of CTG-labeled species (down to 32 µm fraction) should be carried out over several months to identify more precisely if the adults reproduce or if there is an input of propagules during the different periods linked to the hydrodynamics and meteorological context of the bay. An analysis of the quality of organic matter (e.g. C/N ratio), enrichment factors for trace metal elements (e.g. lead, zinc, copper) and hydrocarbons could also provide indications on the contributions of the Loire river inputs, and the local OM production of the mudflat.

3.4 Monthly spatiotemporal monitoring of redox elements and nutrients in the Bourgneuf Bay mudflat

This PhD thesis work highlighted periods of sediment instability (winter Loire flooding, high rainfall, windstorms, high tidal coefficient) and more stable periods (low water level,

summer conditions). The complete 3-year monitoring of 1D geochemical analyses was not shown in detail. Only April and October 2019 in the chapter 4 were detailed to understand the geochemical processes at two contrasted periods. However, the dynamics of redox and nutrient processes is more complex and requires a complete view of the spatiotemporal evolution of the 1D profiles. This work is *in progress* by Metzger et al., (*in preparation*). The 1D profiles are analyzed using a kriging method and spatial interpolation to easily follow the behaviour of nutrients and other species or chemical elements in the mudflat.

Mesocosm experiments with sediments from the Bourgneuf Bay are *in progress* (PhD thesis project of Corentin Guilhermic) to analysed density and micro-distribution of CTG-labeled foraminifera (> 125 µm) following a succession of fine (3-5 mm) and larger (3 cm) sediment deposits. The first results of this two-month experiment seem promising on the foraminiferal response (moving or not, survival or not, dormancy...) following to the deposition of a layer of sediment (to simulate the conditions of post-flooding event as observed in the Bourgneuf Bay). Then, there is also a geochemical part of the experiment which should allow a better understanding of the chemical evolution of the sediments after a higher deposit event.

Bibliography

Barras, C., Mouret, A., Nardelli, M. P., Metzger, E., Petersen, J., La, C., Filipsson, H. L., and Jorissen, F.: Experimental calibration of manganese incorporation in foraminiferal calcite, Geochim. Cosmochim. Acta, 237, 49–64, https://doi.org/10.1016/j.gca.2018.06.009, 2018.

Bernhard, J. and Richardson, E.: FLEC-TEM: Using Microscopy to Correlate Ultrastructure with Life Position of Infaunal Foraminifera, 103 pp., https://doi.org/10.1007/978-4-431-54388-6_7, 2014.

Bernhard, J. M. and Bowser, S. S.: Novel epifluorescence microscopy method to determine life position of foraminifera in sediments, J. Micropalaeontology, 15, 68–68, https://doi.org/10.1144/jm.15.1.68, 1996.

Bird, C., LeKieffre, C., Jauffrais, T., Meibom, A., Geslin, E., Filipsson, H. L., Maire, O., Russell, A. D., and Fehrenbacher, J. S.: Heterotrophic Foraminifera Capable of Inorganic Nitrogen Assimilation, Front. Microbiol., 11, https://doi.org/10.3389/fmicb.2020.604979, 2020.

Choquel, C., Geslin, E., Metzger, E., Filipsson, H. L., Risgaard-Petersen, N., Launeau, P., Giraud, M., Jauffrais, T., Jesus, B., and Mouret, A.: Denitrification by benthic foraminifera and their contribution to N-loss from a fjord environment, Biogeosciences, 18, 327–341, https://doi.org/10.5194/bg-18-327-2021, 2021.

Courtial, J., Metzger, E., Lothier, J., Choquel, C., Limami, A. M., Cukier, C., & Geslin, E. (2021). Kleptoplastic foraminifera : A trophic strategy of life; (N° EGU21-15345). EGU21. Copernicus Meetings. https://doi.org/10.5194/egusphere-egu21-15345.

Debenay, J.-P. and Guillou, J.-J.: Ecological transitions indicated by foraminiferal assemblages in paralic environments, Estuaries, 25, 1107–1120, https://doi.org/10.1007/BF02692208, 2002.

Dijk, I. van, Mouret, A., Cotte, M., Houedec, S. L., Oron, S., Reichart, G.-J., Reyes-Herrera, J., Filipsson, H., and Barras, C.: Chemical Heterogeneity of Mg, Mn, Na, S, and Sr in Benthic Foraminiferal Calcite, Front. Earth Sci., 1, https://doi.org/10.3389/feart.2019.00281, 2019.

Eyre, B. D., Oakes, J. M., and Middelburg, J. J.: Fate of microphytobenthos nitrogen in subtropical subtidal sediments: A 15N pulse-chase study, Limnol. Oceanogr., 61, 2108–2121, https://doi.org/10.1002/lno.10356, 2016.

Froelich, P. N., Klinkhammer, G. P., Bender, M. L., Luedtke, N. A., Heath, G. R., Cullen, D., Dauphin, P., Hammond, D., Hartman, B., and Maynard, V.: Early oxidation of organic matter in pelagic sediments of the eastern equatorial Atlantic: suboxic diagenesis, Geochim. Cosmochim. Acta, 43, 1075–1090, https://doi.org/10.1016/0016-7037(79)90095-4, 1979.

Glock, N., Romero, D., Roy, A. S., Woehle, C., Dale, A. W., Schönfeld, J., Wein, T., Weissenbach, J., and Dagan, T.: A hidden sedimentary phosphate pool inside benthic foraminifera from the Peruvian upwelling region might nucleate phosphogenesis, Geochim. Cosmochim. Acta, 289, 14–32, https://doi.org/10.1016/j.gca.2020.08.002, 2020.

Groeneveld, J. and Filipsson, H. L.: Mg/Ca and Mn/Ca ratios in benthic foraminifera: the potential to reconstruct past variations in temperature and hypoxia in shelf regions, Biogeosciences, 10, 5125–5138, https://doi.org/10.5194/bg-10-5125-2013, 2013.

Jauffrais, T., Mouret, A., Metzger, E., Jesus, B., Jean-Soro, L., Bernhard, J. M., and Geslin, E.: Combined characterization of fine-scale distributions and microenvironments of living protists in intertidal sediment., J. Exp. Biol. Ecol., *in preparation*.

Jauffrais, T., Mouret, A., Metzger, E., Jesus, B., Bernhard, J. M., and Geslin, E.: Two-dimensional paired analyses of fine-scale sediment geochemistry and live benthic protists, and metazoans distributions in mudflat chemoclines., Environ. Sci. Technol., *in preparation*.

Jauffrais, T., Jesus, B., Metzger, E., Mouget, J.-L., Jorissen, F., and Geslin, E.: Effect of light on photosynthetic efficiency of sequestered chloroplasts in intertidal benthic foraminifera (*Haynesina germanica* and *Ammonia tepida*), Biogeosciences, 13, 2715–2726, https://doi.org/10.5194/bg-13-2715-2016, 2016.

LeKieffre, C., Spangenberg, J. E., Mabilleau, G., Escrig, S., Meibom, A., and Geslin, E.: Surviving anoxia in marine sediments: The metabolic response of ubiquitous benthic foraminifera (*Ammonia tepida*), PLOS ONE, 12, e0177604, https://doi.org/10.1371/journal.pone.0177604, 2017.

LeKieffre, C., Spero, H. J., Russell, A. D., Fehrenbacher, J. S., Geslin, E., and Meibom, A.: Assimilation, translocation, and utilization of carbon between photosynthetic symbiotic dinoflagellates and their planktic foraminifera host, Mar. Biol., 165, 104, https://doi.org/10.1007/s00227-018-3362-7, 2018a.

LeKieffre, C., Jauffrais, T., Geslin, E., Jesus, B., Bernhard, J. M., Giovani, M.-E., and Meibom, A.: Inorganic carbon and nitrogen assimilation in cellular compartments of a benthic kleptoplastic foraminifer, Sci. Rep., 8, 10140, https://doi.org/10.1038/s41598-018-28455-1, 2018b.

Mouret, A., Barbe, A., Levrard, R., Charbonnier, C., Cesbron, F., Choquel, C., and Metzger, E.: Two-dimensional determination of dissolved manganese in sediment porewaters, Front. Chem., *in preparation*.

Polovodova Asteman, I. and Schönfeld, J.: Recent invasion of the foraminifer Nonionella stella Cushman & Moyer, 1930 in northern European waters: evidence from the Skagerrak and its fjords, J. Micropalaeontology, 35, 20–25, https://doi.org/10.1144/jmpaleo2015-007, 2015.

Risgaard-Petersen, N., Nielsen, L. P., Rysgaard, S., Dalsgaard, T., and Meyer, R. L.: Application of the isotope pairing technique in sediments where anammox and denitrification coexist, Limnol. Oceanogr. Methods, 1, 63–73, https://doi.org/10.4319/lom.2003.1.63, 2003.

Thibault de Chanvalon, A., Metzger, E., Mouret, A., Cesbron, F., Knoery, J., Rozuel, E., Launeau, P., Nardelli, M. P., Jorissen, F. J., and Geslin, E.: Two-dimensional distribution of living benthic foraminifera in anoxic sediment layers of an estuarine mudflat (Loire estuary, France), Biogeosciences, 12, 6219–6234, https://doi.org/10.5194/bg-12-6219-2015, 2015.

Thibault de Chanvalon, A., Metzger, E., Mouret, A., Knoery, J., Geslin, E., and Meysman, F. J. R.: Two dimensional mapping of iron release in marine sediments at submillimetre scale, Mar. Chem., 191, 34–49, https://doi.org/10.1016/j.marchem.2016.04.003, 2017.

ACTIVITES COMPLEMENTAIRES

Activités complémentaires à mon travail de recherche réalisées au cours de cette thèse de doctorat :

Campagnes d'échantillonnages :

- Deux campagnes d'échantillonnage dans le Gullmar Fjord (Suède) (2 jours en Novembre 2017 et 2 jours en Septembre 2018).
- Campagne d'échantillonnage mensuel (1 journée par mois pendant 2 ans) dans la vasière de la Baie de Bourgneuf au site d'étude « La Coupelasse ».

Travaux collaboratifs avec des laboratoires nationaux et internationaux :

- Deux mois à l'université de Lund (Suède) avec Pr. Helena Filipsson. Ces deux mois m'ont permis de tamiser mes échantillons de sédiments. J'ai pu commencer le travail de taxonomie des espèces de foraminifères du Gullmar Fjord avec l'aide de Dr. Laurie Charrieau et Dr. émérite Karen Luise Knudsen.
- Une semaine à l'université d'Aarhus (Danemark) avec Dr. Nils Risgaard-Petersen (Associate professor). Cette semaine m'a permis de faire les mesures de taux de dénitrification de l'espèce *Nonionella* sp. T1. J'ai pu également mesurer le taux de respiration de plusieurs espèces du Gullmar Fjord.
- Plusieurs jours (l'équivalent d'environ 2 mois) passés au LPG-Nantes à travailler avec Pr. Patrick Launeau sur l'analyse des gels 2D.
- Plusieurs jours à l'IFSTTAR (Institut français des sciences et technologies des transports, de l'aménagement et des réseaux) de Nantes avec Dr. Liliane Jean-Soro pour réaliser des cartes µXRF à partir des plaques de sédiment enrésiné.
- Travail collaboratif en distanciel (environ 1 mois) avec Dr. Emilie Houliez (post-doctorante), avec qui j'ai pu discuter des analyses statistiques/multivariées de ma thèse.
- Travail collaboratif en distanciel (environ 2 mois) avec Dr. Aubin Thibault de Chanvalon pour travailler sur la modélisation des gels 2D.
- Travail collaboratif (environ un mois) avec Franck Mercier de Polytech Angers, pour l'impression en 3D des pièces constituant un splitter humide (Charrieau et al., 2018). J'ai été chargée du bon déroulement des impressions de foraminifères en 3D pour l'exposition « Foraminifères, l'océan à la loupe ».

Communications scientifiques nationales et internationales (congrès et séminaires) :

- Présentation d'un poster au congrès international FORAMS 2018 à Edinburgh (Ecosse).
- Présentation d'un poster au congrès international GOLDSCHMIDT 2019 à Barcelone (Espagne).
- Présentation orale en anglais au congrès nationale RST 2018 (Réunion des Sciences de la Terre) session « Micropaleontology » à Lille (France).
- Séminaire à l'université de Rennes 1 (France) pour présenter mes travaux de recherche sur le Gullmar Fjord en 2019.
- Séminaire de présentation de mon projet de thèse pendant les journées du LPG en 2018.
- J'ai présenté l'avancement de chaque chapitre de ma thèse aux membres du BIAF lors de réunions de travail « brainstorming ».

Communications de vulgarisation scientifique :

- Projet de sciences participative avec des élèves de première du Lycée Mounier. Obtention d'un contrat DCACV « Mission de valorisation de la recherche scientifique 2017-2018 » de 32h (séminaire, visite du laboratoire, participation des élèves au piquage des foraminifères et présentation orale des élèves autour de leurs découvertes, participation à Exposciences avec un groupe d'élèves).
- Nuits des chercheurs 2018 « 1001 HISTOIRES », réalisation d'une bande dessinée (illustrations et textes) à destination du grand public sur les foraminifères.
- Nuits des chercheurs 2019 « Vous aussi, entrez dans l'enquête ! », réalisation d'un jeu ludique autour de la bioindication avec Marie Fouet (doctorante BIAF).
- Participation au concours Ma thèse en 180 secondes. Finale locale angevine et demi-finale régionale Bretagne-Loire édition 2019.
- Participation au journées porte-ouvertes 2019 de l'université pour présenter la licence « parcours géosciences et environnement », les salles de TP, le laboratoire du BIAF.
- Participation à l'exposition « Foraminifères, l'océan à la loupe » Nov. Déc 2021 au Muséum des Sciences Naturelles d'Angers. Participation à l'écriture des textes et idées des schémas associés pour la partie « connaissance de base sur les foraminifères ».

Enseignements contrat DCACE (Activité Complémentaire d'Enseignement)

- Deux contrats de DCACE pendant cette thèse un premier de 64h (2018-2019) et un deuxième de 32h (2019-2020).
  Licence 2 : Enseignement Biostratigraphie (paléo-écologie ; dessins de micro-fossiles (diatomées, radiolaires, foraminifères, ostracodes, ptéropodes).
  Licence 1 : Histoire de la Terre et de la Vie (indices de biodiversité, visite du musée d'histoire naturelle, paléo-biodiversité des Faluns, dessins macro-fossiles (archéocyathes, trilobites, graptolites, stromatolites, anthozoaires, éponges, bryozoaires, brachiopodes, échinodermes, gastéropodes, bivalves, céphalopodes).

Encadrement de stagiaire

- Encadrement de Zofia Stachowska, étudiante Polonaise en 2ème année de licence de Géologie. J'ai co-encadré le stage de Zofia pendant deux mois en 2018, je l'ai guidée pour le lavage, piquage et taxonomie des foraminifères en Baie de Bourgneuf et l'écriture d'un premier mémoire de stage.

Implications administratives

- Déléguée des doctorants au conseil de l'EDSML (Ecole doctorale Sciences de la mer et du Littoral) pendant 3 ans (3 conseils par an).
- Déléguée des doctorants au conseil du collège doctoral d'Angers pendant 3 ans (3 conseils par an).
- Déléguée des contractuels au conseil de Laboratoire LPG-BIAF (Nantes-Angers) pendant un an (2 conseils).

Formations transversales qui m'ont apportée le plus pendant cette thèse :

289 heures de formations ont été réalisées pendant cette thèse (équivalent 132 Ects).

- Doctoriale Bretagne Loire 2018 (valorisation des connaissances et compétences des docteurs dans les secteurs non-académiques).
- Anglais scientifique.
- Gestion du trac dans la prise de parole.
- Communication pédagogique (dans la formation DCACE).

VULGARISATION SCIENTIFIQUE « FORAMSTORY »

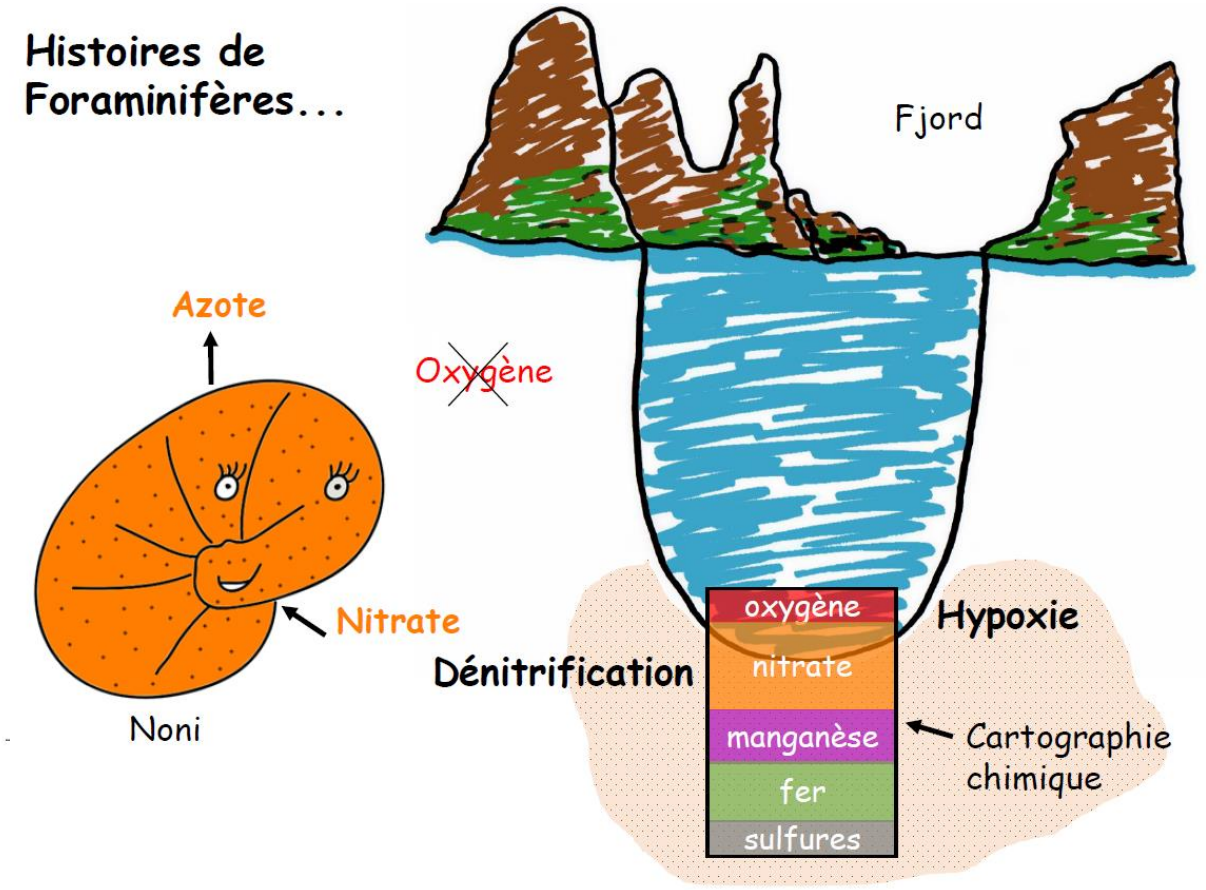

Slide presented to the competition "my thesis in 180 seconds" (MT180s). One of the four winners of the local Angevin competition. Participation in the regional semi-final at Le Mans.

Texte presenté au concours MT180s

En ce moment, sans vous en rendre compte, vous respirez de l'oxygène et expirez du dioxyde de carbone. Mais ce n'est pas exceptionnel... puisque la majorité des êtres vivants utilise ce mode de respiration.

Pendant mes travaux de thèse je m'intéresse à de minuscules organismes marins, capables de vivre temporairement sans oxygène dans les sédiments, ce sable, qui tapisse le fond des mers et des océans. Mais qui sont ces incroyables micro-organismes ? Ce sont des foraminifères, comme *Nonionella,* caricaturé ici par Noni. Ils ressemblent à de petits coquillages mais ce ne sont ni des bactéries ni des animaux.

L'objectif de la 1ère partie de ma thèse est de comprendre la vie de Noni et son environnement chimique. Noni vit dans un Fjord en Suède. Un fjord c'est une cuvette d'eau de mer entre des montagnes. En hiver le tapis roulant des courants marins n'apporte pas suffisamment d'oxygène au fond de la cuvette ce qui crée un manque d'oxygène appelé hypoxie. Et ça c'est une condition extrême pour la vie ! Plusieurs solutions s'offrent alors pour les organismes ; soient ils meurent, soient ils s'enfuient soient ils s'adaptent.

Récemment, des collègues internationaux ont découvert que certains foraminifères en absence d'oxygène, respirent des nitrates et expirent de l'azote, comme Noni, c'est ce qu'on appelle la dénitrification. Alors là vous vous dites nitrates = pollution, pollution oui mais pas que...il ne faut pas oublier que les nitrates sont avant tout une molécule essentielle à la vie marine et à la vie végétale, vous comprenez ? C'est simple pas de nitrates, pas de plancton, pas de plancton pas de sandwich au thon !

Au fond des mers une fois que l'oxygène a été consommé par des bactéries, d'autres molécules se forment : tels que les nitrates mais aussi des métaux comme le manganèse et le fer puis les sulfures. Vous vous imaginez un peu une campagne océanographique en Suède en hiver ? alors déjà il fait froid, il fait nuit et en plus ça sent l'œuf pourri à cause des sulfures ! Bonjour l'ambiance !

Dans le premier article que je suis en train d'écrire, j'ai réussi à quantifier la respiration de Noni et à cartographier son environnement chimique en 2 dimensions. Ainsi j'ai pu montrer que Noni avec ses milliers de frères et sœurs peuvent consommer jusqu'à 100% des nitrates contenu dans le sédiment du Fjord ! Noni pourrait être ainsi considéré comme une espèce bio-indicatrice d'un milieu riche en nitrates et faible en oxygène. Super ! mais au fait à quoi ça sert de savoir ça finalement ?

Vous devez savoir que de nos jours certaines zones de l'océan s'appauvrissent en oxygène à cause de nos activités humaines. Et bien comprendre la vie des foraminifères denitrifiants, dont Noni, permet de suivre sur le long terme l'évolution de ces zones et donne un moyen de comprendre et prédire les impacts sur le fonctionnement des écosystèmes marins, mais là il me faudra plus de 180s pour vous l'expliquer !

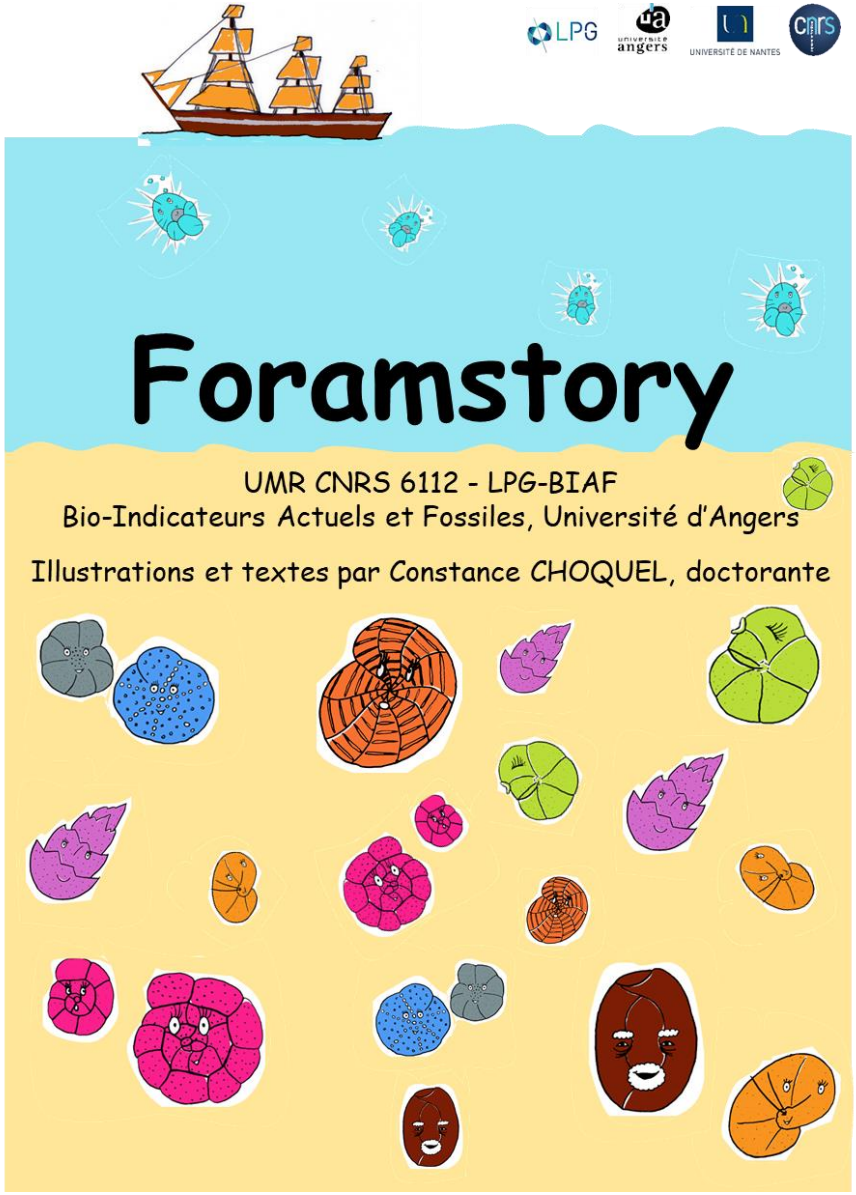

Forams dessins/Forams photos

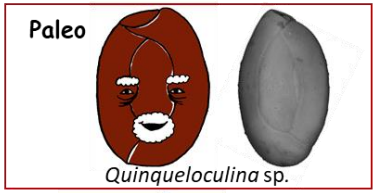

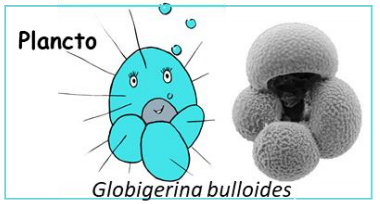

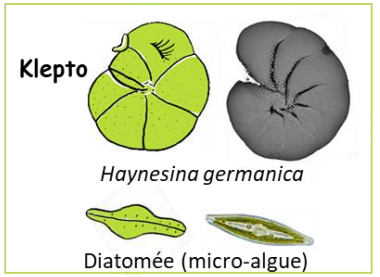

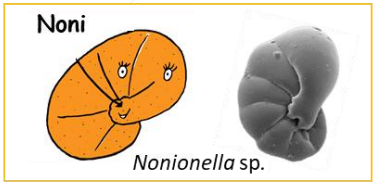

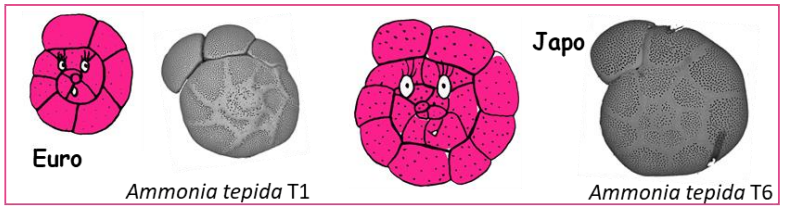

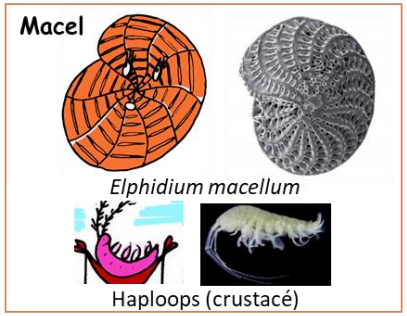

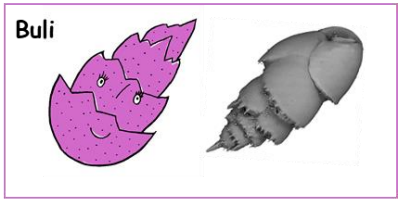

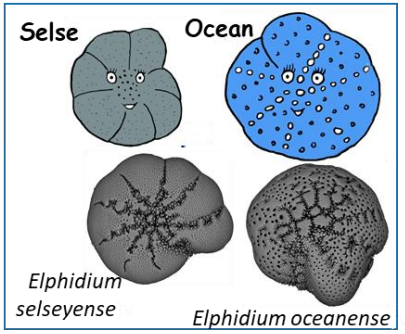

Bienvenue dans le monde des **Foraminifères** ! (ou **Forams** pour les intimes).

Mais que sont les Foraminifères ?

Les Forams sont des **micro-organismes marins** (< 1 mm) vivants dans les **sédiments** (sable, vase) au fond des océans … En grec Foraminifera signifie « qui porte des trous » ; ces trous leur servent à communiquer avec leur environnement extérieur.

Ces petites créatures mystérieuses ne sont ni des bactéries, ni des animaux, ni des végétaux, ils appartiennent à la branche des **Rhizaria**!

Foram story

Les Forams sont connus depuis l'Antiquité, mais c'est au 19ème siècle qu'ils deviennent célèbres grâce au micropaléontologue **Alcide d'Orbigny.**

Le 19ème siècle, c'est aussi l'expédition « **Glomar Challenger** » qui a été, de 1872 à 1876, la première campagne océanographique mondiale. Elle a permis de découvrir plus de 4000 nouvelles espèces !

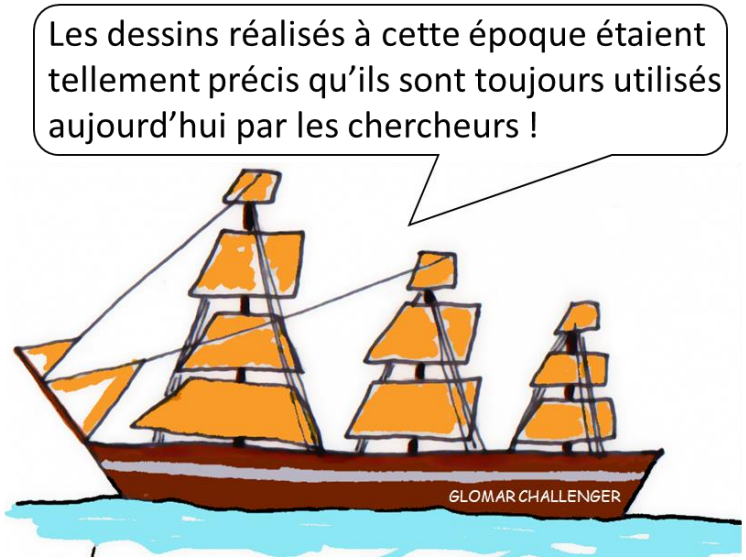

Paleo story

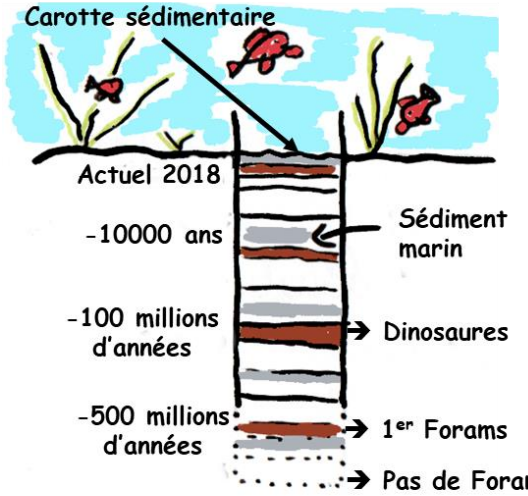

Les Forams sont apparus il y a plus de **500 millions d'années,** bien avant les dinosaures et même avant la vie terrestre !

Pour remonter le temps, les scientifiques étudient des **carottes sédimentaires**. C'est une colonne de sédiment, qui comme un mille feuilles, contient les coquilles des organismes morts dits **« fossiles ».**

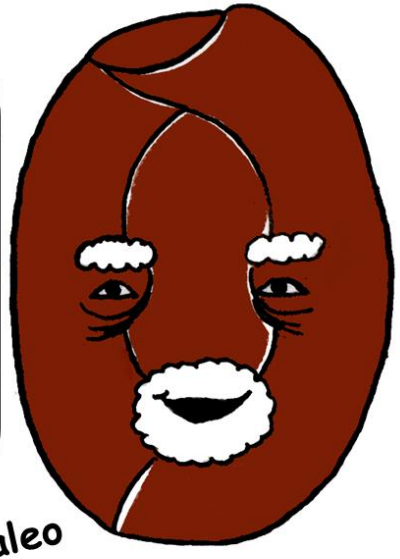

Climat story

Les Forams avec une **coquille** se retrouvent dans les sédiments anciens.

Ainsi les océans du passé peuvent être dévoilés !

Par exemple, plus l'océan est chaud plus les Forams incorporent du **Magnésium (Mg)** dans leur coquille à la place du **Calcium (Ca)**.

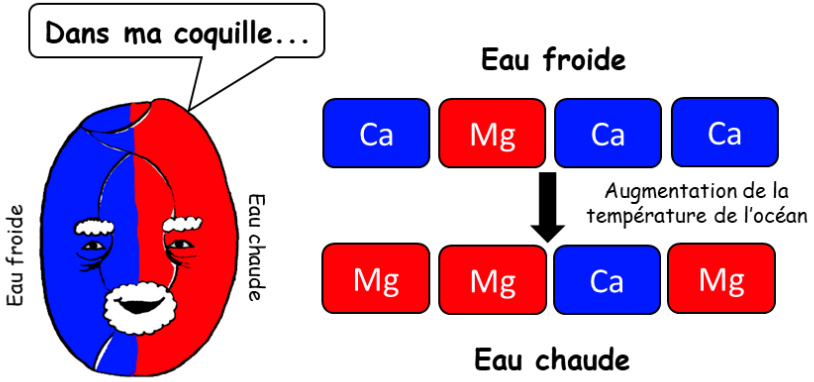

En mesurant les proportions de Magnésium et de Calcium dans la coquille, les chercheurs peuvent retrouver quelle était la température des océans au temps des dinosaures !

Cellule story

Les Forams sont des **eucaryotes unicellulaires** (une cellule avec un noyau)

La cellule du Foram est constituée d'un **noyau** (ADN), de **mitochondries** (respiration), de **lysosomes** (digestion), d'un **appareil de Golgi** et de **reticulum** (fabrication de lipides et protéines), de **pseudopodes** (mobilité)… Bref beaucoup de fonctions dans une seule cellule !

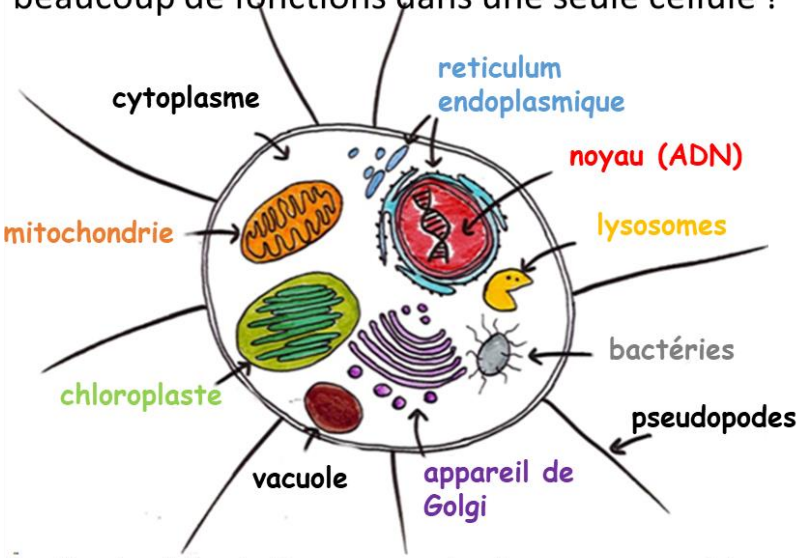

Particularités ! Ils peuvent vivre en symbiose avec des **bactéries** et certains peuvent utiliser des **chloroplastes** volés aux micro-algues !

Plancto story

Parmi les Forams, il y a des espèces **benthiques** qui vivent dans le sédiment (environ 5000 espèces) et aussi des espèces **planctoniques** comme **Plancto** (environ 100 espèces) qui se déplacent au gré des courants dans l'océan de surface (0 à 200m de profondeur).

La moitié des espèces planctoniques vivent en symbiose avec des micro-algues ! Et leurs coquilles sont très étudiées par les paléontologues.

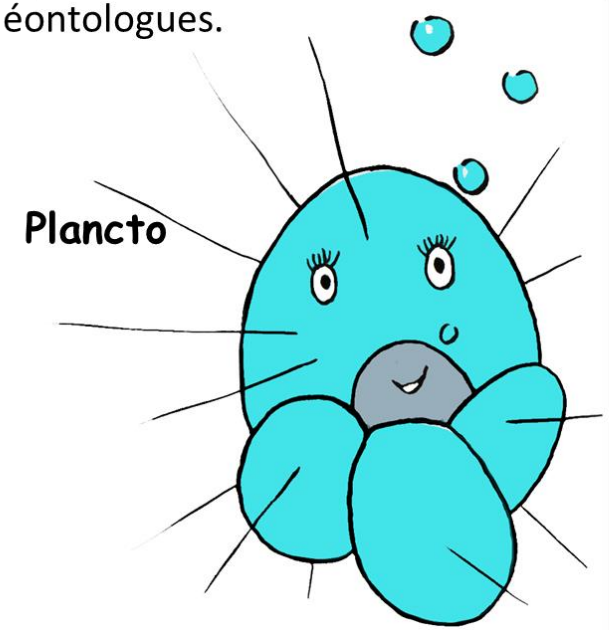

Noni story

Comme tous les organismes (sauf les bactéries), les Forams ont besoin d'oxygène mais certains « respirent » les nitrates comme **Noni** et rejettent de l'azote (gaz). C'est la **dénitrification** !

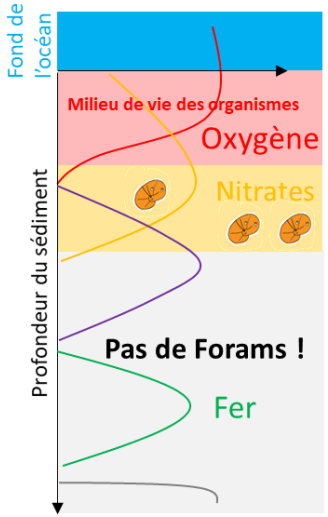

Les nitrates sont les oxydants les plus rentables pour les organismes après l'oxygène.

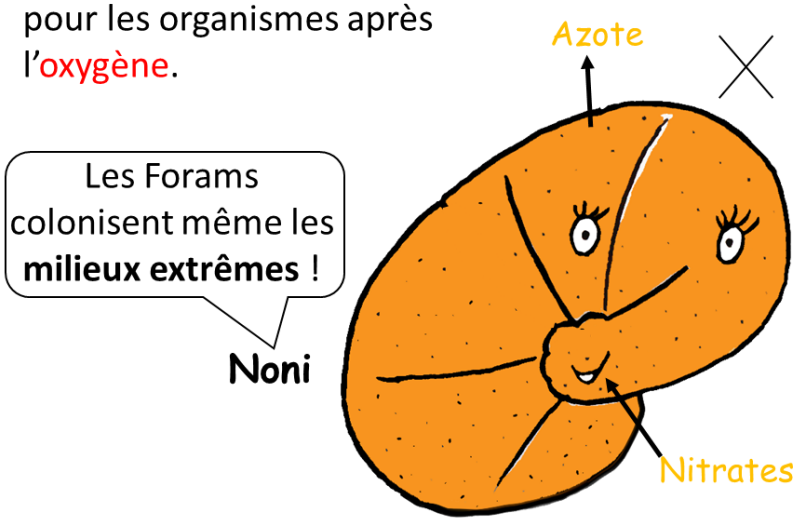

Klepto story

Les diatomées sont des **micro-algues** ; elles sont à la base de la chaine alimentaire marine et produisent, grâce à la **photosynthèse*,** jusqu'à 1/4 de l'oxygène terrestre !

*Photosynthèse =

CO_2 + sels nutritifs + eau → Oxygène + sucre

Les micro-algues peuvent se faire voler leurs **chloroplastes** (sac contenant le sucre de la photosynthèse) par les Forams **kleptoplastes**

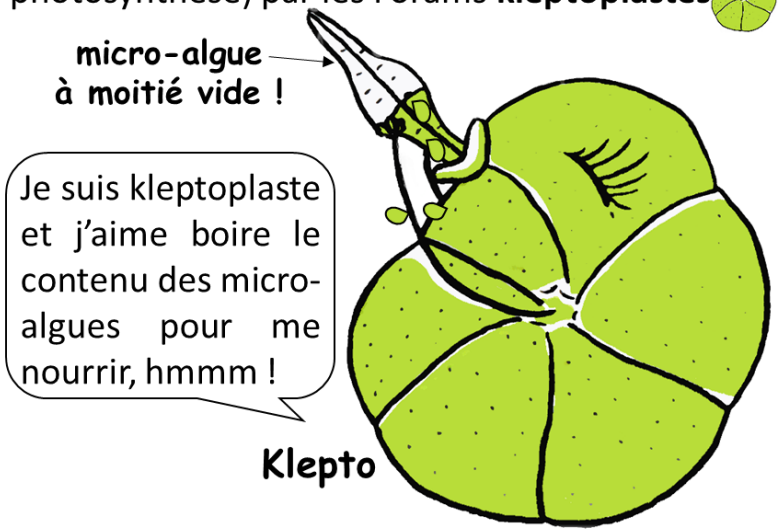

Bio-Indicateur story

Les Forams peuvent être utilisés comme indicateurs de la **qualité** de l'environnement marin. Mais comment est-ce possible ?

Les espèces ne seront pas les mêmes si l'environnement est bon ou mauvais !

Code couleur = échelle de qualité de l'environnement

Mauvais = rouge
Médiocre = orange
Moyen = jaune
Bon = vert
Très bon = bleu

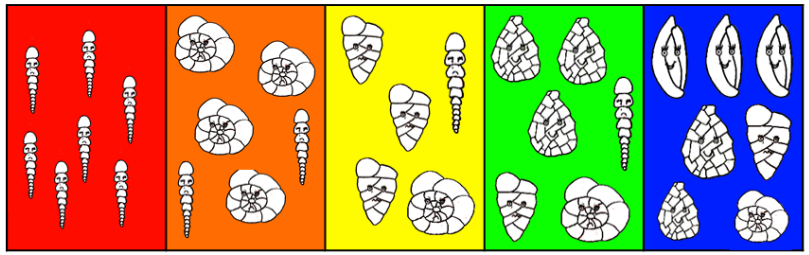

Sur la côte Méditerranéenne française, les principales perturbations sont : trop de **déchets organiques** (débris de végétaux, animaux et micro-organismes), trop de **nutriments** (dû aux activités humaines…) et le manque d'**oxygène**.

Buli story

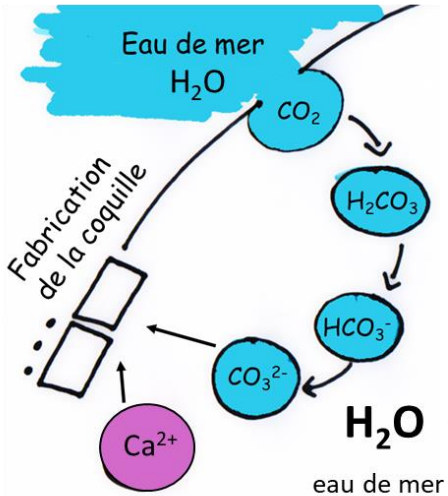

Comment les Forams fabriquent-ils leur coquille ?

Grâce à l'eau de mer et à la chimie des carbonates !

H_2O + CO_2 = H_2CO_3

eau de mer — dioxyde de carbone — acide carbonique

H_2CO_3 → HCO_3^- → CO_3^{2-}

acide carbonique — bicarbonate — ion carbonate

Ces ions carbonates combinés au **calcium** (Ca^{2+}) lui aussi dissous dans l'eau, forment du **calcaire $CaCO_3$.**
Et c'est comme ça que se construit ma coquille !

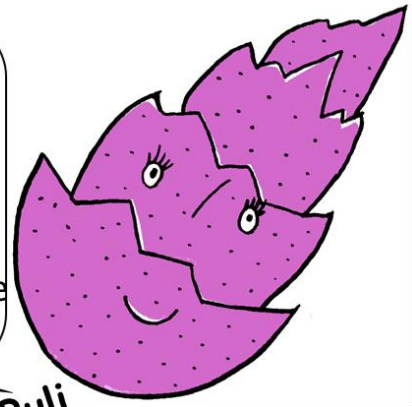

Buli

Invasion story

Involontairement, les Forams peuvent être transportés hors de leur zone de vie naturelle (par bateau, par importation de coquillages…)

Certaines espèces transportées survivent très bien dans leur nouvel habitat. Mais elles peuvent nuire aux espèces **autochtones** (qui vivent sur place) et sont alors considérées comme **invasives**.

L' **Ammonia japonaise** serait arrivée en France au début des années 70 en même temps que les huitres japonaises et a quasiment fait disparaitre l'**Ammonia européenne** !

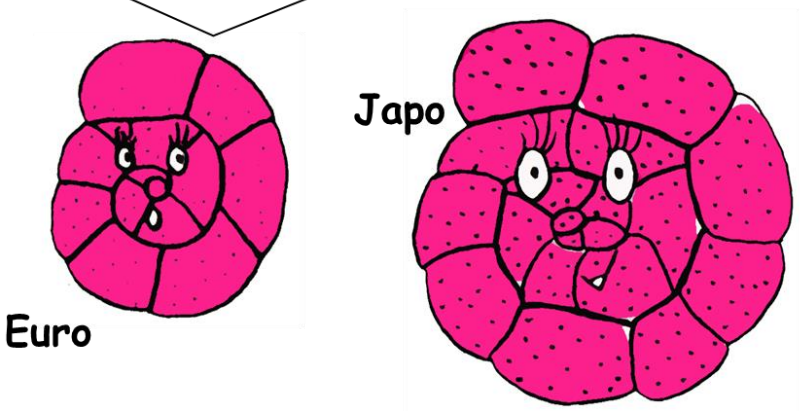

Elphi story

Les Elphi comme **Selse** et **Ocean** sont deux espèces venant de milieux côtiers. Ils se reproduisent en fonction des saisons.

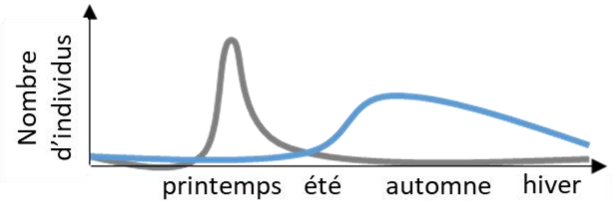

Ces deux espèces n'occupent pas la même **niche écologique,** autrement dit...

Nous avons besoin de conditions de vie différentes (température, salinité, qualité de la nourriture).

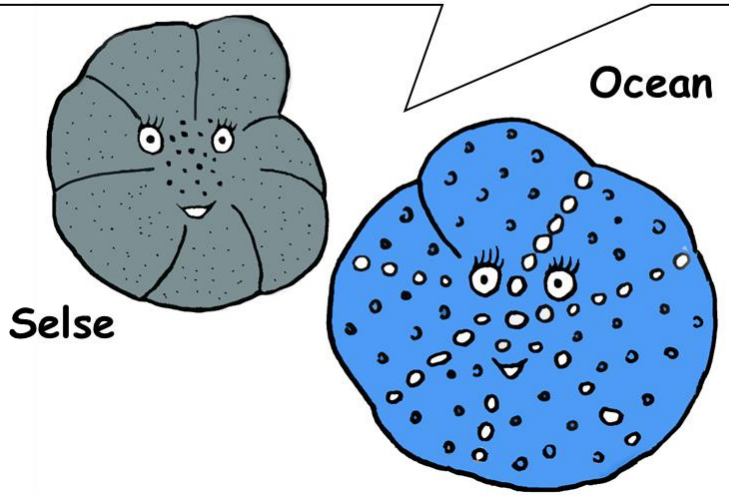

Haploops story

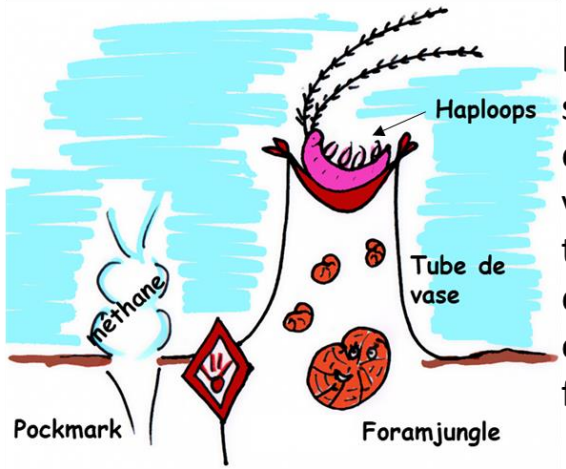

Les **haploops** sont des cousins des crevettes. Ils vivent dans des tubes de vase qu'ils construisent au fond de la mer.

Ces petits tubes servent également de maison aux Forams !

Mais attention ! Si la vie d'un haploops parait paisible ils vivent pourtant à proximité de **Pockmarks** (cavités) contenant un gaz appelé **méthane**.

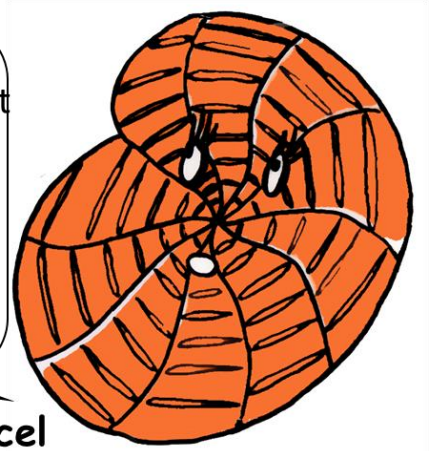

Macel

Les **Foraminifères** sont d'incroyables **micro-organismes marins** faits d'une seule cellule. La Foramstory illustre les diverses thématiques de recherche étudiées par les scientifiques. Par exemple, la **paléontologie** permet de mieux représenter les climats anciens, la **biologie cellulaire** aide à comprendre les métabolismes des cellules vivantes, et l'**écologie** met en relation les organismes et leur environnement.

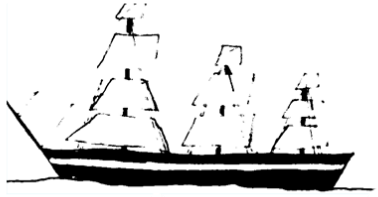

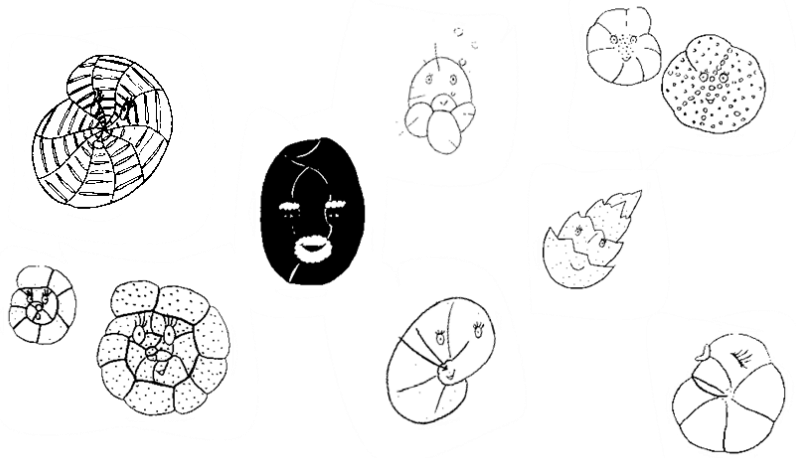

DOCTORAT SCIENCES BRETAGNE DE LA MER LOIRE ET DU LITTORAL

université angers

Titre : Ecologie des foraminifères benthiques, interactions biologiques et géochimiques : approche pluridisciplinaire à différentes échelles

Mots clés : foraminifères benthiques, dynamiques de populations, diatomées, micro-environnements sédimentaires, 2D-DET, denitrification, bioirrigation

Résumé : L'objectif général de cette thèse est d'étudier les micro-environnements sédimentaires et le fonctionnement des écosystèmes de deux zones côtières. Nous avons combiné différentes méthodes à haute résolution spatiale et des analyses multivariées à différentes échelles spatio-temporelles pour révéler les interactions entre les compartiments de la faune benthique et géochimiques. Tout d'abord, nous avons étudié deux stations présentant des conditions contrastées en oxygène, nitrate et manganèse dans le Gullmar Fjord (Suède). Nous avons révélé la forte contribution (50-100 %) des foraminifères benthiques dénitrifiants au cycle de l'azote dans des micro-environnements oxygénés et riches en nitrate. Le cycle de l'azote et du manganèse sont étroitement liés aux conditions d'oxygénation de l'écosystème. Nos résultats ont mis en évidence la forte contribution (87 %) de la bioirrigation engendrée par la macrofaune au cycle du Mn dans des conditions hypoxiques. Deuxièmement, nous nous sommes concentrés sur un suivi mensuel de deux groupes de bioindicateurs écologiques : le microphytobenthos (MPB) et les foraminifères dans la vasière en Baie de Bourgneuf (France). Nous avons montré que les événements de reproduction des foraminifères sont modulés par des conditions défavorables (hydrodynamisme plus fort en conditions hivernales) par rapport à des conditions favorables (hydrodynamisme plus faible en conditions estivales). Nos résultats suggèrent que les espèces de foraminifères se nourrissent préférentiellement des espèces de diatomées en fonction de leur forme, de leur taille et de leur mode de vie. Nous avons également comparé avec des méthodes à haute résolution spatiale les conditions géochimiques de deux mois contrastés, ce qui a permis de clarifier le comportement des espèces redox et des nutriments. De plus, les micro-distributions des foraminifères indiquent l'état d'instabilité *versus* stabilité des sédiments. Enfin, cette recherche doctorale ouvre de nouvelles perspectives dans l'utilisation des hautes résolutions spatiales en 2D/3D pour résoudre des problèmes d'écologie benthique complexes.

Title: Ecology of benthic foraminifera, geochemical and biological interactions: multidisciplinary approach at different scales

Keywords: benthic foraminifera, population dynamics, diatoms, sedimentary micro-environments, 2D-DET, denitrification, bioirrigation

Summary: The overall aim of this PhD thesis was to investigate sedimentary micro-environments and ecosystem functioning of two coastal areas. We combined different high spatial resolution methods and multivariate analyses at different spatio-temporal scales to reveal interactions between benthic faunal and geochemical compartments. Firstly, we investigated two stations with contrasted oxygen, nitrate and manganese conditions in the Gullmar Fjord (Sweden). We revealed the high contribution (50–100 %) of denitrifying benthic foraminifera to the nitrogen cycle in oxygenated and nitrate-rich micro–environments. Nitrogen and manganese cycles are closely related to oxygenation conditions of the ecosystem. Our results highlighted the high contribution (87 %) of macrofaunal bioirrigation to Mn release to the water column under hypoxic conditions. Secondly, we focused on a monthly monitoring of two ecological bioindicators groups; microphytobenthos (MPB) and foraminifera in the Bourgneuf Bay mudflat (France). We showed that foraminiferal reproduction events were modulated by unfavorable conditions (high hydrodynamic and winter conditions) *versus* favorable conditions (low hydrodynamic and summer conditions). We also demonstrated that foraminiferal species fed preferentially on diatom species based on their shape, size and life-forms. We further compared, with high spatial resolution methods, geochemical conditions at two contrasted months, which allowed to clarify the behavior of redox species and nutrients. Then, foraminiferal micro-distributions indicated the state of sediment instability *versus* stability. Finally, this doctoral research opens new perspectives in the use of high spatial resolution in 2D/3D to solve complex benthic ecology problems.